

The role of m⁶A modification on mRNA processing in *Drosophila melanogaster*

Dissertation

submitted to attain the academic degree

“Doctor of Natural Sciences”

at the Department of Biology

of the Johannes Gutenberg University Mainz

by

Tina Lenče

born in Ljubljana

Mainz, January 2021

Dekan:

1. Berichterstatter:

2. Berichterstatter:

Tag der mündlichen Prüfung: 12. January 2021

Table of contents

Table of contents	V
List of Figures	VII
List of Tables	VIII
List of Supplemental data	VIII
List of Abbreviations	IX
Abstract	XI
Zusammenfassung	XIII
1 Introduction	1
1.1 Regulation of gene expression	1
1.1.1 DNA methylation.....	1
1.1.2 Histone modifications	3
1.1.3 Non-coding RNA	4
1.2 mRNA processing	5
1.2.1 pre-mRNA capping and cap associated mRNA processing.....	6
1.2.2 pre-mRNA splicing.....	6
1.2.3 mRNA translation	11
1.2.4 Cytoplasmic mRNA turnover	11
1.3 RNA modifications	13
1.3.1 mRNA modifications	15
1.4 m⁶A modification	21
1.4.1 Identification of the m ⁶ A writer complex-(es)	22
1.4.2 m ⁶ A methylation by the METTL3-METTL14 –dependent complex	24
1.4.3 Other m ⁶ A methyltransferases	27
1.4.4 m ⁶ A methylation by the MIS complex in budding yeast	29
1.4.5 m ⁶ A erasers	30
1.4.6 m ⁶ A reader proteins.....	34
1.4.7 m ⁶ A modification regulates nearly all aspects of mRNA processing.....	41
1.4.8 m ⁶ A modification regulates various cellular and physiological processes	47
1.4.9 Methods for m ⁶ A quantification and mapping	51
1.5 <i>Drosophila melanogaster</i>	54
1.5.1 Developmental stages of <i>D. melanogaster</i>	54
1.5.2 Sex determination and dosage compensation pathways in <i>Drosophila melanogaster</i>	55
1.5.3 Neuronal development	57
2 Aim of the work	60
3 Preliminary remarks	61
4 Results	63
4.1 Identification of the m⁶A writer complex in <i>D. melanogaster</i>	63
4.1.1 Mettl3, Mettl14 and Fl(2)d are required for m ⁶ A methylation of mRNA.....	63
4.1.2 Components of the m ⁶ A writer complex localize to the nucleus.....	65
4.1.3 m ⁶ A levels are dynamic during fly development.....	67
4.2 Identification of m⁶A reader proteins in <i>D. melanogaster</i>	68
4.2.1 Flies encode one nuclear and one cytoplasmic YTH domain protein	68
4.2.2 Putative novel m ⁶ A readers are involved in mRNA turn-over.....	71
4.3 Loss of m⁶A on mRNA affects gene expression and splicing	75
4.3.1 The m ⁶ A writer complex and the Ythdc1 protein regulate alternative splicing	75
4.3.2 m ⁶ A in <i>D. melanogaster</i> is enriched along 5'UTR regions and in coding sequences	76

4.4	Flies lacking m⁶A display severe locomotion defects	80
4.4.1	<i>Mettl3</i> and <i>Mettl14</i> mutant flies are viable, but flightless and die earlier	80
4.4.2	Loss of m ⁶ A leads to altered neuronal functions	81
4.5	m⁶A modification modulates splicing of <i>Sex lethal (Sxl)</i>.....	83
4.6	<i>Ythdc1</i> mutants recapitulate defects observed upon loss of m⁶A.....	85
4.6.1	Loss of <i>Ythdc1</i> results in altered fly locomotion	85
4.6.2	<i>Mettl3</i> and <i>Ythdc1</i> mutant flies regulate many common splicing events.....	86
4.7	Nito is a novel component of the m⁶A writer complex.....	88
4.7.1	<i>Ythdc1</i> interacts with splicing factors and with components of the m ⁶ A writer complex	88
4.7.2	Nito and Vir are conserved components of the writer complex.....	89
4.8	Flacc is required for m⁶A deposition as a component of the MACOM complex.....	92
4.8.1	Nito interacts with many proteins linking m ⁶ A to transcription and mRNA processing	92
4.8.2	Flacc is required for m ⁶ A deposition	92
4.8.3	Flacc regulates similar transcriptome events as other m ⁶ A writer components	94
4.8.4	Flacc regulates splicing of m ⁶ A modified transcripts	95
4.8.5	Flacc is required for proper splicing of <i>Sex lethal</i>	96
4.8.6	Flacc stabilizes the interaction between Nito and Fl(2)d	97
4.8.7	Flacc interactome identifies factors previously linked to m ⁶ A writers and readers	100
4.9	Hakai protein modulates m⁶A deposition by stabilizing the m⁶A writer complex.....	103
4.9.1	Hakai is a conserved protein, required for m ⁶ A deposition	103
4.9.2	Hakai interacts with MACOM components.....	106
4.9.3	Fl(2)d is ubiquitinated and strongly destabilized upon Hakai depletion	107
4.9.4	Hakai depletion strongly affects stability of MACOM components	109
5	Discussion and outlook.....	113
5.1	m⁶A writer complex consists of two sub-complexes MAC and MACOM	114
5.1.1	MAC.....	115
5.1.2	MACOM.....	117
5.1.3	m ⁶ A-independent functions of MACOM components	125
5.1.4	Is MACOM required for methylation of all mRNA sites?	128
5.1.5	What are the functions of other putative m ⁶ A methyltransferases in flies?	131
5.2	m⁶A demethylases in <i>Drosophila melanogaster</i>?.....	134
5.3	m⁶A is decoded by different reader proteins.....	136
5.3.1	<i>Ythdc1</i>	136
5.3.2	<i>Ythdf</i>	138
5.3.3	Other putative m ⁶ A regulated proteins	139
5.4	The mystery behind the m⁶A profile on mRNA	143
5.5	m⁶A modification regulates alternative splicing	146
5.5.1	m ⁶ A modification modulates splicing of <i>Sex lethal (Sxl)</i>	148
5.6	The role of m⁶A mRNA modification during <i>D. melanogaster</i> development	151
5.6.1	Gametogenesis and early embryogenesis	152
5.6.2	m ⁶ A in <i>D. melanogaster</i> is required for proper neuronal functions	153
	Conclusions	159
	Supplemental data.....	160
	Materials and methods	188
	Literature	200
	Appendix 1 - Research article	220
	Appendix 2 - Research article	240
	Acknowledgements.....	267

List of Figures

Figure 1. Scheme of N6-methyltransferases and ALKBH-family demethylases.....	3
Figure 2. Schematic depiction of spliceosome assembly.....	8
Figure 3. Schematic representation of alternative splicing events.....	10
Figure 4. RNA modifications found in three kingdoms of life.....	14
Figure 5. Nucleotide modifications on mRNA.....	15
Figure 6. m ⁶ A and m ⁶ Am modifications show non-random distribution along the mRNA.....	22
Figure 7. Schematic representation of m ⁶ A methyltransferases and their substrates.....	23
Figure 8. Schematic representation of AlkB-family of proteins and their substrates.....	30
Figure 9. Schematic representation of m ⁶ A and m ⁶ Am demethylation by ALKBH5 and FTO.....	31
Figure 10. m ⁶ A reader proteins.....	35
Figure 11. Life cycle of <i>Drosophila melanogaster</i> at 25 °C.....	54
Figure 12. Regulation of sex determination in <i>D. melanogaster</i>	56
Figure 13. Schematic view of <i>D. melanogaster</i> central complex.....	58
Figure 14. Mettl3, Mettl14 and WTAP are required for m ⁶ A methylation of mRNA.....	64
Figure 15. Components of the m ⁶ A writer complex localize to the nucleus and show enrichment in the neuro-ectoderm layer during embryogenesis.....	66
Figure 16. m ⁶ A levels are dynamic during <i>D. melanogaster</i> development.....	67
Figure 17. Nuclear Ythdc1 protein is enriched in the neuroectoderm during embryogenesis.....	68
Figure 18. Expression of both YTH domain-containing proteins correlate with m ⁶ A profile during fly development.....	69
Figure 19. Ythdc1 reader protein preferentially binds m ⁶ A modified RNA probe.....	71
Figure 20. Identification of other potential m ⁶ A binders links m ⁶ A to splicing and polyadenylation.....	73
Figure 21. Loss of m ⁶ A writers or nuclear reader Ythdc1 alters gene expression and splicing.....	75
Figure 22. m ⁶ A in <i>D. melanogaster</i> is enriched along 5'UTR regions and coding sequences.....	77
Figure 23. fl(2)d splicing is regulated by m ⁶ A modification.....	78
Figure 24. Mettl3 and Mettl14 mutant flies are viable, but flightless and die earlier.....	80
Figure 25. Mutant flies lacking m ⁶ A display severe locomotion defects due to altered neuronal functions.....	82
Figure 26. m ⁶ A modulates splicing of the master regulator of sex determination in <i>D. melanogaster</i> , sex lethal (Sxl).....	83
Figure 27. Ythdc1 mutant flies recapitulate locomotion defects of m ⁶ A writer mutants.....	85
Figure 28. Mettl3 and Ythdc1 mutant flies regulate many common splicing events.....	86
Figure 29. Ythdc1 interacts with many splicing factors and with components of the m ⁶ A writer complex.....	88
Figure 30. Ythdc1 regulates splicing of the m ⁶ A modified transcripts.....	89
Figure 31. Nito and Vir are new, conserved components of the writer complex.....	90
Figure 32. Flacc is required for m ⁶ A deposition and regulates m ⁶ A dependent events.....	93
Figure 33. Depletion of Flacc results in similar transcriptome changes as depletion of other m ⁶ A writer components.....	95
Figure 34. Depletion of Flacc leads to similar splicing changes as depletion of other m ⁶ A writer components.....	96
Figure 35. Flacc is required for proper splicing of Sxl.....	97
Figure 36. Flacc stabilizes the interaction between Nito and Fl(2)d writer components.....	99
Figure 37. Flacc interactome analysis identifies factors previously linked to m ⁶ A writers and readers.....	101
Figure 38. Hakai is a conserved RING domain-containing protein, affecting m ⁶ A deposition.....	104
Figure 39. Hakai regulates transcripts that are common with other components of the MACOM complex.....	105
Figure 40. Hakai directly interacts with writer complex components Fl(2)d and Nito.....	107
Figure 41. Fl(2)d is post-translationally ubiquitinated.....	108
Figure 42. Hakai is required for stability of MACOM complex.....	110
Figure 43. Scheme depicting components of MAC and MACOM complexes required for m ⁶ A methylation in <i>D. melanogaster</i>	124
Figure 44. Proteins required for methylation of N6-position of adenosine in representative organisms.....	128
Figure 45. Regulation of Sxl alternative splicing.....	149
Figure 46. Heatmap of m ⁶ A levels and m ⁶ A players during developmental stages of <i>D. melanogaster</i>	151

List of Tables

<i>Table 1. Description of major types of eukaryotic non-coding RNAs and their biological functions.</i>	5
<i>Table 2. Comparison of genome size and extent of alternative splicing in human, mouse and fly.</i>	7
<i>Table 3. U snRNP composition.</i>	7
<i>Table 4. Methods used for m⁶A detection and quantification.</i>	52
<i>Table 5. Evolutionary conserved macromolecular complexes.</i>	114
<i>Table 6. Flies generated and used in this study.</i>	195
<i>Table 7. Oligonucleotides used in this study.</i>	197
<i>Table 8. Plasmids generated and used in this study with corresponding oligonucleotides.</i>	199

List of Supplemental data

<i>Supplemental data 1. Protein interactors with Mettl3, Fl(2)d, Nito, Flacc and Ythdc1 baits.</i>	160
<i>Supplemental data 2. Common protein interactors of writers and Ythdc1 reader.</i>	161
<i>Supplemental data 3. Misregulated transcripts in Mettl3 KO female heads with a predicted m⁶A methylation.</i>	162
<i>Supplemental data 4. Fly locomotion.</i>	163
<i>Supplemental data 5. UCSC tracks showing splicing and methylation of Dsp1 transcript.</i>	164
<i>Supplemental data 6. UCSC tracks showing splicing and methylation of Aldh-III transcript.</i>	165
<i>Supplemental data 7. UCSC tracks showing splicing and methylation of Hairless transcript.</i>	166
<i>Supplemental data 8. Putative m⁶A mRNA methyltransferases.</i>	167
<i>Supplemental data 9. Description of Mettl4 mutant allele.</i>	168
<i>Supplemental data 10. Putative demethylases of m⁶A on mRNA.</i>	169
<i>Supplemental data 11. Description of mutant alleles for putative m⁶A demethylases.</i>	170
<i>Supplemental data 12. Description of mutant allele for Ythdf cytoplasmic reader.</i>	171
<i>Supplemental data 13. Proteins required for methylation of N6-position of adenosine on diverse classes of RNA in representative organisms.</i>	172
<i>Supplemental data 14. Proteins required for recognition and demethylation of N6-position of adenosine on RNA and DNA in representative organisms.</i>	173
<i>Supplemental data 15. Functions of Ythdc1 interactors.</i>	174
<i>Supplemental data 16. Alignment of Mettl3-METTL3 proteins.</i>	175
<i>Supplemental data 17. Alignment of Mettl14-METTL14 proteins.</i>	176
<i>Supplemental data 18. Alignment of Fl(2)d-WTAP proteins.</i>	177
<i>Supplemental data 19. Alignment of Vir-VIRMA proteins (part2/2).</i>	179
<i>Supplemental data 20. Alignment of Nito-RBM15 proteins.</i>	180
<i>Supplemental data 21. Alignment of Flacc-ZC3H13 proteins (part2/2).</i>	182
<i>Supplemental data 22. Alignment of Hakai-HAKAI proteins.</i>	183
<i>Supplemental data 23. Alignment of Ythdc1-YTHDC1 proteins.</i>	184
<i>Supplemental data 24. Alignment of Ythdf-YTHDF3 proteins.</i>	185
<i>Supplemental data 25. Scheme depicting sequence features of human and fly MAC (Mettl3 and Mettl14) and MACOM (Fl(2)d, Nito, Vir, Flacc and Hakai) components.</i>	186
<i>Supplemental data 26. Scheme depicting interactions between MAC and MACOM components.</i>	187

List of Abbreviations

5mC	5-Methylcytosine	FTO	Fat mass and obesity-associated protein
6mA	N6-methyladenine	G3BP1	Ras GTPase-activating protein-binding protein 1
A3SS	Alternative 3`ss usage	GMC	Ganglion mother cell
A5SS	Alternative 5`ss usage	GO	Gene ontology
ac⁴C	N4-cytosine acetylation	GSC	Glioblastoma stem cells
ADAR	Adenosine deaminases acting on RNA	GST	Glutathione-S-transferase
ADAT	Adenosine deaminase acting on transfer RNA	hm⁵C	5-hydroxymethylcytosine
AML	Acute myeloid leukemia	HRP	Horse raddish peroxidase
ANOVA	Analysis of variance	HYB domain	Hakai pTyr-binding domain
BMI	Body Mass Index	I	Inosine
BP	Branch point	icSHAPE	Selective 2'-hydroxyl acylation analysed by primer extension
bprl	Bovine prolactin	IGF2BP	Insulin-like growth factor 2 mRNA-binding proteins
BrU	Bromouridine	IgM	Immunoglobulin-M
CBC	Cap-binding complex	Ime4	Inducer of meiosis
Cbl	Casitas B-lineage Lymphoma	Kar4	Karyogamy-specific transcription factor
CBP20	Cap-binding protein 20	KD	Knock down
CBP80	Cap-binding protein 80	KH	K-homology
CDS	Coding sequence	KO	Knock out
CDS	Coding sequence	KSHV	Kaposi's sarcoma-associated herpesvirus
CITS (A)	Crosslink-induced truncation site at Adenosine	LAIC-seq	Level and isoform-characterization sequencing.
CMTR1 and CMTR2	Cap-specific mRNA 2'-O-methyltransferases 1 and 2	LC-domain	Low complexity domain
CNOT complex	Ccr4-Not complex	m¹A	N1-methyladenosine
CNS	Central nervous system	m¹G	1-methylguanine
CPE	Cytoplasmic polyadenylation element	m^{2,6}A	N2,6-methyladenosine
CPEB	Cytoplasmic polyadenylation element-binding protein 1	m²A	2-methyladenosine
CPSF	Cleavage and polyadenylation specificity factors	m²G	N2-methylguanine
CRISPR-Cas9	Clustered regularly interspaced short palindromic repeats and CRISPR-associated protein 9	m³C	3-methylcytosine
CTIF protein	CBP80/20-dependent translation initiation factor	m⁵C	5-methylcytosine
Ctr	Control	m⁶A	N6-methyladenosine
D.	<i>Drosophila melanogaster</i>	m⁶Am	N6,2'-O-dimethyladenosine
melanogaster		m⁷G	N7-methylguanosine
DART-seq	APOBEC-editing based detection of methylated region	MAC	m ⁶ A-METTL complex
Dcp1 and Dcp2	mRNA-decapping enzyme subunit 1 and 2	MACOM	m ⁶ A-METTL-associated complex
DLG	Disc-large	MAT	Methionine adenosyltransferase
DNA	Deoxyribonucleic acid	MAZTER-seq	MazF RNase assisted cleave of RNA at unmethylated sites within ACA motifs.
DNMT	DNA methyltransferase	MDa	Mega Dalton
dsRNA	Double stranded RNA	MEIOC	Meiosis-specific coiled-coil domain-containing
dsx	Doublesex	MeRIP	m ⁶ A-methylated RNA immunoprecipitation
eIF	Eukaryotic translation initiation factor	mES cells	Mouse embryonic stem cells
FDR	False discovery rate	Mettl14	Methyltransferase Like 14
FI(2)d	Female-lethal(2)d	Mettl3	Methyltransferase Like 3
Flacc	FI(2)d-associated complex component	Mettl4	Methyltransferase Like 4
FMRP	Fragile X mental retardation protein	MG132	Proteasome inhibitor
fru	Fruitless	miCLIP	m ⁶ A-Methylation iCLIP
		mRNA	Messenger RNA

List of abbreviations

MSA	Muscle surface area	s.e.m.	Standard error mean
msl-2	Male-specific lethal-2	SAF-B	Scaffold attachment factor-B
MTase	Methyltransferase	SAH	S-adenosylhomocysteine
mt-mRNA	Mitochondrial mRNA	SAM	S-Adenosyl methionine
MXE	Mutually exclusive exon splicing	SCARLET	Site-specific cleavage (RNaseH) and radioactive-labelling followed by ligation-assisted extraction and thin-layer chromatography.
N6-MTases	N6-type of MTases		
NB	Neuroblasts	scaRNA	Small Cajal body-specific RNA
NER	Nucleotide excision repair	SE	Exon skipping
NGD	No-go decay	shRNA	Short hairpin RNA
NLS	Nuclear localisation signal	Sm-proteins	Small nuclear ribonucleoprotein-associated proteins
Nm	2'-O-ribose methylations	SMRT-seq	Single molecule real time sequencing
NMD	Non-sense mediated decay	SND1	Staphylococcal Nuclease And Tudor Domain Containing 1
NMJ	Neuromuscular junctions	snoRNA	Small nucleolar RNA
NPC	Neplanocin A	SNP	Single-nucleotide polymorphism
NSD	Non-stop decay	snRNA	Small nuclear RNA
Nsun	RNA cytosine C(5)-methyltransferase NSUN2/NOL1/NOP2/Sun domain family member	Spen	Split ends
nt	Nucleotide	SPOC	Spen paralogs and orthologs C-terminal
NXF1	Nuclear RNA export factor 1	ss	Splice site
PABPC1	Polyadenylate-binding protein 1	STAR	signal transduction activator of RNA metabolism
PARP	Poly ADP-ribose polymerase	STH	S-tubercidinylhomocysteine
P-bodies	Processing bodies	Sxl	Sex lethal
PCIF1	PDX1 C-Terminal Inhibiting Factor 1	TE	Transposable elements
PD	Parkinson's disease	TET	Methylcytosine dioxygenase
Pe	Establishment promoter	TLC	Thin layer chromatography
PIC	Pre-initiation complex	TLS	Translesion DNA synthesis
Pm	Maintenance promoter	TNT-seq	Transient N6-methyladenosine transcriptome sequencing
PNS	Peripheral nervous system	Tra	Transformer
poly(A) RNA	Poly-adenylated RNA	Tra-2	Transformer-2
PRC1, PRC2	Polycomb repressive complexes 1 and 2	TREX	TRanscription-EXport
pTEFb	Positive transcription elongation factor-b	TRIBE	ADAR-editing based detection of methylated region
PTM	Posttranslational modifications	tRNA	Transfer RNA
Pus	Pseudouridine synthases	TUTases	Terminal uridylyltransferases
RBM15	RNA Binding Motif Protein 15	U snRNP	Uridine-rich small ribonucleoprotein
RBP	RNA binding protein	Ub	Ubiquitin
RI	Intron retention	UTR	Untranslated region
RING-domain	Really interesting new gene - domain	VCR	Vertebrate specific C-terminal region
RISC	RNA-induced silencing complex	WT	Wild type
RNA	Ribonucleic acid	WTAP	Wilms' tumour 1-associating protein
RNA PolII	RNA polymerase II	WT-CS	Wild-type Canton-S
RPKM	Read per kilobase per million mapped reads	XCI	X chromosome inactivation
RRM	RNA recognition motif	Y	Pseudouridine
rRNA	Ribosomal RNA	YTH	YT521-B homology
RSV	Rous sarcoma virus	YTHDC	YTH Domain-Containing protein
RT step	Reverse transcription step	YTHDF	YTH Domain-containing Family protein
RT-PCR	Reverse transcription-PCR	Zn-finger (ZnF)	Zinc finger
RT-signature	Reverse transcription signature		
s.d.	Standard deviation		

Abstract

Dynamic regulation of gene expression guarantees cellular adaptation, survival and ultimately organismal development. Over 170 known RNA modifications can decorate various RNA molecules and represent one of the layers of gene regulation. N6-methyladenosine (m⁶A) is among the most prevalent modifications in eukaryotic mRNA and is implicated in nearly every step of mRNA biogenesis. Hence, the importance of m⁶A modification is being increasingly recognised in numerous biological processes. m⁶A installation is accomplished by a large protein complex, whose exact composition was long unknown. This modification can be recognised by the so-called YTH domain-containing m⁶A reader proteins that are main mediators of m⁶A functions.

The purpose of this PhD work was to advance the understanding of m⁶A formation, investigate its role on mRNA processing, and examine the importance of this abundant modification during development of a fruit fly (*Drosophila melanogaster*). Molecular biology techniques along with high-throughput sequencing experiments were applied to characterise components of the so-called “m⁶A writer complex”, required for m⁶A deposition, and to identify novel “m⁶A readers”. Gene-specific knockout animals were generated using the CRISPR-Cas9 genome engineering to study m⁶A functions in vivo. This study shows that the m⁶A writer complex in *D. melanogaster* consists of seven subunits that are conserved in higher eukaryotes. Methyltransferase-like protein 3 (Mettl3) carries catalytic activity and forms a heterodimer with the Methyltransferase-like protein 14 (Mettl14). In addition, five accessory proteins were found to be required for efficient target methylation: Fl(2)d, Vir, Nito, Flacc, and Hakai. Mechanistically, Flacc was shown to promote the interaction between Fl(2)d and Nito, whereas Hakai maintained the stability of Vir, Fl(2)d and Flacc. Analysis of m⁶A distribution along mRNA revealed enrichment of modification within 5' UTR regions in an A-rich RRACH sequence motif. Functionally, loss of m⁶A altered alternative splicing of a subset of modified transcripts. Characterisation of m⁶A readers identified the nuclear protein Ythdc1 as one of the key mediators of m⁶A functions in *D. melanogaster* and its loss recapitulated most splicing defects. Among aberrantly spliced transcripts was *Sex lethal (Sxl)*, the master regulator of sex determination and dosage compensation pathways in *D. melanogaster*, which implicated m⁶A in the modulation of these processes. By exploring the importance of m⁶A modification during fly development, this work revealed high levels of m⁶A during early embryogenesis, at the onset of pupation, as well as in heads and ovaries of adult flies. Notably, fly mutants lacking *Mettl3* or *Mettl14* had reduced lifespan and were flightless. In addition, flies lacking m⁶A displayed severe locomotion defects due to altered neuronal functions and loss of Ythdc1 resembled the loss of m⁶A writer components.

Novel findings presented in this study substantially advance our current knowledge on the composition of the m⁶A writer machinery. This work also reveals the requirement of m⁶A in the alternative pre-mRNA splicing of *Sxl* and other targets and highlights the impact of this modification in the nervous system. In addition, numerous findings presented in this work provide an important resource of data for future studies that will allow better characterisation of this abundant mRNA modification at the molecular and organismal level.

Zusammenfassung

Die dynamische Reguli der Genexpression ermöglicht die Anpassung der Zellen, deren Überleben und letztendlich die Entwicklung des Organismus. RNA Moleküle können durch über 170 bekannte RNA-Modifikationen markiert werden und stellen eine der wichtigsten Schichten der Genregulation dar. N⁶-Methyladenosin (m⁶A) gehört zu den am häufigsten vorkommenden Modifikationen in eukaryotischer mRNA und ist an nahezu allen Schritten der mRNA-Biogenese beteiligt. Die Bedeutung der m⁶A-Modifikation findet daher in zahlreichen biologischen Prozessen zunehmend Beachtung. Die m⁶A-Modifikation erfolgt durch einen großen Proteinkomplex, dessen genaue Zusammensetzung lange unbekannt war. Diese Modifikation kann durch die sogenannten YTH-Domäne-enthaltenen m⁶A-Leserproteine erkannt werden, die Hauptmediatoren der m⁶A-Funktionen sind.

Das Hauptziel dieser Doktorarbeit ist es, das Verständnis der m⁶A-Bildung zu verbessern. Zudem soll die Rolle bei der mRNA-Prozessierung und die Bedeutung dieser stark vorkommenden Modifikation während der Entwicklung der Fruchtfliege (*D. melanogaster*) untersucht werden. Hierfür werden molekularbiologische Methoden zusammen mit Hochdurchsatz-Sequenzierungsexperimenten angewendet. Diese Methoden sollen helfen Komponenten des sogenannten "m⁶A-Schreiber-Komplex" der die m⁶A-Modifikation katalysiert, als auch einzelne "m⁶A-Leser", die die Modifikation erkennen und binden können, zu identifizieren und charakterisieren. Genspezifische Knockout-Modelle wurden unter Verwendung des CRISPR-Cas9-Genom-Engineerings erzeugt, um die m⁶A-Funktionen in vivo zu untersuchen. Insgesamt wurden die sieben Untereinheiten des m⁶A-Schreiber-Komplex in *D. melanogaster* identifiziert. Alle Untereinheiten sind in höheren Eukaryoten konserviert. Das Methyltransferase-ähnliche Protein 3 (Mettl3) trägt als einziges katalytische Aktivität und bildet mit dem Methyltransferase-ähnlichen Protein 14 (Mettl14) ein Heterodimer. Neben diesen entscheidenden Proteinen sind fünf weitere für eine effiziente Zielmethylierung erforderlich: Fl(2)d, Vir, Nito, Flacc und Hakai. Hierbei stärkt Flacc die Wechselwirkung zwischen Fl(2)d- und Nito-Proteinen, während Hakai die Stabilität von Vir-, Fl(2)d- und Flacc-Proteinen stabilisiert. Die Analyse der m⁶A-Verteilung entlang der mRNA ergab eine Anreicherung der Modifikation im 5'-UTR- innerhalb eines A-reichen RRACH-Sequenzmotiv. Funktionell veränderte der Verlust von m⁶A das alternative Spleißen einiger modifizierter Transkripte. Durch die Charakterisierung von m⁶A-Lesern wurde das nukleare Ythdc1-Protein als einer der Hauptmediatoren der m⁶A-Funktionen in *D. melanogaster* charakterisiert, dessen Verlust zu Spleißdefekten führt. Unter den fehlerhaft gespleißten Transkripten befand sich unter anderem der Hauptregulator der Geschlechtsbestimmung und der Dosierungskompensationswege, *Sex lethal (Sxl)*, der die Verbindung zwischen m⁶A und der Regulierung dieser Prozesse verdeutlicht. Zusätzlich zeigte die Untersuchung der m⁶A-Modifikation während der Fliegenentwicklung eine hohe Menge der Modifikation während der frühen Embryogenese, zu Beginn der Verpuppung sowie in Köpfen und Eierstöcken erwachsener Fliegen auf. Insbesondere ist die m⁶A-Modifikation für das ordnungsgemäße Funktionieren des Nervensystems erforderlich: Fliegenmutanten ohne Mettl3 oder Mettl14 sind flugunfähig und zeigen schwere Bewegungsdefekte. Der Verlust des nuklearen Ythdc1-Proteins ähnelt dem Verlust von m⁶A-Schreiberkomponenten in diesem Phänotyp.

Zusammenfassend werden in dieser Studie neue Erkenntnisse unseres derzeitigen Wissens über die Zusammensetzung und Funktion der m⁶A-Schreibmaschinerie fundamental erweitert. Diese Arbeit enthüllt den Bedarf an m⁶A für die Regulierung des alternativen prä-mRNA-Spleißens von *Sxl* und anderen Transkripten und unterstreicht damit die Auswirkungen dieser Modifikation auf neuronale Funktionen. Darüber hinaus liefern zahlreiche in dieser Arbeit vorgestellte Ergebnisse eine wichtige

Datenquelle für zukünftige Studien, die eine bessere Charakterisierung dieser mRNA-Modifikation auf molekularer Ebene und hinsichtlich den gesamten Organismus ermöglichen.

1 Introduction

1.1 Regulation of gene expression

Gene expression is a tightly regulated process, crucial for the formation, differentiation and functioning of every cell – a fundamental unit of life. Genetic information of a given organism is encoded in a form of genomic deoxyribonucleic acid (DNA) that is wrapped around histones and saved in a cell nucleus as a compacted chromatin (Iyer et al. 2011). Each individual cell of a multicellular organism carries identical copy of a genome that is passed on to future generations by the germ cells. However, already in the first day of development, the frog embryo forms 69 distinct cell types, highlighting the importance of precise gene expression for cell differentiation and specialization (Briggs et al. 2018). By the central dogma of biology, genetic information is transferred from DNA to messenger RNA (mRNA) and further to proteins that represent main enzymatic and building blocks of the cell (Crick 1958, Crick 1966). Spatial and temporal regulation of gene expression is thus achieved at multiple levels; before and during gene transcription, at the stage of pre-mRNA processing and finally during protein translation and folding. The first determinant of which genes are switched “on” and “off” is encoded within the chromatin state that either permits or inhibits transcription from specific loci. This chromatin landscape is defined by a combinatorial interplay between histone modifications, DNA modifications, regulatory non-coding RNAs, as well as long distance interactions of gene promoter and enhancer elements (Chen et al. 2017). Whether or not a gene is expressed, is ultimately decided by a plethora of sequence and cell type specific transcription factors that can promote the recruitment of RNA polymerase and associated complexes to initiate transcription.

1.1.1 DNA methylation

DNA methylation of cytosines (5mC) represents an epigenetic mark linked to transcriptional repression, when found at high and intermediate dense CpG islands within promoter regions (Meissner et al. 2008, Borgel et al. 2010), and bound by modification specific readers that mediate gene silencing. 5mC can be deposited by DNMT1, a “maintenance” methyltransferase, that recognizes hemi-methylated DNA (Hermann et al. 2004) or by “de-novo” methyltransferases DNMT3A and DNMT3B (Okano et al. 1999). This modification can also be dynamically removed by ten-eleven-translocase (TET) enzymes via hydroxymethyl-cytosine, formyl-cytosine and carboxyl-cytosine intermediates in consecutive reactions of iron and α -ketoglutarate dependent oxidations (Ito et al. 2011, Wu and Zhang 2014). This dynamic removal/deposition is of particular importance during the course of epigenetic reprogramming, when 5mC is erased from DNA in primordial germ cells (PGC) and in the embryo, just prior to its implantation. In mammals, 5mC modification is crucial for genomic imprinting whereby in a given cell one allele of either maternal or paternal origin is permanently repressed, while the other is kept transcriptionally active (Messerschmidt et al. 2014). 5mC is also required for the process of X-chromosome inactivation in females, where one of the two X-chromosomes gets silenced in order to achieve proper dosage compensation (Clemson et al. 1996). While 5mC epigenetic mark is found in many organisms (Zemach et al. 2010, Su et al. 2011), it is not present in yeast, nematodes and flies, consistent with the absence of DNMT1, DNMT3A and DNMT3B enzymes in these species (Goll and Bestor 2005). Albeit, some studies reported identification of 5mC in the *D. melanogaster* genome at

limited levels (Dunwell and Pfeifer 2014). Although 5mC has been gaining most of the attention, it is not the only methylation mark found on DNA. N6-methyladenine (6mA) has been identified on the genomes of many organisms, however its roles in the regulation of gene expression are only beginning to be unveiled (Iyer et al. 2011, Iyer et al. 2016, O'brown and Greer 2016). 6mA was first identified in prokaryotes as one of DNA modifications of the restriction-modification (R-M) system that bacteria use as a tool to discriminate methylated “self” DNA from non-methylated “foreign” DNA (Bickle and Krüger 1993). It was later also shown to be important in the processes of bacterial replication (Abeles et al. 1993), chromosome segregation (Mohapatra et al. 2014) and gene transcription (Casadesús and Low 2006), thereby expanding the regulatory potential of this DNA mark. 6mA methylation can be carried out by various N6-MTases that belong to three groups of enzymes originating from distant prokaryotic ancestors and their viruses (Iyer et al. 2016). Each group can be further divided to clades and sub-clades, based on respective secondary structure predictions (Iyer et al. 2016). One of the three groups contains proteins of evolutionary diverse MT-A70 clade, deriving from bacterial Mui-like R-M MTases. Notably, this clade contains enzymes acting on DNA as well as RNA targets; the Mettl3 and Mettl14 for example deposit m⁶A on mRNA (**Figure 1**) (Iyer et al. 2011, Iyer et al. 2016) (See also *Chapter 1.4.1*).

In most prokaryotes, 6mA modification is found in predicted DNA sequences, consistent with restricted activity of N6-MTases on well-defined and often palindromic recognition sites (Geier and Modrich 1979). This, however, is not the case in eukaryotes, where 6mA is present at low levels in distinct sequence contexts, within coding and non-coding genomic regions. Recruitment of responsible methyltransferases to sites of methylation is therefore likely regulated by distinct mechanisms and does not depend solely on the underlying DNA sequence (Fu et al. 2015, Greer et al. 2015, Zhang G. et al. 2015, Wu et al. 2016, Mondo et al. 2017, Xiao et al. 2018). The 6mA deposition in eukaryotes is associated with nucleosome positioning and active transcription (Fu et al. 2015), transposon expression (Fu et al. 2015, Zhang G. et al. 2015, Wu et al. 2016) as well as with cancer progression (Xiao et al. 2018, Xie et al. 2018). Despite the fact that 6mA has been found in many eukaryotic genomes, only two distinct N6-MTases have been identified to date. DAMT-1 methyltransferase, an ortholog of vertebrate Mettl4 protein and a member of MT-A70 clade, was initially proposed to be required for 6mA formation in *C. elegans* (Greer et al. 2015). Recently its catalytic activity was also confirmed in mammals (Kweon et al. 2019). Additionally, N6AMT1 protein, a member of HemK family, was found responsible for genomic DNA methylation in human cells (Xiao et al. 2018). Notably, as a heterodimer with the Trm112 protein, N6AM1 was shown to methylate amino group of lysine and glutamine residues of the histone H4 (Metzger et al. 2019) and of the eukaryotic release factor eRF1, respectively (Figaro et al. 2008). Most recently, another partner protein of Trm112 was identified, the N6-MTase Mettl5. Mettl5/Trm112 heterodimer catalyses formation of m⁶A, however not on DNA, but on a specific site of 18s rRNA (Van tran et al. 2019, Ignatova et al. 2020, Leismann et al. 2020). Intriguingly, 6mA modification can also be dynamically removed, presumably by the activity of ALKBH1 (Wu et al. 2016, Xiao et al. 2018, Xie et al. 2018) or ALKBH4 demethylases in mammals (Kweon et al. 2019), ALKBH4 ortholog NMAD-1 in *C. elegans* (Greer et al. 2015), and by dTET enzyme in *D. melanogaster* (Zhang G. et al. 2015). Similarly to 5mC modification, the dynamics of 6mA deposition and its removal may as well have important epigenetic functions in different cell types and during distinct developmental processes. Of note, the abundance and biological roles of 6mA in eukaryotes are currently highly debated and findings from two recent studies argue against regulated deposition of this DNA mark. Instead they propose that modification results due to promiscuous activity of the DNA polymerase λ , which can incorporate m⁶dATP (Liu X. et al. 2020, Musheev et al. 2020).

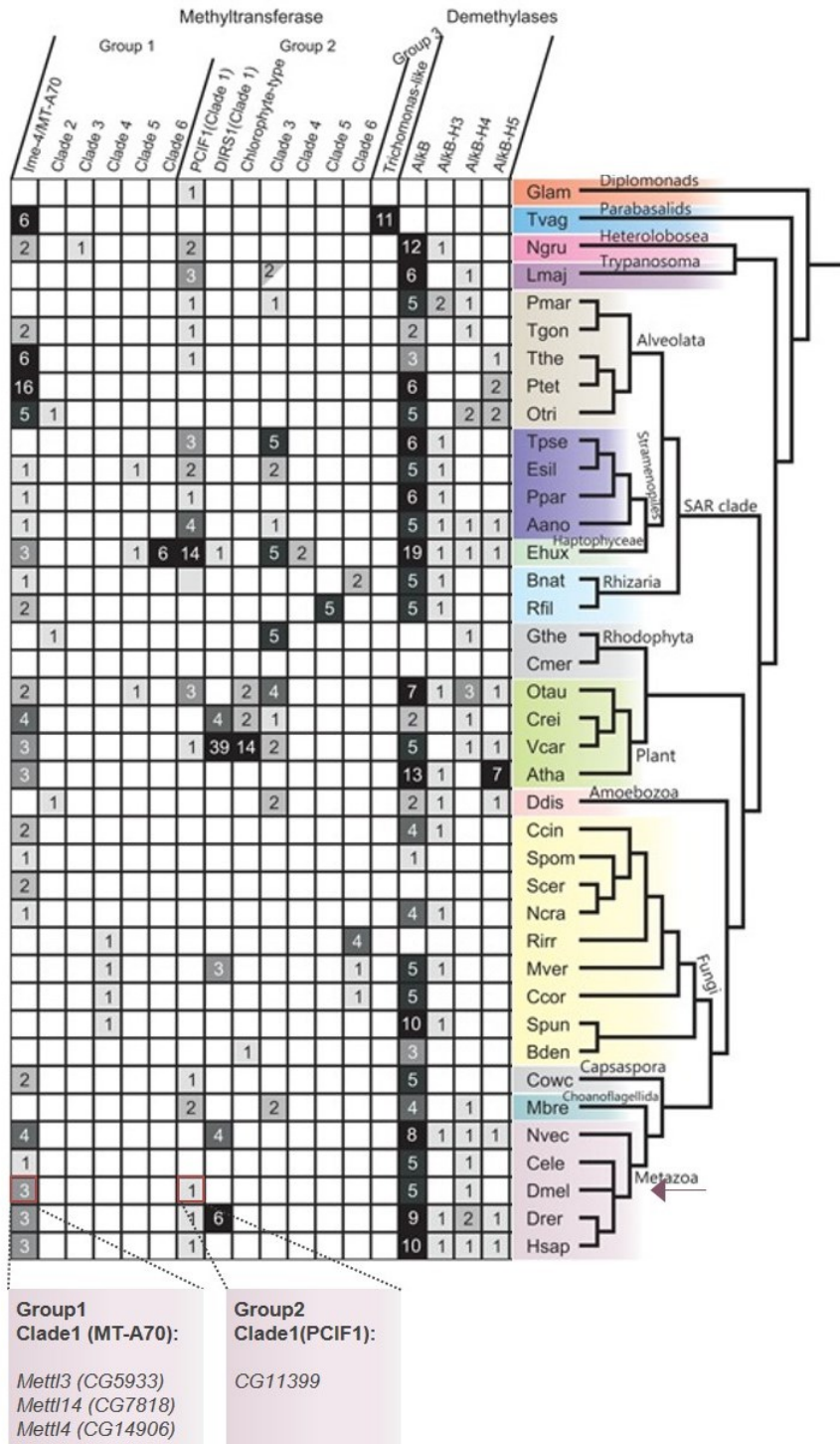


Figure 1. Scheme of N6-methyltransferases and ALKBH-family demethylases.

Phylogenetic tree of species included in the analysis is shown on the right. Group1 and Group2 methyltransferases in *Drosophila melanogaster* (Dmel, red arrow) are listed below. Adapted from (Iyer et al. 2016).

1.1.2 Histone modifications

In the cell nucleus DNA is wrapped around a nucleosome core complex made of histone proteins that assemble in octamer structures composed of two copies of histones H2A, H2B, H3 and H4 (Weintraub et al. 1975). N-terminal histone tails can be post translationally modified by distinct

modifications (methylation, ubiquitination, acetylation and others) that can alter histone charge and thereby directly affect chromatin compaction (Zentner and Henikoff 2013). Different histone modifications were shown to act as a platform for recruitment of specific “reader proteins”, such as chromatin modifiers and transcription factors that affect multiple cellular processes from transcription, chromatin organisation to mitosis, DNA replication and repair (Lawrence et al. 2016). Finally, the chromatin landscape may be transcriptionally accessible, repressed or poised for transcription, depending on the combination of present chromatin marks. While H3K9, H3K27 and H3K20 methylations are normally associated with condensed, repressive chromatin, the H3K4, H3K36 and H3K79 methylations and H3K27 acetylation are linked to open, transcriptionally active chromatin (Kouzarides 2007, Zentner and Henikoff 2013).

1.1.3 Non-coding RNA

Beside chromatin associated proteins that can deposit, remove or bind distinct DNA and histone modifications, a growing list of non-coding RNAs involved in gene regulation are being characterized. They may act as transcriptional enhancers or repressors, by either directly influencing RNA PolII transcription or by guiding the chromatin modifiers to DNA in *cis* or in *trans* (Iyer et al. 2011, Kim et al. 2015). A well-studied example includes a long non-coding RNA *Xist*, required for silencing of inactive X-chromosome in female mammals to achieve dosage compensation (Clemson et al. 1996). *Xist* is transcribed from the inactive X-chromosome and acts in *cis* as a recruiter and activator of chromatin modifiers and scaffolding factors that induce chromatin compaction and repress gene expression (Creamer and Lawrence 2017). Presumably, *Xist* ensures removal of H3K27ac by HDAC3 deacetylase and subsequently deposition and spreading of H2AK119Ub and H3K27me3 marks by Polycomb repressive complexes 1 and 2 (PRC1 and PRC2), respectively (Żylicz et al. 2019) (see also *Chapter 1.4.8.b*). Another well-studied example of RNA mediated chromatin repression represent small non-coding RNAs of the piRNA pathway. The 21-31 nt long piRNAs associate with a family of PIWI proteins and act as guardians of the germ line in different species by repressing transposable elements (TE) in two ways. The piRNA-complexes direct cleavage of transcripts deriving from TE and induce transcriptional silencing of these loci (Iwasaki et al. 2015).

Taken together, combinatorial effects of various epigenetic regulators, including DNA methylation, histone modifications and non-coding RNAs define chromatin compaction, its accessibility, and ultimately the first step in gene expression, the gene transcription. All coding genes are transcribed by the RNA polymerase II (RNA PolII) in a process that consists of three phases, initiation, elongation and termination (Proudfoot 2016, Cramer 2019). All stages of transcription are dynamically regulated, and linked with co-transcriptional assembly of pre-mRNA processing complexes. Thus, transcription itself has an important impact on the outcome of a mature mRNA.

1.2 mRNA processing

Nascent pre-mRNA consists of non-coding untranslated regions (UTR) at its 5' and 3'-ends and an internal sequence composed of coding exons and non-coding introns. Following transcription, pre-mRNA must first undergo a comprehensive co- and post-transcriptional processing that include 5'-capping, intron removal via splicing, and final 3'-end processing and polyadenylation. A mature mRNA is then exported to the cytoplasm where its translation and eventual decay take place. Of all cellular RNAs, mRNAs account for only 2-5 % while the remaining 95 – 98 % represent various non-coding RNAs that are involved in different biological processes either as structural or as regulatory components (Qu and Adelson 2012) (**Table 1**). Many of those are for example constituents of large ribonucleoprotein complexes, such as spliceosome (snRNA) or ribosome (rRNA), while some are involved in different steps of gene repression (*Xist* long ncRNA) or mRNA destabilization (siRNA) (Qu and Adelson 2012).

RNA type	Biological role
snRNA small nuclear RNA	snRNA associates with Sm and various other proteins to form snRNP complexes that are constituents of spliceosomes. Uridine-rich snRNA U1, U2, U4, U5 and U6 form major spliceosome, and U11, U12, U4atac and U6atac form minor spliceosome. (Matera and Wang 2014).
rRNA ribosomal RNA	rRNA serve as structural and functional components of the ribosomes, the cellular translation machinery. The large ribosomal subunit (60S) contains 5S, 5.8S, 25S/28S rRNA and the small subunit (40S) contains 18S rRNA along with a large set of ribosomal proteins (Henras et al. 2015).
tRNA transfer RNA	tRNA are highly modified and structured functional molecules that transfer individual amino acids to ribosomes during translation. Upon stress, the cleavage-induced tRNA-derived fragments can also regulate translation and gene expression (Raina and Ibbá 2014).
snoRNA small nucleolar RNA	snoRNA guide RNA modifying enzymes to defined targeted sites for methylation or pseudouridylation. C/D-box snoRNAs regulate 2'-O-ribose methylation while H/ACA-box snoRNAs guide pseudouridylation to other types of RNA (rRNA, tRNA, U6 snRNA, mRNA) (Kiss-László et al. 1996, Ganot et al. 1997, Dupuis-Sandoval et al. 2015).
scaRNA small Cajal body RNA	scaRNA guide RNA modifying enzymes to RNA PolIII transcribed snRNAs in the Cajal Body for 2'-O-ribose methylation and pseudouridylation (Darzacq et al. 2002).
miRNA micro RNA	miRNA are small RNA species of (~26 nt) of RNAi pathway associated with RISC complex and involved in translational repression of mRNA, by partial base pairing with its targets. They can also function as transcriptional regulators (Catalanotto et al. 2016, Bartel 2018).
siRNA small interfering RNA	siRNA are ~25 nt long double stranded RNA of RNAi pathway. They are of endo- or exogenous origin, associated with RISC complex and involved in mRNA degradation by perfect complementarity. They can also act as transcriptional regulators (Carthew and Sontheimer 2009).
piRNA Piwi RNA	piRNA are 21-31 nt long small RNA associated with PIWI proteins that act as transcriptional repressors of transposable elements in the germ line. They may also induce cleavage of TE derived transcripts (Iwasaki et al. 2015).
circRNA circular RNA	circRNA are very stable covalently closed RNA species formed during mRNA splicing by a back splicing mechanism (downstream 5' splice ligates to upstream 3' splice) or they exist as stable intron lariats that did not undergo debranching. Functions of most circRNA are not known, albeit some examples of circRNA sequestering miRNA and RBPs have been described, as well as examples of circRNA involved in gene regulation and mRNA processing (Li X. et al. 2018).
lncRNA long non-coding RNA	lncRNA are a diverse class of >200 nt long transcripts that do not code for proteins. Many are transcribed from promoter/enhancer/intergenic/gene antisense-regions of the genome and can be involved in numerous biological processes, from regulating gene expression, transcription, translation to protein scaffolding for cellular compartmentalization (Kopp and Mendell 2018).

Table 1. Description of major types of eukaryotic non-coding RNAs and their biological functions.

1.2.1 pre-mRNA capping and cap associated mRNA processing

The very first step of pre-mRNA processing is a co-transcriptional modification of 5'-ends during the so-called capping. Newly formed mRNA cap has an important effect on mRNA stability and on its downstream processing, including splicing, export and translation (Cowling 2009). The most common mRNA cap in eukaryotes consists of 7-methyl-guanosine (m⁷G) coupled to the first transcribed nucleotide by a triphosphate linkage of two corresponding 5'-hydroxyl groups. This type of 5'-5'-connection aids the mRNA resistance from 5' → 3' - exonucleolytic cleavage (Murthy et al. 1991). Addition of mRNA cap is catalysed in a three step enzymatic reaction by a capping complex that interacts with the RNA PolII C-terminal domain and a nascent mRNA of ~20 nt. In this process the so-called cap0 or m⁷G-ppp-N (where “p” represents phosphate and “N” the first nucleotide) is formed. The cap0 is further modified by the cap-specific mRNA 2'-O-methyltransferases 1 and 2 (CMTR1 and CMTR2) that methylate the ribose of the first and the second nucleotide to form the cap1 (m⁷G-ppp-Nm) and the cap2 (m⁷G-ppp-NmNm), respectively. The Nm modification of cap1 and cap2 structures are important for the self/non-self-RNA discriminating mechanism by the RIG-I mediated stimulation of the immune response (Galloway and Cowling 2019). Additionally, if the first nucleotide is adenosine, the N6-position of purine base can be methylated by a PCIF1 methyltransferase that forms the m⁷G-ppp-m⁶Am cap whose functions remain to be characterised (Akichika et al. 2019, Boulias et al. 2019), (Mauer et al. 2019, Sendinc et al. 2019, Sun et al. 2019) (for details see also *Chapter 1.3.1 and 1.4.3.c*). Once deposited, the m⁷G modification is recognised by the cap-binding complex (CBC) composed of two proteins, cap-binding protein 20 (CBP20) that binds m⁷G and cap-binding protein 80 (CBP80) that interact with various mRNA processing factors (Gonatopoulos-Pournatzis and Cowling 2014). CBC association with components of the spliceosome promotes spliceosome assembly (Pabis et al. 2013) and its interaction with U1 snRNA aids to the recognition of the 5' splice site of the very first intron (Lewis et al. 1996). Besides splicing, CBC also enhances the cleavage step during the mRNA 3'-end processing (Flaherty et al. 1997), and additionally, plays an important role in the regulation of mRNA export by binding to protein Aly/REF, a component of the TREX export complex (Cheng et al. 2006). Finally, mRNA m⁷G cap is crucial for efficient translation of the vast majority of transcripts and has an important impact on mRNA turnover by acting as a 5'-end protection from exonucleolytic cleavage.

1.2.2 pre-mRNA splicing

The process of pre-mRNA splicing was discovered in the late 1970s (Berget et al. 1977, Chow et al. 1977) after initial observations showed that the size of many processed and exported mRNAs in the cytoplasm is smaller than the size of the nuclear nascent RNA transcripts (Getz et al. 1975, Herman et al. 1976). It was later demonstrated that genes are composed of coding as well as non-coding units, the so-called exons and introns, respectively. During the process of mRNA splicing introns are removed and the exons are ligated back together to form a mature mRNA. In the case of alternative splicing introns are recognised and excised in various different ways, leading to formation of multiple distinct mRNA isoforms from a single transcript (Pan et al. 2008, Wang et al. 2008). The importance of alternative splicing becomes apparent when comparing the complexity of different organisms, which is not proportional to their genome sizes or to numbers of protein-coding genes (**Table 2**). For instance, human and mouse genomes encode similar numbers of protein-coding genes, albeit the human transcriptome contains two-times more mRNA isoforms, and over 88 % of human genes code for more than two mRNA isoforms. In comparison, the fly genome contains twice less protein-coding genes, but nearly 7-times less mRNA isoforms indicating that the process of alternative pre-mRNA splicing

significantly expands proteome diversity and correlates with organismal complexity (Pan et al. 2008, Wang et al. 2008, Barbosa-Morais et al. 2012, Lee and Rio 2015).

Feature	Human	Mouse	Fly
Genome size	3.300 MB	3.300 MB	165 MB
All genes	63.677	39.179	15.682
Protein-coding genes	22.180	22.740	13.937
Multi-exonic genes	21.144	19.654	11.767
Multi-exonic genes with > 2 mRNA isoforms	88 %	63 %	45 %
mRNA isoforms	215.170	94.929	29.173

Table 2. Comparison of genome size and extent of alternative splicing in human, mouse and fly.
Adapted from (Lee and Rio 2015).

1.2.2.a Spliceosome composition

The splicing reaction involves two catalytic steps that both consist of a chemically simple nucleophilic attack during *trans*-esterification reaction. However, to accomplish this process, a dynamic assembly and disassembly of five uridine-rich small ribonucleoprotein (U snRNP) particles and associated proteins that all together form a major spliceosome machinery, is required. Each U snRNP is composed of one non-coding small nuclear RNA (snRNA) bound by surrounding core proteins. The U1, U2, U4 and U5 snRNAs associate with seven Sm-proteins that form a ring (SmB, SmD1, SmD2, SmF, SmE, SmG and SmD3), whereas the U6 snRNA is bound by the Lsm-ring proteins (Lsm2-Lsm8) (**Table 3**) (Matera and Wang 2014, Lee and Rio 2015). Various other RBPs, helicases and ATP-ases associate with snRNPs to support and regulate different steps of spliceosome assembly. The role of Prp19-associated complex, NineTeen Complex (NTC) in spliceosome remodelling has also been described in recent years (De Almeida and O'keefe 2015).

U snRNP	U snRNA	U snRNA-associated core proteins	Other associated proteins
U1	U1 snRNA	Sm-ring proteins, U1-70K, U1-A, U1-C	Prp39, Prp40, Prp42, Snu71, Nam8, Snu56 and Urn1
U2	U2 snRNA	Sm-ring proteins, U2A', U2B'', SF3a and SF3b complexes	U2AF35, U2AF65, SF1
U4-U6	U4 snRNA, U6 snRNA	U4 snRNA: Sm-ring proteins, U6 snRNA: Lsm2-Lsm8 proteins, Prp3, Prp31, Prp4 and Snu13	
U5	U5 snRNA	Sm-ring proteins, Prp8, Prp6, Prp28, Brr2, Snu114, U5-40K and Dib1	Snu23, Prp38, Prp2, Spp2, Yju2 and Cbc2

Table 3. U snRNP composition.

Composition of U snRNA particles with associated proteins. Adapted from (Lee and Rio 2015).

1.2.2.b Spliceosome assembly and splicing catalysis

The splicing reaction starts by the recognition of correct exon/intron boundaries or splice sites (ss), which are defined by specific consensus sequences. The 5'ss is defined by the **AG/GURAGU** sequence, whereas the 3'ss region is composed of more elements; the 3'ss motif **NCAG/GU**, the **polypyrimidine** tract just upstream of the 3'ss and a branch point sequence (BP) **YNYURAC** that is located 20-40 nt upstream of the splice site. Adenosine (underlined) within the BP, represents the site of an intron lariat formation (Reed 1989). Throughout the splicing reaction, spliceosome constantly remodels and thus exists in various states (**Figure 2**).

The first splicing step involves the association of U1 snRNPs with pre-mRNA to form an early spliceosome complex (complex E). The U1 snRNP is co-transcriptionally recruited to the 5' splice site where U1 snRNA base pairs with a complementary intronic region. At the same time, the 3' splice site is recognised by U2AF35 (binds 3' ss) and U2AF65 (binds poly-pyrimidine tract) proteins, whereas the branch point (BP) is bound by the SF2 protein. SF2 protein (also known as ASF or SRSF1) interacts with the U2AF65 and the U1 snRNP, which triggers formation of a molecular bridge between both sites of the intron, and stabilizes the interaction of U1 snRNP with the 5' ss. In the next step, the ATP-dependent helicases initiate an exchange of SF1 with the U2 snRNA that binds around the branch point adenosine (formation of U2 snRNA/BP duplex). The rearrangement of U1 and U2 snRNPs brings both sites of the intron in a close proximity, which allows formation of the pre-spliceosome complex (complex A) (Matera and Wang 2014, Fica and Nagai 2017). Following the formation of complex A, the U4-U6 and U5 snRNPs join as a tri-RNP sub-complex to assemble a pre-catalytic spliceosome (complex B). With the help of various helicases, major compositional and conformational rearrangements take place, resulting in the formation of activated spliceosome (complex B^{act}) (Fica and Nagai 2017).

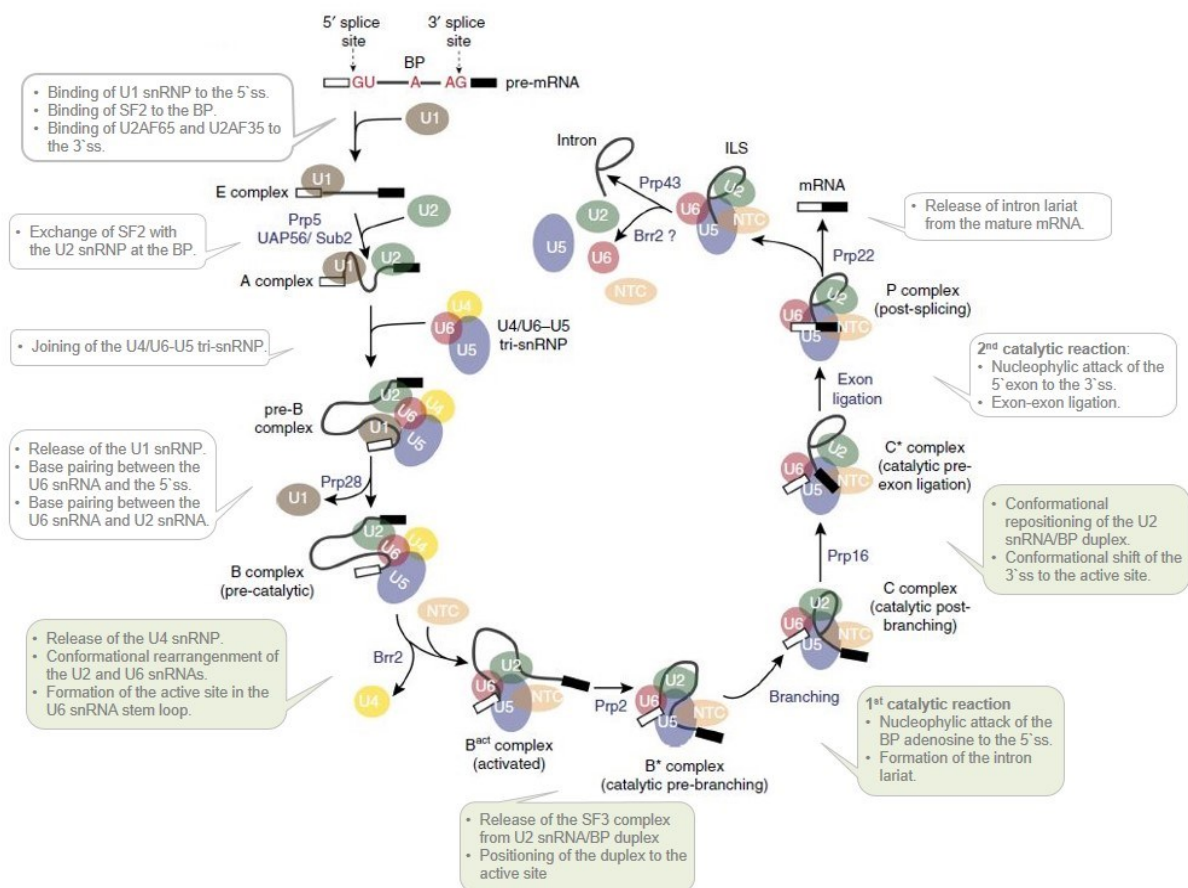


Figure 2. Schematic depiction of spliceosome assembly.

Schematic depiction of spliceosome assembly within one exon-intron-exon sequence. 5'- and 3'-exon are shown as a white and a black block, respectively. A solid line between the exons represents the intronic region. Intronic 5'ss (GU), 3'ss (AG) and branch point (BP) adenosine (A) are depicted with red letters. U snRNPs and the NTC complex are shown as coloured ellipses. Text illustrations summarise main steps of spliceosome formation. Highlighted in green: during transition from B complex to C* complex, the U2 snRNP (U2 snRNA/BP duplex) undergoes major conformational changes. Source and adapted figure: (Fica and Nagai 2017, Van Der Feltz and Hoskins 2019).

Joining of the tri-snRNP disrupts the interaction of U1 snRNA with the 5' splice site (5'ss) that is instead replaced with the U6 snRNA. U6 snRNA also base pairs with the U2 snRNA, and forms an internal stem loop to accommodate two metal ions thereby creating an active site of the spliceosome, required for the first catalytic step. At this stage, conformational changes trigger the release of U1 and U4 snRNPs from the spliceosome and joining of the NTC complex. In addition, the release of SF3 complex uncovers the U2 snRNA/BP duplex and allows its positioning in the active site (Van Der Feltz and Hoskins 2019).

Catalytic complex B* then catalyses the first splicing step, whereby the 2' hydroxyl group of the branch point adenosine carries out a nucleophilic attack to the 5' phosphoryl of the 5'ss, generating a free 5' exon and an intron lariat in the so-called catalytic spliceosome (complex C). Additional RNA helicases and remodelling factors (e.g. Prp16) then rearrange the complex C for the second step of splicing reaction, albeit leaving the catalytic centre in a similar conformation. The U2 snRNA/BP duplex moves away from the catalytic centre, which gets occupied by the 3'ss intron-exon junction (Bertram et al. 2017). In the following step, the free 3' hydroxyl group of the 5'-exon acts as a nucleophile and attacks the 5' phosphoryl of the 3'ss. This results in exon-exon ligation and release of mRNA with the help of Prp22 helicase and other factors. Finally, the U2, U5, and U6 snRNPs are released from the post-splicing complex P and recycled, whereas the intron lariat is debranched and eventually degraded (Figure 2).

Two mechanisms of efficient splice site recognition and splicing completion have been proposed depending on the intron and exon sizes. By the “intron definition” mechanism, spliceosome assembles on a short, nascently transcribed intron and splicing occurs while transcription of its downstream exon is still ongoing. This type of mechanism was demonstrated in yeast, where short introns are flanked by larger exons (Oesterreich et al. 2016). In contrast, most exons in higher eukaryotes are surrounded by much longer introns (from hundreds to thousands of nucleotides) and the “exon definition” mechanism is therefore used. In this case the spliced 5'-exon remains associated with the transcribing RNA PolII and further splicing steps only occur after transcription of an entire downstream exon has been completed, and the U1 snRNA recruited (Nojima et al. 2015, Nojima et al. 2018). In mammals, where the exon definition model prevails, components of the catalytic spliceosome were found to be associated with the Ser5P modified RNA PolII, which shows enrichment at the transcription start sites and over exonic regions (Nojima et al. 2018). These sites of transcription also correlate with reduced RNA PolII kinetics, likely allowing for efficient spliceosome assembly (Jonkers et al. 2014). Notably, the splicing outcome is also directly affected by the splice site recognition mechanism; mutation of the 5'ss results in intron retention if intron definition is used, and in exon skipping in the case of exon definition mechanism (Shukla and Oberdoerffer 2012, Jacob and Smith 2017). Splicing of very long introns can also occur in a stepwise fashion, known as recursive splicing, where the internal 3'ss is followed by an immediate 5'ss (recursive splice site) (Duff et al. 2015, Sibley et al. 2015). In vertebrates, a short exon (RS-exon) is present just downstream of the recursive splice site, enabling the spliceosome association by the exon definition mechanism. The RS-exon is, however, spliced out of the mature mRNA transcript in the following step of recursive splicing (Sibley et al. 2015).

1.2.2.c Regulation of alternative splicing

Alternative splicing enables the formation of multiple different mRNA isoforms from a single pre-mRNA transcript and in this way expands transcriptome and proteome diversity. Differential usage of 5'ss, 3'ss or both, leads to distinct types of alternative splicing events, namely: exon skipping (SE), alternative 5'ss (A5SS) and 3'ss usage (A3SS), mutually exclusive exon splicing (MXE) and intron retention (RI) (Figure 3). One of the very first examples of alternative splicing shed light onto generation

of two distinct immunoglobulin-M (IgM) isoforms important for adaptive immunity during B-lymphocyte maturation; the membrane bound isoform in B-cells, and the secreted one in plasma cells (Alt et al. 1980, Early et al. 1980). Further examples have shown that alternative splicing can be regulated in a developmental- and tissue- specific manner by various cis- and trans- acting elements, which can alter spliceosome recruitment or its assembly in a positive or negative fashion, and during all stages of splicing reaction. Trans-acting factors recognise and bind the cis-regulatory sequences that can be classified into splicing enhancers (SE) and splicing silencers (SS), found within introns (ISE, ISS) or exons (ESE, ESS), respectively.

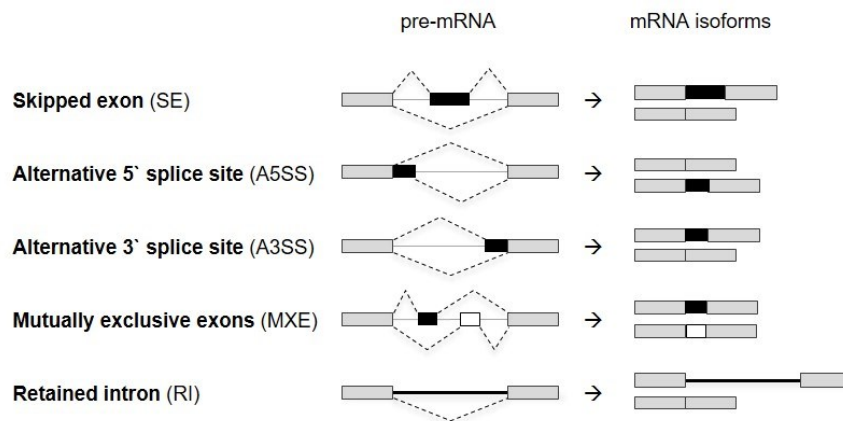


Figure 3. Schematic representation of alternative splicing events.

Two main mRNA isoforms are depicted for each alternative splicing event; skipped exon (SE), alternative 5' splice site (A5SS), alternative 3' splice site (A3SS), mutually exclusive exons (MXE), retained intron (RI).

Among the well-characterised trans-acting factors are RBPs belonging to the group of RS proteins (arginine and serine-rich proteins) and hnRNP proteins. Both can impact constitutive as well as alternative splicing decisions by acting as enhancers or silencers (Busch and Hertel 2012, Howard and Sanford 2015). Importantly, most trans-acting factors regulate splicing in a context dependent manner, as demonstrated by transcriptome wide binding assays and corresponding RNA splicing maps for Nova, TDP-43, TIA, FUS, and many other proteins (Tollervey et al. 1993, Ule and Darnell 2006, Wang et al. 2010, Ishigaki et al. 2012, Rot et al. 2017, Yee et al. 2018). Nova protein for example promotes inclusion of an alternative exon when it is bound to the YCAAY cis-recognition motif in the flanking introns, but silences exon inclusion when it is bound to the same motif within the alternative exon (Ule and Darnell 2006).

pre-mRNA splicing occurs co-transcriptionally and is therefore strongly linked to the state of chromatin and DNA modifications, nucleosome positioning as well as to the speed of RNA PolII transcription, which are cell type- and tissue-specific (Naftelberg et al. 2015) (*Chapter 1.1*). In turn, splicing factors can also directly affect transcription. SRSF2 for example stimulates the pause release and processivity of RNA PolII by promoting the recruitment of the pTEFb (positive transcription elongation factor-b) complex (Ji et al. 2013). Many studies comparing tissue specific alternative splicing found that occurrence of alternative splicing is elevated in the neuronal tissue (Wang et al. 2008) (Merkin et al. 2012), where it affects brain development and synaptic plasticity (Ule and Darnell 2006, Su et al. 2018). Thus, splicing alterations are often the leading cause of diverse neurological defects (Modic et al. 2013, Doxakis 2014, Vuong et al. 2016).

1.2.2.d Additional functions of U1 snRNP

Besides its functions in splice site selection, the U1 snRNP also plays important roles in other aspects of mRNA processing. It can bind to 5`ss like sequences along the nascent transcripts to inhibit the use of pseudo-5`ss and to prevent the occurrence of premature cleavage and polyadenylation. Recruitment of U1 snRNP to the 5`ss-like sequence within the *ATM* transcript for example, blocks this site and in turn promotes the use of correct 5`ss, allowing formation of a functional mRNA to impede development of disease ataxia telangiectasia (Dhir et al. 2010). Additionally, U1 snRNP acts as a general suppressor of premature polyadenylation. By binding upstream of the cryptic polyadenylation signals within introns, the U1 snRNP prevents their recognition (Kaida et al. 2010, Berg et al. 2012, Langemeier et al. 2013). In this way, the U1 snRNP prevents transcript shortening and safeguards the transcriptome (Venters et al. 2019). This function of U1 snRNP, named as telescripting, has a positive impact on transcription elongation of long genes (Oh et al. 2017) and promotes transcription of sense transcripts at bidirectional promoters (Almada et al. 2013). In addition, the snRNP-free U1A and U1-70K proteins can bind stem loop sequences, similar to those present in the U1 snRNA, along certain transcripts. When present in the proximity of polyadenylation signals, they prevent their usage, by interacting with and inhibiting the polyA-polymerase (Gunderson et al. 1998). In this way the U1A protein for example regulates processing and abundance of its own transcript (Boelens et al. 1993).

1.2.3 mRNA translation

In the cytoplasm the cap binding complex (CBC) is involved in the first pioneering round of translation, when mRNA associated proteins get stripped off the transcript to enable efficient translation in consecutive steps (Kim et al. 2009). Binding of CTIF protein (CBP80/20-dependent translation initiation factor) to the CBP80 was suggested to initiate recruitment and assembly of the 43S translation pre-initiation complex (PIC). One of the PIC factors, the eIF3 complex, was shown to be important for the m⁶A-dependent and cap-independent translation under certain stress conditions (Meyer et al. 2015, Lin et al. 2016, Choe et al. 2018, Meyer Kate D. 2019). PIC scans along the 5`UTR until it recognises the AUG codon. At this point, the large 60S ribosomal subunit joins to form a translation initiation complex of the 80S ribosome, which starts the protein synthesis (Hinnebusch 2014). Following the first round of translation, CBC dissociates from mRNA and is imported back to the nucleus, while the m⁷G cap gets bound by a new cap-associated complex eIF4F composed of three subunits; eIF4E, eIF4A and eIF4G. eIF4E binds directly to the m⁷G cap, eIF4A acts as an RNA helicase and eIF4G serves as a scaffolding component. The new, cap-bound eIF4F complex promotes the recruitment of PIC, required for initiation of continuous translation (Hinnebusch 2014). Additionally, the eIF4G interacts with the 3`-poly(A) tail binding protein (PABPC1) thereby connecting the 5`- and the 3`-ends of mRNA in a closed loop during subsequent steps of translation. This enhances ribosome recycling and antagonizes mRNA decay (Amrani et al. 2008, Roy and Jacobson 2013).

1.2.4 Cytoplasmic mRNA turnover

mRNA translation and decay are well connected processes. During the course of translation, each mRNA undergoes a quality control to identify anomalous transcripts that could result in the synthesis of aberrant proteins. Depending on the transcript alteration, different mechanisms of degradation can be initiated. The presence of a premature stop codon triggers the activation of a non-sense mediated decay (NMD) pathway, the lack of a stop codon initiates a non-stop decay (NSD), and translational stalling events lead to the activation of a no-go decay (NGD) pathway (Roy and Jacobson 2013). mRNA

decay can also be triggered by sequence specific 3'UTR RNA binding Puf proteins that inhibit translation and recruit deadenylation complexes (Miller and Olivas 2011), as well as by miRNA mediated recruitment of RISC complex that leads to translation inhibition and subsequent mRNA deadenylation and decapping (Djuranovic et al. 2012). Most mRNA decay pathways are initiated by deadenylation. Shortening of the poly(A) tail is carried out by the Pan2-Pan3 and CNOT (Ccr4-Not) complexes. They are recruited to poly(A) tails of different lengths (>250 nt and <250 nt, respectively) and lead to dissociation of the poly(A) binding protein PABPC1 (Webster et al. 2018, Yi et al. 2018). Once the poly(A) tail reaches a critical length (<25 nt), the transcript becomes translationally inactive. At this stage, the transcript can get (a) stabilised/stored, (b) uridylated and degraded or (c) re-adenylated and returned to the translatable pool.

(a) Stabilization of translationally repressed transcripts is mediated by RBPs that sequester mRNA to cytoplasmic membrane-less compartments, the so-called processing bodies (P-bodies), or upon stress, to the stress bodies (Standart and Weil 2018). P-bodies consist of phase separated mRNA and proteins that contain low complexity domains (LCD). Among associated proteins are translational repressors, deadenylation and decapping factors, as well as other components of the 5' → 3' decay pathway. Nevertheless, how exactly is the balance between mRNA stabilisation, translation and decay in these compartments regulated is currently unknown.

(b) Uridylation of short poly(A) tails is carried out by terminal uridyl transferases or TUTases (TUT4 and TUT7) (Lim et al. 2014), which add oligo U-tails and mark transcripts for degradation via the 3' → 5' or the 5' → 3' pathways. Recognition of the oligo-U-tail by the exosome complex, leads to mRNA decay from the 3' → 5' end (Mugridge et al. 2018). On the other hand, degradation via the 5' → 3' direction requires a prior removal of the m⁷G cap that protects mRNA from the 5'-exonucleases. This step is mediated by the binding of the Lsm1-7 – Pat1 octamer complex to short oligoadenylated or uridylated 3'-RNA ends (Chowdhury et al. 2007). The protein octamer interacts with and recruits decapping factors and exonuclease, which loop towards the 5'-termini. Removal of the m⁷G is carried out by the activity of the Nudix family proteins, such as mRNA-decapping enzyme 2 (Dcp2) (Sheth and Parker 2003, Schoenberg and Maquat 2012, Chen and Shyu 2017). Dcp2 acts on most targets and preferentially binds to the stem loop structure within the transcript's 5'UTR. It hydrolyses the pyrophosphate linkage between the m⁷G and RNA, leaving behind the unprotected 5'-pRNA that can be further degraded by the activity of 5' → 3' exonuclease Xrn1 (Li et al. 2008). Dcp2 activity is strongly stimulated by the Pat1 protein (Patr-1), the Lsm1-7 complex, as well as by the ECD4 (Ge-1) and DDX6 (Dhh1) proteins that all associate with deadenylated and uridylated-mRNAs (Parker and Song 2004, Song and Kiledjian 2007). In summary, a pool of non-translatable mRNAs accumulates with Pat1, Lsm1-7, LSM14, DDX6, XRN1, 4E-T and ECD4 and other decapping and decay activators in the cytoplasmic storage compartments (P-bodies) before they undergo mRNA decay. Notably, despite the fact that these mRNAs are destined for degradation, they may under certain conditions and if not yet decapped, re-associate with ribosomes (Luo Y. et al. 2018).

(c) Translationally inactive transcripts with short poly(A) tails can escape decay if they undergo cytoplasmic polyadenylation by the cytoplasmic poly(A) RNA polymerase GLD-2 that extends poly(A) tails and enables translation reinitiation. Cytoplasmic polyadenylation is promoted by the CPEB protein that binds to CPE element (UUUUUAU) in the transcript's 3'UTR (Ivshina et al. 2014).

1.3 RNA modifications

“The methylated purine bases reported here may be randomly incorporated into the various component nucleic acids in the specimens as the result of incompletely specific enzymatic action. On the other hand, it appears possible that the methylated purines represent functional constituents of particular nucleic acids”

OCCURRENCE OF METHYLATED PURINE BASES IN YEAST RIBONUCLEIC ACID

(Adler et al. 1958).

RNA modifications decorate every known RNA group and represent another important layer in the regulation of gene expression. The first discovery of modified ribonucleotide dates back to 1951, when Cohn and colleagues identified a novel nucleotide isoform in samples of total RNA (Cohn and Volkin 1951). Further characterisation showed that the modified nucleotide in fact represents an isomer of uridine (Yu and Allen 1959) and was therefore named pseudouridine (Ψ) (Cohn and Volkin 1951). In following years many other studies found additional ribonucleotide modifications, such as the 2-methyladenosine (m^2A), N6-methyladenosine (m^6A), N2,6-methyladenosine ($m^{2,6}A$), N2-methylguanine (m^2G), and 1-methylguanine (m^1G), present in highly abundant ribosomal and transfer RNAs (Adler et al. 1958, Littlefield and Dunn 1958). Since those early discoveries, the knowledge about various RNA modifications has grown remarkably. To date, 170 distinct modifications have been identified and all types of known RNA species were shown to be modified (Boccaletto et al. 2018) (**Figure 4**). Notably, over one third of modifications involve methylation, which places methyltransferases among the most abundant RNA modifying enzymes (Motorin and Helm 2011). Diversity of RNA modifications expands the potential for novel properties of modified nucleotides. m^1A modification for example adds a positive charge, geranylation increases hydrophobicity (Dumelin et al. 2012), while adenosine to inosine editing changes the base pairing (Crick 1966). RNA modifications can therefore substantially alter features and biogenesis of modified transcripts. In this way RNAs that carry ribose methylation (Nm) gain protection from alkaline hydrolysis (Parker and Steitz 1989) and pseudouridylated (Ψ) RNAs show increased rigidity, which in turn affects their folding and structure (Davis 1995). Additionally, a large number of studies have recently identified a diverse set of RBPs that specifically recognize and bind, for example, the m^5C and m^6A modifications (Edupuganti et al. 2017, Zhao et al. 2017a). This suggests that RNA modifications can also act as signalling marks for protein recruitment in order to regulate downstream RNA processing.

Amongst the most highly and diversely modified transcripts are rRNA and tRNA. Modifications regulate their folding and stability, and can affect mRNA translation. Many rRNA modifications for example cluster in the functional areas such as the decoding centre, as well as mRNA and tRNA accommodation sites (Natchiar et al. 2017). Modifications on tRNAs accumulate at the wobble anticodon (position 34), expanding the tRNA decoding potential, and just next to anticodon nucleotides (position 37), preventing the frameshifting during translation (Pan 2018). Despite demonstrated importance, less than half of all tRNA modifications have been mapped so far, since many tRNAs are expressed and modified in a cell type specific manner or in response to stress (Pan 2018). Notably, modifications have a strong impact on tRNA half-life. Loss of m^5C for example leads to tRNA destabilization and cleavage, resulting in the formation of so-called tRNA fragments, with significant roles in various biological processes that go beyond mRNA decoding (Kumar et al. 2016). Other classes of small RNA, such as miRNA, siRNA and piRNA, were found to be 2'-O methylated at their 3'-ends, which protects them from the exonuclease degradation (Horowitz et al. 1984, Yu et al. 2005, Kirino and Mourelatos 2007, Saito et al. 2007). Recently, 24 additional modifications have been identified by high sensitivity mass spectrometry in a pool of small RNA species (16-28 nt) isolated from human cells (Lan et al. 2018), which could include tRNA fragments. While further validations are needed to reveal the

exact identity of RNAs, this study nevertheless suggests that certain small RNAs might be modified to a higher extent than previously anticipated.

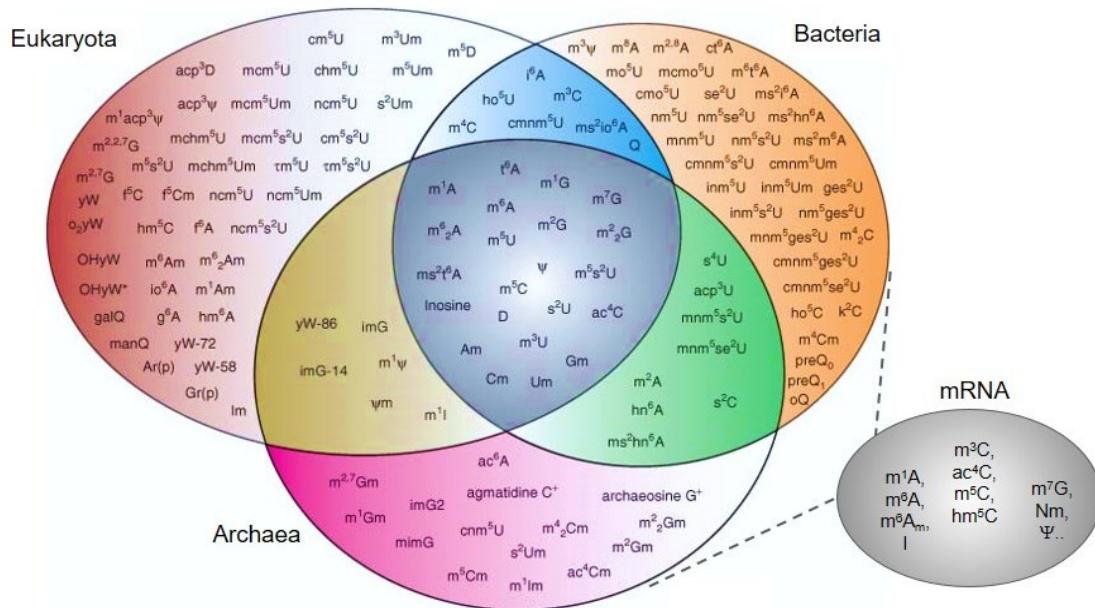


Figure 4. RNA modifications found in three kingdoms of life.

Modifications found on mRNA are listed on the right. Adapted from (Motorin 2015).

Despite the growing number of novel modifications that are being discovered in distinct RNA species, the functional and biological relevance for most of them is not known. However, numerous examples highlight the importance of RNA modification homeostasis in distinct cellular processes. Thus, identification of factors involved in their deposition, from the enzymatic machinery to corresponding cofactors, is likely going to be a major task in the future. Notably, chemically identical modifications found on different RNA molecules are often generated by different, target-specific enzymes that display unique sequence and context requirements. For example, $m^6\text{A}$ in a stem-loop structure of the U6 snRNA is generated by Mett16, whereas a vast majority of $m^6\text{A}$ on mRNA is formed by the activity of MAC-MACOM complex (*Chapter 1.4.2 and 1.4.3.b*). Intriguingly, formation of a particular tRNA modification $m^5\text{U}$ can be generated by different enzymes that require specific methylation precursors. For instance, the $m^5\text{U}$ modification on tRNA at position 54 is in most bacteria catalysed by the TrmA enzyme that uses S-Adenosyl methionine (SAM) as a methyl donor. However, in a gram positive bacteria *B. subtilis*, this modification is formed by a TrmFO flavoprotein that requires methylene-tetrahydrofolate as a methyl group precursor (Schmidt et al. 1975, Urbonavicius et al. 2005, Grosjean 2009). This example of a convergent evolution shows how species can find different ways to ensure correct formation of favourable RNA modifications. It also infers that complexity of enzymatic machinery, required for formation of different RNA modifications, may be even more diverse than are modifications themselves.

1.3.1 mRNA modifications

The first discovery of modifications on coding RNAs dates back to 1974, when a number of laboratories independently found 2'-O-methylated nucleotides as well as internal N6-methylated adenosines in mRNA originating from eukaryotic cells (Desrosiers et al. 1974, Perry and Kelley 1974) and viruses (Furuichi 1974, Shatkin 1974, Wei and Moss 1974). These studies coincided with major discoveries of the mRNA cap structure and its corresponding cap modifications, including m⁷G, Nm and m⁶Am, which were at that time also described as the “bizarre 5'-termini” (Adams and Cory 1975, Furuichi and Miura 1975, Furuichi et al. 1975, Perry et al. 1975, Wei and Moss 1975). Contrary to a great variety of modifications found on tRNA and rRNA, only a dozen were up until now found on mRNA. Recent technological advances enabled their detection and transcriptome wide mapping by various techniques oftentimes employing a step of chemical conversion, or an antibody-based immunoprecipitation, coupled with next generation sequencing (*Chapter 1.4.9*) (reviewed in (Ovcharenko and Rentmeister 2018, Motorin and Helm 2019)). Among more abundant mRNA modifications are inosine (I) (Porath et al. 2014), 2'-O-ribose methylations (Nm) (Dai et al. 2017), pseudouridine (Ψ) (Carlile et al. 2014, Schwartz et al. 2014a) and N6-methyladenosine (m⁶A) (Meyer et al. 2012) (Dominissini et al. 2012). Some others seem to be less prevalent; 5-methylcytosine (m⁵C) (Edelheit et al. 2013) and its derivative 5-hydroxymethylcytosine (hm⁵C) (Delatte et al. 2016), N1-methyladenosine (m¹A) (Dominissini et al. 2016, Li X. et al. 2016, Li X. et al. 2017, Safra et al. 2017b) and the cap-specific N6,2'-O-dimethyladenosine (m⁶Am) (Mauer et al. 2017). Among the most recently identified internal mRNA modifications are N4-cytosine acetylation (ac⁴C) (Arango et al. 2018), 3-methylcytosine (m³C) (Xu L. et al. 2017) and N7-methylguanosine (m⁷G) (Chu et al. 2018, Zhang L.S. et al. 2019) (**Figure 5**). Of note, the prevalence of m¹A, m⁷G and ac⁴C on mRNA in eukaryotes is, however, still highly debated (Grozhik and Jaffrey 2018, Enroth et al. 2019, Sas-Chen et al. 2020).

The ability to finally detect and map modifications on mRNA led to a renewed interest in this field of RNA biology. A boost of research, over the past years, resulted in many significant findings that shed light on this important new layer of gene regulation that was given the name of “Epitranscriptomics” (Roundtree I. A. et al. 2017).

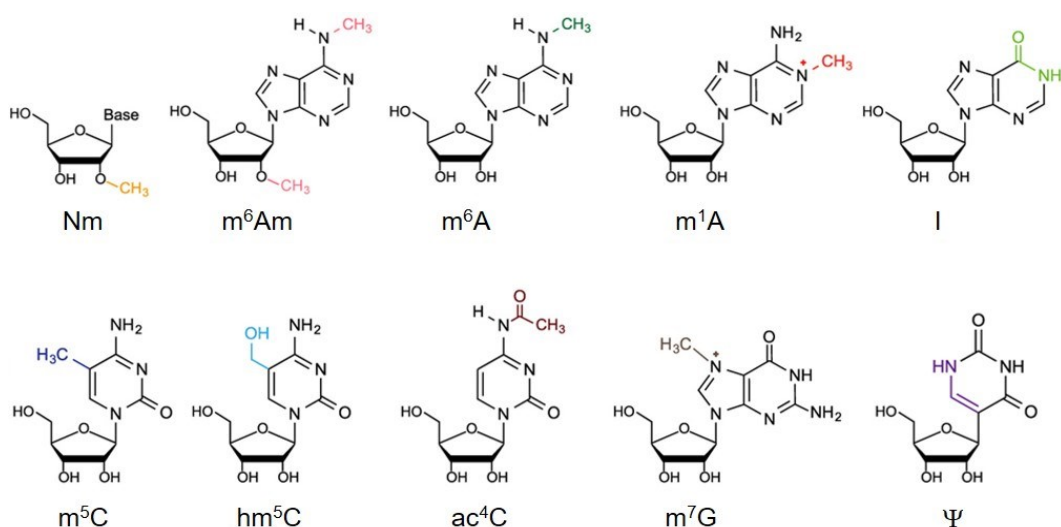


Figure 5. Nucleotide modifications on mRNA.
Adapted from (Song and Yi 2019).

Pseudouridine (Ψ)

Pseudouridine modification is the most abundant RNA modification, and was at first mistakenly thought to be the fifth RNA base (Cohn and Volkin 1951). It was initially found on tRNA, rRNA, snRNA (Spenkuch et al. 2015) and more recently on snoRNA and coding RNA (Carlile et al. 2014, Schwartz et al. 2014a). Pseudouridine is a uridine isomer, in which the glycosidic bond between the pyrimidine ring and the ribose forms via the C4 residue of the ring, and not via the N1 residue like in uridine (Yu and Allen 1959). The imino group of N1 residue can therefore form an additional hydrogen bond, which increases thermal and structural stability of RNA (Davis 1995). Pseudouridine isomerisation requires the activity of pseudouridine synthases (Pus) that belong to different families and act on multiple RNA targets. All known pseudouridine synthases, with the exception of Dyskerin, act as stand-alone enzymes that recognise and modify RNA sites within a defined sequence. Dyskerin on the other hand requires the H/ACA-box snoRNA (or scaRNA) acting as a guide, and its associated proteins. The base pairing between the snoRNA and a target RNA defines the modification site specificity (Li Xiaoyu et al. 2016, Rintala-Dempsey and Kothe 2017) Many pseudouridine synthases have been recently shown to act on mRNA, where pseudouridine is a rather prevalent modification (0,2-0,6 % Ψ /U) (Li et al. 2015). Its transcriptome wide mapping, however, identified only a limited number of reproducible sites, likely due to biological variability of different samples as well as challenges associated with available mapping techniques (Carlile et al. 2014, Schwartz et al. 2014a, Li et al. 2015). Further characterisation of high confidence sites in mRNA identified Trub1 (Safra et al. 2017a) and Pus1 (Carlile et al. 2019) as the main pseudouridine synthases acting on mRNA. While functions of pseudouridine on mRNA are not known yet, its deposition was shown to be dynamic in response to environmental stress (Carlile et al. 2014, Schwartz et al. 2014a) and its presence could potentially alter mRNA decoding (Karijolich and Yu 2011), as well as other aspects of mRNA processing by affecting its stability and structure. Notably, mutations in different Pus enzymes have been associated with occurrence and progression of various cancers, distinct inheritable diseases, as well as with cognitive and neurological impairments (reviewed in (Penzo et al. 2017, Angelova et al. 2018)), highlighting the importance of this modification in non-coding and coding RNAs.

2'-O-ribose methylation (Nm)

2'-O-ribose methylation, also named as the Nm modification, represents the methylation of the ribose at the 2'-hydroxyl position and can be found on all four nucleotides and their derivatives (Boccaletto et al. 2018). Nm modification increases nucleotide hydrophobicity and protects RNA from nucleolytic cleavage (Sproat et al. 1989). Methylation is carried out by 2'-O-methyltransferases that, similarly to pseudouridine synthases, either act on their own as stand-alone enzymes or are guided to target sites by the C/D-box snoRNAs (or scaRNAs) and associated proteins. Many of them act on more than one substrate. Notably, a methyltransferase fibrillarin methylates rRNA targets via the C/D-box snoRNAs guidance (Tollervey et al. 1993), yet it was recently found to also methylate glutamine residues of the histone H2A at the rDNA loci (Tessarz et al. 2014), coupling transcriptionally permissive chromatin landscape and rRNA processing. Nm is highly abundant on rRNA, as well as on other non-coding RNAs. It is part of the 5'-cap1 and cap2 structures on most RNA PolIII transcripts (*Chapter 1.2.1*) contributing to cellular discrimination between self and non-self RNA (Galloway and Cowling 2019). It also decorates 3'-ends of many small RNAs protecting them from degradation (Ji and Chen 2012). In recent years, different methods have been developed for the transcriptome-wide mapping of Nm (Krogh et al. 2016, Dai et al. 2017, Incarnato et al. 2017, Dai Q. et al. 2018) and thousands of putative Nm sites have been identified on mRNA, with vast majority on uridines (0,15 % Um/U) (Dai Q. et al. 2018). In line with this,

the 2'-O-methyltransferase Spt1 in yeast modifies hundreds of mRNA sites, that are predominantly Um (Bartoli et al. 2018). The physiological relevance of internal Nm modification on mRNA is not known yet, however, it was suggested to increase RNA stability, alter its structure and affect protein binding (Bartoli et al. 2018).

5-methylcytosine (m⁵C) and 5-hydroxymethylcytosine (hm⁵C)

Five methyl-cytosine (5mC) is a well-studied epigenetic mark on DNA (*Chapter 1.1.1*). The same base modification (m⁵C) is also found on RNA, where it decorates abundant tRNA and rRNA. To some extent, the modification is also found on non-coding RNA and mRNA (Bohnsack et al. 2019). Like 2'-O-methylation, the m⁵C protects tRNA from cleavage and fragmentation, thereby affecting mRNA decoding, particularly during stress response (Motorin and Helm 2010). Its presence in rRNA was shown to be important for correct ribosome biogenesis (Schosserer et al. 2015). Consistent with assigned functions, alterations in an m⁵C deposition have been linked to the occurrence of various diseases (Blanco and Frye 2014). In recent years, several studies developed different techniques for m⁵C mapping in an attempt to reveal transcriptome-wide m⁵C methylation (Squires et al. 2012, Hussain et al. 2013, Khoddami and Cairns 2013, Legrand et al. 2017). Most studies found the presence of m⁵C on mRNA with the enrichment around translation start sites. However, the number of identified sites and their methylation levels greatly varied (Amort et al. 2017, Legrand et al. 2017, Yang et al. 2017), suggesting that m⁵C deposition might be cell-type and context-dependent. m⁵C RNA modification can be catalysed by eight different proteins, seven members of the Nsun family and the DNMT2 enzyme. Of those, three proteins have been shown to bind mRNA (Castello et al. 2012), the Nsun2, Nsun5 and Nsun1. Nsun2 has been studied by several groups that identified either only a few (Hussain et al. 2013), or thousands of Nsun2-dependent sites (Squires et al. 2012, Yang et al. 2017). How prominent m⁵C really is on mRNA, which methyltransferases are responsible for its formation and how it affects mRNA processing, therefore remains the matter of future research. Intriguingly, recent identification of ALYREF protein as an m⁵C specific reader protein suggests a potential regulatory role of this modification in the mRNA export pathway (Yang et al. 2017). Similarly to 5mC on DNA, the m⁵C modification on RNA can be further demethylated to hm⁵C, f⁵C and ca⁵C by the activity of TET and ALKBH1 proteins acting on mRNA and tRNA sites, respectively (Delatte et al. 2016, Liu F. et al. 2016, Kawarada et al. 2017). Notably, in *Drosophila melanogaster* the hm⁵C methylation on mRNA is formed by the only TET ortholog, dTet (Delatte et al. 2016). dTet and hm⁵C modification are both elevated in neuronal tissue and essential for proper brain development, as well as for fly survival beyond pupation. dTet mutants also display altered locomotion and have defects in circadian rhythm (Delatte et al. 2016, Wang F. et al. 2018). Whether hm⁵C modification is present in other eukaryotes, and whether its functions are conserved, remains an open question.

N1-methyladenosine (m¹A)

N1-methyladenosine modification (m¹A) has been best characterised in tRNA, where a conserved m¹A58 residue is critical for tRNA structure (Safra et al. 2017b). m¹A adds a positive charge and alters base pairing, which can affect mRNA translation and reverse-transcription (Dominissini et al. 2016, Li X. et al. 2016, Li X. et al. 2017, Safra et al. 2017b). Transcriptome-wide mapping of m¹A modification by different approaches resulted in inconsistent conclusions, in regards to its abundance on the mRNA. Hundreds of m¹A sites were first proposed to decorate mRNA with enrichment in the 5'UTR (Dominissini et al. 2016, Li X. et al. 2016, Li X. et al. 2017). A follow-up study, however, classified the vast majority of them as mapping artefacts (Safra et al. 2017b, Grozhik et al. 2019) and the abundance

of m¹A on mRNA was shown to be rather low by some of the studies (m¹A/A: 0,015 % - 0,16 %) (Dominissini et al. 2016, Li X. et al. 2016, Li X. et al. 2017). Most recent validation of m¹A modification identified a single m¹A site in one mitochondrial mRNA (mt-mRNA). The work also implied that antibody cross-reactivity with the m⁷G 5`cap modification is the likely cause of false-positive m¹A mapping in initial studies (Grozhek et al. 2019). Future mapping of m¹A modification with complementary approaches and identification of enzymes responsible for methylation might provide more insights into m¹A biogenesis and its functions, and should help to clarify observed discrepancies. Notably, the cytosolic tRNA methyltransferase complex TRMT6/TRMT61 was suggested to install some of the m¹A sites that reside within a tRNA-like motif in the mRNA (Li X. et al. 2017). Other m¹A methyltransferases are yet to be identified. Notably, m¹A modification can be demethylated by three members of the AlkB family of proteins; FTO and ALKBH1 act on tRNA (Liu F. et al. 2016, Wei J. et al. 2018), while ALKBH3 demethylates m¹A on tRNA and mRNA (Chen Z. et al. 2019). Whether ALKBH1 and FTO also demethylate m¹A on mRNA has not been explored yet, however potential activity of these proteins could account for the observed m¹A profile variability. Interestingly, all demethylation enzymes acting on m¹A have multiple substrates; ALKBH3 can additionally demethylate m³T, m³C and m¹G in single-stranded nucleic acids, as well as m⁶A modification in tRNA (Ueda et al. 2017). ALKBH1, on the other hand, acts on m⁵C in tRNA, but also on 3mC, and 6mA modifications in DNA (Zhang and Jia 2018). Finally, FTO was primarily shown to demethylate m⁶A and m⁶Am modifications on mRNA and snRNA (Jia et al. 2012, Mauer et al. 2017, Wei J. et al. 2018). This type of demethylation promiscuity by the AlkB members suggests a potential cross-talk between different modifications and biological processes in which they are involved (Figure 8).

Inosine

Adenosine can be converted to inosine via oxidative deamination by the activity of Adenosine deaminases acting on RNA (ADAR) and Adenosine deaminase acting on transfer RNA (ADAT) proteins. While ADATs form inosine on ssRNA in tRNA, ADAR enzymes act on intra- or inter-molecular dsRNA regions of various targets (Jin et al. 2009, Grice and Degan 2015). Inosine preferentially base pairs with a cytosine, which alters mRNA decoding. One such example is a single amino acid change from glutamine to arginine in a GluA2 subunit of AMPA receptor, which prevents its calcium permeability, and demonstrates the importance of inosine editing for proper brain functions (Wright and Vissel 2012). Majority of editing events have been attributed to the activity of ADAR1 and ADAR2 homodimers that are expressed in many tissues (Cho et al. 2003). Editing is, however, most prominent in the CNS of different species, including flies, squid and vertebrates. Consistently, loss of the only Adar protein in flies results in various behavioural defects (Palladino et al. 2000). Editing also plays an important role in innate immune response, where inosine acts as a label of the “self” RNA (Liddicoat et al. 2015) and in RNAi pathways during multiple steps of miRNA and siRNA biogenesis (Nishikura 2015). Over 1000 inosine sites have been identified in human cells using transcriptome-wide mapping (Ramaswami and Li 2016). Nearly 95 % were in Alu repeats that reside in introns and UTRs (Levanon et al. 2004), suggesting a general potential function. In squid on the other hand, hundreds of thousands of sites were identified and 10 % of those were in coding regions, thus altering protein decoding (Liscovitch-Brauer et al. 2017). Editing occurs co-transcriptionally and can be affected by splicing in cases where the exon-intron pairing is required for the recognition of a given editing site (Licht et al. 2016). On the other hand, inosine itself can also alter the splicing outcome (Solomon et al. 2013).

N4-cytosine acetylation (ac⁴C)

One of the more recently identified modifications on mRNA is cytosine acetylation (ac⁴C) (Arango et al. 2018). It is deposited by the NAT10A acetyltransferase that was previously known to modify serine and leucine tRNAs as well as 18S rRNA (Ito et al. 2014, Sharma et al. 2015). On mRNA, ac⁴C modification is enriched around the 5'UTR region and CDS and was shown to promote transcript stability, as well as translation efficiency, when present at the wobble position (Arango et al. 2018).

3-methylcytosine (m³C)

One study over the past years detected m³C modification on mRNA and attributed the catalytic activity to the METTL8 enzyme (Xu L. et al. 2017). Two additional m³C methyltransferases, METTL2 and METTL6, were found to modify position 32 of certain tRNAs, however the METTL8 was shown to be restricted to mRNA targets. Further characterisation of METTL8 will likely uncover the potential biological functions of this newly described modification.

N7-methylguanosine (m⁷G)

The m⁷G modification is one of the positively charged modifications. It is co-transcriptionally deposited to RNA PolIII transcripts as part of the 5' RNA cap (*Chapter 1.2.1*). Additionally, m⁷G is found on rRNA, tRNA and was recently identified also on mRNA (Chu et al. 2018, Malbec et al. 2019, Zhang L.S. et al. 2019). METTL1-WDR4 heterodimer that was known to modify tRNA, was shown to be responsible for deposition of a subset of m⁷G sites along mRNA. Modification was mapped in the polyadenylated RNA from mouse and human origin using an antibody enrichment followed by sequencing (Me-RIP-seq and miCLIP-seq), as well as by chemical conversion of m⁷G that caused site-specific misincorporation during the reverse transcription step. Most transcripts carried m⁷G in an AG-rich motif in the proximity of TSS (Malbec et al. 2019), as well as within CDS and 3'UTR regions (Malbec et al. 2019, Zhang L.S. et al. 2019). METTL1 was shown to be highly upregulated upon heat and oxidative stress and m⁷G was notably increased within CDS and 3'UTR regions (Malbec et al. 2019). These initial studies demonstrated that m⁷G is differentially installed upon stress and its abundance positively correlates with translational efficiency, suggesting a role in mRNA translation (Malbec et al. 2019, Zhang L.S. et al. 2019).

N6-methyladenosine (m⁶A)

m⁶A is the most prevalent of all, and best-studied modification on mRNA. Since its discovery in the 1970s, m⁶A has been shown to be required for nearly every aspect of mRNA metabolism and to play crucial roles in numerous biological processes. Alterations in its deposition, removal or decoding result in severe developmental defects and are associated with the occurrence of various diseases. Detailed insights into m⁶A biogenesis and its functions are described in the following sections (*Chapter 1.4*).

N6, 2'-O-dimethyladenosine (m⁶Am)

m⁶Am modification is part of the 5'-terminal cap modification (cap1) of RNA PolIII transcripts (*Chapter 1.2.1*). Modification was recently mapped in a transcriptome wide manner along with the m⁶A modification, using m⁶A-specific antibody and a miCLIP technique (Linder et al. 2015, Mauer et al. 2017). While the methyltransferases responsible for the 2'-O methylation have been known for a long time (Galloway and Cowling 2019), the identity of the methyltransferase acting on N6-position, PCIF1 (also known as CAPAM), was revealed only recently (Akichika et al. 2019) (Boulias et al. 2019, Sendinc et al. 2019, Sun et al. 2019) (*Chapter 1.4.3.c*). m⁶Am was proposed to increase mRNA stability by

interfering with decapping machinery (Mauer et al. 2017), however not all studies shared the same findings (Akichika et al. 2019, Boulias et al. 2019, Sun et al. 2019). In addition, m⁶Am was suggested to regulate mRNA translation in either positive (Akichika et al. 2019), or negative fashion (Sun et al. 2019) and further studies are required to clarify these discrepancies. Notably, m⁶Am can be demethylated to Am by the FTO demethylase that also acts on internal m⁶A sites in mRNA, lncRNA and snRNA (Jia et al. 2011, Mauer et al. 2017, Mauer et al. 2019), and m⁶Am abundance was shown to change in response to stress (Akichika et al. 2019). Whether specific reader proteins can recognise m⁶Am modification has not been investigated yet, but it has been speculated that m⁶Am might alter the recruitment of the known cap-binding proteins to fine tune mRNA processing (Galloway and Cowling 2019, Sendinc et al. 2019). Overall, the main biological functions of m⁶Am and its relevance in vivo remain to be discovered in the future.

Over the past decade, the field of Epitranscriptomics expanded immensely. However, despite all the knowledge that accumulated, many questions remain to be explored. Namely, the molecular and biological functions of most modifications are not yet understood, nor are the enzymatic machineries responsible for their deposition, recognition and removal. Intriguingly, many enzymes, previously known to modify abundant rRNA and tRNA species, have been recently shown to also act on mRNA (Carlile et al. 2014, Schwartz et al. 2014a, Arango et al. 2018). Thus, one can anticipate that out of a plethora of all known RNA modifications, additional ones will likely be identified on coding RNAs in the future. Albeit, these might be present at limited levels and on only a subset of selected mRNA targets. Finally, with the growing list of mRNA modifications, it will be important to consider potential combinatorial effects that all modifications might impose on the fate of modified targets.

1.4 m⁶A modification

m⁶A modification in mRNA was discovered in the 1970s (Wei et al. 1975), and was shown to be the most prevalent internal modification, present in a consensus sequence G/A-m⁶A-C (Wei et al. 1976). Initial studies found that each mRNA on average carries 6-7 methylated nucleotides. Considering the 5'-cap specific m⁷G and 2'-O-methylations, this results in an average of 1-3 internal m⁶A methylations on a single mRNA (Perry and Kelley 1974, Wei et al. 1975). Future studies based on a few individual transcripts from Rous sarcoma virus (RSV) (Kane and Beemon 1985) and a *bovine prolactin (bprl)* (Narayan and Rottman 1988, Carroll et al. 1990) could demonstrate that m⁶A is enriched at the mRNA 3' ends at non-stoichiometric levels (Horowitz et al. 1984). In 2012, an important breakthrough was made by two independent groups that developed a method for transcriptome wide mapping of m⁶A modification, called m⁶A-seq or MeRIP-seq (*Chapter 1.4.9*). They used the advantage of m⁶A-specific antibody to enrich m⁶A containing transcripts, and subjected them to high throughput sequencing (Dominissini et al. 2012, Meyer et al. 2012). Consistent with early reports, m⁶A mapping revealed that distribution of m⁶A along transcripts is not random. In vertebrates, modification is found around start codon and is highly enriched within long internal exons and, in particular, along the first 400 nts of the 3'UTR regions (Dominissini et al. 2012, Meyer et al. 2012, Ke et al. 2015) (**Figure 6**). In yeast, m⁶A shows similar distribution, but is restricted to meiosis (Schwartz et al. 2013), while in plants modification has pronounced enrichment around 3'UTR and 5'UTR regions (Luo et al. 2014). These studies also confirmed that m⁶A resides in a specific consensus sequence **RRACH** (R denotes A or G, and H denotes A, C or U). Distribution of RRACH motif along transcripts appears to be random, with a mild enrichment towards transcript's 3'-ends, albeit less pronounced than m⁶A (Ke et al. 2015). Importantly, not every RRACH motif is methylated, indicating that m⁶A deposition must be highly regulated. Underlying mechanisms that define methylation sites are, however, not yet understood. Thousands of human and mouse transcripts were found to be methylated and their methylomes were highly conserved, suggesting that m⁶A likely plays important functions in shaping the transcriptome.

m⁶A methylation of vast majority sites on mRNA and lncRNA, is carried out by a large multi-subunit m⁶A writer complex, the composition of which has only been characterised in recent years (*Chapter 1.4.1*) (Lence et al. 2019). Intriguingly, m⁶A modification was also shown to be reversible; two proteins of the AlkB-family demethylases, FTO and ALKBH5 can remove m⁶A from a subset of modified sites, which adds another layer to m⁶A complexity (*Chapter 1.4.5*) (Jia et al. 2011, Zheng et al. 2013). Initial findings in the m⁶A field, in regards to m⁶A mapping and discovery of m⁶A writers and erasers, were followed by a rapid exploration of m⁶A functions in various physiological systems. As of now, m⁶A modification was shown to affect nearly every step of mRNA metabolism (*Chapter 1.4.7*) and to play a significant role in various biological processes, as well as in a range of disease (*Chapter 1.4.8*) (Yang et al. 2018). Notably, m⁶A functions can be interpreted by the so called “reader proteins” that either specifically recognise modification, or their binding to certain mRNA is altered due to structural alterations induced by m⁶A (*Chapter 1.4.6*). Proteins of the YTH domain family that bind m⁶A modification have been thoroughly characterised. However, a growing list of newly discovered m⁶A readers keeps further expanding the regulatory potential of this highly abundant modification. The following chapters describe some aspects of m⁶A modification in more detail.

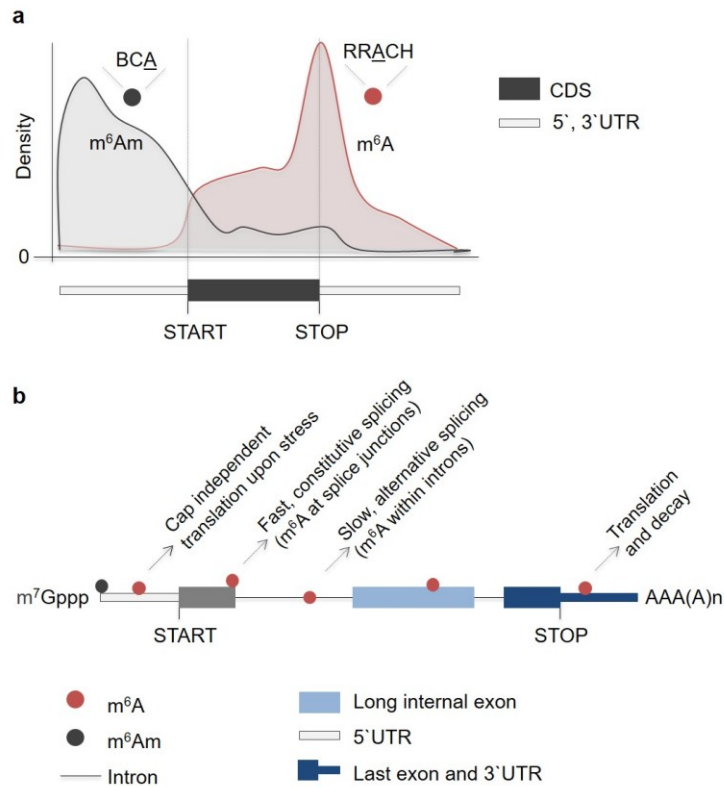


Figure 6. m⁶A and m⁶Am modifications show non-random distribution along the mRNA.

a) Schematics representing distribution profiles of m⁶Am and m⁶A modifications along coding transcripts, within typical motifs BCA and RRACH, respectively (underlined A is targeted for methylation). Source: (Linder et al. 2015). **b)** Schematic representation of m⁶A and m⁶Am localization along the pre-mRNA regions. Arrows highlight a few functions mediated by m⁶A modification, if located in the indicated regions (Meyer et al. 2015, Louloui et al. 2018). CDS – coding sequence, START – start of the CDS, STOP – end of the CDS, m⁷Gppp – 5'-mRNA cap, AAA(A)_n – 3'-polyadenylated tail.

1.4.1 Identification of the m⁶A writer complex-(es)

First discoveries of the m⁶A methyltransferase complex were made in the 1990s, when two laboratories performed chromatographic separations of various cell types and found that m⁶A enzymatic activity resided in the nuclear fraction (Tuck 1992, Bokar et al. 1994, Bokar et al. 1997). They identified two multimeric protein sub-complexes that could efficiently methylate targets only when combined into a nearly 1 MDa large complex (Bokar et al. 1994). **Smaller sub-complex of 200 kDa (MT-A, or now known as MAC)** was shown to contain two proteins. One of them was successfully characterised as a 70 kDa protein called MTA-70 (now renamed to METTL3) with a SAM-binding ability and methylation activity. The **larger sub-complex of 875 kDa (MT-B, or now known as MACOM)** displayed a tendency for nucleic acid binding (Bokar et al. 1994, Bokar et al. 1997), but the identity of its composition remained a mystery for over 20 years. In 2008, a study in plants found the first interactor of METTL3, a protein Fip37, and proposed that it might be one of the MACOM complex subunits (Zhong et al. 2008). Indeed, a few years later corresponding orthologs from yeast and vertebrates (Mum2 and WTAP, respectively) were shown to be conserved components of the m⁶A writer complex. Agarwala and colleagues found that Mum2 was indispensable for m⁶A deposition in *S. cerevisiae* (Agarwala et al. 2012) and three independent groups discovered WTAP in human, mouse and zebrafish (Liu et al. 2014, Ping et al. 2014, Wang Y. et al. 2014). In addition, these studies identified another component of the complex, a methyltransferase METTL14 that is in fact a paralogue of METTL3. They could demonstrate

that METTL3 and METTL14 are the two proteins that form a stable heterodimer (now known as MAC), which interacts with the WTAP protein and other MACOM components to efficiently methylate its RNA targets (Liu et al. 2014, Ping et al. 2014, Wang Y. et al. 2014).

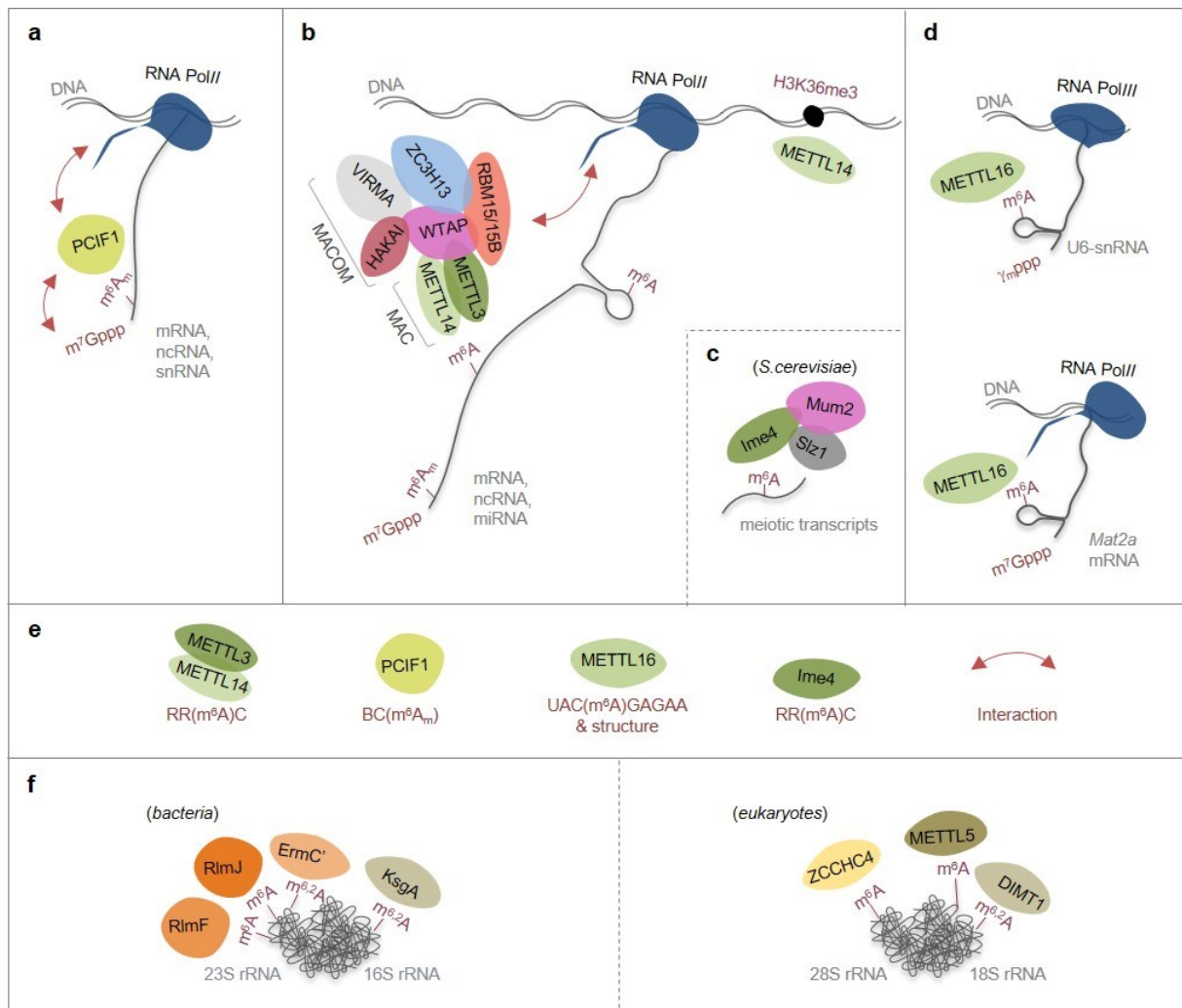


Figure 7. Schematic representation of m⁶A methyltransferases and their substrates.

a) PCIF1 is required for formation of m⁶Am cap modification on RNA PolII transcripts. **b)** MACOM and MAC complexes act cooperatively to methylate RNA PolII transcripts. **c)** MIS methylation complex in *S. cerevisiae* consists of three components (Ime4, Mum2 and Slz1) and is sufficient for m⁶A deposition. **d)** METTL16 methylates structured RNA sequences in the U6 snRNA and in the *Mat2a* mRNA. **e)** Legend depicting methylation motifs of indicated methyltransferases. Red arrow indicates confirmed interactions. **f)** m⁶A and m^{6,2}A methyltransferases acting on rRNA in bacteria (left) and eukaryotes (right). (See also **Supplemental data 13**).

Over the last few years, while this study was ongoing, a major progress towards revealing the complete composition of the m⁶A writer was made by us, and others. Four additional proteins of the larger MACOM complex have been characterised: VIRMA (Schwartz et al. 2014b), RBM15 (Lence et al. 2016, Patil et al. 2016) ZC3H13 (Guo et al. 2018, Knuckles et al. 2018, Wen et al. 2018, Yue et al. 2018), and HAKAI (Růžička et al. 2017) (**Figure 7**). All proteins were shown to be indispensable for efficient m⁶A methylation of mRNA, lncRNA and pri-miRNA, however their exact roles within the complex are to a large extent still unknown. Notably, while the m⁶A writer complex is found in many metazoan, it is absent in nematodes and notable differences in its composition exist in other species (**Supplemental**

data 13). In plants for example, two of the proteins, RBM15 and ZC3H13, are not conserved (Růžička et al. 2017), and in budding yeast, the complex is much simpler and contains only three subunits (Agarwala et al. 2012) (*Chapter 1.4.4*). Beside the large methyltransferase complex mentioned above, other methyltransferases that catalyse formation of m⁶A on mRNA (METTL16), rRNA (TRMT112/METTL5, ZCCHC4), tRNA, snRNA (METTL16, METTL4), as well as on a subset of mRNA, have been identified (**Figure 7**) (*Chapter 1.4.3*).

1.4.2 m⁶A methylation by the METTL3-METTL14 –dependent complex

METTL3 and METTL14 proteins belong to the N6-type of MTases (N6-MTase) that originate from prokaryotic ancestors. They have a typical Rossmann-fold catalytic domain that normally contains a [DNSH]PP[YFW] motif, which enables transfer of the methyl group from the SAM donor to target adenosine via the S_N2-nucleophilic substitution (Iyer et al. 2016). Proteins belonging to N6-MTases are, based on their predicted secondary structures, further classified into three groups that contain several clades and subclades (**Figure 1**). Both, METTL3 and METTL14 belong to the clade 1 of the group 1, which is the most widespread and separates into six subclades. METTL3 and METTL14 are members of subclades 1 and 2, respectively (Iyer et al. 2016). A closely related methyltransferase, METTL4, belongs to a subclade 3 and was recently shown to catalyse m⁶A on U2 snRNA (Chen et al. 2020, Goh et al. 2020, Gu et al. 2020). It was also proposed to form 6mA methylation on DNA in some species (Fu et al. 2015, Greer et al. 2015, Zhang G. et al. 2015, Liu J. et al. 2016, Wu et al. 2016, Mondo et al. 2017, Xiao et al. 2018) (see also *Chapter 1.1.1*). Members of the subclade 2 are often catalytically inactive due to mutations within their active motif, which is indeed the case in METTL14 (Sledz and Jinek 2016). Notably, subclades 4-6 are restricted to unicellular eukaryotes, fungi and plants and are not found in metazoan species (Iyer et al. 2016). Members of these subclades have their MTase domains often fused to different DNA and protein-binding domains, indicating that they might interact with, or act on various distinct substrates.

1.4.2.a METTL3-METTL14 heterodimer structure

In a MAC complex, the METTL3 and METTL14 form a stable asymmetric heterodimer, required for m⁶A deposition (Liu et al. 2014). While METTL3 displays low catalytic activity on its own, the heterodimer can efficiently methylate its targets in vitro and in vivo (Sledz and Jinek 2016, Wang P. et al. 2016, Wang X. et al. 2016). Partial crystal structures of the two enzymes, with a SAM methyl donor, revealed that their dimerization interface is formed via an extensive hydrogen bonding between both MTase domains and two partially disordered loops (Sledz and Jinek 2016, Wang P. et al. 2016, Wang X. et al. 2016). Interestingly, their dimerization is structurally more similar to a homodimer of prokaryotic 6mA DNA methyltransferases, than to other known heterodimers acting on RNA (Sledz and Jinek 2016). From two methyltransferases, only METTL3 is catalytically active and coordinates the SAM methyl donor just next to a DPPW motif. This motif forms interactions with the acceptor adenine residue and activates its amino group for a nucleophilic attack onto the methyl group of the SAM. The METTL14 adopts a similar overall fold to METTL3, but it cannot bind neither SAM nor acceptor adenine due to a few residues that impose critical structural differences. Steric hindrances created by two residues that intrude into SAM binding region, prevent SAM accommodation. Besides, METTL14 lacks residues, which in METTL3 stabilize SAM. METTL14 also cannot accommodate the acceptor adenine because of a few distinct amino acid residues that block its putative binding site. In addition, these residues prevent accessibility to the active motif, which also differs from the one in METTL3; in contrast

to DPPW motif in METTL3, the METTL14 motif EPPL lacks the final aromatic residue that would normally interact with adenine. Thus, METTL14 does not play a catalytic role, but is instead required for RNA binding and complex stability, which in turn increases catalytic activity of METTL3. The interface between the METTL3-METTL14 heterodimer forms a positively charged groove that can accommodate a single stranded RNA substrate and is crucial for m⁶A methylation (Sledz and Jinek 2016, Wang P. et al. 2016, Wang X. et al. 2016). Differences between METTL3 and METTL14 also exist at the level of primary sequences and in the predicted secondary folding. METTL3 contains two N-terminal CCCH-zinc finger motifs that cooperate with the substrate RNA binding, while in METTL14, both N- and C-terminal ends are unstructured and of low complexity, which may, however, contribute to interactions with other proteins or RNA substrates (Iyer et al. 2016). Indeed, recent study demonstrated that a stretch of C-terminal RGG-repeats in the METTL14 strongly improves RNA binding (Scholler et al. 2018). Notably, purification experiments with METTL3 and METTL14 proteins showed that the full-length METTL3 protein is soluble, while the METTL14 forms high molecular weight aggregates (Wang P. et al. 2016). This could contribute to the assembly of multiple m⁶A writer complexes and may explain the observed clustering of m⁶A sites along the transcript (Linder et al. 2015, Meyer Kate D. 2019). The heterodimer localizes to the nucleus, however only METTL3 protein seems to encode a functional NLS in humans (Scholler et al. 2018).

1.4.2.b METTL3-METTL14 posttranslational modifications

Protein functions can be modulated by numerous posttranslational modifications (PTM), such as methylation, phosphorylation, ubiquitination, sumoylation and others. These PTMs can alter protein interactions, induce structural changes, modify protein localisation, affect its activity, or act as a signal for protein degradation. A comprehensive analysis of METTL3 and METTL14 phosphorylation sites in human cells has been reported recently (Scholler et al. 2018), however their functional importance has not been demonstrated yet. Phosphorylations were not required for methylation activity, protein localisation, or interaction with WTAP, suggesting they might not be essential for m⁶A deposition, or that they only modulate a subset of target sites, by altering binding to specific RNA sequences (Scholler et al. 2018). Another study recently analysed sumoylation of METTL3 and identified four modified lysine residues that strongly reduced its catalytic activity (Du et al. 2018), revealing an important mechanism for the regulation of m⁶A deposition.

1.4.2.c METTL3-METTL14 biological roles

METTL3 and METTL14 are highly conserved among eukaryotes (Bujnicki et al. 2002, Iyer et al. 2016) (**Figure 1**). Typically, either both or none of the proteins is present in a genome, which is consistent with their activity as a homodimer. An exception is found in *S. cerevisiae*, where both proteins are encoded and expressed, however Kar4 (METTL14 ortholog) seems not to be required for m⁶A deposition, but is involved in other cellular processes (*Chapter 1.4.4*). METTL3 and METTL14 play fundamental roles during organismal development. Loss of either protein has a detrimental effect on the progress of embryogenesis and gametogenesis in most species studied so far. *S. cerevisiae* lacking Ime4 (the METTL3 ortholog) display sporulation defects during meiosis (Shah and Clancy 1992) and loss of corresponding orthologs in plants results in early developmental arrest and abnormal seed development (Zhong et al. 2008, Bodi et al. 2012). Zebrafish lacking Mettl3 are viable, but show altered gamete maturation leading to reduced fertility in both males and females (Xia et al. 2018). Unexpectedly, Mettl3 depletion using morpholino treatment resulted in embryonic lethality, possibly

due to off-target effects (Zhang C. et al. 2017). Finally, Mettl3 and Mettl14 KO mice die during early embryogenesis at E6.5 (Wang Y. et al. 2014, Chen T. et al. 2015, Geula et al. 2015, Meng et al. 2019).

Conditional removal or depletion of Mettl3 or Mettl14 revealed that their functions are required in diverse biological processes (*Chapter 1.4.8*). They regulate circadian clock (Fustin et al. 2013), cell-cycle progression (Yoon et al. 2017), neurogenesis (Yoon et al. 2017) and axonal regeneration (Weng et al. 2018), among others. Mettl3 and Mettl14 are also indispensable for stem cell self-renewal, as well as for exit from pluripotency, and for coordinated differentiation of various cell types (Meng et al. 2019) (Wang Y. et al. 2014, Geula et al. 2015). The role of Mettl3 and Mettl14 in cell reprogramming has also been demonstrated (Chen T. et al. 2015). Alteration of Mettl3 or Mettl14 expression impairs proper immune response (Li H.-B. et al. 2017), haematopoiesis (Zhang C. et al. 2017), neuronal development (Angelova et al. 2018), and is associated with occurrence of a number of diseases and in a poor cancers prognosis (Dai D. et al. 2018, Liu Z.-X. et al. 2018).

Given that METTL3 and METTL14 act as a heterodimer to methylate their targets, they are in most cases involved in similar biological processes, and loss of one component resembles the loss of the other. Few studies, however, found that both proteins may also function independently of each other. For instance, Mettl3 was shown to partially localise to the cytoplasm and associate with the polysomic fractions, where it was proposed to promote translation, of m⁶A-modified transcripts by interacting with the eIF3b translation initiation factor (Meyer et al. 2015, Lin et al. 2016). This function was independent of its catalytic activity, and of METTL14 and WTAP components. Additionally, Mettl3 was recently detected in protrusions of migrating cells, where it may be involved in the regulation of localised translation (Dermit et al. 2019). Despite the fact that Mettl3 is the only catalytic subunit, the m⁶A profile can be orchestrated by other factors. For example, Mettl3 and Mettl14 both interact with chromatin, but bind different factors and associate with different chromatin sites (Aguilo et al. 2015, Barbieri et al. 2017, Huang et al. 2019). In AML cells Mettl3 is recruited to active gene promoter regions via the CEBPZ transcription factor, independently of Mettl14, which promotes m⁶A deposition along transcript's CDS (Barbieri et al. 2017). On the other hand, in mouse embryonic stem (mES) cells the interaction of Mettl3 with chromatin is regulated by ZFP217 protein that tethers it away from transcription sites in order to maintain low methylation levels of pluripotency factors and ensure mES cell self-renewal (Aguilo et al. 2015). Mettl14 was also recently shown to interact with chromatin. It can directly bind the H3K36me3 histone mark that is enriched at the end of gene segments. In this way Mettl14 was proposed to recruit the remaining subunits of the methyltransferase complex towards the transcript's 3'UTR, which could potentially explain the m⁶A abundance within this region (Huang et al. 2019). In light with these findings, it is possible that certain methylation sites are more dependent on Mettl3, Mettl14 or other factors of the methyltransferase complex. It would be interesting to investigate if the previously identified posttranslational modifications (*Chapter 1.4.2.b*) perhaps regulate Mettl3- and Mettl14-unique interactomes and potentially control m⁶A deposition to only a subset of selected targets.

1.4.2.d WTAP

Wilms' tumour 1-associating protein (WTAP) was shown to interact with METTL3 in plants and yeast (Agarwala et al. 2012, Bodi et al. 2012), many years before its role in m⁶A methylation was discovered. Recent studies in vertebrates revealed that WTAP co-fractionates with the METTL3 and METTL14 proteins and that it is required for heterodimer stabilization and its localization to nuclear speckles (Liu et al. 2014, Ping et al. 2014, Wang Y. et al. 2014). Interaction of WTAP with METTL3 is established via the N-terminal coiled-coil region that binds the N-terminal helix of the METTL3 protein

(Scholler et al. 2018). Consistent with its role within the m⁶A writer complex, WTAP shares over 50 % of RNA binding sites with METTL3 and its depletion results in significant loss of m⁶A on mRNA (Liu et al. 2014, Ping et al. 2014, Wang Y. et al. 2014). WTAP is essential for survival and mice lacking WTAP die during early embryogenesis (E10.5), due to impaired mesoderm and endoderm differentiation (Fukusumi et al. 2008). Likewise, loss of its ortholog, Fip37, in plants leads to developmental arrest and embryonic lethality (Vespa et al. 2004). Flies lacking Fl(2)d, a WTAP ortholog, do not progress post larval stages (Granadino et al. 1990, Granadino et al. 1996) and morpholino-mediated depletion of WTAP in zebrafish results in severe developmental defects and increased apoptosis (Ping et al. 2014). Consistently, its depletion in different cell lines inhibits cell proliferation and differentiation (Small et al. 2006, Fukusumi et al. 2008) by activation of apoptosis (Small and Pickering 2009), while over expression is associated with increased glioblastoma migration and cancer invasion (Jin et al. 2012). WTAP is a nuclear protein, enriched in nuclear speckles where it interacts with different splicing factors and other proteins involved in RNA processing (Small and Pickering 2009, Horiuchi et al. 2013). Its localisation was shown to be dependent on the presence of BCLAF1 and THRAP3 that are part of the DNA damage-induced BRCA1 protein complex (Horiuchi et al. 2013). WTAP depletion results in altered alternative splicing (Small and Pickering 2009), and impairs cell cycle progression (Horiuchi et al. 2006). In flies, Fl(2)d was also shown to colocalize with many splicing factors and is one of the proteins required for proper splicing of *Sxl* and *tra* in female germ and somatic cells (Ortega et al. 2003) (*Chapter 1.5.2*). WTAP is essential for m⁶A deposition together with METTL3-METTL14 heterodimer and four other components of MACOM sub-complex that constitute a complete m⁶A writer complex. However, while the METTL3-METTL14 heterodimer has been studied extensively, much less is known about remaining components and their respective roles within the complex. They are discussed in *Chapter 5.1*, along with our findings from flies.

1.4.3 Other m⁶A methyltransferases

1.4.3.a m⁶A and m^{6,2}A methyltransferases acting on rRNA

N⁶-methyladenosine also known as 6-methylaminopurine (m⁶A) was initially discovered in highly abundant rRNA (Adler et al. 1958, Littlefield and Dunn 1958). Two recently characterised methyltransferases, ZCCHC4 and Mettl5, each methylate a single adenosine of 28S rRNA (A4220) and 18S rRNA (A1832) (Ma et al. 2019, Van tran et al. 2019, Ignatova et al. 2020, Leismann et al. 2020). These modifications are, however, not conserved in yeast (Piekna-Przybylska et al. 2008). m⁶A modification is also present on two sites of bacterial 23S rRNA (Tanaka and Weisblum 1975), where RlmF and RlmJ methyltransferases catalyse its formation on A1618 and A2030 residues, respectively (Sergiev et al. 2008, Golovina et al. 2012).

In some bacteria, 23S rRNA also carries the N^{6,2}-dimethyladenosine (m^{6,2}A) modification at position A2058. This modification, catalysed by the Erm methyltransferase (Denoya and Dubnau 1987), was identified in the 1970s by the Weisblum laboratory that studied bacterial resistance to macrolide antibiotic erythromycin (Lai and Weisblum 1971, Lai et al. 1973). Two additional, conserved m^{6,2}A sites were later also found on bacterial 16S rRNA (A1518 and A1519) and eukaryotic 18S rRNA. Modifications are deposited by the bacterial KsgA methyltransferase and corresponding homologs in other species (Lafontaine et al. 1994, O'farrell et al. 2004) (**Supplemental data 13**) (**Figure 7**).

1.4.3.b Mettl16

Beside MAC-MACOM complex and above-mentioned rRNA methyltransferases, two other m⁶A methyltransferases acting on mRNA, non-coding RNA and snRNA substrates have been identified recently, Mettl16 and Mettl4. Mettl16 is an m⁶A methyltransferase with only two identified targets, the U6 snRNA and *Mat2a* mRNA (Pendleton et al. 2017, Warda et al. 2017, Doxtader et al. 2018), whereas Mettl4 was shown to act on U2 snRNA (Chen et al. 2020, Goh et al. 2020, Gu et al. 2020) and is further discussed in (*Chapter 5.1.5*). Unlike Mettl3-Mettl14 heterodimer, Mettl16 binds and methylates its targets as a homodimer, albeit dimerization is not required for its catalytic activity (Ruszkowska et al. 2018). Notably, Mettl16 can bind triple RNA helix of lncRNA MALAT1 as a homodimer, but does not methylate it (Ruszkowska et al. 2018). Substrate selectivity by the Mettl16 is restricted to the nonamer sequence motif [UACm⁶AGAGAA] located within a stem loop structure of its RNA targets. Intriguingly, Mettl16 regulates expression of *Mat2a*, a SAM-synthetase, in response to changes in intracellular SAM levels. Upon reduced SAM levels, Mettl16 binds a stem loop downstream of an alternative intron within the 3'UTR region of *Mat2a* transcript to promote its splicing. This results in translation of a functional protein and initiates a positive feedback loop to increase synthesis of SAM (Pendleton et al. 2017, Warda et al. 2017, Doxtader et al. 2018). Inversely, high levels of SAM lead to transcript methylation and a quick turnover of Mettl16 from the stem loop, resulting in intron retention and *Mat2a* transcript decay, thereby repressing the SAM production (Pendleton et al. 2017, Warda et al. 2017, Doxtader et al. 2018). While numerous other transcripts were shown to be bound by Mettl16, mostly within intronic regions, so far only two have been found to be also methylated (Warda et al. 2017) (**Figure 7**). Given that Mettl16 promotes *Mat2a* splicing (when SAM levels are low) independently of its catalytic activity, binding to other identified transcripts may also affect their processing independently of m⁶A methylation (Brown et al. 2016, Warda et al. 2017). The crystal structure of Mettl16 revealed an extensive positively charged groove in the N-terminal region and in a part of Rossmann fold, which guides the bound RNA to the SAM-containing catalytic core (Doxtader et al. 2018, Mendel et al. 2018, Ruszkowska et al. 2018). Notably, Mettl16 adopts a similar structure to Mettl3, but shows unique features around the putative m⁶A binding site. This likely explains distinct substrate preferences of the two m⁶A methyltransferases (Ruszkowska et al. 2018). Mettl16 is essential for mouse survival and KO animals die during early embryogenesis at the time of implantation (around E6.5), presumably due to altered SAM synthesis (Doxtader et al. 2018, Mendel et al. 2018). Further characterisation of Mettl16 might reveal its additional functions during development or in other biological processes.

1.4.3.c PCIF1

PCIF1 (Phosphorylated CTD Interacting Factor 1) is a recently identified methyltransferase required for the formation of m⁶Am cap modification on RNA PolIII dependent transcripts (for m⁶Am see also *Chapter 1.3.1*) (Akichika et al. 2019, Boulias et al. 2019, Mauer et al. 2019, Sendinc et al. 2019, Sun et al. 2019). PCIF1 interacts with the m⁷G cap of mRNAs and snRNAs and methylates the N6-position of the first 2'-O-methylated adenosine. The biological significance of m⁶Am modification on mRNA is as of now not known, however potential roles in mRNA translation and stability have been proposed (Mauer et al. 2017, Akichika et al. 2019, Boulias et al. 2019, Sendinc et al. 2019, Sun et al. 2019). Using precise m⁶Am detection with miCLIP technique in PCIF1 KO cells, Senedic and colleagues recently demonstrated that m⁶Am stabilizes a subset of low abundant transcripts and simultaneously acts to repress translation. Its functions might be specifically required during stress, when PCIF1 knock out was shown to have a negative impact on cell survival. The m⁶Am modification and PCIF1 activity are specific for vertebrates. The PCIF1 ortholog (CG11399) is conserved in flies, however no m⁶Am has been detected in this species at the 5'-cap even though the catalytic residues required for methylation

reaction are intact. However, *Drosophila melanogaster* PCIF1 lacks two proline residues required for correct accommodation of the m⁷G modification at the 5'-cap of mRNA, which could explain the absence of m⁶Am modification in flies. Interestingly, the catalytic motif [DPPF] that is found in the vertebrate protein also differs in flies, by the last amino acid residue, which is histidine [DPPH]. The same motif has been previously identified in a bacterial N4mC methyltransferase M.NgoMXV (Radlinska et al. 1999), a protein that belongs to the same clade as N6-Adenine methyltransferases and adopts similar folding of its catalytic site (Iyer et al. 2016). This suggests that *Drosophila melanogaster* PCIF1 ortholog (CG11399) may also be catalytically active, but might act on RNA targets, other than the m⁷G-proximal 2'-O-methylated adenosines and may be restricted to early embryogenesis (0-1 h), when CG11399 transcript expression is particularly high (Graveley et al. 2011).

1.4.4 m⁶A methylation by the MIS complex in budding yeast

m⁶A modification has been well characterized in budding yeast *S. cerevisiae*, where it is specifically required for entry to meiosis during sporulation upon nitrogen starvation (Shah and Clancy 1992, Agarwala et al. 2012). The composition of the m⁶A methyltransferase complex in *S. cerevisiae* differs from other species and consists of three components; Ime4 (Inducer of meiosis), Mum2 and protein Slz1 that has no orthologs in higher eukaryotes (Agarwala et al. 2012). Slz1 serves as an accessory component for tethering the Ime4-Mum2 proteins to the nucleolus where methylation takes place (Schwartz et al. 2013). Timely deposition of m⁶A modification is achieved by restricted expression of Slz1 just prior to meiosis (Schwartz et al. 2013). The closest ortholog of Mettl14 in budding yeast is protein Kar4 (karyogamy-specific transcription factor) (Bujnicki et al. 2002). Even though Kar4 was found to interact with Ime4, in a yeast-two-hybrid screen (Ito et al. 2001), it seems not to be required for establishing m⁶A methylation. Instead, Kar4 acts as a transcriptional activator to promote mating (Lahav et al. 2007). It is currently not known how the MIS components assemble, bind RNA or specify target recognition. Given that Ime4 and Mum2 have high sequence similarity to METTL3 and WTAP, respectively, it would be interesting to compare the structural conformation of the MIS complex with the existing knowledge about the METTL3, METTL14 and WTAP proteins. Interestingly, the methylation profile and motif in yeast are reminiscent to those in vertebrates, with m⁶A enrichment along the 3'UTR regions and in the RGAC sequence motif (Schwartz et al. 2013) (**Figure 7**). Notably, a single m⁶A site within a 3'UTR region of a transcriptional repressor RME1 was recently found to be critical for the entry to meiosis. RME1 blocks transcription of a protein Ime1 that is essential for meiotic DNA replication. Methylation of *rme1* mRNA triggers its degradation, which in turn enables Ime1 activity and induction of meiotic program (Bushkin et al. 2019). However, what triggers the timely expression of Slz1 remains to be shown.

1.4.5 m⁶A erasers

1.4.5.a ALKBH family of proteins

Paralleling the dynamic reversibility of DNA modifications, the m⁶A modification on RNA can also be demethylated. To date two m⁶A mRNA demethylases have been identified, ALKBH5 (AlkB homologue 5) and FTO (fat mass and obesity associated) that belong to the group of AlkB family of Fe(II) and 2-oxoglutarate-dependent oxidative DNA/RNA demethylases (Gerken et al. 2007, Jia et al. 2011, Zheng et al. 2013). The AlkB family contains nine homologues of the bacterial AlkB protein (ALKBH1-ALKBH8 and FTO). Of those, seven members are conserved in all metazoan, however, the most recently evolved enzymes, ALKBH5 and FTO, that demethylate m⁶A on mRNA, are restricted to the vertebrate clade, with the exception of FTO that is also found in diatoms (Sanchez-Pulido and Andrade-Navarro 2007). Notably, archaea, obligate-anaerobic bacteria and *S. cerevisiae* do not encode AlkB proteins (Fedeles et al. 2015). All AlkB family proteins contain a typical N-terminal catalytic core, required for demethylation reaction (Mishina and He 2006, Fedeles et al. 2015, Kal and Que 2017), yet they differ by their substrate and target specificity (**Figure 8**).

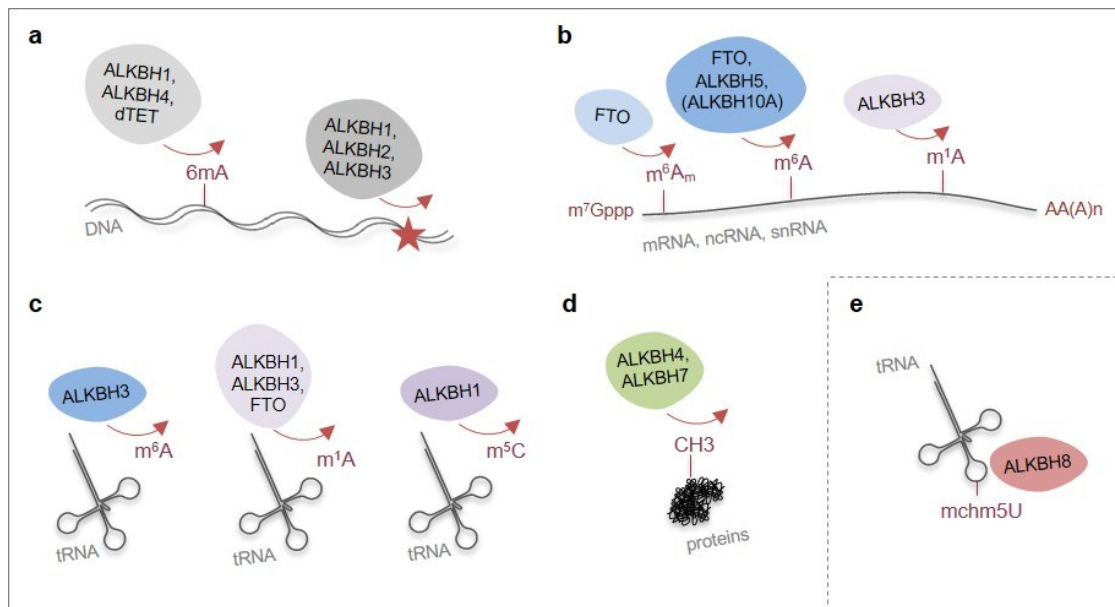


Figure 8. Schematic representation of ALKB-family of proteins and their substrates.

Demethylation activities of different AlkB-family members on **a**) DNA, **b**) mRNA, ncRNA and snRNA, **c**) tRNA targets. **d**) Predicted activity of ALKBH4 and ALKBH7 on protein substrates (Fedeles et al. 2015). **e**) ALKBH8 catalyses the formation of mchm⁵U at tRNA wobble site (Songe-Møller et al. 2010). Of note, dTET is not a member of AlkB-family, but was proposed to demethylate 6mA on DNA in *D. melanogaster* (Zhang G. et al. 2015). Red star in a) denotes DNA damage sites (alkylated bases such as 3mC, 1mA, 1mG).

While ALKBH3, ALKBH1, ALKBH5 and FTO preferentially target single stranded nucleic acids, the ALKBH2 was shown to act on dsDNA (Fedeles et al. 2015). Three members of the AlkB family (ALKBH1-3) protect cells from alkylating DNA damage by catalysing oxidation of alkylated bases (such as m³C, m¹A, m¹G, m³U/T) (Fedeles et al. 2015). ALKBH8 differs from other members by containing an additional methyltransferase domain and is involved in the generation of the mchm⁵U modification at the tRNA wobble position (Songe-Møller et al. 2010). Finally, ALKBH4 and ALKBH7 are believed to demethylate proteins, while the ALKBH6 targets have not been identified yet (Fedeles et al. 2015). Notably, better

characterisation of AlkB proteins has revealed that many of them act on multiple distinct targets and substrates, which may be due to a conformational flexibility of the nucleotide recognition lid, positioned over the active site in most members of the AlkB family (Fedele et al. 2015). For instance, ALKBH3, ALKBH1 and FTO can also act on m¹A in tRNA (Kawarada et al. 2017, Wei J. et al. 2018, Chen Z. et al. 2019), and ALKBH1 can remove m⁵C on tRNA (Zhang and Jia 2018). Additionally, ALKBH1 and ALKBH4 both also demethylate 6mA on DNA (Wu et al. 2016, Xiao et al. 2018, Kweon et al. 2019), while ALKBH3 catalyses the removal of m⁶A on tRNA (Ueda et al. 2017) (*Chapter 1.1.1 and 1.3*). It is therefore important to consider potentially promiscuous activity of individual AlkB protein on different targets and substrates, when their biological functions are being studied. In addition, the extent of their possible redundancy has not been addressed so far. Two m⁶A demethylases, FTO and ALKBH5, that were shown to act on mRNA, can both demethylate only a subset of m⁶A sites along transcripts (Jia et al. 2011, Zheng et al. 2013). In addition, FTO can demethylate m⁶Am modification in mRNA and snRNA (Mauer et al. 2017, Mauer et al. 2019) (**Figure 9**)¹.

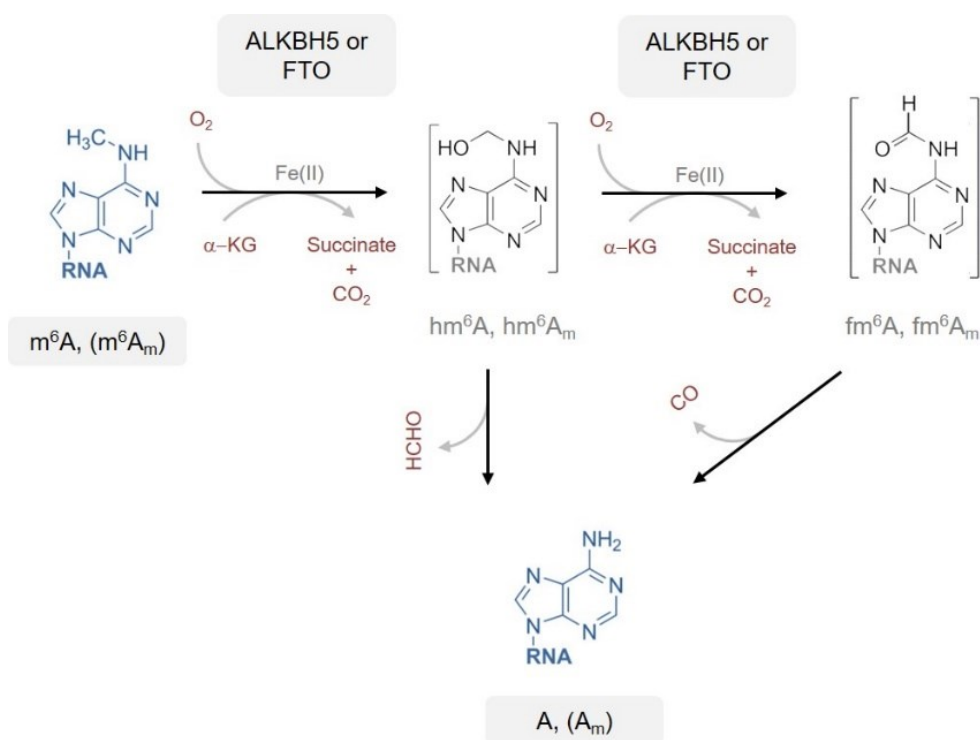


Figure 9. Schematic representation of m⁶A and m⁶Am demethylation by ALKBH5 and FTO.

ALKBH5 and FTO AlkB belong to non-heme iron dioxygenases and catalyse oxidative dealkylation of their substrates. ALKBH5 acts on m⁶A (Zheng et al. 2013), while FTO acts on both m⁶A and m⁶Am. Unstable hm⁶A and fm⁶A intermediates have been detected in FTO mediated reactions (Jia et al. 2011, Mauer et al. 2019). α-KG: α-ketoglutarate.

¹ The AlkB enzymes and other non-heme iron dioxygenases catalyse oxidative dealkylation of their substrates. For ALKBH5 and FTO the reaction starts by the recognition of the substrate and binding of the α-ketoglutarate (α-KG) to the Fe(II) centre in the enzymes' active site. This activates sequentially bound oxygen (O₂) to carry out a nucleophilic attack on the α-KG. Oxidative decarboxylation of α-KG results in a formation of succinate and CO₂, the later of which leaves the reaction. In addition, this generates a reactive iron-oxygen moiety (high valent Fe(IV)=O) that can hydroxylate the alkylated substrate (e.g. methylated substrate). Reactive iron-oxygen attacks the substrate's C-H bond and removes the hydrogen, which results in a formation of a carbon radical. The radical then rebinds the -OH group from the iron and forms unstable hydroxyl-intermediate that over time spontaneously resolves into formaldehyde (HCHO) and a demethylated nucleotide. FTO can further oxidise hydroxyl-intermediate to unstable formyl-intermediate.

FTO and ALKBH5 are expressed in different tissues and consistently, their depletion results in alterations of distinct biological processes (see below). Structurally, both proteins contain a characteristic loop that is not present in other AlkB family members and interferes with the accommodation of double stranded nucleic acid substrates (Han et al. 2010, Chen et al. 2014). FTO also contains an extended alpha-helical C-terminal region that is essential for its stability and catalytic activity (Han et al. 2010). Notably, the two enzymes do not display strict specificity for RRACH sites and target selectivity is achieved by structural constraints between the sequence surrounding the m⁶A site and the RNA binding motif (Zou et al. 2016). Intriguingly, interaction of ALKBH5 with one particular target was shown to be promoted by the transcript's own antisense RNA (Zhang S. et al. 2017), suggesting that recognition of the correct target might require multiple mechanisms. In plants two ALKBH10 paralogs exist, ALKBH10A and ALKBH10B, with the former one acting on m⁶A mRNA modification (Duan et al. 2017). Notably, as mentioned above, three other AlkB members can demethylate N6-methylated adenosines on DNA (ALKBH1 and ALKBH4) and tRNA (ALKBH3) (Ueda et al. 2017) Whether any of them could potentially remove m⁶A also from a subset of mRNA sites, remains to be addressed.

1.4.5.b FTO

FTO (Fat Mass and Obesity-associated) protein exhibits demethylation activity towards m⁶A and m⁶Am modifications on mRNA and snRNA targets (Jia et al. 2011, Mauer et al. 2019). Recently, m¹A modification on tRNA was also shown to be the FTO substrate (Wei J. et al. 2018). FTO is a predominantly nuclear protein and partially co-localizes with splicing factors in nuclear speckles (Jia et al. 2011), suggesting its role in nuclear pre-mRNA processing. Indeed, its depletion in different cell types results in altered alternative splicing and a vast majority of FTO binding sites (74 %) are found in intronic regions (Zhao et al. 2014, Bartosovic et al. 2017). Study by Zhao and colleagues demonstrated that FTO dependent m⁶A sites accumulate at the splice sites and promote binding of SRSF2 splicing regulator, leading to increased inclusion of alternative cassette exons. However, given that FTO also demethylates m⁶A on U6 snRNA, and m⁶Am on U1 and U2 snRNAs (Wei J. et al. 2018, Mauer et al. 2019), it would be important to investigate the possible contribution of altered snRNA methylation on the FTO-dependent splicing outcomes. FTO mediated removal of m⁶A, but not m⁶Am, seems to have a negative effect on mRNA stability (Wei J. et al. 2018), by a so far unknown mechanism. Notably, FTO binding along the mRNA does not follow m⁶A distribution profile, which may indicate a function independent of its catalytic activity, or the presence of m⁶Am modification at sites other than 5' cap (Zhao et al. 2014, Bartosovic et al. 2017). In some cell types, FTO also localizes to the cytoplasm, where it was shown to primarily demethylate m⁶Am modification, and m¹A modification on tRNA (Wei J. et al. 2018). Additionally, FTO was found in the axons of cells belonging to dorsal root ganglia, where it demethylates m⁶A from localized transcripts and in this way regulates their timely translation (Yu et al. 2018).

FTO protein is highly expressed in brain and adipose tissue and alterations in FTO gene have been associated with numerous biological defects. genome-wide association study studies linked mutations in the first intron of the FTO gene to an increased BMI (Body Mass Index), and consequently FTO was proposed to be the driving factor of obesity (Loos and Yeo 2014). Intronic FTO single-nucleotide polymorphisms (SNPs) were later shown to alter expression of a protein *Irx3* that regulates basal cellular metabolism (Smemo et al. 2014), via a long-range enhancer interactions. However, future work indeed demonstrated a direct role of FTO in obesity. FTO mutant mice models display reduced lean and fat mass (Fischer et al. 2009, Gao et al. 2010) whereas FTO overexpression associates with enhanced adiposity and increased food intake (Church et al. 2010). Consistently, FTO demethylation activity is

required for adipocyte differentiation and fat cell maturation (Zhao et al. 2014). Notably, some studies reported that FTO expression is modulated in response to starvation or increased food intake (Poritsanos et al. 2011, Gill et al. 2019), suggesting that both, FTO genetic variants and diet may lead to obesity risk.

Besides its role in metabolism, FTO is important in various neuronal processes and is highly expressed in different brain regions. It is particularly elevated in hypothalamus (Gerken et al. 2007) adult neural stem cells, and mature neurons (Li L. et al. 2017), where it is required for proper neuronal differentiation and adult neurogenesis (Li L. et al. 2017). Consistently, FTO loss of function results in impaired learning and memory consolidation (Widagdo et al. 2016, Li L. et al. 2017). Additionally, mice lacking FTO display postnatal growth retardation (Boissel et al. 2009, Fischer et al. 2009, Gao et al. 2010), reduced brain volume (Li L. et al. 2017) and altered locomotion (Fischer et al. 2009). Notably, neural specific conditional FTO KO mice exhibit similar phenotypes (Gao et al. 2010). Alteration of FTO levels in mice upon induced stress leads to anxiety-like behaviour (Spsychala and R  ther 2019), impaired dopaminergic signalling (Hess et al. 2013) and altered synaptic plasticity (Engel et al. 2018), suggesting that m⁶A (or m⁶Am, m¹A) levels must be tightly regulated during stress adaptation. Finally, accumulating evidence suggests that FTO alterations promote growth and metastasis of different cancer types including acute myeloid leukemia (AML), glioblastoma and endometrial cancer (Chen and Du 2019). Nevertheless, while most studies thus far correlated all of the above-mentioned deficiencies with the misregulation of m⁶A levels, the exact contribution of m⁶Am and m¹A modifications in these processes will have to be adequately analysed in the future. In summary, FTO is implicated in a wide range of biological processes and certainly represents an important pharmacological target for potential drug development (Niu et al. 2018).

1.4.5.c ALKBH5

ALKBH5, another m⁶A mRNA demethylase, is a strictly nuclear protein and partially co-localizes with splicing factors in nuclear speckles (Zheng et al. 2013). Consistently, its depletion alters alternative splicing (Tang et al. 2018). ALKBH5 also regulates mRNA localization and its depletion results in enhanced mRNA export (Zheng et al. 2013). ALKBH5 is highly expressed in testes, where its functions have been best-studied (Zheng et al. 2013, Tang et al. 2018). Loss of ALKBH5 in mice leads to male specific infertility. Males develop smaller testes with abnormal tubular architecture and strongly diminished numbers of spermatozoa that show significantly reduced motility (Zheng et al. 2013). These alterations arise from spermatogenic arrest, as demonstrated by reduced number of pachytene spermatocytes and their increased apoptosis (Zheng et al. 2013). Further studies showed that loss of ALKBH5 increases levels of m⁶A within CDS and around start codons, which results in altered splicing and aberrant transcript shortening. Additionally, high m⁶A levels promote premature transcript decay, which altogether interferes with the progress of spermatogenesis (Tang et al. 2018). Similarly to FTO, ALKBH5 is implicated in poor prognosis of several cancers (Zhang et al. 2016, Zhang S. et al. 2017, Liu Z.-X. et al. 2018, Pinello et al. 2018). Levels of ALKBH5 were shown to be strongly increased under hypoxic conditions that are often present in advanced tumours. Induced hypoxia in breast cancer stem cells leads to ALKBH5 mediated demethylation of a core pluripotency factor, *Nanos*, which elevates its protein levels and consequently promotes BCSC proliferation (Zhang et al. 2016). Levels of ALKBH5 are also high in glioblastoma stem cells (GSC), where demethylation of *FOXM1* transcript, a cell-cycle regulator gene, elevates its protein levels. This resulted in increased GSC proliferation and promoted glioblastoma progression (Zhang S. et al. 2017). Given its role in cancer, ALKBH5 might represent a relevant target for diagnostic or therapeutic purposes.

1.4.6 m⁶A reader proteins

m⁶A modification has a strong impact on the fate of modified RNA by, either directly or indirectly influencing the binding of various RBPs. The main mediators of m⁶A functions are the so-called “reader” proteins that can specifically recognise and accommodate m⁶A modification (*Chapter 1.4.6.a and 1.4.6.b*). Best characterized are members of the YTH (YT521-B homology) domain-containing family of proteins (YTH proteins) (Patil et al. 2017). Different nuclear and cytoplasmic YTH proteins are implicated in nearly every aspect of mRNA processing: from splicing (Xiao et al. 2016) and polyadenylation (Ke et al. 2015), to mRNA export (Roundtree Ian A. et al. 2017). In the cytoplasm, they can promote translation (Wang et al. 2015, Hsu et al. 2017, Shi et al. 2017) and function in the regulation of mRNA stability and decay (Wang et al. 2013, Du et al. 2016, Hsu et al. 2017). Additionally, in specific sequence context m⁶A modification can change local RNA structure and in this way alter RNA-protein interactions in a positive or negative fashion (*Chapter 1.4.6.c*). This type of regulation, also called an “m⁶A-switch”, was shown to impact binding of a number of hnRNP proteins. hnRNPC (Liu et al. 2015), hnRNPA2B1 (Alarcon et al. 2015a), hnRNPG (Liu et al. 2017), and HuR (Spitale et al. 2015) can in this way influence pri-miRNA processing, mRNA splicing and stability (Alarcon et al. 2015a, Liu et al. 2015, Spitale et al. 2015, Liu et al. 2017). Following chapters provide an overview of current knowledge on various RBPs whose binding to RNA was shown to be affected by m⁶A (**Figure 10**).

1.4.6.a YTH domain-containing reader proteins

YTH domain-containing family of proteins were among the first identified m⁶A binders (Dominissini et al. 2012). As revealed by the recent crystal structures, they can specifically accommodate m⁶A modification by an aromatic cage of the YTH domain (Li F. et al. 2014, Luo and Tong 2014, Theler et al. 2014, Xu et al. 2014, Zhu et al. 2014). YTH family members are found in various species, from yeast to human as well as in plants. While their primary sequences outside the YTH domain largely differ, the primary sequence and structure of the YTH domain itself are highly conserved (Stoilov et al. 2002, Huang and Yin 2018). Vertebrates have five YTH proteins, four primarily acting in the cytoplasm (YTHDF1/2/3 and YTHDC2) and one in the nucleus (YTHDC1). However, while budding yeast have only one member (Pho92) (Schwartz et al. 2013), some plants encode up to thirteen paralogs (Arribas-Hernández et al. 2018, Scutenaire et al. 2018, Wei L.-H. et al. 2018). Consistent with the absence of m⁶A modification on mRNA in nematodes and fission yeast, no YTH domain members are found in the former, while the latter contains a single YTH domain protein Mmi1 that, however, cannot specifically accommodate m⁶A-modified RNA via its YTH domain (Wang C. et al. 2016) Vertebrate YTH proteins have been well characterised and were shown to have an important impact on mRNA biogenesis by interacting with various mRNA processing factors and by recruiting them to the target transcript. Among these are different splicing and export factors, translation apparatus, as well as components of the deadenylation complex (**Figure 10**).

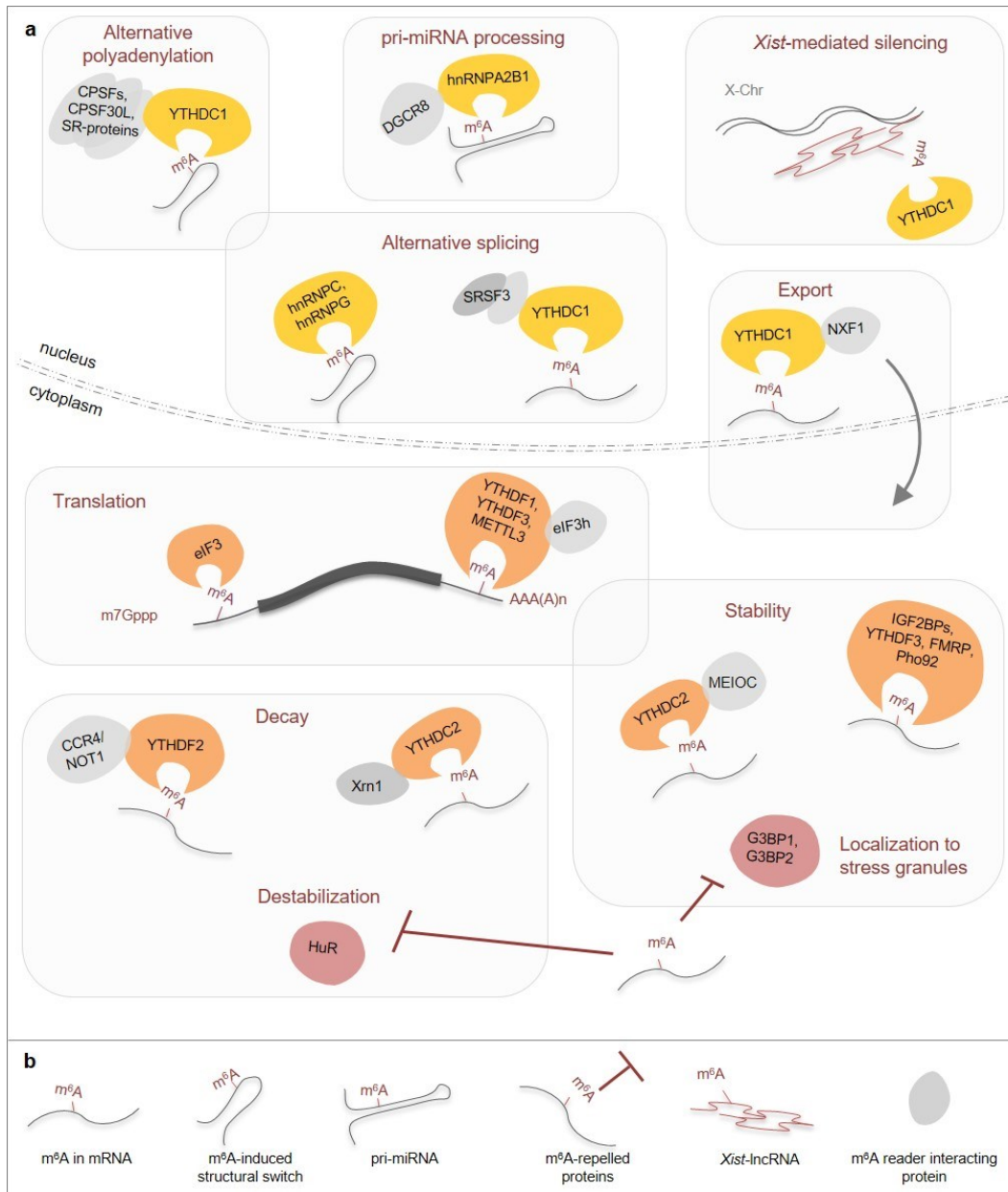


Figure 10. m⁶A reader proteins.

a) Schematic representation of known m⁶A readers and m⁶A-repelled proteins in different RNA processing steps in which they are involved. m⁶A readers in the nucleus and cytoplasm are shown above (in yellow) and below (in orange), respectively. Repelled proteins are shown in red and various interactors in grey. **b)** Figure legend depicting m⁶A in different types of RNA or in different structural contexts.

YTHDC1 proteins

YTHDC1 is the only nuclear YTH domain-containing family member that carries four predicted NLS and several low complexity regions; the N-terminal Q-rich, and C-terminal P- and E/R-rich regions, with the later likely implicated in protein-protein interactions (Hartmann et al. 1999). YTHDC1 was initially found as an interactor of various splicing factors, including SC35, SF2 and TRA2B (Imai et al. 1998, Hartmann et al. 1999). TRA2B is the homolog of a well characterised splicing factor transformer-2 in *D. melanogaster*, suggesting YTHDC1's role in the regulation of pre-mRNA splicing. YTHDC1 resides in the so-called YT-bodies, adjacent to nuclear speckles, along with Sam68 and SAF-B proteins, that couple mRNA transcription to splicing (Hartmann et al. 1999, Nayler et al. 2000). Consistent with these

early observations, YTHDC1 was later found to regulate alternative splicing of a subset of m⁶A modified sites via its interactions with hyper-phosphorylated SRSF-proteins (Xiao et al. 2016). It promotes the recruitment of the splicing enhancer SRSF3 and interferes with the binding of the splicing silencer SRSF10, to enhance exon inclusion (Xiao et al. 2016). Besides its role in splicing, YTHDC1 was also found to interact with factors involved in alternative polyadenylation (SRSF3, SRSF7 and CPSF6) and to control transcripts' 3'UTR length (Kasowitz et al. 2018). Of note, the SRSF3 and SRSF10 were previously shown to regulate 3'UTR lengths in opposite directions (Müller-Mcnicoll et al. 2016). The exact mechanism by which YTHDC1 mediates 3'UTR processing has not been revealed yet. It could either sequester its interactors from their binding sites or promote their recruitment to methylated regions. Besides nuclear processing, YTHDC1 is also involved in mRNA export. It interacts with the hypo-phosphorylated version of the SRSF3 protein that acts as an adaptor for the NXF1 export factor (Müller-Mcnicoll et al. 2016). In line with this, depletion of YTHDC1 results in the accumulation of m⁶A modified mRNA in the nucleus, which can be rescued by the ectopic expression of its C-terminal region required for the interaction with the SRSF3 protein (Roundtree Ian A. et al. 2017). Of note, the YTHDC1 interactor SRSF7 was also shown to promote the recruitment of the NXF1 export factor to a subset of targets (Müller-Mcnicoll et al. 2016).

Another study that recently investigated the involvement of m⁶A in mRNA export, could demonstrate that on a subset of m⁶A sites YTHDC1, as well as m⁶A writer complex, directly interact with the TREX export complex components, suggesting that m⁶A can mark transcripts for nuclear export by multiple ways (Lesbirel et al. 2018). In addition to its interactions with mRNA, the iCLIP analysis of YTHDC1 binding also revealed high overlap with identified m⁶A on snoRNA and nuclear lncRNAs, such as *Malat1*, *Neat1* and *Xist* (Patil et al. 2016). Notably, its binding to *Xist* is required for efficient X-chromosome silencing, albeit the mechanism has not been refined yet (Patil et al. 2016). Overall, despite well-demonstrated roles of YTHDC1 in alternative splicing, polyadenylation and export (**Figure 10**), it is currently not understood what regulates its recruitment to defined set of m⁶A sites, or how its interactions with other proteins are coordinated. The importance of YTHDC1 in numerous biological processes is being increasingly recognised. Like *Mettl3* and *Mettl14* writer components, *Ythdc1* is indispensable for mice survival and most *Ythdc1* KO embryos die in early stages post implantation (E8.5) (Kasowitz et al. 2018). In addition, *Ythdc1* is also essential for gametogenesis in both males and females.

YTHDF proteins

Vertebrates contain three YTHDF paralogs (YTHDF1, YTHDF2 and YTHDF3) that share a high sequence similarity and contain an N-terminal low complexity region with P/Q/N rich repeats, involved in interactions with many mRNA processing factors (Patil et al. 2017) (**Figure 10**). Binding sites of all three YTHDF proteins throughout the transcriptome are highly similar and greatly overlap with identified m⁶A sites on mRNA (Patil et al. 2016). They all localize to the cytoplasm and are involved in the regulation of mRNA translation and turn over. YTHDF2 was the first protein shown to regulate mRNA stability (Wang et al. 2013) by interacting with the CCR4/Not complex (Du et al. 2016). YTHDF2 also co-localizes with decapping and deadenylation components and was suggested to promote mRNA localization from the translatable pool to cellular compartments (e.g. P-bodies), from where they are committed for eventual decay (Wang et al. 2013). YTHDF1 on the other hand was shown to promote translation initiation of m⁶A marked transcripts by interacting with the eIF3 factors, which leads to mRNA looping and increases ribosome loading (Wang et al. 2015). The third member of the YTHDF proteins, YTHDF3, stimulates mRNA processing together with YTHDF1 and YTHDF2 and was proposed to stabilize their binding (Li A. et al. 2017) (Shi et al. 2017). Recent study, however, also demonstrated

that YTHDF3 mediates translation initiation by cooperative binding with PABPC1 and eIF4G2 proteins in the proximity of translation initiation sites, independently of the Mettl3 deposited m⁶A modification (Zhang Yuan et al. 2019). Nevertheless, its m⁶A interacting ability was indispensable for this regulation, suggesting that YTHDF3 might bind m⁶A deposited by other methyltransferases (e.g. Mettl16) or that it binds the m⁶Am modification that resides at the TSS (Mauer et al. 2017). In addition, upon stress the YTHDF3, but not YTHDF1 or YTHDF2, binds m⁶A sites within 5'UTR and tethers transcripts to cytoplasmic stress granules. This results in translational stalling and transcript stabilization (Anders et al. 2018), possibly via a set of Ythdf3-specific interactors that remain to be identified. All three YTHDF proteins share many common target sites and are involved in the same regulatory pathways, albeit it is currently not understood how their binding specificity or target recognition are defined. It was proposed that YTHDF1 and YTHDF3 recognise target mRNAs and promote their translation prior to recruitment of YTHDF2 that subsequently leads mRNA to decay. In this way, fast and efficient mRNA output could be achieved, whenever required (Li A. et al. 2017). Given that none of the proteins shows any sequence specificity, it is possible that other interacting partners are involved in the selection of unique m⁶A targets. Intriguingly, recent findings from Jaffrey and Hanna groups suggest that Ythdf1, Ythdf2 and Ythdf3 proteins act redundantly in a context and dosage-dependent manner, whereby the loss of one reader can be compensated by sufficient expression of the two other Ythdf members (Lasman et al. 2020, Zaccara and Jaffrey 2020). Nevertheless, different spatial and temporal expression patterns of the Ythdf2 makes it indispensable for mouse gametogenesis and viability (Lasman et al. 2020), highlighting that the three proteins are not redundant in all cell types and biological systems. **Pho92** (also known as Mrb1) is the only YTH domain-containing protein in the budding yeast and is a member of the YTHDF family, with cytoplasmic localisation (Schwartz et al. 2013). Similarly to the MIS m⁶A writer complex, its expression is restricted to meiosis (Schwartz et al. 2013). In yeast m⁶A is elevated along the mRNA 3'UTR regions and methylated transcripts are highly enriched in the translatable pool associated with polysomes (Bodi et al. 2015). Early meiotic transcripts have a very short half-life (T Surosky and Esposito 1992) and Pho92 was proposed to mediate their timely decay (Kang et al. 2014). In line with this, Pho92 KO was efficiently rescued by the ectopic expression of YTHDF2 protein (Kang et al. 2014) whose function in mRNA decay has been well demonstrated (Wang et al. 2013). Nevertheless, more studies are needed to decipher the exact mechanism of Pho92 mediated m⁶A-specific transcript destabilization.

YTHDC2

YTHDC2 is the least conserved cytoplasmic member of the YTH-family and unlike the name might suggest, it is not related to the YTHDC1 protein (Bailey et al. 2017, Hsu et al. 2017, Wojtas et al. 2017, Jain et al. 2018). Besides its C-terminal YTH domain, the YTHDC2 contains other unique protein regions, including the R/H rich R3H domain, the DEAH-box helicase core with an Ankyrin repeat and further sequence motifs involved in nucleic acid binding and protein interactions (Jain et al. 2018). YTHDC2 homologs are present in many eukaryotes, however they represent a highly divergent group of proteins. Many members retained overall architecture, but have lost either the YTH domain, or some of the other protein domains. This suggests that YTHDC2 homologs likely have different protein interactors, and have possibly evolved novel functions (Jain et al. 2018). Consistent with the presence of the helicase region, YTHDC2 has an ATP-dependent 3' → 5' unwinding activity, albeit its biological relevance is not known yet (Wojtas et al. 2017, Jain et al. 2018). Similarly to other cytoplasmic YTH-members, YTHDC2 can enhance mRNA translation (Hsu et al. 2017) and regulate stability of m⁶A modified transcripts (**Figure 10**). It acts cooperatively with an interacting partner MEIOC (Bailey et al.

2017, Hsu et al. 2017, Wojtas et al. 2017, Jain et al. 2018) that was previously shown to be required for the progression of meiosis (Abby et al. 2016). In addition, YTHDC2 associates with the Xrn1, a 5' → 3' exoribonuclease via the Ankyrin domain, which may contribute to its proposed function in mRNA decay (Wojtas et al. 2017). However, since YTHDC2 can alter stability of different subsets of methylated transcripts in a positive or a negative fashion, exact mechanisms of its activities remain to be resolved.

1.4.6.b Other m⁶A readers and m⁶A repelled proteins

Most studies that searched for m⁶A readers performed in vitro pull-down experiments in chosen cell lysates using different m⁶A methylated/non-methylated RNA probes, that were followed by mass spectrometry proteomic analysis of recovered proteins (Dominissini et al. 2012, Schwartz et al. 2014b, Arguello et al. 2017, Edupuganti et al. 2017, Baquero-Perez et al. 2019). All studies consistently identified YTH-family members, however, many other RNA binding proteins were also found to preferentially interact with the m⁶A modified RNA sequences (Dominissini et al. 2012, Arguello et al. 2017, Edupuganti et al. 2017, Baquero-Perez et al. 2019). Among them were the FMRP and its homologs FXR1 and FXR2 that have all been previously linked to translational repression (Siomi et al. 1996) as well as IGF2BPs implicated in mRNA stability and translation (Huang et al. 2018).

FMRP: FMRP (Fragile X mental retardation protein) has an important role in neuronal development and its loss of function leads to Fragile X syndrome, a form of intellectual disability (Darnell and Klann 2013). FMRP is a predominantly cytoplasmic protein, although it is also found in the nucleus. Its functions in mRNA metabolism include regulation of alternative splicing, transcript localisation and primarily, translational inhibition (Bagni et al. 2012, Darnell and Klann 2013). FMRP protein contains several RNA binding domains (e.g KH, RGG) and all were shown to be required for binding to m⁶A modified sequences (Edupuganti et al. 2017). The analysis of FMRP targets transcriptome wide revealed that many carry m⁶A modification, suggesting that FMRP acts as a context dependent m⁶A reader protein (Chang et al. 2017). Recent study demonstrated that FMRP interacts with the YTHDF2 reader and proposed that both proteins might regulate mRNA stability of common targets (Zhang F. et al. 2018), however, it is currently not known whether they act cooperatively, competitively or independently.

IGF2BP: Another group of proteins that can recognise m⁶A modified sites are IGF2BP (Insulin-like growth factor 2 mRNA-binding protein) proteins (IGF2BP1, IGF2BP2 and IGF2BP3) (Huang et al. 2018). They share highly homology and carry two RRM and four KH (K-homology) RNA binding domains, with the later ones required for recognition and binding of m⁶A in the consensus sequence RRACH. Their transcriptome wide binding analyses showed that they mostly bind mRNA in their CDS and 3'UTR regions, where m⁶A is highly enriched. In line with this, over 80 % of their targets were m⁶A modified. A vast majority of identified transcripts was bound by at least two IGF2BP members, yet the proteins are not redundant, as individual depletion of each of them results in reduced target stability (Huang et al. 2018) (**Figure 10**). Stabilizing function was proposed to be mediated via IGF2BP interactors that are well characterised mRNA stabilizing proteins (DCP1A, PABPC1, HuR, MATR3, TIAR) and reside in cytoplasmic mRNA storage compartments, such as P-bodies and stress granules (Huang et al. 2018). In addition to their mRNA stabilizing role, IGF2BPs also associate with polysomal fractions and facilitate mRNA translation (Huang et al. 2018).

eIF3: Translation initiation factor eIF3 can specifically bind m⁶A sites at the mRNA 5' UTR region to promote cap-independent mRNA translation upon cellular stress (e.g. heat shock), when the m⁷G-cap-dependent translation is globally suppressed. Under such conditions, a set of stress-inducible transcripts gains the 5'-proximal m⁶A modification. Consequent binding of eIF3 ensures proper cellular

response (Meyer et al. 2015). Notably, eIF3 also contributes to efficient m⁷G-cap-dependent translation of m⁶A-modified transcripts via its interaction with the YTHDF1 and METTL3 proteins at the 3'UTR regions (**Figure 10**). Whether YTHDF1 and METTL3 also recruit eIF3 to the 5' sites during stress has not been investigated yet.

SND1: The Tudor SND1 (Staphylococcal Nuclease And Tudor Domain Containing 1) protein binds viral m⁶A modified transcripts to regulate replication of Kaposi's sarcoma-associated herpesvirus (Baquero-Perez et al. 2019). Some members of Tudor domain proteins contain an aromatic cage that can accommodate methylated histones and is structurally similar to the m⁶A-binding pocket of the YTH domain (Chen et al. 2011). Intriguingly, FMRP, FXR1 and FXR2 that also bind m⁶A, have a Tudor-like domain (Chen et al. 2011, Baquero-Perez et al. 2019). It is thus possible that other Tudor domain proteins recognise m⁶A modified transcripts in a sequence and structure dependent manner. Of note, many Tudor domain-containing (TDRD) proteins are highly expressed in the germ line, where m⁶A plays significant roles (*Chapter 1.4.8.e*).

G3BP1 and G3BP2: Beside m⁶A readers, many pull-down experiments also identified proteins that preferentially interacted with the non-methylated RNA sequences (Arguello et al. 2017, Edupuganti et al. 2017). Among the repelled proteins were G3BP1 and G3BP2 (Ras GTPase-activating protein-binding protein 1 and 2) (Arguello et al. 2017, Edupuganti et al. 2017) along with their interactors (e.g. RBM42, USP10 and CAPRIN) that localise to cytoplasmic stress granules, where mRNA is stored and stabilized upon different stress stimuli (Arguello et al. 2017). This finding suggested that loss of m⁶A might promote transcript stability via G3BP1/2 binding (**Figure 10**). Further characterisation of G3BP1/2 in vivo however revealed that both proteins are repelled by m⁶A modification on a very small subset of sites that reside within a GGACU sequence, while their binding to the GAACU sequence (that differs by a single nucleotide) is equally good in the presence or absence of m⁶A (Edupuganti et al. 2017). In addition, transcriptome wide binding analyses of G3BP1/2 by PAR-CLIP also demonstrated that both proteins are highly enriched in CAACUC sites that contain AAACU m⁶A-motif where their recruitment is m⁶A-independent (Edupuganti et al. 2017). In summary, binding of G3BP1/2 to target mRNA is repelled by m⁶A modification only in a restricted sequence context, where the loss of m⁶A modification promotes the G3BP1/2 mediated stabilization of targeted transcripts.

1.4.6.c “m⁶A-switches”

m⁶A modification does not interfere with Watson-Crick base pairing, however it can destabilize RNA duplex formation (Engel and Von Hippel 1974). In specific sequence contexts, m⁶A can therefore change local RNA structure and in this way influence binding of various RBPs (Alarcon et al. 2015a, Liu et al. 2015, Spitale et al. 2015, Liu et al. 2017). As shown by transcriptome wide RNA structural probing via icSHAPE (selective 2'-hydroxyl acylation analysed by primer extension) experiment, m⁶A in many cases destabilizes base pairing of its surrounding nucleotides (Spitale et al. 2015). RNA binding of a number of hnRNP proteins, including hnRNPC, hnRNPA2B1, hnRNPG, and HuR, were found to be affected by these so-called “m⁶A-switches”, which consequently altered pre-mRNA splicing, miRNA targeting and mRNA stability (**Figure 10**) (Alarcon et al. 2015a, Liu et al. 2015, Spitale et al. 2015, Liu et al. 2017). For instance, thousands of intron-residing U-stretches become exposed by such m⁶A-induced remodelling, allowing for hnRNPC binding and its m⁶A-dependent splicing regulation (Liu et al. 2015). Likewise, the hnRNPG protein regulates splicing by binding to over 10.000 m⁶A-remodeled RNA motifs using its C-terminal low-complexity RGG-repeat region (Liu et al. 2017). Recent study demonstrated that it acts as a bridge between the transcribing RNA PolIII and m⁶A modified sites near exons of the nascent RNA. In this way hnRNPG increases RNAPolIII dwell time and thereby promotes downstream

exon inclusion (Zhou et al. 2019). **hnRNPA2B1** is another example of a protein that binds to sites in a UGAA motif in the proximity of m⁶A-switches and recapitulates alternative splicing outcomes observed upon loss METTL3 (Alarcon et al. 2015a). The most pronounced binding of hnRNPA2B1 is however along the 3`UTR regions, where it generally promotes the usage of proximal alternative polyadenylation sites. Whether this regulation is m⁶A-switch dependent is currently not known (Martinez et al. 2016). In addition to binding mRNA targets, hnRNPA2B1 also recognizes many m⁶A sites that reside in the pri-miRNA sequences and promotes their processing by interacting with the DGCR8 microprocessor subunit (Alarcon et al. 2015a, Alarcon et al. 2015b). This function is however, not conserved in cells of the CNS (Martinez et al. 2016). Contrary to other m⁶A-switch regulated RBP mentioned so far, the **HuR** protein was shown to be repelled from hundreds of its binding sites that overlapped with m⁶A modification within the 3`UTR regions. This resulted in mRNA destabilization, due to increased miRNA targeting (Wang Y. et al. 2014). The impact that m⁶A-switches have on the regulation of RNA processing is likely underscored, and more context dependent examples are expected to be found in the future. Overall, in order to gain better understanding into how different direct and indirect m⁶A readers coordinately shape the transcriptome, additional studies on individual transcript examples will have to be carried out.

1.4.7 m⁶A modification regulates nearly all aspects of mRNA processing

To get the first glimpse into biological functions of m⁶A mRNA methylation, back in the 1970s, researchers took advantage of different SAM inhibitors and monitored the mRNAs processing of known m⁶A modified transcripts¹ (Caboche and Bachellerie 1977, Bachellerie et al. 1978). These early studies proposed the role of m⁶A in pre-mRNA splicing, export and decay albeit not ruling out effects that inhibitors might have on other methylation reactions, which could indirectly lead to the observed outcomes (Sommer et al. 1978, Camper et al. 1984). As of today, we know that m⁶A modification indeed regulates a subset of alternative pre-mRNA splicing and polyadenylation events, as well as that it promotes mRNA export. In addition, its role in nearly every other aspect of cytoplasmic mRNA processing including translation, stability, and decay has been demonstrated. Most of these functions are mediated by the m⁶A reader proteins (*Chapter 1.4.6*) (**Figure 10**). The following chapters summarise some processes shown to be affected by altered m⁶A levels.

1.4.7.a Alternative splicing

Alternative splicing is a co-transcriptional process that enables the formation of multiple distinct mRNA isoforms from a single transcript and represents one of the crucial mechanisms that contribute to proteome diversity. It is regulated by a combinatorial effect of cis-acting elements and trans-acting factors that define splice site selection (*Chapter 1.2.2*). The very first indication that m⁶A might play a role in the process of splicing was made in the early 1980s when modification was mapped to intronic regions of several transcripts (Stoltzfus and Dane 1982, Carroll et al. 1990), revealing that methylation takes place prior to splice site recognition. Indeed, loss of methylation in the pre-mRNA of avian retrovirus envelope protein and in the *bovine prolactin* transcript was found to correlate with poor splicing efficiency (Stoltzfus and Dane 1982, Carroll et al. 1990). Further indications that m⁶A is likely involved in the regulation of alternative splicing came from its transcriptome wide mapping, showing that modification is highly enriched in long internal exons with multiple isoforms (Dominissini et al. 2012, Ke et al. 2015). More recently, several studies demonstrated that m⁶A deposition occurs co-transcriptionally, suggesting that its presence within introns might be more widespread (Barbieri et al. 2017, Ke et al. 2017, Knuckles et al. 2017, Slobodin et al. 2017, Huang et al. 2019). Transcriptome wide RNA binding analyses of METTL3, METTL14 and WTAP also revealed that nearly 30 % of their binding sites reside in introns (Liu et al. 2014, Ping et al. 2014) that are located next to alternatively spliced exons (Ping et al. 2014). These intronic sites, bound by the writer complex, are most likely methylated, however the nature of fast co-transcriptional splicing, interferes with m⁶A recognition by the conventional MeRIP-seq mapping technique (Dominissini et al. 2012, Meyer et al. 2012). Louloupou and colleagues therefore recently developed a method termed TNT-seq (transient N-6-methyladenosine transcriptome sequencing) that enables m⁶A detection in bromouridine (BrU) labelled and enriched nascent pre-mRNA (Louloupou et al. 2018). Using this approach, they could demonstrate that over 50 % of m⁶A sites reside in introns and correlate with slow processing and alternative splicing. In contrast, exonic m⁶A sites located in a close proximity to splice junctions, in particular to 5`ss, were linked to fast

¹ Chemical inhibitors that interfere with SAM biogenesis and counteract with SAM-dependent methylations have been used in order to reduce m⁶A levels. SAM is a methyl donor for numerous DNA, RNA and protein methyltransferases and is synthesised by the methionine adenosyltransferase (MAT) enzyme. SAM turnover results in the formation of S-adenosylhomocysteine (SAH), which is further hydrolysed by the activity of SAH-hydrolase. Early studies investigating m⁶A functions used three classical methylation inhibitors: cycloleucine, neplanocin A (NPC) and S-tubercidinylhomocysteine (STH). Cycloleucine is a competitive inhibitor of MAT. NPC can inhibit SAH hydrolase, which results in accumulation of SAH. This in turn inhibits activity of some methyltransferases that use SAM as a methyl donor. STH is structurally similar to SAH and inhibits methylation by the same mechanism.

and constitutive splicing (Louloupi et al. 2018). Similar findings were obtained by Molinie and colleagues, who developed a method (LAIC-seq) that allows a quantitative analysis of m⁶A-positive and negative fractions. They found that m⁶A promotes inclusion of cassette exons in mature transcripts (Molinie et al. 2016).

Consistent with these observations, numerous studies could show that changes in m⁶A deposition or removal result in altered splicing outcomes (Dominissini et al. 2012, Zhao et al. 2014, Liu et al. 2015, Xiao et al. 2016, Bartosovic et al. 2017, Ke et al. 2017, Tang et al. 2018). Notably, some of the identified splicing events are likely indirect and the exact contribution of m⁶A for most events remains to be determined. However, few examples provide mechanistic insights into m⁶A regulated splicing that is in most cases mediated by different m⁶A reader proteins. A study from Xiao and colleagues demonstrated that a nuclear reader protein YTHDC1 promotes exon inclusion via its interactions with splicing regulators, the SR proteins. On a subset of cassette exons, YTHDC1 recruits splicing enhancer SRSF3 and interferes with the binding of splicing silencer SRSF10 (Xiao et al. 2016). The same mechanism also enhances splicing of the lytic cycle switch protein RSA in the Kaposi's sarcoma-associated herpesvirus, albeit the respective m⁶A sites are in this case located in the intronic region of the RSA pre-mRNA (Ye et al. 2017). In another study, Liu and colleagues identified over 2000 methylated intronic sites that promote hnRNPC binding via a structural m⁶A-switch mechanism and regulate alternative splicing of a subset of flanking exons (Liu et al. 2015). Work from Zhao and colleagues demonstrated how splicing can be regulated by the interplay between the SRSF2 protein and FTO mediated demethylation. They observed m⁶A enrichment in the proximity of splice sites, within exons that overlapped with SRSF2 binding sites. Depletion of FTO promoted SRSF2 binding and led to increased exon inclusion. It is currently not known, if SRSF2 binds m⁶A directly, or if its recruitment to RNA is affected by m⁶A-induced structural changes (Zhao et al. 2014). Bartosovic and colleagues also studied regulation of splicing by FTO mediated demethylation. In line with observations from Louloupi and colleagues, they showed that loss of m⁶A by FTO promotes splicing of internal exons. Additionally, they found that it counteracts with splicing of the last exon, where m⁶A enrichment is typically elevated (Bartosovic et al. 2017). Notably, given that the vast majority of FTO binding sites are in fact in intronic regions, suggests that some of the observed splicing alterations are likely caused by elevated m⁶A that reside in introns (Bartosovic et al. 2017). The importance of regulated m⁶A levels for correct splicing was also demonstrated by studies involving the ALKBH5 demethylase. The ALKBH5 KO for example promotes splicing and leads to shortening of various transcripts during spermatogenesis (Tang et al. 2018).

Another important example of m⁶A mediated splicing regulation was demonstrated for a transcript encoding the SAM-synthase (*Mat2a*) that is methylated by the Mettl16 enzyme in an auto regulatory fashion (Pendleton et al. 2017, Warda et al. 2017, Doxtader et al. 2018). When SAM is present in cells at sufficient levels, Mettl16 methylates *Mat2a* transcript at 3'UTR located stem loops. This results in retention of the upstream intron and subsequent mRNA degradation in the nucleus. Contrary, when levels of SAM are scarce, Mettl16 cannot induce methylation; however, it still recognizes and binds the stem loops of *Mat2a* mRNA and promotes intron splicing. In this way levels of functional *Mat2a* transcript are increased, which in turn elevates its protein levels and enzymatic production of SAM. This important negative feedback loop depends on the levels of available SAM that is required for methylations in various biological processes. Importantly, Mettl16 binds its target sites regardless of whether SAM is present or not, albeit with distinct binding affinity. This indicates that the enzyme can in some way sense and respond to SAM availability, possibly via a structural change induced after SAM binding. Recent structural data showed that Mettl16 can dimerize (Ruszkowska et al. 2018),

however its methylation activity seems to depend only on individual N-terminal methyltransferase region. It will be helpful to determine how is the Mettl16 stalling on the transcript accomplished, and how this promotes splicing. Of note, the vertebrate specific C-terminal region (VCR) of Mettl16 alone is sufficient to induce *Mat2a* intron splicing. It will be also informative to see, if methylation of stem loop is needed to prevent functional splicing or else, if it is only required to ensure fast Mettl16 release from the transcript. Finally, it would be interesting to investigate, if any other SAM-dependent methyltransferase can respond similarly to the reduced levels of SAM, in regards to substrate recognition, binding retention or methylation efficiency.

1.4.7.b Polyadenylation

In vertebrates, m⁶A modification was shown to be highly enriched around the STOP codons and within the 3'UTR regions of coding transcripts (Dominissini et al. 2012, Meyer et al. 2012), where they in most cases also contain the cleavage and polyadenylation sequences. This raised the question whether m⁶A deposition and 3'-end processing are correlated. To address this possibility, Ke and colleagues performed m⁶A mapping with a nucleotide precision using an anti-m⁶A antibody and UV crosslinking (m⁶A-CLIP). They observed that 70 % of all m⁶A sites in mouse and human samples reside in the first 150-400 nts of the last exon, regardless of the location of the stop codon. They next analysed the polyA site choice in the presence and absence of m⁶A writer components (Ke et al. 2015). Among transcripts that changed alternative polyadenylation sites within the last exons, they found that in over 60 % of cases m⁶A had an inhibitory effect on the proximal polyA site usage and has in this way promoted 3'UTR extension (Ke et al. 2015). In line with this, inactivation of FTO, increases m⁶A levels and steady state levels of transcripts with extended 3'UTRs (Bartosovic et al. 2017). Additional insights into the regulation of alternative polyA site usage via m⁶A have been demonstrated in a study that observed an interplay between the m⁶A writer component VIRMA and cleavage and polyadenylation specificity factors CPSF5 and CPSF6 (Yue et al. 2018). VIRMA was proposed to direct methylation of 3'UTR regions. In contrast to Ke and colleagues, loss of VIRMA and m⁶A in most cases promoted the usage of a distal polyA site (Yue et al. 2018), while depletion of CPSF5 increased methylation and led to 3'UTR shortening.

The effect of m⁶A modification on the polyadenylation site choice was shown to be partially mediated by the nuclear reader protein YTHDC1 that interacts with the SRSF3, SRSF7, SRSF10 and CPSF6 proteins (Kasowitz et al. 2018) involved in 3'UTR processing. Of note, the SRSF3 and SRSF10 were previously shown to regulate 3'UTR lengths in opposite directions, resulting in either pA shortening or lengthening, respectively (Müller-Mcnicoll et al. 2016). Beside examples of alternative polyadenylation, a recent study in plants also demonstrated that m⁶A in a subset of transcripts ensures efficient 3'UTR processing and thereby prevents generation of transcript fusions via transcriptional read-through. This is achieved via a nuclear reader protein CPSF30L that contains a YTH domain fused to a 30-kD subunit of the cleavage and polyadenylation specificity factor (Pontier et al. 2019). Extended 3'UTRs can contain features that affect transcript stability or subcellular localization, for example during early embryogenesis and neurogenesis (Elkon et al. 2013). By regulating the polyA site choice m⁶A could provide an additional layer in these processes. However, how exactly m⁶A modification in some cases prevents and in other facilitates the selection of alternative polyadenylation sites remains to be demonstrated on representative examples of biologically relevant transcripts.

1.4.7.c Export

m⁶A modification can act as a signal for nuclear export via the TREX-NXF1 pathway. This pathway relies on the binding of TREX core components (THO complex and UAP56 helicase), export adaptor (e.g. ALYREF, SRSF3, SRSF7) and co-adaptor proteins (e.g. THOC5, CHTOP) that associate with mRNA during different steps of pre-mRNA processing; capping, splicing and polyadenylation. Binding of TREX complex components recruits the export receptor NXF1 that ultimately facilitates mRNA export (Lesbirel and Wilson 2019). First observations that m⁶A may regulate mRNA export were made by the use of methylation inhibitors that delayed cytoplasmic appearance of mature mRNA (Camper et al. 1984). Consistently, future studies could show that depletion of m⁶A demethylase ALKBH5, resulting in increased m⁶A levels, positively correlates with cytoplasmic localization of mRNA (Zheng et al. 2013). The main mediator of m⁶A-facilitated mRNA export was found to be a nuclear reader YTHDC1. It directly interacts with the SRSF3 and SRSF7 proteins and thereby facilitates the recruitment of NXF1 (Müller-Mcnicoll et al. 2016, Roundtree Ian A. et al. 2017, Kasowitz et al. 2018). Consistent with these observations, depletion of YTHDC1 leads to the accumulation of m⁶A modified mRNA in the nucleus (Roundtree Ian A. et al. 2017). Additionally, YTHDC1 as well as m⁶A writer complex were shown to be associated with different components of TREX complex or corresponding adaptors, suggesting that m⁶A may enhance nuclear mRNA export by various parallel ways (Lesbirel et al. 2018, Lesbirel and Wilson 2019). Intriguingly, improved m⁶A-mediated nuclear export was also observed for certain viral transcripts. Upon infection, Zika and HIV viruses can exploit cellular methylation machinery to increase their replication, possibly via the viral specific export mechanisms (Lichinchi Gianluigi et al. 2016, Lichinchi G. et al. 2016).

1.4.7.d Translation

One of the best studied functions of m⁶A is its role in mRNA translation (Wang et al. 2015, Meyer Kate D. 2019). It was first proposed in 1996 by a study that used an in vitro translation system to evaluate whether the presence of m⁶A might have an impact on this process. Indeed they observed a positive effect of m⁶A on protein synthesis (Heilman et al. 1996). In recent years, numerous studies demonstrated that m⁶A can affect translation initiation and elongation steps by different mechanisms (Meyer Kate D. 2019). Translation initiation can be promoted by binding of cytoplasmic m⁶A reader proteins YTHDF1 and YTHDF3 to m⁶A sites within the 3'UTR region. YTHDF1 presumably recruits the translation initiation factor eIF3 and promotes mRNA looping that connects polyA-bound PABPC1 with the cap bound eIF4E and eIF4G (Wang et al. 2015). YTHDF3 on the other hand, was shown to enhance binding of YTHDF1 and in turn promote translation (Shi et al. 2017). YTHDF3 was also proposed to drive translation of circRNA that carry m⁶A within an ORF and require a cap-independent translation mechanism. It was proposed to do so by interacting with the translation initiation factor eIF4G2 (Zhang Yuan et al. 2019). A different mechanism was described to take place in the case of a stress response. Upon heat shock response, translation initiation factor eIF3 can promote cap-independent translation of heat shock induced transcripts. It does so by directly binding to m⁶A sites located within the 5'UTR region (Meyer et al. 2015). Whether this mechanism also takes place during translation of circRNA has not been investigated yet. In addition, a cytoplasmic reader YTHDC2 was recently shown to elevate translation of a subset of transcripts with highly structured 5'UTR regions, possibly via the unwinding activity of its helicase domain, albeit the exact mechanism is not known yet (Tanabe et al. 2016).

A positive effect on translation was also attributed to METTL3 itself (Lin et al. 2016, Choe et al. 2018). Similarly to the YTHDF1 protein, METTL3 was shown to bind a subset of mRNAs at their 3'UTR and was found to interact with the eIF3h subunit of the eIF3 complex (Choe et al. 2018). This promoted

mRNA looping between the 3'UTR and 5'UTR ends, and resulted in a translational boost. While not all mRNA were regulated in this manner, those that responded to METTL3 binding all carried m⁶A modification near a STOP codon (Choe et al. 2018). METTL3 was also shown to regulate translation in case of a heat shock, albeit by a different mechanism. Upon stress response, METTL3 levels elevated and could trigger translation independently of its catalytic activity (Lin et al. 2016). Notably, given that under normal and stress conditions in most cell types the majority of METTL3 protein resides in the nucleus, several mechanistic aspects remain to be addressed. What directs METTL3 to bind a subset of cytoplasmic transcripts, does METTL3 remain bound to selected targets during transfer to the cytoplasm, and whether it localizes alone, or with other m⁶A writer components (Lin et al. 2016, Choe et al. 2018).

A few studies demonstrated that m⁶A modification also affects translation elongation. m⁶A sites located within the CDS of some transcripts were shown to reduce elongation kinetics, by counteracting with the initial step of tRNA selection (Choi et al. 2016). In line with this, ALKBH5 demethylation of *FOXM1* mRNA strongly promoted its translation in the glioblastoma stem-like cells (Zhang S. et al. 2017), whereas FTO-mediated demethylation promoted protein synthesis of axonal transcripts (Yu et al. 2018). Two other studies showed that methylation of CDS is linked to transcription, but can affect mRNA translation in either a negative (Slobodin et al. 2017) or positive fashion (Barbieri et al. 2017). Slobodin and colleagues found that reducing the rate of transcription improved the interaction between RNA PolII and METTL3. This resulted in an increased methylation along the CDS and correlated with poor translation (Slobodin et al. 2017). In contrast, a study from Barbieri and colleagues proposed that METTL3 associates with promoter sites of selected, actively transcribed genes via the CEBPZ protein, in a METTL14 independent manner. This recruitment induced methylation of transcripts along their CDS and resulted in increased translation, presumably due to a release of ribosome stalling at methylated GAN codons (Barbieri et al. 2017). More studies are needed to reveal how all the above-mentioned mechanisms coordinate translation of methylated transcripts that for example contain m⁶A modifications within different regions.

1.4.7.e mRNA turnover

mRNA translation, stability and decay are highly connected processes, and their coordinated regulation is crucial for achieving a desirable protein output. The presence of m⁶A modification can have an important impact on mRNA turnover. m⁶A reader and anti reader proteins can, in specific sequence contexts, define whether mRNA becomes stabilised, destabilised, or destined for a rapid decay. One mechanism by which m⁶A enhances transcript stability is via *IGF2BP* reader proteins (*IGF2BP1*, *IGF2BP2* and *IGF2BP3*). They interact with components of the stress granules and P-bodies and tether bound mRNAs to these cytoplasmic storage compartments (Huang et al. 2018). Another cytoplasmic reader, *YTHDC2* promotes stability of m⁶A modified transcripts during meiosis by interacting with protein MEIOC (Bailey et al. 2017, Hsu et al. 2017, Wojtas et al. 2017, Jain et al. 2018). A different mechanism of m⁶A-mediated mRNA stabilisation was described in *A. thaliana* during osmotic stress. Modified transcripts were protected from nucleolytic cleavage, which enabled a specific response to environmental changes (Anderson et al. 2018).

A few studies also demonstrated that m⁶A can interfere with transcript's stabilization. This has been exemplified by RNA stabilizing proteins (e.g. *G3BP1*, *G3BP2* and *HuR*), whose binding to RNA is altered by m⁶A. These so-called m⁶A-repelled proteins were shown to preferentially stabilize certain non-modified transcripts. Upon stress, *G3BP1/2* proteins bind de-methylated transcripts and mediate their localisation to the cytoplasmic stress granules (Arguello et al. 2017, Edupuganti et al. 2017),

whereas the HuR protein prevents miRNA-mediated mRNA destabilization by binding to non-modified 3'UTR sites (Wang Y. et al. 2014).

One of the best-described roles of m⁶A modification is in the regulation of mRNA decay. Methylated transcripts were shown to be subjected to faster degradation, in various cell types and biological processes, including cell fate determination, gametogenesis, during maternal-to-zygotic transition and neurogenesis (Ivanova et al. 2017, Wojtas et al. 2017, Zhao et al. 2017b, Tang et al. 2018). mRNA decay was shown to be mediated via two cytoplasmic readers, YTHDF2 and YTHDC2. The cytoplasmic reader YTHDF2 interacts with the CCR4/Not1 deadenylation complex (Du et al. 2016). It was proposed to guide transcripts to processing bodies (Wang X. et al. 2014) from where they are eventually destined for degradation. Consistently, depletion of YTHDF2 markedly increases half-life of its targets in various cell types and model systems (Wang X. et al. 2014, Du et al. 2016, Zhao et al. 2017b). Notably, two recent studies showed that all three Ythdf proteins promote mRNA decay and can function redundantly in a context and dosage-dependent manner (Lasman et al. 2020, Zaccara and Jaffrey 2020). Finally, besides Ythdf proteins, binding of YTHDC2 to a subset of mRNA also expedites their decay. This function of YTHDC2 might be mediated via its interaction with the Xrn1 exoribonuclease (Wojtas et al. 2017).

1.4.8 m⁶A modification regulates various cellular and physiological processes

Given the importance of m⁶A modification in numerous post-transcriptional processes mentioned above, it is not surprising that alterations in m⁶A deposition, removal or recognition can affect a plethora of biological functions (Nachtergaele and He 2018). A few examples are summarised below.

1.4.8.a Cell cycle progression

m⁶A modification is important for cell cycle progression. Initially, a study from Horiuchi and colleagues investigated molecular functions of WTAP protein in mice, before it was known that WTAP functions in m⁶A biogenesis. They found that WTAP and its interactors in human cells (RBM15, VIR, HAKAI) stabilize the *cyclin A2* transcript and in this way regulate cell cycle transition from G2 to M phase (Horiuchi et al. 2006). Consistent with these early observations, Yoon and colleagues later showed that depletion of Mettl14 or Mettl3 delays cell progression through the S/G2/M phase, due to altered decay of cell cycle related transcripts (Yoon et al. 2017). This was found to be crucial for a timely cell differentiation of radial glia cells during cortical neurogenesis (Yoon et al. 2017), as well as for differentiation and clonal expansion of adipocytes (Kobayashi et al. 2018). Recent findings from Fei and colleagues described a positive regulatory loop that drives timely mitotic entry and involves YTHDF2-mediated decay of a negative regulator of cell cycle, the kinase WEE1. In addition, they found that YTHDF2 is itself under the control of the cyclin-dependent kinase 1 (CDK1), whereby CDK1 inhibition resulted in YTHDF2 degradation (Fei et al. 2020). This indicated that various different mechanisms can contribute to cell cycle progression. Indeed, in glioblastoma stem cells (GSC), demethylation of a cell-cycle regulator FOXM1 increased *FOXM1* translation, which in turn promoted cell proliferation and glioblastoma progression (Zhang S. et al. 2017). Overall, it is possible that similar m⁶A-mediated pathways as described above also stimulate cycle progression in other cell types.

1.4.8.b Xist-mediated X chromosome inactivation

In most organisms females and males do not carry same sex chromosomes; in mammals females have two X chromosomes whereas males have one X and one Y chromosome. In order to achieve equal expression of X chromosome-encoded genes in both genders, a process of dosage compensation takes place whereby in females one of the X chromosomes (Xi) becomes transcriptionally silenced. A long non coding RNA *Xist* plays a crucial role in this process by mediating the recruitment and activation of chromatin modifiers and Polycomb repressive complexes 1 and 2 (PRC1 and PRC2) to sites of the inactive X chromosome (Xi) (Mira-Bontenbal and Gribnau 2016, Żylicz et al. 2019). In this way *Xist* induces spreading of silencing marks and subsequent X chromosome inactivation (XCI). m⁶A modification was proposed to be involved in the process of XCI by decorating the long non coding RNA *Xist* (Patil et al. 2016). m⁶A sites can be recognised by the Ythdc1 protein that facilitates *Xist*-mediated chromosome silencing (Patil et al. 2016). In support of this model, many studies that screened for novel *Xist*-associated interactors repeatedly found m⁶A reader protein Ythdc1 (Chu et al. 2015, Moindrot et al. 2015) as well as components of the m⁶A writer complex, including Vir (Moindrot et al. 2015) Wtap and Rbm15 (Chu et al. 2015, Moindrot et al. 2015, Graindorge et al. 2019). Ythdc1 was shown to be required for *Xist*-mediated gene silencing, but was not involved in *Xist* localisation to Xi, suggesting that it may facilitate the recruitment of the polycomb repressive complexes PRC1 and PRC2.

1.4.8.c Stress response

Upon different stimuli, bulk levels of m⁶A modification in mRNA were found to elevate (Dominissini et al. 2012, Meyer et al. 2012). Following a heat shock m⁶A becomes increased specifically in the 5'UTR regions of transcripts critical for stress adaptation (Meyer et al. 2015). Modification acts as a means for cap independent translation, by direct recruitment of eIF3b to the modified sites (Meyer et al. 2015). Consistently, Mettl3 rapidly relocates to heat shock induced genes to ensure timely *Hsp70* mRNA turnover and thus cell recovery (Knuckles et al. 2017). Another example of stress response involves targeted RNA methylation upon DNA damage. Mettl3 and Mettl14, but not WTAP, were shown to be recruited to the UV-induced DNA lesions. m⁶A on nascent transcripts facilitates binding of poly ADP-ribose polymerase (PARP) and trans-lesion synthesis DNA polymerase (Pol-κ) to damage sites, which promotes efficient repair of damaged DNA (Xiang et al. 2017). The m⁶A-Pol-κ repair is carried out by a yet unknown mechanism, albeit independently of the canonical Nucleotide excision repair (NER) pathway and Rad18/PCNA-regulated translesion DNA synthesis (TLS) pathway.

1.4.8.d Cell differentiation and reprogramming

m⁶A is required for maintenance of stem cell pluripotency, reprogramming and differentiation of various cell types in part by regulation of crucial transcription factors that drive and determine cell identity (Aguilo et al. 2015, Chen T. et al. 2015, Chen J. et al. 2019). Loss of Mettl3 in naïve mESC prevents their timely exit from pluripotency, whereas Mettl3 loss in primed mESC results in premature differentiation (Geula et al. 2015). Mettl14 knock-out in mouse alters conversion of epiblasts from naïve to primed cell state, which impairs post-implantation embryo development (Meng et al. 2019). Similarly, mice lacking Mettl3 die during early embryogenesis, due to a failure to down-regulate pluripotency marker *Nanog* (Geula et al. 2015). During hematopoietic stem cell differentiation, sufficient upregulation of *Myc* depends on m⁶A methylation (Lee et al. 2019). Mettl3 activity is also required during adipocyte differentiation, by facilitating correct splicing of *RUNX1T1* transcription factor (Zhao et al. 2014) and by promoting cell cycle progression (Kobayashi et al. 2018). Likewise, m⁶A is important for correct cell differentiation in plants. Loss of WTAP ortholog (*Fip37*) leads to over proliferation of stem cells in shoot meristem, required for generation of all aerial parts (Shen et al. 2016).

1.4.8.e Gametogenesis

m⁶A is crucial for male and female gametogenesis in plants, mice, and zebrafish and is indispensable for progression of meiosis in budding yeast. The role of m⁶A during spermatogenesis was well studied and was shown to be important at several stages. In mice, Mettl3 expression is particularly high in undifferentiated spermatogonia. Consistently, removal of m⁶A writers Mettl3 and Mettl14 in germ line dysregulates spermatogonial stem cell proliferation and differentiation (Lin et al. 2017) and loss of Mettl3 blocks initiation of meiosis at zygotene stage resulting in cell apoptosis (Xu K. et al. 2017). Different YTH domain readers were shown to contribute to progression of spermatogenesis. Similarly to m⁶A writers, removal of *Ythdc1* alters spermatogonia differentiation (Kasowitz et al. 2018). *Ythdc2* on the other hand, interacts with the MEIOC protein that was previously shown to regulate meiosis (Abby et al. 2016). Novel insights revealed that *Ythdc2* and MEIOC act together as a complex and promote progression of germ cells during mitotic and meiotic divisions in males and females (Bailey et al. 2017, Hsu et al. 2017, Wojtas et al. 2017, Jain et al. 2018). By binding to m⁶A modified transcripts, *Ythdc2* and MEIOC reduce their stability in mitotic spermatogonial stem cells. In contrast, they can

promote transcript stability during later stages of spermatogenesis in meiotic spermatocytes (Bailey et al. 2017, Hsu et al. 2017, Wojtas et al. 2017). In addition, Ythdc2 interacts with and destabilizes piRNA precursors in spermatocyte germ granules, and co-precipitates with MIWI protein, suggesting it may be involved in the control of piRNA processing (Bailey et al. 2017). Notably, Alkbh5 expression is elevated in testis and its deletion impairs spermatocyte differentiation post meiotic metaphase stage (Zheng et al. 2013), highlighting that m⁶A levels must be tightly regulated during spermatogenesis. In females, Ythdc1 ensures oocyte development post primary follicle stage (Kasowitz et al. 2018), while Ythdf2 controls oocyte maturation (Ivanova et al. 2017). The involvement of m⁶A in gametogenesis is conserved in other species. In zebrafish, loss of Mettl3 impairs oocyte maturation and results in altered sperm maturation and motility (Xia et al. 2018). Finally, loss of WTAP ortholog in rice (OsFIP) leads to defects in spore formation due to abnormal meiosis (Zhang F. et al. 2019), while inactivation of MTA machinery in *A. thaliana* results in a delay of endosperm development (Vespa et al. 2004).

1.4.8.f Neural development and plasticity

m⁶A modification is highly enriched in mammalian neural tissue as compared to other organs. Its levels gradually increase during brain development (Meyer et al. 2012) as well as during brain activity (Widagdo et al. 2016) and memory formation (Walters et al. 2017), suggesting that m⁶A might be important in this tissue. In line with this, numerous studies over the past few years demonstrated that m⁶A is involved in a wide range of neural processes. Precisely regulated levels of m⁶A for example ensure neural stem cell differentiation and proper brain development. Modification is involved in synaptic plasticity, and axonal regeneration and loss of m⁶A machinery leads to diverse neurological defects. Alterations are reflected in compromised learning and memory formation, in behavioural disorders, as well as in aggravated glioblastoma progression (Angelova et al. 2018, Engel and Chen 2018, Jung and Goldman 2018, Flamand and Meyer 2019, Livneh et al. 2020).

Neurogenesis

Importance of m⁶A for neuronal development was first exemplified by studies showing that Mettl3 inactivation strongly impairs neuronal differentiation from hESC (Batista et al. 2014) as well as from embryoid bodies (Geula et al. 2015). In line with this, m⁶A is essential during embryonic and adult neurogenesis. I) During cortex development, conditional deletion of Mettl14 in mouse embryonic neural stem cells (NSCs) decreases self-renewal (Wang Y. et al. 2018) and alters differentiation of cortical neuronal progenitors (Yoon et al. 2017, Wang Y. et al. 2018). This extends neurogenesis to postnatal stages and reduces numbers of mature cortical neurons. Mechanistically, loss of m⁶A, in this context, delays timely decay of transcripts implicated in cell cycle progression (Yoon et al. 2017) and leads to upregulation of many chromatin modifiers associated with either gene silencing (H3K27me3) or activation (H3K27ac) (Wang Y. et al. 2018). Thus, combinatorial effects of several m⁶A-regulated pathways promote spatiotemporal formation of different neuronal subtypes. Notably, similar alterations in cortical neurogenesis were observed upon depletion of Ythdf2 that mediates m⁶A-dependent decay (Li M. et al. 2018), suggesting that functions of this reader are critical for cortex development. II) m⁶A is also important for adult neurogenesis and alterations of m⁶A writers in later stages of brain development can result in impaired learning and memory formation, depression, as well as in occurrence of neurodegenerative diseases. Global levels of m⁶A and its writer components are not equally abundant in all brain regions (Chang et al. 2017, Wang C.-X. et al. 2018). They are elevated in the cerebellum and gradually decrease over the course of mouse cerebellar development from P7 to P20, suggesting critical roles of m⁶A in this region. Indeed, depletion of Mettl3 in mice cerebellum at

stage P7, results in several morphological changes in glia and Purkinje cells that exhibit altered dendrite lengths (Ma et al. 2018). Intriguingly, conditional knock-out (cKO) of *Mettl3* specifically in neuronal cells manifests in particularly increased apoptosis of cerebellar granule cells, resulting in reduced brain size (Wang C.-X. et al. 2018). As a consequence, cKO *Mettl3* mice display severe locomotor defects such as slow, interrupted movement with reduced moving distance and they eventually die at 3 weeks (Wang C.-X. et al. 2018). Notably, loss of *Alkbh5* demethylase also alters cerebellar development, which highlights the need for tight regulation of m⁶A levels in this tissue (Ma et al. 2018). In addition, during adult neurogenesis *Fto* levels increase in developing neurons and *Fto* KO mice display growth retardation. Conditional loss of *Fto* in neurons recapitulates the whole body deletion, which strongly suggests crucial functions of this m⁶A/m⁶Am demethylase in the brain (Gao et al. 2010).

Learning and memory formation

m⁶A has an important role in the regulation of stress response, as well as for learning and memory formation in mice. Loss of *Mettl3* in the adult hippocampus reduces long-term memory formation; however, prolonged training can rescue memory consolidation, pointing towards an important, yet dispensable function of m⁶A in this process (Zhang Z. et al. 2018). Several studies reported the role of *Fto* demethylase for memory acquisition. Neuronal loss of *Fto* alters adult neural stem cell proliferation and differentiation, which impairs short-term memory formation and leads to anxiety (Li L. et al. 2017, Spychala and R  ther 2019). On the other hand, loss of *Fto* in the hippocampus (Walters et al. 2017, Engel et al. 2018) or in the medial prefrontal cortex (Widagdo et al. 2016) enhances memory formation upon fear conditioning and impairs long-term potentiation. Consistently, induced fear-training leads to downregulation of *Fto* in primary cortical neurons and elevated m⁶A levels in genes involved in synaptic plasticity contribute to memory formation (Widagdo et al. 2016). This altogether highlights the importance of activity dependent m⁶A dynamics for behavioural adaptation. m⁶A dependent memory formation is mediated by different reader proteins. YTHDF1 is highly expressed in the hippocampus and is required for correct synaptic transmission and long-term potentiation. It binds numerous neuronal genes and facilitates local translation upon neuronal stimulation, when its levels become elevated in the postsynaptic densities (Shi et al. 2018).

Synaptic plasticity

Following external stimuli, neurons rapidly adjust their transcriptome and proteome to enable synaptic plasticity. m⁶A is involved in these processes via multiple ways. Thousands of localised transcripts were found to be methylated at synapses (Merkurjev et al. 2018), where *Ythdf1*, *Fmr1* and other reader proteins can regulate their translation and stability (Edupuganti et al. 2017, Shi et al. 2018). In addition, *Fto* mediated removal of m⁶A promotes local translation of a subset of methylated targets, which in turn enhances axonal growth (Yu et al. 2018). Loss of *Fto* specifically in dopaminergic neurons increases sensitivity to cocaine due to impaired neuronal signalling and results in altered neuronal activity and behavioural response (Hess et al. 2013). Beyond the role in neuronal development, m⁶A modification also contributes to axon regeneration in CNS and PNS. Upon peripheral nerve injury, m⁶A levels strongly elevate which promotes *Ythdf1* mediated translation of critical transcripts needed for efficient axon regeneration (Weng et al. 2018).

1.4.9 Methods for m⁶A quantification and mapping

In order to understand the biological functions of any RNA modification, it is crucial to know the identity of the modified RNA species as well as sequence and context information surrounding the modified nucleotide. Following the discovery of m⁶A modification in the 1970s, a thin layer chromatography (TLC) in combination with different exo- and endoribonucleases was used to identify precise positions of m⁶A in a limited number of viral and eukaryotic transcripts (Perry et al. 1975). However, despite knowing that modification is one of the most abundant in mRNA, the characterisation of other modified transcripts only became possible with a development of an antibody based immunoprecipitation techniques nearly 30 years later (see below). In recent years, various methods have been established in order to map and quantify m⁶A on targeted RNAs. Some take the advantage of the m⁶A-recognizing antibody (MeRIP, miCLIP, LAIC-seq) or m⁶A-sensitive restriction endonucleases (MAZTER-seq), while others employ metabolic labelling with SAM analogs to induce RT-signature (e.g. propargyl-L selenohomocysteine, allyl-SAM) (Hartstock et al. 2018, Shu et al. 2020), or try to engineer DNases and RTases to discriminate m⁶A from A and induce modification-specific fingerprint (Aschenbrenner et al. 2018, Potapov et al. 2018). More recently fusion proteins of the YTH domain with RNA-editing domains have been successfully used to map m⁶A transcriptome wide (TRIBE, DART-seq) (Meyer K. D. 2019, Worpenberg et al. 2019). Future efforts and hopes for precise and quantitative determination of m⁶A sites are in the single molecule nanopore sequencing methods (**Table 4**) (Grozhiik and Jaffrey 2018, Hartstock et al. 2018, Ovcharenko and Rentmeister 2018, Motorin and Helm 2019).

Anti-m⁶A antibody-based enrichment techniques

One of the major breakthroughs in the m⁶A-field happened in 2012, when Rechavi's and Jaffrey's laboratories independently reported the first transcriptome wide mapping of m⁶A modification on polyA RNA. Both groups developed similar methods that took the advantage of an antibody, which specifically recognized m⁶A modification, and performed m⁶A-methylated RNA immunoprecipitation coupled with next-generation sequencing named as **MeRIP-seq** or **m⁶A-seq** (Dominissini et al. 2012, Meyer et al. 2012). Using this approach, m⁶A containing fragments can be enriched from a pool of randomly fragmented RNAs, reverse transcribed and sequenced. The peak summit of aligned reads represents the approximate location of the putative m⁶A site.

Both groups identified thousands of methylated transcripts and found a high rate of conservation between mouse and human m⁶A methylomes (Dominissini et al. 2012, Meyer et al. 2012). Another important discovery from these two studies was a metagene profile that revealed a strong enrichment of m⁶A around stop codons, within the 3'UTR regions and long internal exons (**Figure 6**). MeRIP-seq provides a broad spatial information about the presence of m⁶A along the transcripts, but it has its limitations. Its resolution is restricted to the initial size of RNA fragments and alignment of reads around the putative m⁶A site. Additionally, since the method relies on immunoprecipitation, stringent washes have to be limited, which often results in reduced specificity and increased background (Schwartz et al. 2013). Another drawback is the requirement of high amounts (microgram) of input material, which is oftentimes not possible (when a limited amount of biological samples is to be analysed). While MeRIP-seq is in general a good method of choice for transcripts with highly abundant m⁶A content, it can suffer from high background when transcripts with low stoichiometry are analysed, due to potential poor RNA recovery. In addition, transcripts with low expression levels might not be efficiently captured, thus MeRIP-seq is by no means a quantitative method. miCLIP was developed in order to overcome some of these limitations (Linder et al. 2015). By taking the advantage of UV crosslinking and iCLIP library preparation protocol (Konig et al. 2011). Linder and colleagues were able to obtain a high resolution

mapping of m⁶A modification in mouse and human samples. In contrast to MeRIP-seq, miCLIP allows stringent immunoprecipitation washing steps and only recovers RNA fragments that covalently crosslink to the antibody, thus providing a more reliable m⁶A map with reduced background. Depending on the antibody choice, during the reverse transcription step of library preparation, an RTase can induce truncation and/or mutation at the site of antibody peptide remnant, which reflects the m⁶A-signature (Linder et al. 2015).

Method	Description	References
2D-TLC	Restriction to nts and thin layer chromatographic separation. <ul style="list-style-type: none"> Quantification of absolute modification levels in chosen RNA sample. Can distinguish m⁶A from m⁶Am. 	(Bodi and Fray 2017)
SCARLET	Site-specific cleavage (RNaseH) and radioactive-labelling followed by ligation-assisted extraction and thin-layer chromatography. <ul style="list-style-type: none"> Quantification of the exact site of interest. Can distinguish m⁶A from m⁶Am. 	(Liu et al. 2013)
LC-MS/MS	Liquid Chromatography with tandem mass spectrometry. <ul style="list-style-type: none"> Restriction to nts, LC separation and MS detection analysis. Quantification of absolute modification levels in chosen RNA sample. Can distinguish m⁶A from m⁶Am. 	(Yuan 2017)
MeRIP	m ⁶ A-methylated RNA immunoprecipitation. <ul style="list-style-type: none"> Ab-based enrichment. Transcriptome-wide mapping. 	(Dominissini et al. 2012, Meyer et al. 2012)
TNT-seq	Transient N6-methyladenosine transcriptome sequencing. <ul style="list-style-type: none"> Ab-based enrichment of the nascent BrU-labelled RNA (input: BrU enriched RNA, IP: BrU and m⁶A enriched RNA). Detection of m⁶A in nascent RNA (improved detection of intronic sites). 	(Louloupi et al. 2018)
miCLIP	Methylation iCLIP. <ul style="list-style-type: none"> Ab-based enrichment and UV crosslinking. Transcriptome-wide mapping with a nt resolution. 	(Linder et al. 2015)
m ⁶ A-LAIC-seq	m ⁶ A-level and isoform-characterization sequencing. <ul style="list-style-type: none"> Ab-based enrichment with external spike-in standards for relative quantification. Transcriptome-wide mapping and relative quantification with no spatial information. 	(Molinie et al. 2016)
MAZTER-seq	MazF RNase assisted cleave of RNA at unmethylated sites within ACA motifs. <ul style="list-style-type: none"> Transcriptome-wide mapping with a nt-resolution and relative quantification. 	(Garcia-Campos et al. 2019)
TRIBE	ADAR-editing based detection of methylated region (A→I). <ul style="list-style-type: none"> Transcriptome-wide mapping (in vivo) and relative quantification. 	(Worpenberg et al. 2019)
DART-seq	APOBEC-editing based detection of methylated region (C→U). <ul style="list-style-type: none"> Transcriptome-wide mapping (in vivo or in vitro) and relative quantification. 	(Meyer K. D. 2019)
SMRT-seq	Single molecule real time sequencing <ul style="list-style-type: none"> RT based detection of a difference in binding of fluorescently labelled nts to m⁶A vs A. Theoretically, detection and quantification of all sites in a single molecule with a nt resolution. 	(Saletore et al. 2012)
Nanopore-based sequencing	Nanopore-forming proteins. <ul style="list-style-type: none"> Direct detection of a current change during RNA travelling through the nanopore. Theoretically, detection and quantification of all sites in a single molecule with a nt resolution. 	(Leger et al. 2019, Liu H. et al. 2019, Pratanwanich et al. 2020)

Table 4. Methods used for m⁶A detection and quantification.

One of the biggest limitations of available antibody-based enrichment techniques, such as MeRIP-seq (Dominissini et al. 2012, Meyer et al. 2012), m⁶A-CLIP (Ke et al. 2015), PA-m⁶A-seq (Chen K. et al. 2015) and miCLIP (Linder et al. 2015) is the fact that they rely on the efficiency of

immunoprecipitation and can therefore not provide quantitative information. Even though iCLIP methodology allows for PCR duplicate removal (Konig et al. 2011), it is not a quantitative method for m⁶A mapping, since the RNA recovery highly depends on the 1) antibody choice, 2) the crosslinking efficiency, as well as on 3) the transcript expression level. Another approach termed m⁶A-LAIC-seq aimed to improve m⁶A quantification via the use of modified spike-in RNA sequences and by sequencing of both, the bound as well as the non-bound fractions (Molinie et al. 2016). When compared to known spike-ins, this approach enabled the quantification of methylated vs. non-methylated RNA fractions of intact, non-fractionated mRNA. However, LAIC-seq still relies on the antibody based immunoprecipitation and, in addition, cannot provide any spatial information in regards to m⁶A position along the RNA. Notably, the extent of methylation within intronic regions is likely underestimated, given that none of the currently available methods, with the exception of TNT-seq, can reliably detect m⁶A modification in introns. Considering the speed of technological advance, it is perhaps not too elusive to expect that a single molecule RNA sequencing on engineered nanopores may become a routine way for the analysis of the complex epi-transcriptome, by providing simultaneous quantification and exact spatial decoding of various RNA modifications.

1.5 *Drosophila melanogaster*

1.5.1 Developmental stages of *D. melanogaster*

Drosophila melanogaster, a “fruit fly”, is a broadly used model organism. Development of sophisticated genetic tools enabled remarkable progress in our understanding of gene regulatory processes that affect development and behaviour of *D. melanogaster*. *D. melanogaster* belongs to the family of Drosophilidae with nearly 4500 other species (TaxoDros Database (Bächli 2015)). Taxonomic classification places *D. melanogaster* into subfamily Drosophilinae, genus *Drosophila* and subgenus *Sophophora* (O’grady and Desalle 2018).

Development of *D. melanogaster* takes approximately ten days at 25 °C and consists of a series of stages that belong to four morphologically distinct states: embryogenesis, larval development, pupation, and adulthood (Figure 11). Following egg fertilisation, seventeen stages of fly embryogenesis occur over the course of 24 hours, before the hatching of the first instar larvae takes place. Development of first and second instar larvae each lasts one day, while maturation of the third instar larvae is completed in two days. Larval development is then followed by four days of metamorphosis during immobile stages of pupation (Tenessen and Thummel 2011) and is terminated by adult fly eclosion. The steroid hormone 20-hydroxyecdysone (20E), formed by the ecdysone from cholesterol, regulates progression through many stages of fly development. A pulse of 20E arrests larval growth and determines the onset of pupation and metamorphosis. Notably, throughout metamorphosis, many tissues of the larvae body including the nervous system, are replaced or become highly reorganised (Tissot and Stocker 2000).

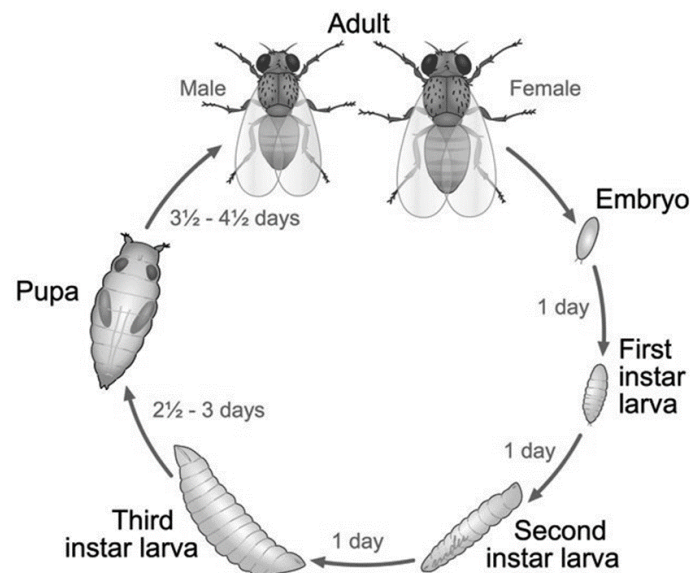


Figure 11. Life cycle of *Drosophila melanogaster* at 25 °C.

The life cycle of *Drosophila melanogaster* at 25 °C is depicted (adapted from (Ong et al. 2014)).

1.5.2 Sex determination and dosage compensation pathways in *Drosophila melanogaster*

Sex determination in *D. melanogaster* is controlled by the master regulatory gene *Sex lethal* (*Sxl*), which is expressed specifically in females. *Sxl* encodes an RNA binding protein (RBP) that regulates expression of genes in a downstream cascade that determine either male or female development, their physiognomy and behaviour (**Figure 12a**) (Penalva and Sánchez 2003, Salz 2011). In females, *Sxl* promotes formation of a functional protein Transformer (*Tra*) via an alternative splicing of *transformer* (*tra*). *Tra* is a female-specific splicing regulator that, together with Transformer-2 (*Tra-2*), establishes expression of transcription factors *doublesex* (*dsx*) and *fruitless* (*fru*). These factors play a major role in defining female vs. male development and behaviour (Pitman et al. 2002, Salz 2011). In addition, *Sxl* represses expression of male-specific lethal-2 (*msl-2*) at the level of splicing, export and translation (Salz 2011). *Msl-2* is an essential gene required for the assembly of the dosage compensation complex in males. In flies, females carry two X-chromosomes whereas males only have one. The dosage compensation process enables hyper transcription of the X-chromosome, which ensures equal expression of X-linked genes in males and females. Overall, levels of *Sxl* must be tightly controlled as sufficient levels of *Sxl* protein are crucial for efficient repression of *Msl-2* and, therefore, female survival.

Sxl transcript contains an alternative exon (L3) that introduces a premature STOP codon. Hence, in females, this exon must be repressed, whereas in males it is included in the final transcript. Initial expression of *Sxl* during early embryo development is controlled through the establishment promoter (*Pe*) and omits exons L2 and L3 (**Figure 12b**). It is driven by several X-chromosome encoded genes that are expressed at 2-fold higher levels in females and this dosage difference drives *Sxl* expression only in females. This is crucial for *Sxl* expression in later stages of development, since *Sxl* can auto-regulate its own splicing in a positive feedback loop. Upon zygotic gene activation, transcription of *Sxl* becomes dependent on the maintenance promoter (*Pm*) in both, males and females and females require efficient mechanisms for the silencing of L3 exon in order to form a functional *Sxl* protein (Moschall et al. 2017).

Sxl contains two RRM domains that are required for its binding to Uridine-rich intronic regions next to L3 exon. With its N-terminal domain it interacts with spliceosome and other splicing factors to prevent L3 exon recognition and inhibit its splicing (Deshpande et al. 1999, Moschall et al. 2017). Among other known factors required for *Sxl*-dependent splicing regulation are U2AF, U1-70K, Snf, PPS, Fl(2)d, Vir as well as more recently identified Nito, Flacc, Ythdc1, Mettl3, and Mettl14 (Hilfiker et al. 1995, Granadino et al. 1996, Nagengast et al. 2003, Johnson et al. 2010, Moschall et al. 2017). The interplay between these factors in the regulation of *Sxl* splicing is not entirely understood, however they were all shown to genetically interact with *Sxl* and some of their loss-of-function alleles strongly compromise female, but not male, viability. Several factors also physically associate with *Sxl* protein, suggesting that these interactions may stabilize *Sxl* binding on *Sxl* transcript or aid in aborting the exon recognition (Moschall et al. 2017). Indeed, Snf is a fly homolog of U1A and U2B^{''} proteins and, thus, a component of the U1 and U2 snRNPs (**Table 3**) (Harper et al. 1992) that interacts not only with *Sxl*, but also with Nito and PPS proteins (Nagengast et al. 2003, Johnson et al. 2010, Guo et al. 2018). A few recent studies, including our work, shed light on the importance of m⁶A modification in the L3 exon silencing. These findings are discussed in the [Chapter 5.5.1](#).

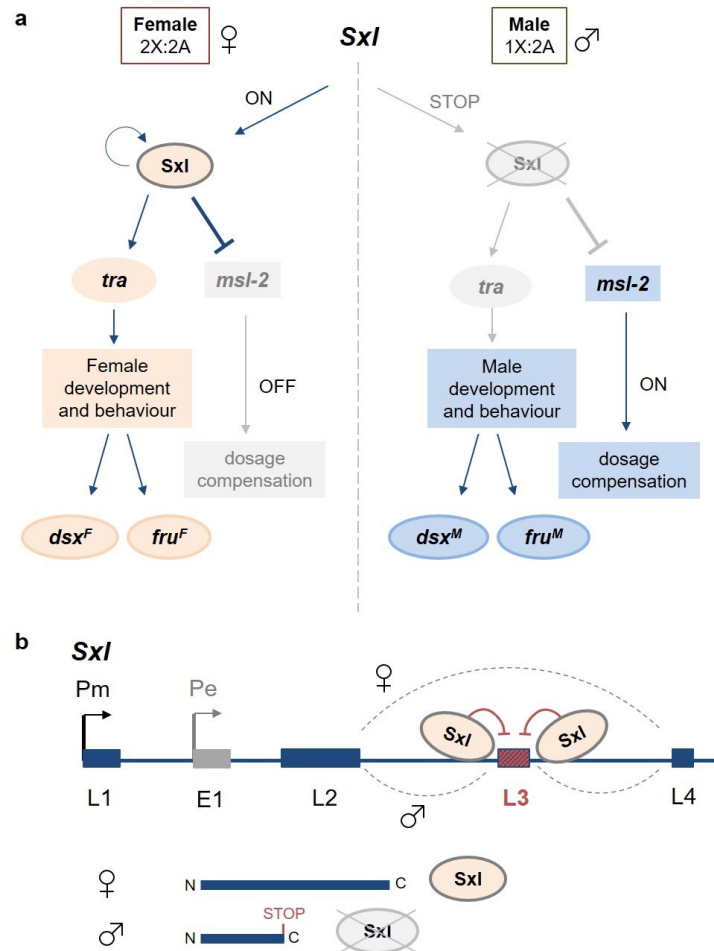


Figure 12. Regulation of sex determination in *D. melanogaster*.

a) Schematic representation of regulatory cascade driving sex determination and dosage compensation in *D. melanogaster*. Female pathway is depicted on the left hand side and male pathway on the right hand side. **b)** Schematic representation of autoregulatory pre-mRNA splicing of *Sex lethal* (*Sxl*) transcript in males and females. In females, Sxl protein represses inclusion of the L3 exon (in red), which carries a premature STOP codon. This results in a translation of a functional Sxl protein. The absence of Sxl in males leads to inclusion of L3 exon, which introduces a premature STOP codon in a final transcript. Hence, no functional Sxl protein is produced in males.

Initial work dissecting mechanisms behind *Sxl* splicing regulation, generated and studied mutant alleles of *Sxl* interacting factors. Two alleles of *fl(2)d* have been described: *fl(2)d¹* has a single point mutation and causes sex specific and temperature-dependent female lethality (Granadino et al. 1992). This allele was described as an antimorph (dominant negative) and is more detrimental for female viability than the null allele *fl(2)d²* (Penalva et al. 2000), possibly due to interference with Sxl activity, leading to *msl-2* derepression. Fl(2)d associates with several spliceosome associated proteins Snf, U1-70K, U2AF50 and U2AF38 (Penn et al. 2008) that act in the 5' and 3'ss recognition during early stages of spliceosome assembly (complex E and A) (Chapter 1.2.2). A fly mutant for Vir, *vir2f*, also leads to female specific lethality. Rescue of these *fl(2)d* and *vir* mutants can be achieved by ectopic expression of Sxl or by repression of *msl-2*. However, such flies develop as pseudomales (Hilfiker and Nothiger 1991), since both, Fl(2)d and Vir, are also involved in the splicing regulation of *transformer* (*tra*) (Granadino et al. 1996, Ortega et al. 2003).

Sxl protein is involved in pre-mRNA processing of several downstream targets (e.g. *tra*, *msl-2*). Splicing of *tra* in a male/female fashion is achieved by an alternative 3' splice site selection. Sxl competes

with the U2AF for the binding to polypyrimidine tract just upstream of the proximal 3' splice site. In this way, Sxl promotes the usage of a downstream splice site and, in turn, ensures the formation of a functional protein in female flies. In the absence of Sxl in males, the use of proximal site leads to the extension of the coding region, but at the same time introduces a premature STOP codon (Valcárcel et al. 1993). Thus, males do not express functional Tra protein. Repression of another Sxl target, *msl-2*, is crucial for female survival and Sxl controls its expression by interfering with splicing, export and translation. At the level of splicing, Sxl binds uridine-rich regions within the first intron of the *msl-2* transcript and promotes intron retention, by competing with Rox8 and U2AF35/50 for binding to the 5' and 3' splice sites, respectively (Förch et al. 2000).

1.5.3 Neuronal development

Neurogenesis in *Drosophila melanogaster* consists of two phases, one during embryogenesis and another during larval development and early pupation. The first phase establishes all larval neurons. It starts at embryonic stage nine (6h) by asymmetric division of neuroblasts (NB) that form new NB and a ganglion mother cell (GMC). GMCs further divide and differentiate into neurons and glia cells starting from the stage 13 (10h) until the end of embryogenesis. NBs on the other hand, undergo mitotic arrest at late embryonic stages and continue to divide only after larval hatching (Tissot and Stocker 2000). The start and extent of the second stage of neurogenesis varies between different regions of larval central nervous system (CNS). NBs in brain optical lobes and the mushroom body (learning and memory centres) divide continuously throughout larval development and metamorphosis (Prokop and Technau 1994, Tissot and Stocker 2000, Homem and Knoblich 2012). NBs in the ventral nerve cord of the thoracic region also extensively proliferate during larval development but then die within the first 18 hours of pupation when they are no longer required (Truman 1990). Most adult-specific neurons that form during the second phase of neurogenesis in sensory systems, mushroom bodies and thoracic ventral nerve cord, are sensory neurons and interneurons responsible for the coordination of complex locomotor functions. On the other hand, large numbers of adult motor neurons have an embryonic origin and represent remodelled larval neurons. They acquire new functions to direct muscles of an adult fly, such as motor neurons required for flight (Truman 1990, Tissot and Stocker 2000).

Fly locomotion, orientation and walking

Spatio-temporal movements require coupling between sensory inputs and body locomotion. In adult flies, this adaptive sensorimotor processing is coordinated by structures in the central nervous system, the so-called **central complex (Figure 13)**. Central complex of the insect brain has been implicated in visual orientation, visual learning, and locomotor control (Strauss 2002, Turner-Evans and Jayaraman 2016). The complex is located in the centre of the brain between the two protocerebral hemispheres. It consists of four highly connected structures; the protocerebral bridge, ellipsoid body, fan-shaped body, and the paired noduli. The ellipsoid body and fan-shaped body are connected to other brain regions, such as lateral accessory lobes, which are further linked to the ventral nerve cord that controls leg and wing movements (Strauss 2002, Turner-Evans and Jayaraman 2016). Fly walking speed is defined by a combination of step length and step frequency. Reduced walking speed was shown to be caused by alterations in the protocerebral bridge of the central complex, whereas ablation of mushroom bodies leads to increased walking activity (Strauss 2002). Fly orientation is controlled by the ellipsoid body and fan-shaped body of the central complex. They both contribute to the formation of

short-term memory that enables landmark orientation during walking (Strauss 2002). Overall numerous fly lines that display defects in the neuronal circuits of the central complex structures and the mushroom bodies suffer from walking and flying disabilities (Jordan et al. 2007).

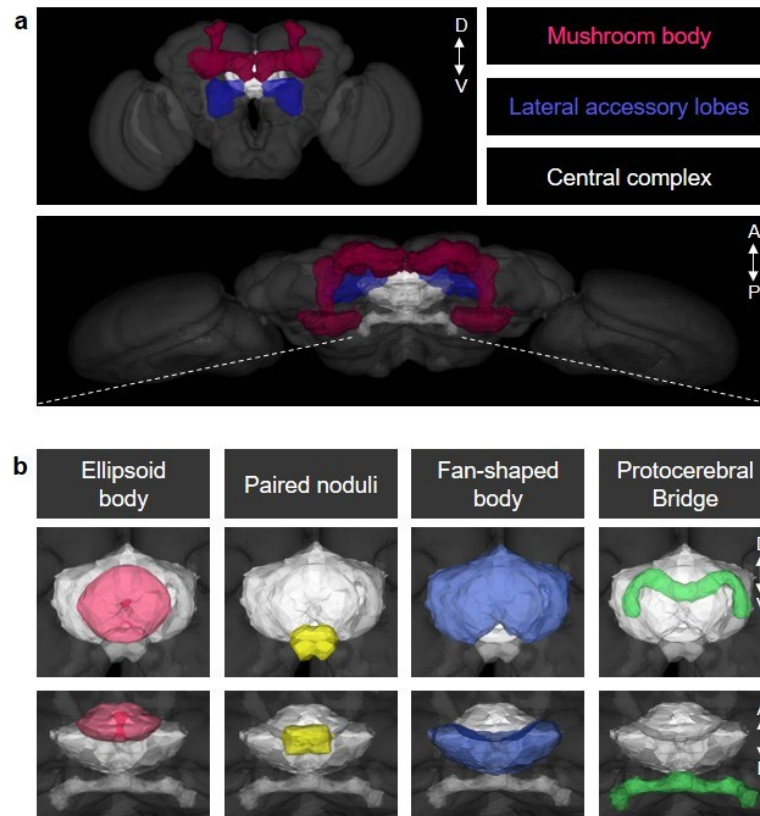


Figure 13. Schematic view of *D. melanogaster* central complex.

a) Scheme of adult fly brain with indicated mushroom body (in magenta), lateral accessory lobes (in dark blue) and central complex (in white). Shown is anterior view (top) and ventral view (bottom). **b)** Scheme of adult fly brain with indicated central complex structures: ellipsoid body (in pink), paired noduli (in yellow), fan-shaped body (in blue) and protocerebral bridge (in green). Shown is anterior view (top) and ventral view (bottom). Arrows indicate orientations: A – anterior, P – posterior, D – dorsal and V – ventral. Figures were generated with the 3D Virtual Fly Brain viewer (v2.virtualflybrain.org) (Milyaev et al. 2011).

Buridan`s paradigm and the negative geotaxis assay are two behavioural tests that have been used throughout this study to address alterations in fly locomotion, orientation and their walking ability. **Buridan`s paradigm** allows for unbiased video tracking and analysis of an individual fly in an open arena. A single fly with clipped wings is placed onto a round platform surrounded by water in a circular arena. Fly in this paradigm walks back and forth, undisturbed, between two black visual targets (stripes) that are perceived as an escape gap in an illuminated surrounding. Over 15 minutes, fly`s walking trajectories are being tracked in order to analyse its orientation, activity, and walking speed (Strauss and Pichler 1998, Colomb et al. 2012). **Negative geotaxis** represents a natural escape response of flies to move against the gravity after being tapped to the bottom of the vial. Analysis of negative geotaxis is a simple and robust behavioural assay that can be used to assess fly locomotion unless flies display severely altered motor functions and cannot climb the wall of the test vial. Notably, the assay is not affected by repeated fly testing, neither by the number of flies tested simultaneously in the same vial (Gargano et al. 2005, Ali et al. 2011).

2 Aim of the work

N6-methyladenosine (m⁶A) is one of the most abundant modifications on mRNA. Over the past years, countless discoveries, including the ones described in this work, revealed critical functions of m⁶A modification in numerous biological processes. The main purpose of my PhD work was to advance the understanding of m⁶A biogenesis, to investigate the role of m⁶A on mRNA processing, and examine the importance of this RNA modification for development of a fruit fly (*Drosophila melanogaster*).

- Aim I:

Characterization of novel modulators required for deposition, recognition and removal of m⁶A modification on mRNA. m⁶A modification was previously shown to be deposited by a large, nearly 1 MDa complex, albeit most components except for methyltransferase (MTA-70 or Mettl3) were not known. In vertebrates, m⁶A was also found to be dynamically erased by two demethylases and a few proteins that specifically interacted with m⁶A were discovered. During my PhD work I, therefore, anticipated to 1) identify components of the large methyltransferase m⁶A writer complex, 2) characterise m⁶A-specific reader proteins and 3) find potential erasers of this modification in *D. melanogaster*.

- Aim II:

Identification of regulatory functions of m⁶A modification on mRNA processing. In vertebrates, m⁶A modification has a non-random distribution along the coding transcript. It is found in exonic as well as intronic regions, suggesting its co-transcriptional deposition and possible roles in pre-mRNA processing. I, therefore, aimed to 1) generate the precise transcriptome-wide map of m⁶A modification in *D. melanogaster*, 2) identify transcriptome changes upon m⁶A loss and finally, study the possible contribution of m⁶A modification on alternative pre-mRNA splicing.

- Aim III:

Exploring the importance of m⁶A modification in vivo during development of *D. melanogaster*. At the time this project had started, functions of m⁶A modification in multicellular organisms had not been investigated yet. One of the goals was therefore to 1) investigate the prevalence of m⁶A modification and its regulators during different stages of *D. melanogaster* development and 2) generate fly mutants lacking critical components required for m⁶A biogenesis in order to characterise the importance of this modification in physiological processes.

3 Preliminary remarks

Parts of results presented in this PhD thesis have been published in peer-reviewed journals in the form of research articles and literature reviews that are listed below. *Chapters 4.1 to 4.7* cover main findings of the *Research article 1*, along with additional unpublished data. *Chapter 4.8* includes main findings of the *Research article 2*, along with additional unpublished data. The final part of this thesis in *Chapter 4.9* covers unpublished findings, with the manuscript in preparation.

- Research article 1 (Appendix 1 of this PhD thesis):

Lence T, Akhtar J, Bayer M, Schmid K, Spindler L, Ho CH, Kreim N, Andrade-Navarro MA, Poeck B, Helm M, Roignant JY (2016). m⁶A modulates neuronal functions and sex determination in *Drosophila*. *Nature*, Dec 8;540(7632):242-247. doi:10.1038/nature20568.

- Research article 2 (Appendix 2 of this PhD thesis):

Knuckles P*, **Lence T***, Haussmann IU, Jacob D, Kreim N, Carl SH, Masiello I, Hares T, Villaseñor R, Hess D, Andrade-Navarro MA, Biggiogera M, Helm M, Soller M, Bühler M# and Roignant J-Y# (2018). Zc3h13/Flacc is required for adenosine methylation by bridging the mRNA binding factor Rbm15/Spenito to the m⁶A machinery component Wtap/FI(2)d. *Genes Dev*, Mar 1;32(5-6):415-429. doi: 10.1101/gad.309146.117.

* - indicates equal contribution, # - indicates joint correspondence

- Reviews:

Lence T, Soller M, Roignant JY (2017). A fly view on the roles and mechanisms of the m⁶A mRNA modification and its players. *RNA Biol*, Review, Mar 29:1-9. doi.org/10.1080/15476286.2017.1307484.

Angelova M*, Dimitrova A*, Dinges N*, **Lence T***, Worpenberg L*, Carre C# and Roignant J-Y# (2018). The emerging field of epitranscriptomics in neurodevelopmental and neuronal disorders. *Front. Bioeng. Biotechnol*, Review, Apr 13;6:46. doi: 10.3389/fbioe.2018.00046.

Lence T*, Paolantoni C*, Worpenberg L* and Roignant J-Y (2019). Mechanistic insights into m⁶A RNA enzymes. *Biochimica et Biophysica Acta (BBA) - Gene Regulatory Mechanisms*, Review, Mar 1862(3):222-229. doi: 10.1016/j.bbagrm.2018.10.014.

* - indicates equal contribution, # - indicates joint correspondence

Contributions

Numerous collaborators provided invaluable advice and experimental support during different stages of this work. Contributions of co-authors are summarized below.

Prof. Dr. Miguel A. Andrade-Navarro (Faculty of Biology JGU and IMB Mainz)

Performed phylogenetic analyses and generated phylogenetic trees.

Marc Bayer (Roignant`s Lab)

Generated and validated the *Ythdc1* mutant allele.

Dr. Anke Busch (IMB Bioinformatics Core Facilities), Dr. Hans Herman Wessels and Prof. Dr. Uwe Ohler (BIMSB and BMC Berlin)

Performed bioinformatics analysis of the miCLIP dataset.

Anja Freiwald (IMB Proteomics Core Facilities) and Dr. Mario Dejung (IMB Proteomics Core Facilities)

Carried out quantitative proteomics and data analysis (Interactomes of Mettl3, Fl(2)d, Nito, Flacc and Ythdc1 proteins and m⁶A-interactome).

Dr. Cheuk Hei Ho (Skirball Institute, NYU School of Medicine)

Performed the NMJ experiments and carried out data analysis.

Dr. Irmgard U. Haussmann (Faculty of Health and Life Sciences, Coventry University) and Dr. Matthias Soller (School of Biosciences, University of Birmingham)

collaborated on the *D. melanogaster* part Flacc/Zc3h13 story

Jan Heidelberger, Prof. Dr. Petra Beli (IMB Mainz)

Carried out quantitative proteomics and data analysis (Hakai dependent ubiquitinome and proteome, detection of Fl(2)d and Nito ubiquitination sites).

Dr. Philip Knuckles and Prof. Dr. Mark Bühler (FMI Basel)

collaborated on the mouse part Flacc/Zc3h13 story

Nastasja Kreim (IMB Bioinformatics Core Facilities)

Performed bioinformatics analysis of all RNAseq, ActD-RNAseq and MeRIP-seq datasets and generated corresponding figures.

Dr. Irene Masiello and Tina Hares (Roignant`s Lab)

Performed phenotype analysis and imaging of Flacc/Fl(2)d/Nito depleted flies.

Dr. Christian Renz and Prof. Dr. Helle Ulrich (IMB Mainz)

Provided advice and reagents for the yeast-two-hybrid experiment.

Dr. Katharina Schmidt, Dominik Jacob and Prof. Dr. Mark Helm (Institute of Pharmacy and Biochemistry JGU Mainz)

Performed LC-MS-MS quantification of m⁶A levels.

Dr. Laura Spindler and Dr. Burkard Poeck (Institute of Zoology III (Neurobiology))

Performed the Buridan assay and carried out data analysis.

Dr. Reymond F. X. Sutandy, Heike Hannel and Dr. Julian König (IMB Mainz)

Provided invaluable advice, reagents and experimental help for the miCLIP experiment.

4 Results

4.1 Identification of the m⁶A writer complex in *D. melanogaster*

In order to identify potential m⁶A methyltransferase enzymes in *Drosophila melanogaster*, we performed an in silico approach and searched for *Drosophila melanogaster* orthologs of human METTL3 methyltransferase. The phylogenetic analysis identified a protein Inducer of meiosis 4 (Ime4) that showed the highest homology to METTL3 (**Figure 14a**). Additionally, we found that among human proteins two other putative methyltransferases, METTL14 and METTL4, shared high similarity and sequence conservation with METTL3. This observation was consistent with the previous study from Bujnicki and colleagues, in which all three proteins were described as MT-A70 family members, belonging to lineages B, C and A, respectively (Bujnicki et al. 2002). As METTL14 and METTL4 could potentially be m⁶A methyltransferases, we also searched for their respective orthologs in *Drosophila melanogaster*, and found proteins CG7818 and CG14906 that have not been characterized before (**Figure 14a**). Notably, all three members of the MT-A70 family are also present in other vertebrate species, but are not conserved in distinct lineages of yeast species. The *S. cerevisiae* (budding yeast) encodes for the two orthologs of METTL3 and METTL14 (ime4 and KAR4, respectively), but lacks the METTL4 ortholog. In contrast, the *S. pombe* (fission yeast) encodes only the METTL4 ortholog (C22G7.07c) and has no orthologs of the other two enzymes (**Figure 14a**), which may suggest a loss of proteins during divergent evolution of the two yeast lineages.

4.1.1 Mettl3, Mettl14 and Fl(2)d are required for m⁶A methylation of mRNA

To investigate the involvement of the three putative methyltransferases, Ime4, CG7818 and CG14906 in m⁶A mRNA methylation in flies, we depleted proteins in *Drosophila melanogaster* Schneider S2R+ cells using dsRNA designed against respective transcripts. In order to quantify levels of m⁶A modification in mRNA, we subjected samples of enriched poly-adenylated (poly(A)) RNA to LC-MS analysis. Levels of m⁶A were significantly reduced (70 %) upon depletion of Ime4 (renamed to Mettl3) (**Figure 14b**), consistent with previously described function of METTL3 protein in vertebrates (Bokar et al. 1994). Intriguingly, we also observed a significant decrease (70 %) of m⁶A levels in samples where CG7818, the closest ortholog of human METTL14 (hereafter renamed to Mettl14), was depleted, suggesting that Mettl14 also acts as an mRNA methyltransferase. However, no change in m⁶A levels was observed when CG14906, the closest ortholog of human METTL4, was depleted (**Figure 14b**). This result is consistent with the current knowledge about the human METTL4, which also does not act on mRNA. It was instead shown to mediate formation of 6mA on DNA (Fu et al. 2015, Greer et al. 2015, Zhang G. et al. 2015) (Liu J. et al. 2016, Wu et al. 2016, Mondo et al. 2017, Xiao et al. 2018) and m⁶A on U2 snRNA (Chen et al. 2020, Goh et al. 2020, Gu et al. 2020) pointing towards distinct enzymatic activity and target recognition of the CG14906 (Mettl4) protein.

Since neither depletion of Mettl3 nor Mettl14 lead to complete loss of m⁶A modification, we reasoned that the two proteins might act redundantly on a subset of methylated sites. We therefore depleted both proteins simultaneously and analysed residual m⁶A levels on mRNA. Surprisingly, levels of m⁶A modification were reduced to the same extent (70 %). This indicated that Mettl3 and Mettl14 proteins are both required for m⁶A methylation of mRNA and that they likely share common targets,

while the residual m⁶A might be present due to activity of other, uncharacterized methyltransferases. Alternatively, it may also represent an experimental artefact due to incomplete depletion of Mettl3 and Mettl14 proteins by dsRNA treatment, or remaining traces of rRNA that is also m⁶A modified. The advance in the m⁶A field at that time led to the discovery of another component of the large methyltransferase complex (see introduction: *Chapter 1.4.1*) by three independent laboratories. A protein WTAP was shown to interact with a METTL3-METTL14 heterodimer and to be required for m⁶A methylation in zebrafish, mouse as well as in human cells (Liu et al. 2014, Ping et al. 2014, Wang Y. et al. 2014). Additionally, previous studies in yeast and plants found that WTAP orthologs in these species (Mum2 and AtFIP37) strongly interact with MTA and Ime4, the respective METTL3 counterparts (Zhong et al. 2008, Agarwala et al. 2012).

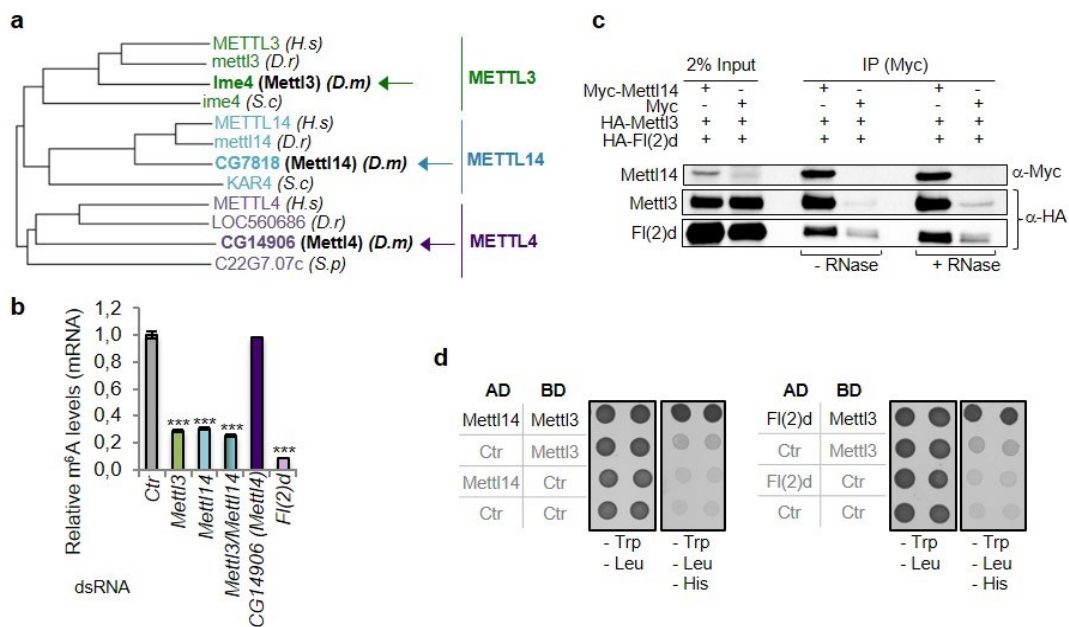


Figure 14. Mettl3, Mettl14 and WTAP are required for m⁶A methylation of mRNA.

a) Phylogenetic analysis of METTL3 orthologs in *D. melanogaster*. Mettl3 (*lme4*), Mettl14 (*CG7818*) and Mettl4 (*CG14906*) are orthologs of human METTL3 (in green), METTL14 (in blue) and METTL4 (in violet) proteins, respectively. Each *D. melanogaster* (D.m) sequence clusters with the corresponding human (H.s), *Danio rerio* (D.r) and fungal ortholog; *Schizosaccharomyces pombe* (S.p) and *Saccharomyces cerevisiae* (S.c). **b**) LC-MS/MS quantification of m⁶A levels in mRNA samples depleted for indicated proteins. Ctr, control. Bar chart represents the mean ± standard deviation (s.d.) of three technical measurements from three biological replicates. ***P < 0.0001 (one-way analysis of variance (ANOVA), Tukey's post-hoc analysis) are shown. Depletion of Mettl3 and Mettl14, but not Mettl4, results in a strong decrease of m⁶A levels. Depletion of Fl(2)d also leads to significant reduction of m⁶A levels on mRNA. **c**) Co-immunoprecipitation experiments between Mettl3, Mettl14 and Fl(2)d. Myc-tagged Mettl14 and HA-tagged Mettl3 or HA-tagged Fl(2)d were expressed in S2R+ cells and their interactions assayed using co-immunoprecipitation experiments with anti-Myc antibody. The three components of the methyltransferase complex interact with each other in an RNase treatment-independent manner. **d**) Yeast two-hybrid assay of Mettl3, Mettl14 and Fl(2)d protein interactions. Proteins were cloned in yeast expression vectors and fused with either DNA-binding domain (BD) or DNA-activation domain (AD). Indicated combinations of vectors were co-expressed in yeast. Empty vectors encoding only activation or binding domain were used as a control (Ctr). Recovered colonies were spotted on plates lacking Leucine and Tryptophan (-Leu, -Trp) as well as on selection plates lacking amino acids Leucine, Tryptophan and Histidine (-Leu, -Trp, -His). BD-Mettl3 specifically interacts with AD-Mettl14, as well as with AD-Fl(2)d (a, b, c - adapted from Lence et al 2016, d - unpublished data).

We therefore investigated the potential involvement of a *D. melanogaster* WTAP ortholog Fl(2)d, in m⁶A biogenesis. Consistent with data from other species, depletion of Fl(2)d in S2R+ cells resulted in a strong reduction of m⁶A levels (90 %) (**Figure 14b**), indicating that function of this protein, in regards

to m⁶A mRNA methylation, is conserved in flies. To explore whether Mettl3 and Mettl14 together with Fl(2)d also form a methyltransferase complex in *D. melanogaster*, the interactions between the three proteins were analysed in S2R+ cells. Corresponding cDNAs were cloned in expression vectors with either C-terminal HA or N-terminal Myc tags and protein interactions were tested by co-immunoprecipitation experiments. Consistent with vertebrate data, the Mettl14 protein efficiently co-precipitated Mettl3 in an RNase-independent manner (**Figure 14c**). Likewise, Fl(2)d was highly enriched in Mettl14 precipitates compared to Myc-alone control pull down experiment, albeit to a lesser extent than Mettl3. To investigate whether the interactions between the three proteins are direct or mediated by other proteins, we performed the yeast-two-hybrid experiment. cDNA sequences were cloned in yeast expression vectors and fused to either GAL4 activation or DNA-binding domains. Different combinations of constructs were co-transfected and expressed in yeast. Recovered colonies were further spotted on selection plates for validation of direct protein-protein interactions. Mettl3 fused to the binding domain strongly interacted with Mettl14 as well as Fl(2)d that were fused to the activation domain (**Figure 14d**). Altogether, these results indicated that a conserved, stable complex composed of Mettl3-Mettl14 heterodimer together with Fl(2)d protein is required for m⁶A methylation of mRNA in flies.

4.1.2 Components of the m⁶A writer complex localize to the nucleus

We next analysed the subcellular localization of the methyltransferase complex components in S2R+ cells. Mettl3, Mettl14 and Fl(2)d proteins were tagged with a C-terminal HA-tag and expressed in cells along with the GFP-tagged Barentsz protein that served as a cytoplasmic marker. All three proteins localized intensely to the nuclear compartment, similar to their vertebrate counterparts (**Figure 15a**). However, while the vertebrate proteins were shown to co-localize with various splicing factors in distinct nuclear speckles (Liu et al. 2014, Ping et al. 2014, Wang Y. et al. 2014), we did not observe any apparent punctuated sub-nuclear localization of fly orthologs. This discrepancy could be due to cell type, or species-driven differences. Alternatively, the overexpressed, tagged versions of fly proteins might not entirely recapitulate the biological localization of endogenous proteins. Overall, the strong nuclear localization of components of the methyltransferase complex in fly and vertebrates, pointed towards a conserved activity of the complex, within the cell nucleus, where m⁶A mRNA methylation takes place. Additionally, this also suggested that m⁶A could play a role in pre-mRNA processing, including splicing and export.

To gain further insights into the m⁶A functions we searched for protein interactors of the Mettl3 and Fl(2)d proteins. Myc-tagged proteins or empty control vector were transfected in SILAC (stable isotope labelling of amino acids in cell culture) S2R+ cells and immuno-precipitated using anti-Myc antibody coupled to magnetic beads. A subsequent mass spectrometry analysis of Mettl3 and Fl(2)d interactors identified 66 and 30 proteins, respectively, that showed more than 1.5-fold enrichment over control (**Figure 15b, Supplemental data 1**). Among them were many proteins previously shown to be involved in different steps of mRNA processing, such as transcription (tousled-like kinase, topoisomerase 2), splicing (Hrb-proteins) and translation (eukaryotic initiation factor eIF-4a). Most enriched category of Fl(2)d interactors included proteins involved in heterochromatin formation (**Figure 14b**). This finding is in line with a screen that identified Fl(2)d as an interactor of HP1 and as an enhancer of gene silencing (Swenson et al. 2016), suggesting that Fl(2)d likely represents an important factor for heterochromatin formation in flies. Whether this function is linked to m⁶A deposition is currently not known. Additionally, proteins required during cellular stress response (heat shock proteins) and for

proper progress through cytokinesis (twinstar, lamin, alpha-cop, hts, Rab11) were identified, potentially linking m⁶A modification to various biological processes.

To address the role of m⁶A writer components Mettl3, Mettl14, and Fl(2)d in vivo, we performed in situ hybridization in wild type (WT) embryos using transcript specific antisense probes. The sense and antisense probes against *elav* transcript served as either a negative or a positive control, respectively. At stages 8-9 (3-4 hours post fertilization), all three components displayed enrichment in the neuroectoderm and endoderm layers (Figure 15c) and at embryonic stage 15 (13 hours post fertilization) transcripts showed a rather ubiquitous expression profile with distinct enrichment in the developing CNS (Figure 15c). This was particularly apparent in the case of *Mettl3* and *fl(2)d* transcripts.

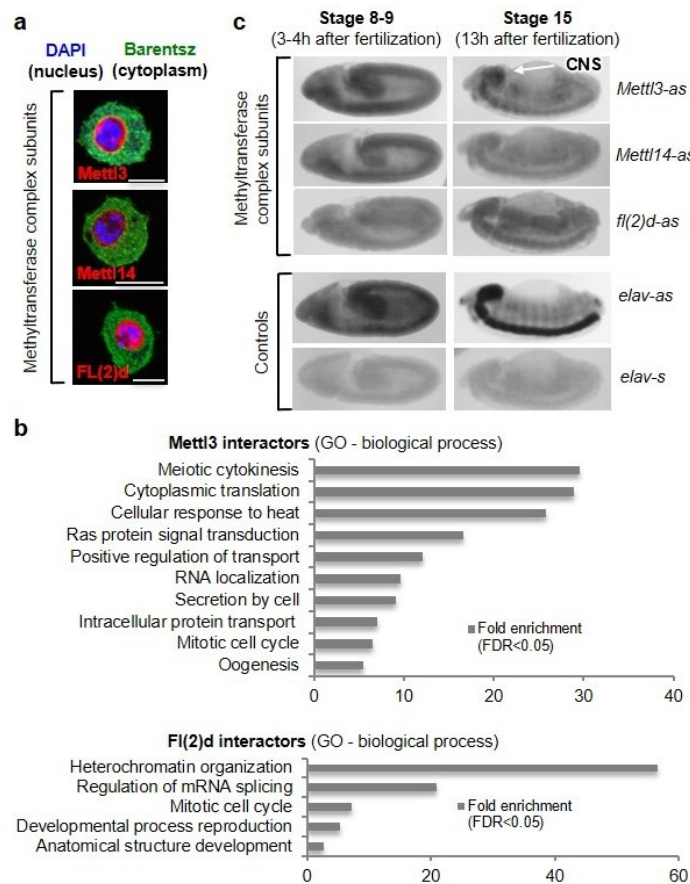


Figure 15. Components of the m⁶A writer complex localize to the nucleus and show enrichment in the neuro-ectoderm layer during embryogenesis.

a) Immunostaining of HA-tagged Mettl3, Mettl14 and Fl(2)d proteins (in red) overexpressed in S2R+ cells. GFP-tagged Barentsz protein served as a cytoplasmic marker. DAPI staining is shown in blue. Three proteins of the methyltransferase complex localize to the nucleus. Scale bars, 10 μ m. **b**) Gene ontology (GO) analysis of Mettl3 and Fl(2)d interacting proteins, identified by immunoprecipitation in S2R+ cells using either Myc-tagged Mettl3 or Fl(2)d proteins as a bait. Proteins that showed more than 1.5-fold enrichment over control were considered. Top GO-terms for biological processes are shown (Tyanova et al. 2016). **c**) In situ hybridization analysis of *Mettl3*, *Mettl14* and *fl(2)d* transcripts in staged *D. melanogaster* embryos using antisense (as) RNA probes. *Elav* sense (s) and antisense (as) probes were used as positive and negative controls, respectively. The three methyltransferase components show enrichment in the central nervous system (CNS) at embryonic stage 15 (a, c - adapted from Lence et al 2016, b - unpublished data).

4.1.3 m⁶A levels are dynamic during fly development

The results of the in situ hybridization experiment suggested a potential function of m⁶A in the nervous system. To get further insights into the prevalence of the modification during fly development, we performed a staging experiment, where mRNA levels of m⁶A writer components as well as levels of m⁶A modification were assayed over the course of *D. melanogaster* development. Levels of *Mettl3* and *fl(2)d* transcripts displayed a prominent enrichment during early embryogenesis, as well as in heads and ovaries of adult female flies (Figure 16). Importantly, levels of m⁶A modification on mRNA correlated well with the expression profile of the m⁶A writer components (*Mettl3*, *fl(2)d*) during all developmental stages. m⁶A modification was highly enriched in the first two hours of fly embryogenesis when transition from maternal to zygotic transition takes place. It then strongly declined and remained low during the remaining course of embryogenesis (6-22 hours) as well as during most larval stages (24-96 hours). Level of m⁶A modification peaked again at early pupation (144 hours), but then declined towards the end of pupation and stayed low in adult male and female flies (Figure 16). Notably, compared to a whole fly, m⁶A was strongly elevated in heads and ovaries, implying that m⁶A mRNA modification likely plays important roles during gametogenesis, early embryogenesis, as well as in the development of the nervous system.

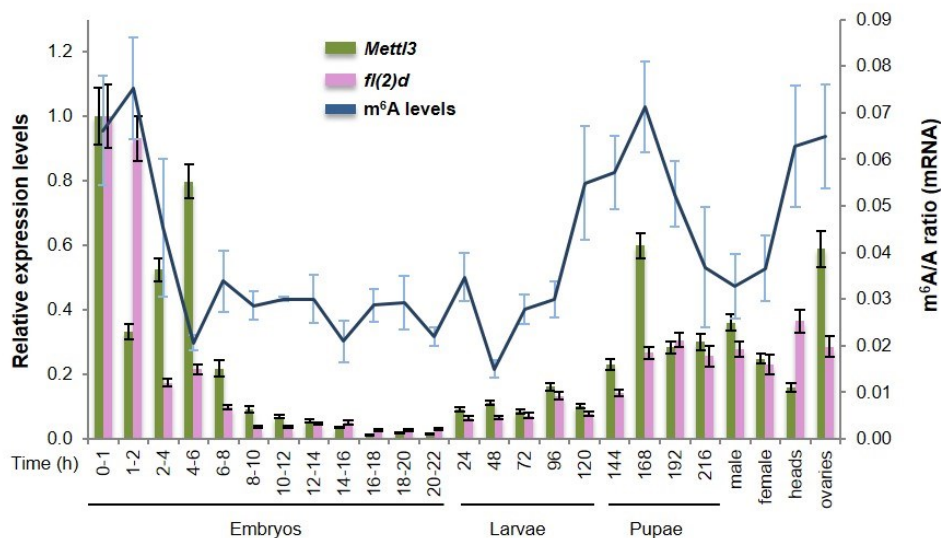


Figure 16. m⁶A levels are dynamic during *D. melanogaster* development.

Relative expression of *Mettl3* and *fl(2)d* transcripts during *D. melanogaster* developmental stages and in adult female heads and ovaries, analysed by qRT-PCR. Levels of m⁶A modification were analysed in the same mRNA samples using LC-MS. Methyltransferase components and m⁶A levels are enriched during first hours of embryogenesis, early pupation as well as in adult heads and ovaries. Bars and line junctions represent the mean \pm standard deviation (s.d.) of three technical measurements from three biological replicates (adapted from Lence et al 2016).

4.2 Identification of m⁶A reader proteins in *D. melanogaster*

4.2.1 Flies encode one nuclear and one cytoplasmic YTH domain protein

After m⁶A modification is deposited to mRNA it can be specifically recognized by a set of so-called reader proteins. The first identified and best-characterized readers belong to the YTH domain-containing family and can accommodate N⁶-methylated adenosine via a hydrophobic pocket formed by aromatic residues of the YTH domain (Liao et al. 2018) (*Chapter 1.4.6.a*). To identify putative YTH domain-containing m⁶A reader proteins in *D. melanogaster*, we performed an in silico analysis and searched for homologs of a human YTHDC1 protein. While vertebrates contain five members of the YTH family proteins, there are only two proteins present in flies. *Ythdc1* is the closest ortholog of human YTHDC1, while a CG6422 protein (that has not been investigated before) has the highest homology to three human YTHDF-proteins (**Figure 17a**).

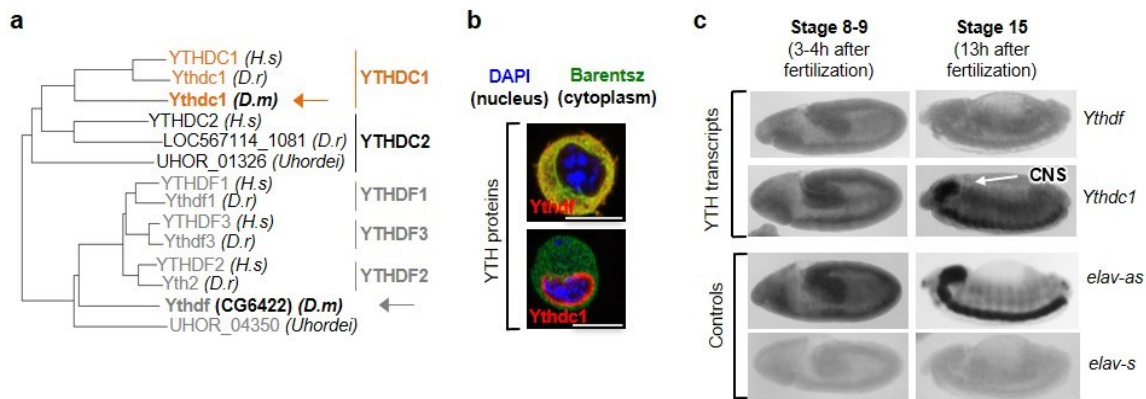


Figure 17. Nuclear *Ythdc1* protein is enriched in the neuroectoderm during embryogenesis.

a) Phylogenetic analysis of YTH domain-containing proteins. *D. melanogaster* *Ythdc1* (also known as YT521-B) is an ortholog of human YTHDC1 protein (in orange), while *Ythdf* (CG6422) is the closest ortholog of YTHDF family of proteins (in grey). Each *D. melanogaster* (D.m) sequence clusters with the corresponding human (H.s), *Danio rerio* (D.r) and fungal ortholog *Ustilago hordei* (Uhordei). **b**) Immunostaining of HA-tagged *Ythdc1* and *Ythdf* proteins (in red) overexpressed in S2R+ cells. GFP-tagged Barentsz protein served as a cytoplasmic marker. DAPI staining is shown in blue. *Ythdc1* localizes to the nucleus and *Ythdf* shows cytoplasmic localization. Scale bars, 10 μ m. **c**) In situ hybridization analysis of *Ythdc1* and *Ythdf* transcripts in staged *D. melanogaster* embryos using antisense (as) RNA probes. *Elav* sense (s) and antisense (as) probes were used as positive and negative controls, respectively. *Ythdc1*, but not *Ythdf*, shows enrichment in the central nervous system (CNS) at embryonic stage 15 (adapted from Lence et al 2016).

To investigate the subcellular localization of both YTH domain-containing proteins we cloned corresponding cDNAs in the expression vector with a C-terminal HA-tag and co-expressed them in *D. melanogaster* S2R+ cells along with a cytoplasmic protein Barentsz fused to the GFP. *Ythdc1* protein localized to the nucleus with an intense enrichment at the nuclear periphery, while the *Ythdf* protein displayed strong cytoplasmic localization (**Figure 17b**). This was consistent with the localization pattern of vertebrate orthologs, where the YTHDC1 is the only nuclear YTH family member and all three YTHDF proteins localized to the cytoplasmic compartment. We next investigated the expression profile of *Ythdc1* and *Ythdf* transcripts in wild type embryos using *in situ* hybridization. The *Ythdc1* transcript showed a similar expression pattern to m⁶A writer components (**Figure 17c**); it was highly expressed at embryonic stage 8-9 (3-4 hours post fertilization) and showed a strong enrichment in the developing

neuro-ectoderm layer of embryos at stage 15 (13 hours post fertilization). On the other hand, the *Ythdf* transcript was expressed at much lower levels during early and late developmental stages (**Figure 17c**).

4.2.1.a Expression profiles of both YTH domain proteins follow m⁶A levels during fly development

To get further insights into the expression profile of *Ythdc1* and *Ythdf* during complete fly development, we examined the transcript abundance in RNA samples from *D. melanogaster* developmental stages, in which we previously analysed m⁶A levels and expression of m⁶A writer complex components. The *Ythdc1* levels (in orange) were highest in the stages of early embryogenesis (0-8 hours) and then steadily decreased, similarly to m⁶A levels (**Figure 18**). *Ythdc1* expression then slightly increased during L1 and L2 larval stages (24-48 hours) and during early pupation (168 hours). The *Ythdc1* levels were low in adult flies, however they were strongly elevated in female heads, but not in ovaries. Levels of *Ythdf* transcript, on the other hand, were very high during the first two hours of embryogenesis and then sharply decreased, and remained low for the rest of embryogenesis and larval development. A mild increase of *Ythdf* levels was observed during pupation (144 hours) and in ovaries, where m⁶A levels are also elevated. Taken together, the two YTH domain-containing proteins in *D. melanogaster* localize to distinct cellular compartments and their transcripts show different expression patterns. During late embryogenesis *Ythdc1* transcript displayed enrichment in the neuro-ectoderm layer whereas *Ythdf* was expressed ubiquitously. Additionally, *Ythdc1* was strongly enriched in adult heads, while *Ythdf* showed highest expression exclusively during the first two hours of embryogenesis. Therefore *Ythdc1* might play important functions in nuclear pre-mRNA processing events, such as splicing and RNA export, possibly in neuronal tissue, while *Ythdf* could be involved in the cytoplasmic processes of mRNA localization, decay or translation during early embryogenesis prior to zygotic gene activation.

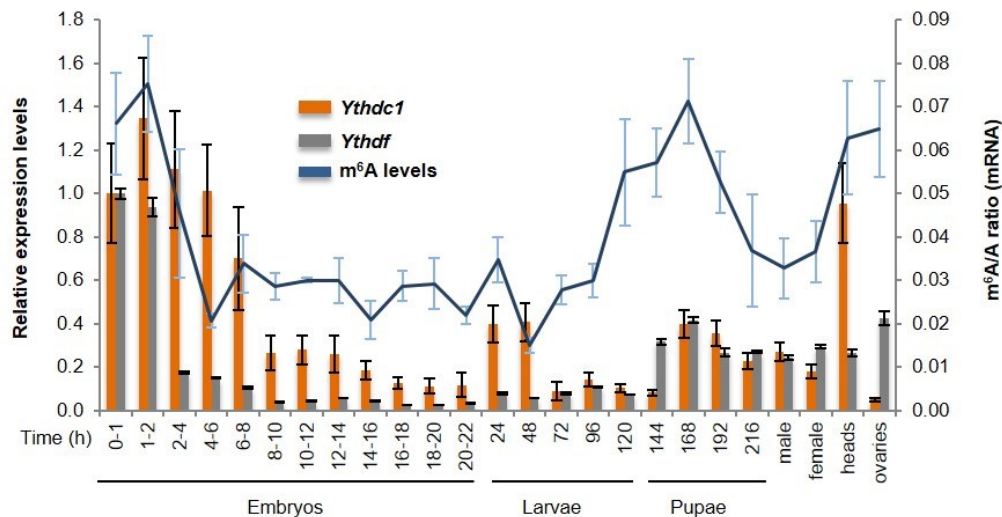


Figure 18. Expression of both YTH domain-containing proteins correlate with m⁶A profile during fly development.

Relative expression of *Ythdc1* and *Ythdf* transcripts during *D. melanogaster* developmental stages and in adult female heads and ovaries, analysed by qRT-PCR. Levels of m⁶A modification were analysed in the same mRNA samples using LC-MS. *Ythdc1* and *Ythdf* components and m⁶A levels are enriched during first hours of embryogenesis and during early pupation. *Ythdc1* and m⁶A levels are also enriched in adult female heads. Bars and line junctions represent the mean \pm standard deviation (s.d.) of three technical measurements from three biological replicates (adapted from Lence et al 2016).

4.2.1.b Ythdc1 reader protein preferentially binds m⁶A modified RNA

The specificity of m⁶A binding by different YTHDC and YTHDF proteins was revealed by resolved crystal structures of YTH domains with short RNA sequences containing m⁶A modification (Li F. et al. 2014, Luo and Tong 2014, Theler et al. 2014, Xu et al. 2014, Zhu et al. 2014, Xu et al. 2015) (*Chapter 1.4.6.a*). We compared the amino acid sequences of Ythdc1 and Ythdf to corresponding human orthologs and found that all residues of the YTH domain, required for m⁶A accommodation, are conserved (**Supplemental data 23** and **Supplemental data 24**). In order to test whether the two YTH domain-containing proteins in *D. melanogaster* also recognize and bind m⁶A modification, we performed an in vitro binding assay using either m⁶A-modified or non-modified RNA probes from a 3'UTR region of the *bovine prolactin* (*bprl*) transcript that carried m⁶A at a known position and a 5'-biotin tag (**Figure 19a**) (Narayan and Rottman 1988). We first analysed binding specificity using a dot-blot assay. Serial dilutions of both RNA probes were heat denatured, spotted on a nylon membrane and crosslinked. Membrane was then incubated with a protein lysate from S2R+ cells expressing either a Myc-tagged GFP, Ythdc1 or Ythdf protein. To evaluate the specificity of the assay, one membrane was also incubated with an anti-m⁶A antibody. As expected, the antibody recognized the m⁶A-containing RNA probe substantially better than the unmodified one. This was particularly apparent at higher RNA amounts (> 0.5 µg) (**Figure 19a**, top). Lysate containing the GFP protein served as a negative control and the protein did not bind any of the two probes (**Figure 19a**, middle), suggesting that despite limited sensitivity the assay may reveal potential m⁶A binders. Among the two YTH domain-containing proteins, the Ythdc1 protein recognized the m⁶A-modified probe better than the non-modified one, similarly to the anti-m⁶A antibody (**Figure 19a**, middle), indicating that *D. melanogaster* Ythdc1 is likely a reader of m⁶A modification. In contrast, we could not observe any difference in the recognition of m⁶A modified or non-modified probes by the Ythdf protein (**Figure 19a**, bottom). This could be due to the presence of a tag interfering with m⁶A accommodation or could reflect the inability of the Ythdf protein to accommodate m⁶A modification in a given sequence and/or structure context of the RNA probe used in this experiment.

To confirm the observation of the dot-blot assay that Ythdc1 protein binds m⁶A modified RNA, we performed the following pull-down experiment. Protein lysates from cells expressing Myc-tagged GFP or Ythdc1 proteins were incubated with same m⁶A-modified or non-modified RNA probes from *bovine prolactin*. Probes were pulled-down with streptavidin-coupled magnetic beads and recovered proteins were analysed by western blot. Consistently with the dot-blot assay, GFP did not bind to any of the two probes, while Ythdc1 was more efficiently recovered with the m⁶A-containing probe (**Figure 19b**). Overall, these results suggested that *D. melanogaster* Ythdc1 preferentially binds the m⁶A-modified *bovine prolactin* transcript. On the other hand, the only YTHDF-member in *D. melanogaster*, Ythdf, showed no preference for m⁶A-modified probes in our assay. Nevertheless, Ythdf might as well bind m⁶A-modified RNA, however in a different sequence or structure context.

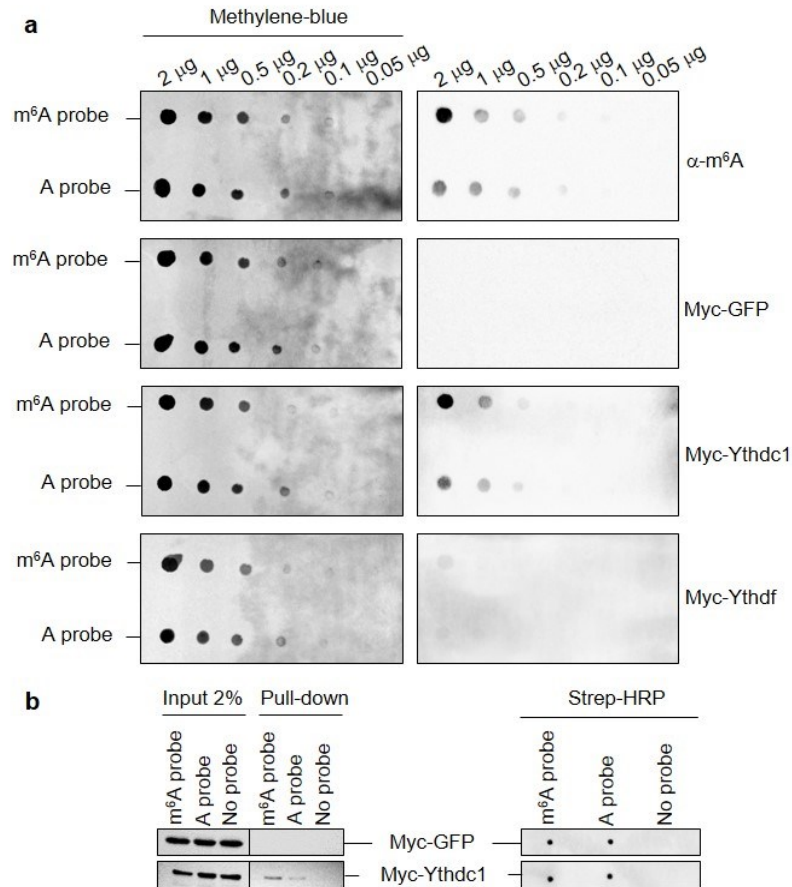


Figure 19. Ythdc1 reader protein preferentially binds m⁶A modified RNA probe.

a) Dot-blot assay using biotinylated probe from *bovine prolactin* transcript with and without m⁶A modification. Protein extracts from S2R+ cells transfected with either Myc-tagged GFP, Ythdc1 or Ythdf were analysed for binding specificity to the cross-linked RNA probes. Left, methylene-blue staining of crosslinked probes. Right, immunostaining using anti-Myc or anti-m⁶A antibody. Ythdc1 protein and anti-m⁶A antibody both show similarly enriched binding to the m⁶A-methylated probe. **b)** Pull-down using biotinylated m⁶A probe from *bovine prolactin* transcripts and protein extracts from S2R+ cells transfected with either Myc-tagged GFP or Ythdc1. The same probe lacking the methylation was used as a negative control. Left, western blot using anti-Myc antibody. Right, dot blot using anti-Streptavidin-HRP antibody. Myc-Ythdc1 was pulled down better with the m⁶A methylated probe. Three independent experiments showed similar results (adapted from Lence et al 2016).

4.2.2 Putative novel m⁶A readers are involved in mRNA turn-over

m⁶A modification was shown to alter binding of various RBPs either in a positive or negative fashion (Dominissini et al. 2012, Edupuganti et al. 2017, Baquero-Perez et al. 2019) (*Chapter 1.4.6.b*). To identify potential m⁶A-interactors other than YTH domain proteins, we performed new pull-down experiments and subjected all recovered proteins to quantitative mass spectrometry proteomics analysis. We incubated *bovine prolactin* RNA probes with protein lysates from SILAC-labelled *D. melanogaster* S2R+ cells. We performed four independent experiments; in three experiments the methylated probe was incubated with lysates from heavy-amino acid labelled cells and the non-modified probe with light-amino acid labelled cells (IP1, IP2, and IP3). To ensure that recovered proteins were not reflecting a possible effect of SILAC labelling on protein expression, we also performed one reverse experiment in which the methylated probe was incubated with lysates from light-amino acid labelled cells and the non-modified probe with heavy-amino acid labelled cells (IP4). Proteins that were identified in all four experiments and were either enriched, or repelled (by more than 1.3-fold) in at

least three experiments were considered as potential m⁶A-regulated RBPs (**Figure 20**). We identified 23 proteins that displayed enrichment for binding to m⁶A probe over the non-modified one and 6 proteins that were m⁶A-repelled. The YTH domain-containing proteins were, however, not among selected candidates. While Ythdc1 protein was enriched above the threshold in two replicates, the Ythdf was enriched only once. This was not entirely unexpected, considering our previous results from the dot-blot and pull-down assays performed with overexpressed YTH-proteins (**Figure 19a, b**) in which the Ythdc1 showed preferential, but not exclusive binding to the m⁶A-modified probe, whereas the Ythdf protein displayed no clear binding to neither methylated nor unmethylated probe (**Figure 19a**).

We wondered why the *bovine prolactin* probe could not efficiently recover YTH domain proteins in any of the assay we have performed (**Figure 19a, b** and **Figure 20b**). Initial study, that identified different m⁶A readers, including YTH domain proteins, performed a similar in vitro pull-down experiment, but used as a bait a sequence of a viral RNA carrying m⁶A modification located in a predicted loop position (Dominissini et al. 2012). Notably, a recent study from Liu and colleagues systematically evaluated m⁶A recognition by an anti-m⁶A antibody or a purified YTH domain when it was located in different RNA substrates/structures. They found that m⁶A located within an RNA duplexes cannot be efficiently bound neither by an anti-m⁶A antibody, nor by a recombinant YTH domain (K_d>50 μM for both, modified and unmodified RNA) (Liu B. et al. 2018). Additionally, they also demonstrated that only when m⁶A is positioned in a single stranded RNA or next to a nucleotide bulge of the same strand, it adopts an accessible conformation that can be specifically and strongly bound by the YTH domain proteins (K_d<0.5 μM for modified and K_d>30 μM for unmodified RNA) (Liu B. et al. 2018).

We thus questioned if structural restrictions might explain why the methylated RNA probe that we used in our study could not adequately recover YTH domain-containing proteins. We analysed the putative secondary structure of the 39 nt long *bovine prolactin* RNA probe using the Fold algorithm of the “RNAstructure” web tool that predicts the lowest free energy structure in a set of low free energy structures for a given sequence (Reuter and Mathews 2010). Intriguingly, we found that the *bovine prolactin* RNA probe is predicted to adopt a strong secondary structure in which m⁶A, at position 21, is embedded in the middle of a 3 nt long RNA duplex (**Figure 20b**) with perfect base pairing of a very high probability (80-90 %). This RNA duplex is surrounded by a short stem loop on one side and by an open, unpaired sequence on the other side (**Figure 20b**). m⁶A modification was previously shown to have a destabilizing effect on RNA duplexes (Spitale et al. 2015), due to unfavourable isomer conformation that adenosine needs to adopt in order to base pair with uridine of the opposite strand. This trans-conformation results in a steric clash within the atoms of adenosine base (between the exocyclic N6-methyl group and the endocyclic nitrogen (N7)) (Roost et al. 2015). In spite of this, NMR studies have shown that self-complementary RNA containing a GGACU sequence motif can adopt a fully paired RNA duplex regardless of its methylation status (Roost et al. 2015). Therefore, it is unlikely that m⁶A in the *bovine prolactin* RNA could destabilize the 3-nt long RNA stem structure in a given GAC sequence context [nt 22 – nt 23], where the upstream guanosine and downstream cytosine nucleotides perfectly base pair with cytosine and guanosine [nt 34 – nt 36], respectively (**Figure 20b**). Thus, it is very likely that Ythdc1 and Ythdf proteins were not efficiently recovered by the *bovine prolactin* sequence, because m⁶A modification in this RNA probe is located in the paired RNA duplex and could not be appropriately accommodated by the corresponding YTH domains (**Figure 19a, b** and **Figure 20a, b**). This is in line with the study from Liu and colleagues (Liu B. et al. 2018). showing that m⁶A recognition is regulated not only by the RRACH motif, but also by structural constraints of the surrounding sequence.

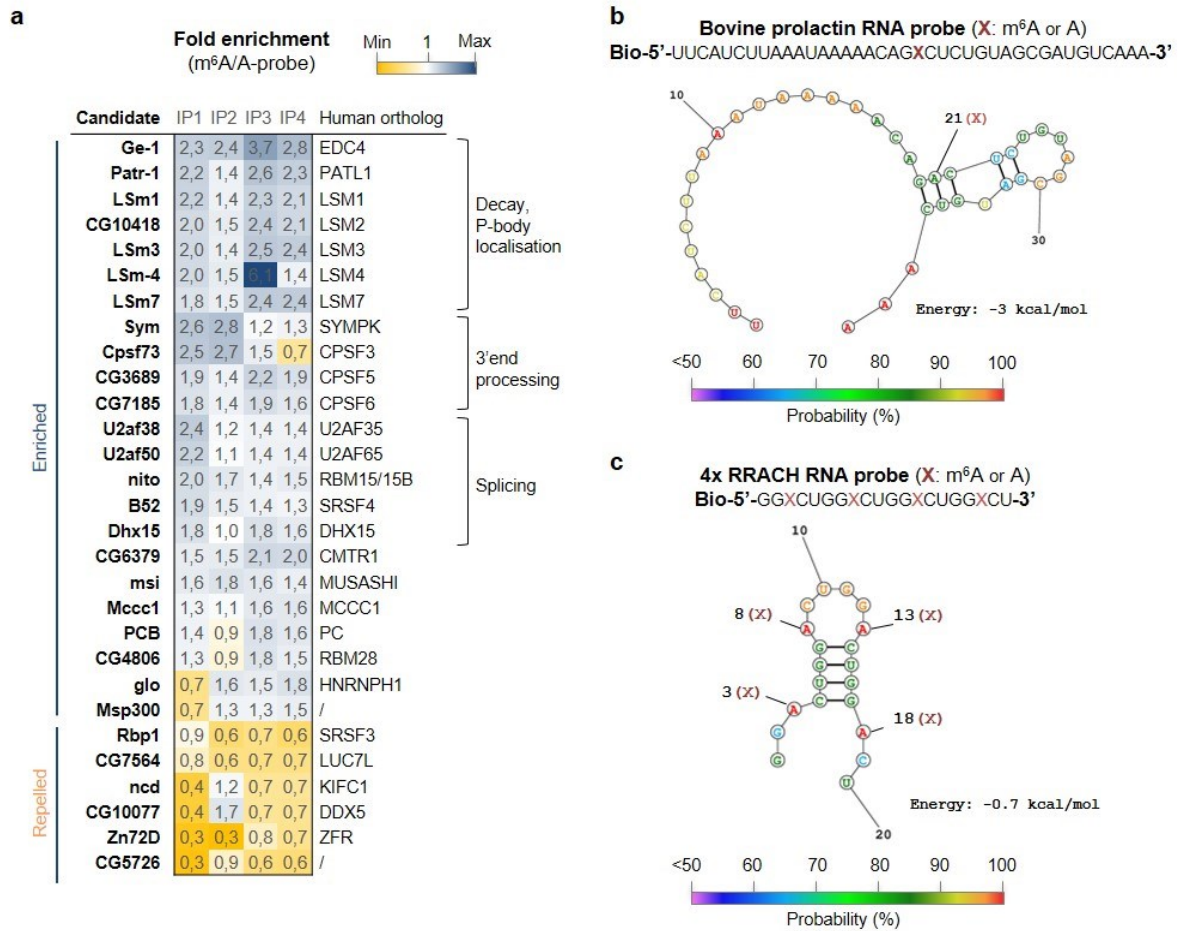


Figure 20. Identification of other potential m⁶A binders links m⁶A to splicing and polyadenylation.

a) Heat map of enriched and repelled proteins identified by a pull-down experiment using biotinylated m⁶A or A containing probes from *bovine prolactin* transcript (shown in (b)) and protein extracts from S2R+ cells. Pulled down proteins from four independent experiments were subjected to MS analysis. Proteins that were more than 1.3-fold enriched (in blue) or repelled (in yellow) with m⁶A-containing probe over A-containing probe in at least three out of four experiments are shown. Corresponding human orthologs are listed on the right. Enriched proteins are involved in various steps of mRNA processing. **b)** Sequence of biotinylated RNA probe from *bovine prolactin* 3'UTR transcript carrying either m⁶A or A at position 21 (above). RNA structure prediction by the “RNAstructure” tool and the Fold algorithm (Reuter 2010). m⁶A is positioned in a closed stem structure of a predicted three nucleotide long stem that shows a high probability (80-90 %) for base pairing. Colour code denotes probability of each nucleotide to adopt displayed paired or unpaired structure. Calculated free energy of predicted structure is shown on the right. **c)** As in (b) for a sequence of biotinylated RNA probe (4xRRACH) containing four consecutive GGACU motifs carrying either m⁶A or A at each adenosine position (above) (unpublished data).

Recent study from Vermeulen lab extensively screened for novel m⁶A reader proteins in various human and mouse cell types (Edupuganti et al. 2017) and found that YTH domain-containing proteins were by far the strongest binders of an RNA probe that contained four consecutive GGACU repeats with four m⁶A sites (Edupuganti et al. 2017). We wondered if perhaps a good m⁶A accessibility in this particular 4x RRACH RNA probe could explain efficient YTH-protein recovery. We analysed the predicted secondary structure of the 4x RRACH probe using the same Fold algorithm (Reuter and Mathews 2010). Indeed, as shown in **Figure 20c**, all four m⁶A sites in this RNA probe appear to be in an unpaired position. Consistent with the findings from Liu and colleagues, it is therefore not surprising that this RNA probe could readily recover YTH domain proteins. Overall, various studies aiming to identify putative m⁶A binders all used different RNA sequences that consequently also adopted different secondary

structures (Dominissini et al. 2012, Edupuganti et al. 2017, Baquero-Perez et al. 2019). This likely contributes to the discrepancy among identified sets of putative m⁶A reader proteins. Albeit, more importantly, it also reveals that distinct proteins can interpret m⁶A functions in a context dependent manner.

Among candidates that we found enriched with the m⁶A probe were Ge-1, Patr-1 and Lsm1-Lsm7 proteins that form a cytoplasmic complex involved in mRNA storage and decay in the P-bodies (Luo Y. et al. 2018), possibly linking m⁶A modified mRNA to these compartments to fine tune their turnover (**Figure 20a**). Highly enriched were also the cleavage and polyadenylation proteins known to suppress polyadenylation site selection (Masamha et al. 2014), as well as various proteins involved in pre-mRNA splicing, including U2af38 and U2af50, previously found to interact with Fl(2)d (Penn et al. 2008). These candidates therefore strongly support the role of m⁶A modification in different steps of mRNA processing. Given that some of the identified proteins interact with each other, it is likely that only one of the proteins within the complex binds the m⁶A modified RNA and subsequently recruits other components. It is possible that these newly identified m⁶A readers preferentially bind to m⁶A modified sites within the paired stem structure and were therefore not found by other studies. For some of the identified proteins a known binding motif was also present in the sequence surrounding the modified adenosine (e.g. msi protein binds UAG motif (Zearfoss et al. 2014)). It might be that m⁶A increases motif accessibility and protein binding specificity, acting as an “m⁶A-switch”, as previously shown for hnRNP proteins; hnRNPC (Liu et al. 2015), hnRNPG (Liu et al. 2017) and hnRNPA2B1 (Alarcon et al. 2015a). How exactly each of these newly identified proteins binds m⁶A modified RNA awaits future studies. Ideally, binding specificity to biologically relevant, m⁶A-modified transcripts should be analysed, rather than to RNA probes composed of repetitive sets of consensus sites.

4.3 Loss of m⁶A on mRNA affects gene expression and splicing

4.3.1 The m⁶A writer complex and the Ythdc1 protein regulate alternative splicing

Results of our protein interactome analysis and newly identified m⁶A binding proteins pointed towards a potential role of m⁶A modification in different steps of mRNA processing. In order to investigate the importance of m⁶A on gene expression and mRNA splicing, we performed transcriptome analysis in S2R+ cells depleted for m⁶A writer components, Mettl3, Mettl14 and Fl(2)d, as well as for nuclear and cytoplasmic YTH domain readers, Ythdc1 and Ythdf. Knockdown of Fl(2)d and Ythdf altered expression of many genes (n=2129 and n=1309), while other components showed a milder effect (n=484, n=230 and n=522) (**Figure 21a**, left). Among differentially expressed genes, 98 were in common between all three components of the writer complex (**Figure 21a**, middle) and of those, many were also deregulated upon loss of Ythdc1 and Ythdf (40 % and 61 %, respectively). This supports the involvement of these two proteins in m⁶A recognition and regulation of downstream processes (**Figure 21a**, right).

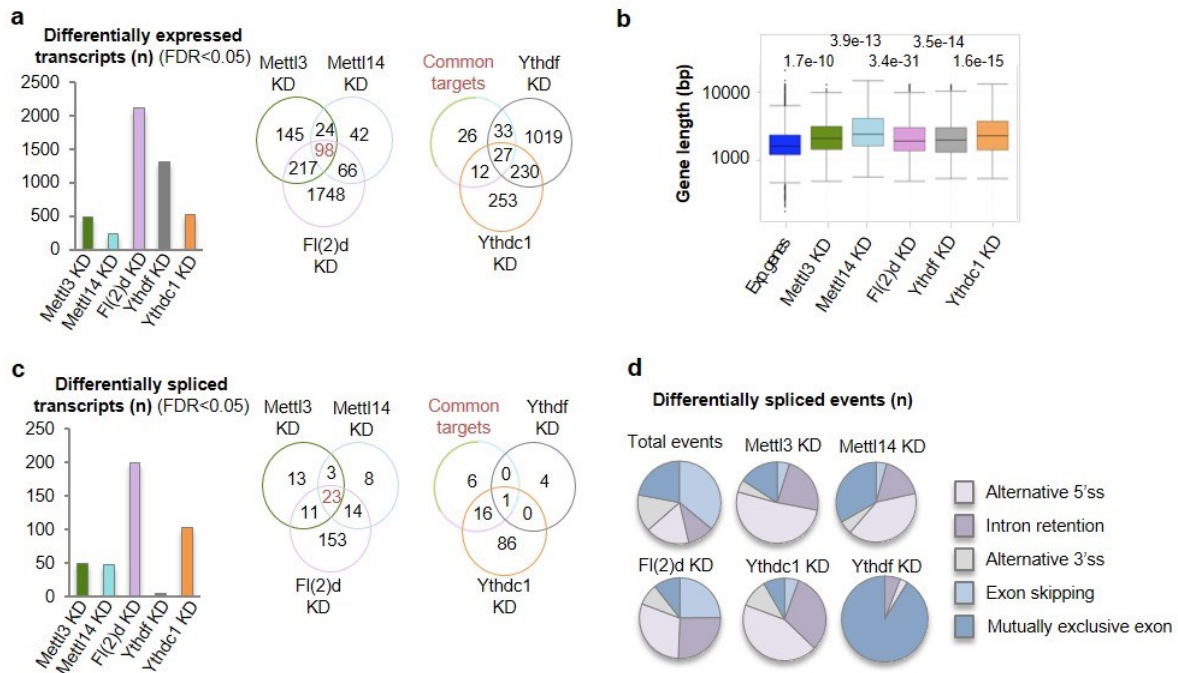


Figure 21. Loss of m⁶A writers or nuclear reader Ythdc1 alters gene expression and splicing.

a) Number of differentially expressed genes upon depletion of indicated proteins. Venn diagram of common misregulated genes upon depletion of Mettl3, Mettl14 and Fl(2)d (left) and YTH domain reader proteins (right). Most common differentially expressed genes by writer components are also misregulated upon depletion of Ythdc1 or Ythdf proteins. **b)** Box plots showing gene length for all expressed genes and differentially expressed genes in indicated knockdowns (KD) (average coverage >1 read per kilobase per million mapped reads (RPKM) in control conditions). Distributions were compared to all expressed genes using the Wilcoxon rank sum test. Expressed genes were down sampled to the same number of genes as in the given knockdown. Differentially expressed genes upon loss of m⁶A or nuclear reader protein Ythdc1 are on average longer. **c)** Number of differentially spliced genes upon depletion of indicated proteins. Venn diagram of common differentially spliced genes upon depletion of Mettl3, Mettl14 and Fl(2)d (left) and YTH domain reader proteins (right). Most common differentially spliced genes by writer components are also differentially spliced upon depletion of Ythdc1. **d)** Pie charts showing distribution of differentially spliced events in each knock down condition. Alternative 5's splice site (5'ss) selection and intron retention are overrepresented events upon loss of m⁶A writers or nuclear reader protein Ythdc1 (Figure 17 - adapted from Lence et al 2016).

Among affected genes were many involved in the regulation of metabolism and organismal development, as well as in processes linked to neuronal functions (axon guidance, synaptic response to stimuli, behaviour), as determined by the Gene ontology term enrichment analysis (**Appendix 1**, ED Fig. 4). Interestingly, even though S2R+ cells are of non-neuronal origin the affected genes were significantly longer as compared to all expressed genes, a feature common for neuronal genes (Zylka et al. 2015) (**Figure 21b**). We next analysed whether depletion of m⁶A components also resulted in differential splicing. While knock down of Fl(2)d altered many splicing events (n=2129), depletion of Mettl3 and Mettl14 had a milder effect (**Figure 21c**, left). Nevertheless, among the common differentially spliced genes, 74 % were also altered upon loss of Ythdc1 (**Figure 21c**, middle and right), indicating that nuclear reader is likely responsible for m⁶A mediated splicing regulation in *D. melanogaster*, as has been previously shown for its mammalian ortholog, Ythdc1 (Xiao et al. 2016). Interestingly, among different classes of splicing events, the intron retention and alternative 5' splice site selection were overrepresented (**Figure 21d**), which has been also observed in human cells (Dominissini et al. 2012).

4.3.2 m⁶A in *D. melanogaster* is enriched along 5'UTR regions and in coding sequences

To identify the sites of m⁶A methylation in *D. melanogaster* S2R+ cells transcriptome wide, we carried out methylated RNA immunoprecipitation followed by next-generation sequencing (MeRIP-seq) (Dominissini et al. 2012, Meyer et al. 2012) using an anti-m⁶A specific antibody. We performed m⁶A enrichment on a polyadenylated fraction of RNA and identified 1120 peaks in 812 genes that showed >1.3-fold enrichment over input. In most of the peaks we found a consensus motif RRACH (n=1027, 92 %), centered on potentially modified adenosine (**Figure 22a**, top). This motif was previously shown to be the most common methylation site in mouse and human cells (Dominissini et al. 2012, Meyer et al. 2012), supporting that peaks we had found are likely valid sites of m⁶A methylation, despite low enrichment. Distribution of identified peaks along transcripts was most prominent within the coding sequence (44,6 %) as well as around stop codons (16,3 %), similar to m⁶A distribution in other species (**Figure 22**, below). Interestingly, a large amount of peaks also fell around start codons (21,8 %) and the enrichment was higher compared to vertebrates (**Appendix 1**: Fig. 2C) (Dominissini et al. 2012, Meyer et al. 2012, Ping et al. 2014). By using the MeRIP-seq technique, we uncovered many putative m⁶A peaks, but we were not able to locate precise positions of m⁶A sites and our enrichment suffered from high background that could potentially result in substantial loss of identified methylation sites as well as in a set of false negative peaks. To overcome these technical drawbacks, we next performed m⁶A mapping using miCLIP (methylation specific individual-nucleotide resolution cross-linking immunoprecipitation) (Linder and Jaffrey 2019). During m⁶A immunoprecipitation, the anti-m⁶A specific antibody was crosslinked to polyadenylated RNA, which allowed stringent washing in order to remove any non-specifically bound RNA fragments. Importantly, crosslinking is expected to induce an indicative m⁶A footprint during the step of reverse transcription, which enables the identification of precise locations of putative m⁶A sites along the transcript (Linder and Jaffrey 2019). We focused on sites that resulted in truncation at adenosines, CITS (A) (crosslink-induced truncation site at Adenosine) and identified nearly 12.000 methylated sites in 3280 genes (**Figure 22b**), which is roughly four times more than the number of genes we mapped by MeRIP-seq. Nevertheless, while 75 % of modified genes identified by MeRIP-seq were also found by miCLIP, this overlap represented only 18.5 % of all genes found by miCLIP, indicating that miCLIP has a markedly better sensitivity (**Figure 22c**).

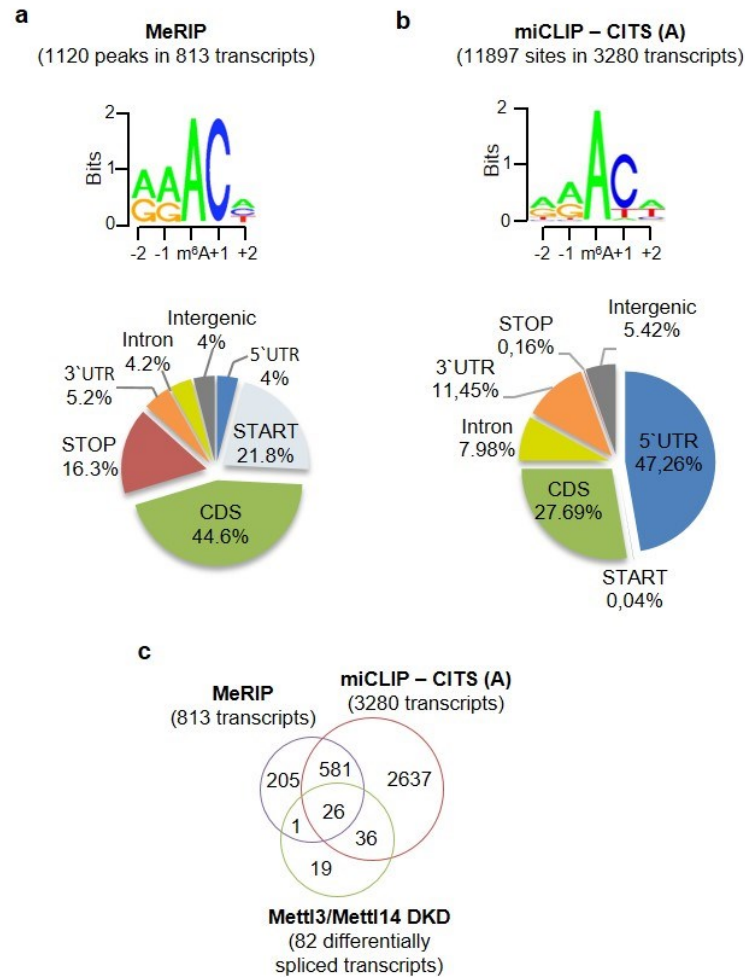


Figure 22. m⁶A in *D. melanogaster* is enriched along 5'UTR regions and coding sequences.

a) MeRIP sequence logo and peak distribution. Sequence logo of deduced consensus motif for most m⁶A peaks centered on the modified adenosine. 1120 peaks were identified in 813 transcripts by MeRIP (top). Pie chart of m⁶A peak distribution in distinct transcript segments identified by MeRIP (below). Start codon (\pm 300 bp window around start), CDS (coding sequence (CDS) excluding 300 bp after start and 300 bp before stop), stop codon (\pm 300 bp window around stop). **b)** miCLIP sequence logo of crosslink induced truncation sites at adenosines (CITS (A)). Shown is a 5-nt region of 20-nt sequence logo of collapsed sequences at diagnostic sites for m⁶A CITS (A) centered on the modified adenosine. See materials and methods for a full sequence logo. 11897 CITS (A) sites were identified in 3280 transcripts by miCLIP (top). Pie chart of m⁶A CITS (A) distribution in distinct transcript segments identified by miCLIP (below). **c)** Overlap between transcripts carrying m⁶A peak identified by MeRIP, CITS (A) identified by miCLIP and a set of common differentially spliced genes upon combined depletion of Mettl3 and Mettl14 proteins. 77 % of transcripts with altered splicing are also m⁶A modified (a - adapted from Lence et al 2016, b, c - unpublished data).

We next compared both datasets to a class of transcripts that were differentially spliced upon simultaneous depletion of Mettl3 and Mettl14 ($n=82$) and found that 77 % of transcripts were m⁶A modified (**Figure 22c**), suggesting that m⁶A might be required for their processing. Of those, 62 transcripts were found in the miCLIP dataset, and 27 also contained a MeRIP peak, with a single transcript not covered by miCLIP. Interestingly, among them was also *fl(2)d* (**Figure 23a**) that can be alternatively spliced into four different RNA isoforms, which code for two protein isoforms. Splicing decision depends on the alternative 5'-splice site (ss) selection of the first intron and on inclusion or exclusion of the alternative exon 2 (Ex2) (**Figure 23**). Use of 5'-splice site three (ss3) extends the sequence of the first exon (Ex1) that carries an upstream start codon and therefore generates longer cDNA isoform.

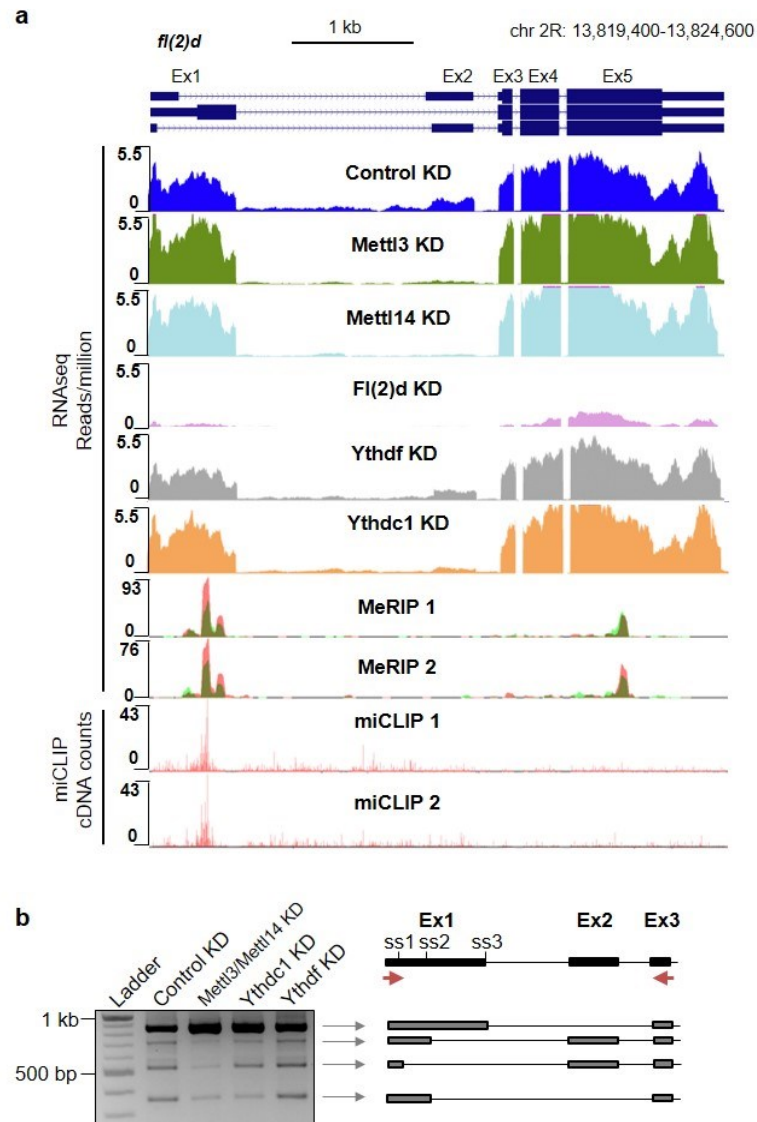


Figure 23. *fl(2)d* splicing is regulated by m⁶A modification.

a) UCSC Genome Browser screenshots of *fl(2)d* transcript showing normalized RNA-seq data from control and indicated knockdown samples in S2R+ cells. The MeRIP and miCLIP tracks of m⁶A positions are shown below. The gene architecture of *fl(2)d* is shown at the top, with thin blue boxes representing the 5' and 3' UTRs, thick blue boxes representing the CDS, and thin lines representing introns. Exon numbers are indicated at the top. Signals are displayed as read per kilobase per million mapped reads. **b)** Usage of different 5' splice sites in exon 1 of *fl(2)d* transcript and skipping of exon 2 upon different knockdowns. Splicing analysis by semi-quantitative RT-PCR using primers in exon 1 and 3 (red arrows in the scheme). ss1, splice site 1; ss2, splice site 2; ss3, splice site3 (adapted from Lence et al 2016).

A few putative m⁶A methylation sites were identified along the transcript, as shown by MeRIP and miCLIP tracks. The most prominent ones were located in the region between the 5' splice site two and three (ss2 and ss3, respectively) (**Figure 23a**). From the RNAseq data, we noticed that depletion of Mettl3, Mettl14, Fl(2)d proteins, or of the nuclear m⁶A reader Ythdc1, resulted in an increased use of downstream 5' splice site 3 (ss3) and in the exon 2 skipping (**Figure 23a**). We could confirm these results by RT-PCR and noticed that alternative splicing generates four major transcript isoforms. The use of 5' ss3 and alternative Ex2 skipping, which produces the longest isoform, is in fact a preferred splicing scenario in a control condition. Upon depletion of m⁶A methyltransferase complex subunits or of the nuclear reader protein, the use of ss1 or ss2 is further reduced (**Figure 23b**). This suggests that the

presence of m⁶A upstream of the ss3 might act as a mechanism to promote ss1 and ss2 usage or to block the ss3 selection, and in this way regulate formation of long vs. short protein isoform. In summary, we generated transcriptome wide m⁶A methylation map at a nucleotide resolution, which together with the results of differential splicing upon loss of m⁶A supports the involvement of m⁶A modification in the regulation of alternative pre-mRNA splicing. In addition, depletion of the nuclear Ythdc1 protein recapitulates splicing outcomes found upon depletion of m⁶A writer components and thus Ythdc1 likely mediates the splice site selection by binding to m⁶A sites.

4.4 Flies lacking m⁶A display severe locomotion defects

4.4.1 *Mettl3* and *Mettl14* mutant flies are viable, but flightless and die earlier

In order to reveal the importance of m⁶A modification in vivo during the course of fly development, we generated mutants for *Mettl3* and *Mettl14* using the CRISPR-Cas9 approach with two gRNAs targeting each of the genes (Figure 24a). To confirm the loss-of-function alleles, we generated antibodies against *Mettl3* and *Mettl14* and analysed fly lysates by western blot. No functional protein was detected neither in the *Mettl3* mutants lacking a large C-terminal part of the CDS including the catalytic core (*Mettl3^{Δcat}*) nor in the complete null allele (*Mettl3^{null}*). Similarly, no protein was detected in the homozygous mutants with a two-nucleotide frameshift deletion of *Mettl14* (*Mettl14^{fs}*) (Figure 24).

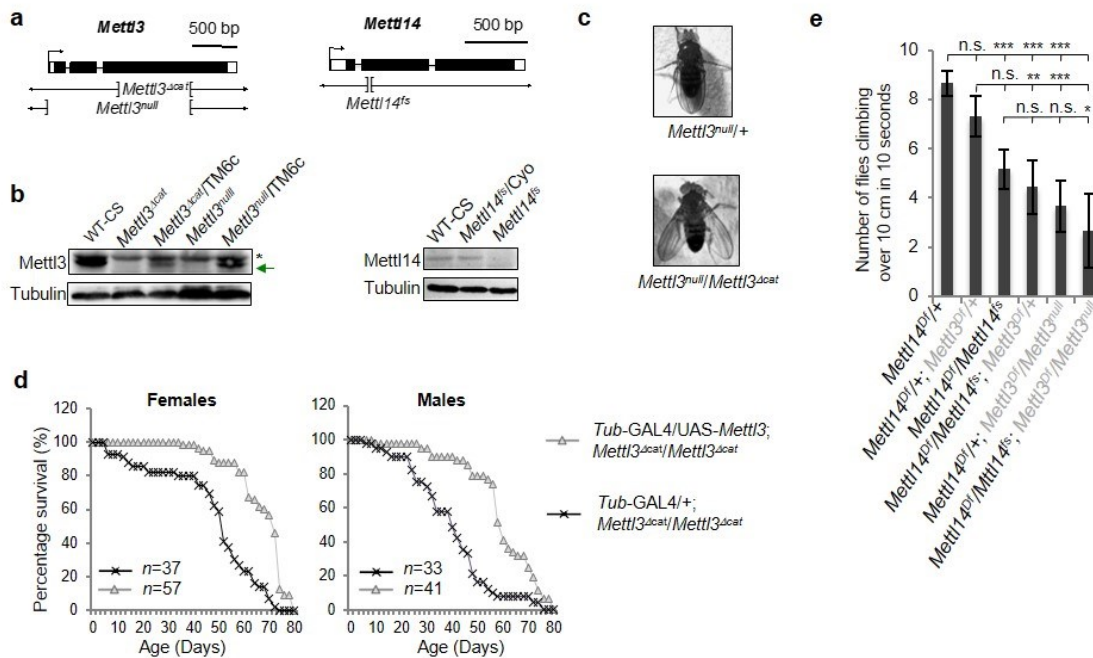


Figure 24. *Mettl3* and *Mettl14* mutant flies are viable, but flightless and die earlier.

a) Schematic of gene loci with indicated deletions for *Mettl3* (left) and *Mettl14* (right). **b**) Validation of loss-of-function alleles for *Mettl3* and *Mettl14* mutants. Protein lysates from control and *Mettl3* (left) and *Mettl14* (right) mutant flies were analysed by western blot using respective antibodies raised against endogenous proteins. Arrow indicates position of *Mettl3* protein size; star denotes unspecific background band (left). Tubulin was used as a loading control. **c**) Flies lacking *Mettl3* protein are flightless and display a held out wing phenotype. **d**) Charts representing a lifespan of female (left) and male (right) *Mettl3* mutant flies (in purple) as well as of *Mettl3* mutant flies expressing ectopically driven *Mettl3* cDNA (in green). **e**) Quantification of fly climbing by negative geotaxis experiment using flies lacking *Mettl3* and/or *Mettl14* proteins. Bars represent the mean \pm s.d. of female flies (n = 10 per condition) that climb over 10 cm in 10 s (six independent measurements). *P < 0.01; **P < 0.001; ***P < 0.0001; n.s., not significant (one-way ANOVA, Tukey's post-hoc analysis) (adapted from Lence et al 2016).

In addition, we generated *fl(2)d* mutant flies and, as shown before, loss of Fl(2)d subunit resulted in lethality with no adult fly survivors (Granadino et al. 1990, Granadino et al. 1996). Surprisingly, flies lacking *Mettl3* or *Mettl14* were viable and displayed no apparent lethality over the course of development. This was in contrast to studies from vertebrates and plants, where depletion or loss of *Mettl3* or *Mettl14* is detrimental during early embryogenesis. (Zhong et al. 2008, Bodi et al. 2012, Wang

Y. et al. 2014, Chen T. et al. 2015, Geula et al. 2015, Meng et al. 2019). Despite these differences, *Mettl3* and *Mettl14* mutant flies exhibited strong locomotion defects that resulted in compromised ability to climb and fly. In addition we observed the appearance of a held-out wing phenotype, resulting from inability to properly close wings over the dorsal body surface (**Figure 24c**). Moreover, mutant male and female flies had a reduced lifespan, as shown for *Mettl3^{null}* allele, which could be rescued by ectopic expression of UAS-*Mettl3* cDNA driven by ubiquitous (*tubulin-GAL4*) driver (**Figure 24e**).

4.4.2 Loss of m⁶A leads to altered neuronal functions

Mettl3 and *Mettl14* mutant flies displayed altered behaviour. To test their locomotion systematically, we performed a negative geotaxis assay, in which flies of selected genotypes were collected in a measuring cylinder and briefly tapped to the bottom. Their climbing ability towards the top was assayed as the number of flies that crossed a defined distance threshold ($d=10$ cm) over the chosen time course ($t=10$ sec). We tested flies lacking either *Mettl3*, *Mettl14* or both proteins in various combinations. While flies missing only one copy of each methyltransferase performed well, every additional removal of *Mettl3* or *Mettl14* resulted in a gradually reduced climbing ability, with double homozygous flies displaying strongly altered climbing (**Figure 24e**). This indicated that sufficient levels of m⁶A modification are required for unaltered locomotion processes. To assess locomotion defects more precisely, we next performed the Buridan paradigm experiment in which the movement of an individual fly in a closed arena is video-tracked over a 15-minute interval. We analysed the walking speed, orientation and activity of control flies, *Mettl3^{Acet}* mutant flies and *Mettl3^{Acet}* mutant flies rescued by ectopic expression of UAS-*Mettl3* cDNA driven by either ubiquitous (*tubulin-GAL4*), pan-neuronal (*elav-GAL4*), or mesoderm specific driver (*24B-GAL4*). Strikingly, all three parameters were strongly altered in mutant flies (**Figure 25a, b and c**). Walking speed was decreased nearly three-fold in comparison to control flies and we were able to completely rescue this defect by ubiquitous or neuronal expression of *Mettl3*, but not by its expression in mesoderm (**Figure 25a**). Likewise, we could restore altered orientation (**Figure 25b**) and activity (**Figure 25c**), indicating that the observed phenotypes were specific to the loss of functional *Mettl3*. Given the strong locomotion defects observed upon loss of m⁶A modification in adult flies, we focused on characterising molecular causes, contributing to this phenotype. We carried out a transcriptome analysis of fly heads from wild type flies and *Mettl3^{Acet}* mutants. A large number of genes was differentially regulated or differentially spliced upon loss of m⁶A ($n=1681$, $FDR<0.05$). Notably, among affected genes 39 % were identified as m⁶A targets in our miCLIP dataset from S2R+ cells and many of those have been previously linked to processes of locomotion and axon guidance ($n=62$) (**Figure 26**) (**Supplemental data 3**). Thus, upon loss of m⁶A modification, a combinatorial effect of various misregulated genes might lead to the observed locomotion phenotype.

Several misregulated genes were previously shown to be required for synapse functionality and for development of larval neuromuscular junctions (NMJ) (e.g. *babo*, *futsch*, *CASK*). We therefore wanted to investigate if neuronal alterations also occur during earlier stages of fly development and analysed neuro-muscular junctions (NMJ) of the late L3-stage larvae. Control and *Mettl3^{null}* larvae were dissected and immunostained with anti-DLG (disc-large, postsynaptic marker), anti-Synaptotagmin (presynaptic marker) and HRP (neuronal membrane marker) to visualize the synaptic connections between motoneurons and muscles, or so-called synaptic boutons. We found a significant increase in the number of boutons per muscle surface area in *Mettl3^{null}* mutant larvae (**Figure 25d**), pointing towards the potential importance of *Mettl3* and m⁶A modification for the synapse growth and possibly

for its functionality. Altogether, these results reveal the importance of m⁶A modification in neuronal functions that control fly locomotion and synapse development.

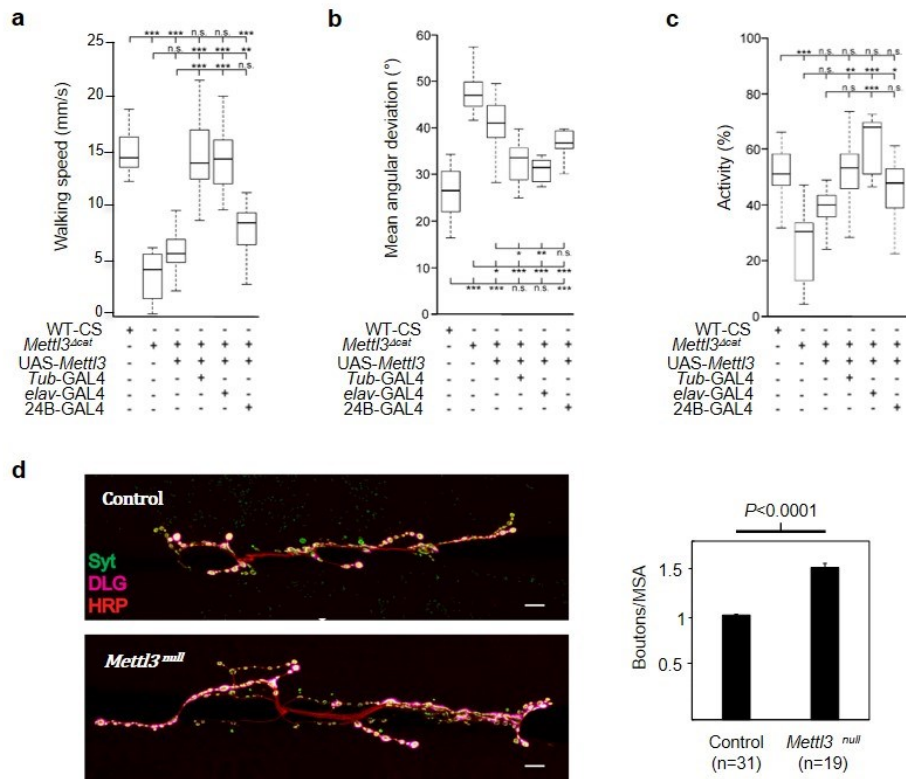


Figure 25. Mutant flies lacking m⁶A display severe locomotion defects due to altered neuronal functions.

a-c) Walking behaviour of Canton-S wild type (WT-CS), *Mettl3^{Δcat}* mutant flies or *Mettl3^{Δcat}* mutant flies expressing *Mettl3* cDNA ubiquitously (*Tub-GAL4*), in neurons (*elav-GAL4*) or in muscles (*24B-GAL4*) analysed by Buridan’s paradigm. Box plots representing **(a)** walking speed, **(b)** orientation, as measured by median angular displacement from the direct approach to one of the stripes, and **(c)** activity, assayed by median fraction of time spent walking during a 15 min test period, of indicated females (n = 15 per condition). Boxes signify 25 %/75 % quartiles, thick lines indicate medians, and whiskers show maximum interquartile range × 1.5. n.s. not significant, *P < 0.05, **P < 0.01, ***P < 0.001 (Kruskal–Wallis analysis of variance with a Bonferroni correction). WT-CS, wild-type Canton-S flies. **d)** Left, Representative confocal images of muscle-6/7 NMJ synapses of abdominal hemisegment A3 for the indicated genotypes labelled with anti-DLG (magenta), anti-Synaptotagmin (green) and HRP (red) to reveal the synaptic vesicles and the neuronal membrane. Right, Quantification of normalized bouton number (total number of boutons/muscle surface area (μm² × 1,000)) of NMJ 6/7 in A3 of the indicated genotypes (right). Error bars show mean s.e.m. P-values were determined with a Student’s t-test. The number of boutons are increased upon *Mettl3* knockout. MSA, muscle surface area (adapted from Lence et al 2016).

4.5 m⁶A modification modulates splicing of *Sex lethal* (*Sxl*)

Another important gene among the top differentially spliced transcripts that caught our attention was *Sex lethal* (*Sxl*). *Sxl* protein is a major regulator of sex determination and dosage compensation in *D. melanogaster*. Its transcript can be alternatively spliced in male and female specific isoforms that differ by the presence of a male specific alternative exon (L3), which introduces a premature stop codon. Therefore, a functional protein is only formed in females, but not in males. *Sxl* auto-regulates its own splicing by binding to flanking introns and preventing L3 exon inclusion. As an RNA binding protein *Sxl* also controls splicing and translation of downstream targets required for female physiognomy and behaviour, and prevents initiation of dosage compensation, thereby allowing female survival (see introduction: *Chapter 1.5.2*).

We analysed the transcriptome from adult female heads and noticed a significantly increased inclusion of L3 exon in *Mettl3* mutant flies, but not in control flies, indicating inefficient repression mechanisms upon loss of m⁶A modification (**Figure 26b**). We confirmed these results by performing an RT-PCR, using primers against L3-flanking exons L2 and L4. Notably, we observed decreased levels of female specific *Sxl* isoform and the appearance of male specific *Sxl* isoform in heads from female mutant flies lacking *Mettl3* or *Mettl14*, while *Sxl* splicing in males was not altered (**Figure 26c**). Thus, these results strongly indicated that m⁶A modification is required for proper splicing of *Sex lethal* transcript. Moreover, splicing of *Sxl* downstream targets, *msl-2* and *tra*, was also affected in mutant females, likely as a result of reduced levels of functional *Sxl* protein (**Appendix 1: ED Fig. 9b and c**).

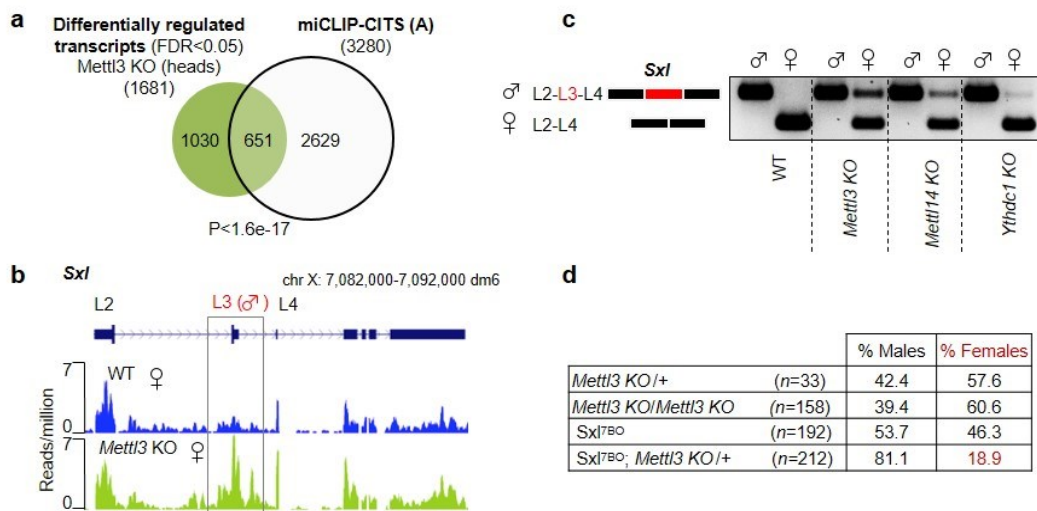


Figure 26. m⁶A modulates splicing of the master regulator of sex determination in *D. melanogaster*, *sex lethal* (*Sxl*).

a) The overlap of common differentially expressed or spliced transcripts in adult female heads lacking *Mettl3*, and of m⁶A modified transcripts. **b)** The UCSC Genome Browser screenshot of *Sex lethal* transcript (*Sxl*). Normalized RNA-seq data from control flies and *Mettl3* mutant flies are shown. The gene architecture is at the top, with thin blue boxes representing the 5' and 3'UTRs, thick blue boxes representing the CDS, thin lines representing introns, and L2, L3 and L4 representing exons. Signals are displayed as read per kilobase per million mapped reads. L3 denotes a male specific exon whose inclusion is highly enriched in *Mettl3* mutant females. **c)** Spliced isoforms of *Sxl* were monitored by semi-quantitative RT-PCR using RNA extracts from male and female heads. The genotypes used are indicated below. Loss of m⁶A or Ythdc1 reader protein leads to inclusion of male specific exon L3. **d)** Table displaying the percentage of males and females hatching for indicated genotypes. *Mettl3* interacts genetically with *Sxl* to control female survival (adapted from Lence et al 2016).

Flies lacking *Mettl3* or *Mettl14* showed no apparent lethality during development and the level of *Sxl* female isoform was only reduced but not absent. Given the importance of sufficient *Sxl* levels for female survival, we wondered if *Mettl3* and *Sxl* might genetically interact, as previously shown for other genes that mediate *Sxl* splicing (Moschall et al. 2017). To test this, we analysed female and male survival of *Mettl3* mutants in a sensitized background, where one copy of *Sxl* was removed. We crossed *Mettl3^{null}* females with *Sxl^{7BO}* males and counted numbers of hatched adult flies. As expected, flies lacking one or both copies of *Mettl3* showed no alterations in fly survival (Female: 57,6 % and 60,6 %, respectively). Likewise, loss of one copy of *Sxl* alone did not result in female lethality (46,3 %). In contrast, strong effect on female survival was observed when *Mettl3* and *Sxl* alleles were combined. Less than 19 % of female flies survived when one copy of *Mettl3* in addition to one copy of *Sxl* were removed (**Figure 26c**), indicating that there is a strong genetic interaction between m⁶A writer and *Sxl*. In conclusion, splicing of *Sxl* transcript is a process, highly regulated at multiple levels, where m⁶A modification acts along with other mechanisms in parallel pathways that altogether ensure sufficient levels of *Sxl* protein in female flies and prevent *Sxl* production in males.

4.6 *Ythdc1* mutants recapitulate defects observed upon loss of m⁶A

4.6.1 Loss of *Ythdc1* results in altered fly locomotion

We noticed severe behavioural defects (**Figure 24** and **Figure 25**) as well as changes in gene expression (**Figure 26**) in mutants lacking m⁶A modification. We therefore wondered if *Ythdc1* that I) also displayed enriched expression in neuroectoderm during embryogenesis (**Figure 15**), II) was shown to preferentially bind m⁶A modification (**Figure 19**) and III) shared most of common splicing defects with writer components in *D. melanogaster* S2R+ cells, could mediate m⁶A functions also in vivo. We therefore generated *Ythdc1* mutant flies using the CRISPR-Cas9 system and two gRNAs targeting the gene region (**Figure 27a**).

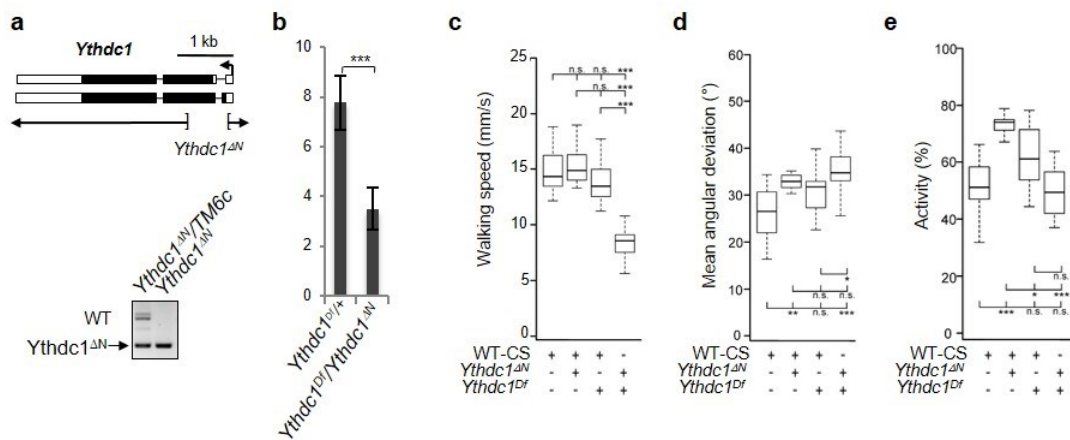


Figure 27. *Ythdc1* mutant flies recapitulate locomotion defects of m⁶A writer mutants.

a) Schematic of gene loci with indicated deletion for *Ythdc1*. Validation of loss of function allele for generated *Ythdc1* mutant (below). PCR using genomic DNA from heterozygous or homozygous *Ythdc1* mutant flies was loaded on agarose gel. Arrow indicates the size of an amplicon representing gene deletion. **b)** Quantification of fly climbing by negative geotaxis experiment using flies lacking *Ythdc1* protein. Bars represent the mean \pm s.d. of female flies ($n = 10$ per condition) that climb over 10 cm in 10 s (six independent measurements). *** $P < 0.0001$; n.s. (Student's t-test). **c-e)** Walking behaviour of control, heterozygous and trans-heterozygous *Ythdc1* mutant flies analysed by Buridan's paradigm. Box plots represent walking speed (**c**), orientation as measured by median angular displacements from the direct approach to one of the stripes (**d**) and activity, assayed by median fraction of time spent walking during a 15 min test period (**e**), of indicated females ($n = 15$ per condition). Boxes signify 25%/75% quartiles, thick lines indicate medians, and whiskers show maximum interquartile range $\times 1.5$. n.s., not significant; * $P < 0.05$, ** $P < 0.01$, *** $P < 0.001$ (one-way ANOVA, Bonferroni post-hoc analysis). WT-CS, wild-type Canton-S flies (adapted from Lence et al 2016).

A deletion within the 5'-end of the gene that removed two start codons of encoded isoforms was confirmed by PCR (**Figure 27a**, below). The *Ythdc1*^{ΔN} mutant flies were viable, but flightless and displayed walking defects, resembling the flies lacking *Mettl3* or *Mettl14*. We therefore analysed fly locomotion by a climbing assay, as described above, and strikingly, noticed that climbing ability of *Ythdc1*^{ΔN} mutants was strongly altered (**Figure 27b**). We next performed the Buridan paradigm and found that the walking speed of trans-heterozygous *Ythdc1*^{ΔN}/*Ythdc1*^{Df} flies was also significantly reduced (**Figure 27c**). Of note, heterozygous *Ythdc1*^{ΔN}/+ flies displayed significantly altered orientation and activity that were not recapitulated in the *Ythdc1*^{Df} deficiency line, thus these phenotypes are likely a result of an off-target effect caused by our CRISPR-Cas9 generated mutant (**Figure 27d, e**). In

summary, these results strongly indicated that the nuclear reader mediates m⁶A functions also in vivo, in regards to adult fly locomotion.

4.6.2 *Mettl3* and *Ythdc1* mutant flies regulate many common splicing events

Given that flies lacking either m⁶A writing components or the nuclear reader *Ythdc1* displayed similar behavioural defects we wanted to identify common molecular targets in vivo. We therefore performed the transcriptome analysis of wild type, *Mettl3*^{null} and *Ythdc1*^{ΔN} mutant adult flies and focused on differential splicing. Loss of *Mettl3* resulted in 397 differentially spliced transcripts and loss of *Ythdc1* in 489 (FDR<0.1). Many transcripts (n=243) were shared between flies lacking *Mettl3* (61 %) and *Ythdc1* (50 %) (**Figure 28a**), suggesting that *Ythdc1* likely regulates m⁶A dependent splicing, not only in S2R+ cells, but also in vivo. Among common transcripts, 70 % (n=170) were m⁶A modified in S2R+ cells, as shown by comparison with our miCLIP dataset (**Figure 28b**). Similarly to splicing alterations found in S2R+ cells, many transcripts displayed differential 5' splice site selection and intron retention. The major class of differentially spliced transcripts was, however, alternative exon skipping (**Figure 28c**). Importantly, *Sxl* whose splicing was shown to be affected in flies lacking *Mettl3*, was also altered in *Ythdc1*^{ΔN} female mutants (**Figure 28c**, last columns). We next analysed the gene ontology of selected 170 transcripts and found that they represented many distinct biological processes, such as cell differentiation, mRNA splicing, vesicle transport, as well as regulation of neurotransmitter transport and secretion (**Figure 28d**). Future work will be required to explore if any of misregulated transcripts contributes to observed neuronal and behavioural phenotypes of m⁶A mutants.

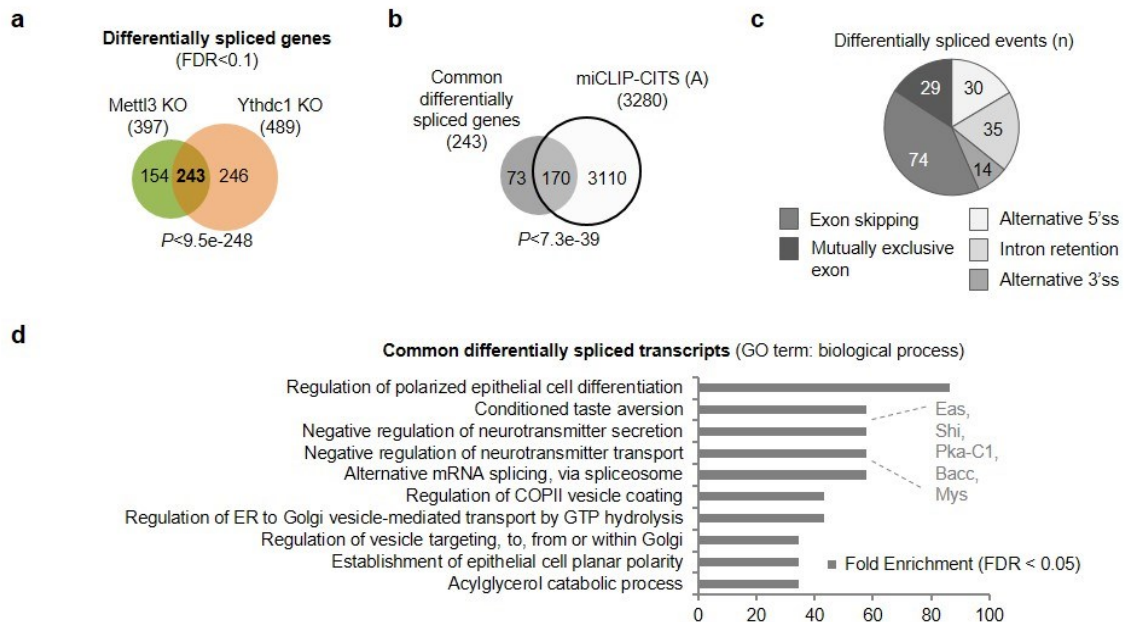


Figure 28. *Mettl3* and *Ythdc1* mutant flies regulate many common splicing events.

a) Venn diagram showing the overlap of differentially spliced transcripts in *Mettl3* and *Ythdc1* knockout flies. **b)** The overlap of common differentially spliced transcripts in flies lacking *Mettl3* or *Ythdc1* and transcripts likely carrying m⁶A modification. **c)** Pie chart showing distribution of differentially spliced events in common, methylated transcripts from (b). Most splicing events include exon skipping. **d)** Gene ontology (GO) analysis of common differentially spliced and methylated transcripts. Top ten terms for biological process are sorted by their fold enrichment (Tyanova et al. 2016). Targets related to neuronal processes are depicted on the right. (a – adapted from Lence et al 2016, b-d – unpublished data).

In summary, we generated mutant flies lacking m⁶A writer components and the nuclear *Ythdc1* that mediates functions of m⁶A modification in vivo via the regulation of alternative splicing. *Mettl3* mutant flies were viable but displayed severe locomotion defects due to impaired neuronal functions and flies lacking *Ythdc1* recapitulated these alterations. *Ythdc1* mutants also shared a substantial number of differentially spliced events with *Mettl3* mutant flies. Notably, among those was *Sxl*, supporting the role of m⁶A modification as an important factor in modulating the sex determination and dosage compensation pathways.

4.7 Nito is a novel component of the m⁶A writer complex

4.7.1 Ythdc1 interacts with splicing factors and with components of the m⁶A writer complex

Given that Ythdc1 regulates m⁶A-dependent splicing events, we wanted to further investigate the underlying mechanism by analysing the Ythdc1 protein interactome. Myc-tagged Ythdc1 was expressed in stable isotope labelled (SILAC) S2R+ cells and immuno-precipitated using anti-Myc antibody coupled to magnetic beads. Recovered proteins were subjected to mass spectrometry analysis, which identified 73 proteins with more than 2-fold enrichment over control in both, forward and reverse experiments (**Figure 29a**). Among them were many predicted mRNA binding proteins (**Supplemental data 1**).

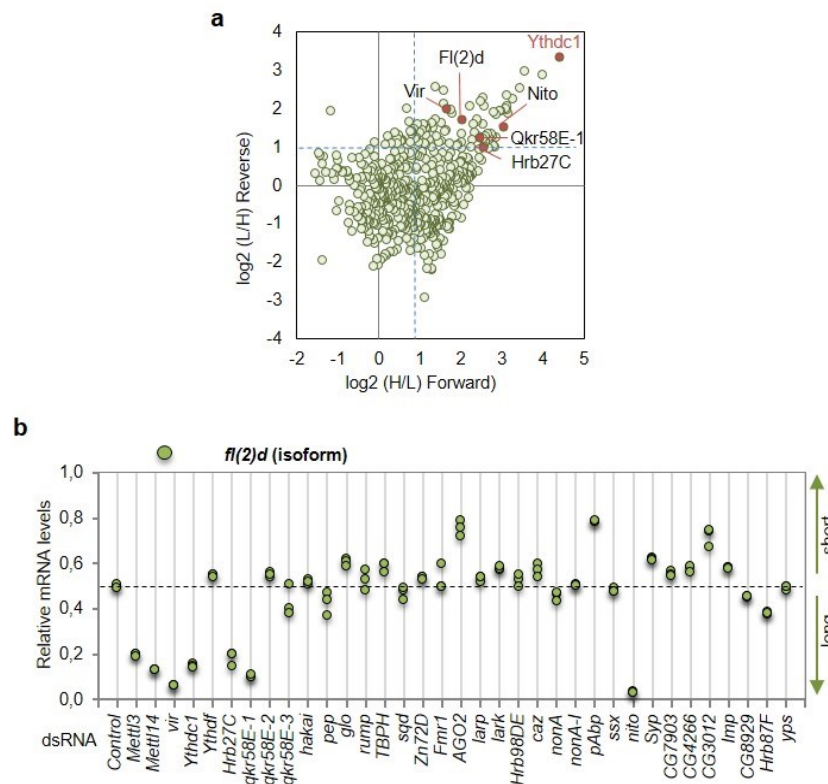


Figure 29. Ythdc1 interacts with many splicing factors and with components of the m⁶A writer complex.

a) SILAC-coupled mass spectrometry analysis using Ythdc1–Myc as a bait. Scatterplot of normalized forward versus inverted reverse experiments plotted on a log₂ scale. The threshold was set to a two-fold enrichment (blue dashed line). Proteins in the top right quadrant were enriched in both replicates. **b)** mRNA quantification of *fl(2)d* isoforms after knockdown of identified Ythdc1-interacting proteins. Four proteins, Hrb27C, Qkr58E-1, Vir and Nito, in addition to m⁶A components, control *fl(2)d* splicing in the same direction. Data points of three technical replicates are shown (adapted from Lence et al 2016).

To identify proteins that might be required for m⁶A-dependent splicing regulation we depleted all candidates in S2R+ cells and analysed splicing outcomes of a previously described transcript *fl(2)d* (**Figure 23d and e**). Depletion of m⁶A, or of the nuclear reader protein, resulted in increased formation of a long *fl(2)d* isoform and we found that depletion of four other proteins, Hrb27c, Qkr58E-1, Vir and

Nito, also altered splicing in the same direction (**Figure 29b**), indicating that they might mediate some of m⁶A-regulated splicing events together with Ythdc1. We next tested the splicing outcomes of other transcripts, with known m⁶A-dependent spliced isoforms from our transcriptome datasets (e.g. *Hairless*, *Aldh-III*, *Dsp1*, *CG8929*, *hts*) (**Supplemental data 5 - 7**). Qkr58E-1 and Hrb27C were not required for the regulation of all splicing events (**Figure 30a**), suggesting that in order to regulate splicing, Ythdc1 likely binds m⁶A and recruits (or interacts with) distinct RBPs, depending on the sequence constraints of a given transcript. Notably, we could confirm that the interaction between Ythdc1 and Qkr58E-1 was RNase independent, via a co-immunoprecipitation experiment (**Figure 30b and c**). However, we did not observe binding of Ythdc1 to Hrb27c (**Figure 30b**), suggesting that either interaction is too weak, or that Hrb27c might also act independently of Ythdc1 to mediate splicing of some m⁶A modified transcripts.

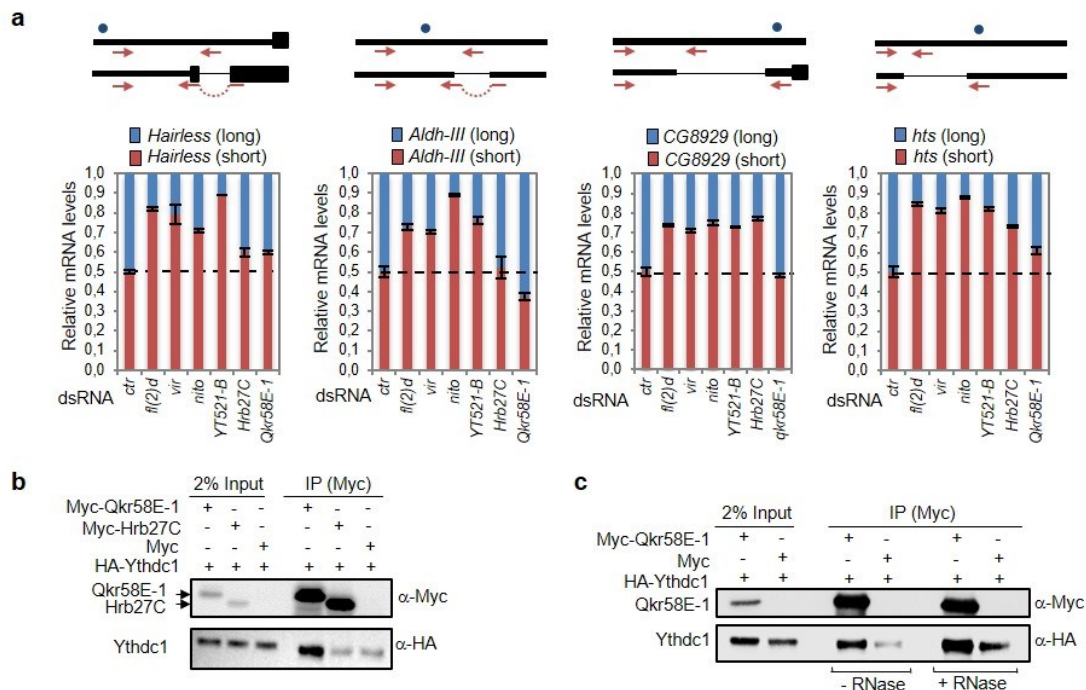


Figure 30. Ythdc1 regulates splicing of the m⁶A modified transcripts.

a) mRNA-isoform quantification of m⁶A-regulated transcripts including *Hairless*, *Aldh-III*, *CG8929*, *hts* upon knockdown of indicated components. Nito controls m⁶A splicing events. The quantification of three technical replicates from two biological experiments is shown as mean \pm s.d. Schematic representation of alternatively spliced transcript regions (5' \rightarrow 3' orientation) is shown above each graph. Blue dots indicate locations of m⁶A and red arrows indicate primer pairs used for RT-qPCR. **b**) Co-immunoprecipitation studies were carried out with lysates prepared from S2R+ cells co-expressing Myc-Qkr58E-1, Myc-Hrb27C and HA-Ythdc1. For control, S2R+ cells were transfected with Myc alone and HA-Ythdc1. Myc-containing proteins were immunoprecipitated using anti-Myc antibody and then immunoblotted with anti-Myc and anti-HA antibodies. **c**) Co-immunoprecipitation of Myc-Qkr58E-1 with HA-Ythdc1 with or without RNase T1. Extracts from S2R+ cells expressing HA-Ythdc1 either with Myc control or with Myc-Qkr58E-1 were immunoprecipitated using anti-Myc antibody. Expression of indicated proteins was monitored by immunoblotting using anti-Myc and anti-HA antibodies (adapted from Lence et al 2016).

4.7.2 Nito and Vir are conserved components of the writer complex

Interestingly, loss of Nito and Vir consistently altered splicing of all transcripts we tested (**Figure 30a**), reminiscent of the loss of m⁶A writer components. Both proteins were previously identified as regulators of *Sxl* splicing (Moschall et al. 2017), suggesting that they might interact with other subunits of the m⁶A writer complex and potentially be constituents of the nearly 1 MDa big methyltransferase

complex (Bokar et al. 1994, Bokar et al. 1997). Notably, depletion of vertebrate ortholog, VIRMA, was shown to reduce m⁶A levels on mRNA in mouse and human cells (Schwartz et al. 2014b), supporting the possibility that the role of Vir in m⁶A pathway could also be conserved in flies. To address this, we first tested if Nito and Vir interact with other components of the writer complex. Indeed, we could co-immunoprecipitate both proteins with FI(2)d in an RNase independent manner (**Figure 31a**).

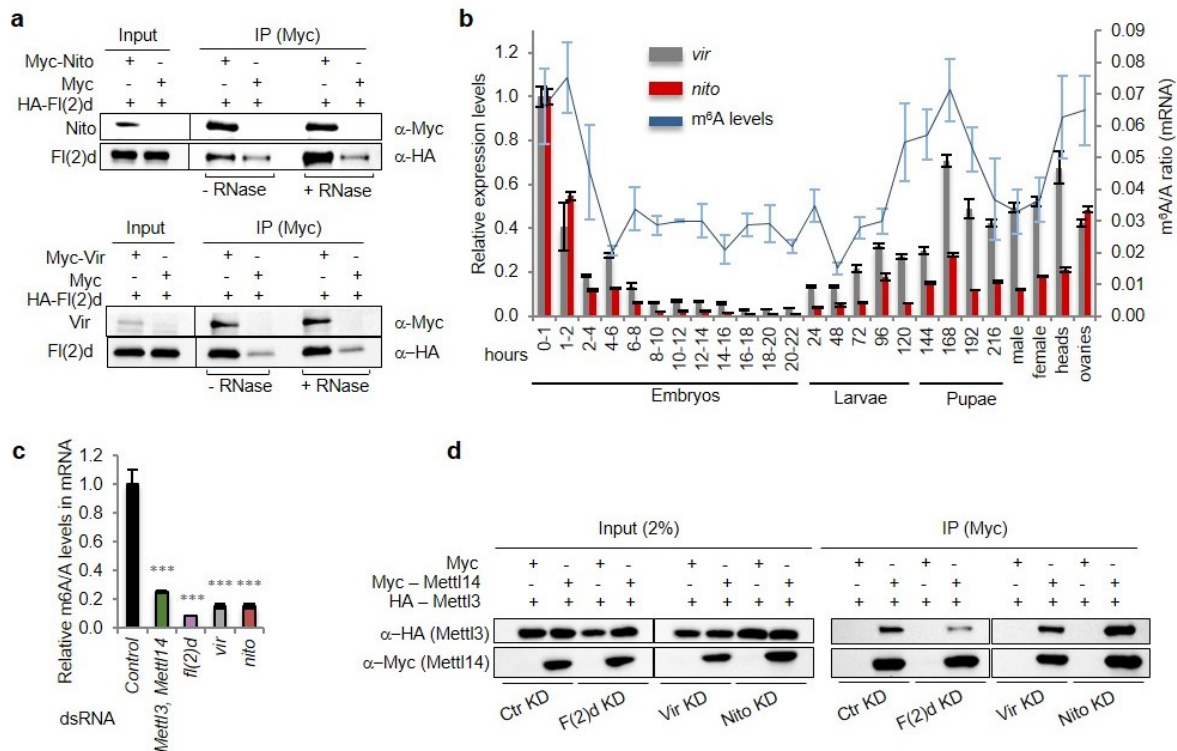


Figure 31. Nito and Vir are new, conserved components of the writer complex.

a) Co-immunoprecipitation of Nito (top) and Vir (bottom) with FI(2)d protein. Extracts from S2R+ cells expressing HA-tagged FI(2)d protein together with Myc alone, Myc–Vir or Myc–Nito were immunoprecipitated using Myc-specific beads. Expression of indicated proteins was monitored by western blot analysis using anti-Myc and anti-HA antibodies. RNaseT1 treatment before immunoprecipitation is indicated at the bottom. Nito and Vir interact with FI(2)d in an RNase independent way. **b**) Relative expression of *nito* and *vir* transcripts during *D. melanogaster* developmental stages and in adult female heads and ovaries, analysed by qRT-PCR. Levels of m⁶A modification were analysed in the same mRNA samples using LC-MS. Methyltransferase components and m⁶A levels are enriched during first hours of embryogenesis, during early pupation as well as in adult heads and ovaries. Bars and line junctions represent the mean ± standard deviation (s.d.) of three technical measurements from three biological replicates. **c**) LC–MS/MS quantification of m⁶A levels in mRNA samples depleted for indicated proteins. Bar chart represents the mean ± standard deviation (s.d.) of three technical measurements from three biological replicates. ***P < 0.0001 (one-way analysis of variance (ANOVA), Tukey’s post-hoc analysis) are shown. Depletion of all components of the methyltransferase complex leads to significant reduction of m⁶A levels on mRNA. **d**) Co-immunoprecipitation studies were carried out with lysates prepared from S2R+ cells co-expressing Myc–tagged Mettl14 and HA–tagged Mettl3 upon control (Ctr) FI(2)d, Vir or Nito knockdown. For control experiments, S2R+ cells were transfected with Myc alone and HA–tagged Mettl3. Lysates were immunoprecipitated using anti-Myc antibody and then detected with anti-Myc and anti-HA antibodies. Knockdown of FI(2)d, but not Nito or Vir, weakens the interaction between Mettl3 and Mettl14 (adapted from Lence et al 2016 Nature).

Additionally, we analysed their expression profiles during *D. melanogaster* developmental stages and observed that they were remarkably similar to the distribution of m⁶A modification. Highest levels were observed in the very first hour of embryogenesis and a steep decrease was seen in the next few hours, and over the following stages of embryogenesis (**Figure 31b**). Recapitulating m⁶A levels, *nito* and

vir peaked again during pupation (168 hours), with levels of *vir* being more pronounced and also higher in remaining stages of pupation, as well as in adults and in fly heads. Like other known components of the writer complex, both transcripts were also highly expressed in ovaries (**Figure 16**), further suggesting their role within the m⁶A complex.

To unambiguously examine, if the two identified proteins are components of the m⁶A writer complex, we analysed m⁶A abundance by LC-MS/MS in mRNA samples from S2R+ cells depleted for Nito, Vir or other known components of the complex. Strikingly, m⁶A levels were significantly reduced in either of the knock down (**Figure 31c**). This strongly supported that Vir and Nito proteins are indeed novel fly components of the m⁶A writer complex, essential for efficient methylation. Importantly, paralleling our findings, two vertebrate orthologs of Nito, RBM15 and RBM15B were also found to be required for m⁶A methylation in human and mouse cells (Patil et al. 2016), highlighting that the complex is likely evolutionary conserved.

To understand how the proteins might interact with each other and affect the complex assembly we depleted Fl(2)d, Vir and Nito in S2R+ cells and assessed the binding between the Mettl3-Mettl14 heterodimer by a series of co-immunoprecipitation experiments. Surprisingly, while knock down of Fl(2)d strongly reduced the interaction between the two methyltransferases, loss of Vir or Nito had no effect (**Figure 31d**). This suggested that Fl(2)d, Nito and Vir proteins may have independent roles within the complex, with Fl(2)d likely stabilizing the Mettl3-Mettl14 heterodimer formation. Importantly, several structural and biochemical studies demonstrated a strong interaction between Mettl3 and Mettl14 proteins in vertebrates and our interactome analysis of Mettl3 protein identified Mettl14 as by far most enriched protein (**Supplemental data 1**), thus further work will be required to explain the apparent destabilisation of the heterodimer upon Fl(2)d depletion in flies. In our current study, we used a co-immunoprecipitation assay, which is not a quantitative method and we ectopically overexpressed tagged proteins. Ideally, similar immunoprecipitation experiments should be performed with endogenous Mettl3 and Mettl14 proteins in either control, Fl(2)d, Nito or Vir depleted condition and by using a quantitative mass spectrometry analysis for the analysis of recovered proteins.

4.8 Flacc is required for m⁶A deposition as a component of the MACOM complex

4.8.1 Nito interacts with many proteins linking m⁶A to transcription and mRNA processing

Deposition of m⁶A modification on mRNA requires nearly 1 MDa methyltransferase complex that has been first described in the 1990s (Bokar et al. 1994, Bokar et al. 1997). Notably, Bokar and colleagues carried out cell fractionation and gel filtration experiments and proposed the existence of two sub-complexes of ~200 kDa and ~800 kDa, however, Mettl3, carrying the catalytic activity, was the only identified subunit at the time. Chuang He and colleagues later confirmed the existence of this large complex by performing similar fractionation followed by mass spectrometry analysis. They also identified additional proteins of the complex, Mettl14 and WTAP (Liu et al. 2014). Follow-up studies by numerous laboratories, including ours, contributed to the identification of further subunits; VIRMA (Vir) and RBM15 (Nito) (Schwartz et al. 2014b, Lence et al. 2016, Patil et al. 2016). Nevertheless, a protein complex composed of these five conserved subunits; Mettl3, Mettl14, Fl(2)d (WTAP), Vir (VIRMA) and Nito (RBM15), would still not add up to a 1 MDa size. This suggested that either other unknown components were yet to be discovered, or else that some of the proteins were present in multiple copies. To identify potential new constituents we decided to search for Nito interacting proteins in *D. melanogaster* S2R+ cells. Myc-tagged Nito protein was expressed in SILAC labelled cells and immunoprecipitated using anti-Myc antibody coupled to magnetic beads. Recovered proteins were subjected to mass spectrometry analysis and 39 proteins with >1.5-fold enrichment over control were identified (**Figure 32a**, top). Importantly, Fl(2)d and Vir were among top hits and many other enriched proteins were involved in mRNA processing and in the regulation of transcription (**Figure 32a**, bottom). One of the candidates that caught our attention was CG7358 that was not yet described in *D. melanogaster*. However, its closest vertebrate ortholog, ZC3H13, was previously found as a strong interacting partner of WTAP (Horiuchi et al. 2013) in several human cell types, yet its link to m⁶A function was not investigated.

4.8.2 Flacc is required for m⁶A deposition

To investigate the potential role of CG7358 in the m⁶A pathway, we first validated interactions of CG7358 with other components of the m⁶A-complex by co-immunoprecipitation. FlagMyc-tagged CG7358 could efficiently precipitate HA-tagged Nito, Fl(2)d and Vir (**Figure 32b and Appendix 2: Fig. S3A, B**) in an RNase independent manner. The CG7358 protein was therefore renamed into **Flacc**, standing for “Fl(2)d-associated complex component”. To see if Flacc was also required for m⁶A methylation, we depleted the protein along with other m⁶A writer components in the S2R+ cells and analysed changes of m⁶A levels on mRNA using LC-MS/MS analysis. Indeed, depletion of Flacc significantly reduced m⁶A levels to a similar extent as knock down of other components (**Figure 32c**).

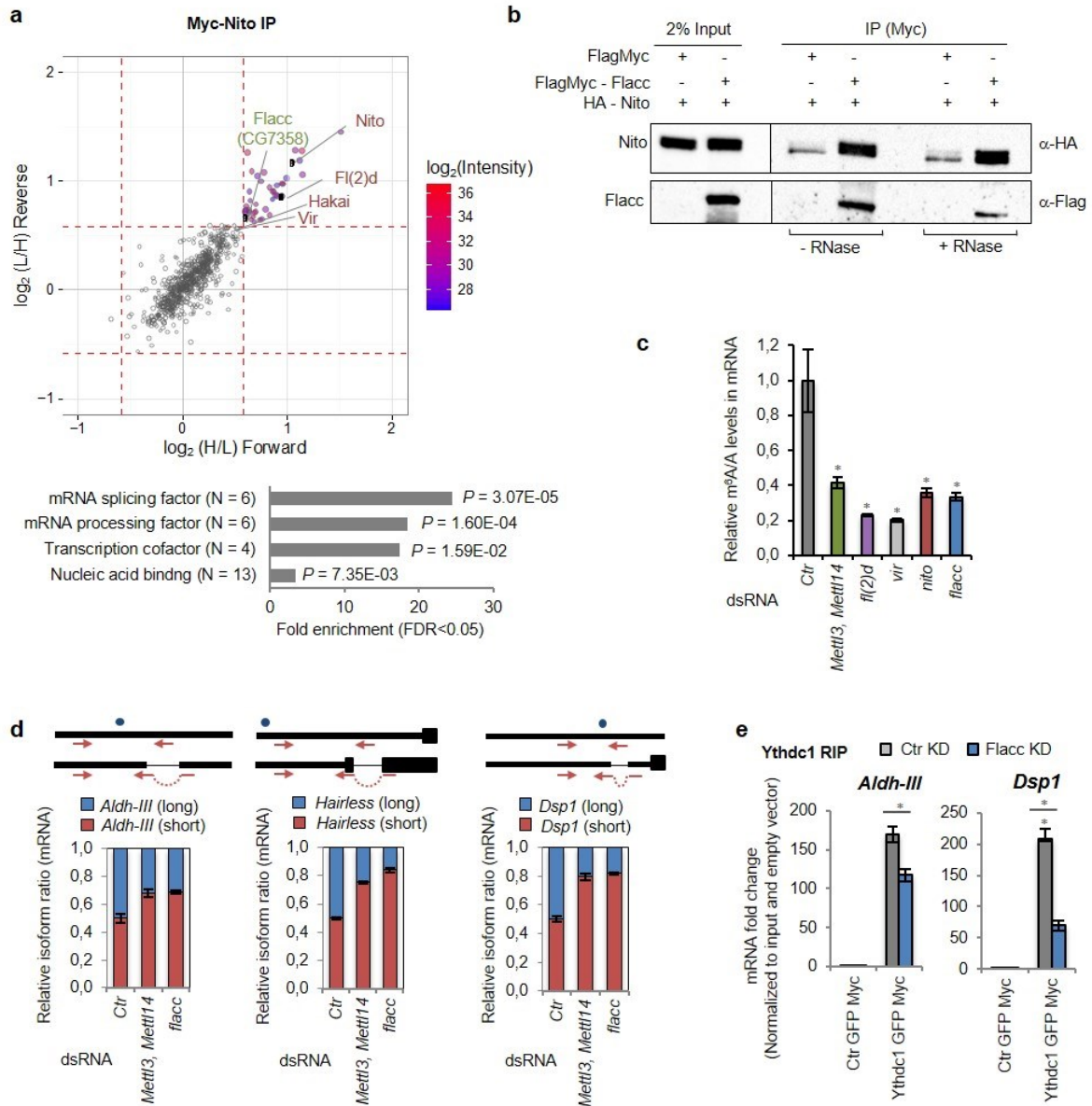


Figure 32. Flacc is required for m⁶A deposition and regulates m⁶A dependent events.

a) SILAC-coupled mass spectrometry analysis using Nito–Myc as a bait. Scatterplot of normalized forward versus inverted reverse experiments plotted on a log₂ scale. The threshold was set to 1,5-fold enrichment (red dashed line). Proteins in the top right quadrant were enriched in both replicates. Gene ontology (GO) term analysis (Tyanova et al. 2016) for enriched proteins is shown below. **b)** Co-immunoprecipitation experiments were carried out with lysates prepared from S2R+ cells transfected with FlagMyc-tagged Flacc and HA-tagged Nito. In control lanes, S2R+ cells were transfected with FlagMyc alone and an identical HA-containing protein. Extracts were immunoprecipitated with anti-Myc antibody and immunoblotted using Flag and HA antibodies. Two percent of input was loaded. The same experiment was repeated in the presence of RNaseT1. Nito and Flacc interact with each other in an RNA-independent manner. **c)** LC-MS/MS quantification of m⁶A levels in either control samples or mRNA extracts depleted for the indicated proteins in S2R+ cells. The bar chart shows the mean of three biological replicates and three independent measurements. Error bars indicate mean ± s.d. (*) P < 0.01, Student's t-test. Knockdown of all indicated proteins significantly reduces m⁶A levels. **d)** Relative isoform quantification of m⁶A-regulated genes (*Aldh-III*, *Hairless*, and *Dsp1*) upon depletion of the indicated components. Error bars represent mean ± s.d. Flacc is required for m⁶A-dependent splicing events. Schematic representation of alternatively spliced transcript regions (5' → 3' orientation) is shown above each graph. Blue dots indicate locations of m⁶A and red arrows indicate primer pairs used for RT-qPCR. **e)** Fold enrichment of m⁶A-regulated transcripts (*Aldh-III* and *Dsp1*) over input in Myc-Ythdc1 RIP after control or Flacc depletion. The bar chart shows the mean of three biological replicates. Errors bars indicate mean ± s.d. (*) P < 0.01; (**) P < 0.001, Student's t-test. Loss of Flacc affects Ythdc1 binding to m⁶A modified transcripts (adapted from Knuckles 2018 G&D).

Additionally, Flacc was required for proper splicing of m⁶A-regulated transcripts, *Aldh-III*, *Hairless* and *Dsp1* (**Figure 32d**) and its depletion resulted in a compromised binding of nuclear reader protein Ythdc1 to methylated sites of *Aldh-III* and *Dsp1* targets (**Figure 32e**), consistent with reduced levels of m⁶A. In parallel to our study in flies, we initiated a collaboration with a laboratory investigating the role of Rbm15 in mouse embryonic stem cells (mESC) (Dr. Philip Knuckles and Prof. Marc Bühler at FMI, Basel). Using a similar approach, they aimed at identifying novel Rbm15 interacting partners and found Zc3h13 protein (closest Flacc ortholog). Importantly, Zc3h13 was, similarly to Flacc in flies, essential for m⁶A methylation in mESC, which strongly suggested that *D. melanogaster* Flacc and mouse Zc3h13 are novel, conserved m⁶A methyltransferase components (**Appendix 2: Fig. 1A, 2A-C** and **Appendix 2: Fig. S4**).

4.8.3 Flacc regulates similar transcriptome events as other m⁶A writer components

We next analysed m⁶A-dependent mRNA processing in a transcriptome wide manner, by performing RNA sequencing upon depletion of every component of the m⁶A writer complex in S2R+ cells. We observed a striking difference between transcriptome changes upon combined depletion of two methyltransferases or of any other component. While knock-down of Mettl3 and Mettl14 changed expression of 300 genes (FDR<0.1), depletion of other m⁶A writer components resulted in more pronounced effect, with over 1500 genes affected in each individual knock-down condition (**Figure 33a**, top). This suggested that Fl(2)d, Nito, Vir and Flacc possibly also regulate gene expression independently of m⁶A methylation, or that depletion of Mettl3 and Mettl14 proteins was not sufficient to recapitulate complete loss of m⁶A modification and corresponding transcriptome changes. Notably, Fl(2)d, Vir and Flacc proteins shared most of their differentially changed genes (94 %, 90 % and 88 %, respectively) with at least one other KD condition (**Figure 33a**, below), suggesting that they act in the same complex. Notably, Nito differed from other components by altering expression of more than 4000 genes. Of those, more than 50 % were unique, indicating that either Nito acts in some pathways independently of other components (see discussion *Chapter 5.1.3*) or that its depletion in S2R+ cells induced an off-target effect. Nevertheless, we found that 706 genes were commonly misregulated upon depletion of any of the four components (**Figure 33a**, below) and these genes changed their expression in the same direction, as demonstrated by the heat map clustering (**Figure 33b**).

Given the similar transcriptome changes observed upon Fl(2)d, Vir, Nito and Flacc depletions, and the fact that the four proteins interacted with each other, as assayed by immunoprecipitation experiments, we reasoned that they likely constitute a protein complex independently of the Mettl3/Mettl14 heterodimer. This would be consistent with previous studies from fractionation and gel filtration experiments in human cells, where two sub-complexes of ~200 and ~800 kDa were shown to be required for m⁶A deposition on mRNA (Bokar et al. 1994, Bokar et al. 1997, Liu et al. 2014). We therefore proposed that the smaller complex represents the stable Mettl3/Mettl14 heterodimer, which we named “MAC” (stated for m⁶A-METTL complex). The larger complex that is composed of Fl(2)d, Vir, Nito, Flacc and potentially additional subunits, was named as MACOM (MAC-associated complex). As shown from the analysis of m⁶A levels, all MAC and MACOM components are required for efficient mRNA methylation (**Figure 32c**). In the following analysis, we focused on the 706 common misregulated transcripts of the MACOM complex and compared them with our miCLIP dataset. Surprisingly, among 253 common up-regulated genes, the majority (80 %, n=203) were methylated (**Figure 33c**, left) and significantly longer than all expressed genes (**Figure 33c**, right). This was consistent with our initial

observations where misregulated genes upon depletion of Mettl3, Mettl14 and nuclear reader Ythdc1 were analysed (**Figure 21b**). In contrast, only 51 % of all common down-regulated genes (n=164) were methylated and only marginally longer than all expressed genes (**Figure 33d**). Thus, it is possible that many down-regulated genes were affected indirectly and that loss of m⁶A in S2R+ cells more likely leads to gene up-regulation. Whether this is a consequence of attenuated transcription or results from reduced transcript turnover is currently not known and will have to be investigated in the future. Of note, our GO-term analysis demonstrated that down-regulated genes were enriched for metabolic processes, whereas up-regulated genes were enriched for embryonic development, epithelial cell differentiation and migration (**Appendix 2: Fig. 3F**), which was in line with our initial transcriptome analysis of S2R+ cells depleted for MAC components (**Appendix 1, ED Fig. 4**).

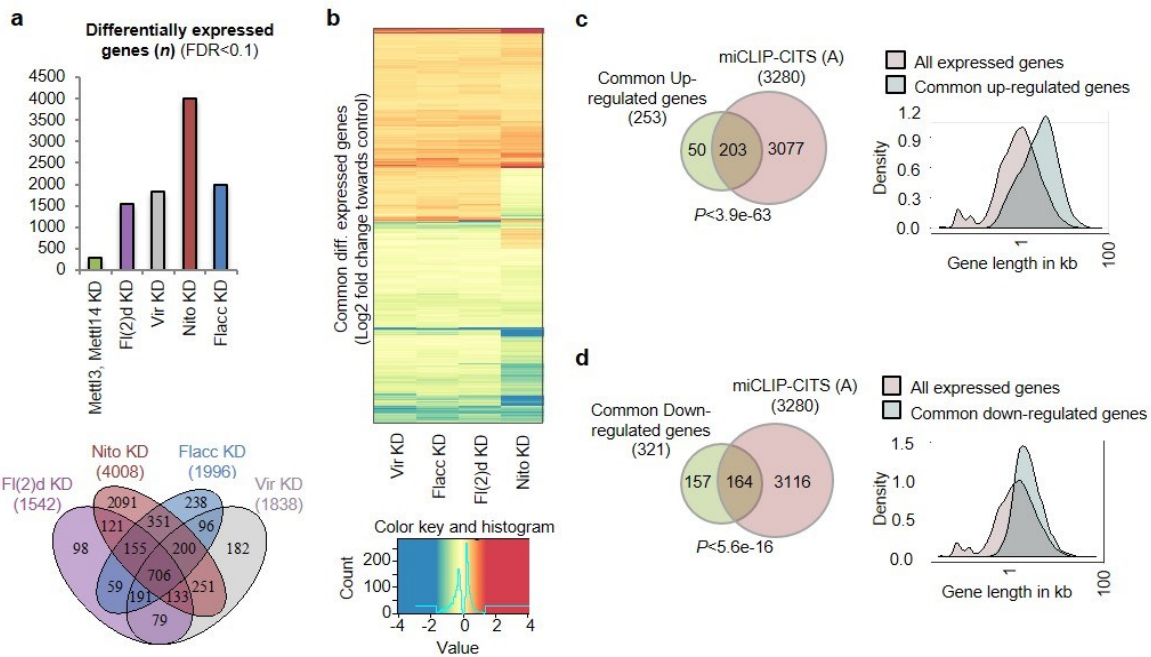


Figure 33. Depletion of Flacc results in similar transcriptome changes as depletion of other m⁶A writer components.

a) Number of differentially expressed genes (false discovery rate [FDR]) upon knockdown of indicated proteins and common differentially expressed targets regulated by components of MACOM (below). **b**) Fold change (log₂) expression of commonly mis-regulated genes. The heat map is clustered according to rows and columns. The colour gradient was adjusted to display the 1 % lowest/highest values within the most extreme colour (lowest values as the darkest blue and highest values as the darkest red). **c**) Overlap between common up-regulated genes and genes that are m⁶A modified (left). Probability density distribution of gene lengths for all genes tested in the differential expression analysis and genes that were up-regulated in all conditions. The distributions were compared using the Kolmogorov-Smirnov test. Most up-regulated genes are m⁶A modified and longer than all expressed genes. **d**) Overlap between common down-regulated genes and genes that are m⁶A modified (left). Probability density distribution of gene lengths for all genes tested in the differential expression analysis and genes that were down-regulated in all conditions. The distributions were compared using the Kolmogorov-Smirnov test. Less downregulated genes are m⁶A modified and their length is larger than length of all expressed genes, albeit to a lesser extent than up-regulated genes (adapted from Knuckles 2018 G&D).

4.8.4 Flacc regulates splicing of m⁶A modified transcripts

We next looked into our transcriptome data from S2R+ cells to analyse the role of Flacc on splicing regulation. More than 100 transcripts were differentially spliced upon combined depletion of Mettl3 and Mettl14, or upon depletion of Vir (**Figure 34a**). Knock-down of Flacc affected 256 genes, whereas depletion of Fl(2)d and Nito had an even more profound effect on over 600 genes with altered

splicing outcome (Figure 34a). Notably, 45 genes were common between all conditions, and belonged to neuron differentiation, cell morphogenesis and cell differentiation processes (Figure 34b). Among 45 common genes all but three were also methylated (Figure 34c), suggesting a role of m⁶A modification on splicing regulation. Most splicing events represented the alternative 5' splice site selection (n=23) or intron retention (n=15). This was consistent with our previous observations when Mettl3, Mettl14, Fl(2)d writer components and Ythdc1 were analysed (Figure 21d), and pointed towards the importance of m⁶A in this particular splicing decision. Of note, many alternative splicing sites were located within, or in close proximity of the 5'UTR regions where m⁶A modification is also highly enriched in *D. melanogaster*, as shown for example in *Dsp1*, *Aldh-III* and *Hairless* transcripts (Supplemental data 5-7).

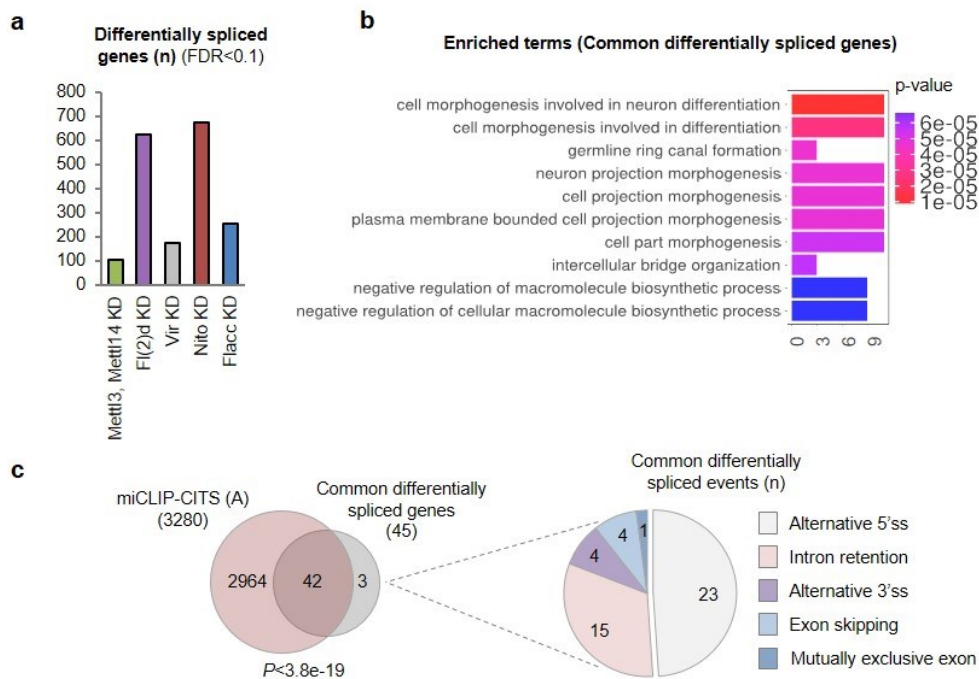


Figure 34. Depletion of Flacc leads to similar splicing changes as depletion of other m⁶A writer components.

a) Number of differentially spliced genes (false discovery rate [FDR]) upon knockdown of indicated proteins. **b**) The GO-term analysis of common differentially spliced genes performed using the package ClusterProfiler. The top 10 terms are displayed. **c**) Overlap between common differentially spliced genes and genes that are m⁶A modified (left). Pie chart showing distribution of common differentially spliced events. Most splicing events include alternative 5' splice site (5'ss) selection and intron retention (Figure 32 a) and b) - adapted from Knuckles 2018 G&D; Figure 32 c) – unpublished data).

4.8.5 Flacc is required for proper splicing of *Sex lethal*

Given that Flacc recapitulated transcriptome changes of other m⁶A writer components, we next wanted to address its role in vivo. We took advantage of two available fly lines carrying dsRNA against Flacc to perform a knock down in a tissue specific manner. We induced Flacc depletion in legs and genitalia discs using a *dome*-GAL4 driver. Strikingly, we noted appearance of male specific sex combs in female forelegs (red arrow), a typical evidence of female masculinization (Figure 35a). Additionally, flies were sterile and their genitalia showed severe transformations, with the appearance of male-like genital structures (red arrowheads). Likewise, depletion of Nito was previously shown to lead to the same type of transformations (Yan and Perrimon 2015) and was therefore used as a positive control.

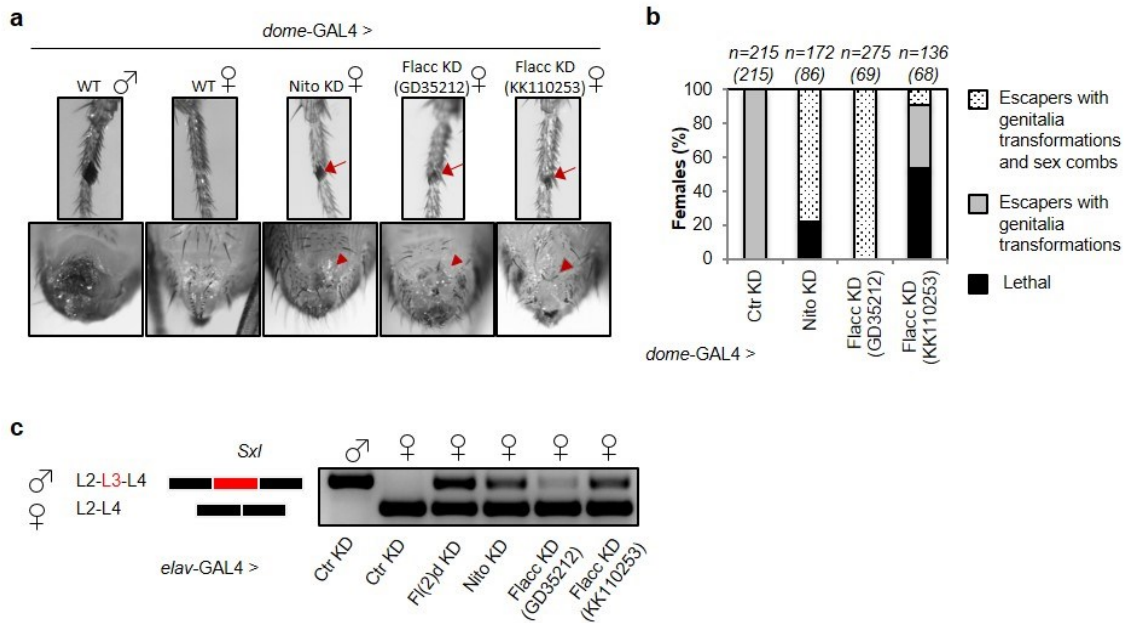


Figure 35. Flacc is required for proper splicing of *Sxl*.

a) *dome-GAL4*-driven expression of shRNA or dsRNA in genital discs and first pair of leg discs against Nito or Flacc, respectively. (Top) Forelegs of a wild-type male fly and female flies depleted for Nito or Flacc show the appearance of male-specific sex comb bristles (red arrow). (Bottom) Depletion of Nito or Flacc results in transformations of female genitalia and loss of vaginal bristles (red arrowhead). **b)** Quantification of female survival and transformations in escapers upon depletion of Nito or Flacc using the *dome-GAL4* driver. (n) The number of analysed flies with the expected number of escapers in brackets. Depletion of Nito and Flacc results in a high level of transformation in female genitalia and the appearance of male specific sex combs on forelegs. **c)** Semi-quantitative RT-PCR analysis of *Sxl* isoforms in male and female heads from flies depleted for Fl(2)d, Nito, or Flacc, respectively, using the *elav-GAL4* driver. Inclusion of male-specific exon L3 is observed in flies lacking m⁶A components (adapted from Knuckles 2018 G&D).

We next quantified the penetrance of the phenotype and observed that one of the dsRNA lines appeared to be stronger (KK110253) leading to 50 % female lethality and with escapers mostly showing genitalia transformations (**Figure 35b**). Using the other dsRNA line (GD35212) resulted in 100 % of female escapers with appearance of genitalia transformations and of male specific sex combs. Similarly, over 80 % of flies with reduced levels of Nito displayed both deformations, while remaining 20 % were lethal, pointing towards a strong requirement of Flacc and Nito proteins in sex determination and dosage compensation pathways. To understand, if observed female transformations and lethality were due to altered splicing of *Sxl*, we analysed RNA extracts from fly heads where either Fl(2)d, Nito or Flacc were depleted using neuronal driver *elav-GAL4*. Indeed, loss of m⁶A writer components lead to strong de-repression of male-specific L3 exon and the appearance of long, non-functional *Sxl* isoform in females (**Figure 35c**). This suggested that Flacc is required for regulation of *Sxl* splicing in vivo along with other m⁶A writer components, and its depletion has a profound effect on female physiognomy and survival.

4.8.6 Flacc stabilizes the interaction between Nito and Fl(2)d

We next wanted to untangle the precise role of Flacc within the methyltransferase complex. Flacc is a large protein (1150 aa) with many repeat regions and no determined structure (**Supplemental data 21**). It displays low homology to its human ortholog ZC3H13 (15,5 % identity) but shares one predicted

coiled-coil region that could be involved in protein-protein binding with other writer complex subunits. We wondered if Flacc could act as a stabilising component of the m⁶A writer complex and we therefore carried out co-immunoprecipitation experiments to systematically test interactions between different components upon depletion of Flacc in S2R+ cells. We previously showed that depletion of Fl(2)d protein, but not Nito or Vir, destabilized the formation of the Mettl3-Mettl14 heterodimer (**Figure 31d**). Depletion of Flacc did not affect this interaction (**Appendix 2: Fig. S8A**), indicating that Fl(2)d is likely the main interactor between MAC and MACOM sub-complexes. We next analysed the stability of the interaction between MACOM components. Flacc depletion had no effect on interactions between Nito protein and Vir, Mettl3 or Mettl14 (**Appendix 2: Fig. S8C, G and H, respectively**). However, we found that the binding of Nito to Fl(2)d was strongly compromised (**Figure 36a**). Since no other interaction between m⁶A writer components was altered in Flacc knock down condition, this indicated that Flacc is specifically required to mediate the binding between Fl(2)d and Nito, possibly to provide a functional link between MAC and MACOM for m⁶A deposition.

To confirm these results, we next tested the binding affinity of Fl(2)d and Nito proteins on known m⁶A modified targets, *Aldh-III*, *Hairless* and *Dsp1*, using RNA immunoprecipitation followed by RT-qPCR. It was previously shown that human ortholog, RBM15, is required for guiding the m⁶A-complex to sites of methylation, by direct recognition of U-rich regions in proximity of m⁶A sites (Patil et al. 2016). We therefore expected that upon Flacc depletion, binding of Fl(2)d to RNA might be more strongly compromised than binding of Nito to RNA. Indeed, upon Flacc KD Fl(2)d recovered significant less RNA as compared to control condition. On the other hand, only a mild decrease in RNA recovery was observed for Nito (**Figure 36b**). Surprisingly, we also found that Vir interacted with both, Nito and Fl(2)d proteins in an RNase independent manner (**Figure 31a** and **Appendix 2, Fig. S8C and E**). These interactions were not altered by Flacc depletion, yet the sole presence of Vir was not sufficient to replace the loss of Flacc in regards to Fl(2)d-Nito binding, consistent with the observation that knock down of Flacc leads to significant reduction of m⁶A levels on mRNA (**Figure 32c**). These results thus suggest that Flacc is indispensable for maintaining the stability of interaction between Fl(2)d and Nito. In the future it will be important to better characterise interactions between all components of the MACOM complex, ideally with purified proteins. In particular it is currently not clear which domains of Flacc are required for interactions with other proteins and whether its binding to Fl(2)d and Nito is indeed direct, or if other components, such as Vir, are also involved.

Given that all components of the m⁶A methyltransferase complex are conserved in higher eukaryotes, we wondered if the function of Flacc, as a stabilizing factor of the Fl(2)d-Nito interaction, might also be conserved for its vertebrate ortholog ZC3H13. We therefore cloned the human isoform of ZC3H13 in *D. melanogaster* expression vector (**Figure 36c**). We then assayed the binding between Fl(2)d and Nito in S2R+ cells upon depletion of Flacc, and a simultaneous ectopic expression of either the ZC3H13 protein or an empty vector. As expected, the interaction was strongly compromised in a control experiment, where only an empty vector was expressed. Strikingly, expression of human ZC3H13 protein could rescue the interaction between *D. melanogaster* Fl(2)d and Nito proteins (**Figure 36d and e**) indicating that, despite low sequence similarity (**Supplemental data 21**), both, Flacc and ZC3H13 proteins carry out a conserved stabilizing function in the MACOM complex assembly. Importantly, in collaboration with Prof. Marc Bühler's laboratory (FMI, Basel) we could also demonstrate that loss of Zc3h13 in mESC compromises the interaction between RBM15 and WTAP, which strongly supports our findings from flies (**Appendix 2, Fig. 6**). Notably, a parallel study characterizing the ZC3H13 protein in human cells showed that depletion of ZC3H13 does not alter interactions between any other components of the m⁶A complex (Wen et al. 2018). While this study

did not investigate the relevance of the RBM15, it is nevertheless possible that the interaction between RBM15 and WTAP is dependent on the presence of ZC3H13 also in human cells.

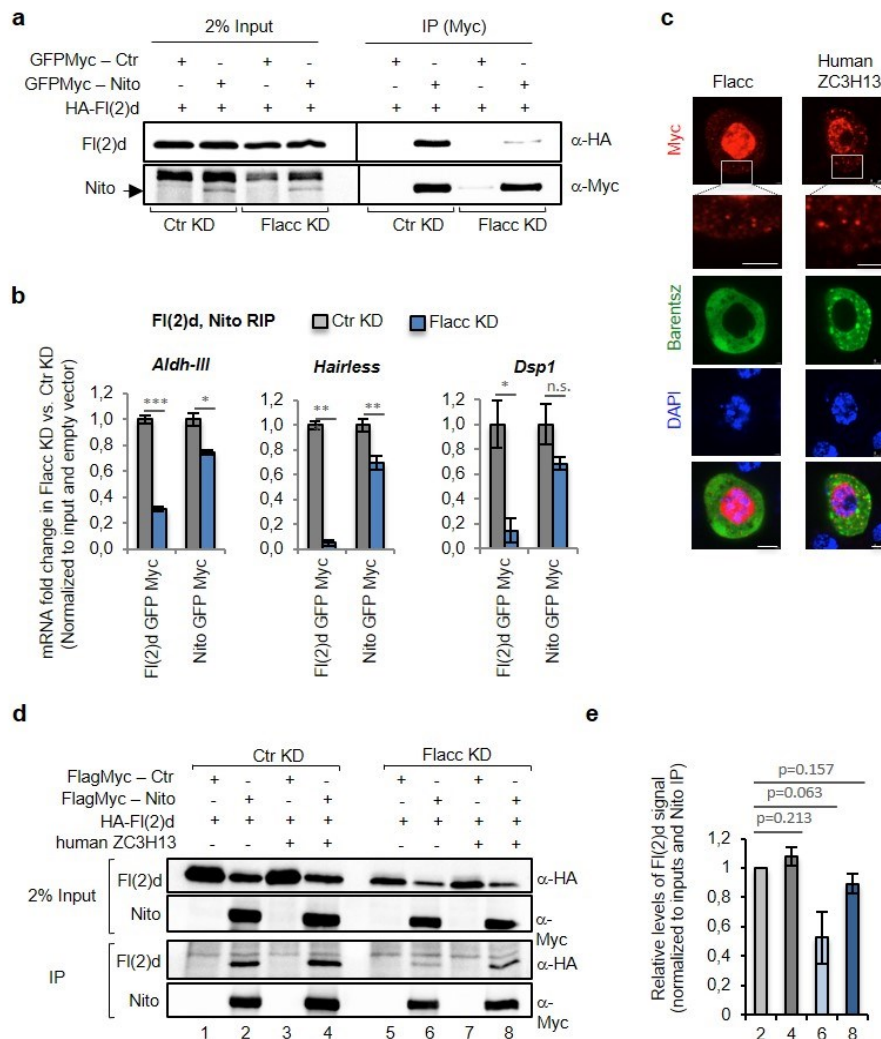


Figure 36. Flacc stabilizes the interaction between Nito and FI(2)d writer components.

a) Co-immunoprecipitation experiments were carried out with lysates prepared from S2R+ cells transfected with GFPMyC-tagged Nito and HA-tagged FI(2)d. In control lanes, S2R+ cells were transfected with Myc alone and an identical HA-containing protein. Extracts were immunoprecipitated with anti-Myc antibody and immunoblotted using anti-Myc and anti-HA antibodies. The same experiment was repeated in Flacc knockdown conditions. Interaction between Nito and FI(2)d is strongly reduced upon depletion of Flacc. **b)** Fold enrichment of m⁶A-regulated transcripts (*Aldh-III*, *Hairless*, and *Dsp1*) over input in Myc-FI(2)d and Myc-Nito RIP upon depletion of Flacc or in control conditions. The bar chart shows the mean of three biological replicates. Errors bars indicate mean \pm s.d. (*) $P < 0.01$; (**) $P < 0.001$; (***) $P < 0.0001$; (n.s.) not significant, Student's t-test. Loss of Flacc strongly affects FI(2)d binding and, to a milder extent, binding of Nito to m⁶A-regulated transcripts. **c)** Immunostaining of Myc-tagged Flacc and human ZC3H13 proteins (in red) overexpressed in S2R+ cells. GFP-tagged Barentsz protein served as a cytoplasmic marker. DAPI staining is shown in blue. Both proteins localize mainly to the nucleus. Zoom-in identifies punctuated localization in the cytoplasm. Scale bars, 5 μ m. **d, e)** Co-immunoprecipitation experiments were carried out with lysates prepared from S2R+ cells transfected with either FlagMyC-tagged Nito or HA-tagged FI(2)d. In control lanes, S2R+ cells were transfected with FlagMyC alone and an identical HA-containing protein. Extracts were immunoprecipitated with Flag antibody and immunoblotted using Myc and HA antibodies. The same experiment was performed upon depletion of Flacc. Human ZC3H13 was transfected in an identical set of experiments. The interaction between Nito and FI(2)d is strongly reduced upon loss of Flacc (lane 6) but can be rescued upon expression of human ZC3H13 protein (lane 8). Quantification of two replicates is shown in d). (a, b, d, e - adapted from Knuckles 2018 G&D, c – unpublished data).

4.8.7 Flacc interactome identifies factors previously linked to m⁶A writers and readers

Aiming to gain a better insight into the functions of MACOM complex, we performed a Flacc protein interactome analysis. Myc-tagged Flacc protein was overexpressed in *D. melanogaster* S2R+ cells and enriched using an anti-Myc antibody coupled to magnetic beads. Following stringent washing, the recovered proteins were subjected to tandem mass spectrometry analysis. Altogether, we identified 87 proteins that were >1,5-fold enriched in both replicates. The strongest interactor was Nito (**Figure 37a**), confirming that the experiment was technically sound. GO-term analysis showed that enriched proteins belonged to various biological processes ranging from nuclear pore organisation and nucleocytoplasmic transport, to different steps of mRNA processing (**Figure 37b**). A large number of identified proteins were constituents of spliceosome, or splicing regulators (**Figure 37c**), supporting our existing observations on m⁶A involvement in the modulation of splicing decision. Interestingly proteins involved in mRNA localization and components of the nuclear pore complex were among enriched proteins, suggesting that Flacc might be required in the regulation of mRNA export or even shuffle with RNA to the cytoplasm.

Unexpectedly, many Flacc interactors were also found to be constituents of the cytoplasmic vesicles, peroxisomes and mitochondria, potentially linking Flacc to distinct cellular processes, where it may function as part of m⁶A writer or independently of other MACOM components. Intriguingly, m⁶A profiling in plants found that nearly 90 % of mitochondria-encoded coding genes carry m⁶A within a typical consensus RRACH site, albeit the metagene profile showed no apparent enrichment towards the 3'-ends of transcripts (Wang et al. 2017). In our miCLIP experiment, we found over 158 m⁶A modified sites on 20 annotated mitochondrial-encoded genes, including 12 out of 13 mRNA transcripts. Most peaks clustered at the very beginning of the transcripts, similar to nuclear encoded genes, however they resided in a non-conventional AT-rich motif. Whether these mitochondrial m⁶A sites are also dependent on the activity of Flacc/MAC/MACOM, or on other methyltransferases, awaits future investigations. Intriguingly, our immunostaining experiments with Flacc, as well as with human ZC3H13 proteins, identified punctuated expression of both proteins in the cytoplasm (**Figure 36c**), which could represent cytoplasmic phase separation of Flacc and ZC3H13 via repeat regions and low complexity domains (**Supplemental data 21**). Notably, human endogenous ZC3H13 protein was also shown to have similar subcellular localization pattern in three different cell types (Human Protein Atlas, (Thul et al. 2017)), suggesting that the fraction of cytoplasmic localized *D. melanogaster* Flacc protein is likely biologically and functionally relevant. Study from Wen and colleagues proposed that in human cells ZC3H13 is required for nuclear localisation of all other components of the MAC and MACOM, therefore it will be interesting to identify the role of the remaining Flacc/Zc3h13 protein residing in the cytoplasm.

We next noticed that many Flacc interactors were previously found to interact with the nuclear reader, Ythdc1, suggesting a link between m⁶A deposition and downstream regulatory processes. To address this possibility, we systematically compared interactome data sets that we obtained for Mettl3, Fl(2)d, Nito, Flacc and Ythdc1 (**Supplemental data 2**). 34 proteins were shared between Ythdc1 and at least one of the writer components, suggesting that some of these common interacting factors, including Ythdc1 itself, might be recruited to sites of methylation simultaneously with the m⁶A writer complex. Among them were proteins involved in the regulation of splicing (Qkr58E-1, Qkr58E-2, Qkr58E-3, Saf-B, nonA), consistent with the proposed role of m⁶A in this process. Additionally, RNA binding proteins that shuttle between nucleus and cytoplasmic compartments were also included.

These were proteins required for RNA localization (rump, homer), translation and stability (Fmr1, pAbp, lark, glo, hang), as well as gene silencing (Ago2) and nuclear pore organisation (Gp210).

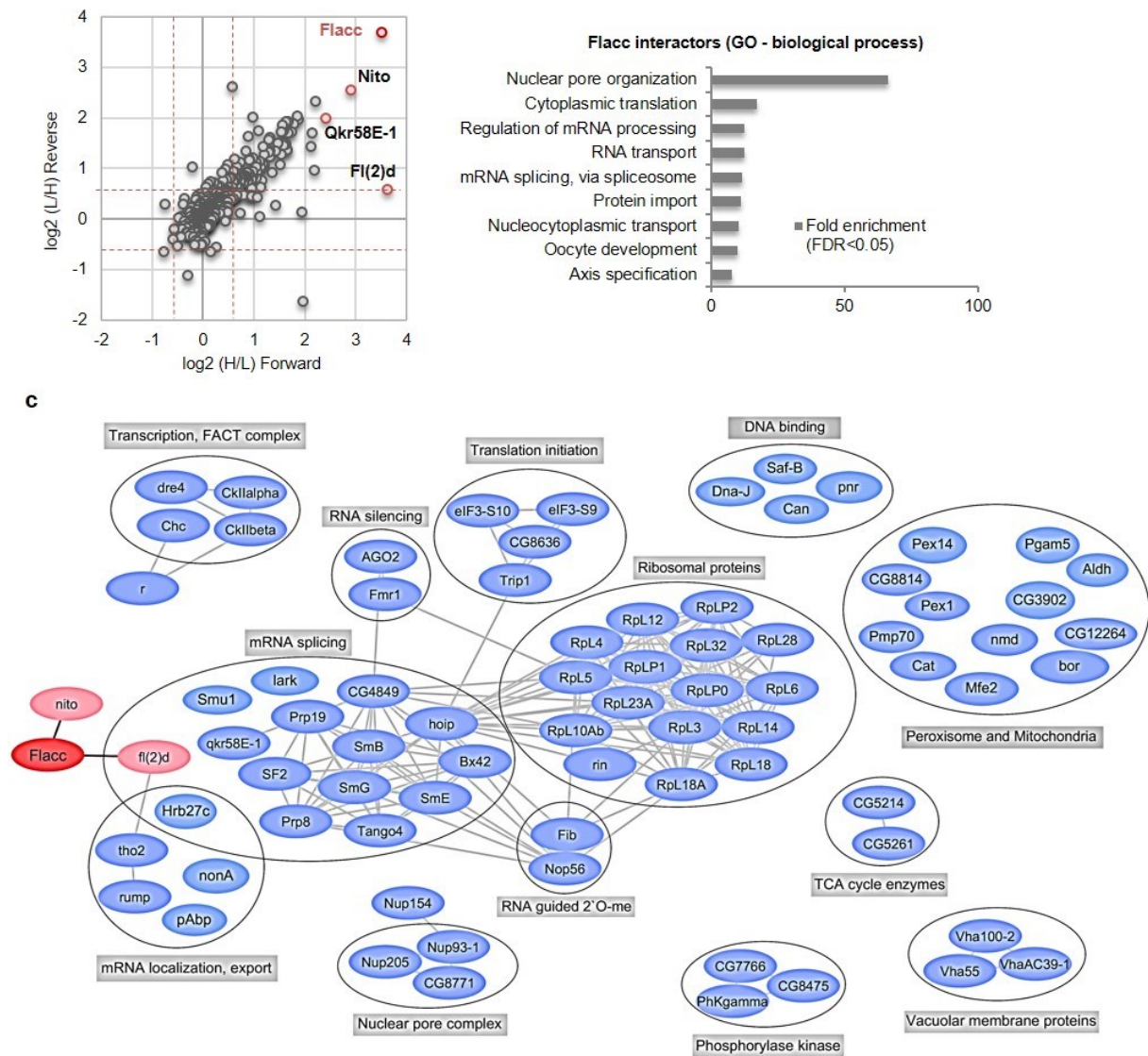


Figure 37. Flacc interactome analysis identifies factors previously linked to m⁶A writers and readers.

a) SILAC-coupled mass spectrometry analysis using Flacc–Myc as a bait. Scatterplot of normalized forward versus inverted reverse experiments plotted on a log₂ scale. The threshold was set to 1,5-fold enrichment (red dashed line). Proteins in the top right quadrant were enriched in both replicates. **b)** Gene ontology (GO) term analysis (Tyanova et al. 2016) for enriched proteins (FDR<0.05). **c)** Flacc interactome network of selected 1.5-fold enriched proteins shown in (b). Each protein is depicted as an individual node. Clusters of nodes represent proteins involved in different RNA processes including transcription, splicing, transport and translation. Edges connect proteins, shown to interact by experimental based evidence (from STRING). Protein nodes and individual proteins that are linked to common cellular processes, are grouped in circles. MACOM complex components are shown in bright red with Flacc in dark red (unpublished data).

Intriguingly, the human FMRP protein (Fmr1 ortholog) was recently shown to interact with the m⁶A reader YTHDF2 and bind m⁶A modified transcripts in the cytoplasm (Zhang F. et al. 2018). This suggests that different m⁶A binding factors may act cooperatively to achieve the same mRNA processing output, or they may function in an opposing manner by competing for the same m⁶A-sites. An interesting common protein was also scaffold attachment factor-B (Saf-B), a component of the nuclear

YT-bodies, where human YTHDC1 was shown to localize along with the Sam68 protein (Qkr58E-1 ortholog) in a phosphorylation dependent manner (Hartmann et al. 1999, Nayler et al. 2000). Saf-B and YT-bodies reside at the sites of active transcription in a close proximity to nuclear speckles (the storage hubs of splicing factors) to regulate co-transcriptional mRNA processing (Nayler et al. 1998). Intriguingly in *D. melanogaster* the Saf-B protein is a constituent of the so-called Omega speckles with Hrb87F, Hrb98DE, other proteins and ncRNA (Singh and Lakhotia 2015). Therefore, Saf-B mediated compartmentalization could potentially link the recruitment of Ythdc1 and associated proteins to co-transcriptionally deposited m⁶A sites. Taken together, our comprehensive interactome analyses of m⁶A writers and the nuclear reader Ythdc1 suggests that they may be required in many biological processes and in different cellular compartments, beyond the main activity in the nucleus.

4.9 Hakai protein modulates m⁶A deposition by stabilizing the m⁶A writer complex

4.9.1 Hakai is a conserved protein, required for m⁶A deposition

m⁶A deposition is mediated by the nearly 1 MDa big writer, composed of two separate sub-complexes, MAC and MACOM. We, and others, have identified and characterised six conserved subunits of this multiprotein complex in flies and vertebrates (Liu et al. 2014, Ping et al. 2014, Schwartz et al. 2014b, Lence et al. 2016, Patil et al. 2016, Lence et al. 2017, Růžička et al. 2017, Guo et al. 2018, Knuckles et al. 2018, Wang Y. et al. 2018, Wen et al. 2018, Yue et al. 2018). The combined composition of Mettl3, Mettl14, Fl(2)d, Vir, Nito and Flacc would, however, only account for ~650-700 kDa (for human orthologs), indicating that either some of the subunits exist in multiple copies, or that additional factors of the complex were yet to be discovered. To address this, we searched over the literature and noticed that Fl(2)d, Flacc and Vir were previously identified as part of the highly conserved macromolecular complex, together with the protein Hakai (Wan et al. 2015). Additionally, in human cells, HAKAI was found as one of the strongest WTAP interactors and both proteins shared a common protein network that included VIR, RBM15, and MAC proteins (Horiuchi et al. 2013). This strongly suggested that HAKAI might associate with, or be a component of the MACOM complex. HAKAI is a highly conserved protein, found in plants, flies and vertebrate lineage and is a predicted E3 ubiquitin ligase (Mukherjee et al. 2012) (**Supplemental data 22**). HAKAI was previously shown to bind E-cadherin, a constituent of cellular adherens junctions. It was proposed to ubiquitinate it and trigger its destabilization, thereby affecting cell-cell adhesion (Fujita et al. 2002, Kaido et al. 2009). For that reason, HAKAI was so far mostly studied in the context of cell migration and cancer progression (Figueroa et al. 2009, Aparicio et al. 2012, Castosa et al. 2018).

To address the possibility that Hakai associates with the m⁶A writer in flies, we first had a look if Hakai was perhaps found in any of our previous protein interactome studies. We noticed that it was indeed just below the 1,5 - fold enrichment threshold in the Nito interactome (**Figure 32a**), suggesting it might bind the MACOM complex. We tested if Hakai is required for m⁶A methylation by depleting it in *D. melanogaster* S2R+ cells along with Mettl3 and Mettl14 proteins, and analysing the change of m⁶A levels in mRNA. In agreement with the potential existence of Hakai in the functional writer complex, its depletion led to a substantial loss of m⁶A (**Figure 38a**). Albeit, the effect was much milder (32 % reduction of m⁶A levels) as compared to Mettl3/Mettl14 knockdown (60 % reduction of m⁶A levels). This result could indicate that Hakai is required for methylation of only a subset of sites, or that residual levels of Hakai protein were still present due to its low knock down efficiency (**Figure 39f**).

While this work was ongoing, two studies found that Hakai is required for m⁶A deposition in plants (Růžička et al. 2017) and human cells (Wen et al. 2018), which was consistent with our observations in flies. Interestingly, plants lacking Hakai only displayed marginal developmental defects and a mild reduction of m⁶A levels, suggesting that Hakai is not an essential component for m⁶A deposition in this species. In *D. melanogaster*, however, protein was previously shown to be indispensable for viability and *hakai null* flies displayed numerous developmental defects due to aberrant cell migration and tissue morphogenesis that led to early embryonic lethality (Kaido et al. 2009).

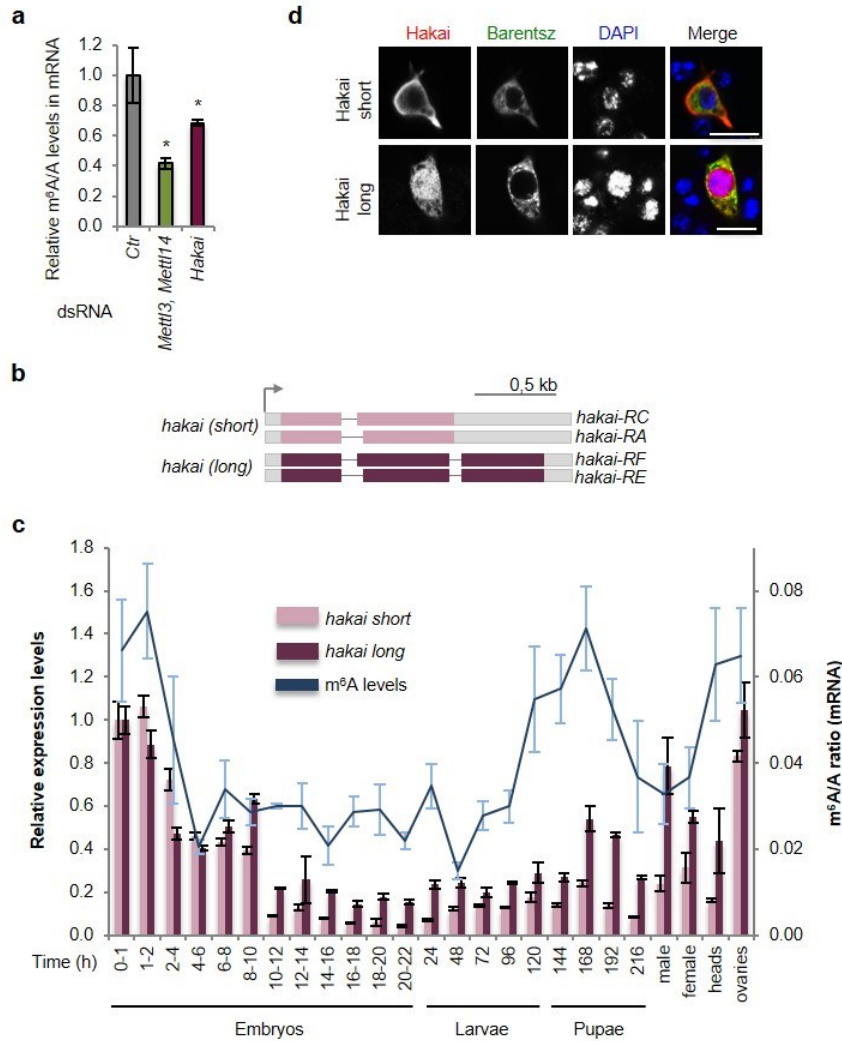


Figure 38. Hakai is a conserved RING domain-containing protein, affecting m⁶A deposition.

a) LC-MS/MS quantification of m⁶A levels in either control samples or mRNA extracts depleted for the indicated proteins in S2R+ cells. The bar chart shows the mean of three biological replicates and three independent measurements. Error bars indicate mean ± s.d. Knockdown of Hakai results in substantial reduction of m⁶A levels. **b)** Schematic representation of two short and two long *hakai* transcript isoforms generated by alternative splicing. 5'UTR and 3'UTR sequences are shown in grey and CDS in colours, connecting lines represent introns. **c)** Relative expression of *hakai* short and long transcript isoforms during *D. melanogaster* developmental stages and in adult female heads and in ovaries, analysed by qRT-PCR. Levels of m⁶A modification were analysed in the same mRNA samples using LC-MS/MS. All *hakai* isoforms and m⁶A levels are enriched during first hours of embryogenesis, during early pupation as well as in adult heads and ovaries. Bars and line junctions represent the mean ± standard deviation (s.d.) of three technical measurements from three biological replicates. **d)** Immunostaining of Myc-tagged Hakai short (Hakai-RC) and long (Hakai-RF) protein isoforms (in red) overexpressed in S2R+ cells. GFP-tagged Barentsz protein served as a cytoplasmic marker. DAPI staining is shown in blue. The short Hakai isoform localizes strictly to the cytoplasm, while the long isoform is expressed in both cellular compartments with enrichment in the nucleus. Scale bars, 10 µm (unpublished data).

Four *hakai* isoforms can be generated in *D. melanogaster* via alternative pre-mRNA splicing, whereby the recognition of an alternative intron can generate two short and two long protein isoforms that differ in their C-terminal region and in the length of the second exon. (Figure 38b). All protein isoforms contain a well characterised RING domain typical for E3 ubiquitin ligases and an adjacent Zn-finger domain. This region is highly conserved in human ortholog HAKAI (Supplemental data 22) and was shown to be required for its dimerization (Mukherjee et al. 2012). Two Zn-fingers from two HAKAI

monomers adopt an atypical fold named as the HYB domain (for “HAKAI pTyr binding”) that is essential for HAKAI binding to phosphorylated Tyrosine residues (pTyr) in a few known interactors (Marengere and Pawson 1994).

In order to investigate the role of Hakai protein in the context of m⁶A modification we analysed the levels of *hakai* transcripts during *D. melanogaster* development and compared them to the m⁶A abundance on mRNA (Figure 38c). All short and long *hakai* isoforms greatly overlapped with the m⁶A profile, displaying high enrichment in the first two hours of embryogenesis and in ovaries. Interestingly, only the long *hakai* isoforms were also highly abundant in males compared to females, implying an important role of Hakai in males. In line with this observation, *hakai* mutants survived until larval stages if paternally contributed Hakai was present (Kaido et al. 2009). Intriguingly, primates have a HAKAI paralog ZNF645 that shares 85 % identity. The protein is expressed exclusively in the testis (Liu et al. 2010) where it might have taken over the functions that are in other organisms still performed by Hakai.

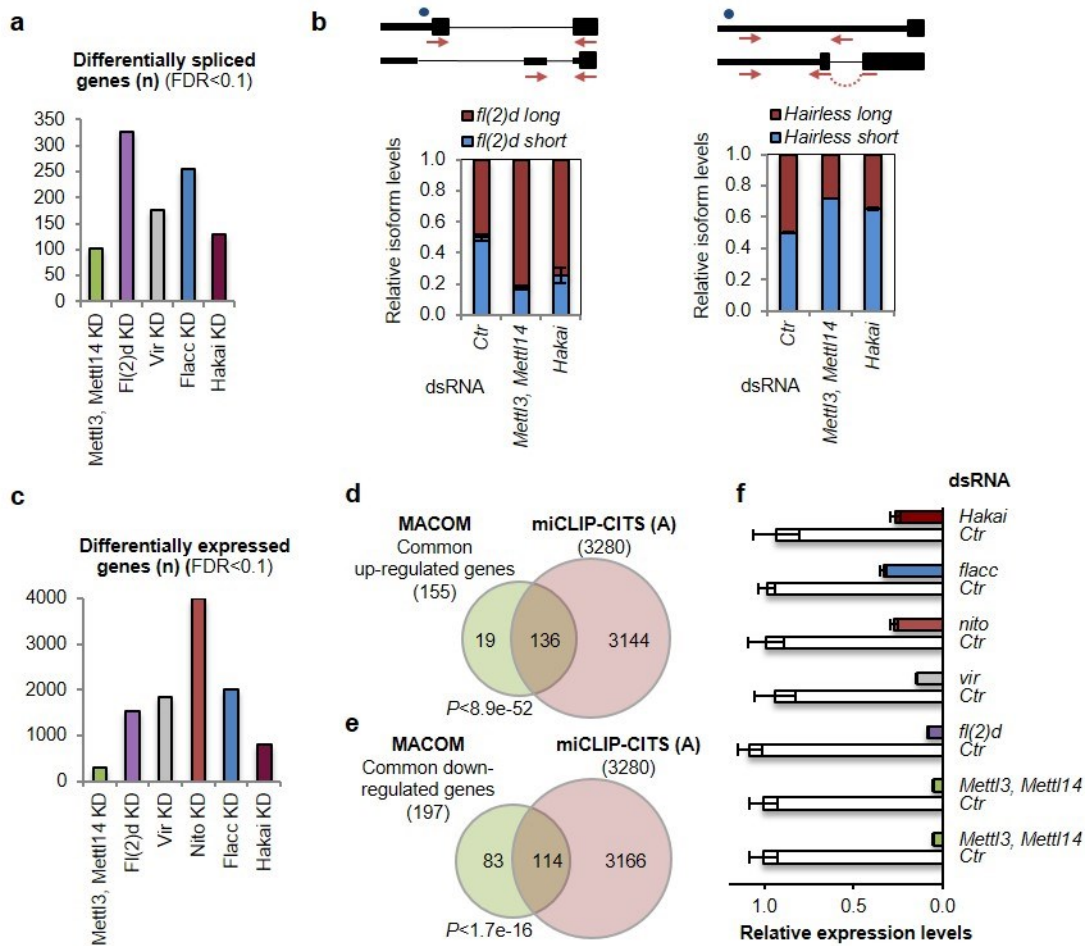


Figure 39. Hakai regulates transcripts that are common with other components of the MACOM complex.

a) Number of differentially spliced genes (false discovery rate [FDR]) upon knockdown of the indicated proteins. **b**) Relative isoform quantification of m⁶A-regulated genes (*fl(2)d* and *Hairless*) upon depletion of the indicated components. Error bars represent mean \pm s.d. Hakai is required for m⁶A-dependent splicing regulation. **c**) Number of differentially expressed genes (false discovery rate [FDR]) upon knockdown of the indicated proteins. **d**) Overlap between common up-regulated genes and genes that are m⁶A modified. **e**) Overlap between common down-regulated genes and genes that are m⁶A modified. **f**) Relative expression levels of indicated transcripts displaying validation of KD efficiency. The mean with standard deviation of three biological replicates and three technical measurements is shown (unpublished data).

To analyse the subcellular localization of Hakai, we next cloned the two Hakai isoforms in a Myc-tag expression vector and expressed them in *D. melanogaster* BG3 cells of neuronal origin. Surprisingly, the short isoform was present exclusively in the cytoplasm with a strong signal at the cellular periphery (**Figure 38d**). The long isoform was predominantly nuclear, but also found in the cytoplasm and resembled the expression pattern observed by Keido and colleagues that used the antibody raised against the endogenous Hakai protein (Kaido et al. 2009). These results thus suggest that two Hakai isoforms might have independent functions, with the longer one likely involved in the regulation of m⁶A deposition.

We next analysed whether Hakai, like other writer components, regulates m⁶A-dependent gene expression in a transcriptome wide manner. Indeed, depletion of Hakai in S2R+ cells resulted in many differentially spliced events (n=128, FDR<0,1) (**Figure 39a**). We validated some of the transcripts that were in common with other writer components by RT-qPCR and observed that depletion of Hakai resulted in similar extent of isoform shift as combined depletion of Mettl3 and Mettl14 (**Figure 39b**), confirming its requirement for m⁶A deposition. Additionally, knock down of Hakai altered expression of 814 genes and 43 % of those were shared with other MACOM subunits (**Figure 39c**). Consistent with our previous observations, common up-regulated genes were more likely to be m⁶A methylated (87,7 %) than down-regulated ones (57,9 %) (**Figure 39d, e**).

4.9.2 Hakai interacts with MACOM components

We next wanted to investigate Hakai binding to other components of the MACOM complex. Given its previously demonstrated interaction with WTAP in human cells (Horiuchi et al. 2013), we first tested if it can co-precipitate with Fl(2)d in S2R+ cells. Indeed HA-tagged Fl(2)d was efficiently pulled down by a Myc-tagged Hakai, but not an empty vector, in an RNase independent manner (**Figure 40a**). In the same way Hakai could precipitate HA-tagged Nito, confirming our Nito-interactome data (**Figure 32a**). This altogether supported that Hakai interacts with the MACOM complex. To validate these results in an unbiased way, we performed a yeast-two-hybrid assay with all seven known writer subunits. We cloned all genes in yeast expression vectors with either Gal4-transcription activation domain (AD) or Gal4-DNA binding domain (BD) and observed a strong signal between Hakai-AD and Fl(2)d-BD, but not in a control conditions, suggesting that Hakai most likely directly binds Fl(2)d. A notable signal, albeit with a higher background, was also observed between Hakai-AD and Nito-BD (**Figure 40b**). No signal was, however, detected with Flacc and the large 180-kDa protein Vir, which was not successfully expressed in yeast. Thus, future binding analyses with purified proteins will be crucial to reveal how proteins interact with each other. Nevertheless, these results suggested that Hakai interacts with at least two MACOM components, Fl(2)d and Nito, to regulate deposition of m⁶A. Additionally, we noticed that Hakai can homo-dimerise. This was consistent with the structural data of human ortholog that self-dimerizes in order to coordinate a Zn-finger motifs of its RING and p-Tyr binding domains (collectively called HYB domain) for a target recognition (Mukherjee et al. 2012). Interestingly, Fl(2)d and Nito were also found to homo-dimerize in a yeast-two-hybrid assay (**Figure 40c**). This has been previously proposed for human ortholog of Fl(2)d (Liu et al. 2014) and will require further validation by biochemical characterisation of the complex. Overall, these results shed light on the likely composition of a functional m⁶A methyltransferase complex consisting of two components of MAC (Mettl3 and Mettl14) and five components of MACOM (Fl(2)d, Vir, Nito, Zc3h13 and Hakai), of which some are likely present as homodimers.

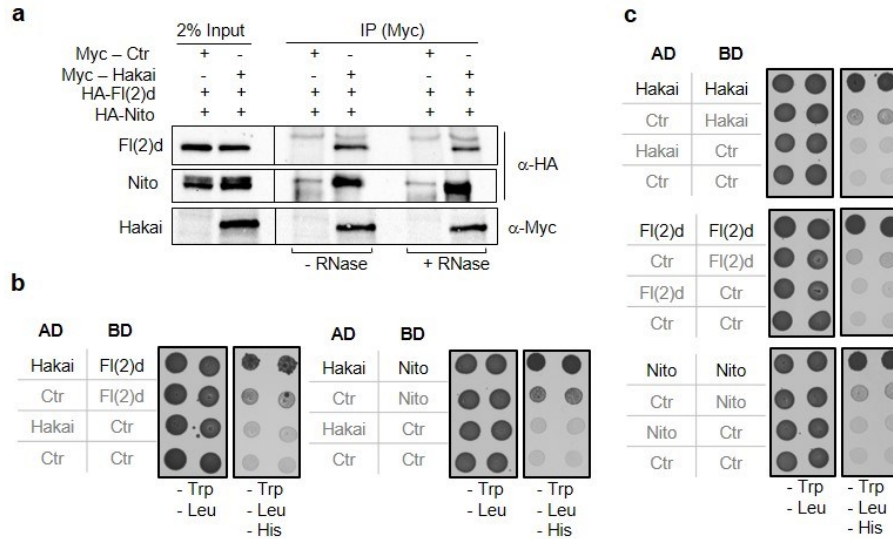


Figure 40. Hakai directly interacts with writer complex components FI(2)d and Nito.

a) Co-immunoprecipitation experiments were carried out with lysates prepared from S2R+ cells transfected with Myc-tagged Hakai (long isoform) and HA-tagged Nito or FI(2)d. In control lanes, S2R+ cells were transfected with Myc alone and an identical HA-containing protein. Extracts were immunoprecipitated with anti-Myc antibody and immunoblotted using anti-Flag and anti-HA antibodies. Two percent of input was loaded. The same experiment was repeated in the presence of RNaseT1. Nito and FI(2)d interact with Hakai in an RNase-independent manner. **b**) Yeast two-hybrid assay to investigate Hakai interaction with Nito and FI(2)d. Proteins were cloned in yeast expression vectors and fused with either Gal4-DNA binding domain (BD) or Gal4-DNA activation domain (AD). Indicated combinations of vectors were co-expressed in yeast and empty vectors encoding only activation or binding domain were used as control (Ctr). Recovered colonies were spotted on plates lacking Leucine and Tryptophan (-Leu, -Trp) as well as selection plates lacking amino acids Leucine, Tryptophan and Histidine (-Leu, -Trp, -His). AD-Hakai interacts with BD-FI(2)d and potentially also with BD-Nito. **c**) Yeast two-hybrid assay same as in **(b)**, to investigate Hakai, Nito and FI(2)d homo-dimerization. Hakai, FI(2)d and Nito all homo dimerize (unpublished data).

4.9.3 FI(2)d is ubiquitinated and strongly destabilized upon Hakai depletion

To understand what may be a potential role of Hakai within the MACOM complex, we turned our focus on its predicted E3 ubiquitin ligase domain. We reasoned that if ubiquitination activity is real, some of the MACOM components might be its direct targets. FI(2)d and Nito have been recently identified among the ubiquitinated proteins in *D. melanogaster* S2R+ cells (Schunter et al. 2017). Given the fact that both proteins interacted with Hakai in the yeast two-hybrid assay (**Figure 40b**) we analysed their ubiquitination status in the presence and absence of Hakai. We cloned FI(2)d and Nito proteins in a GFP-tag containing vector and expressed them in control and Hakai depleted S2R+ cells. We then performed immunoprecipitation under stringent 8M Urea conditions and analysed the ubiquitination by SDS-PAGE and western blot. While we could not detect ubiquitination of Nito, FI(2)d appeared to be polyubiquitinated, as shown by a strong shift of molecular weight of more than 100 kDa (**Figure 41a**). The ubiquitination levels seemed to be reduced in the Hakai knock down condition, however the overall level of immunoprecipitated FI(2)d was also diminished (**Figure 41a and b**). We therefore repeated this experiment and compared ubiquitination levels of FI(2)d in control condition and upon inhibition of proteasome activity using MG132 inhibitor to prevent protein degradation. We could confirm the ubiquitination of FI(2)d in all samples, but surprisingly, FI(2)d was strongly destabilized upon Hakai knock down, when proteasome was not inhibited (**Figure 41c**). This indicated that loss of Hakai results in FI(2)d degradation, at least in part, via the ubiquitin-proteasome pathway. FI(2)d was so strongly destabilized that its input sample was not detected at a given exposure (**Figure 41c**, lane 2), possibly as

a result of very efficient depletion of Hakai (Figure 41d, as compared to Figure 41b). On the other hand, upon proteasome inhibition Fl(2)d was stabilised (Figure 41c, input) and its ubiquitination levels also remained constant (Figure 41c, lane 3 and 4) even though Hakai was strongly depleted (<15 % remaining) (Figure 41d). If ubiquitination of Fl(2)d was indeed Hakai dependent, a decrease of its ubiquitination would have been expected. Thus, these experiments indicated that Hakai is essential for Fl(2)d stabilisation, but not for its ubiquitination.

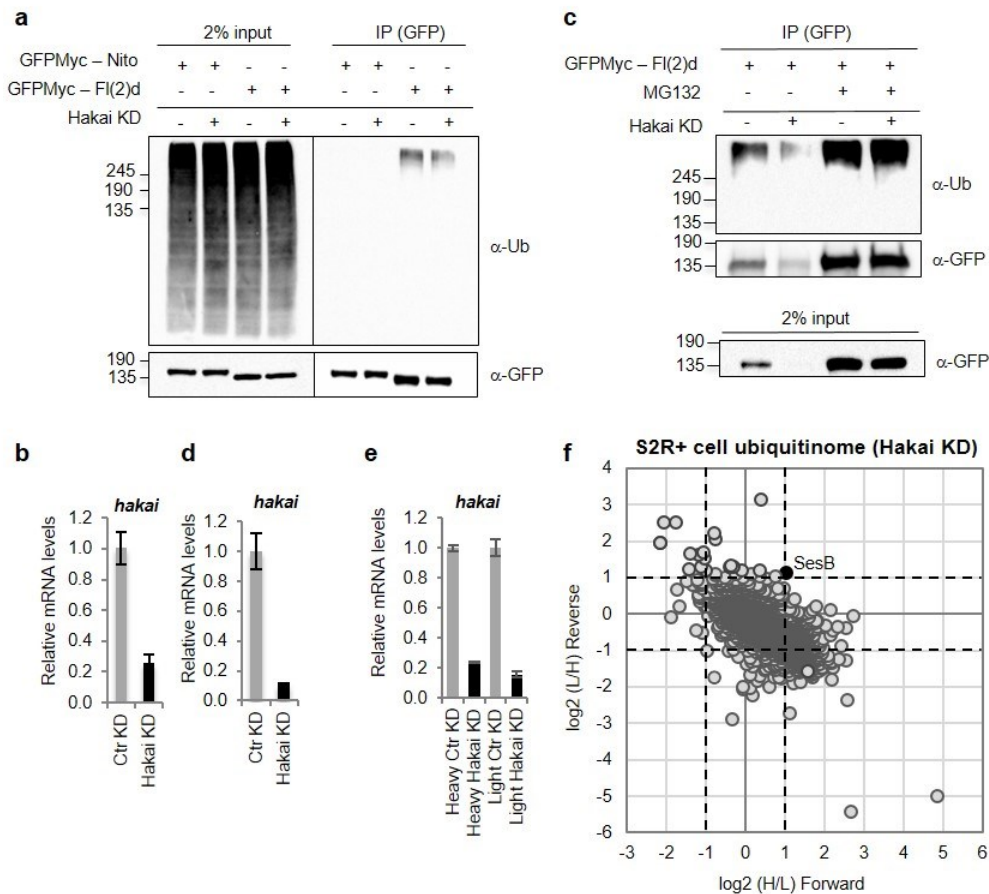


Figure 41. Fl(2)d is post-translationally ubiquitinated.

a, b) Ubiquitination analysis of GFP-tagged Nito and Fl(2)d proteins upon control condition and Hakai depletion. GFP-tagged proteins were immunoprecipitated using anti-GFP-coupled beads under stringent urea conditions and analysed by western blot. Fl(2)d, but not Nito, is ubiquitinated. **b**) Relative expression levels of *hakai* shown as a validation of its KD efficiency. The mean with standard deviation three technical measurements is shown. **c, d**) Ubiquitination analysis of GFP-tagged Fl(2)d protein upon control and Hakai protein depletion, with or without proteasome inhibitor MG132. GFP-tagged Fl(2)d was immunoprecipitated using anti-GFP-coupled beads under stringent urea conditions and analysed by western blot. Fl(2)d stability and ubiquitination are decreased upon Hakai depletion and rescued by inhibition of proteasomal degradation. **d**) Relative expression levels of *hakai* shown as a validation of its KD efficiency. The mean with standard deviation of three technical measurements is shown. **e, f**) MS analysis of Hakai-dependent ubiquitinated proteins in S2R+ cells. Scatter plot of normalized forward versus inverted reverse experiments plotted on a log₂ scale. The threshold was set to a 2-fold enrichment or depletion (red dashed line). One protein in the top right quadrant is enriched in both replicates. **e**) Relative expression levels of *hakai* shown as a validation of its KD efficiency in indicated samples. The mean with standard deviation of three technical measurements is shown. Hakai depletion does not affect global ubiquitination levels in *D. melanogaster* S2R+ cells (unpublished data).

To get a better insight in the function of Hakai as an E3 ubiquitin ligase, we performed a proteome wide ubiquitinome analysis of *D. melanogaster* S2R+ cells in control and Hakai knock-down condition. Cells isotopically labelled with heavy amino acids were depleted for Hakai and cells isotopically labelled with light amino acids served as a control in the forward experiment. A vice versa depletion was performed in the reverse experiment. Proteins were digested with endo-proteinase Lys-C and peptides were further enriched with di-glycine-lysine remnant-recognising resin, to identify ubiquitination sites via LC-MS/MS. We found over 3000 ubiquitination sites, but unexpectedly not a single site was reduced in response to Hakai depletion in a forward and reverse experiment and only one site was 1,5-fold increased (in a SesB protein) (**Figure 41e and f**). Importantly, we noticed that the two replicates, one from heavy and one from light labelled cells, anti-correlate, which most likely reflects the bias in the cell growth and morphology due to labelling (data not shown). Hence, it is possible that Hakai ubiquitinates a subset of targets that were not equally expressed in both types of labelled S2R+ cells, or that its ubiquitination activity depends on specific external stimuli. We also cannot exclude that residual levels of Hakai upon its depletion, were still sufficient to ubiquitinate putative targets. Alternatively, Hakai might not act as an active E3 ubiquitin ligase. Addressing this possibility will require a thorough re-validation of its only known target, protein E-cadherin, and further search for its potential novel targets in other cell types or, ideally, in the *hakai* knock out flies that we generated.

4.9.4 Hakai depletion strongly affects stability of MACOM components

Given the strong effect of Hakai depletion on Fl(2)d stability we wanted to further investigate by which means, other than ubiquitination, could Hakai regulate Fl(2)d protein levels. To confirm that Fl(2)d destabilisation is biologically relevant and not just an artefact of an overexpressed construct, we first analysed levels of the endogenous Fl(2)d protein. In line with previous observations, Hakai depletion strongly destabilized Fl(2)d and its levels were reduced to less than 50 % (**Figure 42a, b and c**). To see if loss of Hakai also destabilizes other components of the m⁶A writer complex or else, if this effect is restricted to Fl(2)d, we analysed protein levels of the Mettl3 and Mettl14, since only antibodies for these two proteins were available. Upon knock down of Hakai, levels of Mettl3 were only marginally reduced, while levels of Mettl14 remained unchanged (**Figure 42a**), indicating that Hakai is required to specifically stabilize Fl(2)d, but not the two components of the MAC complex.

We next wondered if Fl(2)d stability only depends on the presence of Hakai, or whether other components of the methyltransferase complex may regulate its levels as well. To address this possibility, we analysed endogenous Fl(2)d protein upon depletion of Mettl3, a component of MAC, as well as upon depletion of Nito, a component of MACOM. Notably, only knock-down of Hakai, but not Mettl3 or Nito, resulted in a strong decrease of Fl(2)d levels, indicating that this effect is specifically mediated by Hakai (**Figure 42d, e and f**). We repeated the same experiment upon proteasome inhibition (+MG132) and observed a partial, albeit significant recovery of Fl(2)d levels, suggesting that either proteasome inhibition was not complete or that both major protein degradation pathways contribute to destabilization and removal of endogenous Fl(2)d protein; the ubiquitin-proteasome pathway and the autophagy-lysosome pathway.

We next wanted to investigate if Hakai can stabilize other proteins on a global level. We therefore analysed the complete proteome of control and Hakai-depleted S2R+ cells (that was performed from the same cell lysate as ubiquitinome mentioned above). Given that proteasome-dependent protein degradation pathway was inhibited, levels of nearly all proteins remained unchanged. However, protein levels of Hakai were strongly reduced, indicating a successful depletion (**Figure 42g**). Strikingly, we found

that levels of Vir, a component of the MACOM complex, were decreased to the same extent as levels of Hakai (**Figure 42g**). This suggested that reduced levels of Hakai have a particularly strong impact on Vir stability and that upon Hakai depletion Vir is subjected to degradation, most likely, via autophagy-lysosome pathway. Moreover, when having a closer look at all proteins whose levels were decreased by at least 1,4-fold in both replicates upon Hakai depletion, we found that among only eight identified proteins also Fl(2)d and Flacc were present (with 1.41/1.47-fold and 1,64/1,73-fold reduced levels, in Forward/Reverse experiment, respectively) (**Figure 42g and h**).

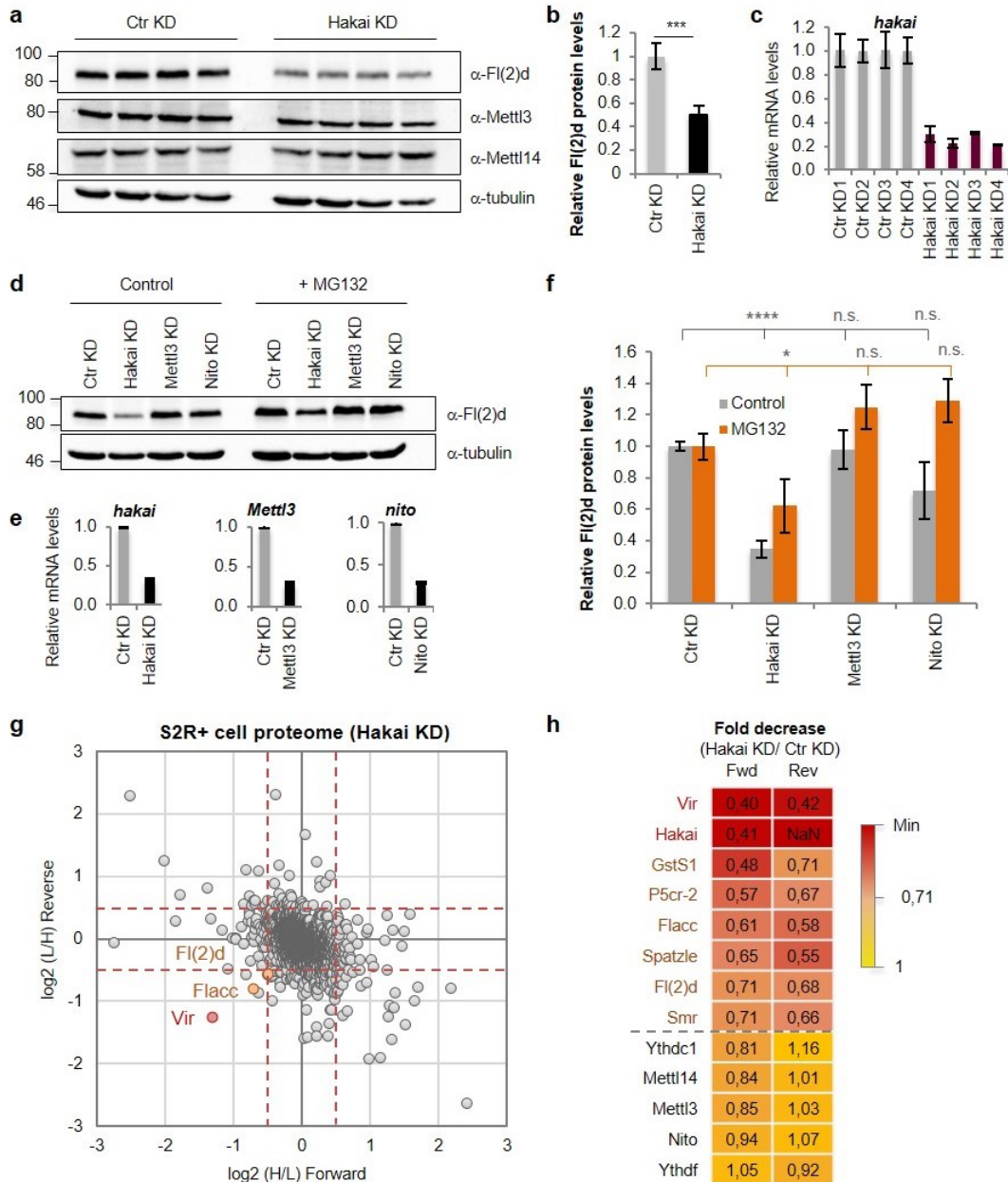


Figure 42. Hakai is required for stability of MACOM complex.

a) Analysis of endogenous Fl(2)d, Mettl3 and Mettl14 protein levels from control cells and cells depleted for Hakai were analysed by western blot. Tubulin was used as a loading control. **b)** Quantification of Fl(2)d, Mettl3 and Mettl14 levels from blots shown in (a). The bar chart shows the mean of four biological replicates. Error bars indicate mean \pm s.d. (***) $P < 0.001$, Student's t-test. Hakai depletion strongly destabilizes Fl(2)d, but not Mettl3 or Mettl14 proteins. **c)** Relative expression levels of *hakai* shown in (a) shown as a validation of its KD efficiency. The mean with standard deviation of three technical measurements is shown. **d)** Analysis of Fl(2)d levels upon Hakai, Mettl3 or Nito depletion with or without proteasome inhibitor

MG132. Protein lysates from control cells and cells depleted for Hakai, Mett13 or Nito were analysed by western blot for levels of endogenous Fl(2)d protein. Tubulin was used as a loading control. One representative experiment is shown and quantification of three independent experiments is shown in (f). **e**) Relative expression levels of *hakai*, *Mett13* and *nito* shown in (d) show as a validation of their KD efficiencies. The mean with standard deviation of three technical measurements is shown. **f**) Quantification of Fl(2)d levels related to experiment in (d). The bar chart shows the mean of three biological replicates. Error bars indicate mean \pm s.d. (*) $P < 0.05$, (****) $P < 0.0001$, n.s. not significant, Student's t-test. Hakai strongly destabilizes Fl(2)d and its levels can be partially rescued by proteasome inhibition. Nito depletion destabilizes Fl(2)d to a much milder extent. **g**) LC-MS/MS analysis of Hakai-dependent proteome in S2R+ cells. Scatter plot of normalized forward versus inverted reverse experiments plotted on a log₂ scale. The threshold was set to a 1,4-fold enrichment or depletion (red dashed line). Proteins in the bottom left quadrant are decreased in both replicates. Hakai and Vir were reduced >2-fold, Flacc >1,5-fold and Fl(2)d >1,4-fold. **h**) Heat map of proteins whose levels were reduced by >1,4-fold in both replicates of the whole proteome analysis shown in (g). Other components of the m⁶A writer complex and reader proteins are shown for comparison. Levels of Mett13, Mett14 and Nito are not changed upon Hakai depletion (unpublished data).

Interestingly, levels of Nito, MAC components or reader proteins were not affected (**Figure 42g** and **h**). This suggested that Hakai is essential for stabilization of three components of the MACOM complex; Vir, Fl(2)d and Flacc that together with Hakai form an evolutionary conserved and stably associated macromolecular complex (Wan et al. 2015). These observations are also in line with our results on MACOM dependent transcriptome analysis, where depletion of Nito had a much stronger effect on gene expression compared to other components (**Figure 33a**), suggesting that Nito is involved in processes independently of the MACOM complex (see discussion *Chapter 5.1.3*).

Of note, isotopically labelled S2R+ cells with heavy amino acids display changed morphology (better cell-cell adhesion and reduced adhesion to surface of the cell culture flask), which likely explains a skewed (anti-correlated) protein expression profile between heavy and light cells, as visible in the plot (**Figure 42g**). Therefore, we also performed an additional, Hakai-dependent proteome analysis using non-labelled S2R+ cells and obtained similar results in regards to Vir destabilization, supporting our initial observations from SILAC labelled cells. Ideally, a ubiquitinome and proteome analysis from *Hakai* fly mutants, that we have generated, should also be performed in the future in order to I) confirm the destabilization effect on Vir, Fl(2)d and Flacc and II) to identify potential biologically relevant ubiquitination targets that might not be expressed in S2R+ cells.

5 Discussion and outlook

Gene regulation has to be tightly controlled to ensure proper development and differentiation at cellular and organismal level. Each cell in the eukaryotic organism carries the same DNA code, yet its chromatin landscape and transcriptome output greatly differ. Dynamic regulation of gene expression is particularly important during stress conditions (e.g. DNA damage, viral infection, starvation, heat shock, malignant deformations), as it guarantees cellular adaptation and survival, and may trigger cell death to ensure removal of anomalous cells. Consistently, alterations of gene expression at chromatin, DNA or RNA level often lead to the occurrence of various diseases or to organismal death. Thus, it is crucial to deeply, and thoroughly understand all mechanisms cells employ, to timely and dynamically regulate their fates (*Chapter 1.1*). Akin to modifications found on DNA, RNA molecules can be heavily modified. In fact, over 170 different RNA modifications have been identified so far in all kingdoms of life. Most are found on highly abundant tRNA and rRNA, and a dozen also decorate less abundant mRNA (*Chapter 1.3*). RNA modifications represent a new layer of gene regulation that has coined a new field of “epitranscriptomics”. N⁶-methyladenosine (m⁶A), known since the 1970s, is one of the most abundant modifications on mRNA. Over the past decade, enzymatic machineries required for its writing, reading and erasing have finally been revealed. Moreover, technological progress enabled transcriptome wide mapping of m⁶A even on scarce RNA species (*Chapter 1.4*). These seminal discoveries allowed further characterisation of roles that m⁶A play at cellular and organismal level. m⁶A is being increasingly recognised as a critical means to rapidly adjust gene expression and regulates nearly every step of mRNA biogenesis. As a result, m⁶A is crucial in numerous biological processes ranging from cell fate determination, cell cycle progression, X-chromosome inactivation, to cellular response to various stress agents (*Chapter 1.4.8*).

In this study, we investigated roles and functions of m⁶A modification in *D. melanogaster* as a model organism. Our findings are discussed in the following sections: *Chapter 5.1* covers characterisation of components of the conserved writer complex, required for m⁶A deposition on mRNA. Our observations about other putative N⁶-methyltransferases and demethylases are discussed in *Chapter 5.1* and *Chapter 5.2*. We also studied YTH domain reader proteins and found other sequence and structure specific m⁶A readers included in *Chapter 5.2*. To investigate roles of m⁶A on mRNA processing, we profiled modification in S2R+ cells and found that it is present in a typical RRACH motif, albeit with a strong enrichment at the 5'UTR regions and with a preference for A-rich sequences. These findings are discussed in *Chapter 5.1.3*. At the molecular level, we could demonstrate that m⁶A in *D. melanogaster* influences splicing of a subset of genes. Link between m⁶A modification and splicing outcome is discussed in *Chapter 5.5*. Finally, to investigate roles of this modification in vivo, we generated several mutants for factors involved in m⁶A deposition and its recognition. We found that modification is not essential for fly survival, yet it modulates sex determination and dosage compensation pathways (*Chapter 1.5.2*). In addition, flies lacking m⁶A-components display severe behavioural defects as a result of altered neuronal functions. These findings are covered by *Chapter 5.6.2*.

5.1 m⁶A writer complex consists of two sub-complexes MAC and MACOM

Early work from the Rottman's group suggested that the vast majority of m⁶A on mRNA is deposited by a large, nearly 1 MDa protein complex, composed of two sub-complexes (Bokar et al. 1994, Rottman et al. 1994, Bokar et al. 1997). One single protein with a catalytic activity, the methyltransferase-like 3 (Mettl3), has been discovered soon after, however, identities of other components remained a mystery. Over the past few years the composition of the so-called "m⁶A writer" complex has been resolved by the identification of seven proteins essential for efficient m⁶A methylation Mettl3 (METTL3), Mettl14 (METTL14), Fl(2)d (WTAP), Vir (VIRMA), Flacc (ZC3H13), Hakai (HAKAI) and Nito (RBM15) (this work and other studies). Biochemical and structural characterisation of these proteins confirmed Rottman's findings and revealed that Mettl3 and Mettl14 heterodimerize and form a complex **MAC (m⁶A-METTL complex)**, while remaining components constitute the larger complex **MACOM (MAC-associated complex)** (reviewed in (Lence et al. 2019)) (**Figure 43** and **Supplemental data 26**). MAC and MACOM are both stable on their own, and interact during m⁶A deposition. Notably, a comprehensive study of evolutionary conserved macromolecular complexes found that Nito primarily resides in a complex with four other RNA-binding proteins, which may be indicative of its involvement in additional cellular processes, independent of MACOM complex (Wan et al. 2015) (**Figure 43** and *Chapter 5.1.3*).

During the course of this study we were able to identify, and to some extent characterise seven components of the m⁶A writer complex in *D. melanogaster*. While functions of some proteins of this large complex have already been revealed, precise roles of most subunits remain enigmatic and await further analyses from genomic, biochemical and structural perspectives (**Table 5**).

Complex	Components	Functions
MAC	Mettl3 (METTL3) Mettl14 (METTL14)	Catalytic subunit Facilitates RNA binding and MAC complex stability
MACOM	Fl(2)d (WTAP) Vir (VIRMA) Flacc (ZC3H13) Hakai (HAKAI)	Interacts with MAC and several splicing factors Large scaffolding protein with repeat-and LC-domain regions Stabilizes interaction between Fl(2)d and Nito Ensures stability of Vir, Fl(2)d and Flacc proteins
*MACOM	*Nito (RBM15/RBM15B) Dhx15 (DHX15) Trmt112 (TRMT112) CG3155 (SUGP1) CG7878 (DDX43)	Promotes RNA binding with RRM domains DEAH-box RNA helicase Activator of protein, rRNA and tRNA methyltransferases Gly-rich domain (G-patch domain) promotes helicase activity DEAD-box helicase

Table 5. Evolutionary conserved macromolecular complexes.

Table of proteins belonging to three conserved macromolecular complexes with components required for m⁶A RNA methylation that have been renamed to MAC and MACOM. Names of human orthologs are shown in brackets. * - star denotes RBM15, RBM15B and Nito proteins that are also part of MACOM complex but were, in addition, shown to exist in a complex with proteins listed below (Dhx15, Trmt112, CG3155 and CG7878) (data source: (Wan et al. 2015).

5.1.1 MAC

To identify putative m⁶A methyltransferases in *D. melanogaster* we searched for orthologs of human METTL3 (or MT-A70) protein, the only known enzyme with a N6-methylation activity towards adenosines in mRNA at that time. By using such an in silico approach, we found a fly protein Mettl3 (or Ime4) as well as two additional, uncharacterised paralogs, METTL14 (Mettl14 or CG7818) and METTL4 (Mettl4 or CG14906) (**Figure 14a**). All three proteins belong to a group of N6-type methyltransferases with a typical catalytic domain consisting of a (DNSH)PP(YFW) motif (Iyer et al. 2016) (**Figure 1**), but act on different targets. We found that Mettl3 and Mettl14 proteins are both required for deposition of m⁶A on mRNA, whereas Mettl4 likely methylates several distinct RNA and DNA substrates (see below *Chapter 5.1.5*). These observations are consistent with functions of their respective orthologs in other species (Lence et al. 2019).

Structural and biochemical studies of vertebrate METTL3 and METTL14 proteins revealed that they form a stable heterodimer (Sledz and Jinek 2016, Wang P. et al. 2016, Wang X. et al. 2016) known as the MAC (m⁶A-METTL-complex). While METTL3 is catalytically active and can accommodate SAM, METTL14 contains a degenerated catalytic centre and facilitates binding of MAC to mRNA, which aids to methylation efficiency (*Chapter 1.4.2.a*). By comparing human and fly protein sequences, we found that regions required for RNA recognition, as well as for a stable interaction between the two proteins, are highly conserved, thus similar mode of dimerization between Mettl3 and Mettl14 most likely also takes place in *D. melanogaster* (**Supplemental data 16, 17 and 25**). In support to this, we found that the two proteins co-immunoprecipitate in an RNA-independent manner and strongly interact with each other in the yeast-two-hybrid assay (**Figure 14c and d**). In addition, we performed Mettl3 and Mettl14 protein interactome analyses, which repeatedly identified the corresponding heterodimer partner as the top interactor (**Supplemental data 1** and data not shown for Mettl14). Interestingly, we observed that removal of one protein (e.g. in *Mettl3* mutant flies) to some extent reduces stability of the other, further implying that they form a stable complex. Similar observations were also reported for human orthologs (Kobayashi et al. 2018), however the mechanism by which Mettl3 and Mettl14 could stabilize each other is currently not known. In line with the notion that Mettl3 and Mettl14 act as a heterodimer, we found that their individual or combined depletion reduces m⁶A levels to a similar extent (**Figure 14b**), suggesting that both proteins are indeed required for methylation of same targets. At the molecular level, we observed that depletion of MAC components results in numerous common misregulated genes and several splicing changes of transcripts that contain m⁶A within a close proximity to alternative splice sites (**Figure 21 and Figure 22**). Analogous findings have been reported in other species (*Chapter 1.4.7*), hence functions of m⁶A modification in regards to mRNA processing are likely conserved in *D. melanogaster*, where it can alter gene expression and modulate splicing of a subset of modified transcripts (see *Chapter 5.5*). Several pieces of data suggest that Mettl3 and Mettl14 primarily act together within the MAC heterodimer to carry out m⁶A deposition. During *D. melanogaster* development for example, expression profiles of *Mettl3* and *Mettl14* transcripts strongly recapitulate the abundance of m⁶A modification on mRNA (**Figure 44**). Likewise both transcripts are enriched in the neuroectoderm at embryonic stage 15 (**Figure 15**). In addition, fly mutants lacking either of the two proteins are viable but display similar developmental defects including reduced lifespan, altered locomotion and inability to fly (see *Chapter 5.6*).

We observed that ectopically expressed Mettl3 and Mettl14 localise to the nucleus in S2R+ cells, which is in line with studies showing that m⁶A deposition on mRNA occurs co-transcriptionally (Barbieri et al. 2017, Knuckles et al. 2017, Slobodin et al. 2017, Huang et al. 2019). Similarly, in vertebrates all components of the m⁶A writer complex are also found in this compartment (Horiuchi et al. 2013,

Scholler et al. 2018). In flies, Mettl3 and Mettl14 both contain a predicted nuclear localisation signal (NLS), however the relevance of these sites in flies has not been confirmed yet (**Supplemental data 16** and **17**). Notably, in human cells a vertebrate-conserved NLS of the METTL3 was shown to be sufficient for tethering the complete MAC heterodimer to the nucleus, whereas the NLS of METTL14 protein was found dispensable (Scholler et al. 2018). An intriguing observation was made in mES cells, where cell fractionation experiments suggested a strong enrichment of MAC complex in the cytoplasm (Wen et al. 2018). Since the cytoplasmic localisation was not apparent by immunofluorescence staining it is possible that the two proteins disperse in that compartment. Further studies should address the biological importance of this cell type-specific localization of MAC in mES cells. Interestingly, in vertebrate METTL3, several sumoylation sites (K177/K211/K212/K215) have been identified within its characterised NLS (209-215 aa), however their mutations had no effect on protein localisation or stability, but instead negatively impacted methylation activity (Du et al. 2018). Even though none of these sites is conserved in fly Mettl3 ortholog, it would be informative to test if this region is important for mediating interaction with any other component of the m⁶A writer complex. Alternatively, sumoylation could promote interaction of Mettl3 with other m⁶A-unrelated proteins, which might, in turn, out-compete its binding with m⁶A writer and in this way compromise methylation output.

Can MAC components act beyond m⁶A methylation?

We performed Mettl3 interactome analysis and surprisingly identified proteins linked to mRNA translation, including eIF4a, eIF2 and several ribosomal subunits (**Supplemental data 1**), suggesting that in addition to its methyltransferase function, Mettl3 may be involved in other cellular processes. Consistently, vertebrate METTL3 was shown to interact with the translation initiation factor eIF3h to promote mRNA translation independently of its catalytic activity or METTL14 (Lin et al. 2016) (Choe et al. 2018). While the region required for binding to this particular factor is absent in flies, interactions with the above-mentioned candidate proteins nonetheless open the possibility that Mettl3 may be implicated in translational regulation in *D. melanogaster*. In addition to translation-related proteins, our Mettl3 interactome study also identified several proteins involved in cytoplasmic vesicle formation (Rab proteins, Chc) and coatome proteins (COP α , COP β , Arf1) (**Supplemental data 1**) that are, for example, required for localisation and sorting of specific mRNAs in neurons (Todd et al. 2013). Mettl3 contains several KKxx motifs that can be recognised by the COP α protein (Arakel and Schwappach 2018), thus it may be involved in RNA-mediated vesicle trafficking from Golgi to ER, or to mitochondria (Zabezhinsky et al. 2016, Béthune et al. 2019). While the biological significance of these putative interactions has not been tested yet, these data nonetheless suggest that, similarly to vertebrate METTL3, a fraction of Mettl3 protein in flies might indeed exist in the cytoplasm, possibly acting as an RBP independently of its catalytic activity.

5.1.2 MACOM

In the current study, we have characterised the so-called MACOM complex (MAC-associated complex) that contains five subunits (Fl(2)d, Vir, Nito, Flacc and Hakai) conserved in flies and vertebrates (**Table 5**). In line with the role of MACOM complex in m⁶A deposition, we found that depletion of any component results in a strong decrease of m⁶A levels on mRNA. The MACOM complex, however, does not contain catalytic activity, but is instead required for stabilization of MAC and likely improves its binding to RNA. In addition, it provides a scaffold that guides MAC to target sites. Notably, the exact mechanism of how specific sites of methylation are selected, is not known yet and MACOM appears to be an important, but not the only factor in determining this process. Current knowledge on mediators that drive m⁶A specificity is discussed in *Chapter 5.4*. Most MACOM components were initially found in a screen searching for WTAP interactors in different human cell lines (Horiuchi et al. 2013), long before their association with m⁶A was discovered. We could show that in mouse cells MACOM components form a functional complex that is stable under high, 350 mM salt conditions. Similarly, all MACOM components in flies co-immunoprecipitate with Nito, indicating that the complex is conserved in these two species (**Appendix 2**, Fig. 1A, B). Many other features of MACOM components further highlight the existence of a stable complex involved in m⁶A methylation: **I**) all components primarily localize in the nucleus, where methylation takes place, **II**) expression profiles of all MACOM subunits strongly correlate with m⁶A levels during fly development (**Figure 46**). High enrichment is observed during early embryogenesis, at the onset of pupation as well as in adult heads and ovaries. **III**) All proteins of the MACOM complex have been implicated in splicing regulation of *Sex lethal (Sxl)*, the master regulator of sex determination in *D. melanogaster* (*Chapter 1.5.2*). **IV**) On a global scale, depletion of each component results in numerous common transcriptome changes (**Figure 39**) and a significant proportion of differentially expressed or spliced transcripts carry m⁶A modification, which strongly suggests that they are indeed direct targets of methylation. This was particularly apparent for genes whose steady state levels were up-regulated upon loss of m⁶A and were enriched for processes involved in embryonic development, cell differentiation and migration (n=136, 87,7 %, P<8,9e-52). Intriguingly, this could be indicative of an important role of m⁶A in the maintenance of the cellular identity as well as in the regulation of cell fate determination during differentiation, similarly to what has been described in numerous other species (Chen J. et al. 2019, Heck and Wilusz 2019). Notably, despite clear indications that MACOM complex is required for m⁶A deposition, several pieces of evidence also point towards separate functions. Most apparent is the early lethality of flies lacking any of the MACOM components, as compared to unaltered viability of flies that lack MAC. These aspects are further discussed in *Chapter 5.6*. Properties of individual MACOM components in flies, with the emphasis on similarities and differences with their orthologs in other species, are described below.

Fl(2)d (WTAP)

Fl(2)d is the fly ortholog of the WTAP protein, that was initially found to associate with the Mettl3 protein in plants, yeast and vertebrate cells (Agarwala et al. 2012, Bodi et al. 2012, Scholler et al. 2018). It encodes a 59 kDa protein with a high sequence similarity to human WTAP. While the structure of WTAP remains mysterious, it was shown to contain a predicted coiled-coil domain that is required for its binding with METTL3 (Scholler et al. 2018) (**Supplemental data 18 and 25**). Since the regions required for mediating the interaction between METTL3 and WTAP proteins are conserved in flies, we expect that the binding mode between Mettl3 and Fl(2)d is likely the same. Indeed, we could confirm that in flies Fl(2)d co-immunoprecipitated with both Mettl3 and Mettl4. However, we only detected direct binding between Fl(2)d and Mettl3, but not Fl(2)d and Mettl4 in a yeast-two-hybrid assay (**Figure 14**).

Likewise, the binding surface between vertebrate WTAP and METTL14 has not been confirmed yet. Intriguingly, we find that depletion of Fl(2)d strongly destabilizes the interaction between Mettl3 and Mettl14 proteins. This is, however, not the case when levels of Nito, Vir or Flacc are reduced (**Figure 31d** and **Appendix 2: Fig. S8A**), suggesting that only Fl(2)d is required for MAC integrity. On the first hand this seems to contradict the accumulated knowledge on MAC heterodimer stability (Sledz and Jinek 2016, Wang P. et al. 2016, Wang X. et al. 2016), thus it would be important to test the in vitro binding affinity between Mettl3 and Mettl14 in the presence and absence of Fl(2)d. Depletion of WTAP in human adipocyte cells, but not mouse ES cells, results in reduced levels of endogenous METTL3 and METTL14 proteins (Kobayashi et al. 2018, Wen et al. 2018), indicating that WTAP may potentially affect MAC formation via several different mechanisms.

Beside its binding to MAC and MACOM, we found that Fl(2)d also co-immunoprecipitated with other factors involved in RNA processing, heterochromatin organisation and cell cycle regulation (**Figure 15** and **Supplemental data 1**). This is in line with earlier studies reporting on Fl(2)d interaction with several splicing factors (Penn et al. 2008). Fl(2)d was also found to bind the heterochromatin associated protein HP1 and to act as an enhancer of gene silencing (Swenson et al. 2016, Kochanova et al. 2020). Intriguingly, we observed that a large fraction of methylated targets were up-regulated upon loss of m⁶A, hence it would be interesting to investigate the potential link between m⁶A deposition and transcriptional output. It is possible that m⁶A writer complex impedes transcription at specific loci and consequently ensures proper target methylation and downstream pre-mRNA processing. Notably, we did not find any association between m⁶A and mRNA stability in flies (data not shown), hence we assume that observed gene misregulation might, to some extent, originate from altered transcription. The link between transcription kinetics and methylation has been already demonstrated in vertebrate system, where reduced RNA PolII kinetics positively affects m⁶A writer recruitment to chromatin and, hence, increases m⁶A deposition on specific targets (Slobodin et al. 2017, Slobodin et al. 2020). Whether such interdependency between the speed of transcription and target methylation also exists in flies is currently not known. In flies, two Fl(2)d isoforms exist that differ in their N-terminal region (**Supplemental data 18**). While their individual functions have not been studied in detail, the long isoform appears to be predominantly expressed in most tissues and contains an extended histidine and glutamine rich region (HQ-rich) that is found in many transcription factors oftentimes promoting protein-protein interactions (Penalva et al. 2000). Notably, only this isoform can interact with the transcription factor Sine Oculis (So) in the eye (Anderson et al. 2014) and altered retinal development in *fl(2)d* mutant cells was in part attributed to elevated expression levels of two target genes of So, the *elav* and *lozenge*. Hence, this further suggests the potential role of Fl(2)d in the regulation of transcription. Of note, even though a small scale yeast-transcriptional-assay failed to prove such activity towards a particular *LacZ*-reporter (Anderson et al. 2014), genome wide approaches may be more appropriate to provide the full picture. Taken together, future work will be required to decipher the involvement of Fl(2)d in the process of transcription and to discriminate if this function is linked to m⁶A deposition, or else, if it acts independently of the m⁶A writer complex.

Vir (VIRMA)

Vir is an essential gene, required for survival and its loss of function leads to embryonic lethality in flies and mice (Schultt et al. 1998, Wu et al. 2019). It codes for the largest, 210 kDa nuclear protein of the MACOM complex with no defined structure or sequence features (**Supplemental data 19**). We found that *Vir* co-immunoprecipitated with Mettl3, Fl(2)d and Nito in an RNase independent manner (**Figure 31a**). Likewise, its human ortholog, VIRMA (also known as KIAA1429) binds WTAP and HAKAI

(Yue et al. 2018) and co-immunoprecipitated with MAC (Schwartz et al. 2014b), indicating that it is a component of the MACOM complex in flies and vertebrates. Notably, these interactions were mediated by its N-terminal region that is partially conserved in flies and was previously shown to be required for fly viability (Niessen et al. 2001). Tethering of N-termini to the reporter was sufficient to induce methylation (Yue et al. 2018), suggesting that this part is required for maintaining the functionality of the MACOM complex. On the other hand, the C-terminal region may be required for RNA binding or for interactions with other factors involved in the guidance of MACOM to methylation sites. The exact role of Vir within the complex is currently not known, but it may act as a scaffold for other MACOM components. We observed that stability of Vir is strongly dependent on Hakai, since depletion of Hakai in S2R+ cells leads to a substantial reduction of its protein, but not RNA levels (**Figure 42**), however the exact mechanism remains to be defined.

Nito (RBM15/RBM15B)

In *D. melanogaster*, Nito (also known as Spenito) is the closest ortholog of two vertebrate paralogs, RBM15 and RBM15B, and encodes a 90 kDa protein. Using co-immunoprecipitation assays, we found that Nito resides in the complex with other MACOM components (**Figure 31a**) and also interacts with MAC and Ythdc1 (**Figure 29** and **Appendix 2**: Fig. S8C, G and H). This is consistent with reports from vertebrates, where RBM15 was shown to interact with other m⁶A writer components (Horiuchi et al. 2013, Patil et al. 2016). In addition, we observed that the interaction between Nito and Fl(2)d is stabilised by Flacc, and intriguingly, this binding mode is conserved in vertebrates (**Figure 36** and **Appendix 2**: Fig. 6). Human and fly proteins contain several predicted NLS, which is consistent with their subcellular distribution and suggests that their localisation might be independent of other interactors (**Supplemental data 20**). Nito, RBM15 and RBM15B proteins are members of the split ends (Spen) family of proteins containing three N-terminal RRM domains and a C-terminal Spen paralogs and orthologs C-terminal (SPOC) domain. These regions are highly conserved, however proteins share low similarity outside of indicated domains. Nito, RBM15 and RBM15B are indispensable for efficient m⁶A deposition (Lence et al. 2016, Patil et al. 2016) and vertebrate counterparts were shown to bind uridine-rich sites in the proximity of m⁶A sites via RRM domains, which was proposed to contribute to methylation specificity (Patil et al. 2016). RBM15 can interact with various chromatin modifiers via the SPOC domain (Ma et al. 2007, Lee and Skalnik 2012, Xiao et al. 2015). It can for example bind the Setd1b H3K4me3 methyltransferase that marks sites of active transcription (Lee and Skalnik 2012, Xiao et al. 2015). Whether this is also the case for Nito has not been explored yet. In vertebrates, levels of RBM15 are regulated by the PRMT1 mediated methylation, followed by ubiquitination. The targeted Arginine residue is however not conserved in Nito, hence, it is currently not known if similar mode of regulation exists in flies. The importance of Nito was previously studied in several developmental processes; it promotes Wingless signalling (Chang et al. 2008) and is required for remodelling of CCAP/bursicon neurons (Gu et al. 2017), whereas elevated levels of Nito in the eye alter photoreceptor development (Jemc and Rebay 2006). In mice, RBM15 is critical for development of heart, spleen and vasculature as well as during haematopoiesis, B-cell and megakaryocyte differentiation (Raffel et al. 2007, Niu et al. 2009, Raffel et al. 2009, Jin et al. 2018). However, whether other components of MAC and MACOM complex are involved in these processes remains to be addressed. Our high throughput mass spectrometry analysis of Nito interactors identified many proteins involved in RNA processing and in particular splicing (**Figure 32a** and **Supplemental data 1**), which is in line with previous studies (Dong et al. 2015, Guo et al. 2018). Notably, RBM15 also interacts with several components of the early

spliceosome (Chu et al. 2015, Zhang L. et al. 2015), hence the involvement of this protein in the regulation of mRNA processing appears to be conserved.

Flacc (ZC3H13)

Flacc or “Fl(2)d associated complex component”, encodes a 1150 aa protein with no defined structure. It contains one predicted coiled-coiled domain embedded in the Arg/Glu-repeats that is partially conserved in its human ortholog ZC3H13 (**Supplemental data 21** and **25**). The importance of this region has not been addressed so far, but it may be targeted by PRMT-mediated methylation and affect protein functionality (Wei et al. 2020). Overall, Flacc shares low sequence similarity with its vertebrate orthologs that contain an N-terminal Zn-finger of unknown function, as well as several extended regions with a compositional bias of different amino acid repeats, which are not present in Flacc. We found that Flacc interacts with MACOM, in particular with Fl(2)d and Nito, as shown by the mass spectrometry analysis (**Figure 37** and **Supplemental data 1**). This is consistent with other parallel studies from flies (Guo et al. 2018), as well as from mES cells, where Zc3h13 forms a complex with Virma, Hakai, Wtap and Rbm15 proteins (**Appendix 2: Fig. 1**) (Wan et al. 2015). Intriguingly, we found that loss of Flacc specifically compromises the interaction between Nito and Fl(2)d, but not between other MAC or MACOM components (**Figure 36**). Importantly, despite the poor sequence similarity with vertebrate orthologs we were able to reconstitute this interaction with the human ZC3H13 protein, suggesting that protein folding, rather than primary sequences, are important for stabilization of MACOM complex. Notably, the final 300 aa of ZC3H13 were shown to be sufficient for interactions with HAKAI, WTAP and VIRMA; however, this region is only partially conserved in Flacc, which further implies that ZC3H13 and Flacc proteins likely share structural similarities. To our surprise, we found that Vir could interact with both, Nito and Fl(2)d independently of Flacc, however this was not sufficient to rescue the binding between the two proteins upon Flacc depletion. We currently do not hold an explanation for this observation, nevertheless, it is important to note that due to the lack of available antibodies, all experiments were performed with ectopically expressed proteins. Hence, it is possible that we were not able to detect some of potentially compromised interactions between endogenous Vir, Nito and Fl(2)d.

An important function that was also attributed to Zc3h13 in mESC, was its requirement for the localisation of other m⁶A writer complex components to the nucleus, albeit the role of Rbm15 was not addressed in this study (Wen et al. 2018). We could show that in Zc3h13 KO mES cells, Rbm15 immunoprecipitated less Wtap, Virma and Hakai proteins than in control cells. This clearly indicated that interactions between Rbm15 and other MACOM components were compromised and could indeed result from aberrant protein localisation (**Appendix 2: Fig. S9**). While we did not observe any changes in subcellular distribution of Fl(2)d and Nito proteins upon depletion of Flacc in *D. melanogaster* S2R+ cells (data not shown), such tethering mechanism might nevertheless exist in other cell types. Indeed, our Flacc interactome analysis identified several proteins that constitute nuclear pore complex (**Figure 37**), hence it would be interesting to test if Zc3h13/Flacc mediated m⁶A writer guidance to the nucleus is cell-type specific. Notably, Flacc and ZC3H13 contain NLS and primarily localize to the nuclei, however a fraction of proteins was also detected in specific punta within the cytoplasm (**Figure 36c**). Our Flacc interactome data from S2R+ cells identified many proteins involved in transcription, RNA splicing and localisation, which is in line with proposed functions of m⁶A modification (**Figure 37**). Unexpectedly, among identified Flacc interactors were also several metabolic enzymes and proteins that constitute vacuoles, peroxisomes and mitochondria. This opens an intriguing

possibility that Flacc may be implicated in cellular processes linked to metabolism and biogenesis of cytoplasmic vesicles.

Hakai (HAKAI)

Hakai protein (named by “destruction” in Japanese) also known as the CBLL1 (for Cbl-like 1 or Cbl Proto-Oncogene-like 1) is highly conserved among metazoan and plants, but absent in yeast (Horiuchi et al. 2013, Růžička et al. 2017, Knuckles et al. 2018). Its functions within the MACOM complex are currently least understood. In *D. melanogaster*, Hakai encodes a 49 kDa protein with two N-terminal domains that display high sequence identity with human ortholog HAKAI (**Supplemental data 22**); the RING-type domain, which is found in many E3 ubiquitin ligases, and the Zn-finger containing region that is required for binding of the phosphorylated-Tyrosine (p-Tyr)-residues (Mukherjee et al. 2012, Růžička et al. 2017). In addition, Hakai in flies contains an N-terminal Arg/Gly-repeats, whereas human ortholog contains a C-terminal Pro-rich region. In plants and vertebrates, Hakai was shown to form a stable homodimer (Mukherjee et al. 2012, Růžička et al. 2017), which is consistent with our results from a yeast-two-hybrid assay, showing that Hakai also homodimerizes in flies (**Figure 40**). Previous studies that characterised partial HAKAI structure in humans, revealed that two HAKAI monomers interact in an antiparallel manner via the highly conserved RING and pTyr-binding domains (Mukherjee et al. 2012). These two domains form a positively charged pocket of the so-called HYB domain (Hakai pTyr-binding), which can accommodate proteins that carry a phosphorylated Tyr residues, surrounded by acidic Asp and Glu amino acids (Mukherjee et al. 2012). Among known binding targets are E-cadherin, contractin and DOK1 that are phosphorylated by the Src-kinase (Mukherjee et al. 2012). In addition, Hakai interacts with constituents of the MACOM complex in vertebrates and plants (Mukherjee et al. 2012, Růžička et al. 2017) and we were able to show that these interactions are conserved in flies. Hakai was for example identified in the Nito interactome (**Figure 32**) and could efficiently co-immunoprecipitate Nito and Fl(2)d proteins in S2R+ cells (**Figure 40a**). We also observed direct binding between ectopically expressed Hakai, Nito and Fl(2)d proteins in a yeast-two-hybrid assay (**Figure 40b**). Intriguingly, Hakai was shown to share many common interactors with WTAP in several different human cell types (Horiuchi et al. 2013) and deletion of a RING domain completely abolished binding with other proteins (Horiuchi et al. 2013). Notably, since this domain contributes to the formation of a stable homodimer, lost interactions most likely reflect a failure of Hakai Δ RING to form contacts with other proteins due to a structural instability of the HYB domain (Mukherjee et al. 2012, Horiuchi et al. 2013). Further details on Hakai HYB and RING domains are discussed in *Chapter 5.1.3*, along with a potential function of Hakai as an active E3 ubiquitin ligase.

Intriguingly, we found that Hakai is crucial for stabilization of Vir, Fl(2)d and Flacc proteins (**Figure 42g, h**). While it is currently not understood how exactly Hakai maintains MACOM homeostasis, it would be informative to investigate, if its loss has the same role in other species. Notably, Hakai depletion only marginally reduced Zc3h13 levels in mES cells, whereas other proteins have not been analysed (Wen et al. 2018). Intriguingly, in flies, Hakai had the strongest impact on levels of Vir that contains a predicted tyrosine phosphorylation site (Y307), located within an acidic amino acid sequence DYEDD (**Supplemental data 19**) (Zhai et al. 2008). This reinforces the idea that the interaction between Vir and Hakai is most likely direct. Of note, levels of the two MAC components and Nito were not affected, which supports previous findings that Mettl3 and Mettl14 form a stable complex on their own and that Nito is involved in additional processes, not linked to the MACOM complex (see below *Chapter 5.1.3*). Depletion of Hakai in vertebrates and flies leads to a significant reduction of m⁶A levels in mRNA (Růžička et al. 2017, Yue et al. 2018), hence, we propose that Hakai protein is an essential constituent

of the m⁶A writer complex and is crucial for m⁶A deposition, by ensuring stability of the MACOM complex.

Similarly to other MACOM components, HAKAI is highly enriched in the nucleus in plants and in most vertebrate cell types (Horiuchi et al. 2013, Růžička et al. 2017). Intriguingly, in several human epithelial cell lines, a fraction of HAKAI was also found in the cytoplasm at sites of cell-cell contacts along the membrane, where it co-localised with E-cadherin, a constituent of adherens junctions (Fujita et al. 2002). In flies, Hakai protein exists in four different isoforms, two longer and two shorter, which differ in their C-terminal region. All isoforms contain the HYB domain (**Figure 38b** and **Supplemental data 22**) and were able to bind ectopically expressed Fl(2)d and Nito in a yeast-two-hybrid assay (**Figure 40b** and data not shown for the short isoform). Despite these similarities, we found that subcellular localisation of short and long Hakai proteins is different. In *D. melanogaster* BG3 cells, the long isoform is expressed ubiquitously with a clear enrichment in the nucleus and resembles the expression pattern that was previously observed in S2R+ cells (Kaido et al. 2009). On the other hand, the short Hakai isoform is restricted to the cytoplasm and enriched at the cellular membrane (**Figure 38d**). While it is important to note that we used ectopically expressed proteins to assess their localisation, these results nevertheless suggest that long and short Hakai proteins might be involved in different cellular processes. Notably, since none of the two Hakai isoforms contains NLS, they are most likely tethered to distinct cellular compartments via a distinct set of interactors. Intriguingly however, work by Keido and colleagues previously demonstrated that co-expression of E-cadherin and the long Hakai isoform in *D. melanogaster* S2R+ cells was sufficient to promote the re-localisation of this isoform from the nucleus to sites of cell-cell junctions (Kaido et al. 2009). This strongly suggests that short and long Hakai isoforms can also act redundantly and that their localisation most likely depends on the temporal cellular proteome. Indeed, in vertebrates HAKAI displays distinct subcellular distribution in different human cell lines and can dynamically change upon various stimuli (Figuroa et al. 2009, Horiuchi et al. 2013, Díaz-Díaz et al. 2017). It is currently not understood why short and long Hakai isoforms in flies localise to distinct cellular compartments under unperturbed conditions and whether this is biologically relevant. In order to decipher the unique roles of the two Hakai proteins, several important questions remain to be addressed:

- Do short and long Hakai isoforms localise to different compartments in all cell types? Which other proteins, beside E-cadherin, can affect their distribution?
- What are isoform specific interactors? Does the short Hakai isoform preferentially interact with the E-cadherin (or other cell-cell contact proteins) in BG3 cells?
- Do both isoforms display the same affinity to other MACOM components? Can both isoforms rescue protein levels of Vir, Fl(2)d and Flacc in *Hakai null* cells? Which of the two isoforms can potentially replace Hakai loss in plants and vertebrates?

To investigate the role of different Hakai isoforms *in vivo*, we generated flies with specifically deleted long isoform as well as *Hakai null* flies. As shown before, Hakai is indispensable for survival and flies lacking both isoforms die during larval stages ((Kaido et al. 2009) and our unpublished data). In addition, previous study from Kaido and colleagues demonstrated that germline loss of Hakai leads to embryonic lethality with variable penetrance (Kaido et al. 2009). Several developmental processes, including dorsal closure and ectoderm organisation were shown to be altered, likely resulting from impaired epithelial formation and cell motility. Notably, many embryos displayed deteriorated epithelial integrity, which was most apparent at regions that require morphological changes (tracheal invagination, segmental furrow formation) (Kaido et al. 2009). Aberrant cell migration also contributed

to defects in midgut formation where endoderm and visceral mesoderm failed to reach proper positions, whereas in migrating tracheal cells, Hakai was required for F-actin organisation and cell motility. The importance of Hakai protein in the epithelial development was, in addition, supported by a large genetic screen where Hakai was found as a modifier of a rough eye phenotype. Its inactivation enhanced the defects in organisation of the eye epithelium (Ketosugbo et al. 2017). Taken together, Hakai likely functions in distinct cell types to control cell migration, regulate cellular connectivity and maintain tissue homeostasis. Hence, upon loss of Hakai, a combination of different defects leads to early fly lethality. Of note, we found that flies lacking only the long isoform are viable, whereas Kaido and colleagues obtained a partial rescue of *Hakai null* flies by ectopic expression of the long Hakai isoform. These results, hence, strongly suggest the two Hakai isoforms can act redundantly also in vivo. Which processes are preferentially regulated by a short or long Hakai isoform, is currently not known, and will need to be investigated in the future.

HAKAI has been also studied in plants, where it co-purifies with VIR and FIP37 (WTAP ortholog), and localizes exclusively in the nuclei (Růžička et al. 2017). Complete loss of MAC components, FIP37 or VIR leads to developmental arrest during seed development and results in embryonic lethality (Bodi et al. 2012). Surprisingly, HAKAI mutant plants are viable, with no apparent defects and with only marginally decreased m⁶A levels (Růžička et al. 2017), suggesting that its functions are not essential for plant development. Nevertheless, a strong genetic interaction was observed between HAKAI and FIP37 trans-heterozygous plants, which failed to produce homozygous seedlings. In addition, removal of HAKAI in MTA (Mettl3 ortholog) mutants strongly deteriorated the severity of growth phenotype (Růžička et al. 2017). This altogether indicates that in plants HAKAI mediates m⁶A functions, albeit it is not a crucial component of the m⁶A writer complex. Whether it affects stability of other MACOM components is currently not known. In vertebrates, HAKAI was found to be highly enriched in the proliferating tissue as well as in many cases of malignancies (Figueroa et al. 2009, Aparicio et al. 2012, Castosa et al. 2018) and was recently proposed as a potential novel target for cancer treatment (Díaz-Díaz et al. 2017, Castosa et al. 2018). In the future it will be important to investigate, which proteins might be regulated by HAKAI-mediated ubiquitination and whether this activity is required for functional m⁶A methylation (see *Chapter 5.1.3*).

How do MAC and MACOM complexes assemble and interact?

Existing data indicate that Fl(2)d is the main bridging factor that connects MACOM with the MAC complex (**Figure 43** and **Supplemental data 26**). However, given that there are currently no structural insights of the MACOM complex, it remains possible that other components also contribute to MAC binding. In fact, exact assembly and connectivity between MACOM components are to a large extent still unknown. Likewise, protein stabilities appear strongly interdependent. Most of the data from our work and other studies suggest that Fl(2)d directly interacts with Vir and Hakai, whereas its interaction with Nito strongly depends on the presence of Flacc. Given the protein size and currently known interactions, it is conceivable that Vir potentially functions as a scaffold, connecting other components. Notably, depletion of Virma in mES cells leads to substantially diminished levels of Wtap and Zc3h13 proteins (Wen et al. 2018, Yue et al. 2018). In addition, depletion of Wtap or Hakai independently of Virma also results in Zc3h13 reduction, suggesting that each of these subunits contributes to MACOM stability and functionality (**Figure 43** and **Supplemental data 26**). Notably, we found that in flies and mES cells depletion of Flacc (Zc3h13) destabilizes the interaction between Fl(2)d (Wtap) and Nito (Rbm15), however, protein levels of all components remain unperturbed. This infers that binding between Wtap-

Vir-Hakai might be independent of Flacc and Nito. Indeed, plants do not encode Nito and Flacc orthologs (**Figure 44**), hence these three components possibly form a stable “minimal” MACOM complex on their own (Růžička et al. 2017). In addition, upon loss of Flacc in mES cells, Wtap, Vir and Hakai can still interact, even though they are retained in the cytoplasm (Wen et al. 2018). Intriguingly, depletion of any of these proteins also leads to cytoplasmic retention of Mettl3 and Mettl14 proteins, strongly suggesting that a completely assembled “minimal” MACOM complex is in fact needed for the interaction with MAC heterodimer within the nuclei. Nonetheless, further characterisation of each individual component will be required to precisely define binding surfaces and interdependencies between them.

We found that in addition to Hakai, also Mettl14, Fl(2)d and Nito can form homodimers (**Figure 40** and data not shown), which is consistent with observations from plants (Růžička et al. 2017). These interactions could promote clustering of the m⁶A writer within a particular region of the selected transcript to enrich methylation at certain loci. Indeed, m⁶A mapping data from flies and vertebrates identified areas with prominent m⁶A clusters in most methylated transcripts (Linder et al. 2015) (**Supplemental data 7**). Thus, to understand mechanisms for m⁶A site selection, it will be informative to validate and further investigate these observations. In summary, structural and biochemical studies of MAC and MACOM complexes will be required to uncover the exact spatial positioning of each component and to shed light on the precise contribution of individual protein in the formation and stability of m⁶A writer.

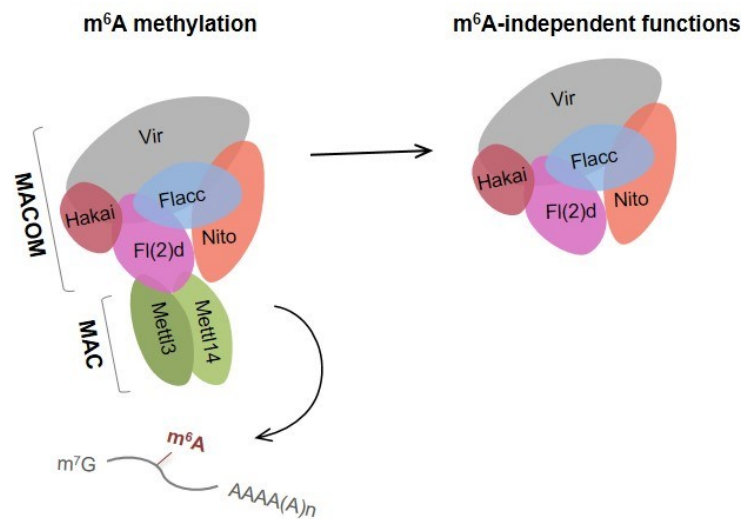


Figure 43. Scheme depicting components of MAC and MACOM complexes required for m⁶A methylation in *D. melanogaster*. MAC and MACOM complexes interact and form a functional methyltransferase complex in order to deposit m⁶A on targeted RNA (left). MACOM is also involved in m⁶A-independent processes (right). For details see also **Supplemental data 26**.

5.1.3 m⁶A-independent functions of MACOM components

As discussed in previous chapters, MACOM complex is crucial for efficient m⁶A deposition to a vast majority of sites. However, molecular and genetic characterisation of MACOM components clearly indicates that they are involved in additional, m⁶A-independent processes. I) We find that depletion of any MACOM component in S2R+ cells results in more severe gene misregulation than depletion of MAC (**Figure 39**). Among misregulated genes, nearly 30 % were not methylated, suggesting that those transcripts might represent their m⁶A-independent targets. It is important to note that these conclusions are based on gene depletion experiments, which may not entirely recapitulate a clear effect of a loss-of-function allele. Hence, it is possible that gene expression changes reported in current work reflect the non-ideal KD efficiencies. II) A clear distinction between MAC and MACOM components is also apparent *in vivo*. While *Mettl3* and *Mettl14* KO flies are viable, the loss of any MACOM component results in lethality during early stages of development, prior to pupation. III) In addition, flies with reduced levels of MACOM components also exhibit more pronounced effects on splicing of *Sex lethal* transcript. We observed that depletion of Nito or Flacc in legs and genitalia discs results in a strong female masculinisation (**Figure 35**). In contrast, flies lacking MAC components show none of these phenotypic characteristics, even though splicing of *Sxl* is altered to some extent (**Figure 26**). These differences may originate from an independent role of MACOM in *Sxl* splicing or an additional function in the regulation of downstream targets within the *Sxl* cascade (See *Chapter 5.5.1*). IV) Given that Fl(2)d, Nito, Vir interact with many splicing factors and spliceosome-associated proteins (**Supplemental data 1**), MACOM might be involved in modulating splicing independently of m⁶A. To address this possibility, it will be important to obtain a precise record depicting transcriptome wide binding of each individual component of MAC and MACOM. In addition to the above-mentioned m⁶A-independent roles of the complete MACOM complex, some unique features of Nito and Hakai also suggest that these proteins may act individually in unrelated pathways.

Nito

Several pieces of evidence suggest that Nito may be involved in processes that are independent of both, m⁶A deposition and MACOM complex. Nito was the only MACOM component, not destabilized upon Hakai KD in our proteome study (**Figure 42h**) and its depletion misregulated a large number of genes that were not shared with other m⁶A writer subunits (**Figure 39**). We observed that depletion of Flacc only marginally affects binding of Nito to m⁶A target transcripts, as demonstrated by the RIP-qPCR experiments. This suggests that its binding to RNA is, at least to some extent, independent of the remaining MACOM components. Of note, binding of Fl(2)d to the same RNA targets was significantly altered, confirming that its interaction with RNA is more dependent on the stable MACOM complex (**Figure 36b**). Another piece of data in favour of Nito having MACOM independent functions, comes from a large study on conserved macro-molecular complexes, in which Nito (and human RBM15 and RBM15B) was found in a complex with a different set of proteins (Wan et al. 2015). Among them were RNA/DNA binding proteins and helicases Dhx15 (DHX15), Trmt112 (TRMT112), CG3155 (SUGP1) and CG7878 (DDX43) (**Table 5**). While the relevance of these interactions is yet to be confirmed, it would, nevertheless, be interesting to see if any of these proteins can modulate or interfere with m⁶A deposition. Finally, in our search for novel m⁶A reader proteins, Nito and Dhx15 were efficiently recovered with the m⁶A modified RNA probe, which suggests that Nito may act in processes downstream of m⁶A writing, potentially as m⁶A reader on a subset of m⁶A sites (**Figure 20**). In summary, further work may decipher putative roles of Nito beyond m⁶A methylation.

Hakai

Contrasting other MACOM components, localisation of the two Hakai isoforms is not restricted to the nuclear compartment. In flies, the long Hakai isoform displays ubiquitous expression with a prominent localisation in the nucleus, whereas the short isoform is enriched in the cytoplasm at cellular membrane (**Figure 42**). Such distinct expression strongly suggests that Hakai is involved in processes within the cytoplasm independently of the MACOM complex. Notably, Hakai contains a conserved RING (really interesting new gene) domain that is found in many active E3 ubiquitin ligases and was, therefore, proposed to act as one (Fujita et al. 2002). Thus far, the only target shown to be bound and supposedly ubiquitinated by HAKAI, is a protein E-cadherin (Fujita et al. 2002). It encodes a transmembrane protein that mediates cell-cell adhesion at sites of adherens junctions. E-cadherin is highly expressed in epithelial cells and plays central roles in epithelial cell polarity as well as in the regulation of cell motility during development, tissue remodeling, carcinogenesis and epithelial-mesenchymal transition (EMT) (Takeichi 1995). Using its extracellular domain, E-cadherin homodimerizes with another E-cadherin on the neighbouring cell. On the other hand, its intracellular domain is required for interactions with p120 catenin and β -catenin that stabilise E-cadherin at the cellular membrane and connect it with the actin cytoskeleton (Takeichi 1995). Hakai can bind E-cadherin that is phosphorylated at a specific Tyrosine residue (pTyr) within its intracellular region (Fujita et al. 2002, Mukherjee et al. 2012). Mechanistically, upon E-cadherin phosphorylation, binding of catenins is outcompeted by Hakai that promotes E-cadherin ubiquitination. Once ubiquitinated, E-cadherin gets cleaved, endocytosed and degraded, which consequently leads to the loosening of cellular contacts (Fujita et al. 2002).

Hakai (also known as Cbl-like-1) was initially proposed to act as an E3 ubiquitin ligase because of its sequence similarity with the well characterised E3 ubiquitin ligase, Cbl (Casitas B-lineage Lymphoma). Both proteins contain a RING domain, pTyr-binding domain and a C-terminal Pro-rich region. However, the RING and p-Tyr domains in Hakai and Cbl are in reversed order and adopt entirely different folding (Dou et al. 2012). In Cbl, the pTyr-binding domain (also known as SH2 domain) consists of a Zn-finger that can accommodate pTyr-containing targets (Joazeiro et al. 1999). Downstream RING domain then facilitates ubiquitin transfer from the ubiquitin conjugating enzyme (E2) to the bound target by acting as a scaffold that connects E2 with its substrates (reviewed in (Metzger et al. 2012, Cooper et al. 2015)). In contrast to Cbl, Hakai has to homodimerize in order to create an atypical pTyr binding module at the interface of two proteins. Notably, several residues of the RING domain are also required for homodimer stabilisation (Mukherjee et al. 2012). Two RING domains and two pTyr domains of the Hakai dimer, fold in the so-called HYB domain that is essential for interactions with other proteins (**Supplemental data 22**), including components of the MACOM complex (Mukherjee et al. 2012, Horiuchi et al. 2013). HYB domain can also specifically accommodate proteins with pTyr residues surrounded by acidic residues.

Several studies demonstrated that Hakai binds phosphorylated E-cadherin and other proteins via its HYB domain, however a direct evidence for its ubiquitination activity is currently missing (Fujita et al. 2002, Mukherjee et al. 2012). The ubiquitination of E-cadherin can be elevated upon simultaneous overexpression of Src-kinase and Hakai (Fujita et al. 2002), however by such indirect approach one cannot rule out that ubiquitination is carried out by another E3 ligase. Indeed, E-cadherin can be ubiquitinated by at least two other E3 ubiquitin ligases, MDM2 and RNF43, in a p-Tyr dependent manner (Yang et al. 2006, Zhang Y. et al. 2019). It is therefore possible that Hakai uses the HYB domain to bind p-Tyr targets and then acts as a bridging factor that mediates transfer of the bound protein to another E3 ligase. Notably, in vertebrates Hakai immunoprecipitated with RNF20 and RNF40

(Mukherjee et al. 2012), whereas in *D. melanogaster* it was shown to interact with several E3 ligases such as Parkin, Ariadine1 and Ariadine2 (Aguilera et al. 2000, Giot et al. 2003, Gradilla et al. 2011). Nevertheless, it remains possible that Hakai acts as an ubiquitin ligase in certain cell types or on a limited subset of its interactors. Of note, Hakai does not directly interact with and ubiquitinate E-cadherin in *D. melanogaster*, despite the fact that they co-immunoprecipitate and colocalise at sites of cell-cell junctions (Kaido et al. 2009). Hence other ubiquitin ligases must mediate E-cadherin internalisation and subsequent degradation in flies.

To identify potential ubiquitinated targets of Hakai in flies, we performed a quantitative ubiquitinome analysis of control and Hakai depleted S2R+ cells. To our surprise, we did not find any Hakai dependent ubiquitination-sites that would consistently change in both replicates (**Figure 41**). Notably, many sites were differentially ubiquitinated in a single replicate, however, given that the heavy and light amino acid labelled cells displayed morphological differences it is more likely that these sites simply reflect the effect of cell labeling, rather than relevant Hakai-dependent ubiquitination. Nevertheless, in order to find any potential targets that might not be expressed in S2R+ cells, it will be important to perform ubiquitinome analysis in non-labelled cells, preferentially originating from *Hakai* mutant flies that we had generated. In summary, despite having a RING domain and being initially proposed to act as an active E3 ubiquitin ligase, it will be important to unambiguously confirm that Hakai indeed carries out ubiquitination of proteins it binds. To address this, it will be crucial to:

- Identify the E2 ubiquitin conjugating enzyme involved in ubiquitination reaction(s).
- Confirm that ubiquitination of E-cadherin in vertebrates is indeed carried out by Hakai and characterise other putative ubiquitinated targets.
- Uncouple the pTyr binding role from the ubiquitination role of the HYB domain.
- Specify the exact interaction sites between Hakai and other MACOM components in order to understand if ubiquitination plays any role in the process of m⁶A deposition.

Taken together, the combined biochemical and transcriptome analyses, along with phenotypical characterizations of all seven proteins of the writer complex suggest that they reside in two separate complexes, the MAC and the MACOM (**Figure 43** and **Supplemental data 26**). MACOM complex has significant roles beyond m⁶A deposition that will have to be systematically investigated in the future. Keeping this in mind it will be crucial to uncouple functions of individual MACOM components that occur due to alterations in m⁶A deposition from the ones that are m⁶A independent. In addition, Mettl3 and Mettl14 were implicated in processes that do not require MACOM components (see below *Chapter 5.1.4*), implying that MAC may also act on specific targets in a MACOM independent fashion. Future work may provide better understanding of regulatory mechanisms that define how and when MAC and MACOM complexes interact and deposit m⁶A.

5.1.4 Is MACOM required for methylation of all mRNA sites?

We could demonstrate that depletion of any subunit of MACOM leads to a significant reduction of m⁶A levels in mRNA, indicating that MACOM complex is indispensable for m⁶A deposition. However, a few examples discussed below, indicate that methylation of some sites may, nevertheless, not depend on all MACOM subunits.

m⁶A writer composition

Regulated deposition, decoding and removal of m⁶A mRNA modification is crucial for proper development and functioning of most eukaryotic organisms studied thus far. Yet, notable differences exist in regards to the composition of the m⁶A writer complex as well as in a variety of reader proteins and in the presence or absence of m⁶A demethylases. **Figure 44** and a table in the **Supplemental data 13** summarize our current knowledge about different m⁶A methyltransferases and their substrate preferences in some of the model organisms. Dissimilarities in the composition of MAC and MACOM complexes in different organisms raise the question, whether all MACOM components are equally important for m⁶A deposition on mRNA.

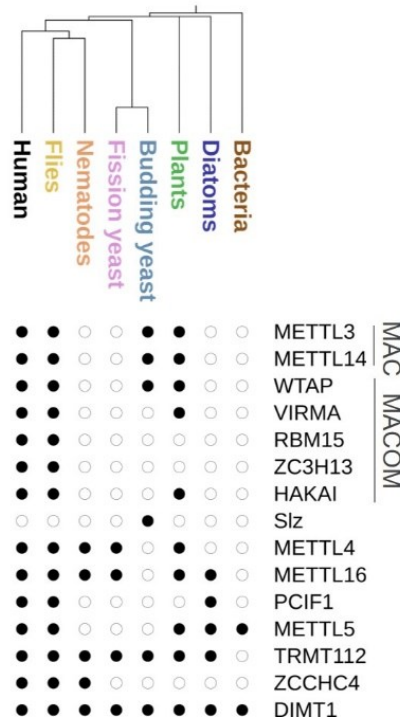


Figure 44. Proteins required for methylation of N⁶-position of adenosine in representative organisms.

Phylogenetic tree is shown on the left, whereas m⁶A methyltransferases and associated proteins are listed on top. Full dots represent the presence of the indicated protein. PCIF1 acts on Am and forms m⁶Am modification. DIMT1 adds m^{6,2}A instead of m⁶A and different bacterial Erm enzymes can form m⁶A or m^{6,2}A modifications. See also Supplemental data 13. Figure was generated with iTOL tool (Letunic and Bork 2019).

As described in previous sections, in flies and vertebrates, seven proteins constitute MAC and MACOM. Plants, on the other hand, do not encode orthologs of RBM15 and ZC3H13 components and methylation is efficiently carried out with only five subunits. Notably, different methylation motif (UGUAHH) has been identified in plants (Li Y. et al. 2014, Wei L.-H. et al. 2018, Zhang F. et al. 2019, Wang et al. 2020), however it is currently not known if this is due to different composition of the m⁶A-

complex, or if the genome context and other possible interactors drive methylation within this particular sequence. Nevertheless, it would be interesting to study if ectopic expression of ZC3H13 and RBM15 proteins could induce differential methylation in plants. Another interesting example of the m⁶A writer complex, with different composition also comes from budding yeast, where the so-called MIS complex only consists of three subunits; Mum2 (Wtap), Ime4 (Mettl3) and a yeast specific factor Slz (*Chapter 1.4.4*) (Agarwala et al. 2012). Notably, despite this obvious difference in the complex composition, the methylation motif as well as m⁶A enrichment along the mRNA appear to be the same as in vertebrates (Schwartz et al. 2013). It will be of great interest to structurally characterise m⁶A writer complexes from different species and compare their selective binding to mRNA along with their putative associations with the chromatin. Such findings would without a doubt shed light onto why the very same catalytic enzyme in *S. cerevisiae* only requires two accessory proteins, whereas in higher eukaryotes efficient methylation depends on the large MACOM complex.

Cytoplasmic methylation

In most cell types, MAC and MACOM components show predominantly nuclear localization, as inferred by immunostaining experiments. In contrast, the cell fractionation analysis of mES cells, found a strong cytoplasmic localization of MAC, but not MACOM components (Wen et al. 2018), suggesting that MAC might carry out cytoplasmic methylation of specific targets independently of MACOM. Interestingly, numerous reports identified m⁶A on transcripts originating from ssRNA viruses of *Flaviviridae* family that replicate exclusively in the cytoplasm (e.g. HCV, DENV, ZIKV, KSHV, and others) (Gokhale et al. 2016, Lichinchi G. et al. 2016, Dang et al. 2019). This raises several possibilities for their methylation: **I)** cytoplasm-located MAC complex is sufficient for m⁶A deposition, **II)** a certain amount of functional MAC-MACOM complexes exists in the cytoplasm or **III)** MAC and MACOM components localize to the cytoplasm upon infection. **IV)** Alternatively, methylation could be carried out by a different cytoplasmic methyltransferase. To discriminate which of these possibilities holds true, it would be informative to monitor the localisation of each component upon viral infection and to analyse potential changes in the complex composition. Intriguingly, in mES cells Zc3h13 was shown to be required for nuclear localization of other m⁶A writer components (Wen et al. 2018), therefore its regulated re-localisation to the cytoplasm could, in principle, enable the formation of a complete methylation machinery in this compartment. Alternatively, since loss of ZC3H13 was shown to specifically destabilize only the interaction between WTAP and RBM15 (**Figure 36**), a stable and catalytically competent complex of MAC, WTAP, VIR, ZC3H13 and HAKAI proteins might still exist in the cytoplasm. Such complexes could carry out methylation of viral and other potential targets. Characterisation of mechanisms that drive cytoplasmic methylation of viral RNA could have important implications for future development of potential antiviral treatments.

m⁶A methylation upon cellular stress

Findings from a few studies suggest that under certain cellular conditions MACOM complex is not required for m⁶A methylation. Upon UV-induced DNA damage, m⁶A levels rapidly increase at sites of DNA lesions (peaking at two minutes post laser-induced DNA damage), which in turn promotes DNA repair via DNA polymerase- κ (Pol- κ) dependent mechanism (Xiang et al. 2017). Under these circumstances, Mettl3 and Mettl14 were shown to be essential for m⁶A deposition, however Wtap protein was found dispensable, suggesting that MACOM may not be required. Although it is not possible to exclude that other MACOM components facilitated MAC recruitment to sites of methylation, this work, nevertheless, demonstrates that co-transcriptional deposition of m⁶A in certain cellular

conditions does not require all MACOM components. Of note, this study characterised methylated RNA species by MeRIP sequencing (restricted to polyA+ RNA) and found enrichment of m⁶A at 5' UTR regions within the RRACH and other motifs. Thus, future work implementing precise mapping of MAC/MACOM binding before and after DNA damage, and characterisation of MAC-interacting proteins during DNA damage, might shed light onto the exact mechanism of m⁶A-mediated DNA repair. Intriguingly, in human cells, WTAP and HAKAI co-precipitate with splicing-associated proteins THRAP3 and BCLAF1 (Horiuchi et al. 2013). In the context of UV-induced DNA damage, these two proteins were found to be rapidly excluded from damage sites (within two minutes after laser-induced DNA damage), which in turn promoted cellular resistance to genotoxic stress (Beli et al. 2012). It would be interesting to test if THRAP3 and BCLAF1 proteins perhaps mediate the removal of MACOM complex from DNA damage sites prior to methylation of nascent transcripts, and to further investigate the potential interplay between THRAP3/BCLAF1 proteins and m⁶A methylation. Intriguingly, since no orthologs of THRAP3 or BCLAF1 proteins neither of Pol-κ exist in *D. melanogaster*, it might be informative to investigate if MAC mediated m⁶A methylation upon DNA damage also occurs in flies and if so, how are methylation and repair regulated (Sekelsky 2017).

5.1.5 What are the functions of other putative m⁶A methyltransferases in flies?

In flies and other species, Mettl3 and Mettl14 proteins are part of the conserved methylation complex that is required for deposition of a majority of m⁶A on mRNA. Besides, several other m⁶A methyltransferases that can act on different RNA and DNA targets have also been characterised in recent years (*Chapter 1.4.3*) (**Supplemental data 14**). When we initiated this project only the function of Mettl3 was known and we therefore decided to screen for additional m⁶A mRNA methyltransferases that could potentially act on mRNA. We searched for fly proteins that contained the N6-MTase sequence motif (Prosite: PS00092) (Timinskas et al. 1995, Sigrist et al. 2013). Beside two closest Mettl3 paralogs, Mettl14 (CG7818) and Mettl4 (CG14906), we found six other uncharacterised proteins (CG9531, CG9966, CG9154, CG9666, CG1074 and CG7544), whose functions in flies were not known (**Supplemental data 8**). We tested all proteins for m⁶A-activity by depleting them in *D. melanogaster* S2R+ cells and by measuring residual m⁶A levels on mRNA. Unlike depletion of Mettl3 and Mettl14 that strongly reduced m⁶A levels, KD of other candidates showed no evident change (**Supplemental data 8**). Intriguingly, Mettl16, a vertebrate ortholog of CG7544 protein was later found to specifically methylate U6 snRNA and one particular mRNA target in human cells (*Mat2a*), whereas Mettl5, an ortholog of CG9666 protein was recently characterised as an exclusive 28s rRNA m⁶A methyltransferase (Van tran et al. 2019, Ignatova et al. 2020, Leismann et al. 2020). Such restricted substrate selectivity of Mettl16 and Mettl5 proteins likely explains why no change in m⁶A levels was observed in our enzyme depletion-LC/MS assay. Nevertheless, it is possible that also in flies, CG7544 and other putative m⁶A methyltransferases act on a limited set of mRNA targets. Different approaches, such as characterisation of transcriptome wide RNA binding sites and analysis of m⁶A levels in different RNA species, should enable identification of relevant targets and shed light on molecular functions of these methyltransferases in the future.

Among other uncharacterised methyltransferases, Mettl4 (CG14906) is a nuclear protein that belongs to the same clade of N6-MTases as Mettl3 and Mettl14 proteins (**Figure 1**) and shares high sequence similarity with the two proteins within the MT-A70 domain. Thus, we assumed that it might act as a potential m⁶A methyltransferase and decided to investigate its functions in vivo. Using the CRISPR-Cas9 system we generated a mutant allele (*Mettl4 Δ 2*) that lacked a large part of the CDS including the translation start site (**Supplemental data 9**). Flies lacking Mettl4 were homozygous viable and displayed no obvious developmental defects indicating that Mettl4 is not essential for fly survival. This observation is consistent with other alleles that have been described thus far (Silva 2017, Gu et al. 2020). We analysed transcript expression levels during fly development and noticed that *Mettl4* levels are particularly high in the first hour of embryogenesis. *Mettl4* is also elevated during the transition from late larvae to pupation (120 h) and is rather high in adult flies (**Supplemental data 9**), suggesting that Mettl4 might be important during these developmental stages.

Intriguingly, a few recent studies provided novel insights into the role of this methyltransferase. Mettl4 was found to act as an N6-adenosine methyltransferase in human HEK293 cells, where it forms the m⁶Am modification of U2 snRNA by methylating the pre-existing Am residue at position A30 (Chen 2020 Cell Research, Goh 2020 Biorxiv). Consistently, a recent study in flies also identified the activity of Mettl4 as an m⁶A methyltransferase of the U2 snRNA, acting on site A30 (Gu et al. 2020). Notably, in collaboration with Prof. Suzuki's group (The University of Tokyo), we were able to confirm that our *Mettl4 Δ 2* mutant flies indeed lack m⁶A methylation in U2 snRNA at the position A30, as well as at the following position A31 (unpublished data). In light of these recent reports, it would be interesting to functionally compare the human and fly Mettl4 orthologs since the activity of human METTL4 was

found to be strongly elevated by the Nm modification, which is not present at these positions in flies. All studies also reported alterations in pre-mRNA splicing upon loss of Mettl4, albeit direct involvement of the N6-methylation has not been demonstrated and the mechanism is, as of now, unknown. Intriguingly, the A30 site (A30, A31 in *D. melanogaster*) of the U2 snRNA is part of the flexible linker located just between the region that interacts with the pre-mRNA branch point sequence on one side (U2/BS helix) and the U6 snRNA on the other side (U2/U6 helix Ia) (Sashital et al. 2007). A30 was previously shown to be the spot that allows rotation of the entire downstream region of U2 snRNP (U2/BS helix) during the spliceosome transition from B^{act}-, C- to C*-complexes (**Figure 2**) (Bao et al. 2017). Thus, m⁶A may promote flexibility that ensures the rearrangement of the branch site within the catalytic centre. Notably, recent reports showed that only a subset of splicing events were Mettl4 dependent and most represented cassette exons (Goh et al. 2020). Thus, a study using an in vitro splicing assay in the presence/absence of this modification might shed light on the exact mechanism. Given the close proximity of the A30 to the branch point sequence, m⁶A may alter the splicing efficiency depending on the sequence surrounding the branch point motif. Of note, budding yeast does not encode Mettl4 and a less diverse set of branch point sequences has been reported in this organism (Lim and Burge 2001). It is also important to note that U2 snRNA genes exist in multiple copies and their expression is spatially and temporarily regulated. A five nucleotide deletion in one the U2 snRNA genes, which included the A30 site, was shown to alter splicing of a subset of small introns specifically in the mouse cerebellum, which in turn resulted in neuron degeneration (Jia 2012 cell). It would be interesting to explore if all U2 snRNA genes are m⁶A modified and whether some cells or splicing events are more susceptible to the loss of this particular m⁶A modification than others. In summary, future work will be required to reveal the importance of this conserved U2 snRNA methylation site on pre-mRNA processing in different cell types, as well as during normal and stress conditions.

In recent years, several studies reported an additional N6-methylation activity of METTL4 resulting in the formation of 6mA modification on DNA substrates in different organisms, including human and *C. elegans* (*Chapter 1.1.1*) (Greer et al. 2015, Kweon et al. 2019). In *Drosophila melanogaster*, a 6mA demethylase DMAD (also known as dTet) has been found (Zhang G. et al. 2015), while the 6mA methyltransferase has not been characterised yet. To investigate, if the function of Mettl4 as a 6mA methyltransferase is conserved in flies we measured 6mA levels in DNA samples from WT and *Mettl4Δ2* mutant female ovaries, as well as from S2R+ cells where Mettl4 was depleted. 6mA levels in all samples were rather low (<0,0015 % 6mA/T) and loss of Mettl4 in flies did not further reduce 6mA levels, neither in S2R+ cells nor in ovaries (**Supplemental data 9**). Whether Mettl4 is a functional 6mA methyltransferase in *Drosophila melanogaster*, therefore, remains the matter of future investigations. It is possible that Mettl4 deposits 6mA at restricted DNA sites, in specific cell types, developmental stages, or only under particular stress conditions. Notably, recent studies in vertebrates argue against the existence of an enzymatic machinery depositing 6mA in a regulated manner and, instead, suggest that the main source of this rare epigenetic mark is DNA polymerase λ , which incorporates m⁶dATP in a cell cycle dependent manner (Liu X. et al. 2020, Musheev et al. 2020).

5.2 m⁶A demethylases in *Drosophila melanogaster*?

Akin to the reversibility of m⁵C DNA methylation, m⁶A modification on RNA can be demethylated to adenosine via the activity of a few ALKBH-family of proteins. Table in **Supplemental data 14** summarizes currently known enzymes with enzymatic activity against N6-methyladenosine in different species. ALKBH5 and FTO display demethylation activity towards m⁶A on mRNA, snRNA and lncRNA. Besides, FTO can demethylate m⁶Am modification that is found as a part of a 5'-cap at the first nucleotide of mRNA and RNA PolIII-transcribed snRNA (*Chapter 1.4.5.b*). ALKBH5 and FTO are found only in vertebrate species. The exception to this is FTO that also exists in unicellular diatoms (Sanchez-Pulido and Andrade-Navarro 2007). Interestingly, none of the MAC or MACOM components is conserved in diatom species, however, they encode two paralogs of the PCIF1 enzyme, required for m⁶Am formation. This might speak in favour of recent findings, suggesting that the primary substrate of FTO is m⁶Am, rather than m⁶A (Mauer et al. 2017, Mauer et al. 2019). It is important to note that the epitranscriptome landscape of m⁶A or m⁶Am modifications has not been investigated in diatoms thus far, but may nevertheless be informative. Of note, like in flies, both PCIF proteins in diatoms carry atypical catalytic motifs with a histidine residue [DPPH] (*Chapter 1.4.3.c*). Thus, diatoms would represent an ideal system to address I) if this Histidine residue abrogates enzymatic activity for m⁶Am formation, and II) in case m⁶Am indeed exists in this species, whether it is a preferred substrate of FTO demethylase.

Besides FTO and ALKBH5, a few additional ALKBH members were also shown to demethylate m⁶A on other types of RNA and DNA substrates. ALKBH1 and ALKBH4 act on 6mA modification in DNA, whereas ALKBH3 reverses m⁶A on tRNA (Ueda et al. 2017). Whether any of these enzymes can also demethylate m⁶A on specific mRNA targets, has not been addressed yet. Throughout this work, we investigated if any of the seven ALKBH-members present in *Drosophila melanogaster* might act on mRNA substrates (**Supplemental data 10**). To this end, we depleted all proteins in S2R+ cells and analysed changes in m⁶A content on mRNA. While none of the ALKBH members affected bulk m⁶A levels, we cannot exclude that some of them might act only on a restricted subset of mRNA targets. Notably, as mentioned above, vertebrate orthologs of AlkB and CG4036 (ALKBH1 and ALKBH4, respectively) were recently shown to demethylate 6mA on DNA, which makes them intriguing candidates for potential activity towards m⁶A on mRNA. On the other hand, catalytic activities of CG6144 and CG14130 proteins, and of their corresponding vertebrate proteins ALKBH6 and ALKBH7 are not known yet and only a few reports addressed their functions thus far. In human, *ALKBH6* transcript is highly expressed in testis and pancreas (Tsujikawa et al. 2007), while in *Drosophila melanogaster* expression of *CG6144 (Alkbh6)* is elevated during early embryogenesis (Flybase modENCODE (Brown et al. 2014)). Any further molecular or biological relevance of this protein is, as of now, unknown. More is, however, known about the ALKBH7 protein. It is highly expressed in the human pancreas, spleen, and prostate. A particular SNP has been associated with prostate cancer (Tsujikawa et al. 2007), whereas its loss of function in mice leads to obesity (Solberg et al. 2013). Upon DNA damage, ALKBH7 initiates programmed necrosis by triggering mitochondrial membrane collapse. As a result, cells lacking ALKBH7 can become resistant to DNA damage-induced cell death, which strongly suggests its role as a cancer suppressor (Fu et al. 2013). While its targets are not known, structural studies revealed that it lacks a characteristic nucleotide-recognition lid and has a catalytic site exposed to the solvent, suggesting it might not be a typical RNA/DNA demethylase and may also act on other substrates (Wang G. et al. 2014).

Given the lack of knowledge about these two ALKBH-members, we wanted to reveal functions of CG6144 (*Alkbh6*) and CG14130 (*Alkbh7*) in flies and have therefore generated corresponding mutant alleles (**Supplemental data 11**). Large deletion of *CG6144Δ2* (*Alkbh6Δ2*) allele removed nearly complete CDS including the translation start site and resulted in fly lethality. We found no adult escapers, nor did we notice any apparent pupae survival. While we cannot exclude a possible off-target effect that could arise during mutant generation, this observation is, nevertheless, in line with the high expression of *CG6144* (*Alkbh6*) during embryogenesis (Flybase modENCODE) (Brown et al. 2014) and suggests a potential importance of this protein for early fly development. The mutant allele that we generated for *CG14130* gene removed a C-terminal part of the AlkB domain including the α -ketoglutarate binding residues. *CG14130Δ6* (*Alkbh7Δ6*) flies were, however, viable with no apparent developmental delay.

Besides, we created expression constructs of HA-tagged CG6144 (*Alkbh6*) and CG14130 under the UAS promoter and generated corresponding fly lines. If driven with a particular GAL4-driver, these constructs enable ectopic protein expression in a chosen cell type. Expression of constructs with an *actin*-GAL4 driver in the S2R+ cells revealed that CG6144 is localised ubiquitously throughout nuclear and cytoplasmic compartments (**Supplemental data 11**). CG14130 (*ALKBH7*), on the other hand, displayed cytoplasmic localisation that most likely represented mitochondria. This is consistent with the presence of a predicted mitochondrial localisation signal in both, fly and vertebrate orthologs. It is thus possible that CG14130 (*Alkbh7*) functions are required during stress, starvation or upon DNA damage as demonstrated for human ALKBH7 (Fu et al. 2013). Notably, several modifications on mt-RNA are crucial for adequate adaptation to different environmental cues and many mutations in mt-RNA modifying enzymes have been previously linked to the occurrence of various mitochondrial diseases (Bohnsack and Sloan 2018).

In summary, no m⁶A demethylase has been so far identified in flies. Tools that we have generated, including mutant flies and rescue constructs, will enable further investigation into the potential involvement of the two poorly characterised ALKBH-members (CG6144 (*Alkbh6*) and CG14130 (*Alkbh7*)) in the epitranscriptomic and epigenetic field. Given the rapid advance in the LC-MS and other detection techniques, a plethora of distinct modifications can be simultaneously analysed even from a limited amount of RNA or DNA samples (Lan et al. 2018). Thus, one could potentially screen for the demethylation activity of these enzymes towards various modifications in different tissue samples, developmental stages, or upon particular stress conditions.

5.3 m⁶A is decoded by different reader proteins

Once deposited, m⁶A modification can be recognised by reader proteins that may interact with and recruit other RNA processing factors, and in this way mediate the fate of modified transcript. Alternatively, m⁶A can also change local RNA structure and indirectly affect binding of various RBPs by the so-called RNA-switch mechanism (*Chapter 1.4.6*). Among the best described m⁶A readers are the YTH domain-containing proteins that can specifically accommodate m⁶A via a hydrophobic pocket of the YTH domain (Li F. et al. 2014, Luo and Tong 2014, Theler et al. 2014, Xu et al. 2014, Zhu et al. 2014). All YTH domain-containing proteins that have been investigated so far, displayed m⁶A binding ability. The only known exception is the Mmi protein from fission yeast that carries a mutation in the YTH domain, which interferes with m⁶A accommodation (Wang C. et al. 2016). Notably, *S. pombe* does not encode components of the m⁶A writer machinery (**Supplemental data 14**) and has no m⁶A on mRNA.

In this study, we aimed to identify and characterise proteins that can decode m⁶A in *D. melanogaster* (*Chapter 4.2*). By in silico analysis, we initially found two fly orthologs of the YTH domain-containing proteins, Ythdc1 and Ythdf that showed a high sequence similarity to corresponding human orthologs, the YTHDC1 and YTHDF1/2/3 proteins, respectively (**Supplemental data 23 and 24**). While the homologies within the YTH domains were very high, sequences outside these regions differed. We performed several in vitro assays to investigate if two *D. melanogaster* proteins can bind m⁶A. Using m⁶A modified RNA probe from the *bovine prolactin* containing a known methylation site (*Chapter 4.2.1.b*) we were able to confirm that Ythdc1 preferentially binds m⁶A. However, our results for Ythdf were not conclusive (**Figure 19**). Of note, similar observations were obtained in an independent study from Kan and colleagues who analysed RNA binding specificities of purified YTH domains. Only Ythdc1, but not Ythdf, was efficiently recovered by m⁶A-containing RNA probe in an EMSA assay (Kan et al. 2017). Intriguingly, sequence alignments of all fly and human orthologs unequivocally show that all residues, required for m⁶A accommodation, are conserved (**Supplemental data 23 and 24**). This led us to assume that Ythdc1 and Ythdf in *D. melanogaster* perhaps only bind m⁶A in a specific sequence and structure context. In line with these predictions, a recent study demonstrated that the YTH domain cannot accommodate m⁶A modification if it is located in a stable RNA duplex (Liu B. et al. 2018). This is indeed the case for the *bovine prolactin* RNA probe that we have used in the current study (**Figure 20b**) and most likely explains a poor binding of YTH proteins to this RNA probe. Notably, two recent studies from flies confirmed that Ythdc1 and Ythdf can bind m⁶A, when located in a different sequence (4xGGACU) which adopts an open conformation (**Figure 20c**) (Kan et al. 2020, Soldano et al. 2020). Thus, we can conclude that in *D. melanogaster* both YTH domain-containing proteins are functional, albeit context dependent, m⁶A readers.

5.3.1 Ythdc1

Ythdc1 is the only nuclear YTH domain-containing protein and shares high sequence similarity with its human ortholog YTHDC1, in particular within the region adjacent to the YTH domain (**Supplemental data 23**). The entire N-terminal part and a vast majority of the C-terminal part are of low complexity with no predicted secondary structure. Instead, they are expected to constitute a flexible disordered region (as predicted by NetSurfP-2.0 software) (Klausen et al. 2019), likely involved in protein-protein interactions. In our interactome study from S2R+ cells, we found that Ythdc1 associates with numerous proteins, many of which are RBPs involved in different RNA processing steps (**Figure 29** and **Supplemental data 1**), potentially linking Ythdc1 to pre-mRNA splicing, polyadenylation and export.

Consistently, vertebrate YTHDC1 interacts with various splicing factors (Imai et al. 1998, Hartmann et al. 1999, Xiao et al. 2016) and was, in addition, proposed to be involved in the regulation of mRNA export (Lesbirel and Wilson 2019). Human and fly Ythdc1 proteins interact with several common RBPs, suggesting that some functions of Ythdc1 may be conserved. Among them were for example members of the STAR family of proteins (Signal Transduction and Activators of RNA), such as the Sam68 and several QKI-proteins, that link signal transduction with post-transcriptional gene regulation. Another example was the scaffold attachment factor-B (Saf-B) protein that couples pre-mRNA transcription and splicing (Nayler et al. 2000) (**Supplemental data 1**). Interestingly, in human cells YTHDC1, Sam68 and Saf-B proteins reside in the so-called YT-bodies, adjacent to nuclear speckles and influence splicing in a phosphorylation dependent manner (Hartmann et al. 1999, Nayler et al. 2000, Rafalska et al. 2004). Whether such mode of regulation also exists in flies is not known, however we could identify interactions between Ythdc1, Saf-B and several orthologs of the Sam68 protein (Qkr58E-1, -2, -3), strongly suggesting that similar protein complex, involved in splicing regulation, also exists in flies (**Figure 29 and Figure 30**). Notably, Qkr58E-1 was also one of the proteins that influenced splicing of many Ythdc1 targets, indicating that the two proteins likely act cooperatively to achieve efficient splicing outcome of a subset of methylated transcripts (**Figure 30**). Indeed, their combined depletion in S2R+ cells had more prominent effect on the splicing alteration of the *fl(2)d* transcript compared to individual depletion of either Mettl3, Ythdc1 or Qkr58E-1 proteins (**Supplemental data 15**). Importantly however, loss of Qkr58E-1 did not alter all Ythdc1-dependent events, signifying the existence of other parallel mechanisms that mediate splicing together with the Ythdc1 (see *Chapter 5.5*).

From our interactome analysis, we also noticed that Ythdc1 in flies interacts with the cap-binding proteins CBP20 and CBP80. Interestingly, their depletion in S2R+ cells shifted splicing of methylated targets in the opposite way than did depletion of m⁶A machinery, or of the Ythdc1 reader (**Supplemental data 15**). However, m⁶A levels remained unchanged, indicating that cap-binding proteins (CBPs) do not stimulate m⁶A deposition. Instead, these observations may suggest a competition between the CBPs and Ythdc1 for methylated sites, or could point toward CBP20/80 - mediated tethering of Ythdc1 away from sites of methylation. Of note, a vast majority of m⁶A in flies reside within the 5'UTR regions in a proximity to the mRNA cap (**Figure 22**) and many differentially spliced events were also found in the 5'-regions (**Supplemental data 5, 6 and 7**). The putative interplay between CBP20/80 - Ythdc1 therefore provides an exciting possibility to adjust the extent of Ythdc1 binding to m⁶A sites and in this way mediate downstream pre-mRNA processing.

Interplay between m⁶A writers and Ythdc1

We found that Ythdc1 protein represents one of the main mediators of m⁶A functions in flies. Consistent with its role in splicing, over 70 % of differentially spliced transcripts were shared between Mettl3 and Ythdc1 depleted cells (**Figure 21 and Figure 23**). Likewise, its removal in vivo resembled the loss of m⁶A writer machinery in regards to altered pre-mRNA processing (**Figure 28**). Furthermore, *Ythdc1* KO flies displayed similarly compromised adult locomotor abilities (**Figure 27**). During the course of fly development *Ythdc1* expression recapitulated the profile of m⁶A modification and the writer complex (**Figure 16 and Figure 18**) (see also *Chapter 5.6*), highlighting the importance of this nuclear reader protein in maintaining accurate m⁶A interpretation. It is currently not known to what extent Ythdc1 binds m⁶A sites in flies, hence, it will be important to generate an accurate RNA binding map and compare it with the m⁶A profile in order to clearly evaluate its direct contribution in posttranscriptional regulation.

Our comprehensive interactome analysis of m⁶A writer components and of the Ythdc1 protein revealed that they share many common interactors, which is highly suggestive of the interplay between m⁶A writers and readers in downstream mRNA processing (**Supplemental data 2**). Ythdc1 for example efficiently precipitated most components of the MACOM complex, including Nito, Fl(2), Vir and Flacc (**Supplemental data 1**). Consistently, in several human cell lines HAKAI and WTAP enriched the YTHDC1 protein (Horiuchi et al. 2013). Among the common proteins that we found interacting with Ythdc1 and at least one of the writer components were RBPs involved in the regulation of splicing in line with the proposed role of m⁶A in this process. Additionally, proteins that shuttle between nucleus and cytoplasmic compartments were also identified, such as those required for nuclear pore organisation, mRNA localization, stability translation as well as gene silencing (**Supplemental data 2**). Intriguingly, several common proteins (e.g. Saf-B Hrb87F, Hrb98DE) constitute the so-called Omega speckles that represent chromatin associated co-transcriptional mRNA processing hubs in flies (Singh and Lakhota 2015). It is currently not known how does the Ythdc1 protein recognise and bind the “accurate” set of methylated transcripts, however, given the accumulated data, we envision a formation of non-membranous compartments that expedite the recruitment of Ythdc1 and its associated proteins to co-transcriptionally deposited m⁶A sites. Whether Ythdc1 also directly interacts with any of the MACOM components, or else if additional bridging factors are involved, remains the matter of future investigations. Taken together, the link between m⁶A writing and reading does not seem so elusive and it may well be that many other m⁶A specific binders are recruited to sites of methylation via the writer complex. Nevertheless, further work will be required to unambiguously address which of the identified interactions are biologically relevant and how is the binding of writers and readers regulated.

5.3.2 Ythdf

In contrast to vertebrates, flies encode a single cytoplasmic YTH domain protein, Ythdf (CG6422) (**Figure 17**) that has not been functionally characterised before. In vertebrates, three YTHDF proteins regulate translation, stability and decay of their targets (Hazra et al. 2019). To this end, we investigated the role of *D. melanogaster* Ythdf ortholog in S2R+ cells, where its depletion leads to a up-regulation (n=545) and down-regulation (n=797) of many transcripts (**Figure 21**), with nearly half of them also being m⁶A modified. To investigate, if Ythdf affects mRNA turnover, we carried out RNA stability assay, using Actinomycin D transcriptional inhibitor and analysed mRNA levels at different time points in control, Ythdf and Mettl3/Mettl14 depleted S2R+ cells. Our unpublished data show that loss of m⁶A and Ythdf has no overall effect on mRNA stability. However, we cannot exclude that some targets are under the control of m⁶A-dependent decay or that this may be the case in different cell types. In human cells iCLIP analysis demonstrated that transcriptome wide binding of three YTHDF-proteins highly overlap (Patil et al. 2016), suggesting that they might act redundantly. Indeed, two recent studies demonstrated that the loss of one YTHDF reader can be compensated by two other YTHDF members in a dosage-dependent manner (Lasman et al. 2020, Zaccara and Jaffrey 2020). However, this does not seem to be the case in all cellular contexts and the unique expression pattern of the Ythdf2 during mouse development makes it indispensable for mouse gametogenesis and viability (Lasman et al. 2020). In addition, tethering of YTHDF2 and YTHDF3 to a reporter transcript either facilitated its decay or translation, respectively (Rauch et al. 2018). Besides, loss of yeast YTH domain protein Pho92 that is required for timely mRNA turnover, was efficiently rescued by the YTHDF2 (Kang et al. 2014). Thus, to investigate if *D. melanogaster* Ythdf protein is, to some extent, involved in transcript stability, decay or translation, similar tethering experiments could be carried out. In addition, by expressing a fly Ythdf

protein in *YTHDF1*, *YTHDF2* or *YTHDF3* KO cells one could anticipate that Ythdf protein may rescue some aspects of gene regulation, which could help at interpreting its functions.

We aimed at investigating Ythdf roles in vivo and found that during fly development, *Ythdf* expression strongly correlated with m⁶A levels and was, similarly to *Ythdc1*, most abundant during early embryogenesis (**Figure 18**). In particular, its levels peaked during the first two hours and were elevated in ovaries, suggesting its maternal deposition. To understand the importance of this cytoplasmic reader in fly development, we initially generated a mutant allele with a deletion close to three translation start sites that should interfere with translation of functional proteins. In the *YthdfΔ5* mutant, deletion introduced a premature stop codon after a few translated amino acids (**Supplemental data 12**). *YthdfΔ5* mutant flies were viable and to our surprise, fertile. Even though we found elevated *Ythdf* expression in embryos and ovaries, observations from mutant flies speak against the essential role of this protein in fly gametogenesis and during maternal to zygotic transition. In contrast, different Ythdf members in mice and zebrafish have crucial roles in these processes (*Chapter 1.4.8.e*). Nevertheless, similar findings were recently made by a study from Kan and colleagues who generated *Ythdf* mutants with comparable 5'-end deletions (Kan et al. 2017). Intriguingly, we observed that *YthdfΔ5* flies displayed defects in adult mushroom body development (Soldano et al. 2020). However, due to a small deletion of *YthdfΔ5* allele there was a possibility that an alternative downstream translation start site could be used to generate a truncated protein with an intact YTH domain. If expressed, such protein could either still be functional, or could act as a dominant negative. Thus, a new allele lacking an entire YTH domain was generated (Soldano et al. 2020). Intriguingly, *ΔYTH-Ythdf* mutant flies recapitulated mushroom body phenotypes of the *YthdfΔ5* allele and have since been thoroughly characterised to reveal biological and molecular functions of this cytoplasmic reader (Soldano et al. 2020).

5.3.3 Other putative m⁶A regulated proteins

YTH domain-containing proteins are among best described m⁶A readers and their binding preference for m⁶A modification has been explicitly demonstrated by structural characterisation of the YTH domain (Li F. et al. 2014, Luo and Tong 2014, Theler et al. 2014, Xu et al. 2014, Zhu et al. 2014). Albeit, with a growing volume of studies searching for novel m⁶A readers, it is becoming increasingly recognised that m⁶A can affect RNA binding of many other RBPs (Dominissini et al. 2012, Edupuganti et al. 2017, Baquero-Perez et al. 2019). In certain sequence contexts, these proteins may directly recognise m⁶A. Often times, however, modification enforces structural changes, which can in turn readily expose or hide their RNA recognition sites along the transcripts (Micura et al. 2001, Alarcon et al. 2015a, Liu et al. 2015, Spitale et al. 2015, Liu et al. 2017, Liu B. et al. 2018). Several proteins have been identified whose RNA binding is impacted by m⁶A in a positive (hnRNPs, eIF3, FMRP, IGF2BP) or negative manner (HuR, G3BP1) (Dominissini et al. 2012, Edupuganti et al. 2017, Baquero-Perez et al. 2019). One of these non-conventional m⁶A readers, **FMRP**, can preferentially, but not exclusively, bind m⁶A modified RNAs (Edupuganti et al. 2017). FMRP plays important roles in proper neuronal development and altered FMRP functions are the leading cause of the Fragile X syndrome, a form of intellectual disability (Darnell and Klann 2013). Hence, the interplay between m⁶A and FMRP received a lot of attention over the past few years. FMRP was implicated in mediating the export and stability of methylated mRNA, in part, with the cytoplasmic Ythdf2 protein (Zhang F. et al. 2018, Hsu et al. 2019). Notably, FMRP strongly interacts with other YTH domain proteins, which raises the question, to what extent does FMRP act autonomously as an m⁶A reader? Intriguingly, in flies we found that Fmr1 interacts with the nuclear Ythdc1 protein as well as with MACOM components (**Supplemental data 2**),

whereas, a recent work from Soldano and colleagues revealed that it also binds the cytoplasmic Ythdf protein. This study further highlighted the importance of this interplay for proper neuronal development (Soldano et al. 2020). It is thus possible that FMRP associates with some m⁶A modified transcripts already in the nuclei and shapes their processing along the way to the cytoplasm.

To identify novel m⁶A binding proteins in *D. melanogaster*, we performed an in vitro pull-down assay followed by mass spectrometry analysis of recovered proteins. We used an RNA probe from the 3'UTR of the *bovine prolactin (bprl)* transcript that contains a well characterised m⁶A site (Carroll et al. 1990), (**Figure 20a**). Based on our in silico structure prediction, m⁶A site in the *bprl* is embedded within a stem loop conformation (**Figure 20b**). In many cases, m⁶A modification can obstruct the formation of RNA duplexes and, hence, sites in the proximity of m⁶A tend to be unpaired (Liu B. et al. 2018). However, based on currently available studies (Roost et al. 2015), this does not seem to be the case for the *bprl* sequence, where m⁶A in the GGACU motif is surrounded by a perfect RNA duplex (See also *Chapter 4.2.2*). Importantly, YTH domains cannot efficiently accommodate m⁶A sites that are located within the RNA duplex (Liu B. et al. 2018) and indeed, neither Ythdc1 nor Ythdf were among recovered proteins in our mass spectrometry assay (**Figure 20a**). Thus, we propose that proteins enriched by the methylated probe represent RBPs or protein complexes that directly recognise m⁶A modified *bprl* sequence independently of YTH domain-containing readers.

mRNA decay

Intriguingly, proteins that displayed preferential binding to m⁶A modified probe, were Ge-1 (EDC4), Patr-1 (PATL1) and Lsm1, Lsm2, Lsm3, Lsm4, Lsm5 and Lsm7 proteins (Lsm1-7) (**Figure 20a**) that constitute a complex involved in the regulation of mRNA storage and decay in the cytoplasmic foci termed P-bodies (Luo Y. et al. 2018). Patr-1 (Protein associated with topo II related-1) is one of the core components of the P-bodies, where it engages with various different proteins. The Ge-1 (also known as EDC4, Enhancer of decapping 4) is a scaffolding protein that interacts with and activates decapping proteins Dcp1 and Dcp2 (Mugridge et al. 2018). Lsm1-7 proteins form a ring shaped structure that, together with the Patr-1 protein, associate with short adenylated or uridylated 3'ends of transcripts, which are poised for 5' → 3' mediated decay (see *Chapter 1.2.4*). This heterooctameric complex promotes the recruitment of decapping enzymes Dcp1 and Dcp2, which in turn stimulates mRNA degradation. In vertebrates, the link between m⁶A and mRNA degradation has been already demonstrated (Lee et al. 2020). Briefly, m⁶A carrying transcripts can be bound by the Ythdf2 reader that facilitates tethering of m⁶A-carrying transcripts to the P-bodies. In addition, Ythdf2 recruits the Ccr4-Not complex and, hence, promotes mRNA deadenylation and subsequent turnover (Lee et al. 2020). However, whether there is a direct connection between m⁶A and the following steps of mRNA processing, namely uridylation and decapping, has not been addressed thus far.

Importantly, our findings might provide the missing link that potentially connects m⁶A-mediated mRNA deadenylation (via Ythdf) with mRNA decapping (via Patr-1/Lsm1-7). We propose that deadenylated m⁶A-carrying transcripts can be directly recognised by the Patr-1/Lsm1-7 protein complex, which subsequently accelerates the recruitment of decapping machinery and promotes mRNA turnover of a subset of m⁶A modified transcripts. Notably, while we were not able to find the connection between m⁶A and overall mRNA stability (unpublished data) it remains possible that only selected transcripts are destabilised in this way. Given that in flies a vast majority of m⁶A sites reside in the 5'UTR regions, it would be important to investigate if perhaps transcripts that carry m⁶A specifically within their 3'UTR regions are predisposed for such regulation. Intriguingly, in vertebrates, m⁶A

modification is highly abundant within the 3'UTR regions, hence, we envision that such mechanism may be conserved and of particular importance in the regulation of mRNA turnover in higher organisms.

In summary, our preliminary data provide an intriguing possibility that the Patr-1/Lsm1-7 protein complex is involved in destabilization of methylated transcripts via its ability to directly bind m⁶A sites. Recent studies suggest that Patr-1 enhances mRNA binding of Lsm1-7 proteins to mRNA (Lobel and Gross 2020) and its depletion in flies results in exuberant growth of synaptic boutons at NMJ (Pradhan et al. 2012), a phenotype that is apparent in mutants lacking m⁶A (see *Chapter 1.5.3*). Hence, the role of Patr-1/Lsm1-7 mediated transcript decay may be specifically important for selected set of mRNAs in the nervous system, where rapid adjustment of transcript levels is of particular importance. Future studies will, however, need to decipher whether and how the heterooctamere complex binds m⁶A and to which extent this mechanism contributes to the fine-tuning of mRNA decay.

Polyadenylation machinery

Highly enriched were also components of the cleavage and polyadenylation machinery, including the **Sym** (SYMPK), **Cpsf73** (CPSF3), **CG3679** (CPSF5) and **CG7185** (CPSF6) proteins (**Figure 20a**), which was unexpected, given the poor enrichment of m⁶A in 3'UTR region in flies. Notably, CPSF5 was previously shown to act as a broad repressor of proximal poly(A) site usage (Masamha et al. 2014). While it is currently not known to what extent these sites might overlap with m⁶A, this is nevertheless in line with the study that showed global 3'UTR shortening upon loss of m⁶A (Ke et al. 2015). We identified one single transcript that displayed altered polyadenylation in response to m⁶A loss in *D. melanogaster* S2R+ cells. Intriguingly, this was the *Ythdc1* transcript and the usage of its proximal poly(A) site was increased upon m⁶A loss, consistently with the potential CPSF5 mediated mechanism (unpublished data, (Bayer 2016)). It remains possible, however, that m⁶A affects alternative polyadenylation in a broader range, albeit in other cell types or in particular developmental processes. Of note, in the *bprl* transcript, the preferential CPSF5 binding motif 5'UGUA is located in a loop only 4 nt downstream of the m⁶A site (**Figure 20b**), strongly suggesting that CPSF5 may indeed directly recognise m⁶A modification. Of note, these observations are only partially consistent with a recently published study where CPSF5 depletion was proposed to induce 3'UTR shortening but at the same time also promote efficient m⁶A deposition (Yue et al. 2018).

Splicing factors

Among proteins enriched with the m⁶A probe were also several factors involved in the regulation of splicing, which is in line with a growing evidence of the role of m⁶A in this process (see *Chapter 1.4.7.a* and *Chapter 5.5*). **U2af38** (U2AF35) and **U2af50** (U2AF65) are, for example, required for the recognition of 3' splice elements during the early spliceosome assembly and interact with Fl(2)d, suggesting that their binding to m⁶A sites may be functionally relevant (Penn et al. 2008). In addition, **B52** (SRSF4), **Nito** (RBM15), **Dhx15** (DHX15) and **CG6379** (CMTR1) were also previously implicated in alternative splicing (Venables et al. 2012). Intriguingly in human cells **CMTR1** and **DHX15** form a stable complex and influence activities of each other. DHX15, the DEAH (Asp-Glu-Ala-His)-box RNA helicase is activated by the 2'-O-methyltransferase CMTR1 (Inesta-Vaquera et al. 2018) and, in turn, CMTR1 requires DHX15 helicase for methylation of highly structured 5'UTRs (Toczydlowska-Socha et al. 2018). It is thus possible that m⁶A in some sequence contexts provides a platform for the recruitment of DHX15 helicase, which then mediates structure unwinding and exposes sequence motifs to increase accessibility for other RBPs.

Repelled proteins

A few proteins were also repelled by the presence of m⁶A modification. Of those, Zn72D (ZFR) is a particularly interesting candidate, since it is a known dsRNA binding protein that was just recently implicated in the regulation of RNA editing in flies and vertebrates (Freund et al. 2020, Sapiro et al. 2020). Zn72D was shown to bind a large set of Adar targets and could to some extent promote mRNA editing. Interestingly, *Zn72D* and *Adar* mutant flies resembled alterations in locomotion and NMJ formation that we observed in flies lacking *Mettl3*. However, defects in *Zn72D KO* flies were more pronounced, indicating additional editing-independent functions of this protein. Intriguingly, in our interactome data we found that Zn72D interacts with the Ythdc1 reader (**Supplemental data 1**). Since none of the two proteins can efficiently bind m⁶A within the *bprl* sequence context, their interaction might indeed be relevant, implicating Zn72D in the m⁶A-related processes. Of note, the negative correlation between m⁶A and editing has been already demonstrated, however the mechanistic insights are not entirely understood (Xiang et al. 2018). It is possible that m⁶A modification modulates editing in a sequence and context dependent manner, whereby the presence of m⁶A could destabilize RNA duplex formation and, thus, alter Adar association. Alternatively, it could preclude binding of Zn72D and consequently Adar in cases where dsRNA structure remains unaffected by m⁶A. In the future, it will be interesting to confirm the Ythdc1-Zn72D interaction and further explore the interplay between m⁶A and editing in the context of neuronal development.

Taken together, these newly identified m⁶A-enriched and m⁶A-repelled candidates open up a few exciting possibilities on how m⁶A may modulate several mRNA processing steps. Future studies will uncover the exact mechanisms by which these proteins potentially bind and accommodate m⁶A modification. In a surge to identify new m⁶A-binders, the RNA probe-based in vitro pull-down approaches proved as a powerful tool. However, limitations clearly arise from sequence and structure-dependent binding preferences of individual RBP (Lewis et al. 2017). Hence, upcoming screens for novel m⁶A-regulated RBPs should, at best, include biologically relevant transcripts carrying methylation at well-known sites. In combination with rigorous validation of novel candidates, such methodologies will provide further insights into how the m⁶A code is interpreted by the cell.

5.4 The mystery behind the m⁶A profile on mRNA

Transcriptome-wide mapping of m⁶A modification was one of the major breakthroughs in the field of epitranscriptomics. In 2012, two independent groups found that in vertebrates m⁶A is highly enriched in the RRACH motif and is not randomly distributed along mRNA, but is instead highly enriched around 3'UTR regions, STOP codons and within long internal exons (Dominissini et al. 2012, Meyer et al. 2012). To gain molecular insights into m⁶A deposition along mRNA in *D. melanogaster*, we mapped modification in S2R+ cells by two approaches that, both, take the advantage of an anti-m⁶A-specific antibody to immunoprecipitate m⁶A modified transcripts. We initially employed a low-resolution MeRIP-seq method and later performed a high-resolution miCLIP technique that incorporates UV-crosslinking step prior to immunoprecipitation, and thus highly improves mapping specificity (Linder et al. 2015) (see *Chapter 1.4.9*). Using both methods, we came to the following findings: **I)** m⁶A in *D. melanogaster* resides in an A-rich RRACH motif, resembling RRACH motif found in other species, and **II)** m⁶A in flies is highly enriched along 5'UTR regions.

By MeRIP-seq we initially showed that most peaks (92 %; n=1120 in 812 genes) contain the conserved RRACH consensus motif (**Figure 22**). The m⁶A distribution along mRNA was identified in the coding sequences (~40 %) and around STOP codons (~15 %). In addition, we found that over 20 % of m⁶A peaks were also in the proximity of START codons, which contrasts the methylation profile in vertebrates (Dominissini et al. 2012, Meyer et al. 2012). However, it is important to consider that, due to weak enrichment of peaks over input (>1.3-fold), many low stoichiometry m⁶A sites might have been missed and some of highly abundant transcripts may have been detected as false positives. Using miCLIP technique we later found that m⁶A modification is more prevalent than initially thought. By focusing on sites with truncations at adenosines (CITS (A)) we identified over 12.000 putative m⁶A peaks in 3280 genes. Since the majority of modified genes found in MeRIP were also identified by miCLIP (75 %) we used miCLIP data for all further analyses. Intriguingly, over 50 % of all CITS (A) sites were in 5'UTR regions, whereas only 11 % were present in the 3'UTR regions (**Figure 22**). This strongly suggested that in *D. melanogaster* the m⁶A profile is biased towards the transcripts' 5'-ends and is in this way distinct from the profile generally observed in other species. Nevertheless, the sequence logo surrounding collapsed m⁶A sites was the adenosine rich RRACH, that falls into a typical RRACH-motif recognised by the MAC complex. Similar observations were also obtained by the E. Lai group that performed m⁶A mapping in *D. melanogaster* embryos (Kan et al. 2017) (see also below).

m⁶A at 5'UTR is also found in other systems

m⁶A in the proximity of 5' ends has been, to some extent, also observed in a few other systems. For instance, m⁶A enrichment within the START codons was detected in fully differentiated cells from mouse cerebral cortex (Chang et al. 2017), liver (He et al. 2017), and muscles (Kudou et al. 2017), as well as in plants (Li Y. et al. 2014, Luo et al. 2014). This indicates that m⁶A profile might be cell type, rather than species-specific and is likely orchestrated by the temporary cellular transcriptome. In support of this, in the hippocampus of two weeks old mice many m⁶A sites are found in the first exon, whereas in a six weeks old adult mice, m⁶A is predominantly located in the last exon (Li L. et al. 2017). Notably, the m⁶A profile was shown to gradually change also during fly embryogenesis. In early embryonic stages, similar m⁶A abundance was observed at 5'UTR and 3'UTR regions, however towards the end of embryogenesis, a majority of m⁶A sites were detected within the 5'UTR regions (Kan et al. 2017). The mechanism and relevance of such methylome shift is currently not known, albeit it likely reflects the gradual transcriptome changes of maternal-to-zygotic transition (MZT) (Kwasnieski et al.

2019). Another example of a dynamic switch of m⁶A profile was also reported in vertebrate cells that were subjected to different stress conditions (Meyer et al. 2015, Zhou et al. 2018). Heat shock and starvation induced a global and rapid increase of m⁶A levels within the 5'UTR regions and these newly deposited sites were required for the regulation of selective translation. It is important to note that many vertebrate transcripts carry m⁶Am modification at the very first or second nucleotide. Given that anti-m⁶A antibody cannot distinguish between the m⁶A and m⁶Am modifications, methylomes obtained by immunoprecipitation based techniques need to be interpreted with caution.

Which factors are currently known to regulate m⁶A deposition?

One of the open questions in the m⁶A-field that remains to be solved is: What are determining factors that shape the m⁶A profile? It is clear that m⁶A along mRNA is not located randomly, but rather displays a distinct enrichment in defined segments; e.g. at 3'UTRs in vertebrates and 5'UTRs in flies. A common feature for most m⁶A sites appears to be the RRACH motif (or A-rich motif in flies), yet the motif alone is insufficient to explain the methylation profile since distribution of RRACH sequences is equal along the transcript (Linder et al. 2015) and a vast majority of such sites are not methylated. In recent years, several mechanisms have been proposed that may contribute to m⁶A installation, however, exact "instructions" for methylation of an individual site are likely context-dependent.

I) **m⁶A writer complex:** several m⁶A writer components can bind RNA and display some degree of specificity. For instance, the Mettl3-Mettl14 heterodimer binds ssRNA with a positively charged groove at the interface of both methyltransferase domains. In addition, two zinc-finger domains (ZnF1 and ZnF2) in Mettl3 bind RNA containing RRACH motif, whereas C-terminal RGG repeats of Mettl14 contribute to RNA binding, but do not seem to provide any specificity (*Chapter 1.4.2.a*). Notably, the ZnF1 of Mettl3 in *D. melanogaster* contains a 70-nt extended region, thus it would be interesting to test if this extension contributes to preferred methylation of the A-rich AAACA motif in flies (**Supplemental data 16**). In addition, a single position of Mettl14 (R298) was shown to direct binding to the RRACH motif (towards the position of C) and its mutation (R298A) diminishes methylation efficiency (Wang P. et al. 2016, Wang X. et al. 2016). Importantly, beside the RRACH motif, other substrate sequences were also shown to be recognised by the Mettl3/14 heterodimer in vitro (Wang P. et al. 2016, Wang X. et al. 2016). For example, GGAUU sites can be methylated, albeit at a lower efficiency than GGACU sites (Wang P. et al. 2016, Wang X. et al. 2016, Pratanwanich et al. 2020). Nevertheless, they most likely represent some of m⁶A modified motifs. In our miCLIP dataset, this is reflected by the sequence context of all CITS (A) sites, where the nucleotide following m⁶A is not exclusively C, but to a lesser extent, also U (**Figure 22**). This has been also previously observed in human methylome determined by miCLIP (Linder et al. 2015) and more recently by an antibody-independent mapping assays (Pratanwanich et al. 2020, Wang et al. 2020). Additional RNA recognition was proposed to be defined by MACOM components, whereby binding of RBM15 to U-rich sequences guides methylation machinery towards RRACH sites in the proximity of Uridine-stretches (Patil et al. 2016), whereas the RNA-dependent association of Virma with cleavage and polyadenylation factors promotes m⁶A deposition at the 3'UTR (Yue et al. 2018). Since Fl(2)d (WTAP) and Flacc (Zc3h13) also bind RNA, it is likely that they contribute to the specificity of m⁶A methylation. Future studies resolving the structure of the complete m⁶A writer complex should provide novel insights.

II) **METTL14 binding to H3K36me3:** In vertebrates, METTL14 was shown to interact with chromatin and directly bind the H3K36me3 histone mark (Huang et al. 2019). This was proposed to be a driving mechanism for m⁶A deposition within the 3'UTR region. Given that binding sites for interaction with the H3K36me3 are conserved in *D. melanogaster* Mettl14 protein (**Supplemental data 17**), it would

be interesting to investigate if such association also occurs in flies, where H3K36me3 modification is similarly enriched at the 3'UTR regions (Bell et al. 2007), but the m⁶A profile is nonetheless different (Figure 22).

III) Transcriptional rate of RNA PolII: Several studies demonstrated that m⁶A methylation occurs co-transcriptionally, but it is currently not clear if this can influence the specificity of the m⁶A profile. Work from Slobodin and colleagues provided some insights by showing that impeded transcriptional rate, due to slow or paused RNA PolII, allows better recruitment of methylation complex and, hence, contributes to elevated methylation (Slobodin et al. 2017). Such pausing is observed at TES or along the exons of mRNA where m⁶A levels were shown to be high (Jonkers and Lis 2015). In concordance with these findings, less pausing is detected along the TES of lincRNA as compared to mRNA and no enrichment of m⁶A has been detected along the 3'UTR of lincRNA (Schlackow et al. 2017). However, since methylation of transcripts originating from RNA viruses has also been reported, m⁶A deposition cannot depend solely on the link with chromatin. Future work will be required to elucidate to which extent transcriptional speed, in combination with chromatin state, specifies the underlined m⁶A profile in different systems.

IV) RNA sequence context: An intriguing insights on m⁶A methylation profile were obtained by a recent m⁶A mapping technique, MAZTER-seq, employing a restriction endonuclease MazF, which cleaves RNA specifically at unmethylated sites occurring at ACA motifs (Garcia-Campos et al. 2019). By thorough experimental and computational analysis of sequences surrounding the modified sites, researcher found that m⁶A methylation and its stoichiometry in yeast and mammals can be predicted in *cis* by an extended sequence code flanking the putative m⁶A site (positions -4 to +4) and its local structure. A bias toward an A at position -4, T at position +4, and G at positions -2, -1 appears to be a conserved feature.

Notably, an important insight into m⁶A methylation specificity also comes from an early study that demonstrated a successful methylation of an *in vitro* transcribed RNA by a nuclear cell lysate (Narayan and Rottman 1988) (Rana and Tuck 1990). Methylation sites along the studied transcript were identical to those identified *in vivo*, albeit with reduced stoichiometry. This suggests that transcription might not affect methylation specificity, but rather its efficiency. Since currently available m⁶A mapping techniques cannot accurately determine methylation levels, future studies employing novel quantitative techniques (e.g. nanopore sequencing) might shed light onto methylation stoichiometry in connection with RNA transcription, chromatin status and local m⁶A site environment.

5.5 m⁶A modification regulates alternative splicing

m⁶A modification has been implicated in all steps of mRNA life cycle, from transcription, nuclear processing, to its export, translation and decay. Alternative splicing is one of the main sources of proteome diversification, as well as a means to expand regulatory potential of the transcriptome (Lee and Rio 2015). A growing list of studies could demonstrate the involvement of m⁶A in this posttranscriptional process, whereby m⁶A depletion was not prone to any particular alternative splicing event (*Chapter 1.4.7*). Consistently, we found that in *D. melanogaster* the loss of m⁶A alters a large number of splicing events, in S2R+ cells as well as in vivo (**Figure 21** and **Figure 28**). Consistent with the involvement of m⁶A in the process of alternative splicing, nearly all common differentially spliced transcripts, upon the loss of m⁶A writer components, were also methylated (n=42/45 (**Figure 34a**)). In S2R+ cells, we observed enrichment for alternative 5' ss selection and intron retention events, however this was not readily apparent in vivo, suggesting that m⁶A may modulate different steps of splicing reaction. Of note, we propose the involvement of m⁶A modification in splicing based on the correlation between methylation states of transcripts that display m⁶A-dependent splicing changes, but we lack the explicit mechanistic insights. Thus, it is plausible that some splicing defects may be an indirect consequence of other processes (e.g. altered levels of splicing regulators, altered transcription, and export). Nevertheless, based on the currently available information from this and other studies, we envision several possible scenarios by which m⁶A could potentially affect splicing.

m⁶A writer complex interacts with several splicing factors

Components of the m⁶A writer complex interact with several splicing factors involved in the assembly of the early spliceosome (Complex E and A) during the step of splice site recognition (**Figure 2**). In particular, Fl(2)d was shown to interact with core components of the U1 snRNP [Snf, U1-70K] and U2 snRNP [Snf, U2AF50, and U2AF38] that bind the 5' and 3' ss, respectively (Penn et al. 2008) (**Table 3** and **Figure 2**). Likewise, Nito and Flacc co-precipitate with the Snf protein (Yan and Perrimon 2015, Guo et al. 2018). Our interactome data are consistent with these studies and we find that Nito interacts with the ortholog of Prp39 (CG1646) and with U2A', which form the U1 and U2 snRNP, respectively (**Supplemental data 1**). Intriguingly, our Flacc interactome revealed interactions with several factors that constitute the U5/U4-U6 tri-snRNP [Hoip (SNU13), CG4849 (EFTUD2), Prp8 (PRP8)] and the NTC complex [Bx42 (SNW1), Prp19 (PRP19)]. All these components associate with spliceosome in later stages, during the formation of Complex B and B^{act} (**Table 3** and **Figure 2**), suggesting that MACOM may be implicated in several steps of spliceosome assembly. Consistent, with findings from flies, WTAP and RBM15 were also identified as components associated with the active spliceosome in vertebrates (Zhou et al. 2002), highlighting the involvement of MACOM in the regulation of splicing. In addition, RBM15 was shown to bind numerous intronic sites (55 %) and to promote the recruitment of U2 snRNP components [SF3B1 and the U2AF], which increased splice site recognition and splicing efficiency (Chu et al. 2015, Zhang L. et al. 2015). Overall, current data suggest that spliceosome assembly may be modulated already at the step of m⁶A deposition. Hence, certain splicing changes might be at least in part explained by the numerous interactions between MACOM complex and various splicing factors. Of note, depletion of Fl(2)d and Nito resulted in a substantially greater number of differentially spliced transcripts (n>600) as compared to depletion of MAC components (n<100). This likely reflects the fact that MACOM components are also implicated in m⁶A-independent functions (see *Chapter 5.1.3*).

m⁶A reader proteins

m⁶A is recognised by different reader proteins, either directly or by an m⁶A-imposed structural switch. There are many pieces of evidence that point towards the direct involvement of the nuclear Ythdc1 reader in the process of splicing. We found a significant overlap between differentially spliced transcripts in *Mettl3 KO* and *Ythdc1 KO* flies (50 % and 61 %, respectively), suggesting that this protein is an important mediator of m⁶A-mediated splicing (**Figure 28** and **Figure 30**). In vertebrates, some m⁶A-dependent splicing events could be clearly attributed to the interplay between Ythdc1 and two SR-proteins. Ythdc1 was shown to recruit the splicing enhancer SRSF3 to promote alternative exon inclusion and at the same time interfere with the binding of SRSF10 in order to prevent exon skipping (Xiao et al. 2016). In *D. melanogaster*, these two SR-proteins are not conserved, hence a different mechanism must take place. In our screens for m⁶A-mediators, we found that Ythdc1 interact with proteins that have been previously linked to splicing [QKI proteins, hnRNPs and others] (**Supplemental data 1**). In addition, several putative reader proteins, previously implicated in splicing, have also been identified by our m⁶A-pull down experiment [U2af38 (U2AF35) and U2af50 (U2AF65), B52 (SRSF4), Dhx15 (DHX15) and CG6379 (CMTR1)] (**Figure 20**). Future studies will reveal to what extent is their binding to RNA modulated by m⁶A modification.

Examples in flies

In *D. melanogaster* m⁶A is highly enriched in 5'UTR regions and many examples displayed altered splicing in close proximity to m⁶A sites. For instance, in the *Dsp1*, *Aldh-III* and *Hairless* transcripts the loss of m⁶A resulted in the use of alternative 5'ss and substantially increased splicing (**Supplemental data 5-7**). While the underlying mechanisms that drive splicing alterations are currently not known, we propose that in some of these examples the presence of m⁶A (or its deposition) obstructs splicing. In the case of *Dsp1*, m⁶A perfectly overlaps with the 3'ss that is recognised only upon m⁶A depletion (**Supplemental data 5**). Likewise, several prominent m⁶A peaks are located upstream of the 5'ss that becomes preferentially used when m⁶A is depleted. It is possible that m⁶A acts as a platform that recruits RBPs, which abrogate proper binding of U1 snRNP and U2 snRNP to splice sites. In the example of *Hairless* transcript, m⁶A loss promotes the use of a downstream 5'ss and upstream 3'ss, which results in a CDS extension (**Supplemental data 6**). In this case, m⁶A sites are not adjacent to any splice site, hence modification may either act to promote or block the use of alternative splice sites. Similarly, alternative intron is found in the 5'UTR of the *Aldh-III* transcript where two m⁶A peaks are located upstream of the 5'ss (**Supplemental data 7**). Notably, loss of m⁶A in the *Dsp1* and *H* transcripts enables efficient splicing of very short introns (34 nt and 85 nt, respectively). In short introns, where the 5'ss and branch point sequence are in close proximity (<56 nt), the conformational rearrangements required for the spliceosome to progress from the complex B to the activated complex B^{act} are inefficient, due to limited flexibility (Keiper et al. 2019). Two proteins, Smu1 and RED, were found to facilitate spliceosome activation by releasing structural constraints. Their removal results in a global retention of short introns (Keiper et al. 2019). Intriguingly, the Smu1 protein was found in our Ythdc1 interactome study, hence it is possible that, in some cases, Ythdc1 tethers the Smu1 away from the spliceosome and in this way precludes efficient splicing of short introns. Overall, these examples indicate that m⁶A deposition might interfere with spliceosome assembly and splice site recognition. On one hand via the MACOM complex and its numerous interactions with different spliceosome components and on the other hand via the m⁶A reader proteins. In particular by the Ythdc1 protein and its binding partners. Hence, m⁶A should perhaps be viewed as a novel cis-acting element that can serve as a splicing enhancer or silencer in a context dependent manner.

In summary, loss of m⁶A modification does not seem to have a substantial role in constitutive splicing, but rather affects only a subset of splicing events. The levels of m⁶A are elevated in brain tissue (Meyer et al. 2012) where alternative splicing is of critical importance as it represents one of the mechanisms that contribute to a rapid transcriptome adjustment upon external stimuli and promote neuronal plasticity (Merkin et al. 2012, Su et al. 2018). Altered splicing has been implicated in neuronal defects and is a driving cause of numerous diseases (Vuong et al. 2016). Hence, understanding how m⁶A may help in shaping the transcriptome is of significant value. As of now, a very few individual events have been investigated in detail and more mechanistic studies are clearly required to decipher the exact contribution of m⁶A in this process. Notably, precise and single-nucleotide resolution mapping along with clearly defined stoichiometry of each individual site will provide more conclusive insights in the future. In this respect, the use of long read, single molecule sequencing will, with no doubt, greatly expand our knowledge (Parker et al. 2020). However, one limitation in the interpretation of m⁶A - splicing interplay that remains to be solved, is the lack of a reliable method that could efficiently and quantitatively capture m⁶A within intronic sites. Given the fast mode of co-transcriptional splicing, development of a novel approach that would allow mapping of m⁶A within pre-captured intron lariats, might potentially overcome this limitation.

5.5.1 m⁶A modification modulates splicing of *Sex lethal* (*Sxl*)

Sex lethal (*Sxl*) is a master regulator of sex determination in *D. melanogaster* (Penalva and Sánchez 2003, Moschall et al. 2017) (*Chapter 1.5.2*) that encodes a female specific RNA binding protein Sxl. By posttranscriptional regulation of its downstream targets, Sxl drives female physiognomy. In addition, it acts as the main inhibitor of the dosage compensation pathway and, hence, ensures female survival. In contrast, its aberrant expression in males hinders their viability. Controlled expression of Sxl protein in both, males and females, is thus of utmost importance. It is achieved by an alternative splicing of male specific exon (L3) that comprises a premature stop codon. Skipping of this exon permits translation of a functional Sxl protein in females, whereas its inclusion in males, prevents Sxl formation, and in turn activates the process of dosage compensation. Sxl can auto-regulate splicing of its own transcript, by binding to the Uridine-rich regions in the proximity of the alternative exon L3 (Moschall et al. 2017). By interaction with other proteins (e.g. Snf, PPS, MACOM components), Sxl inhibits spliceosome assembly and precludes exon inclusion.

In our current study, we found that splicing of *Sxl* is altered in flies lacking m⁶A writer components and results in increased inclusion of L3 exon in mutant females (**Figure 26c**), which implicates m⁶A in the sex determination and dosage compensation pathways. Notably, same observations were also reported by Soller and Lai laboratories that, in addition, mapped m⁶A modification in intronic regions flanking the L3 exon (Haussmann et al. 2016, Kan et al. 2017). While the exact role of m⁶A modification in this splicing context is not yet entirely understood, it is critical to note that *Sxl* splicing was also found to be altered upon the loss of the m⁶A reader protein Ythdc1 (**Figure 26c**). It is thus unambiguous that m⁶A deposition as well as its recognition contribute to efficient inhibition of the exon L3. Interestingly, Haussmann and colleagues demonstrated that ectopic expression of Ythdc1 in S2R+ cells, which are of male origin, could repress the L3 exon inclusion and change the *Sxl* splicing outcome into the female isoform (Haussmann et al. 2016). This finding is unexpected, as it suggests that despite the absence of a functional Sxl protein in these cells, splicing of L3 exon can be efficiently silenced. It is possible that I) *Sxl* transcript is efficiently methylated, but the endogenous levels of Ythdc1 are in general low in this cell type and, therefore, only its ectopic expression was able to saturate all intronic m⁶A sites, which

then interfered with the spliceosome assembly. II) Alternatively, we found that Ythdc1 interacts with MACOM components (**Supplemental data 1**), therefore it is possible that ectopic expression of Ythdc1 was sufficient to trigger their recruitment, which led to L3 exon repression.

Given that Sxl directly interacts with MACOM components (*Chapter 1.5.2*), it is possible that m⁶A writer complex amplifies the inhibition of exon recognition by stabilizing Sxl binding on RNA. Notably, depletion of any MACOM component, results in stronger alteration of Sxl splicing compared to the loss of MAC, suggesting that MACOM complex is required for L3 exon silencing beyond its function in m⁶A deposition (Hilfiker et al. 1995, Granadino et al. 1996, Nagengast et al. 2003, Johnson et al. 2010, Yan and Perrimon 2015, Guo et al. 2018, Knuckles et al. 2018). This is further exemplified by the fact that depletion of Nito or Flacc in in genital discs results in transformations of female genitalia, and depletion in the first pair of leg discs leads to the appearance of male-specific sex comb bristles at the forelegs (**Figure 35a**). In contrast, we found no evidence of female masculinization in *Mettl3* or *Mettl14* KO flies. Among proteins that regulate splicing of Sxl and interact with Snf is also PPS (Protein Partner of Sans fille) (Johnson et al. 2010). It encodes a large protein containing a SPOC, PHD and other domains and was proposed to provide a link to the chromatin. PPS, however, acts independently of other MACOM components as its depletion in S2R+ cells has no effect on m⁶A levels (**Supplemental data 15**). These observations altogether highlight the complexity of Sxl splicing, which is controlled by several parallel pathways. In this way different regulatory mechanisms complement each other and ensure that in females levels of functional Sxl protein remain above the minimum threshold (but also within the optimal window (Suissa et al. 2011) that still guarantees female viability. Notably, our analyses of different genetic interactions revealed that the loss of MAC components strongly compromised female viability, albeit only in a sensitised background, where Sxl expression has already been reduced (**Figure 26**). This points towards a mild contribution of m⁶A in Sxl splicing on its own and to its rather modulatory role in this process.

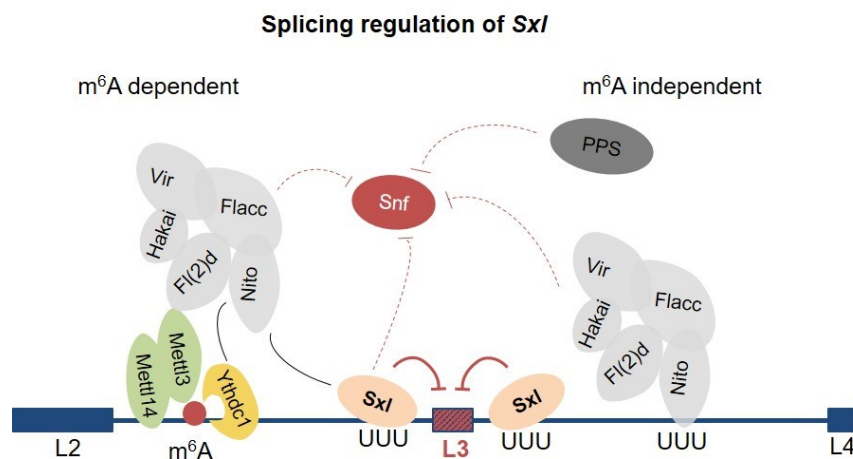


Figure 45. Regulation of Sxl alternative splicing.

Scheme depicting splicing regulation of Sxl in m⁶A dependent and independent manner. In females, several mechanisms contribute to the inhibition of male specific exon L3 (in red). Full lines indicate identified and predicted interactions between Sxl and MACOM components as well as between Ythdc1 and MACOM components ((Guo et al. 2018), **Supplemental data 2**). Red dotted red lines indicate interactions of Sxl, MACOM and PPS with Snf protein. These interactions prevent binding of U1 snRNP and U2 snRNP to the 5'ss and 3'ss of exon L3 and, thus, inhibit its inclusion in the final Sxl transcript.

Nevertheless, in line with reduced levels of functional Sxl protein, we found that splicing of Sxl downstream targets, *msl-2* and *tra*, was also affected in *Mettl3/Mettl14* mutants (**Appendix 1**: ED Fig. 9b and c). In females, splicing of *msl-2* is under the control of Sxl that promotes intron retention and, hence, inhibits Msl-2 expression. In the case of *tra*, two alternative 3' splice sites can be used and inhibition of the proximal site by Sxl enables the formation of a functional Tra protein in female flies (*Chapter 1.5.2*). Notably, it was previously shown that splicing of *tra* is not only under the control of Sxl, but is in parallel also regulated by Fl(2)d and Vir (Granadino et al. 1996, Ortega et al. 2003, Guo et al. 2018). We therefore wondered if the processing of *msl-2* and *tra* might be regulated via the m⁶A-mediated mechanism, similarly to what we observed for *Sxl* transcript. From our miCLIP data, we noticed that *tra* carries two m⁶A sites in the region between the proximal and distal 3' splice sites. Thus, it would be interesting to investigate, if Ythdc1 can indeed bind these m⁶A sites to modulate the splice site decision. Ythdc1 could either block the proximal splice site or promote the usage of the distal splice site. Interestingly, we also found that *msl-2* contains a putative m⁶A peak, which directly overlaps with the adenosine of the potential branch point sequence of the retained intron. Thus, it is possible that splicing of *msl-2* is, in part, also regulated by the m⁶A-Ythdc1 pathway that may interfere with branch point sequence recognition and, hence, with spliceosome assembly. Other targets of Sxl include *notch*, *nanos*, *e(r)*, on which Sxl imposes less decisive outcome (Moschall et al. 2017). Sxl for example inhibits *notch* translation, however this effect can be weakened by the activity of Hrb27C (Hrp48), that reduces Sxl levels to allow Notch expression in specific cell types (Suissa et al. 2011). Likewise, in the germline Sxl mediates translational repression of *nanos*, which has to be tightly regulated. Activity of Sxl, along with other repressors, is required only in germ stem cells (GSC) that are leaving the stem cell niche. At that stage, reduced levels of Nanos allow their differentiation to oocyte. Such restricted action of Sxl is crucial for the balance between GSC differentiation vs. self-renewal and is also important in later stages of oogenesis, when expression of Nanos protein is again required. Notably, GSCs lacking *Sxl* fail to differentiate and, instead, over proliferate and give rise to germ line tumors. Such ovarian defects have been also reported in flies deficient for *Snf* or *MACOM* components (Granadino et al. 1992, Salz 1992, Schultt et al. 1998, Yan and Perrimon 2015, Guo et al. 2018), but were not detected in *MACOM* mutants (**Appendix 1**: ED Fig. 8a). This indicates that m⁶A does not contribute significantly to the regulation of *Sxl* splicing in the germline, whereas *MACOM* complex is essential and it further highlights that *MACOM* acts beyond its role in m⁶A deposition. In support to this, we found that *Sxl* splicing in ovaries of *Mettl3* flies was only marginally affected (**Appendix 1**: ED Fig. 9a), whereas its splicing was strongly altered in fly heads (**Figure 26** and **Appendix 1**: Fig. 4c).

In light of the modulatory role of m⁶A in *Sxl* splicing, it is plausible that a predominant role of m⁶A in posttranscriptional mRNA processing is to adjust, rather than control gene expression. m⁶A mark on a given transcript is most likely interpreted in a context dependent manner, whereby m⁶A readers along with a plethora of RBP concomitantly shape its fate. m⁶A thus appears to represent an additional layer of regulation that acts in parallel with other mechanisms to ensure the optimal transcript output. The benefit of such a cooperative regulatory programme may be that it offers a larger “buffering zone”, whereby a defect in one regulatory pathway may still be partially rescued by other functional pathways. In addition, with a growing set of potential m⁶A-recognising RBPs, m⁶A on a given transcript can serve as a platform that enables a switch from one reader (promoting the outcome A) to another reader (promoting the outcome B). Such a mechanism may facilitate a rapid cellular response when needed (e.g. changing condition, stress, differentiation).

5.6 The role of m⁶A mRNA modification during *D. melanogaster* development

The life cycle of a fruit fly consists of embryogenesis, larval development, metamorphosis during pupation and finally adulthood (see *Chapter 1.5.1*). We found that in *Drosophila melanogaster* m⁶A levels on mRNA are strongly elevated during early embryogenesis (0-2 hours) and at the onset of pupation (120-192 hours), while they are much lower in other developmental stages. In adult flies, m⁶A is strongly enriched in heads and ovaries as compared to the full fly (**Figure 46**). While we cannot rule out that m⁶A modification might also be enriched in some other tissue, our findings nevertheless suggest that m⁶A may be particularly important during fly oogenesis, early embryonic development and in the nervous system. Notably, we find that transcript levels of all factors involved in m⁶A deposition (MAC and MACOM) follow the trend of m⁶A modification. Consistently, their protein levels were also found to be highly enriched during early embryonic stages (Becker et al. 2018). Similarly, transcripts levels of YTH domain-containing m⁶A readers *Ythdc1* and *Ythdf* to a large extent resemble the expression pattern of m⁶A in mRNA. Most apparent differences are observed in adult flies, where *Ythdc1* is particularly enriched in heads, whereas levels of *Ythdf* are elevated in ovaries (**Figure 46**).

A peak of m⁶A levels is also noticeable during pupation (120-192 hours) and might reflect important roles of modification during metamorphosis when a remarkable tissue reorganisation takes place. In particular, the second phase of neurogenesis that is required for the formation of adult sensory and interneurons (INs) occurs during these developmental stages. These newly formed neurons regulate the coordination of complex locomotor functions in adult flies (see *Chapter 1.5.3*). Thus, given the apparent behavioural defects that we observed in m⁶A writer or m⁶A reader lacking flies (see below), it would be interesting to investigate if methylation of some particular targets perhaps contributes to the progression of neurogenesis throughout pupation.

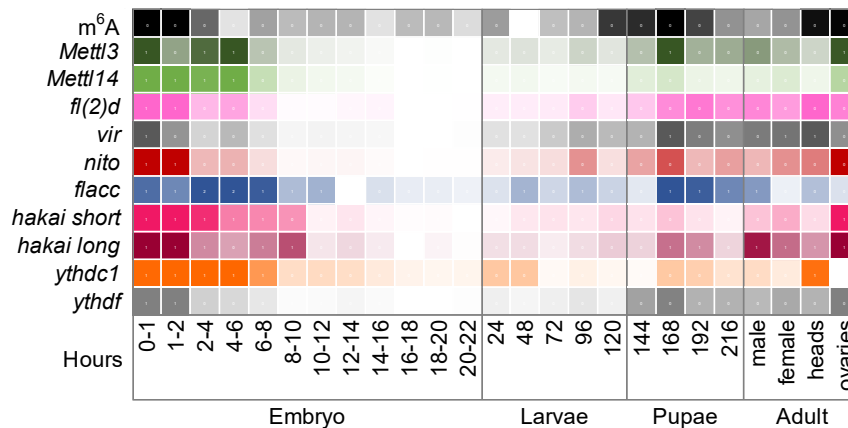


Figure 46. Heatmap of m⁶A levels and m⁶A players during developmental stages of *D. melanogaster*.

Heatmap represents levels of m⁶A modification on mRNA and relative expression levels of m⁶A writer components and readers during *D. melanogaster* developmental stages.

To uncover the importance of m⁶A modification in *D. melanogaster* development, we generated mutants of several proteins involved in m⁶A-deposition and recognition: *Mettl3*, *Mettl14*, *Fl(2)d*, *Hakai*, *Ythdc1* and *Ythdf*. Adult flies lacking MAC components were viable but displayed several deficiencies.

In addition to altered locomotion, flies were flightless and had a reduced life span. *Ythdc1* mutants recapitulate defects observed in MAC mutants, suggesting that in *D. melanogaster* this protein, to a large extent, mediates m⁶A functions in vivo. Mutants lacking *Fl(2)d* developed until larval stages and died before pupation, similarly to what has been described before for different *fl(2)d* alleles (Penalva et al. 2000). Likewise, loss of function alleles for *nito*, *flacc*, *vir* and *hakai* were previously shown to cause lethality during larval development (Hilfiker and Nothiger 1991, Kaido et al. 2009, Yan and Perrimon 2015, Guo et al. 2018). This indicates that MACOM, but not MAC, complex is required for progression through metamorphosis independently of its role in m⁶A-deposition. In line with this, our *hakai* null flies, that lacked both *hakai* isoforms, did not survive post larval stages. Intriguingly, *hakai long* mutants, in which only the long isoform was deleted were viable, suggesting that both protein isoforms may act redundantly. Alternatively, the long protein isoform may not be required for functions determining fly survival that are possibly linked to m⁶A-independent roles of the MACOM complex.

5.6.1 Gametogenesis and early embryogenesis

In our analysis of developmental stages, we found particularly high m⁶A levels during the first two hours of embryogenesis. This time frame corresponds to embryonic development before maternal-to-zygotic transition (**Figure 46**) when embryo progression depends solely on maternally deposited mRNA. Hence, it would be interesting to test if, during these early stages, m⁶A imposes a positive effect on translation of abundantly methylated mRNA in order to boost, much needed, protein production. At the onset of zygotic gene activation, m⁶A levels drastically decrease, which is suggestive of a rapid removal of the existing pool of maternally deposited and methylated transcripts. Notably, the role of m⁶A in the process of maternal-to-zygotic transition has been well studied in zebrafish and mice, where modification indeed contributes to timely decay of maternal transcriptome via the *Ythdf2* reader protein. m⁶A loss therefore leads to early embryonic lethality (Ivanova et al. 2017, Zhao et al. 2017b). To this end, we did not investigate the importance of m⁶A during embryogenesis, however, we did observe that mating of homozygous *Mettl3* mutants resulted in a remarkably lower number of surviving larvae as compared to crosses between heterozygous flies. Since we did not analyse embryo hatching rates we cannot rule out that other factors (e.g. fly mating, embryo laying) had predetermined such an outcome. In order to clearly demonstrate the importance of m⁶A modification during early stages of fly development, it will be crucial to systematically test and discriminate between potential alterations originating from maternal and/or paternal origin. Of note, the importance of maternally deposited *Mettl3* has been elucidated in the context of Sex determination, where only flies that lacked maternal *Mettl3* genetically interacted with the *Sxl*, whereas flies that lacked paternal copy showed no effect (Hausmann et al. 2016, Lence et al. 2016).

We also observed that m⁶A levels were elevated in ovaries, suggesting that modification might be important during oogenesis. Indeed numerous reports from vertebrates, yeast as well as plants have demonstrated the crucial role of m⁶A in male and female gametogenesis (see *Chapter 1.4.8.e*). Early study in flies from Hongay and colleagues in fact reported severe lethality of *Mettl3* mutants, whereby rare escaper females displayed defects during oogenesis. These alterations included aberrant ovarioles with fused egg chambers and were fully rescued by ectopic expression of Notch protein (Hongay and Orr-Weaver 2011). In contrast, our viable homozygous mutants lacking both, *Mettl3* and *Mettl14* components, showed no such ovarian abnormalities (**Appendix 1**, ED Fig. 8). In line with our observations, similar findings were also reported by two other groups that generated independent *Mettl3* mutants (Hausmann et al. 2016, Kan et al. 2017). Nevertheless, Kan and colleagues found that

upon loss of *Mettl3*, nearly 50 % of ovarioles contained egg chambers of earlier stages compared to those of wild type flies, indicating that m⁶A might be important for timely egg chamber maturation. Ovariole maturation undergoes 14 stages of egg chamber development that can be separated into three phases: mitotic (st. 1-6), endocycle (st. 7-10a) and gene amplification phase (st. 10b-13) (Jia et al. 2015). After careful re-analysis of our ovary immunostaining data, we indeed observed that *Mettl3* and *Mettl14* mutant ovarioles on average contain reduced numbers of egg chambers that lack different intermediate stages (**Appendix 1**, ED Fig. 8). This was suggestive of a mild negative effect of m⁶A loss on ovariole development, albeit with a variable penetrance. Notch signalling pathway is an important regulator of a phase transition switch during egg chamber development and we find that *notch* is m⁶A modified in S2R+ cells. In addition, in osteosarcoma cells, loss of Virma leads to diminished Notch levels, suggesting it may be a common m⁶A-regulated target in different systems (Han et al. 2020). It is possible that severe developmental and oogenesis defects, observed in *Mettl3* mutants generated by Hongay and colleagues (Hongay and Orr-Weaver 2011), were, in fact, apparent due to sensitised genetic background in which Notch levels may have already been diminished. An additional loss of m⁶A then resulted in further reduction of *notch* below critical levels. Nonetheless, to get better mechanistic insights into the exact contribution of m⁶A methylation during fly oogenesis, it will be important to determine m⁶A profile at different stages of oogenesis and to characterise relevant m⁶A targets that may be involved in egg chamber development and its progression throughout different phases of maturation.

5.6.2 m⁶A in *D. melanogaster* is required for proper neuronal functions

m⁶A is required for development of neuromuscular junctions

To investigate the potential role of m⁶A in synaptic functions, we analysed neuromuscular junctions (NMJ) in late larval stages. *Drosophila* NMJ is a well-established system that enables studying of the synapse formation, functionality and plasticity and consists of predominantly glutamatergic synapses (Menon et al. 2013). We found that *Mettl3* mutants display increased numbers of synaptic boutons and active zones per bouton in muscle-6/7 of abdominal hemisegment A3 (**Figure 25**), suggesting that m⁶A modification is important for synaptic architecture and potentially neurotransmission. Whether functionality of NMJs is also affected, has not been analysed in our current work and remains a topic of future investigations. Notably, we also analysed NMJs of *Ythdc1* mutant larvae but did not observe any defects (Cheuk Hei Ho; data not shown), thus, other reader proteins likely regulate m⁶A-mediated NMJ synapse formation in muscle-6/7 of abdominal hemisegment A3. Intriguingly, a similar phenotype as observed in *Mettl3* NMJs was previously reported in mutants lacking *Fmr1*, a recently characterised m⁶A reader protein (Edupuganti et al. 2017). *Fmr1* controls synaptic structure by posttranscriptional regulation of several factors required for NMJ formation (e.g. *CamKII*, *chic*, *dscam*, *futsch* and others) (reviewed in (Drozd et al. 2018)). We found that levels of these transcripts are misregulated upon loss of *Mettl3* and they are all m⁶A methylated in S2R+ cells (**Supplemental data 3**). However, future studies will reveal if this is also the case in vivo and if *Fmr1* binding to modified transcripts may at least partially explain altered NMJ formation in *Mettl3* mutants. Interestingly, Nito was recently shown to control axon outgrowth, branching and synaptic bouton formation in the CCAP/bursicon neurons, however it is currently not known if this function is linked to m⁶A deposition (Gu et al. 2017).

One of the proteins that we found downregulated upon Hakai depletion in S2R+ cells was Spätzle (Spz) encoding a neurotrophin that is required for synaptic plasticity at the neuromuscular junctions. Spz is expressed in the body wall muscles and targets Toll1 receptors in motoneurons via a retrograde transport (Sutcliffe et al. 2013). Loss of Spz leads to NMJ overgrowth and increased numbers of synaptic boutons with reduced active zones, which results in altered neurotransmission. In our miCLIP data we find that *spz* contains several prominent m⁶A sites, hence it might be one of the relevant candidates that potentially contribute to altered NMJ formation in m⁶A-lacking flies. Several putative candidates were also among proteins that interact with m⁶A writer proteins (**Supplemental data 2**). Hangover (*hang*) for example is a nuclear RBP expressed in motoneurons and acts as a negative regulator of NMJ bouton growth by reducing the levels of *FasII* transcript (Schwenkert et al. 2008). A transmembrane FasII protein is involved in synapse remodelling pathway and its transcript is m⁶A modified in S2R+ cells. Thus, it would be interesting to test if its levels are regulated by m⁶A-Hangover interplay.

Locomotion of adult flies

Beside aberrant NMJ at larval stages, several abnormalities were also apparent in adult flies lacking m⁶A writer or Ythdc1 reader proteins. *Mettl3* and *Ythdc1* mutants displayed locomotion defects evident by reduced activity, slow walking speed and disorientation. Importantly, these phenotypes were rescued by ectopic expression of *Mettl3* cDNA in neurons, but not in muscles (**Figure 24** and **Figure 27**). In addition, we observed that m⁶A levels were strongly elevated in heads of adult flies, highlighting the importance of m⁶A for neural functions. Adaptive sensimotor processing is controlled by the so-called central complex in the CNS that consists of spatially connected structures; the Protocerebral Bridge, ellipsoid body, fan-shaped body, and the paired noduli, which coordinate different aspects of body locomotion (*Chapter 1.5.3*). Whether only particular brain regions or a subset of neurons are responsible for the observed defects, awaits future investigations. Notably, our transcriptome-wide sequencing from *Mettl3* KO fly heads identified dozens of misregulated transcripts that have been previously linked to locomotion and behavioural defects (**Supplemental data 3**). Most likely, a combinatorial effect of several genes, altered by the loss of m⁶A, is a driving cause for the observed phenotypes. Nevertheless, many of these genes were shown to be modified in S2R+ cells and they might also carry m⁶A in vivo, however, future analysis of neuronal methylome will be crucial for characterization of biologically relevant targets. Recent technological advances in m⁶A detection techniques (e.g. nanopore sequencing, MAZTER-seq and DART-seq) allow m⁶A identification with minimal RNA requirements (Meyer K. D. 2019, Wang et al. 2020). Thus, if combined with single-cell RNA sequencing, these approaches may enable more precise mapping of m⁶A in chosen neuronal populations. Importantly, m⁶A is also implicated in mRNA export and translation, hence, beside a steady state RNA analysis, incorporation of proteomic approaches to monitor protein expression changes may prove useful.

In addition to altered walking, orientation and activity, adult flies lacking *Mettl3* or the nuclear reader protein *Ythdc1* also displayed compromised climbing ability in response to negative geotaxis. We were able to recapitulate climbing defects by depletion of m⁶A writer components, *Mettl3* and *Flacc*, in different types of neurons, indicating that altered climbing indeed results from the absent m⁶A pathway. We used several cell type specific Gal4-driver lines and observed that flies were most sensitive to simultaneous depletion of m⁶A in serotonergic and dopaminergic neurons (**Supplemental data 4**). Notably, individual depletion of m⁶A in serotonergic and dopaminergic neurons or in other types of neurons resulted in less pronounced effects, suggesting that serotonergic and dopaminergic neurons are particularly sensitive to the loss of m⁶A in regards to negative geotaxis response. In the future, it

will be important to confirm these findings by rescue experiments in individual neuronal subtypes, which may also help in elucidating what are exact targets driving such an impaired locomotion.

m⁶A and Parkinson's disease

Parkinson's disease (PD) is a progressive neurodegeneration disorder associated with pathologic accumulation of protein aggregates (Lewy bodies) and mitochondrial dysfunction specifically in dopaminergic neurons resulting in consequent loss of affected neurons. These defects lead to muscle rigidity, altered movement, cognitive impairment and disruption of sleep-wake cycle (Schapira and Jenner 2011). Aetiology of PD involves genetic and environmental factors, however mutations in several genes (α -synuclein, parkin, LRRK-2, PINK-1, and others) were found to be the major cause for the onset of familial forms of disease. Many of these genes encode factors involved in the response to oxidative stress and in the ubiquitin-proteasome system of protein quality control. Parkin for example is an E3 ubiquitin ligase that is involved in mitochondrial quality control and in the control of oxidative stress in dopaminergic neurons. Excess levels of dopamine that are not captured by cellular vesicles, prompt dopaminergic neurons highly susceptible to Parkinson's disease. The accumulation of free dopamine in the cytosol of dopaminergic neurons represents a serious cytotoxic stress (Segura-Aguilar and Paris 2014). In a free form, dopamine can be degraded by several ways; it can be stepwise enzymatically oxidised at the outer membrane of the mitochondria, albeit with the side production of hydrogen peroxide. Alternatively, dopamine can also spontaneously oxidise to highly reactive dopamine o-semiquinone and further to aminochrome. Toxicity of aminochrome is exemplified by the fact that it can form adducts with different proteins (e.g. α -synuclein) or may for example inhibit the activity of E3 ubiquitin ligase parkin. Several mechanisms exist that can inactivate toxic dopamine products. Among them is the glutathione-S-transferase (GST) that can conjugate glutathione to both, dopamine o-semiquinone and aminochrome, and the corresponding products can be further degraded and secreted. Thus, GST can protect dopaminergic neurons from neurotoxicity (Smeyne and Smeyne 2013, Segura-Aguilar and Paris 2014).

Glutathione-S-transferase S1 (GstS1) is the closest ortholog of the GST protein in *D. melanogaster*. It was one of the few reduced proteins that we identified in the proteome analysis of S2R+ cells upon Hakai depletion (**Figure 42**). This could suggest the potential role of m⁶A in the onset of PD. In flies, GstS1 catalyses conjugation of reduced glutathione to a variety of substrates and is involved in the control of oxidative stress. Loss of GstS1 enhances neurodegeneration of dopaminergic neurons in *parkin* mutant flies that represent a fly model of Parkinson disease, whereas GstS1 overexpression specifically in dopaminergic neurons alleviates neurodegeneration symptoms (Whitworth et al. 2005). In addition, flies lacking one copy of *GstS1* in *parkin* null background display reduced locomotion during geotaxic climbing behaviour and have shortened life span (Whitworth et al. 2005). Intriguingly, similar behavioural phenotypes were observed in flies lacking *Mettl3* (**Figure 24**), signifying a possible contribution of m⁶A loss in the PD. As mentioned before, we found that depletion of m⁶A writer components, specifically in dopaminergic and serotonergic neurons, significantly alters fly climbing (**Supplemental data 4**). Of note, *parkin* mutants do not display changes in brain volume, since only a subset of DA neurons in CNS undergo neurodegeneration. In line with this, we did not observe any loss of brain volume or appearance of brain vacuoles in adult *Mettl3* mutant females (at day 3 day and day 10) (data not shown). Interestingly, in a large yeast-two-hybrid screen of *D. melanogaster* protein interactions, Hakai was found with to interact with parkin (Giot et al. 2003), which may also suggest an independent role of Hakai in parkin-mediated mitochondrial homeostasis. In the future it will be important to investigate if GstS1 levels are indeed reduced in *Mettl3* mutants, and particularly, if GstS1

protein is under the control of m⁶A modification in dopaminergic neurons. In addition, elevated levels of carbonylated mitochondrial proteins are indicative of oxidative stress in PD and other neurodegenerative disorders (Bizzozero 2009). Thus, analysis of protein carbonylation in *Mettl3* mutant brain could serve as a simple read-out to assess if loss of m⁶A contributes to the onset of neurodegeneration (Fedorova et al. 2014). Notably, in support of the possible role of m⁶A misregulation in the pathogenesis of PD, a recent study detected reduced m⁶A levels in the brain of a rat model of PD (Chen X. et al. 2019).

Fly models of PD also display alterations in non-motor behaviour. These symptoms include compromised learning and memory formation as well as disrupted circadian rhythm (Seugnet et al. 2009, Balija et al. 2011). In mice, m⁶A has been implicated in the short and long term memory acquisition as well as in the control of circadian rhythm, hence it would be of interest to investigate if these aspects of PD are also present in *Mettl3* mutant flies. Intriguingly, an impairment in short term memory acquisition has been recently demonstrated in flies lacking the cytoplasmic Ythdf protein, however the exact molecular mechanisms remain to be discovered (Kan et al. 2020). Due to simplicity of the fly neural circuits, *D. melanogaster* represents a favourable model to study potential contribution of m⁶A in the onset and progression of PD.

Longevity and flight

In addition to locomotion defects, we also observed that flies lacking *Mettl3* have a reduced life span and display a held-out wing phenotype. They are unable to fold their wings over the thorax and abdomen, and cannot fly (**Figure 24**). Direct flight muscles (DFM) and fast contracting indirect flight muscles (IFMs) in the thorax, control wing positioning and movement, and in this way contribute to flight activity (Clayton et al. 1998, Kozopas and Nusse 2002). Below we describe a few putative candidates that may contribute to shortened lifespan and flight alterations upon loss of m⁶A modification. Their involvement will, however, need to be verified in the future. **I)** As discussed above, *notch* is modified in S2R+ cells and loss of *Mettl3* results in diminished Notch levels in ovaries (Hongay and Orr-Weaver 2011). Intriguingly, adult flies with reduced levels of Notch in the CNS, display shortened lifespan and altered flying (Presente et al. 2001). **II)** GstS1 protein whose levels are decreased upon Hakai depletion, is abundant in IFMs. These muscles contain large numbers of mitochondria and are highly susceptible to oxidative damage, therefore they may be more dependent on functional GstS1 protein (Clayton et al. 1998). In addition, ectopic expression of GstS1 in wing discs results in aberrant wing development (Toba et al. 1999). Finally, in a genomic screen, GstS1 was shown to be required for extended longevity (Seong et al. 2001), hence it represents a potential candidate gene that may contribute to several phenotypes observed in flies lacking m⁶A. In the future, it will be important to unambiguously determine the importance of m⁶A modification for the stability of GstS1 protein in vivo. **III)** Finally, a gene *held out wings* (*how*) encodes a nuclear RNA binding protein that regulates muscle development. As the name implies, *how* mutants exhibit abnormal wing positioning, albeit the exact mechanism leading to such defects is currently unknown (Baehrecke 1997). Its transcript also contains a prominent m⁶A peak and thus may be regulated by the m⁶A pathway. **IV)** Aberrantly positioned held-out wings and flight impairment have also been reported in several mutants lacking different components of the chromatin remodelling complex BAP (e.g. *brahma*, *moira*, *osa*) (Brizuela and Kennison 1997, Vázquez et al. 1999, Ragab et al. 2006). These factors regulate the expression of *Antennapedia* (*Antp*), a trithorax group gene that is, among other functions, required for a proper wing development. Abnormal wing positioning was also observed in mutants for several factors (e.g. *tara*, *stretch*) that genetically interact with BAP complex and *Antennapedia* (Calgaro et al. 2002, Yazdani et

al. 2008). Since many of these factors are m⁶A modified in S2R+ cells, it would be of interest to investigate if functionality of the BAP remodelling complex, in the context of wing positioning and flight activity, is perhaps compromised in flies lacking m⁶A.

Summary

In summary, our findings from flies with disrupted m⁶A pathway highlight a particular importance of m⁶A modification in the fly nervous system. Severely altered locomotion and orientation, flight insufficiency, as well as aberrant synapse morphology at the NMJ are most likely just some of the defects resulting from a loss of m⁶A deposition. Further efforts will be required to better characterise causative factors leading to this apparently elevated dependency of the nervous system on the presence of m⁶A modification. It is important to note that we do not currently have any proof on whether transcripts that we found methylated in S2R+ cells are also methylated in any other fly tissue. A recent study performed a comprehensive analysis of m⁶A landscape across different tissue and cell types in mouse and human. Their findings showed that m⁶A methylation in the brain is conserved between mouse and human, but distinct from other tissue, possibly reflecting a unique and highly specialised transcriptome of neural cells. Surprisingly, however, results from all other tissues demonstrated that m⁶A methylome of non-neuronal cells is more similar within a given species than between mouse and human (Liu J. et al. 2020). Hence it will be important to characterise *D. melanogaster* methylome in other cell types of neuronal origin or from neuronal tissue.

Since neurons are highly specialised and polarised cells that assemble into complex cellular networks to ensure efficient signal transmission and functioning, they may be more reliant on mechanisms that enable flexible adjustment of gene expression at different levels. Notably, several other post-transcriptional processing events also occur at higher frequency in the nervous system as compared to other tissue; these include alternative splicing and polyadenylation, recursive splicing, the formation of circRNA as well as localised translation and translation of microexons (Furlanis and Scheiffele 2018, Lennox et al. 2018, Su et al. 2018). This infers that numerous mRNA processing events may cooperatively enable greater diversification of transcriptome and proteome and a rapid spatiotemporal adjustment in response to various stimuli and environmental cues. Given that m⁶A can modulate at least some of these processes, it most likely serves as an additional layer of gene regulation that strongly contributes to proper neuronal development, functioning and plasticity.

The importance of m⁶A modification in the nervous system is, however, not unique to *D. melanogaster* and over the past few years numerous studies demonstrated that correct deposition of m⁶A is critical for normal development and functioning of the nervous system in other species (*Chapter 5.6.2*) (reviewed in (Angelova et al. 2018, Engel and Chen 2018, Jung and Goldman 2018, Flamand and Meyer 2019, Livneh et al. 2020)). Similarly to our observations, m⁶A levels were found elevated in the developing brain in mice (Meyer et al. 2012) and region-specific methylation has already been characterised in the cortex (Widagdo et al. 2016, Chang et al. 2017, Yoon et al. 2017, Li M. et al. 2018, Wang Y. et al. 2018), cerebellum (Chang et al. 2017, Ma et al. 2018, Wang C.-X. et al. 2018), hippocampus (Walters et al. 2017, Engel et al. 2018, Zhang Z. et al. 2018). By conditional inhibition of m⁶A writers and readers, these studies described numerous alterations and highlighted the requirement of m⁶A in diverse neuronal processes including embryonic and adult neurogenesis (Yoon et al. 2017, Wang C.-X. et al. 2018, Wang Y. et al. 2018), axon guidance (Zhuang et al. 2019) and regeneration (Weng et al. 2018), but also for cognitive functions during memory formation (Engel et al. 2018, Koranda et al. 2018, Zhang Z. et al. 2018). Several studies could demonstrate the molecular mechanisms underlying neuronal alterations and most m⁶A functions have been assigned to YTH

readers. Ythdf2 is for example indispensable for timely decay of methylated transcripts during cortical neurogenesis (Yoon et al. 2017, Li M. et al. 2018), whereas Ythdf1 facilitates local translation of methylated targets in postsynaptic densities of hippocampal neurons to ensure correct synaptic transmission (Shi et al. 2018) and controls translation of *Robo3.1* mRNA for accurate axon guidance in spinal commissural neurons (Zhuang et al. 2019). Notably, restricted activities of different m⁶A readers highlight the need for detailed dissection of m⁶A in different cell populations. Precise mapping of m⁶A in selected neuronal subtypes, however, awaits future endeavours.

D. melanogaster provides a valuable genetic model to studying development and functioning of the nervous system, as well as behavioural response. Our work revealed first phenotypical and genetic evidence that m⁶A modification regulates processes linked to neuronal functioning. The relevance of our findings has been confirmed by independent studies from Soller and Lai Laboratories (Hausmann et al. 2016, Kan et al. 2017). Notably, two recent studies found that loss of m⁶A in flies also impairs cognitive functions during aging (Kan et al. 2020) and controls axonal growth in PNS and CNS via the cytoplasmic Ythdf reader (Soldano et al. 2020). Despite intriguing findings in regards to behavioural and locomotor abnormalities resulting from m⁶A loss (Hausmann et al. 2016, Lence et al. 2016, Kan et al. 2017), the causative factors that drive these defects are to a large extent still unknown. Hence, future studies may attempt careful analysis of different candidate targets identified in this work. In addition, a systematic examination of conditional loss of m⁶A writers in selected neuronal subtypes might provide novel mechanistic insights into factors driving m⁶A-dependent development in the central and peripheral nervous system. Ultimately, a functional dissection of individual m⁶A sites will be needed to prove their roles in specific biological processes.

Intriguingly, a set of novel approaches for targeted addition, removal and recognition of m⁶A modification in a chosen transcript have been developed in recent years (Shi et al. 2019, Wei and He 2019). For example, fusions of m⁶A effectors with dCas9 and dCas13 proteins have enabled site specific methylation, demethylation (Liu X.-M. et al. 2019) and m⁶A binding (Rauch et al. 2018). In another approach, target-specific m⁶A readers were constructed from proteins originating entirely from the human genome. The so-called “CRISPR-Cas-inspired RNA targeting system (CIRTS)”, therefore holds promise for a potential therapeutic use in the future (Rauch et al. 2019). These novel technologies will undoubtedly prove valuable to decipher the significance of a single methylation site on the transcript processing and its fate in a context dependent manner.

Conclusions

The aim of this PhD work was to characterise m⁶A modification in flies from a broad perspective and by following several directions in order to identify factors involved in m⁶A biogenesis, to reveal the roles of m⁶A modification on pre-mRNA processing and to investigate the importance of this modification during development of *Drosophila melanogaster*. Novel findings presented in this study substantially advance our current knowledge on the composition of the m⁶A writer machinery. This work also revealed the requirement of m⁶A in the alternative pre-mRNA splicing of *Sxl* and other targets and highlighted the impact of this modification for neuronal functions. In addition, numerous unpublished findings presented in this work provide an important resource of data that will further future explorations to better characterise this abundant mRNA modification at the molecular and organismal levels. Main findings of this study are summarised below.

Aim I: Characterization of novel modulators required for deposition, recognition and removal of m⁶A modification on mRNA

- m⁶A writer complex in *Drosophila melanogaster* consists of two sub-complexes: MAC (Mettl3, Mettl14) and MACOM (Fl(2)d, Vir, Nito, Flacc, Hakai) that are conserved in higher eukaryotes.
- Nito and Flacc are novel factors, essential for m⁶A deposition.
- Flacc stabilizes the interaction between Fl(2)d and Nito proteins.
- Hakai maintains stability of Vir, Flacc and Fl(2)d proteins.
- Ythdc1 is a nuclear m⁶A reader and one of the main mediators of m⁶A functions in flies.

Aim II: Identification of regulatory functions of m⁶A modification on mRNA processing.

- Distribution of m⁶A in flies is highly enriched in 5'UTR regions.
- m⁶A resides in a conserved consensus A-rich RRACH motif.
- Modification facilitates alternative splicing of a subset of modified transcripts.

Aim III: Exploring the importance of m⁶A modification in vivo during development of a fruit fly (*Drosophila melanogaster*).

- Modification is highly enriched during early embryogenesis, at the onset of pupation, as well as in heads and ovaries of adult flies.
- m⁶A writers and readers follow the expression profile of m⁶A modification during fly development.
- Fly mutants lacking Mettl3 and Mettl14 are flightless and display severe locomotion defects.
- Loss of nuclear reader protein Ythdc1 resembles the loss of m⁶A writer components.
- m⁶A is required for proper splicing of *Sxl* (*Sex lethal*) transcript in females and in this way modulates sex determination and dosage compensation pathways.

Supplemental data

Supplemental data 1

Mettl3			Fl(2)d			Nito			Flacc				Ythdc1							
Gene_names	Fwd	Rev	Gene_names	Fwd	Rev	Gene_names	Fwd	Rev	Gene_names	Fwd	Rev	Gene_names	Fwd	Rev	Gene_names	Fwd	Rev			
Mettl3	229	0.0	fl(2)d	1.0	0.0	nito	2.1	0.4	Flacc	11.0	0.1	52 RpLP1	2.0	0.6	Ythdc1	21.1	0.1	60 homer	3.0	0.6
1 Mettl14	12.7	0.0	1 Hrb98DE	2.1	0.1	1 CG3548	2.9	0.4	1 fl(2)d	12.3	1.5	53 CG8814	2.0	0.4	1 CG9641	16.1	0.1	61 P32	3.3	0.6
2 CG33303	5.3	0.2	2 BRWD3	5.0	0.2	2 Hsp60	2.2	0.5	2 nito	7.5	0.2	54 CG6479	2.0	0.2	2 qkr58E-2	11.8	0.1	62 RpL22	3.3	0.6
3 Psa	4.9	0.3	3 Top2	2.5	0.2	3 GIP	2.2	0.4	3 qkr58E-1	5.4	0.3	55 Fmr1	2.0	0.5	3 GIP	10.8	0.2	63 CG8929	3.2	0.4
4 PyK	4.4	0.2	4 ball	2.6	0.2	4 CG1646	2.2	0.4	4 homer	4.6	0.2	56 CG3902	1.9	0.6	4 CG5787	9.7	0.2	64 vir	3.1	0.2
5 RnrL	4.4	0.1	5 mod	2.4	0.2	5 gag	2.1	0.4	5 didum	4.5	0.5	57 Vha55	1.9	0.7	5 rump	8.8	0.3	65 flacc	3.1	0.4
6 Cct5	4.4	0.2	6 bocksbeutel	4.8	0.2	6 CG7611	2.0	0.5	6 VhaAC39-1	4.4	0.3	58 hoip	1.9	0.7	6 Pep	8.7	0.3	66 CG11148	3.0	0.2
7 Rab7	4.2	0.4	7 D1	2.9	0.2	7 hang	1.9	0.5	7 gag	4.3	0.4	59 Myo31DF	1.9	0.7	7 CG30122	8.7	0.2	67 MLE	3.0	0.2
8 Ca-P60A	4.2	0.3	8 dre4	4.0	0.2	8 tlk	1.9	0.5	8 RpL32	3.9	3.1	60 RpL6	1.9	0.5	8 lark	8.7	0.2	68 LD23634	3.0	0.6
9 T-cp1	4.1	0.2	9 CG4236;Caf1	2.4	0.3	9 fl(2)d	1.9	0.6	9 nmd	3.9	0.9	61 CG9684	1.9	0.4	9 Hrb98DE	8.5	0.2	69 CG1646	2.9	0.3
10 CG3523	4.0	0.3	10 tlk	5.3	0.3	10 CLIP-190	1.9	0.6	10 CG3884-RB	3.7	0.3	62 RpL10Ab	1.9	0.7	10 nito	8.3	0.3	70 tral	2.9	0.5
11 Rop	4.0	0.3	11 CG8878	3.5	0.3	11 CG7668-RA	1.9	0.5	11 Ckllbeta	3.6	0.2	63 Aldh	1.9	0.4	11 Hrb7F	7.8	0.3	71 RpS15	2.9	0.6
12 Gp93	3.7	0.4	12 Hrb7F	2.1	0.3	12 Ulp1	1.9	0.5	12 Nup154	3.4	0.3	64 RpL4	1.9	0.3	12 sqd	7.8	0.3	72 Nop60B	2.8	0.5
13 eIF-2alpha	3.7	0.2	13 glo	3.0	0.3	13 CG5599	1.8	0.5	13 Gp210	3.4	0.3	65 AGO2	1.8	0.6	13 sxx	7.3	0.4	73 Xe7	2.7	0.6
14 Hsc70-4	3.7	0.2	14 Gnf1	3.9	0.3	14 Mtor	1.8	0.6	14 SF2	3.2	0.3	66 Fib	1.8	0.6	14 qkr58E-3	7.3	0.3	74 CG5641	2.7	0.4
15 RpL3	3.5	0.5	15 CG42232	3.6	0.3	15 qkr54B	1.8	0.5	15 Kkllalpha	3.2	0.3	67 RpLP2	1.8	0.5	15 unk	7.1	0.5	75 caz	2.6	0.2
16 Chc	3.4	0.3	16 CG8289	7.7	0.4	16 mRpS22	1.8	0.6	16 PhKgamma	3.1	0.4	68 nonA	1.8	0.4	16 CG1677	7.0	0.5	76 CG5792	2.6	0.3
17 sesB	3.4	0.2	17 Msp300	3.7	0.4	17 Pabp2	1.8	0.5	17 Pxn-RD	3.1	0.4	69 BEST-LD30049	1.8	0.6	17 baf	7.0	0.3	77 CG3542	2.6	0.5
18 RpS3	3.4	0.2	18 CG4747	2.1	0.4	18 RAF2	1.7	0.6	18 Acn	3.1	0.3	70 RpL14	1.8	0.6	18 Ote	6.9	0.4	78 Gp210	2.5	0.6
19 Hsp68	3.4	0.2	19 sle	3.9	0.4	19 tlk	1.7	0.5	19 CG8475	3.1	0.4	71 Sm B	1.7	0.6	19 Ars2	6.7	0.4	79 CG13903	2.5	0.4
20 Hel25E	3.4	0.2	20 Ssrp	3.5	0.4	20 Tm1	1.7	0.6	20 Nup93-1	3.0	0.4	72 Sm G	1.7	0.7	20 bocksbeutel	6.5	0.4	80 tyf	2.5	0.5
21 alphaCop	3.3	0.4	21 CG5746	7.2	0.5	21 Flo-1	1.7	0.5	21 r	3.0	0.4	73 eIF3ga	1.7	0.6	21 eIF-4E	6.4	0.4	81 Tdrd3	2.5	0.3
22 hts	3.3	0.3	22 CG5787	2.2	0.5	22 CG3714	1.7	0.6	22 Pmp70	3.0	0.3	74 eIF3-S10	1.7	0.6	22 Cbp20	6.4	0.5	82 CG7194	2.4	0.4
23 betaCop	3.2	0.3	23 Pep	2.4	0.5	23 CG9641	1.6	0.5	23 zip	3.0	0.3	75 ncd	1.7	0.6	23 His4	6.3	0.4	83 Gnf1	2.3	0.4
24 Rack1	3.1	0.2	24 Lam	1.7	0.5	24 qkr58E-3	1.6	0.6	24 Saf-B	2.9	0.3	76 Prp19	1.7	0.5	24 Lam	6.1	0.5	84 CG6701	2.2	0.5
25 Fan	3.1	0.3	25 RpL7	1.6	0.6	25 qkr58E-1	1.6	0.6	25 Nup205	2.9	0.4	77 Sm E	1.7	0.6	25 Imp	6.1	0.5	85 Tango5	2.2	0.6
26 Vha68-2	3.0	0.2	26 rump	3.0	0.6	26 Top1	1.6	0.6	26 CG15784	2.9	0.3	78 RpL28	1.7	0.6	26 His2B	6.0	0.4	86 CG4266	2.2	0.3
27 betaTub60D	3.0	0.2	27 Rcc1	3.7	0.6	27 Arp2	1.6	0.7	27 Vha100-2	2.9	0.5	79 dre4	1.7	0.9	27 CG10077	6.0	0.2	87 SG07683	2.2	0.4
28 Arf79F	3.0	0.3	28 RpL13A	4.3	0.6	28 glo	1.6	0.6	28 HDC14603	2.8	0.4	80 rin	1.7	0.5	28 pAbp	5.9	0.5	88 CG7903	2.2	0.4
29 Tcp-1eta	2.9	0.3	29 RpL4	3.0	0.6	29 CG5214	1.6	0.5	29 Smu1	2.7	0.8	81 Cat	1.7	0.6	29 His1	5.9	0.3	89 lig3	2.2	0.5
30 Rab2	2.8	0.2	30 qkr58E-1	2.0	0.6	30 Grip71	1.6	0.6	30 gag	2.7	0.4	82 eIF3-S9	1.6	0.6	30 Hrb27C	5.9	0.5	90 Upf1	2.2	0.3
31 Hsp83	2.7	0.6			31 UZA	1.6	0.6	31 CG8771	2.6	0.5	83 RpL12	1.6	0.7	31 His2Av	5.9	0.4	91 ball	2.1	0.3	
32 RpL9	2.7	0.5			32 Mes2	1.6	0.6	32 lark	2.5	0.3	84 Pex14	1.6	0.5	32 Syp	5.8	0.2	92 CG11505	2.1	0.4	
33 ETUM	2.7	0.2			33 mre11	1.6	0.5	33 CG5261	2.5	0.4	85 RpL5	1.6	0.6	33 eIF-3p66	5.7	0.6	93 Saf-B	2.1	0.5	
34 CG7033	2.6	0.3			34 qkr58E-2	1.6	0.6	34 Mec2	2.5	0.4	86 Trip1	1.6	0.5	34 Rcc1	5.6	0.2	94 btz	2.1	0.6	
35 sta	2.6	0.3			35 Set1	1.5	0.4	35 CG7766	2.4	0.4	87 Past1	1.6	0.6	35 eIF4G	5.5	0.5	95 enc	2.0	0.4	
36 Vap-33-1	2.6	0.2			36 CG7065	1.5	0.6	36 Chc	2.4	0.3	88 RpL18	1.6	0.5	36 rngi	5.5	0.6	96 CG9987	2.0	0.6	
37 RpL5	2.6	0.5			37 Arpc1	1.5	0.6	37 tho2	2.3	0.4	89 RpL23A	1.6	0.6	37 qkr58E-1	5.5	0.4	97 l(2)35Df	2.0	0.5	
38 CG17337	2.5	0.3			38 CG7358	1.5	0.6	38 LKR	2.3	0.5	90 CG12264	1.6	0.7	38 His3	5.4	0.4	98 Ostgamma	1.9	0.6	
39 CG4169	2.5	0.4			39 ORF1	1.5	0.6	39 Pex1	2.3	0.4	91 PPO2	1.6	0.6	39 nonA	5.3	0.3	99 CG6422	1.9	0.3	
40 betaTub56D	2.5	0.2					40 GIP	2.2	0.5	92 CG4849	1.6	0.7	40 CG5746	5.3	0.3	100 Top2	1.9	0.4		
41 Rab1	2.5	0.5					41 Nop56	2.2	0.6	93 DnaJ-1	1.6	0.5	41 Iarp	5.1	0.4	101 CG8142	1.9	0.6		
42 E2b	2.4	0.5					42 Rump	2.2	0.6	94 RpL3	1.6	0.6	42 bor	5.0	0.3	102 ISWI	1.8	0.4		
43 Lam	2.4	0.6					43 Tango4	2.2	0.5	95 RpLP0	1.5	0.4	43 AGO2	4.9	0.4	103 CG8478	1.8	0.4		
44 eIF-4a	2.3	0.2					44 Bap60	2.2	1.0	96 Mfe2	1.5	0.6	44 Cbp80	4.8	0.5	104 eIF4G2	1.8	0.4		
45 RpL18A	2.3	0.6					45 bor	2.1	0.5	97 Bx42	1.5	0.5	45 glo	4.7	0.2	105 RfC3	1.8	0.5		
46 R	2.2	0.2					46 CG43088	2.1	0.3	98 RpL18A	1.5	0.6	46 rin	4.6	0.6	106 Top3beta	1.8	0.4		
47 alphaTub84D	2.2	0.2					47 pnr	2.1	0.5	99 Rme-8	1.5	0.5	47 mtSSB	4.5	0.6	107 FK506-bp1	1.8	0.6		
48 Rab11	2.1	0.6					48 pAbp	2.1	0.5	100 CG5077	1.5	0.7	48 lig	4.2	0.6	108 CG9684	1.8	0.6		
49 RpS17	2.1	0.3					49 Pgam5	2.1	0.6	101 CG17544	1.5	0.8	49 Atx2	4.1	0.5	109 NAT1	1.7	0.4		
50 Hsc70-3	2.1	0.3					50 hrp48	2.1	0.5	102 Prp8	1.5	0.6	50 CG5726	4.1	0.5	110 hang	1.7	0.4		
51 Gapdh1	2.1	0.6					51 CG5214	2.0	0.5			51 Ep63E	4.1	0.7	111 Ddx1	1.7	0.6			
52 RpL21	2.1	0.6									52 Fmr1	4.1	0.4	112 RhoGAP19D	1.7	0.4				
53 RpS4	2.0	0.3									53 fl(2)d	4.1	0.3	113 nocte	1.7	0.5				
54 Tsr	2.0	0.4									54 bel	4.0	0.6	114 Parp	1.7	0.3				
55 Tctp	2.0	0.5									55 Patr-1	3.8	0.5	115 cup	1.6	0.2				
56 RpL27	1.9	0.5									56 yps	3.8	0.5	116 par-1	1.5	0.5				
57 RpL30	1.8	0.5									57 Zn72D	3.5	0.3	117 pont	1.5	0.6				
58 RpS7	1.8	0.3									58 nonA-I	3.4	0.5	118 4E-T	1.5	0.6				
59 blw	1.8	0.3									59 La	3.0	0.5							
60 Gale	1.7	0.2																		
61 Prosalphat	1.7	0.3																		
62 RpS16	1.7	0.5																		
63 Mec2	1.7	0.4																		
64 lost	1.7	0.3																		
65 AGO2	1.6	0.4																		
66 RpL22	1.6	0.4																		
68 RpS13	1.5	0.5																		

Supplemental data 1. Protein interactors with Mettl3, Fl(2)d, Nito, Flacc and Ythdc1 baits.

Proteins with >1,5 fold enrichment (bait/control) in forward (Fwd) and reverse (Rev) experiments are shown. Numbers in red represent intensity ratios for proteins that were detected with one peptide in the control condition of the respective experiment.

Supplemental data 2

Common protein interactors			
Fly protein	Human ortholog	Predicted function	Reference
AGO2	Ago2	Component of the RISC complex, siRNA pathway	FBgn0087035 (Martinez and Tuschl 2004)
ball (NHK-1)	VRK1	Ser/Thr kinase, H2A and BAF phosphorylation, chromatin condensation. Mitotic spindle organisation. Progression of meiosis and mitosis. Neuronal stem cell population maintenance.	FBgn0027889 (Cullen et al. 2005, Nikalayevich and Ohkura 2015)
bocksbeutel	-	Unknown (LEM domain, possible nuclear lamina associated protein)	FBgn0037719 (Barton et al. 2014)
Bor	ATAD3A	Mitochondrial ATPase. Mitochondria maintenance.	FBgn0287225 (Harel et al. 2016)
CG1646	PRPF39	Unknown (predicted 5' ss recognition).	FBgn0039600
CG5746	-	-	FBgn0039186
CG9641	-	-	FBgn0031483
CG9684	-	Unknown (TDRD1 family protein)	FBgn0037583
copia/GIP	-	Retrotransposon gene, required for RNA dependent DNA intergartion. Abundant in MB alpha/beta neurons.	FBgn0013437
FI(2)d	WTAP	MACOM component	FBgn0037583 (Knuckles et al. 2018)
Flacc	ZC3H13	MACOM component	FBgn0030974 (Knuckles et al. 2018)
Fmr1	FMRP	Regulation of mRNA localization, translation. Neuronal development and synaptic plasticity.	FBgn0028734 (Drozd et al. 2018)
glorund	hnRNPH/F	oskar mRNA localisation, repression of nanos mRNA translation. Dorsal-ventral and anterior-posterior axis specification.	FBgn0259139 (Piccolo et al. 2014)
Gnf1	RFC1	Unknown (predicted DNA binding, PCNA association)	FBgn0004913
Gp210	NUP210	Unknown (predicted nuclear pore organisation)	FBgn0266580
hang	-	RBP, regulates response to cellular stress and ethanol tolerance via binding and stabilization of dnc-RA mRNA. Negative regulation of NMJ bouton growth, possibly via reduction of FasII expression.	FBgn0026575 (Schwenkert et al. 2008, Ruppert et al. 2017)
homer	HOMER2	RBP important for oskar anchoring at the post pole, binds glutamate receptor at post-synaptic part. Control of locomotor activity.	FBgn0025777 (Diagana et al. 2002)
Hrb87F (hrp36)	hnRNPA2B1	Unknown (predicted splicing regulator. Involved in female gonad development and stress response). Interacts with non-A and pep proteins.	FBgn0004237 (Reim et al. 1999, Piccolo et al. 2014)
Hrb98DE (hrp38)	hnRNPA2B1	RBP, 5UTR binding of DE-cadherin for translational regulation. Control of GSC self-renewal and oocyte localisation.	FBgn0001215 (Ji and Tulin 2012, Piccolo et al. 2014)
lark	RBM4B	RBP involved in positive regulation of translation of circadian clock transcripts.	FBgn0011640 (Huang et al. 2014)
Nito	RBM15/15B	MACOM component	FBgn0027548
nonA	SFPQ/NONO	Regulation of circadian rhythm via stabilization of cpx pre-mRNA. Interacts with hrb87F and pep proteins. Vertebrate SFPQ/NONO homo- and heterodimerize and are implicated in various mRNA processing steps including splicing. Human SFPQ is found in cytoplasmic aggregates in neurodegenerative disorders.	FBgn0004227 (Reim et al. 1999, Luo W. et al. 2018) (Knott et al. 2016)
pAbp (PABPC1)	pAbp	Regulation of mRNA translation, localization.	FBgn0265297 (Vazquez-Pianzola and Suter 2012, Marygold et al. 2017)
Pep	-	Protein on ecdysone puffs. Interacts with non-A and Hrb87F proteins. DNA and RNA binding protein, acts on ecdysone response loci.	FBgn0004401 (Reim et al. 1999)
qkr58E-1	KHDRBS3	Unknown (KH domain, predicted RNA splicing)	FBgn0022986 (Lence et al. 2016)
qkr58E-2	KHDRBS1	Unknown (KH domain, predicted RNA processing)	FBgn0022985
qkr58E-3 (kep1)	KHDRBS1	Regulation of alternative splicing.	FBgn0022984 (Katzenberger et al. 2009)
Rcc1	RCC1	Regulator of chromosome condensation 1. RanGTPase, regulation of nucleocytoplasmic transport. Differentiation of lateral neurons. Regulation of mitotic spindle formation.	FBgn0002638 (Carazo-Salas et al. 1999, Shi and Skeath 2004)
Rin (Rasputin)	G3BP1	Localisation of mRNA to stress granules. Regulation of dorsal-ventral axis during oogenesis, presumably via the translational activation of orb mRNA. Context dependent m ⁶ A repelled RBP.	FBgn0015778(Costa et al. 2013, Edupuganti et al. 2017)
Rpl22	RPL22	Large ribosomal subunit	FBgn0015288
rump	hnRNPM	Regulation of splicing (exonic splicing enhancers), binds and localizes oskar and nanos mRNA. Regulation of anterior/posterior axis specification.	FBgn0267790 (Jain and Gavis 2008, Sinsimer et al. 2011)
Saf-B	SAFB	Scaffold attachment factor B. Regulation of splicing.	FBgn0039229 (Park et al. 2004)
Top2	TOP2A-B	DNA and RNA binding.	FBgn0284220 (Strick et al. 2000)

Supplemental data 2. Common protein interactors of writers and Ythdc1 reader.

List of protein interactors that were >1,5 fold enriched and identified with at least two of the baits: Mettl3/FI(2)d/Nito/Flacc and Ythdc1 (see also **Supplemental data 1**). Corresponding human orthologs and predicted functions are shown in columns on the right.

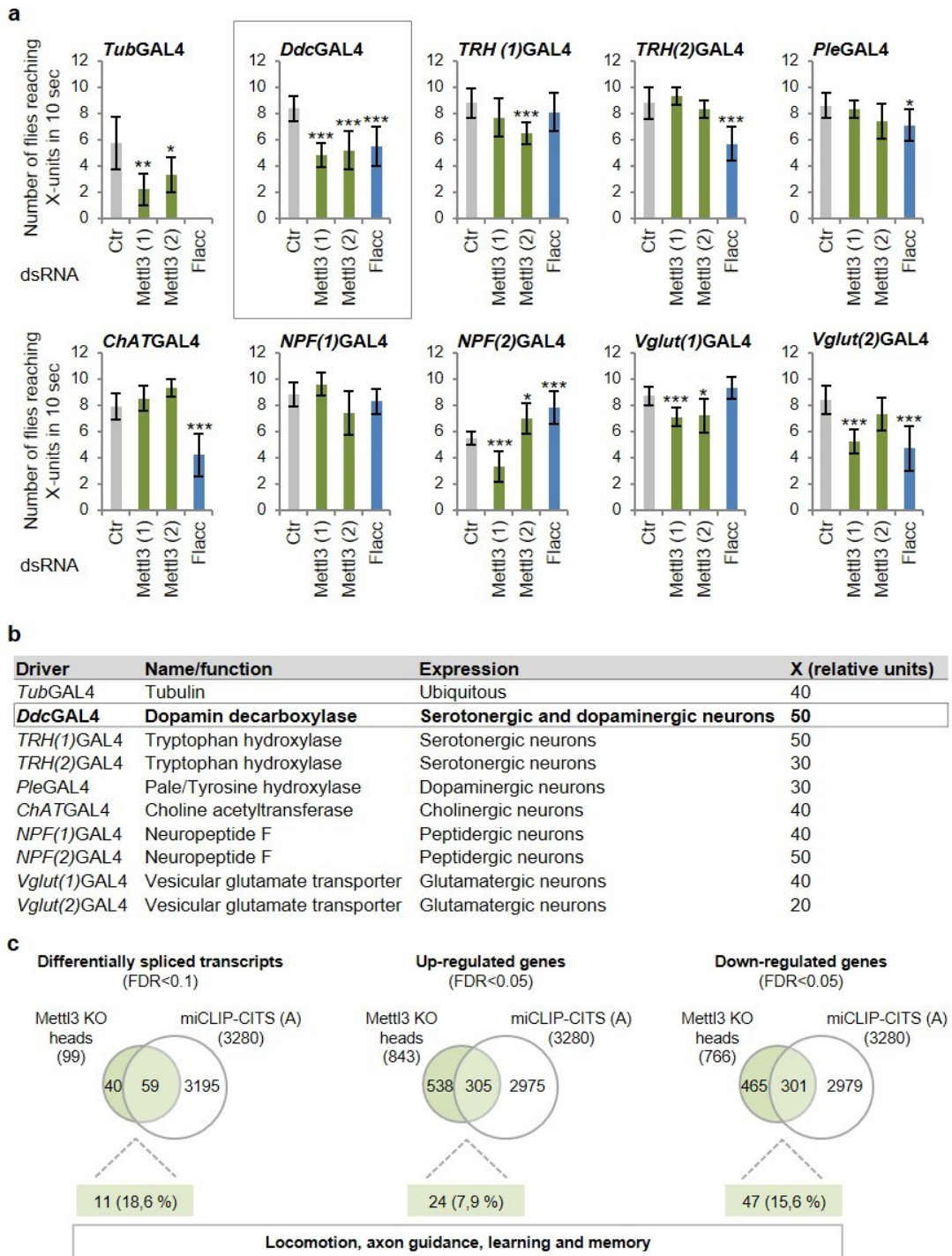
Supplemental data 3

Mis-regulated transcripts in <i>Mettl3</i> KO female heads with a miCLIP peak					
Locomotion			Axon guidance		
Gene			Gene		
18w	UP	18-wheeler, Toll-like receptor.	babo	DN	Receptor protein serine/threonine kinase
aop	DN	Ets DNA-binding protein pokkuri	brat	DN	Brain tumor protein
awd	UP	Nucleoside diphosphate kinase	Bsg	AS	Basigin
babo	DN	Receptor protein serine/threonine kinase	Cam	UP	Calmodulin
brat	DN	Brain tumor protein	Caps	DN	Capricious
Bsg	AS	Basigin	Cdc42	UP	Cdc42 homolog
Cam	UP	Calmodulin	chic	UP	Profilin
Caps	DN	Capricious	dlp	UP	Dally-like
CASK	DN	Peripheral plasma membrane protein CASK	dock	DN	Dreadlocks
Cdc42	UP	Cdc42 homolog	Dscam1	AS	Down syndrome cell adhesion molecule 1
chic	UP	Profilin	egh	DN	Beta-1,4-mannosyltransferase egh
csw	DN	Tyrosine-protein phosphatase corkscrew	eIF-2beta	UP	Eukaryotic translation initiation factor 2 subunit 2
disp	DN	Protein dispatched	fend	DN	Transmembrane protein fend
dlp	UP	Dally-like,	FER	DN	Tyrosine-protein kinase Fer
dock	DN	Dreadlocks,	ImpL2	DN	Neural/ectodermal development factor IMP-L2
dom	DN	Helicase domino	kis	DN	Kismet, isoform C
Dscam1	AS	Down syndrome cell adhesion molecule 1	Lar	DN	Tyrosine-protein phosphatase Lar
EcR	DN	Ecdysone receptor	Mical	DN	[F-actin]-methionine sulfoxide oxidase Mical
egh	DN	Beta-1,4-mannosyltransferase egh	mmps	DN	Protein mini spindles
eIF-2beta	UP	Eukaryotic translation initiation factor 2 subunit 2	PlexA	DN	Plexin A, isoform A
fend	DN	Transmembrane protein fend	pod1	DN	Coronin
FER	DN	Tyrosine-protein kinase Fer	Rac1	UP	Ras-related protein Rac1
gish	AS	Gilgamesh	Rho1	UP	Ras-like GTP-binding protein Rho1
hipk	DN	Homeodomain interacting protein kinase	sbb	AS	Scribbler, isoform J
ImpL2	DN	Neural/ectodermal development factor IMP-L2	Sema-1a	DN	Semaphorin-1A
Jafrac1	UP	Peroxiredoxin 1	sli	DN	Protein slit
kis	DN	Kismet, isoform C	sm	DN	Smooth, isoform T
Lar	DN	Tyrosine-protein phosphatase Lar	Smox	DN	Mothers against decapentaplegic homolog
mask	DN	Ankyrin repeat and KH domain-containing protein mask	trio	DN	Trio, isoform A
Mical	DN	[F-actin]-methionine sulfoxide oxidase Mical	unc-104	DN	Kinesin-like protein unc-104
mmps	DN	Protein mini spindles	wgn	UP	Tumor necrosis factor receptor superfamily member wengen
nonA	AS, DN	Protein no-on-transient A	Wnk	DN	Wnk kinase
norpA	DN	1-phosphatidylinositol 4,5-bisphosphate phosphodiesterase	Learning or memory		
nudE	UP	Nuclear distribution protein nudE homolog	Gene		
PlexA	DN	Plexin A	Adf1	AS	Transcription factor Adf-1
pod1	DN	Coronin	arm	DN	Armadillo segment polarity protein
qm	AS	Quemao	arr	DN	Arrow
Rab11	UP	Drab11	aru	DN	Arouser
Rac1	UP	Ras-related protein Rac1	be	UP	Ben
Rac2	UP	Ras-related protein Rac2	Cam	UP	Calcium/calmodulin-dependent protein kinase type II α -chain
Rala	UP	Ras-related protein Ral-a	CASK	DN	Peripheral plasma membrane protein CASK
Rho1	UP	Ras-like GTP-binding protein Rho1	CG18769	UP	Calcium uniporter protein, mitochondrial
sbb	AS	Scribbler	CrebB	AS	Cyclic AMP response element-binding protein B
Sema-1a	DN	Semaphorin-1A	eas	UP	Ethanolamine kinase
sesB	UP	ADP/ATP carrier protein	EcR	DN	Ecdysone receptor
sgl	UP	UDP-glucose 6-dehydrogenase	Fdh	UP	Alcohol dehydrogenase class-3
shep	DN	Protein alan shepard	futsch	DN	Microtubule-associated protein futsch
shi	AS	Dynamin	Gclm	DN	GH03051p
slgA	DN	Proline dehydrogenase 1, mitochondrial	gish	AS	Gilgamesh
sli	DN	Protein slit	kis	DN	Kismet
sm	DN	Smooth	Mob2	DN	MOB kinase activator-like 2
Smox	DN	Mothers against decapentaplegic homolog	Pka-C1	DN	cAMP-dependent protein kinase catalytic subunit
sqh	UP	Myosin regulatory light chain sqh	ps	AS	Presenilin homolog
stai	DN	Stathmin	Rac1	UP	Ras-related protein Rac1
Syn1	DN	IP02644p	Sap47	AS, DN	Synapse-associated protein of 47 kDa
trbd	DN	Ubiquitin thioesterase trabid	shi	AS	Dynamin
trio	DN	Trio	Syn1	DN	Synapsin
tsr	UP	Cofilin/actin-depolymerizing factor homolog	Tomosyn	DN	Tomosyn ortholog
unc-104	DN	Kinesin-like protein unc-104	wnd	DN	Mitogen-activated protein kinase kinase kinase
wgn	UP	Tumor necrosis factor receptor superfamily member wengen			
Wnk	DN	Wnk kinase			
yuri	UP	Yuri gagarin			

Supplemental data 3. Misregulated transcripts in *Mettl3* KO female heads with a predicted m⁶A methylation

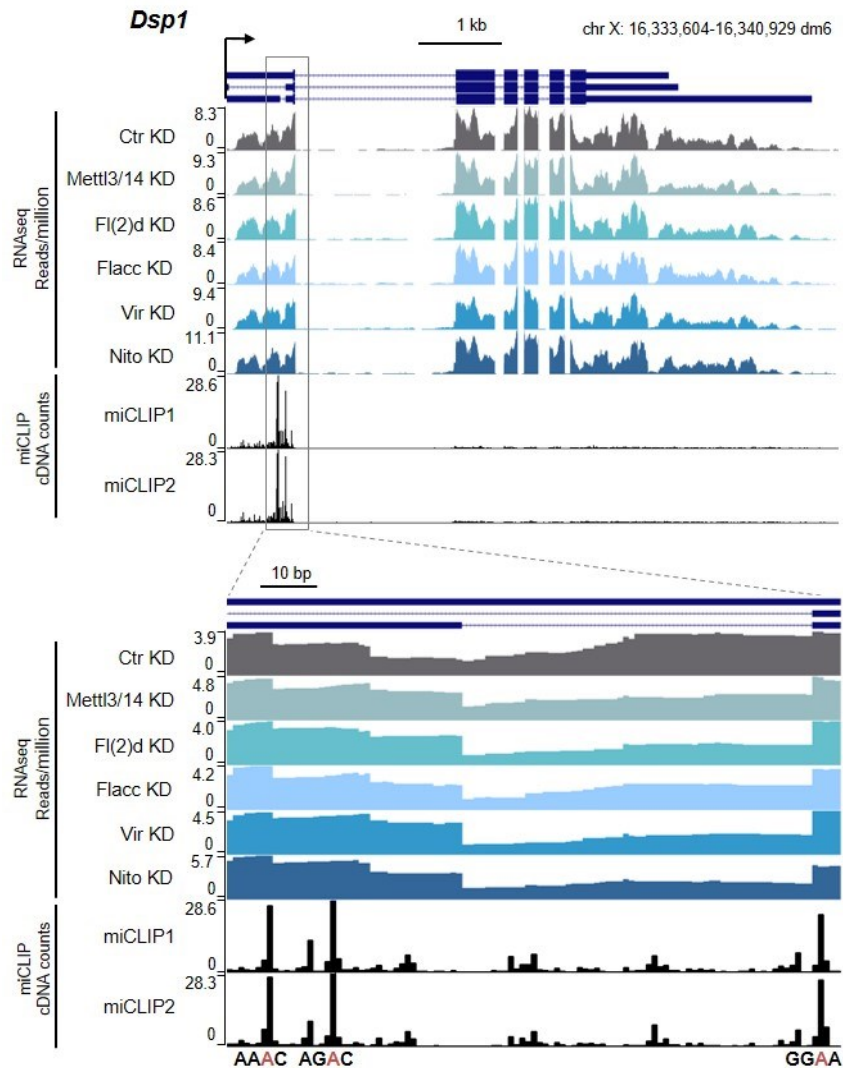
List of misregulated transcripts from *Mettl3* KO female heads that also have m⁶A methylation peak. (Inferred from miCLIP data from S2R+ cells based on truncation peaks (miCLIP-A)) and are involved in fly locomotion, axon guidance, or learning and memory formation, source: FlyBase. UP – up-regulated genes (FDR<0,05), DN – down-regulated genes (FDR<0,05), AS – alternatively spliced genes (FDR<0,1).

Supplemental data 4

**Supplemental data 4. Fly locomotion.**

a and b) Quantification of fly climbing by negative geotaxis experiment using flies depleted for Mettl3 or Flacc proteins. Bars represent the mean \pm s.d. of female flies ($n = 10$ per condition) that climb over X-units (see (b)) in 10 seconds (10 independent measurements). * $P < 0.01$; ** $P < 0.001$; *** $P < 0.0001$ (two sided Student's t-test, equal variances). **b)** Description of GAL4 drivers used for expression of *Mettl3* and *flacc* dsRNAs ubiquitously, or in specific neurons. **c)** Related to Supplemental data 3. Venn diagram displaying the overlap differentially spliced, up-regulated or down-regulated genes (in heads from *Mettl3 KO* flies) and genes that are m^6A modified in S2R+cells. Number of genes for each overlap that have a role in locomotion, axon guidance or learning and memory formation based on GO-terms analysis of biological process (FDR<0,05) is displayed below (Tyanova et al. 2016).

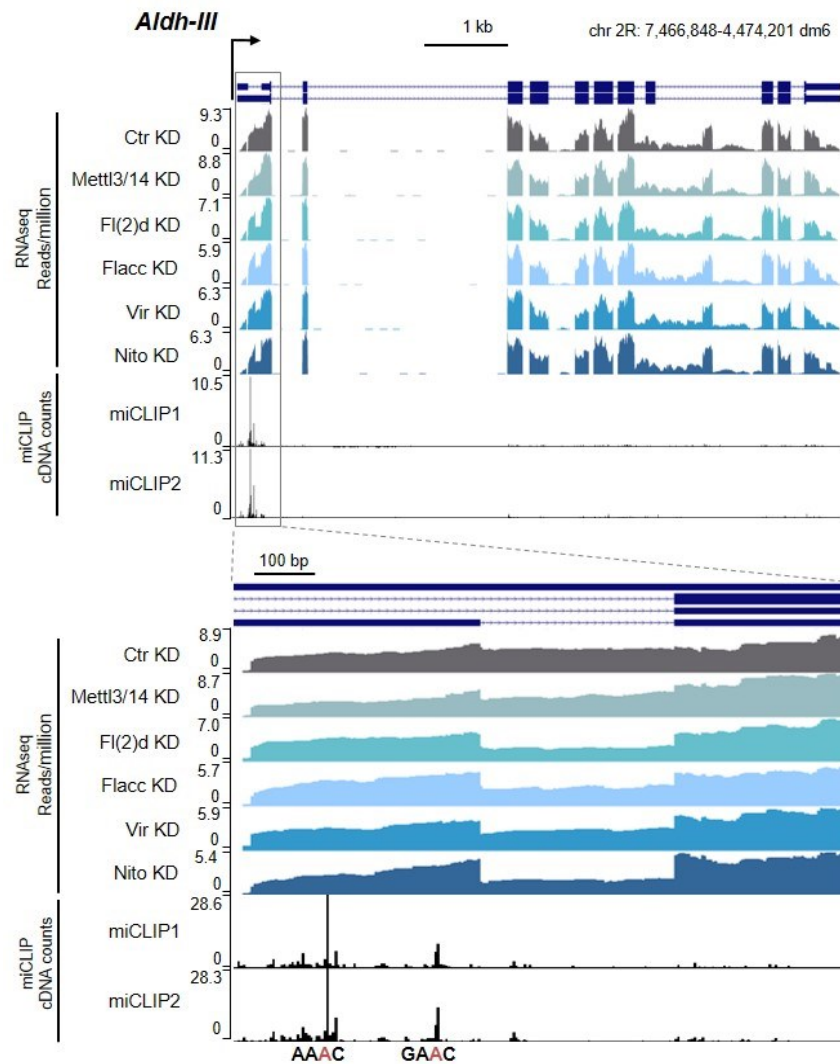
Supplemental data 5



Supplemental data 5. UCSC tracks showing splicing and methylation of *Dsp1* transcript.

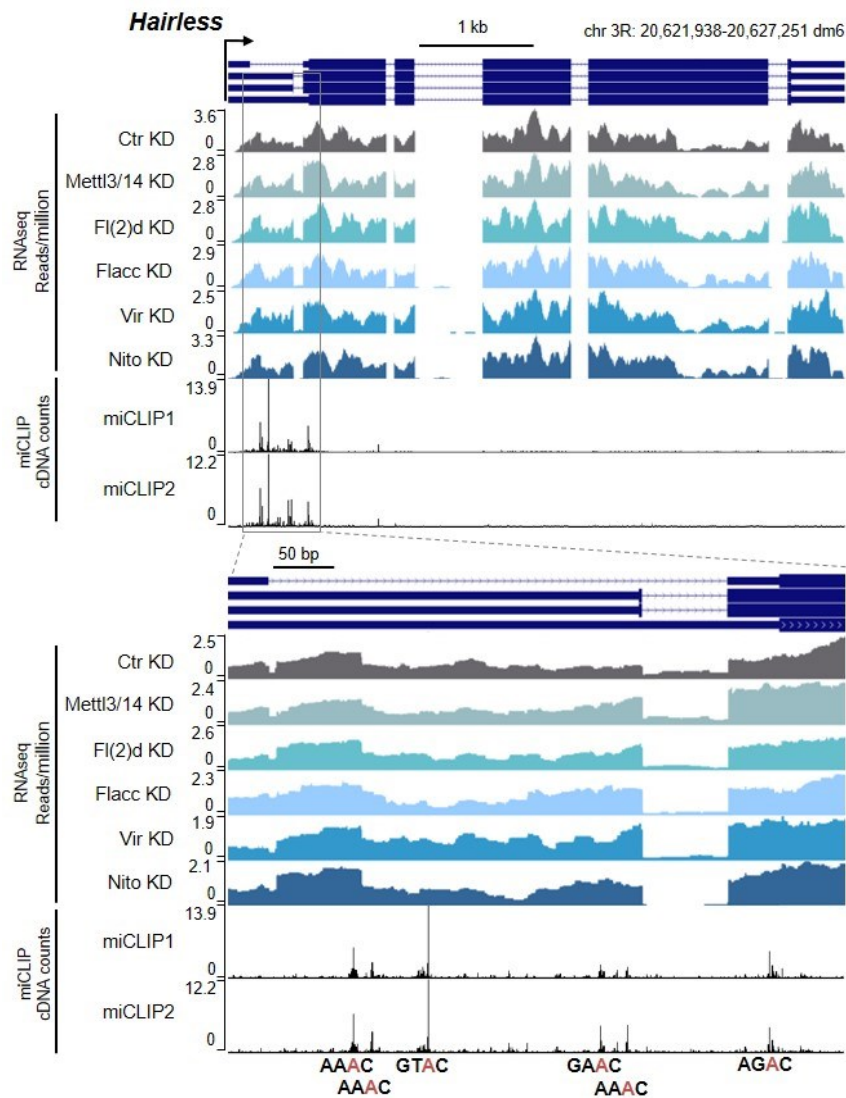
UCSC Genome Browser screenshots. Normalized RNA-seq data from control and indicated knockdown samples in S2R+ cells are shown. The miCLIP tracks showing cDNA counts of predicted m⁶A positions are shown below. Gene architecture of *Dsp1* is depicted above, with thin blue boxes representing the 5' and 3' UTRs, thick blue boxes representing the CDS, and thin lines representing introns. Zoom-in view of the selected region is shown below. Motifs of putative m⁶A methylation sites are listed below each miCLIP cDNA count peak signal. Adenosines predicted to be modified are labelled in red.

Supplemental data 6

Supplemental data 6. UCSC tracks showing splicing and methylation of *Aldh-III* transcript.

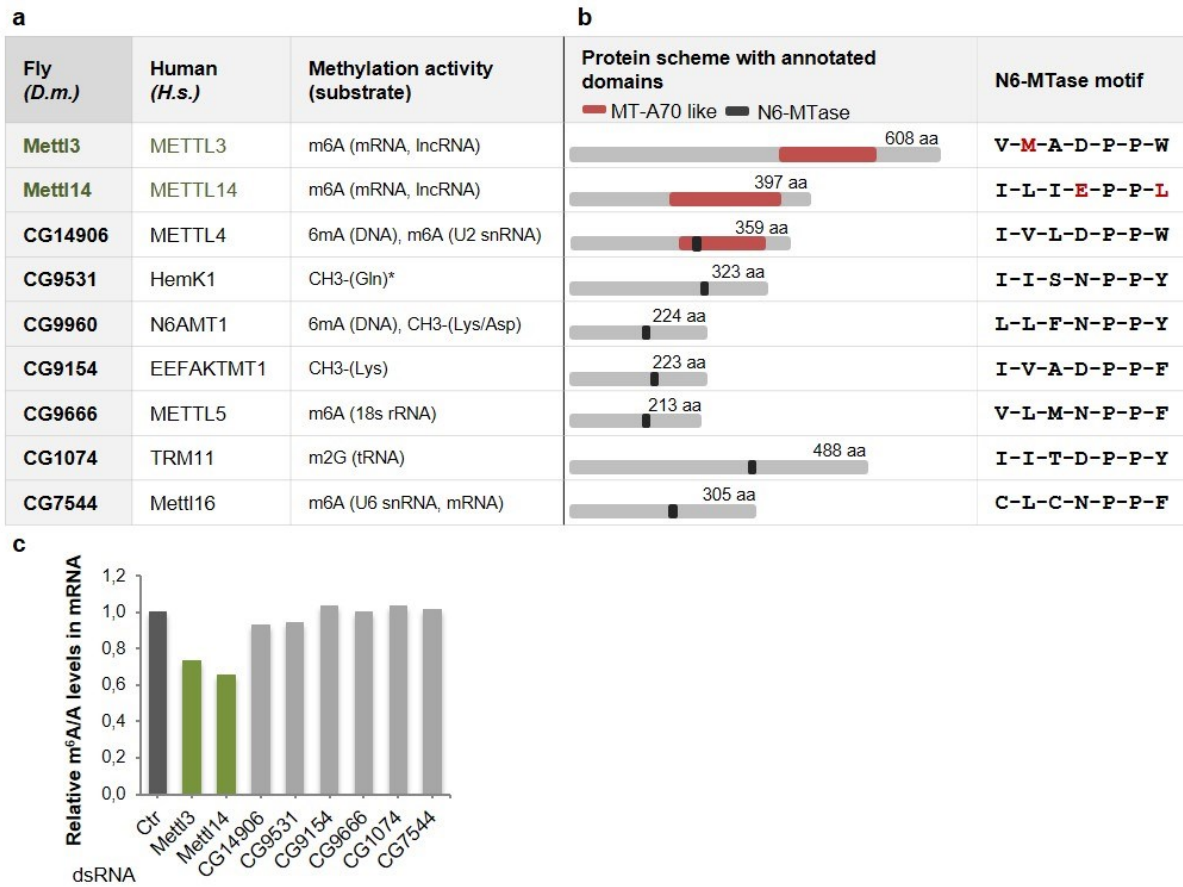
UCSC Genome Browser screenshots. Normalized RNA-seq data from control and indicated knockdown samples in S2R+ cells are shown. The miCLIP tracks showing cDNA counts of predicted m⁶A positions are shown below. Gene architecture of *Aldh-III* is depicted above, with thin blue boxes representing the 5' and 3' UTRs, thick blue boxes representing the CDS, and thin lines representing introns. Zoom-in view of the selected region is shown below. Motifs of putative m⁶A methylation sites are listed below each miCLIP cDNA count peak signal. Adenosines predicted to be modified are labelled in red

Supplemental data 7

**Supplemental data 7. UCSC tracks showing splicing and methylation of *Hairless* transcript.**

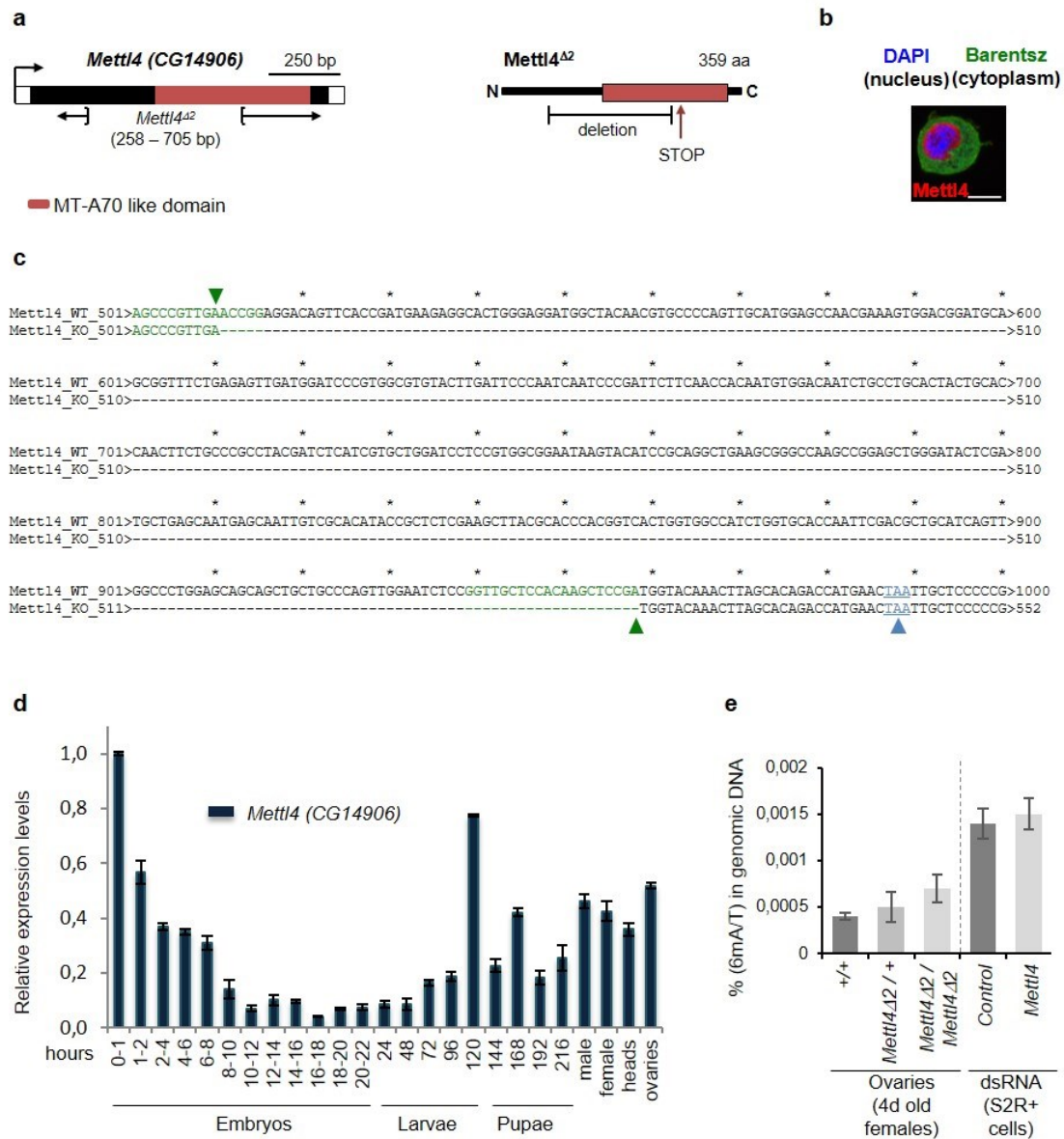
UCSC Genome Browser screenshots. Normalized RNA-seq data from control and indicated knockdown samples in S2R+ cells are shown. The miCLIP tracks showing cDNA counts of predicted m⁶A positions are shown below. Gene architecture of *Hairless* is depicted above, with thin blue boxes representing the 5' and 3' UTRs, thick blue boxes representing the CDS, and thin lines representing introns. Zoom-in view of the selected region is shown below. Motifs of putative m⁶A methylation sites are listed below each miCLIP cDNA count peak signal. Adenosines predicted to be modified are labelled in red.

Supplemental data 8

Supplemental data 8. Putative m⁶A mRNA methyltransferases.

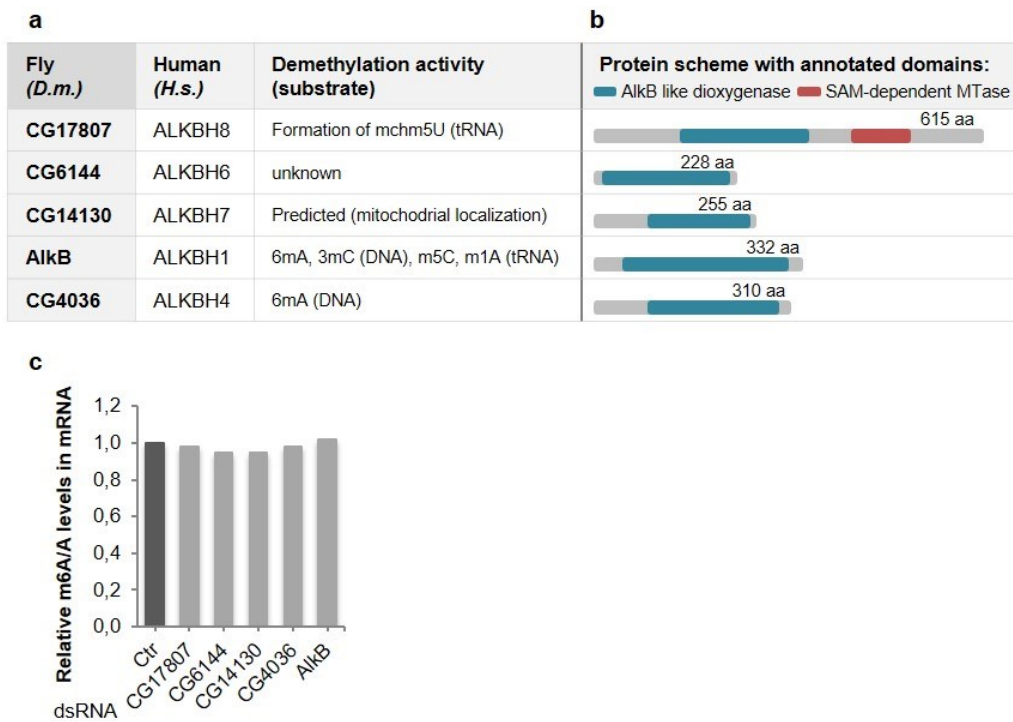
a) List of putative N6-methyltransferases in *Drosophila melanogaster* (*D.m.*), based on the presence of the N6-MTase motif: [LIVMAC]-[LIVFYWA]-{DYP}-[DN]-P-P-[FYW] (Prosites: PS00092) (Timinskas et al. 1995, Sigrist et al. 2013). Human (*H.s.*) orthologs and attributed methylation activities with targets are listed for each protein. * - predicted function based on its yeast ortholog (Polevoda et al. 2006). **b)** Schematics of each methyltransferase, with indicated protein size and the N6-MTase motif (in black). Proteins of the MT-A70 clade (Iyer et al. 2016) share high sequence similarity with the Mettl3 (also known as MT-A70) protein in their c-terminal region (MT-A70-like, in red). Exact amino acid residues of the N6-MTase motif are shown on the right. Degenerate N6-MTase motifs of Mettl3 and Mettl14 proteins contain amino acids that do not comply and are coloured in red. **c)** LC-MS/MS quantification of m⁶A levels in either control samples or mRNA extracts depleted for the indicated proteins in S2R+ cells. Only depletion of Mettl3 and Mettl14 proteins, but of no other candidates, reduces m⁶A levels on mRNA.

Supplemental data 9

Supplemental data 9. Description of *Mettl4* mutant allele

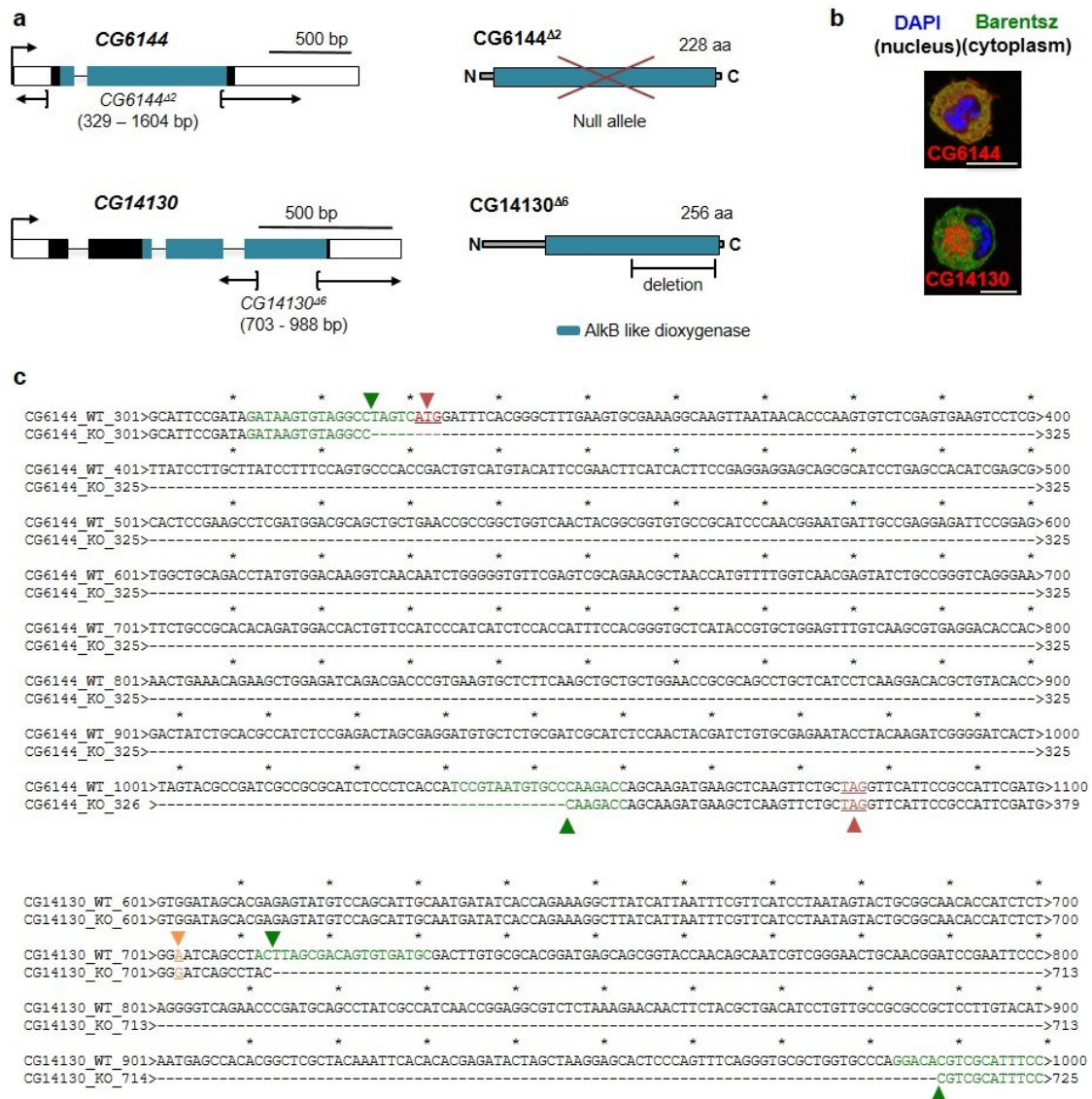
a) Schematic representation of genomic (left) and protein (right) region of generated mutant allele for putative m^6A mRNA methyltransferase CG14906 (*Mettl4*). The MT-A70-like domain is shown in red. Large deletion of *Mettl4Δ2* allele introduces a premature stop codon within the methyltransferase region. **b)** Immunostaining of HA-tagged *Mettl4* protein (in red) overexpressed in S2R+ cells. GFP-tagged Barentsz protein served as a cytoplasmic marker. DAPI staining is shown in blue. *Mettl4* localizes to the nucleus. Scale bars, 10 μ m. **c)** Alignment of wild type (*Mettl4_WT*) and mutant (*Mettl4_KO*) DNA alleles. Regions targeted by gRNAs are shown in green with arrowheads indicating beginning and end of deletion. Premature stop codon of *Mettl4_KO* is shown in blue. **d)** LC-MS/MS quantification of dm^6A levels in genomic DNA extracts from 4 days old female flies of indicated genotypes (left) or from S2R+ cells depleted for the indicated proteins. 6mA levels were not significantly different from controls.

Supplemental data 10

Supplemental data 10. Putative demethylases of m⁶A on mRNA.

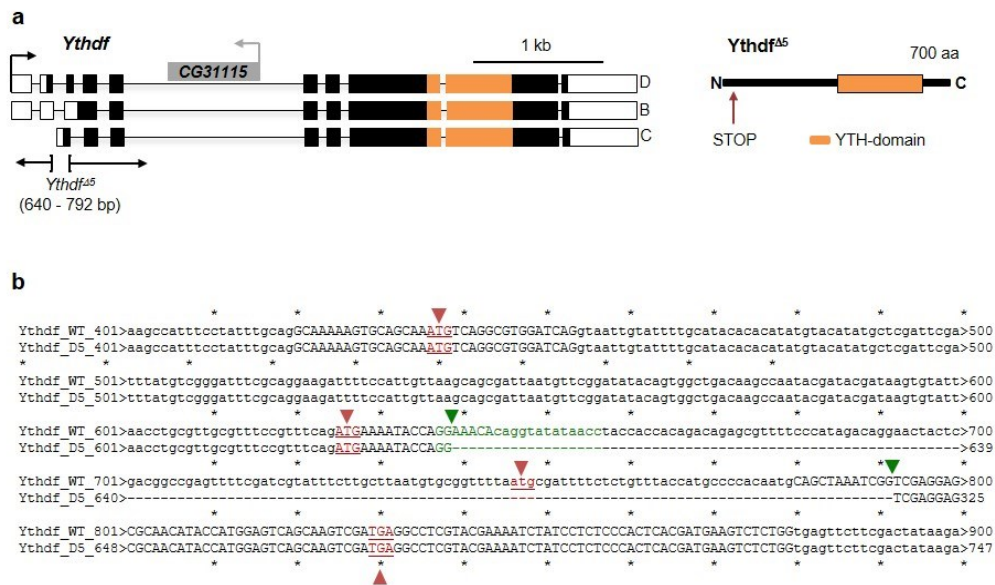
a) List of putative ALKBH-family demethylases in *Drosophila melanogaster* (*D.m.*), based on the presence of the AlkB-like dioxygenase region (InterPro: IPR037151). Human (*H.s.*) orthologs with described demethylation activities and their targets are listed for each protein (Fedele et al. 2015, Zhang G. et al. 2015, Alemu et al. 2016, Mitchell et al. 2019). **b)** Schematics of each demethylase, with indicated protein size and the AlkB-like region denoting an iron and α -ketoglutarate-dependent dioxygenase (in blue). CG17807 protein contains additional SAM-dependent methyltransferase type 11 domain (InterPro: IPR013216). **c)** LC-MS/MS quantification of m⁶A levels in mRNA extracts depleted for the indicated proteins in S2R+ cells. Depletion of neither candidate elevated m⁶A levels on mRNA.

Supplemental data 11

Supplemental data 11. Description of mutant alleles for putative m⁶A demethylases.





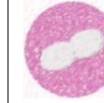
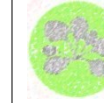

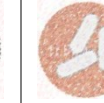
a) Schematic representation of genomic (left) and protein (right) loci of generated mutant alleles for putative m⁶A mRNA demethylases CG6144 (Alkbh6) and CG14130 (Alkbh7). The AlkB-like region is shown in blue. Large deletion of *CG6144Δ2* (null) allele removes complete coding sequence (top). Deletion of *CG14130Δ6* allele leads to truncation of the protein and removes a large part of the encoded C-terminal AlkB like region. **b)** Immunostaining of HA-tagged CG6144 and CG14130 proteins. CG6144 is ubiquitously expressed, while the CG14130 shows predicted mitochondrial localisation. Scale bars, 10 μm. **c)** Alignment of wild type (CG14130_WT, CG6144_WT) and mutant (CG14130_KO, CG6144_KO) alleles. Regions targeted by gRNAs are shown in green with arrowheads indicating beginning and end of deletion. Start and stop codons of CG6144_WT are labelled in red, and the mutation in CG14130_KO is depicted in orange.

Supplemental data 12

**Supplemental data 12. Description of mutant allele for Ythdf cytoplasmic reader.**

a) Schematic representation of genomic (left) and protein (right) loci of generated mutant alleles for Ythdf cytoplasmic reader. YTH domain is shown in orange. Three isoforms are depicted (D, B and C). Deletion in the 5' region of *Ythdf Δ 5* mutant allele introduces a premature stop codon to remove nearly complete CDS. A short (<11 aa) peptide can be translated. **b)** Alignment of wild type (*ythdf_WT*) and mutant (*Ythdf_Δ5*) alleles. One region targeted by gRNAs is shown in green with arrowheads indicating beginning and end of deletion. Start and premature stop codons are depicted in red and with arrowheads.




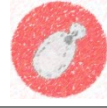


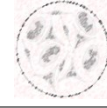

Supplemental data 13

Human	Flies	Nematodes	Fission yeast	Budding yeast	Plants	Diatoms	Bacteria	Targets
								
<i>Homo sapiens</i>	<i>Drosophila melanogaster</i>	<i>Caenorhabditis elegans</i>	<i>Schizo. pombe</i>	<i>Saccharomyces cerevisiae</i>	<i>Arabidopsis thaliana</i>	<i>Thalassiosira pseudonana</i>	<i>Escherichia coli</i>	Targets
METTL3	Mettl3	/	/	Ime4	MTA	/	/	mRNA ncRNA circRNA viral RNA (Zhong et al. 2008, Agarwala et al. 2012, Dominissini et al. 2012, Meyer et al. 2012, Schwartz et al. 2014b, Lichinchi G. et al. 2016, Zhou et al. 2017)
METTL14	Mettl14	/	/	Kar4	MTB	/	/	
WTAP	Fl(2)d	/	/	Mum2	Fip37	/	/	
VIRMA	Vir	/	/	/	Virilizer	/	/	
RBM15/15B	Nito	/	/	/	/	/	/	
ZC3H13	Flacc	/	/	/	/	/	/	
HAKAI	Hakai	/	/	/	Hakai	/	/	
/	/	/	/	Slz1	/	/	/	mRNA (Agarwala et al. 2012)
<i>Homo sapiens</i>	<i>Drosophila melanogaster</i>	<i>Caenorhabditis elegans</i>	<i>Schizo. pombe</i>	<i>Saccharomyces cerevisiae</i>	<i>Arabidopsis thaliana</i>	<i>Thalassiosira pseudonana</i>	<i>Escherichia coli</i>	Targets
METTL4	Mettl4 (CG14906)	Damt-1	C22G7.07c	/	F18O14.6	/	/	DNA, U2 snRNA (Gu et al. 2020) (Goh et al. 2020, unpublished data.)
METTL16	Mettl16 (CG7544)	METT-10	Mtl16	/	FIO1	THAPSDRAFT_11744	/	mRNA, U6 snRNA (Pendleton et al. 2017, Shima et al. 2017, Warda et al. 2017)
PCIF1	CG11399	/	/	/	/	THAPSDRAFT_20873, THAPSDRAFT_24679	/	mRNA, snRNA (m ⁶ Am) (Akichika et al. 2019, Boulias et al. 2019, Sendinc et al. 2019)
METTL5	Mettl5 (CG9666)	Mettl5 (C38D4.9)	/	/	/	THAPSDRAFT_36249	L11 MTase	18S rRNA (Van tran et al. 2019, Ignatova et al. 2020, Leismann et al. 2020)
TRMT112	Trmt112	C04H5.1	trm112	TRM112	TRM112A, TRM112B	THAPSDRAFT_36108, THAPSDRAFT_36539	/	
ZCCHC4	CG12863	F33A8.4	/	/	/	/	/	28S rRNA (Ma et al. 2019)
DIMT1	CG11837	E02H1.1	Dim1	Dim1	DIM1A	THAPSDRAFT_28300	KsgA	16S, 18S rRNA (m ⁶² A) (Lafontaine et al. 1994, O'farrell et al. 2004)
hMT10	/	/	/	/	/	/	RlmF	23S rRNA (Sergiev et al. 2008)
/	/	/	/	/	/	/	RlmJ	23S rRNA (Golovina et al. 2012)
/	/	/	/	/	/	/	Erm	23S rRNA (m ⁶ A or m ⁶² A) (Denoya and Dubnau 1987)

Supplemental data 13. Proteins required for methylation of N6-position of adenosine on diverse classes of RNA in representative organisms.

Components of MAC and MACOM complexes are shown on top, whereas other m⁶A methyltransferases are listed below. PCIF1 acts on Am and forms m⁶Am modification. DIMT1 adds m^{6,2}A instead of m⁶A and different bacterial Erm enzymes can form m⁶A or m^{6,2}A modifications. Figures were created based on templates from BioRender.

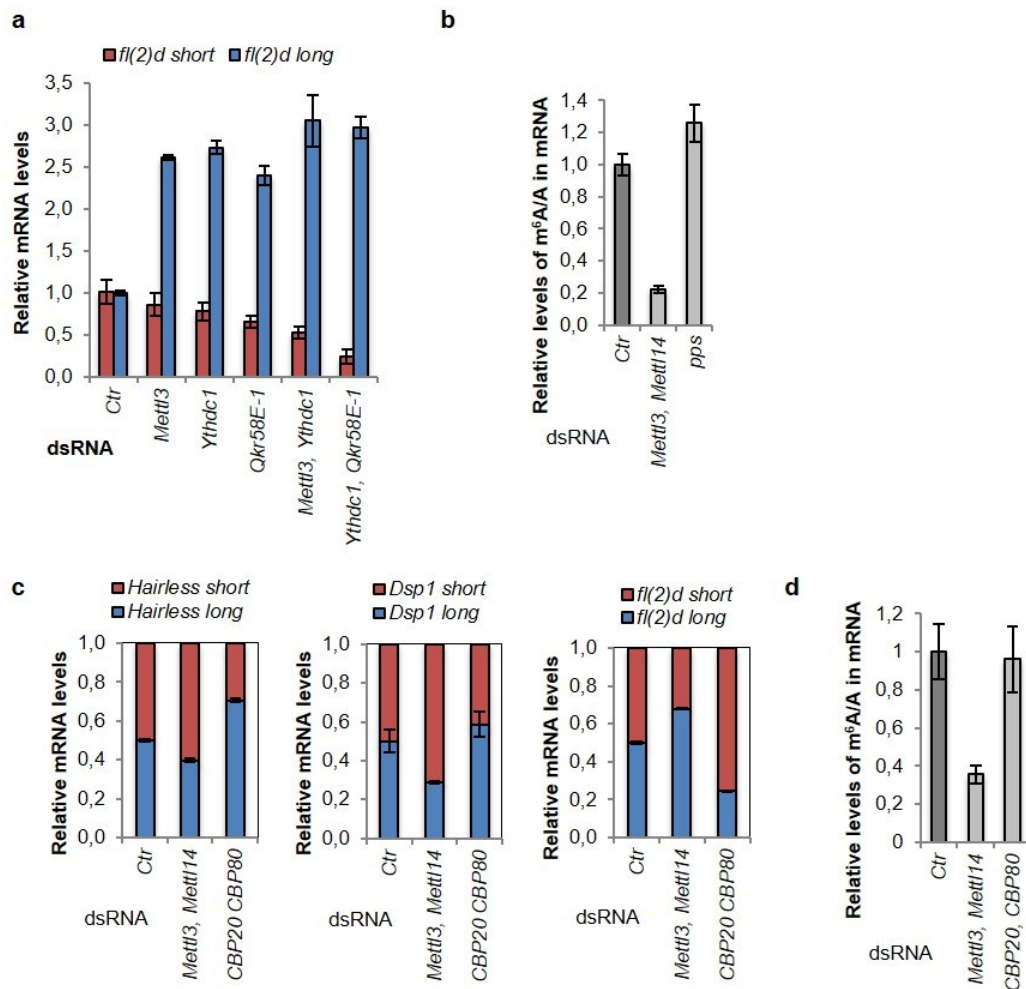
Supplemental data 14

	Human	Flies	Nematodes	Fission yeast	Budding yeast	Plants	Diatoms	Bacteria	
									
	<i>Homo sapiens</i>	<i>Drosophila melanogaster</i>	<i>Caenorhabditis elegans</i>	<i>Schizo. pombe</i>	<i>Saccharomyces cerevisiae</i>	<i>Arabidopsis thaliana</i>	<i>Thalassiosira pseudonana</i>	<i>Escherichia coli</i>	Targets
YTH domain readers	YTHDC1	Ythdc1	/	Mmi	/	ECT12, CPSF30	/	/	m ⁶ A (Xiao et al. 2016)
	YTHDC2	Bgcn*	F52B5.3*	/	/	AAB01660.1 *	/	/	m ⁶ A (Tanabe et al. 2016) (Bailey et al. 2017)
	YTHDF1, YTHDF2, YTHDF3	Ythdf	/	/	Pho92	ECT2, ECT3, ECT4, ECT5** to ECT11**	/	/	m ⁶ A (Dominissini et al. 2012)
Demethylases	ALKBH5	/	/	/	/	ALBH9B, ALKBH10B	/	/	m ⁶ A (mRNA, ncRNA) (Zheng et al. 2013, Duan et al. 2017)
	FTO	/	/	/	/	/	THAPSDRAFT_261481	/	m ⁶ A, m ⁶ Am (mRNA, ncRNA, snRNA) (Sanchez-Pulido and Andrade-Navarro 2007, Jia et al. 2011, Mauer et al. 2017, Mauer et al. 2019)
	ALKBH1	AlkB	alkb-1	Alkb homolog	/	alkB	/	AlkB	6mA (DNA) (Wu et al. 2016)
	ALKBH4	CG4036	nmad-1	/	/	/	/	/	6mA (DNA) (Kweon et al. 2019)
	ALKBH3	/	/	/	/	/	THAPSDRAFT_42543	/	m ⁶ A (tRNA) (Ueda et al. 2017)

Supplemental data 14. Proteins required for recognition and demethylation of N6-position of adenosine on RNA and DNA in representative organisms.

YTH domain-containing proteins are shown on top, whereas m⁶A or 6mA demethylases are listed below. * - *Drosophila melanogaster* Bgcn, *Caenorhabditis elegans* F52B5.3 and *Arabidopsis thaliana* AAB01660.1 are the closest orthologs of YTHDC2 protein, but lack the YTH domain. ** - m⁶A binding has not been confirmed yet. Figures were created based on templates from BioRender.

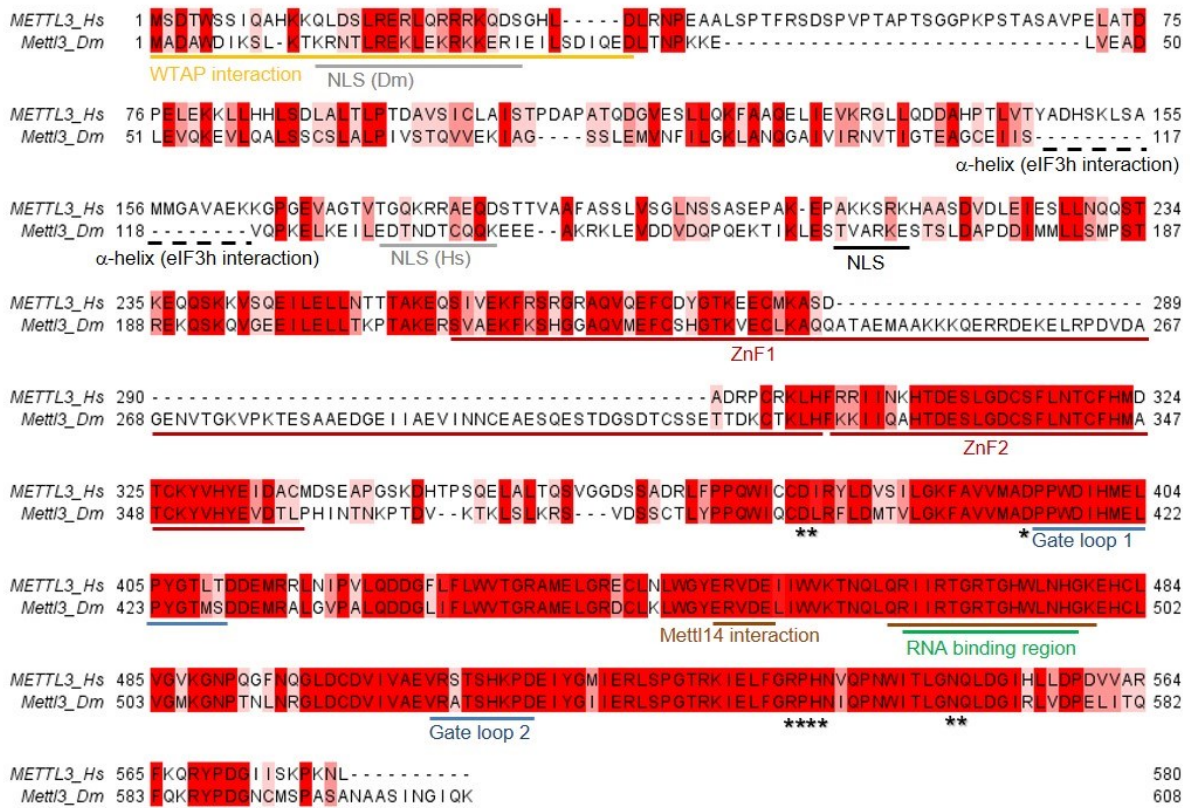
Supplemental data 15



Supplemental data 15. Functions of Ythdc1 interactors.

- a)** Splicing changes of *fl(2)d* transcript upon depletion of indicated proteins, alone or in different combinations. Combined depletion of Qkr58E-1 and Ythdc1 proteins has the strongest effect on transcript upregulation and differential isoform splicing.
- b)** Relative m⁶A levels on mRNA upon depletion of indicated proteins. Loss of *pps* has no effect on m⁶A levels.
- c)** Splicing changes of *Hairless*, *Dsp1* and *fl(2)d* transcript upon depletion of indicated proteins. Loss of CBP20-CBP80 proteins changes splicing of m⁶A-dependent transcripts in the opposite direction than the loss of m⁶A writer components Mettl3 and Mettl14.
- d)** Relative m⁶A levels on mRNA upon depletion of indicated proteins. Loss of CBP20 and CBP80 proteins has no effect on m⁶A levels.

Supplemental data 16



Supplemental data 16. Alignment of Mettl3-METTL3 proteins.

Alignment of Mettl3 protein sequences from *D. melanogaster* (Mettl3_Dm: Q9VCE6-1) and human (METTL3_Hs: Q86U44-1), with 43.4 % identity. Protein alignments were generated in Jalview 2.10.5 (Waterhouse et al. 2009) with ClustalO version 1.2.4 using default parameters (Larkin et al. 2007). Coloured by degree of amino acid conservation in each column with a 50 % cut off threshold. Underlined regions indicate: validated nuclear localization signal in METTL3 (NLS, black), ZnF1 and ZnF2 (red), Gate loop 1 and 2 (blue), interaction with Mettl14 (brown), WTAP (yellow) and RNA (green). Stars(*) denote SAM-binding residues (Sledz and Jinek 2016, Wang P. et al. 2016, Wang X. et al. 2016). Interrupted underlined regions indicate predicted α-helix required for a direct interaction with eIF3h protein (Choe et al. 2018). Predicted NLS are shown in grey with indications for fly (*Dm*) and human (*Hs*) proteins (Obtained by cNLS Mapper (Kosugi et al. 2009)).

Supplemental data 17

<i>METTL14_Hs</i>	1	MDSRLQEIRERQKLRRLAQQLGAEASDSGAVLNSKDEQREIAETRETCRASDYDTSAPNAKIKYLDEIETDED	75
<i>Mettl14_Dm</i>	1	SDVKKSSQERSRKRRLLAGTLLSSVDDKKAIGNAEDINS-----S ^{grey} QLNSG ^{grey} QREEE	56
		NLS (Dm) NLS (Hs)	
<i>METTL14_Hs</i>	76	KMEEYKDELEMQQDEENLPYEIEIKDSS ^{grey} TFLKGTQSLNPHNDYCOHFVDTQHRPQNFIRDVGLADRFE ^{grey} EYPKLR	150
<i>Mettl14_Dm</i>	57	-----DGGASSSKKTPNEIIRDSS ^{grey} TFLKGTQSLNPHNDYCOHFVDTQHRPQNFIRDVGLADRFE ^{grey} EYPKLR	122
		H3K36me3 binding	
<i>METTL14_Hs</i>	151	ELIRLKDELTAKSNTPMYLQADIEAFDIREITPKFDVILLEPPLEEYFETGIT-----ANEKCHTWDDIMKLE	220
<i>Mettl14_Dm</i>	123	ELIKLKKLIDQTASAPMYLQADIKSLQVKTGAKFDVILLEPPLEEVARAAPSVATVGGAPRVFVNWDDILNLD	197
		H3K36me3 binding	
<i>METTL14_Hs</i>	221	IDETAAPRSFIFLWCGSGEGLDLQVCLRWGYRRCEDICWIKTKNINFGKTTLDPKAVFORTKEHCLMGIKGT	295
<i>Mettl14_Dm</i>	198	VGEIAAHRSFVFLWCGSSEGLDMGRNCLK ^{grey} WGFRRCEDICWIRTNINKFGHSIQLEPKAVFORTKEHCLMGIKGT	272
		RNA binding region Mettl3 interaction	
<i>METTL14_Hs</i>	296	KRSTDGD ^{grey} FIHANVDIDLITTEEP ^{grey} IGNIEKPV ^{grey} EIFHI ^{grey} IEHFCLGRRRLHLFGRDSTIRPGWLV ^{grey} VGPTLTNSNY	370
<i>Mettl14_Dm</i>	273	RRSTDGD ^{grey} FIHANVDIDLISEE ^{grey} IFGSF ^{grey} EKPI ^{grey} EIFHI ^{grey} IEHFCLGRRRLHLFGRDSSIRPGWLV ^{grey} VGPELTNSNF	347
		RNA binding region	
<i>METTL14_Hs</i>	371	AE ^{grey} T ^{grey} AS ^{grey} YS ^{grey} APNSYL ^{grey} TC ^{grey} TEE ^{grey} IER ^{grey} LRPKS ^{grey} PPP ^{grey} K ^{grey} SDRGG ^{grey} - -APRGG ^{grey} RRGGTSAGRGRERNRSNFRGERGGFRG	443
<i>Mettl14_Dm</i>	348	SEL ^{grey} L ^{grey} QTY ^{grey} IAEA ^{grey} - -PATGC ^{grey} ISR ^{grey} IEL ^{grey} LRPKS ^{grey} PPP ^{grey} NS ^{grey} VLRGR ^{grey} RGF ^{grey} RR ^{grey} RR ^{grey} PR ^{grey} -----	397
		RNA binding region	
<i>METTL14_Hs</i>	444	GRGGAHRGGFPPR	456
<i>Mettl14_Dm</i>		-----	

Supplemental data 17. Alignment of Mettl14-METTL14 proteins.

Alignment of Mettl14 protein sequences from *Drosophila melanogaster* (Mettl14_Dm: Q9VLP7-1) and human (Mettl14_Hs: Q9HCE5-1), with 55.5 % identity. Protein alignments were generated in Jalview 2.10.5 (Waterhouse et al. 2009) with ClustalO version 1.2.4 using default setting (Larkin et al. 2007). Coloured by degree of amino acid conservation in each column with a 50 % cut off threshold. Underlined regions indicate interaction with H3K36me3 (blue), Mettl3 (brown) and RNA (green) (Sledz and Jinek 2016, Wang P. et al. 2016, Wang X. et al. 2016, Huang et al. 2019). Predicted NLS are shown in grey with indications for fly (*Dm*) and human (*Hs*) proteins (Obtained by cNLS Mapper (Kosugi et al. 2009)).

Supplemental data 18

```

WTAP_Hs 1 -----MTNEEP L P K K V R L S E T D F K 19
F(2)d_Dm 1 MSVAAMTMDQRP CMNSYDKMPP TKYEQNLN I LNSSQNSGATGGPASP T P S G L E D H H H H H H P H P H H H H H H Q E Q Q Q Q 75
                                                NLS (Hs)

WTAP_Hs 20 V M A R D E L I L R W K - - - - Q Y - E A Y V Q - - A L E G K Y T D L N S N D V T G L R E S E E K L K Q Q Q E S A R R E N I L V M R L A T K E Q E M 87
F(2)d_Dm 76 Q Q Q Q Q H L Q Q Q Q Q Q Q Q Q H A A A V A E A V A A E Q R Q R L L E D E I E N L K L E Q V R M A Q Q C A D A Q R R E K I L M R R L A N K E Q E F 150
                                                *

WTAP_Hs 88 Q E C T T Q I Q Y L K Q V Q Q P S V A Q L R S T M V D P A I N L F F L K M K G E L E Q T K D K L E Q A Q N E L S A W K F T P D S Q T G K K L M A K C R 162
F(2)d_Dm 151 Q Q Y V S Q I A E Y K A Q Q A P T A L A L R T A L L D P A V N L L F E R L K K E L K A T K A K L E E T Q N E L S A W K F T P D S N T G K R L M A K C R 225
                                                *

WTAP_Hs 163 M L I Q E N Q E L G R Q L S Q G R I A Q L E A E L A L Q K K Y S E E L K S S Q D E L N D F I I Q L D E E V E G M Q S T I L V L Q Q L K E T R Q Q L A 237
F(2)d_Dm 226 L L Y Q E N E E L G K M T S N G R L A K L E T E L A M Q K S F S E E V K K S Q S E L D D F L Q E L D E D V E G M Q S T I L F L Q Q E L K T R D R I Q 300
                                                * *
                                                Coiled-coil region

WTAP_Hs 238 Q Y Q Q Q Q S Q A S A P S T S R T T A S - - - - - E P V E Q S E A T S K D C S R L T N G P S N G S S S R Q R T S G S G F H R E G N T T E D D F 303
F(2)d_Dm 301 T L E K E N A Q L K Q A I K D E V V A P A A T N G G T N T T I N K L E T I H E D - A C M A N N P T N P D C Y - - - - - N G N T N N E Q I 363

WTAP_Hs 304 - - - P S S P G N G N K S S - N S S E E R T G R G G S G Y V N Q L - S A G Y E S V D S P T G S E N S L T H Q - - - - - 352
F(2)d_Dm 364 A A V P Q I P L S D D G S N M N G N A A R L A R K - R N Y Q E E E A L P T V V V V P T P T P V G N N V Q E A P P I R E V T A P R T L P P K K S K L R G 437

WTAP_Hs 353 - - - - - S N D T D S S H D P Q E - - - - - E K A V S G K G N R T V G - - - S - - - - - R H V Q N G L D S S V N V Q G - - - - - 393
F(2)d_Dm 438 I T T R R N S Q L E E D H P F V T T P V A V P M I V D N A V A G M A S E E A A A A A A V N N S N T G I I P E T G V Q V G V P V E G G D P G A P A A P 512

WTAP_Hs 394 - S V L - - - - - 396
F(2)d_Dm 513 G R I L T R R R S V R M Q Q N G S G A V D Y S T 536

```

Supplemental data 18. Alignment of Fl(2)d-WTAP proteins.

Alignment of Fl(2)d protein sequences from *Drosophila melanogaster* (Fl(2)d_Dm: Q9Y091-1) and human (WTAP_Hs: Q15007-1), with 26.4 % identity. Protein alignments were generated in Jalview 2.10.5 (Waterhouse et al. 2009) with ClustalO version 1.2.4 using default settings (Larkin et al. 2007). Coloured by degree of amino acid conservation in each column with a 50 % cut off threshold. Stars (*) denote ubiquitination sites in Fl(2)d that were identified in this study. Underlined regions indicate coiled-coil regions (blue) predicted by program COILS (Lupas et al. 1991). Predicted NLS are shown in grey with indications for fly (*Dm*) and human (*Hs*) proteins (Obtained by cNLS Mapper (Kosugi et al. 2009)).

Supplemental data 19

<i>VIRMA_Hs</i>	1	MADSDSMEELLFLDTFKIPSAEQSSHIDVIRFCVYVINEYRVIFPCVRAHSSLIDNRAYEETSHTFQDLFFIN	75
<i>Vir_Dm</i>	1	MADYDDSEELLFDTFSHEEVT-DINLDLYQEFKPFITQVRIIPLCARVQADFVGGVRLIATNSKIDLEFFVND	75
<i>VIRMA_Hs</i>	76	VSKFSAPVFDRLQSLDEDETSIIIFR-PNSKVNFDGLVLRGWYNCLTLAIYGSVDRVISHDRDSPPPPPPPPQ	150
<i>Vir_Dm</i>	76	LGMFAASAENLGLRINQDCIHLDCSQEIVFDGLVLRGWYSTITLAIYGIFTNSVTEPIASHTLCEIVGPEI	151
<i>VIRMA_Hs</i>	151	PPPSL----KR-----NFKH-----ADKEKEDQFNGSPPR-----PQPRGPRTPPG	187
<i>Vir_Dm</i>	152	ANLAGEVLLQEDVVKDEWQEMQAEELLTAHKGNSVDYDPEDMEYMSRHYHQHAAEQEQREMRRLRRSTHSIDHS	227
<i>VIRMA_Hs</i>	188	PPPPDDED-----DPVPVPSGDKKEDAPHR-EDYFEPISPD-----RNSVPOVGGQYSDEGEVEEQQEEGEDE	252
<i>Vir_Dm</i>	228	PPPPRRSHTHSESNREYVRCRDKGSRDWSRSEPESSHRSRKRSESRSVVDLHKVPRTPPASIDSP-PTRPRSP	302
<i>VIRMA_Hs</i>	253	DDVVEEEEDDEDRRTVDSIP----SEEEEDSEEEGEDEEGEGDDGYEQSSDEDGADLRETF----KYP	319
<i>Vir_Dm</i>	303	ITMAYED---ESRSHYKMQSHYRHSSLSLRGERDRDDEDRSCTPQEQFEPVLSODEIIGDDIEDDAVDAAAAIA	375
		Y307 phospho site	
<i>VIRMA_Hs</i>	320	NFDVVEYTAEDLSVPMFTYDPYDRELVPLLYFSOPYKTTREIEISRMVDQGPDKENSGAIEASVKLTLLDLYRED	395
<i>Vir_Dm</i>	376	EYERELE--AAAAAAPAIDAFEPWQKPLLVFEGDMAAHRCKELETLLLFKLVL-----QTRCENVNFAFSE	442
<i>VIRMA_Hs</i>	396	RSKQWTA--LEEPSLIKGLSYLQLKNTKQ-----DSGLVDWTMQLNLLVALR-QPIILNVFQL	456
<i>Vir_Dm</i>	443	HGASVDEREQFVYVGEQNNQGLAQAHYKRRNFVLQQFFGNDELHRLAANVLQIALSFAACMQPQPFKIRHI	518
<i>VIRMA_Hs</i>	457	AATKLVSSLAECGA--IGVTGLLQAGVISGLLELFDADHYSSSLKLNAFKALDSVISMTEGMEALRGRQNEKS	530
<i>Vir_Dm</i>	519	PLARMAELLSSEELFHLLKEHKFDIFEAVRILYHEPYMALSIKLLQLLAVYALLDTRMGIHEMGAK---NNS	591
<i>VIRMA_Hs</i>	531	YKLLLELLLDQTVRVVTGSAIILQVCFYEVSEIKRLGDHIAEKTSSLPNHSEPDDHDAGLERTNPEYENEVE	606
<i>Vir_Dm</i>	592	YQMIVEAKTAKLTBTKYALQAIIKLLLWEGESVQIWGRRFVDRIIIPGNRDQMEDTVITCQQIE-----FA	661
<i>VIRMA_Hs</i>	607	ASIDMDLSESSNTSEGEIEFLINLLEEVIHLMETAPHTMIQQPVKSFPTMARIIGFPERDDPYPVIFRYLHSHHF	682
<i>Vir_Dm</i>	662	FELMDALFSSQLSYLQPRFPLVSK-KIE-----VVDFDTAQRSFGNAIQSYLQGNSLA	715
<i>VIRMA_Hs</i>	683	ELVTLLELISIPVTSAHPGVLQATKIVLKFIAQSQKGLLFIMSEYEA-TNLIIRALCHFY-----DQ-----	741
<i>Vir_Dm</i>	716	ESLLVMAN-CKELPATTYLSMLQLMHTILRSHVYIDYVDDAFVVTQTVAIILGLDEVPRNPEEKKEKAEKSDA	790
<i>VIRMA_Hs</i>	742	-----DEEEQLQSDVVD--AFALW-----LQDSTQT-----QCIT-ELF	775
<i>Vir_Dm</i>	791	EDKAMEVENEAVEAGGKPTPPTADEEQKPAAPISVPAPAAAPQVRPRPILRPVLPRLARLGIEMSYKQTRYHL	866
<i>VIRMA_Hs</i>	776	SHFQRCTSEETIHSDLGTLNLYLIIFNVVGRSAVGHVFSLEKNLQSLITLMEYYSKALGDSK-----SKKSV	846
<i>Vir_Dm</i>	867	DAIAYAAAPAYAVKLAATHMHAIVSQVCDPAGHQHTVEILGNNNLKIFMDLIKKEQRLQTQRLLSSPGTKYKSP	942
<i>VIRMA_Hs</i>	847	AYNTACILLVVYQSSSDVQMLEQHAASLLKLCADEN-----NAKLOELGKWLEPLKNLRF-EINCPNIIYVK	916
<i>Vir_Dm</i>	943	VLSYAVDMVDACRYCEQLDYIEHGGVILEALNHETFEPSVSVLVQEMVYMKPLEAINVFVYDDIMPVVEVIG	1018

Alignment of Vir-VIRMA proteins (part1/2).

Description on next page.

Supplemental data

```

VIRMA_Hs 917 QNIDNLMPEVGGTTALRVLCNVACPPPVVE-----QQKDLWNLAVTQLFSREGMDTFIRVLOKLNLSILTDHW 987
Vir_Dm 1019 RSLDYLTTFPG-DIMAMRILRYLSIS-KLAPQKAPPVTEELHRFVALQLYADGVQLCQIMERLCAYFEQFG 1092

VIRMA_Hs 988 RLHVNMGTTLHRVTTISMARCT-----ETLLKTMTELRRGGSFEFKDMRVPSAEVTLHMLLCSIFLSGRLDSE 1057
Vir_Dm 1093 AHAPA-----LMTIQGVHCCQIMLPTQIIRRELSYALCRDGTYSKDLTAIDHLELVKVVYLYYFTRCQAGPEV 1161

VIRMA_Hs 1058 QKIQNDIIDILLTFTQGVNEKLTISEETANNTNSLMLKEVLSSILKVEGFFSGLILSELLPLPLMQTTQV-- 1131
Vir_Dm 1162 EQCKMEVVQTLAYTCPN---EQDEESLHKSLWTMIREVLKNV-DGFAHFIPBLKLAELLPLPLMPQPLCDQ 1232

VIRMA_Hs 1132 IEPHDISVALNTRKPLWSMHLHVAKLQEVRSFSGTTCQPIQHMLRRIIVQLCDLASPITALLMRTVLDLIVEDL 1207
Vir_Dm 1233 LQQQHKQRLITERKLSAHLHPISGQIAKLEALAPSSFPQLSELLQRYMQLSDLAPNMTLLAKTITELLCNEY 1308
M1283K (vir 2f)

VIRMA_Hs 1208 CSTSEDKEKQYTSQTTRLALLDALASHKACKLAILHLINGTIKGDERYAEITFDLAVRSPGDSVIRQOCVEY 1283
Vir_Dm 1309 TSNICIPT---TNLERLRFSTRCAFAPLSSMSILS-----GKFWELFQSLAINEF---NDVSNLQEA 1371

VIRMA_Hs 1284 TSLQSLCQDDIALPLPSSEGSISELEQLSNSLPNKEIMTSCDCLLATLANSISSYNCLLTCVRTMMFIAEHQY 1359
Vir_Dm 1372 HRLDSFLDSGSLSHKSTA--SPALNIAAALPPELIPRIIDAVFSNLSVIVTHGISLAVRNLVIITEHDF 1444

VIRMA_Hs 1360 GLFHLKSSIRKNSALHSLLKRVVSTFSKDT-GELASFEFEMQILNSDTIGCCGDDNGLMEVEGAHTSRTMSIN 1434
Vir_Dm 1445 TFYHLAQLKQKI TEFQAWMEVILHNETVEYNAI ESLILLLSLITQIEPP-----PAMSAHPHRTLKG 1510

VIRMA_Hs 1435 AAEKQLQSKES-----PENLFLLEKLVLEHSKDDNLSLLDSVVGKQMLESSQD 1489
Vir_Dm 1511 ATELAQVVEFQDI ELAKPPVLSRILTVMEKHKAVANAALSDEKQIILQASKQELIAGT-----STETPPAEAE 1581

VIRMA_Hs 1490 PLIL-----SDQDVEPVISAPESIQNLFNNTAYVL---ADVMDQKLSMIFTFQASEIDTDL---DLVKVDLI 1553
Vir_Dm 1582 ANSASSCSASLTVEYIPQAGIVTQYEAPIETRFCAENAQAQLTARYLDELPIELLEDMNEPIYERACDIT 1657
E1426K (vir ts)

VIRMA_Hs 1554 EISEKCCSDFDLH--SELESFLSEPSRGR---KKTGKFKLGGKHKHTFITSSGKSEYIEAKRAHVPPPRG 1623
Vir_Dm 1658 DIANVILN-PDINVAGDSKRV-MNLSGRQSNREMPTAPCFRRRVEVPA---TGR-----E-KKMFSS--V 1720

VIRMA_Hs 1624 RGRGFGFGQIRPHSIFRQKQNTSRPPSMHYDDFVAESKEVVDQGIPPPRLKVSQKISSRGGFS-GNRGGG 1698
Vir_Dm 1721 RGRGFARPPSRGDLFRSEPPNTRSRPPLHYDDFLALETCGAQITGPTGYNISML-----RQSRVGRNRGSI 1790

VIRMA_Hs 1699 ---AFHSINRFFTPPASKGNYSRREGTRGSSSAQNTPRNINNESRGGQINFNRPGLPPLRPLSSTGVRPSFRDRA 1771
Vir_Dm 1791 SAAAFRKKMM-----RI-GSPSSWAESP---GSYRSASD--SHSSSD---SHYSAPHISGRFRGRG 1845

VIRMA_Hs 1772 SFGGGLGFSWASANSVGGSGSRGKFSVGGSGRGRHVSFTR 1812
Vir_Dm 1846 LSS-----PSYLR----- 1854

```

Supplemental data 19. Alignment of Vir-VIRMA proteins (part2/2).

Alignment of Vir protein sequences from *Drosophila melanogaster* (Vir_Dm: Q9W1R5-1) and human (VIRMA_Hs: Q69YN4-1), with 22.2 % identity. Protein alignments were generated in Jalview 2.10.5 (Waterhouse et al. 2009) with ClustalO version1.2.4 using default settings (Larkin et al. 2007). Coloured by degree of amino acid conservation in each column with a 50 % cut off threshold. Vir contains a putative phosphorylation site Y307 within a DYEDD sequence context (Zhai et al. 2008). Two *vir* mutations (*vir 2f* M1283K and *vir ts* E1426K) are indicated with a star (Niessen et al. 2001).

Supplemental data 20

<i>RBM15_Hs</i>	1	MRTAGRDPVPRRSPRWRAVPLCETSAGRRVTQLRGDDLRRPATMKGKERSPVKAKRSRGGEDSTSRGERSK	75
<i>Nito_Dm</i>	1	-----MSSHRDGAGADRIT I-----KIH	18
<i>RBM15_Hs</i>	76	GSGGNSGSSGKTDSSGSRRLHLDKSSSRGGSEYDTGGSSSSRLHSYSPSTKNSSGGGESRSSRGGGGE	150
<i>Nito_Dm</i>	19	NMK-----RSASRSPGASRSSLSR---NSRSMGRGYDNGSGVPGDSPERLSPERMRRR----LDRSPSRYG--S	79
<i>RBM15_Hs</i>	151	SRSSGAASSAFGGDGAAYKTKIISLGSQLSDEAVEDGLFHEFKRFQDVSVKISHLSSGSGSDERVAFVNFRRP	225
<i>Nito_Dm</i>	80	PHREPYMRGPPAERPAGYKVLCSVALPPKAPDDFI EETLYREYKFGDFSRLAHD-----LDERVAYVCFRTP	149
		<u>RRM 1</u>	
<i>RBM15_Hs</i>	226	EDARA AKHARGRLVLYDRPLKIEAVYVSRRRSR-----SPLDKDTYPPSASVVGASVVG-GHRHPPGGG---G	288
<i>Nito_Dm</i>	150	EDARE AKHKPRLI IYQKMAIVEPYKSTTRPEYRPRGHSMPDYEYHYSRSPMGQVPLDHRPPIDPYDRY	224
<i>RBM15_Hs</i>	289	QQRSLSPGGAALGYRDYRLQQLALGRLP PPPPLPRD-----LERERDYPFVERVRPAYSLEPRVAG-----A	353
<i>Nito_Dm</i>	225	GPPHMHF--HAVHPRDYRLPHDY--PHPRGPPHRRGGHPHLLHGHAPPHOAPMR--PLAPRPHAPYEKPE	292
<i>RBM15_Hs</i>	354	-GAAPFREVD EISPEDDQRANRTLFLGNLDITVTESDLRRAFDRFGVITVDIKRPSRQSTSTYGFLKFE NLDMS	427
<i>Nito_Dm</i>	293	KKDKFPNYLHHVQPEDDPLSTRTLFAGNLEVTIADDELRRIFGKYGVVDDIDIKRPPGTGNAF AFVRYQNLDM	367
		<u>RRM 2</u>	
<i>RBM15_Hs</i>	428	HRAKLAAMSGKIIRNPKIIGYGKATPTTRLWVGGLGPVPLAA LAREFDRFGTIRTI DYRKGDSDWAYIQYESLDA	502
<i>Nito_Dm</i>	368	HRAKIELSGQYIGKFCCKIGYKVTPTATRMWIGGLGAWTSVQLEREFDRFGAIKKIEYQKGEPIYAYIQYETVEA	442
		<u>RRM 3</u>	
<i>RBM15_Hs</i>	503	AHAATHMRGFPLGGPDRRLRVDFADTEHRYQQQYLQPLPLTHYELVTDAFGHRAPDPLRGARDRTPLL YRDRD	577
<i>Nito_Dm</i>	443	ATAAVKEMRGFPLGGPERRLRTDFAELPGATPAAPF-----KSSKPPYD-----ESALEYRPE	496
<i>RBM15_Hs</i>	578	RD L-----YPSDVPVPPVVRERSRTRTAATSVPAYEPLDSDLRRRGGNSLDRDRGDRDLPSSRDQPRKRRL	644
<i>Nito_Dm</i>	497	YDPYEEESAAYARGGYSPYPRG-----GY-RGRGGYR-GRGRGMYHYHNDVHRP---PH	547
		NLS (Hs)	
<i>RBM15_Hs</i>	645	PEESGRHLDRSPESDRPRKRHCAPS DRSPELSSSRDRYNSDNDRSSRLLLERPSP I RDRRGSLEKSSQDKRDR	719
<i>Nito_Dm</i>	548	PGSLAGSSS-----SVPPP-----GGVEDEWR-----RPPGESYDR	578
		NLS (Hs) NLS (Hs)	
<i>RBM15_Hs</i>	720	KNSAS AERDRKHRTTAPTEGKSP LKKEDRS DGSAPS TSTASSK LKSPSQKQDGTAPVASASP LCLAWQGM LLL	794
<i>Nito_Dm</i>	579	GARS SR---EPGVERSRSRSP LKRA-RSPGSDSDTSTRN-----DALASASTVPDVARCSTVWTGALIL	641
		NLS (Dm)	
<i>RBM15_Hs</i>	795	KNSNFP SNMHLQGD LQVASSLLVEGSGTGKVAQLK I TQRLRLDQPKLDEVTRR I KVAGPNGYAI LLAVPSSSDS	869
<i>Nito_Dm</i>	642	KSSLFPAKFHYTDGDTDIVESLMRDEE---GKHNLR I TQRLRLDPPKLDVQKRIASSSS--HAIFMGLAGSTND	711
		SPOC domain	
<i>RBM15_Hs</i>	870	RSSSSSAASDTATSTQRPLRNLVSYLKQKQAAGVISLPVGGNKDKENTGVLHAFPPCFESQQF DSPAKALAKS-	943
<i>Nito_Dm</i>	712	-----TNCDDASVQTRPLRNLVSYLKQKEAAGVISLL---NKETAATGVLYAFPPCFESTELKRTCHS LTEEG	777
<i>RBM15_Hs</i>	944	-EEDYLVM I I VRGFGFQIGVRYENKKRENALATLL	977
<i>Nito_Dm</i>	778	LKEDHLV I VVVRGTA-----	793

Supplemental data 20. Alignment of Nito-RBM15 proteins.

Alignment of Nito protein sequences from *Drosophila melanogaster* (Nito_Dm:Q7KMJ6-1) and human (RBM15_Hs:Q96T37-1), with 30.2 % identity. Protein alignments were generated in Jalview 2.10.5 (Waterhouse et al. 2009) with ClustalO version 1.2.4 using default settings (Larkin et al. 2007). Coloured by degree of amino acid conservation in each column with a 50 % cut off threshold. Underlined regions indicate interaction with RRM domains (green, PROSITE: PS50102) and SPOC domain (blue, PROSITE: PS50917). Predicted NLS are shown in grey with indications for fly (*Dm*) and human (*Hs*) proteins (Obtained by cNLS Mapper (Kosugi et al. 2009)).

Supplemental data

ZC3H13_Hs	875	SLSPSHLTEDRQGRWKEEDRKPERKESRRRYEEQELKEKVSVDKQREQTE I LESSRMRAQDI IGHHSQSEDRET-	948
Flacc_Dm	451	AYLDARYSSREREAWLEARELRERELQGREYRDLETEDTLYPDERE-----RLIRDRE-RDRERE	509
ZC3H13_Hs	949	SDRAHDEKKKKAKIQKKPKIKKK--KEDDVGIERG-NIETTS-EDGQVFSPPKQKKKKSIE-----KKRKKKSG	1012
Flacc_Dm	510	RDRERERNI-GPRGDFRPEWEREWEEGAGGGPGGPGSGTPGRPGGFVGGPKRQKPPAHAGGGPPSQQHHSASEP	583
		NLS (Hs)	NLS (Hs)
ZC3H13_Hs	1013	SDISDEE-----AAQSKKKRGRPTPTTTTKEELVEMCNKNGKI LEDSDKKKEDTAFSDWSDE	1070
Flacc_Dm	584	DWDADERERERERERDRERDRDRPTGGGGA GDRPSIKNEPAWLEHDQ--REKPRGWQQSSNSGGDWRDN	656
ZC3H13_Hs	1071	VDPDRTEVT-----EAEHTATTTTPGS--TSPFLSSLPPPPVPATATA---TTV	1115
Flacc_Dm	657	DAPPAPSHPHASPHHHVHPRGERGSGRGRFRGGHGDHGERPGYRSHPPPLMTLPVQ-PPGGYSRQFPHKRL	730
ZC3H13_Hs	1116	ATLAATTAAATSFSSTAITISTATPTNTTNTTFANEDSRKCHRTRVEKVETPHYTIEDAQHRKFMQDKRSS	1190
Flacc_Dm	731	YGSGRD--G-----AALGARDGGLPG---SSTFLKKHTA---PLVSPQTPLLNPL-LNAAKFNAAAQAS	788
ZC3H13_Hs	1191	SLGSNRSNRSHTSGRRLRSPSNDSAHRSQDDQSGRKRVLHSGARDRETKSLEITGERKSRIDQLKRGEFSSRSTSS	1265
Flacc_Dm	789	AVAAATTAVAA-----AKAAQAANATTNPGILAQVS---KLNTRYCKQEDA---SEDSAGTPELG---	844
ZC3H13_Hs	1266	DRQDSRSHSSRRSSPESDRQVHSRSGSFDSDRDLQERDRYEHDRERERERRDTRQREWDRDADKDWFRNRDRDR	1340
Flacc_Dm	845	AQD-----SPTQSLNL---NQLSSEGN-----PVKQ--ELI	871
		Coiled-coil region	
ZC3H13_Hs	1341	ERERERERDRKRRDLDRERERLISDSVERDRDRDRDRRTFESSQIESVKRCEAKLEGEHERDLESTSRDSLALDKE	1415
Flacc_Dm	872	TSAVEGE-----L-----SEISD-----SDDILNKTDKVR-----PKNELPTETEQE-----	910
ZC3H13_Hs	1416	RMDKDLGSLVQGFEEETNKSERTESELEGDDESKLDDAHSVSGSAG--EGYEPISDDELEILAGDAEKREDQQDEE	1487
Flacc_Dm	911	MDTNADEV-----KSEAL-----HIVAGHPKKEEGEDEVLDLEEISDGELE-----EDA	954
ZC3H13_Hs	1488	KMPDPLDVIDVDWSGLMPKHPKEPREPG-----AALLKFTPGAVMLRVGISKKLAGSELFVAKVETCQRL	1552
Flacc_Dm	955	RHKGIGDALGVDMQGLIAETROQASDAQAAQQGVDRGTSAKQRMQYRVLLDLGLISFGMAGEGYARCVMEEARQQ	1029
ZC3H13_Hs	1553	EKPQADNL--FE-----HELGALNMAALLRKEERASLL-SNLGPGCKALCFR	1598
Flacc_Dm	1030	LQKEQGGQRELDGDEEPPAKIPSPLLDYREFLASQQLEPLACVQMGRLRSAAVERQRLVGNVCGPGSRAISAR	1104
ZC3H13_Hs	1599	RDSATRKQLVKNEKGTIKQAYTSAPMVDNELRSLRLLFKRKTTCAPGHEKTEDNKLSSQSSIQQELCVS	1668
Flacc_Dm	1105	QLRLRRQLCGLPARE-CEFPKRVPIVGEGLRNLAMQMFQRLLDVK-----	1150

Supplemental data 21. Alignment of Flacc-ZC3H13 proteins (part2/2).

Alignment of Flacc protein sequences from *Drosophila melanogaster* (Flacc_Dm: Q9VWN4-1) and human (ZC3H13_Hs: Q5T200-1), with 15.5 % identity. Protein alignments were generated in Jalview 2.10.5 (Waterhouse et al. 2009) with ClustalO version 1.2.4 using default settings (Larkin et al. 2007). Coloured by degree of amino acid conservation in each column with a 50 % cut off threshold. Underlined regions indicate Zinc-finger (red), coiled-coil regions (blue) predicted by program COILS (Lupas et al. 1991). Predicted NLS are shown in grey with indications for fly (*Dm*) and human (*Hs*) proteins (Obtained by cNLS Mapper (Kosugi et al. 2009)).

Supplemental data 22

```

HAKAI_Hs 1 -----M DHT-----D N- 6
Hakai_Dm 1 MDTEEVKRGRGRGRGTRARGRGRGRGRGKK IDSS I ADAALAASSCAALEDSPGRLDASEDSVMQELDKIGE 75

HAKAI_Hs 7 -----E LQGTNSSS L GGLDVRRR I P I K L I S K Q A N K A K P A P R T Q R T I N R M P A K A P P G D E E G F D Y N E -----E E R Y D 72
Hakai_Dm 76 LETPGA L E E P L P H C A L G A V A A S G N M -----T P A T Q Q P Q V L Q Q V P P V M S Q T T I S L S L A R A V D M E A D I S 138

HAKAI_Hs 73 C K G E L F A N Q --- R R F P G H L F M D F Q I N T L G E I D D T F - V M F C D K I G L P T K I Y G R M I P C K H V F Q Y D C A I L H E K K G D 142
Hakai_Dm 139 Q L E A P T T T L S R G P P E M L R L K I N H K V S L I G E R V L N P M I H C C D Q Q D K P I L V Y G R M I P C K H V F C L K C A R A E --- P I 210

                                                                                               RING-type domain

HAKAI_Hs 143 F M C P G S D P Q R I E C T R S L F M C S I -----V Q G C K R T Y L S Q R D L Q A H I N H R H M R A G K P V T R A S L E N V H P P I A I 211
Hakai_Dm 211 K S C R P T T D K L R V E S G L G T V E M C T H G G S R Y G S S C R R T Y L S Q R D L Q A H I N H R H V A P Q P P L Q P Q P Q L S A M A E Q E 285

                                                                                               Zn-finger                               p-Tyr binding domain

HAKAI_Hs 212 P P T E I P E R F I M P P D K H M -----S H I P K Q H I - M M P P P L Q H V P H E H Y N Q P H E D I R A P P A E L S M A P P P P R S V S Q E 280
Hakai_Dm 286 K M T D L G G - V G L G L E L K Q R K L S E S V E I S V S A S I A S R V S R L E L T G G V -----Q N I G S I G S I P P P - G A A A A 351

                                                                                               End of short isoform

HAKAI_Hs 281 T F R I S T R K H S N I I T V P I Q D D S I S G A R E P P P P A P A P A H H H P E Y Q G Q P V V S P H H I M P P Q Q H Y A P P P P P P P I S H P M 355
Hakai_Dm 352 Q N A I - H G G H S T L T L A N I T R I N A N Q E -----C H G K A S L H I ----- 387

HAKAI_Hs 356 P H P P Q A A G T P H L V Y S Q P P P P M T S A P P I T P P P G H I I A Q M P P Y M N H P P P P P Q H G P P V T P P P H H Y N P N S L P 430
Hakai_Dm 388 --- T L K K G T P H Q S E S V I D A S Y Y -----S S V L A S F G S A A G N P G S G --- P P G G - G A T A A Q P A N --- P S G S H 442

HAKAI_Hs 431 Q F T E D Q G T L S P P F T Q I G M S P I I T P A P R G P P P P R L Q G P P S Q T P L P G P H P D Q T R Y R P Y T Q 491
Hakai_Dm 443 S A V G P G A L I G G S T D A T I G S S N I Q Q S Q -----Y Y R 473

```

RING-type domain - C3HC4:

C-X(2)-C-X(9-39)-C-X(1-3)-H-X(2-3)-C-X(2)-C-X(2-48)-C-X(2)-C

Hs: CDKCGLPKIYGRMIPCKHVFYDCAILHEKKGDKMCPGCS

Dm: CDQCDKPILVYGRMIPCKHVFCLKCARAE---PIKSCPRCT

Zn-finger – C2H2:

X(2)-C-X(2-4)-C-X(12)-H-X(3-5)-H

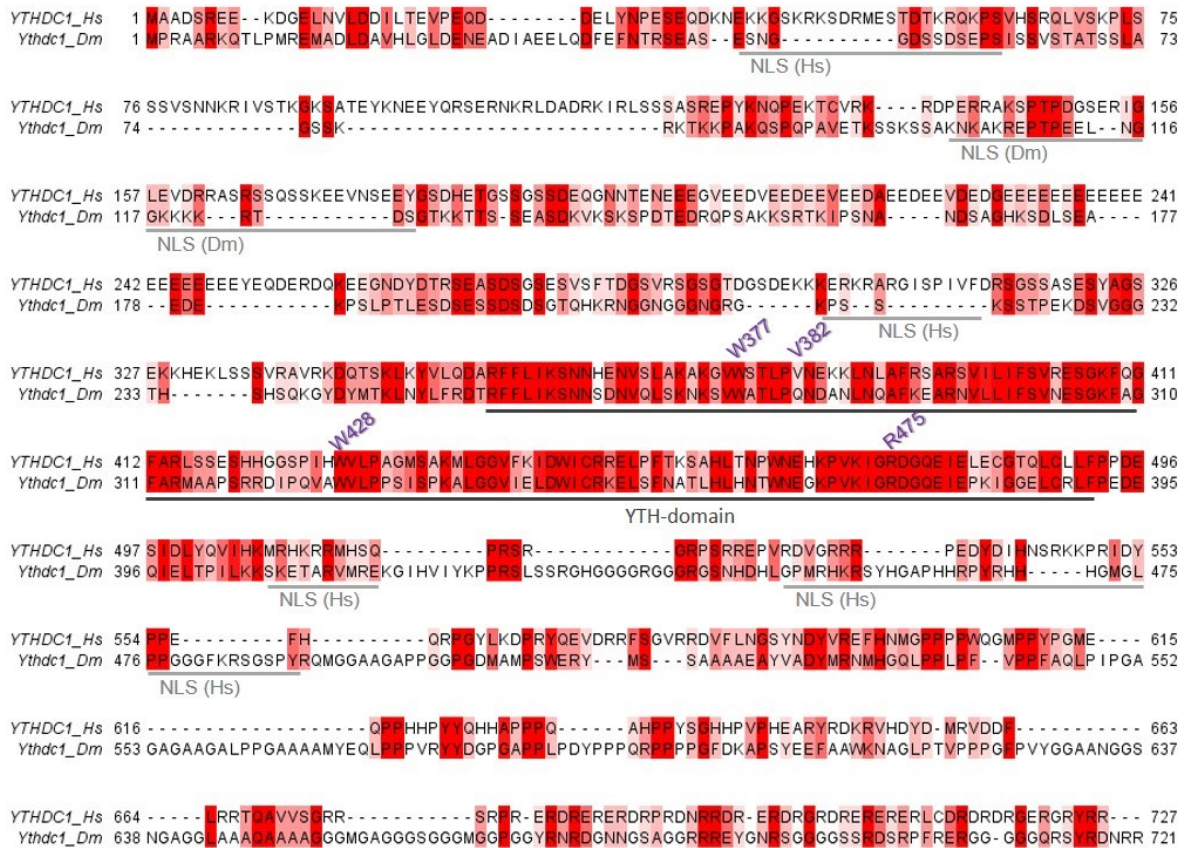
Hs: FMCSI-----VQGCKRITYLSQRDLQAHINHRH

Dm: FMCTHGGSSRYGSSGCRRTYLSQRDLQAHINHRH

Supplemental data 22. Alignment of Hakai-HAKAI proteins.

Alignment of Hakai protein sequences from *Drosophila melanogaster* (Hakai_Dm: M9PBE2-1) and human (HAKAI_Hs: Q75N03-1), with 19.5 % identity. Protein alignments were generated in Jalview 2.10.5 (Waterhouse et al. 2009) with ClustalO version 1.2.4 using default settings (Larkin et al. 2007). Coloured by degree of amino acid conservation in each column with a 50 % cut off threshold. Underlined regions indicate RING-type domain (blue), phospho-Tyrosine (p-Tyr) binding domain (light green) with corresponding Zn-finger (dark green). Both, the RING domain and p-Tyr binding domain are required for Hakai homodimerization and together constitute the so-called **HYB domain** (Mukherjee et al. 2012).

Supplemental data 23



Supplemental data 23. Alignment of Ythdc1-YTHDC1 proteins.

Alignment of Ythdc1 protein sequences from *Drosophila melanogaster* (Ythdc1_Dm: Q9VZQ1-1) and human (YTHDC1_Hs: Q96MU7-1), with 23.8 % identity. Protein alignments were generated in Jalview 2.10.5 (Waterhouse et al. 2009) with ClustalO version 1.2.4 using default settings (Larkin et al. 2007). Coloured by degree of amino acid conservation in each column with a 50 % cut off threshold. Underlined regions indicate YTH domain (grey, PROSITE: PS50882) and m⁶A-accommodating residues (purple) (Xu et al. 2014). Predicted NLS are shown in grey with indications for fly (*Dm*) and human (*Hs*) proteins (Obtained by cNLS Mapper (Kosugi et al. 2009)).

Supplemental data 24

```

Ythdf2_Hs 1 MSASSLLEQRPKGQGNKVQNGSVHQKDGLNDDDFEYLSLSPQARPNNAYTAMSDSYLPSYYSPLGFIYSLGEAA 74
Ythdf_Dm 1 -----MSGVDQMKLPGNTA----KVEERNIP 23

Ythdf2_Hs 75 MSTGGITAMPYLTSYGOVSNGEPHFLPDA MFQQPGALGSTPFLGQHG FNFPPSGIDFSAGGNNSSQIQSTQSS 148
Ythdf_Dm 24 MSQQVDEA-----SYENLSSPT----HEVSGNDN---SMQ-FQYPPFNFKKE--NCNTPNIMNK-GRKAN--A 79

Ythdf2_Hs 149 YSSNAYAPSSLGGAMLDGQSAFAEITLNKAPGMMTIDQGMA LKLGTEVASNVKVVGS AVGSGSITSNI VA 222
Ythdf_Dm 80 NHDSRR-----HGHSIP-----NTRRDEHQVLPWNSRKPAAQ--FRNENDQF-----STKLDNRTS 131

Ythdf2_Hs 223 SNSLPPATIPPKPASVADIASKPAKQPKLKT---KNGIASSLPPPP---IKHNMIDGTNDKGPVA--KA 287
Ythdf_Dm 132 DEAQNQEVVAPKKTWASLASQPAKLTSRRAASTTNSKKKIPGMPPPMVPGKHLLDVNVQLPNNKPPVPS 205

Ythdf2_Hs 288 PSQALVQNIQPTQ-----GSPQPVVQQNNNS-----PPVAQASVG-----QQT----- 326
Ythdf_Dm 206 PPSPL--DLQYSDLSSDFSISSNTAPLLARAEKVHKDTENFLKYEHKGLGNNNNFSRAKVSP TGPVRRNLGPQ 277

Ythdf2_Hs 327 QPLPPPPQPAQL-----SVQQQA AOPTRWAP----RNFGGFGHN-----GVDGNGVGSQASGSGS 380
Ythdf_Dm 278 QPVHHAAPRPATNAGFGPPNARRHDGPHFSRNSERSGNYSFRGSEIESASKFEYRDENQSRPVEATSATEE 351

Ythdf2_Hs 381 TPSEPHPVLEKRSINNYNPKDFWNL-KHGRVFIKSYSEDDIHRSLKYNIWCSTEHGKRLDAFYRSMNG-K 452
Ythdf_Dm 352 LPVDSQLVLDKDKNNYNPKVLDLKKAGSARFVVKSYSEDDIHRSLKYEIWCSTDHGKRLDAFKERHEEG 499
WA486
WA491
WA32
YTH-domain

Ythdf2_Hs 527 RDTQEVPLKAKQVLIKTIASVKHTSIFDDFSHYEQRQEEEVYKERQGRGK----- 579
Ythdf_Dm 500 RDTQEVPLNDKGI EVLQLHSHYNSHSIFDDFHYEQRQEEEVSKRPPMHGPDGNNHAPAPLARSFNRQADDKD 573

Ythdf2_Hs -----
Ythdf_Dm 574 RDRDGRGGMSQKHFNSGGGAGFRNPGHRGAGSGGSHNNYSEYRRGFDIHKSSSDYQFKDRDGPDFDRENDFGS 647

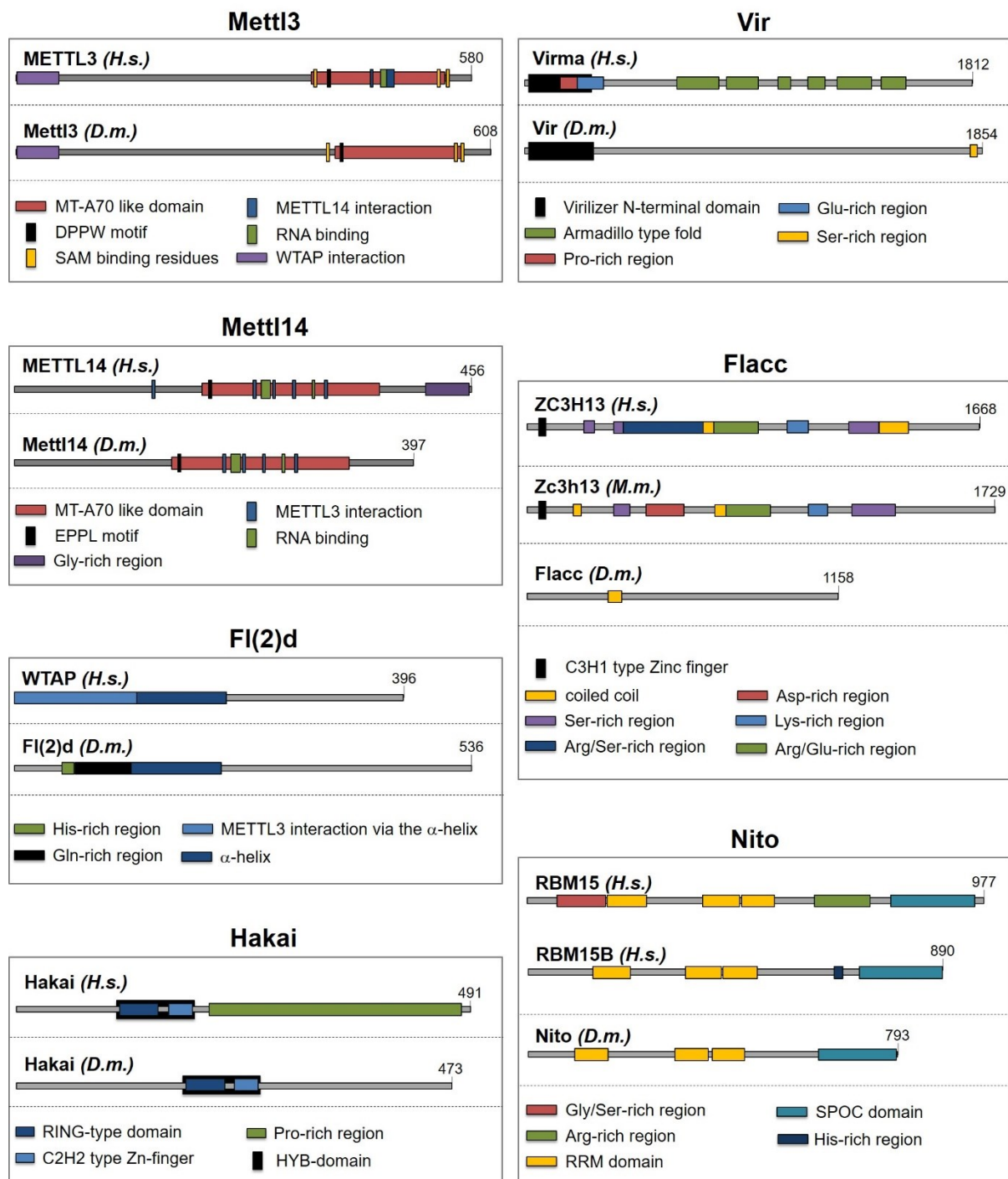
Ythdf2_Hs -----
Ythdf_Dm 648 HYGSNNRKNEYKHNNNTNKARLKTDRDFSTEQIKIGVRFKDTDKDKMRSNEYS 700

```

Supplemental data 24. Alignment of Ythdf-YTHDF3 proteins.

Alignment of Ythdf protein sequences from *Drosophila melanogaster* (Ythdf_Dm: Q9VBZ5-1) and human (YTHDF3_Hs: Q7Z739-1), with 24.3 % identity. Protein alignments were generated in Jalview 2.10.5 (Waterhouse et al. 2009) with ClustalO version 1.2.4 using default settings (Larkin et al. 2007). Coloured by degree of amino acid conservation in each column with a 50 % cut off threshold. Underlined regions indicate YTH domain (grey) and m⁶A-accommodating residues (purple) (Li F. et al. 2014).

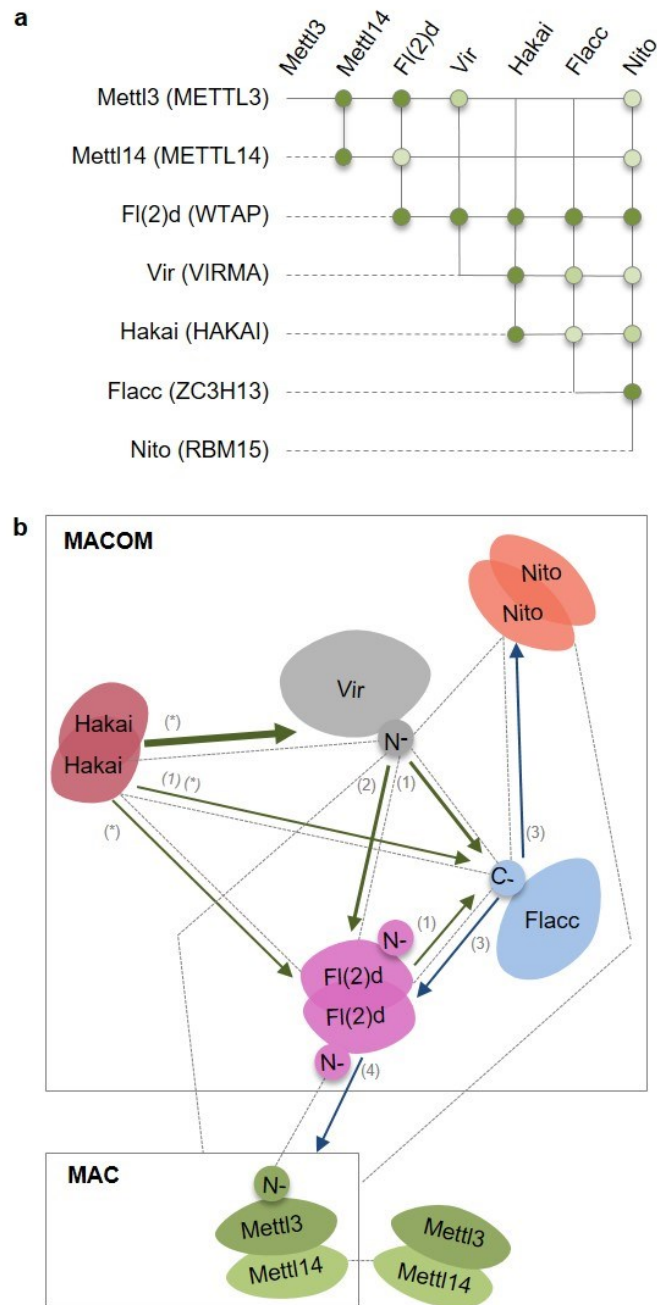
Supplemental data 25



Supplemental data 25. Scheme depicting sequence features of human and fly MAC (Mettl3 and Mettl14) and MACOM (Fl(2)d, Nito, Vir, Flacc and Hakai) components.

See also Supplemental data 16-24. *D.m.* denotes *Drosophila melanogaster*, *M.m.* *Mus musculus* and *H.s.* *Homo sapiens*.

Supplemental data 26

**Supplemental data 26. Scheme depicting interactions between MAC and MACOM components.**

a) Predicted interactions between MAC and MACOM components, based on available data from mouse, human and fly orthologs, are depicted with a dot. Interaction was considered to be plausible, if detected by Co-immunoprecipitation assay, binding assay with purified proteins or by a yeast-two-hybrid assay. Interactions that have been reported by one assay are shown in light green, whereas those reported by more than one assay are shown in dark green. Source: this work, (Liu et al. 2014, Ping et al. 2014, Wang Y. et al. 2014, Yan and Perrimon 2015, Lence et al. 2016, Guo et al. 2018, Knuckles et al. 2018, Wen et al. 2018, Yue et al. 2018). **b)** Interactions between individual components of MAC and MACOM complexes are shown by dotted lines. Green arrows indicate stabilizing effect of protein on the interacting protein, blue arrows indicate positive effect of protein on protein-protein interaction (Flacc stabilizes the interaction between Nito and Fl(2)d; Fl(2)d stabilizes the interaction between Mettl3 and Mettl14). Source: (*) - this work, (1) - (Wen et al. 2018), (2) - (Yue et al. 2018), (3) - (Knuckles et al. 2018), (4) - (Lence et al. 2016).

Materials and methods

In silico phylogenetic analysis

The phylogenetic trees were constructed with ClustalX (Larkin et al. 2007) from multiple sequence alignments generated with MUSCLE (Edgar 2004) of the *Drosophila* sequences with homologs from representative species.

D. melanogaster stocks and genetics

Drosophila melanogaster fly stocks used in this study are listed in **Table 6**. UAS-cDNA-HA flies were generated by injection of UAS cDNA-HA vectors at Bestgene Inc. Mutant alleles for *Mettl3*, *Mettl14*, *Fl(2)d*, *Ythdc1*, *Ythdf*, *CG6144*, *CG14130*, *Hakai* were generated using the CRISPR-Cas9 system following the previously described procedure (Kondo and Ueda 2013) and were injected in house. Two independent guide RNAs per gene were designed using the gRNA design tool: www.crisprflydesign.org (**Table 8**). Oligonucleotides were annealed and cloned into pBFv-U6.2 vector (National Institute of Genetics, Japan). Vectors were injected into embryos of *TBX-0002* ($\gamma 1$ v1 P{nos-phiC31}int.NLS}X; attP40 (II)) flies. All flies were crossed with *TBX-0008* ($\gamma 2$ cho2 v1/Yhs-hid; Sp/CyO) flies to identify positive recombinant flies by eye color marker. Males were further crossed with *CAS-0001* ($\gamma 2$ cho2 v1; attP40(nos-Cas9)/CyO) females. Males carrying nos-Cas9 and U6-gRNA transgenes were screened for the expected deletion and further crossed with the balancer strain *AptXa/CyoGFP-TM6c*. For the analysis of male to female transformations, flies of selected genotypes were chosen randomly.

D. melanogaster climbing test

2-3 day old flies were gender-separated and placed into measuring cylinders to assess their locomotion using the climbing assay reported in (Bahadorani and Hilliker 2008). Flies were tapped to the bottom and the number of flies that climbed over a defined threshold in 10 second intervals were counted. Ten female flies were used per experiment and six independent measurements were performed.

D. melanogaster staging

Staging experiment was performed using *Drosophila melanogaster* W1118 flies that were kept in a small fly cage at 25°C. Flies laid embryos on big apple juice plates that were exchanged every 2 hours (h). Before each start of collection, one-hour pre-laid embryos were discarded in order to remove all retained eggs and embryos from the collection. All following plates with embryos of 1 h or 2 h lay were further incubated at 25°C between 0 h and 20 h, with 2 h increment, in order to get all embryonic stages. For the collection of larval stages, L1 larvae (~30 larvae/stage) were transferred onto a new apple juice plate and were further incubated at 25°C till they reached a defined age (24 to 110 h, 2 hour intervals). Similarly, pupal stages were obtained by the transfer of L3 larvae (~30/stage) in a fresh vial, that were kept at 25°C and left to develop into a defined stage between 144 and 192 hours in 2 h increment. 1-3 day old adults were collected and gender separated. Heads and ovaries from 50 females were also collected. A total of three independent samples were collected for each *Drosophila* stage as well as for heads and ovaries. Samples from the staging experiment were used for RNA extraction to analyse m⁶A abundance in mRNA and expression levels of different transcripts during *Drosophila* development.

Ovary immunostaining

For ovary immunostaining, ovaries from 3-5 days old females were dissected in ice-cold PBS and fixed in 5 % formaldehyde for 20 min at RT. After a 10 min wash in PBT1 % (1 % Triton X-100 in PBS), ovaries were further incubated in PBT1 % for 1h at RT. Ovaries were then blocked with PBTB (0.2 % Triton, 1 % BSA in PBS) for 1 hour at RT and later incubated with the primary antibodies in PBTB O/N at 4°C: Rabbit anti-Vasa, 1:250 (gift from Lehmann lab), mouse anti-ORB 1:30 (#6H4 DSHB). The following day, ovaries were washed 2 times for 30 min in PBTB and blocked with PBTB containing 5 % Donkey serum (Abcam) for 1h at RT. Secondary antibody was added later in PBTB with Donkey serum and ovaries were incubated for 2h at RT. Five washing steps of 30 min were performed with 0.2 % Triton in PBT and ovaries were mounted onto slides in Vectashield (Vector Labs).

NMJ immunostaining

For NMJ staining, third instar larvae were dissected in calcium free HL-3 saline and fixed in 4 % paraformaldehyde in PBT (PBS + 0.05 % Triton X-100). Larvae were then washed briefly in 0.05 % PBT for 30 min and incubated overnight at 4°C with the following primary antibodies: Rabbit anti-Synaptotagmin, 1:2000 (Littleton et al. 1993); mouse anti-DLG, 1:100 (#4F3, DSHB); TRITC-conjugated anti-HRP, 1:200 (Jackson ImmunoResearch). Secondary antibodies conjugated to Alexa-488 (goat anti-rabbit, Jackson ImmunoResearch) and Alexa-647 (goat anti-mouse, Jackson ImmunoResearch) were used at a concentration of 1:200 and incubated at RT for 2 h. Larvae were finally mounted in Vectashield. Images from muscles 6-7 (segment A3) were acquired with a Leica Confocal Microscope SP5. Serial optical sections at 512×512 or 1024×1024 pixels were obtained at 0.38 μm with the 63× objective. Different genotypes were processed simultaneously and imaged using identical confocal acquisition parameters for comparison. Bouton number was quantified in larval abdominal segment A3, muscles 6 and 7, of wandering third instar larvae. ImageJ software (version 1.49) was used to measure the area of the Synaptotagmin positive area.

RNA in situ hybridization

For in situ hybridization *Drosophila melanogaster* W1118 flies were kept at 25°C in conical flasks with apple juice agar plates and embryos were collected every 24 h. Embryos were transferred in a sieve and dechorionated for 2 min in 50 % sodium hypochloride. After 5 min wash in water, embryos were permeabilized with PBST (0.1 % Tween X-100 in PBS) for 5 min. Embryos were transferred in 1:1 mixture of heptane (Sigma) and 8 % formaldehyde (Sigma) and fixed for 20 min with constant shaking at room temperature (RT). After fixation the lower organic phase was removed and 1 volume of MeOH was added to the aqueous phase containing fixed embryos. Following 5 min of extensive shaking all liquid was removed and embryos were washed 3 times with 100 % MeOH. At this point embryos were stored at -20°C or used for further analysis. For in situ hybridization MeOH was gradually replaced with PBST with 10 min washes and with three final washes in PBST. Embryos were further washed for 10 min at RT with 50 % HB4 solution (50 % formamide, 5x SSC, 50 µg/mL heparin, 0.1 % Tween, 5 mg/mL torula yeast extract) diluted in PBST. Blocking was performed with HB4 solution, first for 1h at RT and next for 1 h at 65°C. In situ probes were prepared with DIG DNA labeling Kit (Roche) following the manufacturer's protocol. 2 µL of the probe were diluted in 200 µL of HB4 solution, heated up to 65°C to denature the RNA secondary structure and added to blocked embryos for further O/N incubation at 65°C. The next day, embryos were washed 2 times for 30 min at 65°C with formamide solution (50 % formamide, 1x SSC in PBST) and further 3 times for 20 min at RT with PBST. Embryos were then incubated with anti-DIG primary antibody (Roche) diluted in PBST (1:2000) for 2h at RT and later washed 5 times for 30 min with PBST. In order to develop the staining, embryos were rinsed with AP buffer (100 mM Tris pH 9.5, 50 mM MgCl₂, 100 mM NaCl, 0.1 % Tween) and incubated with NBT/BCIP solution in AP buffer (1:100 dilution) until the intense staining was observed. Reaction was stopped with several 15 min PBST washes. Prior to mounting, embryos were incubated in 20 % glycerol and later visualized on Leica M205-FA stereomicroscope.

Lifespan assay

For lifespan assay, 2-3 day old flies were gender-separated and kept at 25°C in flasks with apple juice medium (<20 flies/tube). Number of flies tested: Females (37, *lme4Δcat/lme4Δcat*; 57, *Tubulin-GAL4/UAS-lme4*); Males (33, *lme4Δcat/lme4Δcat*; 41, *Tubulin-GAL4/UAS-lme4*). To monitor their survival rate over time, flies were counted and transferred into a new tube every 2 days.

Buridan paradigm

Behavioural tests were performed on 2-5 day old females with Canton-S as wild-type control. Wings were cut under cold anaesthesia to 1/3 of their length in the evening prior to the experiment. Walking and orientation behaviour was analysed using Buridan's paradigm as described in (Strauss et al. 1992). Dark vertical stripes of 12° horizontal viewing angle were shown on opposite sides of an 85-mm diameter platform surrounded by water. The following parameters were extracted by a video-tracking system (5Hz sampling rate): total fraction of time spent walking (activity), mean walking speed taken from all transitions of a fly between the visual objects, and number of transitions between the two stripes. The visual orientation capacity (mean angular deviation) of the flies was assessed by comparing all 0.2-s path increments per fly (4500 values in 15 min) to the respective direct path toward the angular wise closer of the two dark stripes. All statistical groups were tested for normal distribution with the Shapiro-Wilk-test. Multiple comparisons were performed using the Kruskal-Wallis analysis of variance or one-way ANOVA with a post-hoc Bonferroni correction. n=15 for all genotypes. The sample size was chosen based on a previous study (Poeck et al. 2008) and its power was validated with result analysis. Blinding was applied during the experiment.

Generation of antibodies

Antibodies against *lme4* and *dMettl14* were generated at Eurogentec. For anti-*lme4* sera guinea pig was immunized with a 14 amino acid-long peptide (163-177 AA); for anti-*dMettl14* sera a rabbit was immunized with a 14 amino acid-long peptide (240-254 AA). Both serums were affinity-purified using peptide antigens cross linked to sepharose columns.

Immunostaining in S2R+ cells

For staining of *Drosophila* S2R+ cells, cells were transferred to the poly-lysine pretreated 8-well chambers (Ibidi) at the density of 2 x 10⁵ cells/well. After 30 min, cells were washed with 1x DPBS (Gibco), fixed with 4 % Formaldehyde for 10 min and permeabilized with PBST (0.2 % Triton X-100 in PBS) for 15 min. Cells were incubated with mouse anti-Myc (1:2000; #9E10, Enzo) in PBST supplemented with 10 % of Donkey serum at 4°C, O/N. Cells were washed 3x for 15 min in PBST and then incubated with secondary antibody and 1x DAPI solution in PBST supplemented with 10 % of Donkey serum for 2 h at 4°C. After three 15 min washes in PBST, cells were imaged with Leica SP5 confocal microscope using 63x oil immersion objective.

Cell culture, RNAi and transfection

Drosophila melanogaster S2R+ cells were grown in Schneider's medium (Gibco) supplemented with 10 % FBS (Sigma) and 1 % Penicillin-Streptomycin (Sigma). For RNAi experiments, PCR templates for the dsRNA were prepared using T7 megascript Kit (NEB). S2R+ cells were seeded at the density of 10⁶ cells/mL in serum-free medium and 7.5 µg of dsRNA was added to 10⁶ cells. After 6 h of cell starvation, serum supplemented medium was added to the cells. dsRNA treatment was repeated after

48 and 96 h and cells were collected 24 h after the last treatment. Effectene (Qiagen) was used to transfect vector constructs in all overexpression experiments following the manufacturer's protocol.

RNA isolation, mRNA purification and RT-PCR

Total RNA from S2R+ cells was isolated using Trizol reagent (Invitrogen) and DNA was removed with DNase-I treatment (NEB). mRNA was purified with Oligotex mRNA Kit (Qiagen) or by using two rounds of purification with Dynabeads® Oligo (dT)25 (Invitrogen). cDNA for RT-qPCR was prepared using M-MLV Reverse Transcriptase (Promega) and transcript levels were quantified using Power SYBR® Green PCR Master Mix (Invitrogen) and oligos indicated in Supplementary Table 9. For RNA isolation from fly heads, 20 female flies were collected in 1.5 mL Eppendorf tubes and flash frozen in liquid nitrogen. Heads were first removed from the body by spinning the flies on vortex and then collected via the 0.63 mm sieve at 4°C. Fly heads were homogenized using a pestle and total RNA was isolated with Trizol reagent. DNA was removed by DNase-I treatment and RNA was further purified using RNeasy Kit (Qiagen). RNA from adult flies and dissected ovaries was prepared as described above by skipping the head separation step.

LC-MS/MS analysis of m⁶A levels

mRNA samples from S2R+ cells depleted for indicated proteins or from *Drosophila* staging experiments were prepared following the aforementioned procedures. Three-hundred nanograms of purified mRNA was digested using 0.3 U Nuclease P1 from *Penicillium citrinum* (Sigma-Aldrich, Steinheim, Germany) and 0.1 U Snake venom phosphodiesterase from *Crotalus adamanteus* (Worthington, Lakewood, USA). RNA and enzymes were incubated in 25 mM ammonium acetate, pH 5, supplemented with 20 µM zinc chloride for 2 h at 37 °C. Remaining phosphates were removed by 1 U FastAP (Thermo Scientific, St Leon-Roth, Germany) in a 1 h incubation at 37 °C in the manufacturer supplied buffer. The resulting nucleoside mix was then spiked with ¹³C stable isotope labelled nucleoside mix from *Escherichia coli* RNA as an internal standard (SIL-IS) to a final concentration of 6 ng/µl for the sample RNA and 10 ng/µl for the SIL-IS. For analysis, 10 µl of the before mentioned mixture were injected into the LC-MS/MS machine. Generation of technical triplicates was obligatory. All mRNA samples were analysed in biological triplicates. LC separation was performed on an Agilent 1200 series instrument, using 5 mM ammonium acetate buffer as solvent A and acetonitrile as buffer B. Each run started with 100 % buffer A, which was decreased to 92 % within 10 min. Solvent A was further reduced to 60 % within another 10 min. Until minute 23 of the run, solvent A was increased to 100 % again and kept at 100 % for 7 min to re-equilibrate the column (Synergi Fusion, 4 µM particle size, 80 Å pore size, 250 × 2.0 mm, Phenomenex, Aschaffenburg, Germany). The ultraviolet signal at 254 nm was recorded via a DAD detector to monitor the main nucleosides. MS/MS was then conducted on the coupled Agilent 6460 Triple Quadrupole (QQQ) mass spectrometer equipped with an Agilent JetStream ESI source which was set to the following parameters: gas temperature, 350 °C; gas flow, 8 l/min; nebulizer pressure, 50 psi; sheath gas temperature, 350 °C; sheath gas flow, 12 l/min; and capillary voltage, 3,000 V. To analyse the mass transitions of the unlabelled m⁶A and all ¹³C m⁶A simultaneously, we used the dynamic multiple reaction monitoring mode.

Dot blot assays

Serial dilutions of biotinylated RNA probe of bPRL containing m⁶A or A were spotted and crosslinked on nitrocellulose membrane (Biorad) with UV 245 light (3x 150 mJ/cm²). RNA loading was validated with methylene blue staining. Membranes were blocked with 5 % milk in PBST for 1h at RT and washed in PBST prior to incubation with the proteins of interest. S2R+ cells were transfected with either Myc-Ythdc1 or Myc-GFP constructs. 48 h post transfection cells were collected, washed with PBS and pelleted by centrifugation at 400 g for 10 min. The cell pellet was lysed in 1 mL of lysis buffer (10 mM Tris-HCl, pH 7.4, 150 mM NaCl, 0.5 % NP-40). 3 mg of the protein lysate were mixed with 2 % BSA in lysis buffer and incubated with the membrane over night at 4 °C. For control dot-blot rabbit anti-m⁶A antibody (Synaptic Systems) was used. The next day membranes were washed 3x in lysis buffer. Membranes with bound proteins were further crosslinked with UV 245 light (3x 150 mJ/cm²) and analysed using anti-Myc antibody.

In vitro pull-down assay

S2R+ cells were transfected with either Myc-Ythdc1 or Myc-GFP constructs. 48 h post transfection cells were collected, washed with PBS and pelleted by centrifugation at 400 g for 10 min. The cell pellet was lysed and processed in 1 mL of pull-down lysis buffer (10 mM Tris-HCl, pH 7.4, 150 mM NaCl, 2 mM EDTA, 0.5 % Triton-X100, and 0.5 mM DTT). For individual pull-down, 1.5 mg of protein were incubated with either 3 µg of biotinylated RNA probe of bPRL containing m⁶A or not, or without probe, as a control in 0.5 mL of pull-down buffer supplemented with protease inhibitor mix and 10 U of Murine RNase Inhibitor (NEB) and incubated 2 h at 4°C. 5 µL of Streptavidin beads (M-280, Invitrogen) were added and pull-down samples were incubated for additional 1 h at 4°C. Following 3 washes for 15 min with pull-down buffer, beads were re-suspended in 400 µL of pull-down buffer. 100 µL were used for RNA isolation and dot blot analysis of recovered RNA probes with anti-Strep-HRP. The remaining 300 µL of the beads were collected on the magnetic rack and IP proteins were eluted by incubation in 1x SDS buffer (ThermoFischer) at 95°C for 10 min. IP proteins as well as input samples were analysed by Western blot.

In vitro pull-down assay followed by MS protein analysis

S2R+ cells were grown in Schneider medium (Dundee Cell) supplemented with either heavy (Arg8, Lys8) or light amino acids (Arg0, Lys0) (Sigma). The cell pellets from heavy and light labelled cells were lysed and processed in 1 mL of pull-down lysis buffer (10 mM Tris-HCl, pH 7.4, 150 mM NaCl, 2 mM EDTA, 0.5 % Triton-X100, and 0.5 mM DTT). For individual pull-down, 1.5 mg of protein were incubated with either 3 µg of biotinylated RNA probe of bPRL containing m⁶A, or not in 0.5 mL of pull-down buffer supplemented with protease inhibitor mix and 10 U of Murine RNase Inhibitor (NEB) and incubated 2 h at 4°C. 5 µL of Streptavidin beads (M-280, Invitrogen) were added and pull-down samples were incubated for additional 1 h at 4°C. Following 3 washes for 15 min with pull-down buffer, beads were re-suspended in 400 µL of pull-down buffer. 100 µL were used for RNA isolation and dot blot analysis of recovered RNA probes with anti-Strep-HRP. The remaining 300 µL of the heavy and light lysates were combined in 1:1 ratio and eluted with 1x NuPAGE LDS buffer. Samples were then subjected to MS analysis as described previously (Bluhm et al. 2016). Raw files were processed with MaxQuant (version 1.5.2.8) and searched against the Uniprot database of annotated *Drosophila* proteins (*Drosophila melanogaster*: 41850 entries, downloaded 8.1.2015).

Co-IP assay and western blot analysis

For the co-IP assay, different combinations of vectors with indicated tags were co-transfected in S2R+ cells seeded in 10 cm cell culture dish as described above. 48 h post transfection cells were collected, washed with DPBS and pelleted by 10 min centrifugation at 400 g. The cell pellet was lysed in 1 mL of lysis buffer (50 mM Tris-HCl, pH 7.4, 150 mM NaCl, 0.05 % NP-40) supplemented with protease inhibitors (1 µg/mL Leupeptin, 1 µg/mL Pepstatin, 1 µg/mL Aprotinin and 1 mM PMSF) and rotated head-over-tail for 30 min at 4°C. Nucleus were collected by 10 min centrifugation at 1000x g at 4°C re-suspended in 300 µL of lysis buffer and sonicated with 5 cycles of 30 s ON, 30 s OFF low power setting. Cytoplasmic and nuclear fractions were joined and centrifuged at 18000x g for 10 min at 4°C to remove the remaining cell debris. Protein concentrations were determined using Bradford reagent (Bio-Rad). For IP, 2 mg of proteins were incubated with 7 µL of anti-Myc Ab coupled to magnetic beads (Cell Signalling) in lysis buffer and rotated head-over-tail O/N at 4°C. The beads were washed 3x for 15 min with lysis buffer and IP proteins were eluted by incubation in 1x NuPAGE LDS buffer (ThermoFischer) at 70°C for 10 min. Eluted IP proteins were removed from the beads and DTT was added to 10 % final volume. IP proteins and input samples were analysed by Western blot after incubation at 70°C for additional 10 min. For Western blot analysis, proteins were separated on 7 % SDS-PAGE gel and transferred on Nitrocellulose membrane (Bio-Rad). After blocking with 5 % milk in PBST (0.05 % Tween in PBS) for 1h at RT, the membrane was incubated with primary antibody in blocking solution O/N at 4°C. Primary antibodies used were: mouse anti-Myc 1:2000 (#9E10, Enzo); mouse anti-HA 1:1000 (#16B12, COVANCE); mouse anti-Tubulin 1:2000 (#903401, Biolegend); Guinea pig anti-Ime4 1:500 and rabbit anti-dMettl14 1:250. The membrane was washed 3x in PBST for 15 min and incubated 1 h at RT with secondary antibody in blocking solution. Protein bands were detected using SuperSignal™ West Pico Chemiluminescent Substrate (Thermo Scientific).

SILAC experiment and LC-MS/MS analysis

For SILAC experiments (Mettl3, Fl(2)d, Nito and Ythdc1 May-tagged baits), S2R+ cells were grown in Schneider medium (Dundee Cell) supplemented with either heavy (Arg10, Lys8) or light amino acids (Arg0, Lys0) (Sigma). For the forward experiment, Myc-Ythdc1 was transfected in heavy labelled cells and Myc-alone in light labelled cells. The reverse experiment was performed vice versa. The co-IP experiment was done as described above. Before elution, beads of the heavy and light lysates were combined in 1:1 ratio and eluted with 1x NuPAGE LDS buffer that was subject to MS analysis as described previously (Bluhm et al. 2016). Raw files were processed with MaxQuant (version 1.5.2.8) and searched against the Uniprot database of annotated *Drosophila* proteins (*Drosophila melanogaster*: 41850 entries, downloaded 8.1.2015).

Immunoprecipitation and ubiquitination analysis

S2R+ cells were transfected with either GFP-tagged Nito or Fl(2)d proteins as described above. 48 hours post transfection attached cells in the 10 cm cell culture dish were washed 2x with cold PBS on ice. Cells were lysed with 1 mL of modified RIPA lysis buffer (50 mM Tris-HCl pH 7.5, 150 mM NaCl, 1 mM EDTA, 1 % NP-40, 0.1 % Na-deoxycholate), supplemented with complete protease inhibitor cocktail, 5 mM β-glycerophosphate, 5 mM NaF, 1 mM Na-orthovanadate, 10 mM N-ethylmaleimide. Cells were then collected and incubated for 10 minutes on ice and centrifuged 15 minutes at 16,000xg at 4°C. Supernatant was transferred to a new tube and protein concentration measured using Bradford. 1.5 mg of proteins were incubated with 20 µL of washed GFPTrap-A beads (Chromotec) for 1h at 4 °C end-over-end mixing. Beads were collected by centrifugation (3,000 rpm, 1 min) and the supernatant removed. Beads were washed 1x with dilution buffer (10 mM Tris-HCl pH 7.5, 150 mM NaCl, 0.5 mM EDTA, 1x Protease Inhibitor (Sigma), 10 mM N-ethylmaleimide), 3x with stringent wash buffer (8 M Urea, 1 % SDS in 1x PBS) and 1x with wash buffer (1 % SDS in 1x PBS). 40 µL of 2xLDS sample buffer (Invitrogen) supplemented with 1 mM DTT was added and beads were incubated for 10 min at 70°C. Eluted proteins were alkylated with 5.5 mM CAA for 30 min at RT in the dark and subjected to in-gel digestion and MS analysis as described previously (Schunter 2017 Plos One).

Ubiquitinome and proteome analysis

Ubiquitinome and proteome analysis of control and Hakai depleted S2R+ cells was performed as described previously (Schunter 2017 Plos One). Following modifications were made: S2R+ cells were grown in Schneider medium (Dundee Cell) supplemented with either heavy (Arg8, Lys8) or light amino acids (Arg0, Lys0) (Sigma). Depletion of Hakai was performed as

described above “Cell culture, RNAi and transfection” by omitting starvation and scaling up to obtain 50 mg of proteins per replicate (8-10, 15-cm cell culture dishes). 6 hours prior to cell lysis, the MG132 proteasome inhibitor was added to a final concentration of 15 μ M. Cells were lysed in modified RIPA lysis buffer (50 mM Tris-HCl pH 7.5, 150 mM NaCl, 1 mM EDTA, 1 % NP-40, 0.1 % Na-deoxycholate) supplemented with complete protease inhibitor cocktail (Roche), 5 mM β -glycerophosphate, 5 mM NaF, 1 mM Na-orthovanadate, 10 mM N-ethylmaleimide. 1.5 mL of buffer was used per each 15-cm dish. All lysates of the same transfection were combined in a falcon and protein concentrations were measured by Bradford. 100 μ g of each protein sample were collected for WB analysis. Heavy and light replicates were joined in a 1:1 ratio and 50 μ g were collected for proteome analysis. For forward experiment Heavy labelled cells with control KD and light labelled cells with Hakai KD were joined, and vice versa for reverse experiment. Finally, ice-cold acetone was added to 80 % final conc. (4xV) and precipitated O/N at -20 °C. Ubiquitin pull downs, ubiquitination analysis and proteome analysis was performed following the procedure described in detail in (Ref Schunter 2017 Plos One).

Yeast-two-hybrid assay (Y2H)

Yeast-two-hybrid assay was performed using *S. cerevisiae* yeast strain [trp1-901, leu2-3,112, ura3-52, his3-200, gal4 Δ , gal80 Δ , LYS2::GAL1-HIS3, GAL2-ADE2, met2::GAL7-lacZ]. cDNAs of all tested genes (*Mettl3*, *Mettl14*, *Fl(2)d*, *Vir*, *Nito*, *Flacc*, *Hakai*, *Er*) were cloned in vectors pGAD424-GW and pGBT9-GW, with *Leu2* and *Trp1* markers (kindly provided by Helle Ulrich, IMB Mainz) to express all candidates with either the C-terminal Gal4-activation domain or the C-terminal Gal4-DNA binding domain, respectively. Briefly, yeast cells were grown in YPD medium until they reached O.D. = 0.6. Cells were centrifuged at 3500 rpm for 7min at RT and washed 1x with water, 1x with 250 mL of SORB (100 mM LiOAc, 10 mM Tris pH 8.0, 1 mM EDTA pH 8.0, 1 M Sorbitol) and 1x with 100 mL of SORB. Pellets were resuspended in 3.6 mL of SORB and 400 μ L of ssDNA carrier was added to competent cells. 50 μ L aliquots of cells were mixed with 100 ng of plasmid DNA. 6x volumes of PEG solution (10 mM Tris pH 8.0, 1 mM EDTA pH 8.0, 40 (w/v)-% PEG 3350) were then added to the cell-DNA mixture that was further incubated at RT for 30 min. Next, 1/9 of DMSO were added to cells that were subjected to 15 min heat shock at 42 °C. Following 2 min centrifugation at 4000 rpm and RT, the cell pellet was resuspended in 500 μ L of water and 100 μ L of cell solution was plated onto Trp-/Leu- selection agar plates. After 3 days of incubation at 30 °C, 5 colonies of each transformation were resuspended in 500 μ L of water and 4 μ L were spotted on selection agar plates (Trp-/Leu- and Trp-/Leu-/His-). Plates were imaged every 24-hour interval.

RNA immunoprecipitation (RIP)

S2R+ cells were transfected with Myc-tagged constructs using Effectene reagent. 72 h post transfection cells were washed with ice cold PBS and collected by 5 min centrifugation at 1000x g. The cell pellet was lysed in 1 ml of lysis buffer (50 mM Tris-HCl, pH 7.4, 150 mM NaCl, 0.05 % NP-40) supplemented with protease inhibitors, rotated head-over-tail for 30 min at 4 °C and centrifuged at 18,000x g for 10 min at 4 °C to remove the remaining cell debris. Protein concentrations were determined using Bradford reagent (Bio-Rad). For RNA immunoprecipitation, 2 mg of proteins were incubated with 2 μ g of anti-Myc antibody coupled to protein-G magnetic beads (Invitrogen) in lysis buffer and rotated head-over-tail for 4h at 4 °C. The beads were washed 3 times for 5 min with washing buffer. One fourth of immunoprecipitated protein – RNA complexes were eluted by incubation in 1x NuPAGE LDS buffer (Thermo Fisher) at 70 °C for 10 min for protein analysis. RNA from the remaining protein-RNA complexes was further isolated using Trizol reagent.

RNA sequencing and computational analysis

For samples from S2R+ cells (*Mettl3*, *Mettl14*, *Mettl3/Mettl14*, *Fl(2)d*, *Ythdc1*, *Ythdf* KDs) and for full fly RNA samples, Illumina TruSeq Sequencing Kit (Illumina) was used. For *Drosophila* head samples, NEBNext Ultra Directional RNA Kit (NEB) was used. Libraries were prepared following the manufacturer’s protocol and sequenced on Illumina HiSeq 2500. The read-length was 71 bp, paired end. The RNA-seq data was mapped against the *Drosophila* genome assembly BDGP6 (Ensembl release 79) using STAR (Dobin et al. 2013) (version 2.4.0). After mapping, the bam files were filtered for secondary alignments using samtools (version 1.2). Reads on genes were counted using htseq-count (version 0.6.1p1). After read counting, differential expression analysis was done between conditions using DESeq2 (version 1.6.3) and filtered for a false discovery rate (FDR) < 5 %. Differential splicing analysis was performed using rMATS (3.0.9) and filtered for FDR < 10 %. The data from fly heads were treated as above but cleaned for mitochondrial and rRNA reads after mapping before further processing. The sample lme4hom_3 was excluded as an outlier from differential expression analysis.

For samples from S2R+ cells (*Mettl3/Mettl14*, *Fl(2)d*, *Vir*, *Nito*, *Flacc*, *Hakai* KDs) Illumina TruSeq Sequencing Kit (Illumina) was used. The RNA libraries were sequenced on a NextSeq500 with a read length of 85 bp. The data was mapped against Ensembl release 90 of *Drosophila Melanogaster* using STAR (v2.5.1b). Counts per gene were derived using featureCounts (v.1.5.1). Differential expression analysis was performed using DESeq2 (v. 1.16.1) and filtered for an FDR < 1 %. Differentially splicing analysis was performed using rMATS (v 3.2.5) and filtered for an FDR < 10 %. Sequencing depth normalised coverage tracks were generated using bedtools (v.2.25.0), samtools (v.1.3.1) and kentutils (v.302).

m⁶A RNA immunoprecipitation (MeRIP) and computational analysis

MeRIP was performed using the previously described protocol (Deng et al. 2015) with the following modifications. 8 μ g of purified mRNA from *Drosophila* S2R+ cells was incubated with 5 μ g of anti-m⁶A antibody (Synaptic Systems) in m⁶A-IP buffer

(150 mM NaCl, 10 mM Tris-HCl pH 7.4, 0.1 % NP-40) supplemented with 5 U/mL of Murine RNase inhibitor (NEB) for 2 h at 4°C. In control m⁶A-IP experiment, no antibody was used in the reaction mixture. 5 µL of A+G magnetic beads were added to all m⁶A-IP samples for 1 h at 4°C. On bead digestion with RNase T1 (Thermo Fisher) at final concentration 0.1 U/mL was performed for 15 min at RT. Beads with captured RNA fragments were then immediately washed 3 times with 500 µL of ice-cold m⁶A-IP buffer and further eluted with 100 µL of elution buffer (0.02 M DTT, 150 mM NaCl, 50 mM Tris-HCl pH 7.4, 1 mM EDTA, 0.1 % SDS, 5 U/mL Proteinase K) at 42°C for 5 min. Elution step was repeated 4 times and 500 µL of acidic phenol/chloroform pH 4.5 (Ambion) was added to 400 µL of the combined eluate per sample in order to extract captured RNA fragments. Samples were mixed and transferred to Phase Lock Gel Heavy tubes (5Prime) and centrifuged for 5 min at 12000x g. Aqueous phase was precipitated O/N, -80°C. On the following day, samples were centrifuged, washed twice with 80 % EtOH and re-suspended in 10 µL of RNase-free H₂O (Ambion). Recovered RNA was analysed on RNA Pico Chip (Agilent) and concentrations were determined with RNA HS Qubit reagents. Since no RNA was recovered in the m⁶A-IP control samples, libraries were prepared with 30 ng of duplicate m⁶A-IPs and duplicate input mRNA samples. MeRIP-qPCR was performed on the fraction of eluted IP RNA and equal amount of input mRNA. cDNA for RT-qPCR was prepared using M-MLV Reverse Transcriptase (Promega) and transcript levels were quantified using Power SYBR[®] Green PCR Master Mix (Invitrogen) using oligonucleotides indicated in **Table 7**.

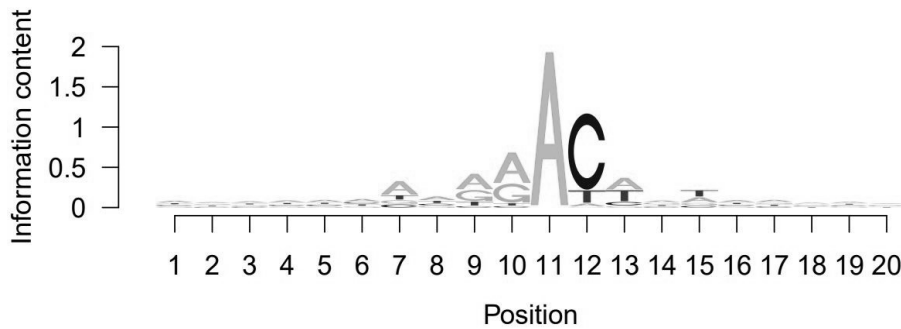
For MeRIP-seq, NEBNext Ultra Directional Kit was used, omitting the RNA fragmentation step for recovered MeRIP samples and following the manufacturer's protocol for input samples. Libraries were sequenced on an Illumina MiSeq as 68 bp single read in one pool on two flow cells. The MeRIP-seq data were processed following the same protocol as the RNA samples for mapping and filtering of the mapped reads. After mapping, peaks were called using MACS (version 1.4.1) (Zhang et al. 2008). The genome size used for the MACS was adjusted to reflect the mappable transcriptome size based on Ensembl-annotated genes (Ensembl release 79). After peak calling, peaks were split into subpeaks using PeakSplitter (version 1.0, <http://www.ebi.ac.uk/research/bertone/software>). Consensus peaks were obtained by intersecting subpeaks of both replicates (using BEDTools, version 2.25.0). For each consensus peak, the coverage was calculated as counts per million (CPM) for each of the samples and averaged for input and MeRIP samples. Fold changes for MeRIP over input were calculated based on these. Peaks were filtered for a minimal fold change of 1.3 and a minimal coverage of 3 CPM in at least one of the samples. Peaks were annotated using the ChIPseeker and the GenomicFeatures package (based on R/Bioconductor) (Yu et al. 2015).

miCLIP and computational analysis

miCLIP was performed following previously described method (Linder et al. 2015) (Sutandy et al. 2016) using 10 µg of purified mRNA from *Drosophila* S2R+ cells and 5 µg of anti-m⁶A antibody (Synaptic Systems, Lot# 202003/2-82). Immunoprecipitations were performed in quadruplicates and as a control one immunoprecipitation was performed where UV-crosslinking was omitted. Of note, this sample produced a library of very limited complexity, reflecting a low amount of background mRNA binding. Briefly, total RNA was isolated using Trizol reagent (Invitrogen) and DNA was removed with DNase-I treatment (NEB). Polyadenylated RNA was purified by two rounds of binding to Oligo (dT)25 magnetic beads (NEB) and mRNA was fragmented with RNA fragmentation solution (Ambion) using 1 µL of solution per 2 µg of mRNA and with 7 min incubation at 70 °C. Immunoprecipitation was performed at 4°C in 500 µL of binding buffer (BB) (50 mM Tris-HCl pH 7,4, 150 mM NaCl, 0,5 % NP-40). First, isolated mRNA and antibody were incubated for 2h. Samples were then transferred to individual well of a 12 well cell culture plate and crosslinked on ice (two-times, 150 ml/cm²). Next, 60 µL of magnetic ProteinG beads (Invitrogen) were resuspended in 500 µL of BB and added to the IP sample. Samples were then incubated for another 2h at 4 °C, before washed with cold solutions as follows: 1x with BB, 2x with high salt buffer (50 mM Tris-HCl pH 7,4, 1 M NaCl, 1 % NP-40, 0,1 % SDS), 1x BB, 2x with PNK buffer (20 mM Tris-HCl pH 7,4, 10 mM MgCl₂, 0,2 % Tween). All washes were performed by gentle pipetting and by 1min incubation on ice, washes with HSB were rotated at 4 °C for 2 min. 40 µL of final wash was used for WB analysis of immunoprecipitation efficiency and 860 µL were used for library preparation. All following steps of library preparation were performed as previously described (Sutandy et al. 2016). Data analysis was performed as described in (Linder et al. 2015).

Two input-control libraries using the same mRNA as for miCLIP were prepared with the NEBNext Ultra Directional RNA Library Prep Kit for Illumina (NEB). To address potential bias that ZnCl₂ fragmentation might impose on read truncation analysis, we generated the following two libraries: one library was prepared using ZnCl₂ fragmented mRNA (the very same as for immunoprecipitation), while another library was prepared using intact mRNA that was fragmented during the library preparation by 1st strand cDNA synthesis buffer as per manufacturer instructions. Of note, the ZnCl₂ fragmented mRNA was first purified using the 1.8X volume of RNAClean XP beads (Beckman Coulter). Following the 20 min incubation at RT, captured RNA was washed 3x with 80 % EtOH and eluted in 20 µL of RNase-free water. The library was prepared using ~50 ng of cleaned, fragmented mRNA using the NEBNext Ultra Directional RNA Library Prep Kit for Illumina (NEB), by omitting the RNA fragmentation step and following the manufacturer's protocol. Both libraries were amplified by 11 PCR cycles.

For miCLIP, data analysis was performed as described in Ref (Linder et al. 2015). The full 20-nt sequence logo (collapsed sequence content) of CITS (A) sites is shown below, with predicted m⁶A site at position 11.



Flies generated and used in this study

	Stock name	Line description	Chr.	Source	Comment
gRNA lines	Mettl3 cris (gRNA 1+2)/cyo	Mettl3 gRNA (1+2)	II	this study	in house injection
	Mettl3 cris (gRNA 0+2)/cyo	Mettl3 gRNA (0+2)	II	this study	in house injection
	Mettl14 cris (gRNA 1+2)/cyo	Mettl14 gRNA (1+2)	II	this study	in house injection
	Mettl14 cris (gRNA 0+2)/cyo	Mettl14 gRNA (0+2)	II	this study	in house injection
	Mettl4 cris (gRNA 1+2)/cyo	Mettl4 gRNA	II	this study	in house injection
	CG6144 cris (gRNA 1+2)/cyo	CG6144 gRNA	II	this study	in house injection
	CG14130 cris (gRNA 1+2)/cyo	CG14130 gRNA	II	this study	in house injection
	Fl(2)d cris (gRNA 1+2)/cyo	Fl(2)d gRNA	II	this study	in house injection
	Ythdc1 cris (gRNA 1+2)/cyo	Ythdc1 gRNA	II	this study	in house injection
	Ythdf cris (gRNA 1+2)/cyo	Ythdf gRNA	II	this study	in house injection
	Hakai cris (gRNA 1+2)/cyo #M1	Hakai gRNA (1+2)	II	this study	BestGene injection
	Hakai cris (gRNA 1+2)/cyo #M4	Hakai gRNA (1+2)	II	this study	BestGene injection
	Hakai cris (gRNA 2+3)/cyo #M3	Hakai gRNA (2+3)	II	this study	BestGene injection
	Hakai cris (gRNA 2+3)/cyo #M4	Hakai gRNA (2+3)	II	this study	BestGene injection
UAS cDNA lines	UAS Mettl3-HA (1)/TM6c	Mettl3 cDNA	III	this study	BestGene injection
	UAS Mettl3-HA (5)/TM6c	Mettl3 cDNA	III	this study	BestGene injection
	UAS Mettl14-HA/TM6c	Mettl14 cDNA	III	this study	BestGene injection
	UAS Mettl4-HA (1)/cyo GFP	Mettl4 cDNA	II	this study	BestGene injection
	UAS Mettl4-HA (2)/cyo GFP	Mettl4 cDNA	II	this study	BestGene injection
	UAS Mettl4-HA (3)/TM6c	Mettl4 cDNA	III	this study	BestGene injection
	UAS CG17807-HA (1)/TM6c	CG17807 cDNA	III	this study	BestGene injection
	UAS CG17807-HA (2)/cyo GFP	CG17807 cDNA	II	this study	BestGene injection
	UAS CG6144-HA (1)/cyo GFP	CG6144 cDNA	II	this study	BestGene injection
	UAS CG6144-HA (2)/cyo GFP	CG6144 cDNA	II	this study	BestGene injection
	UAS CG14130-HA (1)/cyo GFP	CG14130 cDNA	II	this study	BestGene injection
	UAS CG14130-HA (2)/cyo GFP	CG14130 cDNA	II	this study	BestGene injection
	UAS Ythdc1 - FlagMyc/TM6c	Ythdc1 cDNA	III	this study	BestGene injection
Mutant fly lines	Mettl3 Dcat (9C2)/TM6c	Mettl3 mutant Dcat	III	this study	W1118 background
	Mettl3 Dcat/TM6c	Mettl3 mutant Dcat	III	this study	Oregon-R background
	Mettl3 Dcat/TM3, Sb	Mettl3 mutant Dcat	III	this study	Oregon-R background
	Mettl3 null (2A2)/TM6c	Mettl3 mutant null	III	this study	W1118 background
	Mettl3 null null/TM6b	Mettl3 mutant null	III	this study	Oregon-R background
	Mettl3 null null/TM6c	Mettl3 mutant null	III	this study	Oregon-R background
	Mettl14 fs/cyo GFP	Mettl14 mutant (frame shift)	II	this study	Oregon-R background
	Mettl14 Dcut/cyo	Mettl14 mutant (deletion)	II	this study	
	Fl(2)d D52/cyo GFP	Fl(2)d mutant	II	this study	
	Fl(2)d D23/cyo GFP	Fl(2)d mutant	II	this study	
	Fl(2)d D24/cyo GFP	Fl(2)d mutant	II	this study	
	Mettl4 D2/Mettl4 D2	Mettl4 mutant (null)	III	this study	Oregon-R background
	Ythdc1 D34/dfd EYFP TM3, Sb	Ythdc1 mutant	III	this study	
	Ythdc1 D34/TM6b	Ythdc1 mutant	III	this study	Oregon-R background
	Ythdf D5/TM6c	Ythdf mutant	III	this study	
	Ythdf D5 (5B1)/TM6c	Ythdf mutant	III	this study	W1118 background
	CG6144 D2/cyo GFP	CG6144 mutant	II	this study	
	CG14130 D6/CG14130 D6	CG14130 mutant	III	this study	
	Hakai mutant (MS - ha'/cyo GFP)	Hakai mutant	II	Matthias Soller	
	Hakai mutant (MS - 7526/cyo GFP)	Hakai mutant	II	Matthias Soller	
sxlM8/sxl7B0	Sxl mutant	X	Matthias Soller		
Recombined lines	24BGal4, Mettl3 Dcat /TM6c	24BGAL4 driver, Mettl3 mutant Dcat	II; III	this study	
	ElavGAL4 (x); Mettl3 Dcat /TM6c	ElavGAL4 driver Mettl3 mutant Dcat	X; III	this study	
	TubGAL4/cyo; Mettl3 Dcat /TM6c	Tubulin GAL4 driver, Mettl3 mutant Dcat	II; III	this study	
	UAS Mettl3-HA/cyo; Mettl3 Dcat /TM6c	Mettl3 cDNA, Mettl3 mutant Dcat	II; III	this study	
	W+, UAS Mettl3-HA; Mettl3 Dcat /S-T	Mettl3 cDNA, Mettl3 mutant Dcat	II; III	this study	
	UAS Mettl3-HA/cyoGFP; Mettl3 null/TM6c	Mettl3 cDNA, Mettl3 mutant null	II; III	this study	Oregon-R background
	TubGAL4/cyoGFP; Mettl3 null /TM6c	Tubulin GAL4 driver, Mettl3 mutant null	II; III	this study	Oregon-R background
	Mettl14 fs/cyo GFP; Mettl3 Dcat/TM6b	Mettl14 mutant fs, Mettl3 mutant Dcat	II; III	this study	
	Def Mettl14/cyo; Mettl3 Dcat/TM6b	Mettl14 deficiency, Mettl3 mutant Dcat	II; III	this study	
TubGAL4/cyoGFP; Ythdc1 D34/TM6b	Tubulin GAL4 driver, Ythdc1 mutant	II; III	this study	Oregon-R background	

Materials and methods

	Stock name	Line description	Chr.	Source	Comment
Deficiency and RNAi lines	dsMettl3 (1) (#80448)	Mettl3 RNAi (y1 v1; P{TRiP.HMS06028}attP2)		Bloomington	
	dsMettl3 (2) (#41590)	Mettl3 RNAi (y1 v1; P{TRiP.GL01126}attP2/TM3, Sb1)		Bloomington	
	shmir Nito (#34848)	Nito shRNA		DRSC, Harvard	
	shmir Fl(2)d (#55674)	Fl(2)d shRNA		DRSC, Harvard	
	shmir GFP (#41552)	GFP shRNA		Bloomington	
	dsFlacc (KK110253) (#v110253)	Flacc RNAi (P{KK105583}VIE-260B)		VDRC, Vienna	
	dsFlacc (GD35212) (#v35212)	Flacc RNAi (w1118; P{GD12212}v35212)		VDRC, Vienna	
	Def Mettl3/TM6b (Df(3R)Exel6197)	Mettl3 deficiency		Bloomington	
	Def Mettl14/Cyo (Df(2L)BSC200/Cyo)	Mettl14 deficiency		Bloomington	
	Def Ythdc1/TM6c (Df(3L)Exel6094)	Ythdc1 deficiency		Bloomington	
Driver lines	DomeGAL4;UASGFP/FM7i	leg discs, genitalia discs driver		Erica Bach	
	Tub-GAL4	ubiquitous driver		Bloomington	
	elavC155-GAL4	neuronal driver		Bloomington	
	how24B-GAL4	muscular driver		Bloomington	
	DdcGAL4	serotonergic, dopaminergic neuronal driver		lab stock	
	Trh(1)GAL4	serotonergic neuronal driver		lab stock	
	Trh(2)Gal4	serotonergic neuronal driver		lab stock	
	PleGAL4	dopaminergic neuronal driver		lab stock	
	ChATGAL4	cholinergic neuronal driver		lab stock	
	NPF(1)GAL4	peptidergic neuronal driver		lab stock	
	NPF(2)GAL4	peptidergic neuronal driver		lab stock	
	Vglut(1)GAL4	glutamatergic neuronal driver		lab stock	
	Vglut(2)GAL4	glutamatergic neuronal driver		lab stock	
Other fly lines	W1118	W1118 WT flies		lab stock	
	Canton-S	Canton-S		lab stock	
	Oregon-R	Oregon-R		lab stock	
	AptXa/CyoGFP-TM6c	balancer line		lab stock	
	CAS0001	Cas9 line		DGRC, Indiana	
	TBX0008	balancer line		DGRC, Indiana	
	TBX0002	transformation line		DGRC, Indiana	

Table 6. Flies generated and used in this study.

Note: Oligonucleotides used for cloning and generating gRNA plasmids for gRNA lines are listed in **Table 8**.

Oligonucleotides used in this study

Primers used for qPCR validations of transcript levels		Primers used for splicing validations	
Name	Sequence 5'--> 3'	Name	Sequence 5'--> 3'
CBP20 qF	GGGGTTATGGCAAACGTGTTG	FI(2)d 5UTR-1 prox-ss qF	tttccaccgacctgtcac
CBP20 qR	GGGGGCTTATAGTCTTTACAGTCA	FI(2)d 5UTR qR	ggacctgttccagcttgagat
CBP80 qF	ttccagactgtgctgaatttg	FI(2)d 5UTR-2 dist-ss qF	AGCAGCAGCAACATGCAG
CBP80 qR	cacggaataccgaatggaat	FI(2)d 5UTR all isoforms F	CAGCAGCAAACGAGAAATCA
CG7358 short qPCR F	tgatttcgaatggatgaacg	CG8929 5UTR qF	TTGCCAATAAAACGTTAACAGC
CG7358 short qPCR R	cggcaatgatttcgctctttg	CG8929 5UTR long qR	GCTCTGGCAATTATGTAAACGA
CG7358 long qPCR F	TACTGGCTCAGGTAAGCAAACATA	CG8929 5UTR short qR	CGCGAACACACTTTACCA
CG7358 long qPCR R	GTGCGGATTAGCTCCTGTTT	H 5UTR qF	GTGCCCAAAACATGAAAT
ZC3H13 qF	ACATCAGGGAAGGAATGACG	H spliced 5UTR qR	ACGTCATTAAGCAGGGCCATT
ZC3H13 qR	CCCGATCTCTCTCTAGCC	H 5UTR qR	tccaaccgcattataggaca
Hakai short qR	tggtcctaactaagctgtcc	Dsp1 5UTR qF	TGCATCATACATTTCGCTTT
Hakai split long qF	AAGCAGCGCAAGCTCCTCGA	Dsp1 spliced 5UTR qR	TTCTATATCTTTACITTTTATTACC
Hakai common qR	CTACCGATGTTACCGACACC	Dsp1 5UTR qR	ttagtttagcacaagtagct
Mettl3 qF	AAGGAACTCGTTGAGGCTGA	hts 5UTR qF	GCACTTCTTTTTCGCTTC
Mettl3 qR	CACCTGTGTGGAGACAATGG	hts spliced 5UTR qR	TGGTTTTACAGCCGTAATTC
Mettl14 qF	AAGCGCTGTTTGTCTTATG	hts 5UTR qR	aaaattgcccgtcctaacag
Mettl14 qR	GCATTACCAAAGCCTTTTTTC	Aldh-III 5UTR qF	CGGTGAACGGTTGTCAAAG
Mettl4 qF2	TTGAAATGCAAAAAGAAAATGA	Aldh-III spliced 5UTR qR	TCGTTTCTGGTTCTGGTACTC
Mettl4 qR2	CGGTAGCTAATTTACCTCCTCT	Aldh-III 5UTR qR	gcacggcaaatgtaaacac
FI(2)d qF	CGGTCAATCTCCTGTTCGAG	dl 5UTR prox ss qF	TGCTTTAAGCTTCCGCTCTC
FI(2)d qR	GACAGCTGTTCTGGGTCTC	dl 5UTR exon qR	CAAGGAGTGATCGAAATCTCG
Ythdf qF	CCGAGAAAGTGCAAAAGGAT	dl 5UTR dist ss qF	CGAATAATCGAAAACAAAAACA
Ythdf qR	AAACCTTGGCTCTGCTGAAG	Sxl-L2-F	ACACAAGAAAGTTGAACAGAGG
Ythdc1 qF	GGCTCGAGTTATGCGAGAAA	Sxl-4-R	CATTCCGGATGGCAGAGAATGG
Ythdc1 qR	GGTGTGTGATTTGATCTCT		
Hrb27C qF	CGATCTGGGACCTTCTTA	Primers used for validation of MeRIP peaks	
Hrb27C qR	GCGGACTTCTTCTCTCT	Name	Sequence 5'--> 3'
Vir qF	CTGATGACCATCCAGGGAGT	Rpl15 MeRIP qF	AGGATGCATTTATGGCAAGC
Vir qR	GATGGCTGTGAGGTCCTTGT	Rpl15 MeRIP qR	GCGCAATCCAATACGAGTTC
Nito qF	GCCAGTACGGTTCCAGATGT	BRWD3 MeRIP qF	GCAAAAACCTCCTCCTCCTC
Nito qR	CCGTCCGCAAAATGAAACTT	BRWD3 MeRIP qR	GCTGTTCCGATGGAGTTAT
Qkr58E-1 qF	GTGCTCAGAGACCCCTGA	Vinc MeRIP qF	GCTGGTGTCTCATCTGAGG
Qkr58E-1 qR	ACGCGTTGGTCTTCTCATT	Vinc MeRIP qR	GCGGCTGAGACAGGAACTA
Flacc qF	ACGAGACGAGAGCGGACCC	CG4165 MeRIP qF	GGCAGGACTTCTCTGGAC
Flacc qR	TCTTGGTGGTGGTAGTG	CG4165 MeRIP qR	AAGACTGAGCTCCGACTTG
Rpl15-qF	AGGATGCATTTATGGCAAGC	Fak MeRIP qF	GAGTTGGGTCTCTGCAAAC
Rpl15-qR	GCGCAATCCAATACGAGTTC	Fak MeRIP qR	CACGAACTATTCAGCGGATAA
Hakai qF	caagaaaatcgacgacagca	CG3267 MeRIP qF	CAGGAGATTGCCCAAGAAAA
Hakai qR	ctcctcatgaccgaatctt	CG3267 MeRIP qR	TCCGAAGTGCAGTTGTCTG
CG17807 qF	GGAGACGTGCTTTGGTTTA	Hairless MeRIP qF	GCCAACTTAAGCAGGACGAC
CG17807 qR	CTGCTCAGTGGTACGCTCT	Hairless MeRIP qR	GGCAAAAAGCCATTTGAGG
CG6144 qF	GGCAAGTTAATAACACCCAAAGT	AldhIII MeRIP qF	CAACACAGCTTTCGACTACA
CG6144 qR	GCAAGGATAACGAGGACTTCA	AldhIII MeRIP qR	AGGTGTTGGGGTCAAGTA
CG14130 qF	TGATATCCAGAACAGAACTCCT	Primers used for in situ probes	
CG14130 qR	ATGGCACCTCTCAAAATGT	Name	Sequence 5'--> 3'
Mettl4 qF	TTCAATATCGGAAATGTTGAAAT	elav SP6 F	attaggtgacactatagaagagGTGAAGCTGATACGCGACAA
Mettl4 qR	CTTGTGATCCGAAACACTCG	elav T7 R	ttaatagctactactataggagagGGCTTTGTTGGTCTTGAAGC
CG4036 qF	ACATCAATGGCGTAGACATCC	Mettl3 SP6 F	attaggtgacactatagaagagCAGCTGGAGATGGTGAAC
CG4036 qR	TTTATTGCCAGAAATCTGAGACTT	Mettl3 T7 R	ttaatagctactactataggagagTCAGGCTCGACTGACTTTGTG
CG33250-AIkB qF	TGCAAAAGTACCAGTCTGATTT	Mettl14 T7 F	ttaatagctactactataggagagTAATCAGAAATGCCGCCACTA
CG33250-AIkB qR	TTTCTTGATCATCCCTTGA	Mettl14 SP6 R	attaggtgacactatagaagagCCCAAGCAGAAATGTTTCGAT
CG1074 qF	AGGCGGCTACTCACCTATGA	FI(2)d T7 R-long isoform	ttaatagctactactataggagagTCGATCTCATCTTCGAGCAA
CG1074 qR	TACCGATCCCTGAAATCCTG	Ythdf T7 F	ttaatagctactactataggagagACCGATCAGCGCAATAAGAG
CG7544 qF	GACGCCGACTATACAAAA	Ythdf SP6 R	attaggtgacactatagaagagGACCGCCGATTTAATTTGT
CG7544 qR	CACAGAAACCTTGCCATTGA	Ythdc1 T7 F	ttaatagctactactataggagagCGAATCGAATGGTGGAGACT
CG9154 qF	TGTTTATTGATTTGAATGCTC	Ythdc1 SP6 R	attaggtgacactatagaagagCCGTGTCTCGGAATAGGT
CG9154 qR	CGAGATGCTGCTGCCATAA	Flacc SP6 R	attaggtgacactatagaagagGCCAGATCCATAAGGCAATC
CG9531 qF	GCCGATGGTGAAGACCATTA	Flacc T7 F	ttaatagctactactataggagagAGTACCGTACCTCGAAACG
CG9531 qR	CGAATCTCTCGCTGATAC	Hakai SP6 R	attaggtgacactatagaagagGTATTGCGACTGCTGCCAGTTGC
CG9666 qF	TCGAAGGATATTGAGGTGGA	Hakai T7 F	ttaatagctactactataggagagCCTTAAGTGAACCACAAGGTTG
CG9666 qR	TGTCCAAAATAAATGCAACTGA		
CG9960 qF	GCGAGCATTTGTGCATACTG	Templates obtained from DRSC RNAi Screening centre	
CG9960 qR	ATTTGATGCTATTGACAGGAGTC	Gene	Amplicon
		Hrb27C	DRSC32136
		nonA	DRSC20357
		nonA-1	DRSC25387
		CG4266	DRSC04456
		CG7903	DRSC16338
		nonA	DRSC17017
		caz	DRSC23280
		pAbp	DRSC07659
		ssx	DRSC38980
		Nito	DRSC05943
		Syp	DRSC29126
		CG30122	DRSC34694
		Ago2	DRSC31769
Primers used for RIP			
Name	Sequence 5'--> 3'		
FI(2)d qF	CGGTCAATCTCCTGTTCGAG		
FI(2)d qR	GACAGCTCGTTCTGGGTCTC		
FI(2)d 5UTR qF	tttccaccgacctgtcac		
FI(2)d 5UTR qR	AGCAGCAGCAACATGCAG		
Hairless qF	GTGCCCAAAACATGAAAAAT		
Hairless qR	tccaaccgcattataggaca		
Dsp1 qF	TGCATCATACATTTCGCTTT		
Dsp1 qR	ttagtttagcacaagtagct		
AldhIII qF	CAACAGCGTTCGACTACA		
AldhIII qR	AGGTGTTGGGGTCAAGTA		

Materials and methods

Primers used for dsRNA synthesis			
Name	Sequence 5' --> 3'	Name	Sequence 5' --> 3'
Mettl3 T7 F	ttaatacgactcactatagggagacagcctggagatggtgaaact	Zn72D T7 R	ttaatacgactcactatagggagattcgtgtattgtcgggttc
Mettl3 T7 R	ttaatacgactcactatagggagatcaggcactcagcttttgg	Qkr58E-3 T7 F	ttaatacgactcactatagggagaccccaagcaggttactgag
Mettl3 T7 F2	ttaatacgactcactatagggagacactggctcattggctaaac	Qkr58E-3 T7 R	ttaatacgactcactatagggagagccgcatagctttcattgctcag
Mettl3 T7 R2	ttaatacgactcactatagggagacatctggataaacgctcttggga	TBPH T7 F	ttaatacgactcactatagggagacgacttgcgagatatttc
Mettl14 T7 F	ttaatacgactcactatagggagataatcagaaatgccccaacta	TBPH T7 R	ttaatacgactcactatagggagattttggcttcgacgttgt
Mettl14 T7 R	ttaatacgactcactatagggagatgatcagttccctcaacttgg	rump T7 F	ttaatacgactcactatagggagagctcaagcaggtctcaaacg
Mettl14 T7 F2	ttaatacgactcactatagggagataacagtagtcgacagtgaaattcc	rump T7 R	ttaatacgactcactatagggagaccgactctcggaaactgttc
Mettl14 T7 R2	ttaatacgactcactatagggagactcagcaaataggtctgtatagc	CG8929 T7 F	ttaatacgactcactatagggagactcattaccctggaaagc
Mettl4 T7 F	ttaatacgactcactatagggagacgaagcatatgacgaaatitaagc	CG8929 T7 R	ttaatacgactcactatagggagaggatattggcgactggac
Mettl4 T7 R	ttaatacgactcactatagggagatgggtgcaatgttactactttacg	yps T7 F	ttaatacgactcactatagggagagcaacgacacagagaggat
Mettl4 T7 F2	ttaatacgactcactatagggagactgggagatggctacaac	yps T7 R	ttaatacgactcactatagggagatggaccattgttgaagttgc
Mettl4 T7 R2	ttaatacgactcactatagggagacatctctgtaaggctcttc	fmr1 T7 F	ttaatacgactcactatagggagagccagcaggaagatggaga
Fl(2)d F T7	ttaatacgactcactatagggagacggactctaataaccggcaaaa	fmr1 T7 R	ttaatacgactcactatagggagatcttcggtgtgtgtgtgt
Fl(2)d R T7	ttaatacgactcactatagggagaggtgtgtcactggctgatg	Hakai T7 F	ttaatacgactcactatagggagacttaagtggaaaccaagggtg
Fl(2)d T7 F2	ttaatacgactcactatagggagaccctatgaaaagcaacag	Hakai T7 R	ttaatacgactcactatagggagatttgcgacttgcgcaattgc
Fl(2)d T7 R2	ttaatacgactcactatagggagagatcgagcagagcagtg	Hrb27C T7 F	ttaatacgactcactatagggagaggaagcagagaggggcaaaa
Ythdf T7 F	ttaatacgactcactatagggagaccgatcaccgcaataagag	Hrb27C T7 R	ttaatacgactcactatagggagaccaccaggaagacccttcta
Ythdf T7 R	ttaatacgactcactatagggagacacgcccgaattttatgtt	Flacc T7 F	ttaatacgactcactatagggagagtaccgtgacctgaaaccg
Ythd1 T7 F2	ttaatacgactcactatagggagactctgagctgctcggctaga	Flacc T7 R	ttaatacgactcactatagggagagccagcagcagcagcagc
Ythdf T7 R2	ttaatacgactcactatagggagacgcaatttatgtgtcgagag	CBP80 T7F	ttaatacgactcactatagggagacctggaactgcaactagag
Ythdc1 T7 F	ttaatacgactcactatagggagacgaatcgaatggtggagact	CBP80 T7R	ttaatacgactcactatagggagaattgacgaacgctgaaac
Ythdc1 T7 R	ttaatacgactcactatagggagaccgtgtgtcggaaataggt	CBP20 T7F	ttaatacgactcactatagggagacacagcagatctccgaact
Ythdc1 T7 F2	ttaatacgactcactatagggagacggagaccacaccatc	CBP20 T7R	ttaatacgactcactatagggagacctgctgctattcatctc
Ythdc1 T7 R2	ttaatacgactcactatagggagatcccgaattccgatagcc	CG17807-ds-F	ttaatacgactcactatagggagatcaaaaagtgactgaggtgtctcc
Vir T7 F	ttaatacgactcactatagggagatactttgaggcgggtgtcc	CG17807-ds-R	ttaatacgactcactatagggagactgaaagtgactgcaattctaccg
Vir T7 R	ttaatacgactcactatagggagaaacatgaccagcagggattc	CG6144-ds-F	ttaatacgactcactatagggagaggatttaccgggctttgaaatgc
Vir T7 F2	ttaatacgactcactatagggagacatcacactggccatctaccg	CG6144-ds-R	ttaatacgactcactatagggagaggtggaaatctgaggatcacgctcg
Vir T7 R2	ttaatacgactcactatagggagatgcccttcaaaagaccaaca	CG14130-ds-F	ttaatacgactcactatagggagacggtggaagcaacgctataaaagc
Hrb87F T7 F	ttaatacgactcactatagggagactaccgacacagatgatg	CG14130-ds-R	ttaatacgactcactatagggagactctcgtttttaaaggccattcagtc
Hrb87F T7 R	ttaatacgactcactatagggagattgaatctccaccaccac	CG7544-T7 F	ttaatacgactcactatagggagagtttgggtgccacattagc
Qkr58E-2 T7 F	ttaatacgactcactatagggagaccatcaagctgtcccaaaa	CG7544-T7 R	ttaatacgactcactatagggagatagtggtcggagtggaag
Qkr58E-2 T7 R	ttaatacgactcactatagggagactctctctcctgcaccacta	CG9154-T7 F	ttaatacgactcactatagggagagagagatcaaaaagcggaaag
Hrb98DE T7 F	ttaatacgactcactatagggagactaccgtaccaccgacgag	CG9154-T7 R	ttaatacgactcactatagggagaaacttggctgcccagattgc
Hrb98DE T7 R	ttaatacgactcactatagggagactttgtccacgggatcgta	CG9531-T7 F	ttaatacgactcactatagggagacaggtcaactatggcacaac
lark T7 F	ttaatacgactcactatagggagattcatcgggaaattcttgacg	CG9531-T7 R	ttaatacgactcactatagggagaccagggcattaaagttctca
lark T7 R	ttaatacgactcactatagggagacatccatgatcgggtcacc	CG1074-T7 F	ttaatacgactcactatagggagactaccgcccaactcaacaaat
Pep T7 F	ttaatacgactcactatagggagaggctaaagatcgacagcagcag	CG1074-T7 R	ttaatacgactcactatagggagagtttttaggtgctcgcaga
Pep T7 R	ttaatacgactcactatagggagatctccacgctcctgctcacc	CG9960-T7 F	ttaatacgactcactatagggagacttgagcccagaagatttccg
sqd T7 F	ttaatacgactcactatagggagaccattcgacaagcaaaagt	CG9960-T7 R	ttaatacgactcactatagggagatgaaacttcaagcccggaaac
sqd T7 R	ttaatacgactcactatagggagaccgcatagtagtcgccata	CG9666-T7 F	ttaatacgactcactatagggagattggaacagatccccactcc
glo T7 F	ttaatacgactcactatagggagatctgccaagcctgatgaac	CG9666-T7 R	ttaatacgactcactatagggagaaactttagctgagctgagat
glo T7 R	ttaatacgactcactatagggagagccgacattgtgttttct	CG33250-T7 F	ttaatacgactcactatagggagacaaatgccagggctttaaact
larp T7 F	ttaatacgactcactatagggagagaatctggtgcccaaaatg	CG33250-T7 R	ttaatacgactcactatagggagaaaattgaggggttgcacaact
larp T7 R	ttaatacgactcactatagggagaaagAACGACAGCAAGCGGTA	CG4036-T7 F	ttaatacgactcactatagggagagctgcgaacagagactttcat
Imp T7 F	ttaatacgactcactatagggagacaaaactcggccacaacaa	CG4036-T7 R	ttaatacgactcactatagggagatcccggtaggctacacaaac
Imp T7 R	ttaatacgactcactatagggagacaaagcaactcaaccgtga	CG11837-T7 F	ttaatacgactcactatagggagaaaccaccatgctggagaaag
Qkr58E-1 T7 F	ttaatacgactcactatagggagacatacCAAAGCCCGAGATA	CG11837-T7 R	ttaatacgactcactatagggagaaattgaaagccagcagagag
Qkr58E-1 T7 R	ttaatacgactcactatagggagatgctgccaatagatttggaa	CG42631-T7 F	ttaatacgactcactatagggagacagccaggaacagccttag
Qkr58E-1 T7 F2	ttaatacgactcactatagggagatgcttcttcaaaagcccaaaag	CG42631-T7 R	ttaatacgactcactatagggagacgatcttctggaggaagcag
Qkr58E-1 T7 R2	ttaatacgactcactatagggagaggtgtgaaatagttgatttga	CG3910-T7 F	ttaatacgactcactatagggagagggcccaactatagcaccaaa
Zn72D T7 F	ttaatacgactcactatagggagataaccaatgccacctacgc	CG3910-T7 R	ttaatacgactcactatagggagacagagagcgggtagactctcg

Table 7. Oligonucleotides used in this study.

Note: Oligonucleotides used for cloning and generating plasmids are listed Table 8

Plasmids generated and used in this study

Construct Name	cloned gene	Plasmid backbone	Resistance	Fwd oligo	Rev oligo
Actin-GAL4	Actin-GAL4	Actin-GAL4	Amp	-	-
pGAD424 GW *	-	gateway pGAD424	Amp, Cm	-	-
er pGAD424 GW	e(r)	gateway pGAD424	Amp	see pENTR-D-TOPO	see pENTR-D-TOPO
Mettl3 pGAD424 GW	Mettl3	gateway pGAD424	Amp	see pENTR-D-TOPO	see pENTR-D-TOPO
Mettl14 pGAD424 GW	Mettl14	gateway pGAD424	Amp	see pENTR-D-TOPO	see pENTR-D-TOPO
Fl2 d long pGAD424 GW	Fl2 d long	gateway pGAD424	Amp	see pENTR-D-TOPO	see pENTR-D-TOPO
Nito pGAD424 GW	Nito	gateway pGAD424	Amp	see pENTR-D-TOPO	see pENTR-D-TOPO
Vir pGAD424 GW	Vir	gateway pGAD424	Amp	see pENTR-D-TOPO	see pENTR-D-TOPO
Hakai short pGAD424 GW	Hakai short	gateway pGAD424	Amp	see pENTR-D-TOPO	see pENTR-D-TOPO
Hakai long pGAD424 GW	Hakai long	gateway pGAD424	Amp	see pENTR-D-TOPO	see pENTR-D-TOPO
Flacc pGAD424 GW	Flacc long	gateway pGAD424	Amp, Cm	-	-
pGB9T GW *	-	gateway pGB9T	Amp, Cm	-	-
er pGB9T GW	e(r)	gateway pGB9T	Amp	see pENTR-D-TOPO	see pENTR-D-TOPO
Mettl3 pGB9T GW	Mettl3	gateway pGB9T	Amp	see pENTR-D-TOPO	see pENTR-D-TOPO
Mettl14 pGB9T GW	Mettl14	gateway pGB9T	Amp	see pENTR-D-TOPO	see pENTR-D-TOPO
Fl2 d long pGB9T GW	Fl2 d long	gateway pGB9T	Amp	see pENTR-D-TOPO	see pENTR-D-TOPO
Nito pGB9T GW	Nito	gateway pGB9T	Amp	see pENTR-D-TOPO	see pENTR-D-TOPO
Vir pGB9T GW	Vir	gateway pGB9T	Amp	see pENTR-D-TOPO	see pENTR-D-TOPO
Hakai short pGB9T GW	Hakai short	gateway pGB9T	Amp	see pENTR-D-TOPO	see pENTR-D-TOPO
Hakai long pGB9T GW	Hakai long	gateway pGB9T	Amp	see pENTR-D-TOPO	see pENTR-D-TOPO
Flacc pGB9T GW	Flacc long	gateway pGB9T	Amp	see pENTR-D-TOPO	see pENTR-D-TOPO
ctr gateway-UAS-FlagMyc	-	gateway-UAS-FlagMyc	Amp	-	-
Mettl3-UAS-FlagMyc	Mettl3	gateway-UAS-FlagMyc	Amp	see pENTR-D-TOPO	see pENTR-D-TOPO
Mettl14-UAS-FlagMyc	Mettl14	gateway-UAS-FlagMyc	Amp	see pENTR-D-TOPO	see pENTR-D-TOPO
Mettl4-UAS-FlagMyc	Mettl4	gateway-UAS-FlagMyc	Amp	see pENTR-D-TOPO	see pENTR-D-TOPO
CG6144-UAS-FlagMyc	CG6144	gateway-UAS-FlagMyc	Amp	see pENTR-D-TOPO	see pENTR-D-TOPO
CG17807-UAS-FlagMyc	CG17807	gateway-UAS-FlagMyc	Amp	see pENTR-D-TOPO	see pENTR-D-TOPO
CG14130-UAS-FlagMyc	CG14130	gateway-UAS-FlagMyc	Amp	see pENTR-D-TOPO	see pENTR-D-TOPO
Fl2 d-short-UAS-FlagMyc	Fl2 d-short	gateway-UAS-FlagMyc	Amp	see pENTR-D-TOPO	see pENTR-D-TOPO
Yhd1-UAS-FlagMyc	Yhd1	gateway-UAS-FlagMyc	Amp	see pENTR-D-TOPO	see pENTR-D-TOPO
Yhd1-UAS-FlagMyc	Yhd1	gateway-UAS-FlagMyc	Amp	see pENTR-D-TOPO	see pENTR-D-TOPO
Flacc-UAS-FlagMyc	Flacc long	gateway-UAS-FlagMyc	Amp	see pENTR-D-TOPO	see pENTR-D-TOPO
ZC3H13-UAS-FlagMyc	ZC3H13 human	gateway-UAS-FlagMyc	Amp	see pENTR-D-TOPO	see pENTR-D-TOPO
Nito-UAS-FlagMyc	Nito	gateway-UAS-FlagMyc	Amp	-	-
Mettl3-UAS-HA	Mettl3	gateway-UAS-HA	Amp	see pENTR-D-TOPO	see pENTR-D-TOPO
Mettl14-UAS-HA	Mettl14	gateway-UAS-HA	Amp	see pENTR-D-TOPO	see pENTR-D-TOPO
Mettl4-UAS-HA	Mettl4	gateway-UAS-HA	Amp	see pENTR-D-TOPO	see pENTR-D-TOPO
CG6144-UAS-HA	CG6144	gateway-UAS-HA	Amp	see pENTR-D-TOPO	see pENTR-D-TOPO
CG17807-UAS-HA	CG17807	gateway-UAS-HA	Amp	see pENTR-D-TOPO	see pENTR-D-TOPO
CG14130-UAS-HA	CG14130	gateway-UAS-HA	Amp	see pENTR-D-TOPO	see pENTR-D-TOPO
Fl2 d-short-UAS-HA	Fl2 d-short	gateway-UAS-HA	Amp	see pENTR-D-TOPO	see pENTR-D-TOPO
Yhd1-UAS-HA	Yhd1	gateway-UAS-HA	Amp	see pENTR-D-TOPO	see pENTR-D-TOPO
Yhd1-UAS-HA	Yhd1	gateway-UAS-HA	Amp	see pENTR-D-TOPO	see pENTR-D-TOPO
Nito-UAS-HA	Nito	gateway-UAS-HA	Amp	see pENTR-D-TOPO	see pENTR-D-TOPO
Vir-UAS-HA	Vir	gateway-UAS-HA	Amp	see pENTR-D-TOPO	see pENTR-D-TOPO
Flacc-actin-FlagHA	Flacc long	gateway-actin-FlagHA	Amp	see pENTR-D-TOPO	see pENTR-D-TOPO
ZC3H13 human actin-Myc	ZC3H13 human	gateway-actin-Myc	Amp	aa agcggcgccttbaagacacacacajgttctggt	aa agcggcgccttbaagacacacacajgttctggt
Hrb27C-UAS-HA	Hrb27C	gateway-UAS-HA	Amp	see pENTR-D-TOPO	see pENTR-D-TOPO
pENTR-D-TOPO-Mettl3	Mettl3	gateway-UAS-HA	Amp	see pENTR-D-TOPO	see pENTR-D-TOPO
pENTR-D-TOPO-Fl2 d-short	Fl2 d-short	pENTR-D-TOPO	Kn	CGTGGAGTAGTCCAGCTCCGCT	CGTGGAGTAGTCCAGCTCCGCT
pENTR-D-TOPO-Fl2 d-long	Fl2 d-long	pENTR-D-TOPO	Kn	GGTGGAGTAGTCCAGCTCCGCT	GGTGGAGTAGTCCAGCTCCGCT
pENTR-D-TOPO-Yhd1	Yhd1	pENTR-D-TOPO	Kn	GGCCTGTGTCCTCCGATAGCT	GGCCTGTGTCCTCCGATAGCT
pENTR-D-TOPO-Yhd1-RB	Yhd1	pENTR-D-TOPO	Kn	TGAATAITTCATTCCTCCGATTT	TGAATAITTCATTCCTCCGATTT
pENTR-D-TOPO-Yhd1-RC	Yhd1	pENTR-D-TOPO	Kn	TGAATAITTCATTCCTCCGATTT	TGAATAITTCATTCCTCCGATTT
pENTR-D-TOPO-Vir	Vir	pENTR-D-TOPO	Kn	TCTCAGTAGGATGGCTGGAA	TCTCAGTAGGATGGCTGGAA
pENTR-D-TOPO-Nito	Nito	pENTR-D-TOPO	Kn	GGCCTGTGTCCTCCGATAGCT	GGCCTGTGTCCTCCGATAGCT
pENTR-D-TOPO-Hakai short	Hakai short	pENTR-D-TOPO	Kn	TCGTAGTATTGGACGTCTGCCA	TCGTAGTATTGGACGTCTGCCA
pENTR-D-TOPO-Hakai long	Hakai long	pENTR-D-TOPO	Kn	GGAGCCATAGTACCCTGCCCT	GGAGCCATAGTACCCTGCCCT
pENTR-D-TOPO-Flacc	Flacc long	pENTR-D-TOPO	Kn	TTTGACATCCAGAAAGCTGGCT	TTTGACATCCAGAAAGCTGGCT

Literature

- A Alemu E., He C. and Klungland A. (2016). ALKBHs-facilitated RNA modifications and de-modifications. *DNA Repair (Amst)* 44: 87-91.
- Abby E., Tourpin S., Ribeiro J., Daniel K., Messiaen S., Moison D., Guerquin J., Gaillard J.C., Armengaud J., Langa F., Toth A., Martini E. and Livera G. (2016). Implementation of meiosis prophase I programme requires a conserved retinoid-independent stabilizer of meiotic transcripts. *Nat Commun* 7: 10324.
- Abeles A., Brendler T. and Austin S. (1993). Evidence of two levels of control of P1 oriR and host oriC replication origins by DNA adenine methylation. *J Bacteriol* 175(24): 7801-7807.
- Adams J.M. and Cory S. (1975). Modified nucleosides and bizarre 5'-termini in mouse myeloma mRNA. *Nature* 255(5503): 28-33.
- Adler M., Weissmann B. and Gutman A.B. (1958). Occurrence of methylated purine bases in yeast ribonucleic acid. *J Biol Chem* 230(2): 717-723.
- Agarwala S.D., Blitzblau H.G., Hochwagen A. and Fink G.R. (2012). RNA methylation by the MIS complex regulates a cell fate decision in yeast. *PLoS Genet* 8(6): e1002732.
- Aguilera M., Oliveros M., Martínez-Padrón M., Barbas J.A. and Ferrús A. (2000). Ariadne-1: a vital Drosophila gene is required in development and defines a new conserved family of ring-finger proteins. *Genetics* 155(3): 1231-1244.
- Aguilo F., Zhang F., Sancho A., Fidalgo M., Di Cecilia S., Vashisht A., Lee D.F., Chen C.H., Rengasamy M., Andino B., Jahouh F., Roman A., Krig S.R., Wang R., Zhang W., Wohlschlegel J.A., Wang J. and Walsh M.J. (2015). Coordination of m(6A) mRNA Methylation and Gene Transcription by ZFP217 Regulates Pluripotency and Reprogramming. *Cell Stem Cell* 17(6): 689-704.
- Akichika S., Hirano S., Shichino Y., Suzuki T., Nishimasu H., Ishitani R., Sugita A., Hirose Y., Iwasaki S., Nureki O. and Suzuki T. (2019). Cap-specific terminal N(6)-methylation of RNA by an RNA polymerase II-associated methyltransferase. *Science* 363(6423): eaav0080.
- Alarcon C.R., Goodarzi H., Lee H., Liu X., Tavazoie S. and Tavazoie S.F. (2015a). HNRNPA2B1 Is a Mediator of m(6A)-Dependent Nuclear RNA Processing Events. *Cell* 162(6): 1299-1308.
- Alarcon C.R., Lee H., Goodarzi H., Halberg N. and Tavazoie S.F. (2015b). N6-methyladenosine marks primary microRNAs for processing. *Nature* 519(7544): 482-485.
- Ali Y.O., Escala W., Ruan K. and Zhai R.G. (2011). Assaying locomotor, learning, and memory deficits in Drosophila models of neurodegeneration. *J Vis Exp*(49): 2504.
- Almada A.E., Wu X., Kriz A.J., Burge C.B. and Sharp P.A. (2013). Promoter directionality is controlled by U1 snRNP and polyadenylation signals. *Nature* 499(7458): 360-363.
- Alt F.W., Bothwell A.L.M., Knapp M., Siden E., Mather E., Koshland M. and Baltimore D. (1980). Synthesis of secreted and membrane-bound immunoglobulin mu heavy chains is directed by mRNAs that differ at their 3' ends. *Cell* 20(2): 293-301.
- Amort T., Rieder D., Wille A., Khokhlova-Cubberley D., Riml C., Trixl L., Jia X.Y., Micura R. and Lusser A. (2017). Distinct 5-methylcytosine profiles in poly(A) RNA from mouse embryonic stem cells and brain. *Genome Biol* 18(1): 1.
- Amrani N., Ghosh S., Mangus D.A. and Jacobson A. (2008). Translation factors promote the formation of two states of the closed-loop mRNP. *Nature* 453(7199): 1276-1280.
- Anders M., Chelysheva I., Goebel I., Trenkner T., Zhou J., Mao Y., Verzini S., Qian S.B. and Ignatova Z. (2018). Dynamic m(6A) methylation facilitates mRNA triaging to stress granules. *Life Sci Alliance* 1(4): e201800113.
- Anderson A.M., Weasner B.P., Weasner B.M. and Kumar J.P. (2014). The Drosophila Wilms Tumor 1-Associating Protein (WTAP) homolog is required for eye development. *Developmental biology* 390(2): 170-180.
- Anderson S.J., Kramer M.C., Gosai S.J., Yu X., Vandivier L.E., Nelson A.D.L., Anderson Z.D., Beilstein M.A., Fray R.G., Lyons E. and Gregory B.D. (2018). N6-Methyladenosine Inhibits Local Ribonucleolytic Cleavage to Stabilize mRNAs in Arabidopsis. *Cell Reports* 25(5): 1146-1157.e1143.
- Angelova M.T., Dimitrova D.G., Dinges N., Lence T., Worpenberg L., Carré C. and Roignant J.-Y. (2018). The Emerging Field of Epitranscriptomics in Neurodevelopmental and Neuronal Disorders. *Frontiers in Bioengineering and Biotechnology* 6(46).
- Aparicio L.A., Valladares M., Blanco M., Alonso G. and Figueroa A. (2012). Biological influence of Hakai in cancer: a 10-year review. *Cancer Metastasis Reviews* 31(1-2): 375-386.
- Arakel E.C. and Schwappach B. (2018). Formation of COPI-coated vesicles at a glance. *Journal of Cell Science* 131(5): jcs209890.
- Arango D., Sturgill D., Alhusaini N., Dillman A.A., Sweet T.J., Hanson G., Hosogane M., Sinclair W.R., Nanan K.K., Mandler M.D., Fox S.D., Zengeya T.T., Andresson T., Meier J.L., Collier J. and Oberdoerffer S. (2018). Acetylation of Cytidine in mRNA Promotes Translation Efficiency. *Cell*.
- Arguello A.E., DeLiberto A.N. and Kleiner R.E. (2017). RNA Chemical Proteomics Reveals the N6-Methyladenosine (m6A)-Regulated Protein-RNA Interactome. *Journal of the American Chemical Society* 139(48): 17249-17252.
- Arribas-Hernández L., Bressendorff S., Hansen M.H., Poulsen C., Erdmann S. and Brodersen P. (2018). An m6A-YTH Module Controls Developmental Timing and Morphogenesis in Arabidopsis. *The Plant Cell*.
- Aschenbrenner J., Werner S., Marchand V., Adam M., Motorin Y., Helm M. and Marx A. (2018). Engineering of a DNA Polymerase for Direct m6A Sequencing. *Angewandte Chemie International Edition* 57(2): 417-421.
- Bachelier J.P., Amalric F. and Caboche M. (1978). Biosynthesis and utilization of extensively undermethylated poly(A)+ RNA in CHO cells during a cycloleucine treatment. *Nucleic acids research* 5(8): 2927-2943.
- Bächli G. (2015, 21-1-2020). "TaxoDros."
- Baehrecke E.H. (1997). who encodes a KH RNA binding protein that functions in muscle development. *Development* 124(7): 1323-1332.
- Bagni C., Tassone F., Neri G. and Hagerman R. (2012). Fragile X syndrome: causes, diagnosis, mechanisms, and therapeutics. *The Journal of Clinical Investigation* 122(12): 4314-4322.
- Bahadorani S. and Hilliker A.J. (2008). Cocoa confers life span extension in Drosophila melanogaster. *Nutrition research* 28(6): 377-382.
- Bailey A.S., Batista P.J., Gold R.S., Chen Y.G., de Rooij D.G., Chang H.Y. and Fuller M.T. (2017). The conserved RNA helicase YTHDC2 regulates the transition from proliferation to differentiation in the germline. *eLife* 6.
- Balija M.B.G., Griesinger C., Herzig A., Zweckstetter M. and Jäckle H. (2011). Pre-Fibrillar α -Synuclein Mutants Cause Parkinson's Disease-Like Non-Motor Symptoms in Drosophila. *PLoS One* 6(9).
- Bao P., Höbartner C., Hartmuth K. and Lührmann R. (2017). Yeast Prp2 liberates the 5' splice site and the branch site adenosine for catalysis of pre-mRNA splicing. *RNA (New York, N.Y.)* 23(12): 1770-1779.
- Baquero-Perez B., Antanaviciute A., Yonchev I.D., Carr I.M., Wilson S.A. and Whitehouse A. (2019). The Tudor SND1 protein is an m6A RNA reader essential for replication of Kaposi's sarcoma-associated herpesvirus. *eLife* 8: e47261.
- Barbieri I., Tzelepis K., Pandolfini L., Shi J., Millán-Zambrano G., Robson S.C., Aspris D., Migliori V., Bannister A.J., Han N., De Braekeleer E., Ponstingl H., Hendrick A., Vakoc C.R., Vassiliou G.S. and Kouzarides T. (2017). Promoter-bound METTL3 maintains myeloid leukaemia by m6A-dependent translation control. *Nature* 552: 126.
- Barbosa-Morais N.L., Irimia M., Pan Q., Xiong H.Y., Gueroussov S., Lee L.J., Slobodeniuc V., Kutter C., Watt S., Çolak R., Kim T., Misquitta-Ali C.M., Wilson M.D., Kim P.M., Odom D.T., Frey B.J. and Blencowe B.J. (2012). The Evolutionary Landscape of Alternative Splicing in Vertebrate Species. *Science* 338(6114): 1587-1593.
- Bartel D.P. (2018). Metazoan MicroRNAs. *Cell* 173(1): 20-51.

- Bartoli K., Schaening C., Carlile T. and Gilbert W. (2018). Conserved Methyltransferase Spb1 Targets mRNAs for Regulated Modification with 2'-O-Methyl Ribose, bioRxiv.
- Barton L.J., Wilmington S.R., Martin M.J., Skopec H.M., Lovander K.E., Pinto B.S. and Geyer P.K. (2014). Unique and shared functions of nuclear lamina LEM domain proteins in *Drosophila*. *Genetics* 197(2): 653-665.
- Bartosovic M., Molaes H.C., Gregorova P., Hrossova D., Kudla G. and Vanacova S. (2017). N6-methyladenosine demethylase FTO targets pre-mRNAs and regulates alternative splicing and 3'-end processing. *Nucleic acids research* 45(19): 11356-11370.
- Batista P.J., Molinie B., Wang J.K., Qu K., Zhang J.J., Li L.J., Bouley D.M., Lujan E., Haddad B., Daneshvar K., Carter A.C., Flynn R.A., Zhou C., Lim K.S., Dedon P., Wernig M., Mullen A.C., Xing Y., Giallourakis C.C. and Chang H.Y. (2014). m(6)A RNA Modification Controls Cell Fate Transition in Mammalian Embryonic Stem Cells. *Cell Stem Cell* 15(6): 707-719.
- Bayer M. (2016). Investigating the role of m6A RNA modification in 3' UTR polyadenylation. Master Thesis, JGU.
- Becker K., Bluhm A., Casas-Vila N., Dinges N., Dejung M., Sayols S., Kreutz C., Roignant J.-Y., Butter F. and Legewie S. (2018). Quantifying post-transcriptional regulation in the development of *Drosophila melanogaster*. *Nature Communications* 9(1): 4970.
- Beli P., Lukashchuk N., Wagner S.A., Weinert B.T., Olsen J.V., Baskcomb L., Mann M., Jackson S.P. and Choudhary C. (2012). Proteomic investigations reveal a role for RNA processing factor THRAP3 in the DNA damage response. *Molecular cell* 46(2): 212-225.
- Bell O., Wirbelauer C., Hild M., Scharf A.N.D., Schwaiger M., MacAlpine D.M., Zilbermann F., van Leeuwen F., Bell S.P., Imhof A., Garza D., Peters A.H.F.M. and Schübeler D. (2007). Localized H3K36 methylation states define histone H4K16 acetylation during transcriptional elongation in *Drosophila*. *The EMBO journal* 26(24): 4974-4984.
- Berg M.G., Singh L.N., Younis I., Liu Q., Pinto A.M., Kaida D., Zhang Z., Cho S., Sherrill-Mix S., Wan L. and Dreyfuss G. (2012). U1 snRNP determines mRNA length and regulates isoform expression. *Cell* 150(1): 53-64.
- Berget S.M., Moore C. and Sharp P.A. (1977). Spliced segments at the 5' terminus of adenovirus 2 late mRNA. *Proceedings of the National Academy of Sciences of the United States of America* 74(8): 3171-3175.
- Bertram K., Agafonov D.E., Liu W.-T., Dybkov O., Will C.L., Hartmuth K., Urlaub H., Kastner B., Stark H. and Lührmann R. (2017). Cryo-EM structure of a human spliceosome activated for step 2 of splicing. *Nature* 542: 318.
- Béthune J., Jansen R.-P., Feldbrügge M. and Zarnack K. (2019). Membrane-Associated RNA-Binding Proteins Orchestrate Organelle-Coupled Translation. *Trends in Cell Biology* 29(2): 178-188.
- Bickle T.A. and Krüger D.H. (1993). Biology of DNA restriction. *Microbiological reviews* 57(2): 434-450.
- Bizzozero O. (2009). Protein carbonylation in neurodegenerative and demyelinating CNS diseases. *Handbook of neurochemistry and molecular neurobiology*.
- Blanco S. and Frye M. (2014). Role of RNA methyltransferases in tissue renewal and pathology. *Current opinion in cell biology* 31: 1-7.
- Bluhm A., Casas-Vila N., Scheibe M. and Butter F. (2016). Reader interactome of epigenetic histone marks in birds. *Proteomics* 16(3): 427-436.
- Boccaletto P., Machnicka M.A., Purta E., Piątkowski P., Bagiński B., Wirecki T.K., de Crécy-Lagard V., Ross R., Limbach P.A., Kotter A., Helm M. and Bujnicki J.M. (2018). MODOMICS: a database of RNA modification pathways. 2017 update. *Nucleic Acids Research* 46(D1): D303-D307.
- Bodi Z., Bottley A., Archer N., May S.T. and Fray R.G. (2015). Yeast m6A Methylated mRNAs Are Enriched on Translating Ribosomes during Meiosis, and under Rapamycin Treatment. *PLoS One* 10(7): e0132090.
- Bodi Z. and Fray R.G. (2017). Detection and Quantification of N6-Methyladenosine in Messenger RNA by TLC. *RNA Methylation: Methods and Protocols*. A. Lusser. New York, NY, Springer New York: 79-87.
- Bodi Z., Zhong S., Mehra S., Song J., Graham N., Li H., May S. and Fray R.G. (2012). Adenosine Methylation in Arabidopsis mRNA is Associated with the 3' End and Reduced Levels Cause Developmental Defects. *Frontiers in plant science* 3: 48.
- Boelens W.C., Jansen E.J.R., van Venrooij W.J., Striepecke R., Mattaj I.W. and Gunderson S.I. (1993). The human U1 snRNP-Specific U1A protein inhibits polyadenylation of its own pre-mRNA. *Cell* 72(6): 881-892.
- Bohnsack K.E., Höbartner C. and Bohnsack M.T. (2019). Eukaryotic 5-methylcytosine (m⁵C) RNA Methyltransferases: Mechanisms, Cellular Functions, and Links to Disease. *Genes* 10(2): 102.
- Bohnsack M.T. and Sloan K.E. (2018). The mitochondrial epitranscriptome: the roles of RNA modifications in mitochondrial translation and human disease. *Cell Mol Life Sci* 75(2): 241-260.
- Boissel S., Reish O., Proulx K., Kawagoe-Takaki H., Sedgwick B., Yeo G.S., Meyre D., Golzio C., Molinari F., Kadhom N., Etchevers H.C., Saudek V., Farooqi I.S., Froguel P., Lindahl T., O'Rahilly S., Munnich A. and Colleaux L. (2009). Loss-of-function mutation in the dioxygenase-encoding FTO gene causes severe growth retardation and multiple malformations. *American journal of human genetics* 85(1): 106-111.
- Bokar J.A., Rath-Shambaugh M.E., Ludwiczak R., Narayan P. and Rottman F. (1994). Characterization and partial purification of mRNA N6-adenosine methyltransferase from HeLa cell nuclei. Internal mRNA methylation requires a multisubunit complex. *Journal of Biological Chemistry* 269(26): 17697-17704.
- Bokar J.A., Shambaugh M.E., Polayes D., Matera A.G. and Rottman F.M. (1997). Purification and cDNA cloning of the AdoMet-binding subunit of the human mRNA (N6-adenosine)-methyltransferase. *RNA* 3(11): 1233-1247.
- Borgel J., Guibert S., Li Y., Chiba H., Schübeler D., Sasaki H., Forné T. and Weber M. (2010). Targets and dynamics of promoter DNA methylation during early mouse development. *Nature Genetics* 42: 1093.
- Boulias K., Toczyłowska-Socha D., Hawley B.R., Liberman N., Takashima K., Zaccara S., Guez T., Vasseur J.J., Debart F., Aravind L., Jaffrey S.R. and Greer E.L. (2019). Identification of the m(6)Am Methyltransferase PCIF1 Reveals the Location and Functions of m(6)Am in the Transcriptome. *Mol Cell* 75(3): 631-643.e638.
- Briggs J.A., Weinreb C., Wagner D.E., Megason S., Peshkin L., Kirschner M.W. and Klein A.M. (2018). The dynamics of gene expression in vertebrate embryogenesis at single-cell resolution. *Science* 360(6392): eaar5780.
- Brizuela B.J. and Kennison J.A. (1997). The *Drosophila* homeotic gene *moira* regulates expression of engrailed and *HOM* genes in imaginal tissues. *Mechanisms of development* 65(1-2): 209-220.
- Brown J.A., Kinzig C.G., DeGregorio S.J. and Steitz J.A. (2016). Methyltransferase-like protein 16 binds the 3'-terminal triple helix of MALAT1 long noncoding RNA. *Proceedings of the National Academy of Sciences* 113(49): 14013-14018.
- Brown J.B., Boley N., Eisman R., May G.E., Stoiber M.H., Duff M.O., Booth B.W., Wen J., Park S., Suzuki A.M., Wan K.H., Yu C., Zhang D., Carlson J.W., Cherbas L., Eads B.D., Miller D., Mockaitis K., Roberts J., Davis C.A., Frise E., Hammonds A.S., Olson S., Shenker S., Sturgill D., Samsonova A.A., Weiszmann R., Robinson G., Hernandez J., Andrews J., Bickel P.J., Carninci P., Cherbas P., Gingeras T.R., Hoskins R.A., Kaufman T.C., Lai E.C., Oliver B., Perrimon N., Graveley B.R. and Celniker S.E. (2014). Diversity and dynamics of the *Drosophila* transcriptome. *Nature* 512(7515): 393-399.
- Bujnicki J.M., Feder M., Radlinska M. and Blumenthal R.M. (2002). Structure Prediction and Phylogenetic Analysis of a Functionally Diverse Family of Proteins Homologous to the MT-A70 Subunit of the Human mRNA:m6A Methyltransferase. *Journal of Molecular Evolution* 55(4): 431-444.
- Busch A. and Hertel K.J. (2012). Evolution of SR protein and hnRNP splicing regulatory factors. *Wiley interdisciplinary reviews. RNA* 3(1): 1-12.
- Bushkin G.G., Pincus D., Morgan J.T., Richardson K., Lewis C., Chan S.H., Bartel D.P. and Fink G.R. (2019). m6A modification of a 3' UTR site reduces RME1 mRNA levels to promote meiosis. *Nature Communications* 10(1): 3414.

- Caboche M. and Bachellerie J.-P. (1977). RNA Methylation and Control of Eukaryotic RNA Biosynthesis. *European Journal of Biochemistry* 74(1): 19-29.
- Calgano S., Boube M., Cribbs D.L. and Bourbon H.-M. (2002). The *Drosophila* gene *taranis* encodes a novel trithorax group member potentially linked to the cell cycle regulatory apparatus. *Genetics* 160(2): 547-560.
- Camper S.A., Albers R.J., Coward J.K. and Rottman F.M. (1984). Effect of undermethylation on mRNA cytoplasmic appearance and half-life. *Molecular and cellular biology* 4(3): 538-543.
- Carazo-Salas R.E., Guarguaglini G., Gruss O.J., Segref A., Karsenti E. and Mattaj J.W. (1999). Generation of GTP-bound Ran by RCC1 is required for chromatin-induced mitotic spindle formation. *Nature* 400(6740): 178-181.
- Carlile T., Martinez N., Schaening C., Su A., Bell T., Zinshteyn B. and Gilbert W. (2019). mRNA structure determines modification by pseudouridine synthase 1. *Nature Chemical Biology* 15: 1-9.
- Carlile T.M., Rojas-Duran M.F., Zinshteyn B., Shin H., Bartoli K.M. and Gilbert W.V. (2014). Pseudouridine profiling reveals regulated mRNA pseudouridylation in yeast and human cells. *Nature* 515(7525): 143-146.
- Carroll S.M., Narayan P. and Rottman F.M. (1990). N6-methyladenosine residues in an intron-specific region of prolactin pre-mRNA. *Molecular and Cellular Biology* 10(9): 4456-4465.
- Carthew R.W. and Sontheimer E.J. (2009). Origins and Mechanisms of miRNAs and siRNAs. *Cell* 136(4): 642-655.
- Casadesús J. and Low D. (2006). Epigenetic gene regulation in the bacterial world. *Microbiology and molecular biology reviews* : MMBR 70(3): 830-856.
- Castello A., Fischer B., Eichelbaum K., Horos R., Beckmann Benedikt M., Strein C., Davey Norman E., Humphreys David T., Preiss T., Steinmetz Lars M., Krijgsveld J. and Hentze Matthias W. (2012). Insights into RNA Biology from an Atlas of Mammalian mRNA-Binding Proteins. *Cell* 149(6): 1393-1406.
- Castosa R., Martínez-Iglesias O., Roca-Lema D., Casas-Pais A., Díaz-Díaz A., Iglesias P., Santamarina I., Graña B., Calvo L., Valladares-Ayerbes M., Concha Á. and Figueroa A. (2018). Hakai overexpression effectively induces tumour progression and metastasis in vivo. *Scientific Reports* 8(1): 3466.
- Catalanotto C., Cogoni C. and Zardo G. (2016). MicroRNA in Control of Gene Expression: An Overview of Nuclear Functions. *International journal of molecular sciences* 17(10): 1712.
- Chang J.L., Lin H.V., Blauwkamp T.A. and Cadigan K.M. (2008). Spenito and Split ends act redundantly to promote Wingless signaling. *Developmental biology* 314(1): 100-111.
- Chang M., Lv H., Zhang W., Ma C., He X., Zhao S., Zhang Z.W., Zeng Y.X., Song S., Niu Y. and Tong W.M. (2017). Region-specific RNA m(6)A methylation represents a new layer of control in the gene regulatory network in the mouse brain. *Open Biol* 7(9).
- Chen C.-Y.A. and Shyu A.-B. (2017). Emerging Themes in Regulation of Global mRNA Turnover in *cis*. *Trends in Biochemical Sciences* 42(1): 16-27.
- Chen C., Nott T.J., Jin J. and Pawson T. (2011). Deciphering arginine methylation: Tudor tells the tale. *Nature Reviews Molecular Cell Biology* 12(10): 629-642.
- Chen H., Gu L., Orellana E.A., Wang Y., Guo J., Liu Q., Wang L., Shen Z., Wu H., Gregory R.I., Xing Y. and Shi Y. (2020). METTL4 is an snRNA m6Am methyltransferase that regulates RNA splicing. *Cell Research*.
- Chen J. and Du B. (2019). Novel positioning from obesity to cancer: FTO, an m(6)A RNA demethylase, regulates tumour progression. *Journal of cancer research and clinical oncology* 145(1): 19-29.
- Chen J., Wang C., Fei W., Fang X. and Hu X. (2019). Epitranscriptomic m6A modification in the stem cell field and its effects on cell death and survival. *Am J Cancer Res* 9(4): 752-764.
- Chen K., Lu Z., Wang X., Fu Y., Luo G.-Z., Liu N., Han D., Dominissini D., Dai Q., Pan T. and He C. (2015). High-resolution N(6) -methyladenosine (m(6) A) map using photo-crosslinking-assisted m(6) A sequencing. *Angewandte Chemie (International ed. in English)* 54(5): 1587-1590.
- Chen T., Hao Y.J., Zhang Y., Li M.M., Wang M., Han W., Wu Y., Lv Y., Hao J., Wang L., Li A., Yang Y., Jin K.X., Zhao X., Li Y., Ping X.L., Lai W.Y., Wu L.G., Jiang G., Wang H.L., Sang L., Wang X.J., Yang Y.G. and Zhou Q. (2015). m(6)A RNA methylation is regulated by microRNAs and promotes reprogramming to pluripotency. *Cell Stem Cell* 16(3): 289-301.
- Chen W., Zhang L., Zheng G., Fu Y., Ji Q., Liu F., Chen H. and He C. (2014). Crystal structure of the RNA demethylase ALKBH5 from zebrafish. *FEBS Letters* 588(6): 892-898.
- Chen X., Yu C., Guo M., Zheng X., Ali S., Huang H., Zhang L., Wang S., Huang Y., Qie S. and Wang J. (2019). Down-Regulation of m6A mRNA Methylation Is Involved in Dopaminergic Neuronal Death. *ACS Chemical Neuroscience* 10(5): 2355-2363.
- Chen Z., Li S., Subramaniam S., Shyy J.Y.-J. and Chien S. (2017). Epigenetic Regulation: A New Frontier for Biomedical Engineers. *Annual Review of Biomedical Engineering* 19(1): 195-219.
- Chen Z., Qi M., Shen B., Luo G., Wu Y., Li J., Lu Z., Zheng Z., Dai Q. and Wang H. (2019). Transfer RNA demethylase ALKBH3 promotes cancer progression via induction of tRNA-derived small RNAs. *Nucleic acids research* 47(5): 2533-2545.
- Cheng H., Dufu K., Lee C.-S., Hsu J.L., Dias A. and Reed R. (2006). Human mRNA Export Machinery Recruited to the 5-End of mRNA. *Cell* 127(7): 1389-1400.
- Cho D.-S.C., Yang W., Lee J.T., Shiekhhattar R., Murray J.M. and Nishikura K. (2003). Requirement of Dimerization for RNA Editing Activity of Adenosine Deaminases Acting on RNA. *Journal of Biological Chemistry* 278(19): 17093-17102.
- Choe J., Lin S., Zhang W., Liu Q., Wang L., Ramirez-Moya J., Du P., Kim W., Tang S., Sliz P., Santisteban P., George R.E., Richards W.G., Wong K.-K., Locker N., Slack F.J. and Gregory R.I. (2018). mRNA circularization by METTL3-eIF3h enhances translation and promotes oncogenesis. *Nature* 561(7724): 556-560.
- Choi J., Jeong K.-W., Demirci H., Chen J., Petrov A., Prabhakar A., O'Leary S.E., Dominissini D., Rechavi G., Soltis S.M., Ehrenberg M. and Puglisi J.D. (2016). N(6)-methyladenosine in mRNA disrupts tRNA selection and translation-elongation dynamics. *Nature structural & molecular biology* 23(2): 110-115.
- Chow L.T., Gelinas R.E., Broker T.R. and Roberts R.J. (1977). An amazing sequence arrangement at the 5-ends of adenovirus 2 messenger RNA. *Cell* 12(1): 1-8.
- Chowdhury A., Mukhopadhyay J. and Tharun S. (2007). The decapping activator Lsm1p-7p-Pat1p complex has the intrinsic ability to distinguish between oligoadenylated and polyadenylated RNAs. *RNA* 13(7): 998-1016.
- Chu C., Zhang Qiangfeng C., da Rocha Simão T., Flynn Ryan A., Bharadwaj M., Calabrese J.M., Magnuson T., Heard E. and Chang Howard Y. (2015). Systematic Discovery of Xist RNA Binding Proteins. *Cell* 161(2): 404-416.
- Chu J.-M., Ye T.-T., Ma C.-J., Lan M.-D., Liu T., Yuan B.-F. and Feng Y.-Q. (2018). Existence of Internal N7-Methylguanosine Modification in mRNA Determined by Differential Enzyme Treatment Coupled with Mass Spectrometry Analysis. *ACS Chemical Biology* 13(12): 3243-3250.
- Church C., Moir L., McMurray F., Girard C., Banks G.T., Teboul L., Wells S., Brüning J.C., Nolan P.M., Ashcroft F.M. and Cox R.D. (2010). Overexpression of Fto leads to increased food intake and results in obesity. *Nature genetics* 42(12): 1086-1092.
- Clayton J.D., Cripps R.M., Sparrow J.C. and Bullard B. (1998). Interaction of tropinin-H and glutathione S-transferase-2 in the indirect flight muscles of *Drosophila melanogaster*. *Journal of Muscle Research & Cell Motility* 19(2): 117-127.
- Clemson C.M., McNeil J.A., Willard H.F. and Lawrence J.B. (1996). XIST RNA paints the inactive X chromosome at interphase: evidence for a novel RNA involved in nuclear/chromosome structure. *The Journal of cell biology* 132(3): 259-275.
- Cohn W.E. and Volkin E. (1951). Nucleoside 5'-Phosphates from Ribonucleic Acid. *Nature* 167(4247): 483-484.
- Colomb J., Reiter L., Blaszkiewicz J., Wessnitzer J. and Brembs B. (2012). Open Source Tracking and Analysis of Adult *Drosophila* Locomotion in Buridan's Paradigm with and without Visual Targets. *PLOS ONE* 7(8): e42247.

- Cooper J.A., Kaneko T. and Li S.S.C. (2015). Cell regulation by phosphotyrosine-targeted ubiquitin ligases. *Molecular and cellular biology* 35(11): 1886-1897.
- Costa A., Pazman C., Sinsimer K.S., Wong L.C., McLeod I., Yates J., Haynes S. and Schedl P. (2013) Rasputin functions as a positive regulator of orb in *Drosophila* oogenesis. *PloS one* 8, e72864 DOI: 10.1371/journal.pone.0072864.
- Cowling V.H. (2009). Regulation of mRNA cap methylation. *The Biochemical journal* 425(2): 295-302.
- Cramer P. (2019). Organization and regulation of gene transcription. *Nature* 573(7772): 45-54.
- Creamer K.M. and Lawrence J.B. (2017). XIST RNA: a window into the broader role of RNA in nuclear chromosome architecture. *Philosophical transactions of the Royal Society of London. Series B, Biological sciences* 372(1733): 20160360.
- Crick F.H.C. (1958). On protein synthesis, *Symp Soc Exp Biol*.
- Crick F.H.C. (1966). Codon—anticodon pairing: The wobble hypothesis. *Journal of Molecular Biology* 19(2): 548-555.
- Cullen C.F., Brittle A.L., Ito T. and Ohkura H. (2005). The conserved kinase NHK-1 is essential for mitotic progression and unifying acentrosomal meiotic spindles in *Drosophila melanogaster*. *The Journal of Cell Biology* 171(4): 593-602.
- Dai D., Wang H., Zhu L., Jin H. and Wang X. (2018). N6-methyladenosine links RNA metabolism to cancer progression. *Cell Death & Disease* 9(2): 124.
- Dai Q., Moshitch-Moshkovitz S., Han D., Kol N., Amariglio N., Rechavi G., Dominissini D. and He C. (2017). Nm-seq maps 2'-O-methylation sites in human mRNA with base precision. *Nature Methods* 14: 695.
- Dai Q., Moshitch-Moshkovitz S., Han D., Kol N., Amariglio N., Rechavi G., Dominissini D. and He C. (2018). Corrigendum: Nm-seq maps 2'-O-methylation sites in human mRNA with base precision. *Nature Methods* 15: 226.
- Dang W., Xie Y., Cao P., Xin S., Wang J., Li S., Li Y. and Lu J. (2019). N(6)-Methyladenosine and Viral Infection. *Frontiers in microbiology* 10: 417-417.
- Darnell J.C. and Klann E. (2013). The translation of translational control by FMRP: therapeutic targets for FXS. *Nature Neuroscience* 16: 1530.
- Darzacq X., Jády B.E., Verheggen C., Kiss A.M., Bertrand E. and Kiss T. (2002). Cajal body-specific small nuclear RNAs: a novel class of 2'-O-methylation and pseudouridylation guide RNAs. *The EMBO journal* 21(11): 2746-2756.
- Davis D.R. (1995). Stabilization of RNA stacking by pseudouridine. *Nucleic Acids Research* 23(24): 5020-5026.
- de Almeida R.A. and O'Keefe R.T. (2015). The NineTeen Complex (NTC) and NTC-associated proteins as targets for spliceosomal ATPase action during pre-mRNA splicing. *RNA biology* 12(2): 109-114.
- Delatte B., Wang F., Ngoc L.V., Collignon E., Bonvin E., Deplus R., Calonne E., Hassabi B., Putmans P., Awe S., Wetzel C., Kreher J., Soin R., Creppe C., Limbach P.A., Gueydan C., Kruys V., Brehm A., Minakhina S., Defrance M., Steward R. and Fuks F. (2016). Transcriptome-wide distribution and function of RNA hydroxymethylcytosine. *Science* 351(6270): 282-285.
- Deng X., Chen K., Luo G.Z., Weng X., Ji Q., Zhou T. and He C. (2015). Widespread occurrence of N6-methyladenosine in bacterial mRNA. *Nucleic Acids Res* 43(13): 6557-6567.
- Denoya C.D. and Dubnau D. (1987). Site and substrate specificity of the ermC 23S rRNA methyltransferase. *J Bacteriol* 169(8): 3857-3860.
- Dermit M., Dodel M., Lee F.C.Y., Azman M.S., Schwenzler H., Jones J.L., Blagden S.P., Ule J. and Mardakheh F.K. (2019). Subcellular mRNA localization regulates ribosome biogenesis in migrating cells. *bioRxiv*: 829739.
- Deshpande G., Calhoun G. and Schedl P.D. (1999). The N-terminal domain of Sxl protein disrupts Sxl autoregulation in females and promotes female-specific splicing of tra in males. *Development* 126(13): 2841-2853.
- Desrosiers R., Friderici K. and Rottman F. (1974). Identification of methylated nucleosides in messenger RNA from Novikoff hepatoma cells. *Proc Natl Acad Sci U S A* 71(10): 3971-3975.
- Dhir A., Buratti E., van Santen M.A., Lührmann R. and Baralle F.E. (2010). The intronic splicing code: multiple factors involved in ATM pseudoexon definition. *The EMBO journal* 29(4): 749-760.
- Diagna T.T., Thomas U., Prokopenko S.N., Xiao B., Worley P.F. and Thomas J.B. (2002). Mutation of *Drosophila* homer disrupts control of locomotor activity and behavioral plasticity. *J Neurosci* 22(2): 428-436.
- Díaz-Díaz A., Casas-Pais A., Calamia V., Castosa R., Martínez-Iglesias O., Roca-Lema D., Santamarina I., Valladares-Ayerbes M., Calvo L., Chantada V. and Figueroa A. (2017). Proteomic Analysis of the E3 Ubiquitin-Ligase Hakai Highlights a Role in Plasticity of the Cytoskeleton Dynamics and in the Proteasome System. *Journal of Proteome Research* 16(8): 2773-2788.
- Djuranovic S., Nahvi A. and Green R. (2012). miRNA-mediated gene silencing by translational repression followed by mRNA deadenylation and decay. *Science (New York, N.Y.)* 336(6078): 237-240.
- Dobin A., Davis C.A., Schlesinger F., Drenkow J., Zaleski C., Jha S., Batut P., Chaisson M. and Gingeras T.R. (2013). STAR: ultrafast universal RNA-seq aligner. *Bioinformatics* 29(1): 15-21.
- Dominissini D., Moshitch-Moshkovitz S., Schwartz S., Salmon-Divon M., Ungar L., Osenberg S., Cesarkas K., Jacob-Hirsch J., Amariglio N., Kupiec M., Sorek R. and Rechavi G. (2012). Topology of the human and mouse m6A RNA methylomes revealed by m6A-seq. *Nature* 485: 201.
- Dominissini D., Nachtergaele S., Moshitch-Moshkovitz S., Peer E., Kol N., Ben-Haim M.S., Dai Q., Di Segni A., Salmon-Divon M., Clark W.C., Zheng G., Pan T., Solomon O., Eyal E., Hershkovitz V., Han D., Doré L.C., Amariglio N., Rechavi G. and He C. (2016). The dynamic N1-methyladenosine methylome in eukaryotic messenger RNA. *Nature* 530: 441.
- Dong L., Nian H., Shao Y., Zhang Y., Li Q., Yi Y., Tian F., Li W., Zhang H., Zhang X., Wang F. and Li X. (2015). PTB-associated splicing factor inhibits IGF-1-induced VEGF upregulation in a mouse model of oxygen-induced retinopathy. *Cell and Tissue Research* 360(2): 233-243.
- Dou H., Buetow L., Hock A., Sibbet G.J., Vousden K.H. and Huang D.T. (2012). Structural basis for autoinhibition and phosphorylation-dependent activation of c-Cbl. *Nature structural & molecular biology* 19(2): 184-192.
- Doxakis E. (2014). RNA binding proteins: a common denominator of neuronal function and dysfunction. *Neuroscience bulletin* 30(4): 610-626.
- Doxtader K.A., Wang P., Scarborough A.M., Seo D., Conrad N.K. and Nam Y. (2018). Structural Basis for Regulation of METTL16, an S-Adenosylmethionine Homeostasis Factor. *Molecular Cell* 71(6): 1001-1011.e1004.
- Drozdz M., Bardoni B. and Capovilla M. (2018) Modeling Fragile X Syndrome in *Drosophila*. *Front Mol Neurosci* 11, 124 DOI: 10.3389/fnmol.2018.00124.
- Du H., Zhao Y., He J., Zhang Y., Xi H., Liu M., Ma J. and Wu L. (2016). YTHDF2 destabilizes m6A-containing RNA through direct recruitment of the CCR4-NOT deadenylase complex. *Nature Communications* 7: 12626.
- Du Y., Hou G., Zhang H., Dou J., He J., Guo Y., Li L., Chen R., Wang Y., Deng R., Huang J., Jiang B., Xu M., Cheng J., Chen G.Q., Zhao X. and Yu J. (2018). SUMOylation of the m6A-RNA methyltransferase METTL3 modulates its function. *Nucleic Acids Res* 46(10): 5195-5208.
- Duan H.-C., Wei L.-H., Zhang C., Wang Y., Chen L., Lu Z., Chen P., He C. and Jia G. (2017). ALKBH10B is An RNA N6-Methyladenosine Demethylase Affecting Arabidopsis Floral Transition. *The Plant Cell* 29: tpc.00912.02016.
- Duff M.O., Olson S., Wei X., Garrett S.C., Osman A., Bolisetty M., Plocik A., Celniker S.E. and Graveley B.R. (2015). Genome-wide identification of zero nucleotide recursive splicing in *Drosophila*. *Nature* 521: 376.
- Dumelin C.E., Chen Y., Leconte A.M., Chen Y.G. and Liu D.R. (2012). Discovery and biological characterization of geranylated RNA in bacteria. *Nature Chemical Biology* 8: 913.

- Dunwell T.L. and Pfeifer G.P. (2014). Drosophila genomic methylation: new evidence and new questions. *Epigenomics* 6(5): 459-461.
- Dupuis-Sandoval F., Poirier M. and Scott M.S. (2015). The emerging landscape of small nucleolar RNAs in cell biology. *Wiley Interdisciplinary Reviews: RNA* 6(4): 381-397.
- Early P., Rogers J., Davis M., Calame K., Bond M., Wall R. and Hood L. (1980). Two mRNAs can be produced from a single immunoglobulin gene by alternative RNA processing pathways. *Cell* 20(2): 313-319.
- Edelheit S., Schwartz S., Mumbach M.R., Wurtzel O. and Sorek R. (2013). Transcriptome-wide mapping of 5-methylcytidine RNA modifications in bacteria, archaea, and yeast reveals m5C within archaeal mRNAs. *PLoS genetics* 9(6): e1003602-e1003602.
- Edgar R.C. (2004). MUSCLE: multiple sequence alignment with high accuracy and high throughput. *Nucleic Acids Res* 32(5): 1792-1797.
- Edupuganti R.R., Geiger S., Lindeboom R.G.H., Shi H., Hsu P.J., Lu Z., Wang S.-Y., Baltissen M.P.A., Jansen P.W.T.C., Rossa M., Müller M., Stunnenberg H.G., He C., Carell T. and Vermeulen M. (2017). N6-methyladenosine (m6A) recruits and repels proteins to regulate mRNA homeostasis. *Nature Structural & Molecular Biology* 24: 870.
- Elkon R., Ugalde A.P. and Agami R. (2013). Alternative cleavage and polyadenylation: extent, regulation and function. *Nature Reviews Genetics* 14: 496.
- Engel J.D. and Von Hippel P.H. (1974). Effects of methylation on the stability of nucleic acid conformations. Monomer level. *Biochemistry* 13(20): 4143-4158.
- Engel M. and Chen A. (2018). The emerging role of mRNA methylation in normal and pathological behavior. *Genes, brain, and behavior* 17(3): e12428.
- Engel M., Eggert C., Kaplick P.M., Eder M., Röh S., Tietze L., Namendorf C., Arloth J., Weber P., Rex-Haffner M., Geula S., Jakovcevski M., Hanna J.H., Leshkowitz D., Uhr M., Wotjak C.T., Schmidt M.V., Deussing J.M., Binder E.B. and Chen A. (2018). The Role of m(6)A/mRNA Methylation in Stress Response Regulation. *Neuron* 99(2): 389-403.e389.
- Enroth C., Poulsen L.D., Iversen S., Kirpekar F., Albrechtsen A. and Vinther J. (2019). Detection of internal N7-methylguanosine (m7G) RNA modifications by mutational profiling sequencing. *Nucleic Acids Research* 47(20): e126-e126.
- Fedeles B.I., Singh V., Delaney J.C., Li D. and Essigmann J.M. (2015). The AlkB Family of Fe(II)/ α -Ketoglutarate-dependent Dioxigenases: Repairing Nucleic Acid Alkylation Damage and Beyond. *The Journal of biological chemistry* 290(34): 20734-20742.
- Fedorova M., Bollineni R.C. and Hoffmann R. (2014). Protein carbonylation as a major hallmark of oxidative damage: update of analytical strategies. *Mass spectrometry reviews* 33(2): 79-97.
- Fei Q., Zou Z., Roundtree I.A., Sun H.-L. and He C. (2020). YTHDF2 promotes mitotic entry and is regulated by cell cycle mediators. *PLOS Biology* 18(4): e3000664.
- Fica S.M. and Nagai K. (2017). Cryo-electron microscopy snapshots of the spliceosome: structural insights into a dynamic ribonucleoprotein machine. *Nature Structural & Molecular Biology* 24: 791.
- Figaro S., Scrima N., Buckingham R.H. and Heurgué-Hamard V. (2008). HemK2 protein, encoded on human chromosome 21, methylates translation termination factor eRF1. *FEBS Letters* 582(16): 2352-2356.
- Figueroa A., Fujita Y. and Gorospe M. (2009). Hacking RNA: Hakai promotes tumorigenesis by enhancing the RNA-binding function of PSF. *Cell cycle* 8(22): 3648-3651.
- Fischer J., Koch L., Emmerling C., Vierkotten J., Peters T., Bruning J.C. and Ruther U. (2009). Inactivation of the Fto gene protects from obesity. *Nature* 458(7240): 894-898.
- Flaherty S.M., Fortes P., Izaurralde E., Mattaj J.W. and Gilmartin G.M. (1997). Participation of the nuclear cap binding complex in pre-mRNA 3' processing. *Proceedings of the National Academy of Sciences of the United States of America* 94(22): 11893-11898.
- Flamand M.N. and Meyer K.D. (2019). The epitranscriptome and synaptic plasticity. *Curr Opin Neurobiol* 59: 41-48.
- Förch P., Puig O., Kedersha N., Martínez C., Granneman S., Séraphin B., Anderson P. and Valcárcel J. (2000). The apoptosis-promoting factor TIA-1 is a regulator of alternative pre-mRNA splicing. *Mol Cell* 6(5): 1089-1098.
- Freund E.C., Sapiro A.L., Li Q., Linder S., Moresco J.J., Yates J.R. and Li J.B. (2020). Unbiased Identification of trans Regulators of ADAR and A-to-I RNA Editing. *Cell Reports* 31(7): 107656.
- Fu D., Jordan J.J. and Samson L.D. (2013). Human ALKBH7 is required for alkylation and oxidation-induced programmed necrosis. *Genes & development* 27(10): 1089-1100.
- Fu Y., Luo G.-Z., Chen K., Deng X., Yu M., Han D., Hao Z., Liu J., Lu X., Doré Louis C., Weng X., Ji Q., Mets L. and He C. (2015). N6-Methyldeoxyadenosine Marks Active Transcription Start Sites in *Chlamydomonas*. *Cell* 161(4): 879-892.
- Fujita Y., Krause G., Scheffner M., Zechner D., Leddy H.E., Behrens J., Sommer T. and Birchmeier W. (2002). Hakai, a C-bfl-like protein, ubiquitinates and induces endocytosis of the E-cadherin complex. *Nature cell biology* 4(3): 222-231.
- Fukusumi Y., Naruse C. and Asano M. (2008). Wtap is required for differentiation of endoderm and mesoderm in the mouse embryo. *Developmental dynamics : an official publication of the American Association of Anatomists* 237(3): 618-629.
- Furlanis E. and Scheiffele P. (2018). Regulation of Neuronal Differentiation, Function, and Plasticity by Alternative Splicing. *Annual Review of Cell and Developmental Biology* 34(1): 451-469.
- Furuichi Y. (1974). "Methylation-coupled" transcription by virus-associated transcriptase of cytoplasmic polyhedrosis virus containing double-stranded RNA. *Nucleic Acids Res* 1(6): 809-822.
- Furuichi Y. and Miura K.-I. (1975). A blocked structure at the 5' terminus of mRNA from cytoplasmic polyhedrosis virus. *Nature* 253: 374.
- Furuichi Y., Morgan M., Shatkin A.J., Jelinek W., Salditt-Georgieff M. and Darnell J.E. (1975). Methylated, blocked 5 termini in HeLa cell mRNA. *Proceedings of the National Academy of Sciences of the United States of America* 72(5): 1904-1908.
- Fustin J.M., Doi M., Yamaguchi Y., Hida H., Nishimura S., Yoshida M., Isagawa T., Morioka M.S., Kakeya H., Manabe I. and Okamura H. (2013). RNA-methylation-dependent RNA processing controls the speed of the circadian clock. *Cell* 155(4): 793-806.
- Galloway A. and Cowling V.H. (2019). mRNA cap regulation in mammalian cell function and fate. *Biochimica et Biophysica Acta (BBA) - Gene Regulatory Mechanisms* 1862(3): 270-279.
- Ganot P., Bortolin M.-L. and Kiss T. (1997). Site-Specific Pseudouridine Formation in Preribosomal RNA Is Guided by Small Nucleolar RNAs. *Cell* 89(5): 799-809.
- Gao X., Shin Y.-H., Li M., Wang F., Tong Q. and Zhang P. (2010). The fat mass and obesity associated gene FTO functions in the brain to regulate postnatal growth in mice. *PloS one* 5(11): e14005-e14005.
- Garcia-Campos M.A., Edelheit S., Toth U., Safra M., Shachar R., Viukov S., Winkler R., Nir R., Lasman L., Brandis A., Hanna J.H., Rossmanith W. and Schwartz S. (2019). Deciphering the "m⁶A Code" via Antibody-Independent Quantitative Profiling. *Cell*.
- Gargano J.W., Martin I., Bhandari P. and Grotewiel M.S. (2005). Rapid iterative negative geotaxis (RING): a new method for assessing age-related locomotor decline in *Drosophila*. *Experimental Gerontology* 40(5): 386-395.
- Geier G.E. and Modrich P. (1979). Recognition sequence of the dam methylase of *Escherichia coli* K12 and mode of cleavage of Dpn I endonuclease. *Journal of Biological Chemistry* 254(4): 1408-1413.
- Gerken T., Girard C.A., Tung Y.-C.L., Webby C.J., Saudek V., Hewitson K.S., Yeo G.S.H., McDonough M.A., Cunliffe S., McNeill L.A., Galvanovskis J., Rorsman P., Robins P., Prieur X., Coll A.P., Ma M., Jovanovic Z., Farooqi I.S., Sedgwick B., Barroso I., Lindahl T., Ponting C.P., Ashcroft F.M., O'Rahilly S. and Schofield C.J. (2007). The obesity-associated FTO gene encodes a 2-oxoglutarate-dependent nucleic acid demethylase. *Science (New York, N.Y.)* 318(5855): 1469-1472.
- Getz M.J., Birnie G.D., Young B.D., MacPhail E. and Paul J. (1975). A kinetic estimation of base sequence complexity of nuclear poly(A)-containing RNA in mouse friend cells. *Cell* 4(2): 121-129.
- Geula S., Moshitch-Moshkovitz S., Dominissini D., Mansour A.A., Kol N., Salmon-Divon M., Hershkovitz V., Peer E., Mor N., Manor Y.S., Ben-Haim M.S., Eyal E., Yunger S., Pinto Y., Jaitin D.A., Viukov S., Rais Y.,

- Krupalnik V., Chomsky E., Zerbib M., Maza I., Rechavi Y., Massarwa R., Hanna S., Amit I., Levanon E.Y., Amariglio N., Stern-Ginossar N., Novershtern N., Rechavi G. and Hanna J.H. (2015). m6A mRNA methylation facilitates resolution of naïve pluripotency toward differentiation. *Science* 347(6225): 1002-1006.
- Gill R., Stratigopoulos G., Lee J.H. and Leibel R.L. (2019). Functional genomic characterization of the FTO locus in African Americans. *Physiological genomics* 51(11): 517-528.
- Giot L., Bader J.S., Brouwer C., Chaudhuri A., Kuang B., Li Y., Hao Y.L., Ooi C.E., Godwin B., Vitols E., Vijayadamar G., Pochart P., Machineni H., Welsh M., Kong Y., Zerhusen B., Malcolm R., Varrone Z., Collis A., Minto M., Burgess S., McDaniel L., Stimpson E., Spriggs F., Williams J., Neurath K., Ioine N., Agee M., Voss E., Furtak K., Renzulli R., Aanensen N., Carrolla S., Bickelhaupt E., Lazovatsky Y., DaSilva A., Zhong J., Stanyon C.A., Finley R.L., Jr., White K.P., Braverman M., Jarvie T., Gold S., Leach M., Knight J., Shimkets R.A., McKenna M.P., Chant J. and Rothberg J.M. (2003). A protein interaction map of *Drosophila melanogaster*. *Science* 302(5651): 1727-1736.
- Goh Y.T., Koh C.W.Q., Sim D.Y., Roca X. and Goh W.S.S. (2020). METTL4 catalyzes m6Am methylation in U2 snRNA to regulate pre-mRNA splicing. *bioRxiv*: 2020.2001.2024.917575.
- Gokhale N.S., McIntyre A.B.R., McFadden M.J., Roder A.E., Kennedy E.M., Gandara J.A., Hopcraft S.E., Quicke K.M., Vazquez C., Willer J., Ilkayeva O.R., Law B.A., Holley C.L., Garcia-Blanco M.A., Evans M.J., Suthar M.S., Bradrick S.S., Mason C.E. and Horner S.M. (2016). m6A-Methyladenosine in Flaviviridae Viral RNA Genomes Regulates Infection. *Cell Host & Microbe* 20(5): 654-665.
- Goll M.G. and Bestor T.H. (2005). EUKARYOTIC CYTOSINE METHYLTRANSFERASES. *Annual Review of Biochemistry* 74(1): 481-514.
- Golovina A.Y., Dzama M.M., Osterman I.A., Sergiev P.V., Serebryakova M.V., Bogdanov A.A. and Dontsova O.A. (2012). The last rRNA methyltransferase of *E. coli* revealed: the yhiR gene encodes adenine-N6 methyltransferase specific for modification of A2030 of 23S ribosomal RNA. *RNA* 18(9): 1725-1734.
- Gonatopoulos-Pournatzis T. and Cowling V.H. (2014). Cap-binding complex (CBC). *The Biochemical journal* 457(2): 231-242.
- Gradilla A.C., Mansilla A. and Ferrús A. (2011). Isoform-specific regulation of a steroid hormone nuclear receptor by an E3 ubiquitin ligase in *Drosophila melanogaster*. *Genetics* 189(3): 871-883.
- Graindorge A., Pinheiro I., Nawrocka A., Mallory A.C., Tsvetkov P., Gil N., Carolis C., Buchholz F., Ulitsky I., Heard E., Taipale M. and Shkumatava A. (2019). In-cell identification and measurement of RNA-protein interactions. *Nature Communications* 10(1): 5317.
- Granadino B., Campuzano S. and Sanchez L. (1990). The *Drosophila melanogaster* fl(2)d gene is needed for the female-specific splicing of Sex-lethal RNA. *EMBO J* 9(8): 2597-2602.
- Granadino B., Penalva L.O. and Sanchez L. (1996). The gene fl(2)d is needed for the sex-specific splicing of transformer pre-mRNA but not for double-sex pre-mRNA in *Drosophila melanogaster*. *Molecular & general genetics* : MGG 253(1-2): 26-31.
- Granadino B., San Juan A., Santamaria P. and Sanchez L. (1992). Evidence of a dual function in fl (2) d, a gene needed for Sex-lethal expression in *Drosophila melanogaster*. *Genetics* 130(3): 597-612.
- Graveley B.R., Brooks A.N., Carlson J.W., Duff M.O., Landolin J.M., Yang L., Artieri C.G., van Baren M.J., Boley N., Booth B.W., Brown J.B., Chervas L., Davis C.A., Dobin A., Li R., Lin W., Malone J.H., Mattiuzzo N.R., Miller D., Sturgill D., Tuch B.B., Zaleski C., Zhang D., Blanchette M., Dudoit S., Eads B., Green R.E., Hammonds A., Jiang L., Kapranov P., Langton L., Perrimon N., Sandler J.E., Wan K.H., Willingham A., Zhang Y., Zou Y., Andrews J., Bickel P.J., Brenner S.E., Brent M.R., Chervas P., Gingeras T.R., Hoskins R.A., Kaufman T.C., Oliver B. and Celniker S.E. (2011). The developmental transcriptome of *Drosophila melanogaster*. *Nature* 471(7339): 473-479.
- Greer E.L., Blanco M.A., Gu L., Sendinc E., Liu J., Aristizábal-Corrales D., Hsu C.-H., Aravind L., He C. and Shi Y. (2015). DNA Methylation on N6-Adenine in *C. elegans*. *Cell* 161(4): 868-878.
- Grice L.F. and Degan B.M. (2015). The origin of the ADAR gene family and animal RNA editing. *BMC evolutionary biology* 15(1): 4-4.
- Grosjean H. (2009). DNA and RNA modification enzymes. *Landes Bioscience*, Austin, Texas: 289-302.
- Grozhih A.V. and Jaffrey S.R. (2018). Distinguishing RNA modifications from noise in epitranscriptome maps. *Nature Chemical Biology* 14(3): 215-225.
- Grozhih A.V., Olarerin-George A.O., Sindelar M., Li X., Gross S.S. and Jaffrey S.R. (2019). Antibody cross-reactivity accounts for widespread appearance of m1A in 5'UTRs. *Nature Communications* 10(1): 5126.
- Gu L., Wang L., Chen H., Hong J., Shen Z., Dhall A., Lao T., Liu C., Wang Z., Xu Y., Tang H.-W., Chakraborty D., Chen J., Liu Z., Rogulja D., Perrimon N., Wu H. and Shi Y. (2020). CG14906 (mettl4) mediates m6A methylation of U2 snRNA in *Drosophila*. *bioRxiv*: 2020.2001.2009.890764.
- Gu T., Zhao T., Kohli U. and Hewes R.S. (2017). The large and small SPEN family proteins stimulate axon outgrowth during neurosecretory cell remodeling in *Drosophila*. *Developmental biology* 431(2): 226-238.
- Gunderson S.I., Polycarpou-Schwarz M. and Mattaj I.W. (1998). U1 snRNP Inhibits Pre-mRNA Polyadenylation through a Direct Interaction between U1 70K and Poly(A) Polymerase. *Molecular Cell* 1(2): 255-264.
- Guo J., Tang H.W., Li J., Perrimon N. and Yan D. (2018). Xio is a component of the *Drosophila* sex determination pathway and RNA N(6)-methyladenosine methyltransferase complex. *Proc Natl Acad Sci U S A* 115(14): 3674-3679.
- Han Q., Yang J., Yang H., Li C., Li J. and Cao Y. (2020). KIAA1429 promotes osteosarcoma progression by promoting stem cell properties and is regulated by miR-143-3p. *Cell cycle* 19(10): 1172-1185.
- Han Z., Niu T., Chang J., Lei X., Zhao M., Wang Q., Cheng W., Wang J., Feng Y. and Chai J. (2010). Crystal structure of the FTO protein reveals basis for its substrate specificity. *Nature* 464: 1205.
- Harel T., Yoon W.H., Garone C., Gu S., Coban-Akdemir Z., Eldomery M.K., Posey J.E., Jhangiani S.N., Rosenfeld J.A., Cho M.T., Fox S., Withers M., Brooks S.M., Chiang T., Duraine L., Erdin S., Yuan B., Shao Y., Moussallem E., Lamperti C., Donati M.A., Smith J.D., McLaughlin H.M., Eng C.M., Walkiewicz M., Xia F., Pippucci T., Magini P., Seri M., Zeviani M., Hirano M., Hunter J.V., Srour M., Zanigni S., Lewis R.A., Muzny D.M., Lotze T.E., Boerwinkle E., Baylor-Hopkins Center for Mendelian G., University of Washington Center for Mendelian G., Gibbs R.A., Hickey S.E., Graham B.H., Yang Y., Buhas D., Martin D.M., Potocki L., Graziano C., Bellen H.J. and Lupski J.R. (2016). Recurrent De Novo and Biallelic Variation of ATAD3A, Encoding a Mitochondrial Membrane Protein, Results in Distinct Neurological Syndromes. *Am J Hum Genet* 99(4): 831-845.
- Harper D.S., Fresco L.D. and Keene J.D. (1992). RNA binding specificity of a *Drosophila* snRNP protein that shares sequence homology with mammalian U1-A and U2-B' proteins. *Nucleic acids research* 20(14): 3645-3650.
- Hartmann A.M., Nayler O., Schwaiger F.W., Obermeier A. and Stamm S. (1999). The Interaction and Colocalization of Sam68 with the Splicing-associated Factor YT521-B in Nuclear Dots Is Regulated by the Src Family Kinase p59fyn. *Molecular Biology of the Cell* 10(11): 3909-3926.
- Hartstock K., S. N.B., Anna O., V. C.N., Nikolai P., Ann-Marie L.D., A. L.S. and Andrea R. (2018). Enzymatic or In Vivo Installation of Propargyl Groups in Combination with Click Chemistry for the Enrichment and Detection of Methyltransferase Target Sites in RNA. *Angewandte Chemie International Edition* 57(21): 6342-6346.
- Hausmann I.U., Bodi Z., Sanchez-Moran E., Mongan N.P., Archer N., Fray R.G. and Soller M. (2016). m6A potentiates Sxl alternative pre-mRNA splicing for robust *Drosophila* sex determination. *Nature* 540: 301.
- Hazra D., Chapat C. and Graille M. (2019). m6A mRNA Destiny: Chained to the rHYTHm by the YTH-Containing Proteins. *Genes* 10(1): 49.
- He S., Wang H., Liu R., He M., Che T., Jin L., Deng L., Tian S., Li Y., Lu H., Li X., Jiang Z., Li D. and Li M. (2017). mRNA N6-methyladenosine methylation of postnatal liver development in pig. *PLoS one* 12(3): e0173421-e0173421.
- Heck A.M. and Wilusz C.J. (2019). Small changes, big implications: The impact of m(6)A RNA methylation on gene expression in pluripotency and development. *Biochim Biophys Acta Gene Regul Mech* 1862(9): 194402.

- Heilman K.L., Leach R.A. and Tuck M.T. (1996). Internal 6-methyladenine residues increase the in vitro translation efficiency of dihydrofolate reductase messenger RNA. *The International Journal of Biochemistry & Cell Biology* 28(7): 823-829.
- Henras A.K., Plisson-Chastang C., O'Donohue M.-F., Chakraborty A. and Gleizes P.-E. (2015). An overview of pre-ribosomal RNA processing in eukaryotes. *Wiley interdisciplinary reviews. RNA* 6(2): 225-242.
- Herman R.C., Williams J.G. and Penman S. (1976). Message and non-message sequences adjacent to poly(A) in steady state heterogeneous nuclear RNA of HeLa cells. *Cell* 7(3): 429-437.
- Hermann A., Goyal R. and Jeltsch A. (2004). The Dnmt1 DNA-(cytosine-5)-methyltransferase Methylates DNA Processively with High Preference for Hemimethylated Target Sites. *Journal of Biological Chemistry* 279(46): 48350-48359.
- Hess M.E., Hess S., Meyer K.D., Verhagen L.A., Koch L., Bronneke H.S., Dietrich M.O., Jordan S.D., Saletore Y., Elemento O., Belgardt B.F., Franz T., Horvath T.L., Ruther U., Jaffrey S.R., Kloppenburg P. and Bruning J.C. (2013). The fat mass and obesity associated gene (Fto) regulates activity of the dopaminergic midbrain circuitry. *Nat Neurosci* 16(8): 1042-1048.
- Hilfiker A., Amrein H., Dübendorfer A., Schneiter R. and Nöthiger R. (1995). The gene *virilizer* is required for female-specific splicing controlled by *Sxl*, the master gene for sexual development in *Drosophila*. *Development* 121(12): 4017-4026.
- Hilfiker A. and Nöthiger R. (1991). The Temperature-Sensitive Mutation *Virts* (*Virilizer*) Identifies a New Gene Involved in Sex Determination of *Drosophila*. *Roux Arch Dev Biol* 200(5): 240-248.
- Hinnebusch A.G. (2014). The Scanning Mechanism of Eukaryotic Translation Initiation. *Annual Review of Biochemistry* 83(1): 779-812.
- Homem C.C. and Knoblich J.A. (2012). *Drosophila* neuroblasts: a model for stem cell biology. *Development* 139(23): 4297-4310.
- Hongay C.F. and Orr-Weaver T.L. (2011). *Drosophila* Inducer of MEiosis 4 (*IME4*) is required for Notch signaling during oogenesis. *Proc Natl Acad Sci U S A* 108(36): 14855-14860.
- Horiuchi K., Kawamura T., Iwanari H., Ohashi R., Naito M., Kodama T. and Hamakubo T. (2013). Identification of Wilms' Tumor 1-associating Protein Complex and Its Role in Alternative Splicing and the Cell Cycle. *Journal of Biological Chemistry* 288(46): 33292-33302.
- Horiuchi K., Umetani M., Minami T., Okayama H., Takada S., Yamamoto M., Aburatani H., Reid P.C., Housman D.E., Hamakubo T. and Kodama T. (2006). Wilms' tumor 1-associating protein regulates G2/M transition through stabilization of cyclin A2 mRNA. *Proceedings of the National Academy of Sciences of the United States of America* 103(46): 17278-17283.
- Horowitz S., Horowitz A., Nilsen T.W., Munns T.W. and Rottman F.M. (1984). Mapping of N6-methyladenosine residues in bovine prolactin mRNA. *Proceedings of the National Academy of Sciences of the United States of America* 81(18): 5667-5671.
- Howard J.M. and Sanford J.R. (2015). The RNAissance family: SR proteins as multifaceted regulators of gene expression. *Wiley interdisciplinary reviews. RNA* 6(1): 93-110.
- Hsu P.J., Shi H., Zhu A.C., Lu Z., Miller N., Edens B.M., Ma Y.C. and He C. (2019). The RNA-binding protein FMRP facilitates the nuclear export of N (6)-methyladenosine-containing mRNAs. *J Biol Chem* 294(52): 19889-19895.
- Hsu P.J., Zhu Y., Ma H., Guo Y., Shi X., Liu Y., Qi M., Lu Z., Shi H., Wang J., Cheng Y., Luo G., Dai Q., Liu M., Guo X., Sha J., Shen B. and He C. (2017). *Ythdc2* is an N6-methyladenosine binding protein that regulates mammalian spermatogenesis. *Cell Research* 27: 1115.
- Huang H., Weng H., Sun W., Qin X., Shi H., Wu H., Zhao B.S., Mesquita A., Liu C., Yuan C.L., Hu Y.-C., Hüttelmaier S., Skibbe J.R., Su R., Deng X., Dong L., Sun M., Li C., Nachtergaele S., Wang Y., Hu C., Ferchen K., Greis K.D., Jiang X., Wei M., Qu L., Guan J.-L., He C., Yang J. and Chen J. (2018). Recognition of RNA N(6)-methyladenosine by IGF2BP proteins enhances mRNA stability and translation. *Nature cell biology* 20(3): 285-295.
- Huang H., Weng H., Zhou K., Wu T., Zhao B.S., Sun M., Chen Z., Deng X., Xiao G., Auer F., Klemm L., Wu H., Zuo Z., Qin X., Dong Y., Zhou Y., Qin H., Tao S., Du J., Liu J., Lu Z., Yin H., Mesquita A., Yuan C.L., Hu Y.-C., Sun W., Su R., Dong L., Shen C., Li C., Qing Y., Jiang X., Wu X., Sun M., Guan J.-L., Qu L., Wei M., Müschen M., Huang G., He C., Yang J. and Chen J. (2019). Histone H3 trimethylation at lysine 36 guides m6A RNA modification co-transcriptionally. *Nature*.
- Huang J. and Yin P. (2018). Structural Insights into N(6)-methyladenosine (m(6)A) Modification in the Transcriptome. *Genomics, proteomics & bioinformatics* 16(2): 85-98.
- Huang Y., McNeil G.P. and Jackson F.R. (2014) Translational regulation of the DOUBLETIME/CKIδ/ε kinase by LARK contributes to circadian period modulation. *PLoS genetics* 10, e1004536 DOI: 10.1371/journal.pgen.1004536.
- Hussain S., Sajini A.A., Blanco S., Dietmann S., Lombard P., Sugimoto Y., Paramor M., Gleeson J.G., Odom D.T., Ule J. and Frye M. (2013). NSun2-mediated cytosine-5 methylation of vault noncoding RNA determines its processing into regulatory small RNAs. *Cell reports* 4(2): 255-261.
- Ignatova V.V., Stolz P., Kaiser S., Gustafsson T.H., Lastres P.R., Sanz-Moreno A., Cho Y.L., Amarie O.V., Aguilar-Pimentel A., Klein-Rodewald T., Calzada-Wack J., Becker L., Marschall S., Kraiger M., Garrett L., Seisenberger C., Hölter S.M., Borland K., Van De Logt E., Jansen P., Baltissen M.P., Valenta M., Vermeulen M., Wurst W., Gailus-Durner V., Fuchs H., Hrabe de Angelis M., Rando O.J., Kellner S.M., Bultmann S. and Schneider R. (2020). The rRNA m(6)A methyltransferase METTL5 is involved in pluripotency and developmental programs. *Genes Dev* 34(9-10): 715-729.
- Imai Y., Matsuo N., Ogawa S., Tohyama M. and Takagi T. (1998). Cloning of a gene, *YTS21*, for a novel RNA splicing-related protein induced by hypoxia/reoxygenation. *Molecular Brain Research* 53(1): 33-40.
- Incarnato D., Morandi E., Anselmi F., Simon L.M., Basile G. and Oliviero S. (2017). In vivo probing of nascent RNA structures reveals principles of cotranscriptional folding. *Nucleic acids research* 45(16): 9716-9725.
- Inesta-Vaquera F., Chaugule V.K., Galloway A., Chandler L., Rojas-Fernandez A., Weidlich S., Peggie M. and Cowling V.H. (2018). *DHX15* regulates *CMTR1*-dependent gene expression and cell proliferation. *Life Science Alliance* 1(3): e201800092.
- Ishigaki S., Masuda A., Fujioka Y., Iguchi Y., Katsuno M., Shibata A., Urano F., Sobue G. and Ohno K. (2012). Position-dependent FUS-RNA interactions regulate alternative splicing events and transcriptions. *Scientific reports* 2: 529-529.
- Ito S., Horikawa S., Suzuki T., Kawauchi H., Tanaka Y., Suzuki T. and Suzuki T. (2014). Human NAT10 is an ATP-dependent RNA acetyltransferase responsible for N4-acetylcytidine formation in 18S rRNA. *Journal of Biological Chemistry*.
- Ito S., Shen L., Dai Q., Wu S.C., Collins L.B., Swenberg J.A., He C. and Zhang Y. (2011). Tet proteins can convert 5-methylcytosine to 5-formylcytosine and 5-carboxylcytosine. *Science (New York, N.Y.)* 333(6047): 1300-1303.
- Ito T., Chiba T., Ozawa R., Yoshida M., Hattori M. and Sakaki Y. (2001). A comprehensive two-hybrid analysis to explore the yeast protein interactome. *Proceedings of the National Academy of Sciences of the United States of America* 98(8): 4569-4574.
- Ivanova I., Much C., Di Giacomo M., Azzi C., Morgan M., Moreira P.N., Monahan J., Carrieri C., Enright A.J. and O'Carroll D. (2017). The RNA m(6)A Reader YTHDF2 Is Essential for the Post-transcriptional Regulation of the Maternal Transcriptome and Oocyte Competence. *Molecular Cell* 67(6): 1059-1067.e1054.
- Ivshina M., Lasko P. and Richter J.D. (2014). Cytoplasmic Polyadenylation Element Binding Proteins in Development, Health, and Disease. *Annual Review of Cell and Developmental Biology* 30(1): 393-415.
- Iwasaki Y.W., Siomi M.C. and Siomi H. (2015). PIWI-Interacting RNA: Its Biogenesis and Functions. *Annual Review of Biochemistry* 84(1): 405-433.
- Iyer L.M., Abhiman S. and Aravind L. (2011). Chapter 2 - Natural History of Eukaryotic DNA Methylation Systems. *Progress in Molecular Biology and Translational Science*. X. Cheng et al., Academic Press. 101: 25-104.
- Iyer L.M., Zhang D. and Aravind L. (2016). Adenine methylation in eukaryotes: Apprehending the complex evolutionary history and functional potential of an epigenetic modification. *BioEssays: news and reviews in molecular, cellular and developmental biology* 38(1): 27-40.

- Jacob A.G. and Smith C.W.J. (2017). Intron retention as a component of regulated gene expression programs. *Hum Genet* 136(9): 1043-1057.
- Jain D., Puno M.R., Meydan C., Lailier N., Mason C.E., Lima C.D., Anderson K.V. and Keeney S. (2018). *ketu* mutant mice uncover an essential meiotic function for the ancient RNA helicase YTHDC2. *eLife* 7.
- Jain R.A. and Gavis E.R. (2008). The *Drosophila* hnRNP M homolog Rumpelstiltskin regulates nanos mRNA localization. *Development* 135(5): 973-982.
- Jemc J. and Rebay I. (2006). Characterization of the split ends-like gene *spenito* reveals functional antagonism between SPOC family members during *Drosophila* eye development. *Genetics* 173(1): 279-286.
- Ji L. and Chen X. (2012). Regulation of small RNA stability: methylation and beyond. *Cell research* 22(4): 624-636.
- Ji X., Zhou Y., Pandit S., Huang J., Li H., Lin C.Y., Xiao R., Burge C.B. and Fu X.-D. (2013). SR Proteins Collaborate with 7SK and Promoter-Associated Nascent RNA to Release Paused Polymerase. *Cell* 153(4): 855-868.
- Ji Y. and Tulin A.V. (2012) Poly(ADP-ribose) controls DE-cadherin-dependent stem cell maintenance and oocyte localization. *Nature communications* 3, 760 DOI: 10.1038/ncomms1759.
- Jia D., Huang Y.-C. and Deng W.-M. (2015). Analysis of cell cycle switches in *Drosophila* oogenesis. *Drosophila Oogenesis*, Springer: 207-216.
- Jia G., Fu Y., Zhao X., Dai Q., Zheng G., Yang Y., Yi C., Lindahl T., Pan T., Yang Y.G. and He C. (2011). N6-methyladenosine in nuclear RNA is a major substrate of the obesity-associated FTO. *Nature chemical biology* 7(12): 885-887.
- Jia Y., Mu J. and Ackerman S. (2012). Mutation of a U2 snRNA Gene Causes Global Disruption of Alternative Splicing and Neurodegeneration. *Cell* 148: 296-308.
- Jin D.I., Lee S.W., Han M.E., Kim H.J., Seo S.A., Hur G.Y., Jung S., Kim B.S. and Oh S.O. (2012). Expression and roles of Wilms' tumor 1-associating protein in glioblastoma. *Cancer science* 103(12): 2102-2109.
- Jin S., Mi Y., Song J., Zhang P. and Liu Y. (2018). PRMT1-RBM15 axis regulates megakaryocytic differentiation of human umbilical cord blood CD34(+) cells. *Experimental and therapeutic medicine* 15(3): 2563-2568.
- Jin Y., Zhang W. and Li Q. (2009). Origins and evolution of ADAR-mediated RNA editing. *IUBMB Life* 61(6): 572-578.
- Joazeiro C.A., Wing S.S., Huang H., Levenson J.D., Hunter T. and Liu Y.C. (1999). The tyrosine kinase negative regulator c-Cbl as a RING-type, E2-dependent ubiquitin-protein ligase. *Science (New York, N.Y.)* 286(5438): 309-312.
- Johnson M.L., Nagengast A.A. and Salz H.K. (2010). PPS, a large multidomain protein, functions with sex-lethal to regulate alternative splicing in *Drosophila*. *PLoS genetics* 6(3).
- Jonkers I., Kwak H. and Lis J.T. (2014). Genome-wide dynamics of Pol II elongation and its interplay with promoter proximal pausing, chromatin, and exons. *eLife* 3: e02407.
- Jonkers I. and Lis J.T. (2015). Getting up to speed with transcription elongation by RNA polymerase II. *Nature reviews. Molecular cell biology* 16(3): 167-177.
- Jordan K.W., Carbone M.A., Yamamoto A., Morgan T.J. and Mackay T.F.C. (2007). Quantitative genomics of locomotor behavior in *Drosophila melanogaster*. *Genome Biology* 8(8): R172.
- Jung Y. and Goldman D. (2018). Role of RNA modifications in brain and behavior. *Genes, brain, and behavior* 17(3): e12444-e12444.
- Kaida D., Berg M.G., Younis I., Kasim M., Singh L.N., Wan L. and Dreyfuss G. (2010). U1 snRNP protects pre-mRNAs from premature cleavage and polyadenylation. *Nature* 468: 664.
- Kaido M., Wada H., Shindo M. and Hayashi S. (2009). Essential requirement for RING finger E3 ubiquitin ligase Hakai in early embryonic development of *Drosophila*. *Genes to Cells* 14(9): 1067-1077.
- Kal S. and Que L. (2017). Dioxygen activation by nonheme iron enzymes with the 2-His-1-carboxylate facial triad that generate high-valent oxoiron oxidants. *Journal of biological inorganic chemistry : JBIC : a publication of the Society of Biological Inorganic Chemistry* 22(2-3): 339-365.
- Kan L., Grozhik A.V., Vedanayagam J., Patil D.P., Pang N., Lim K.-S., Huang Y.-C., Joseph B., Lin C.-J., Despic V., Guo J., Yan D., Kondo S., Deng W.-M., Dedon P.C., Jaffrey S.R. and Lai E.C. (2017). The m(6)A pathway facilitates sex determination in *Drosophila*. *Nature Communications* 8: 15737.
- Kan L., Ott S., Joseph B., Park E.S., Dai C., Kleiner R., Claridge-Chang A. and Lai E.C. (2020). A neural m⁶A/YTHDF pathway is required for learning and memory in *Drosophila*. [bioRxiv: 2020.03.20.2007.982090](https://doi.org/10.1101/2020.03.20.2007.982090).
- Kang H.J., Jeong S.J., Kim K.N., Baek I.J., Chang M., Kang C.M., Park Y.S. and Yun C.W. (2014). A novel protein, Pho92, has a conserved YTH domain and regulates phosphate metabolism by decreasing the mRNA stability of PHO4 in *Saccharomyces cerevisiae*. *The Biochemical journal* 457(3): 391-400.
- Karijolic J. and Yu Y.-T. (2011). Converting nonsense codons into sense codons by targeted pseudouridylation. *Nature* 474: 395.
- Kasowitz S.D., Ma J., Anderson S.J., Leu N.A., Xu Y., Gregory B.D., Schultz R.M. and Wang P.J. (2018). Nuclear m6A reader YTHDC1 regulates alternative polyadenylation and splicing during mouse oocyte development. *PLoS genetics* 14(5): e1007412-e1007412.
- Katzenberger R.J., Marengo M.S. and Wassarman D.A. (2009). Control of alternative splicing by signal-dependent degradation of splicing-regulatory proteins. *The Journal of biological chemistry* 284(16): 10737-10746.
- Kawarada L., Suzuki T., Ohira T., Hirata S., Miyauchi K. and Suzuki T. (2017). ALKBH1 is an RNA dioxygenase responsible for cytoplasmic and mitochondrial tRNA modifications. *Nucleic acids research* 45(12): 7401-7415.
- Ke S., Alemu E.A., Mertens C., Gantman E.C., Fak J.J., Mele A., Haripal B., Zucker-Scharff I., Moore M.J., Park C.Y., Vågbo C.B., Kusnierzcyk A., Klungland A., Darnell J.E., Jr. and Darnell R.B. (2015). A majority of m6A residues are in the last exons, allowing the potential for 3' UTR regulation. *Genes Dev* 29(19): 2037-2053.
- Ke S., Pandya-Jones A., Saito Y., Fak J.J., Vågbo C.B., Geula S., Hanna J.H., Black D.L., Darnell J.E., Jr. and Darnell R.B. (2017). m(6)A mRNA modifications are deposited in nascent pre-mRNA and are not required for splicing but do specify cytoplasmic turnover. *Genes & development* 31(10): 990-1006.
- Keiper S., Papsaikas P., Will C.L., Valcárcel J., Girard C. and Lührmann R. (2019). Smu1 and RED are required for activation of spliceosomal B complexes assembled on short introns. *Nature Communications* 10(1): 3639.
- Ketosugbo K.F., Bushnell H.L. and Johnson R.I. (2017). A screen for E3 ubiquitination ligases that genetically interact with the adaptor protein Cindr during *Drosophila* eye patterning. *PloS one* 12(11): e0187571-e0187571.
- Khoddami V. and Cairns B.R. (2013). Identification of direct targets and modified bases of RNA cytosine methyltransferases. *Nature biotechnology* 31(5): 458-464.
- Kim K.M., Cho H., Choi K., Kim J., Kim B.-W., Ko Y.-G., Jang S.K. and Kim Y.K. (2009). A new MIF4G domain-containing protein, CTIF, directs nuclear cap-binding protein CBP80/20-dependent translation. *Genes & development* 23(17): 2033-2045.
- Kim T.-K., Hemberg M. and Gray J.M. (2015). Enhancer RNAs: a class of long noncoding RNAs synthesized at enhancers. *Cold Spring Harbor perspectives in biology* 7(1): a018622-a018622.
- Kirino Y. and Mourelatos Z. (2007). Mouse Piwi-interacting RNAs are 2'-O-methylated at their 3' termini. *Nature Structural & Molecular Biology* 14: 347.
- Kiss-László Z., Henry Y., Bachelier J.-P., Caizergues-Ferrer M. and Kiss T. (1996). Site-Specific Ribose Methylation of Preribosomal RNA: A Novel Function for Small Nucleolar RNAs. *Cell* 85(7): 1077-1088.
- Klausen M.S., Jespersen M.C., Nielsen H., Jensen K.K., Jurtz V.I., Sønnderby C.K., Sommer M.O.A., Winther O., Nielsen M., Petersen B. and Marcátilli P. (2019). NetSurfP-2.0: Improved prediction of protein structural features by integrated deep learning. *Proteins: Structure, Function, and Bioinformatics* 87(6): 520-527.

- Knott G.J., Bond C.S. and Fox A.H. (2016). The DBHS proteins SFPO, NONO and PSP1: a multipurpose molecular scaffold. *Nucleic acids research* 44(9): 3989-4004.
- Knuckles P., Carl S.H., Musheev M., Niehrs C., Wenger A. and Bühler M. (2017). RNA fate determination through cotranscriptional adenosine methylation and microprocessor binding. *Nature Structural and Molecular Biology* 24: 561.
- Knuckles P., Lence T., Haussmann I.U., Jacob D., Kreim N., Carl S.H., Masiello I., Hares T., Villaseñor R., Hess D., Andrade-Navarro M.A., Biggiogera M., Helm M., Soller M., Bühler M. and Roignant J.-Y. (2018). Zc3h13/Flacc is required for adenosine methylation by bridging the mRNA-binding factor Rbm15/Spenito to the m6A machinery component Wtap/Fl(2)d. *Genes & Development* 32(5-6): 415-429.
- Kobayashi M., Ohsugi M., Sasako T., Awazawa M., Umehara T., Iwane A., Kobayashi N., Okazaki Y., Kubota N., Suzuki R., Waki H., Horiuchi K., Hamakubo T., Kodama T., Aoe S., Tobe K., Kadowaki T. and Ueki K. (2018). The RNA Methyltransferase Complex of WTAP, METTL3, and METTL14 Regulates Mitotic Clonal Expansion in Adipogenesis. *Molecular and cellular biology* 38(16): e00116-00118.
- Kochanova N.Y., Schauer T., Mathias G.P., Lukacs A., Schmidt A., Flatley A., Schepers A., Thomae A.W. and Imhof A. (2020). A multi-layered structure of the interphase chromocenter revealed by proximity-based biotinylation. *Nucleic Acids Research* 48(8): 4161-4178.
- Kondo S. and Ueda R. (2013). Highly improved gene targeting by germline-specific Cas9 expression in *Drosophila*. *Genetics* 195(3): 715-721.
- Konig J., Zarnack K., Rot G., Curk T., Kayikci M., Zupan B., Turner D.J., Luscombe N.M. and Ule J. (2011). iCLIP—transcriptome-wide mapping of protein-RNA interactions with individual nucleotide resolution. *J Vis Exp*(50).
- Kopp F. and Mendell J.T. (2018). Functional Classification and Experimental Dissection of Long Noncoding RNAs. *Cell* 172(3): 393-407.
- Koranda J.L., Dore L., Shi H., Patel M.J., Vaasjo L.O., Rao M.N., Chen K., Lu Z., Yi Y., Chi W., He C. and Zhuang X. (2018). Mettl14 Is Essential for Epitranscriptomic Regulation of Striatal Function and Learning. *Neuron* 99(2): 283-292.e285.
- Kosugi S., Hasebe M., Tomita M. and Yanagawa H. (2009). Systematic identification of cell cycle-dependent yeast nucleocytoplasmic shuttling proteins by prediction of composite motifs. *Proceedings of the National Academy of Sciences of the United States of America* 106(25): 10171-10176.
- Kouzarides T. (2007). Chromatin Modifications and Their Function. *Cell* 128(4): 693-705.
- Kozopas K.M. and Nusse R. (2002). Direct flight muscles in *Drosophila* develop from cells with characteristics of founders and depend on DWnt-2 for their correct patterning. *Developmental biology* 243(2): 312-325.
- Krogh N., Jansson M.D., Häfner S.J., Tehler D., Birkedal U., Christensen-Dalsgaard M., Lund A.H. and Nielsen H. (2016). Profiling of 2'-O-Me in human rRNA reveals a subset of fractionally modified positions and provides evidence for ribosome heterogeneity. *Nucleic Acids Res* 44(16): 7884-7895.
- Kudou K., Komatsu T., Nogami J., Maehara K., Harada A., Saeki H., Oki E., Maehara Y. and Ohkawa Y. (2017). The requirement of Mettl3-promoted MyoD mRNA maintenance in proliferative myoblasts for skeletal muscle differentiation. *Open biology* 7(9): 170119.
- Kumar P., Kuscic C. and Dutta A. (2016). Biogenesis and Function of Transfer RNA-Related Fragments (tRFs). *Trends in Biochemical Sciences* 41(8): 679-689.
- Kwasnieski J.C., Orr-Weaver T.L. and Bartel D.P. (2019). Early genome activation in *Drosophila* is extensive with an initial tendency for aborted transcripts and retained introns. *Genome research* 29(7): 1188-1197.
- Kweon S.-M., Chen Y., Moon E., Kvederaviciute K., Klimasauskas S. and Feldman D.E. (2019). An Adversarial DNA N6-Methyladenine-Sensor Network Preserves Polycomb Silencing. *Molecular Cell* 74(6): 1138-1147.e1136.
- Lafontaine D., Delcour J., Glasser A.-L., Desgres J. and Vandenhaute J. (1994). The DIM1 Gene Responsible for the Conserved m6Am62A Dimethylation in the 3'-Terminal Loop of 18 S rRNA is Essential in Yeast. *Journal of Molecular Biology* 241(3): 492-497.
- Lahav R., Gammie A., Tavazoie S. and Rose M.D. (2007). Role of transcription factor Kar4 in regulating downstream events in the *Saccharomyces cerevisiae* pheromone response pathway. *Molecular and cellular biology* 27(3): 818-829.
- Lai C.J., Dahlberg J.E. and Weisblum B. (1973). Structure of an inducibly methylatable nucleotide sequence in 23S ribosomal ribonucleic acid from erythromycin-resistant *Staphylococcus aureus*. *Biochemistry* 12(3): 457-460.
- Lai C.J. and Weisblum B. (1971). Altered methylation of ribosomal RNA in an erythromycin-resistant strain of *Staphylococcus aureus*. *Proc Natl Acad Sci U S A* 68(4): 856-860.
- Lan M.-D., Xiong J., You X.-J., Weng X.-C., Zhou X., Yuan B.-F. and Feng Y.-Q. (2018). Existence of Diverse Modifications in Small-RNA Species Composed of 16–28 Nucleotides. *Chemistry – A European Journal* 24(39): 9949-9956.
- Langemeier J., Radtke M. and Bohne J. (2013). U1 snRNP-mediated poly(A) site suppression: beneficial and deleterious for mRNA fate. *RNA biology* 10(2): 180-184.
- Larkin M.A., Blackshields G., Brown N.P., Chenna R., McGettigan P.A., McWilliam H., Valentin F., Wallace I.M., Wilm A., Lopez R., Thompson J.D., Gibson T.J. and Higgins D.G. (2007). Clustal W and Clustal X version 2.0. *Bioinformatics* 23(21): 2947-2948.
- Lasman L., Krupalnik V., Geula S., Zerbib M., Viukov S., Mor N., Aguilera Castrejon A., Mizrahi O., Shashank S., Nachshon A., Schneir D., Aigner S., Shankar A., Mueller J., Stern-Ginossar N., Yeo G.W., Novershtern N. and Hanna J.H. (2020). Context-dependent functional compensation between Ythdf m6A readers. *bioRxiv*: 2020.2006.2003.131441.
- Lawrence M., Daujat S. and Schneider R. (2016). Lateral Thinking: How Histone Modifications Regulate Gene Expression. *Trends in Genetics* 32(1): 42-56.
- Lee H., Bao S., Qian Y., Geula S., Leslie J., Zhang C., Hanna J.H. and Ding L. (2019). Stage-specific requirement for Mettl3-dependent m6A mRNA methylation during haematopoietic stem cell differentiation. *Nature Cell Biology* 21(6): 700-709.
- Lee J.-H. and Skalnik D.G. (2012). Rbm15-Mkl1 interacts with the Setd1b histone H3-Lys4 methyltransferase via a SPOC domain that is required for cytokine-independent proliferation. *PLoS one* 7(8): e42965-e42965.
- Lee Y., Choe J., Park O.H. and Kim Y.K. (2020). Molecular Mechanisms Driving mRNA Degradation by m(6)A Modification. *Trends in genetics : TIG* 36(3): 177-188.
- Lee Y. and Rio D.C. (2015). Mechanisms and Regulation of Alternative Pre-mRNA Splicing. *Annual Review of Biochemistry* 84(1): 291-323.
- Leger A., Amaral P.P., Pandolfini L., Capitanich C., Capraro F., Barbieri I., Migliori V., Luscombe N.M., Enright A.J., Tzelepis K., Ule J., Fitzgerald T., Birney E., Leonardi T. and Kouzarides T. (2019). RNA modifications detection by comparative Nanopore direct RNA sequencing. *bioRxiv*: 843136.
- Legrand C., Tuorto F., Hartmann M., Liebers R., Jacob D., Helm M. and Lyko F. (2017). Statistically robust methylation calling for whole-transcriptome bisulfite sequencing reveals distinct methylation patterns for mouse RNAs. *Genome research* 27(9): 1589-1596.
- Leismann J., Spagnuolo M., Pradhan M., Wacheul L., Vu M.A., Musheev M., Mier P., Andrade-Navarro M.A., Graille M., Niehrs C., Lafontaine D.L. and Roignant J.Y. (2020). The 18S ribosomal RNA m(6) A methyltransferase Mettl5 is required for normal walking behavior in *Drosophila*. *EMBO reports*: e49443.
- Lence T., Akhtar J., Bayer M., Schmid K., Spindler L., Ho C.H., Kreim N., Andrade-Navarro M.A., Poec B., Helm M. and Roignant J.-Y. (2016). m6A modulates neuronal functions and sex determination in *Drosophila*. *Nature* 540: 242.
- Lence T., Paolantoni C., Worpenberg L. and Roignant J.-Y. (2019). Mechanistic insights into m6A RNA enzymes. *Biochimica et Biophysica Acta (BBA) - Gene Regulatory Mechanisms* 1862(3): 222-229.
- Lence T., Soller M. and Roignant J.Y. (2017). A fly view on the roles and mechanisms of the m6A mRNA modification and its players. *RNA biology*: 1-9.

- Lennox A.L., Mao H. and Silver D.L. (2018). RNA on the brain: emerging layers of post-transcriptional regulation in cerebral cortex development. *Wiley Interdisciplinary Reviews: Developmental Biology* 7(1): e290.
- Lesbirel S., Viphakone N., Parker M., Parker J., Heath C., Sudbery I. and Wilson S.A. (2018). The m6A-methylase complex recruits TREX and regulates mRNA export. *Scientific Reports* 8(1): 13827.
- Lesbirel S. and Wilson S.A. (2019). The m(6)A-methylase complex and mRNA export. *Biochim Biophys Acta Gene Regul Mech* 1862(3): 319-328.
- Letunic I. and Bork P. (2019). Interactive Tree Of Life (iTOL) v4: recent updates and new developments. *Nucleic Acids Research* 47(W1): W256-W259.
- Levanon E.Y., Eisenberg E., Yelin R., Nemzer S., Hallegger M., Shemesh R., Fligelman Z.Y., Shoshan A., Pollock S.R., Szybel D., Olshansky M., Rechavi G. and Jantsch M.F. (2004). Systematic identification of abundant A-to-I editing sites in the human transcriptome. *Nature Biotechnology* 22: 1001.
- Lewis C.J.T., Pan T. and Kalsotra A. (2017). RNA modifications and structures cooperate to guide RNA-protein interactions. *Nature Reviews Molecular Cell Biology* 18(3): 202-210.
- Lewis J.D., Izaurralde E., Jarmolowski A., McGuigan C. and Mattaj J.W. (1996). A nuclear cap-binding complex facilitates association of U1 snRNP with the cap-proximal 5' splice site. *Genes & Development* 10(13): 1683-1698.
- Li A., Chen Y.-S., Ping X.-L., Yang X., Xiao W., Yang Y., Sun H.-Y., Zhu Q., Baidya P., Wang X., Bhattarai D.P., Zhao Y.-L., Sun B.-F. and Yang Y.-G. (2017). Cytoplasmic m(6)A reader YTHDF3 promotes mRNA translation. *Cell research* 27(3): 444-447.
- Li F., Zhao D., Wu J. and Shi Y. (2014). Structure of the YTH domain of human YTHDF2 in complex with an m6A mononucleotide reveals an aromatic cage for m6A recognition. *Cell Research* 24(12): 1490-1492.
- Li H.-B., Tong J., Zhu S., Batista P.J., Duffy E.E., Zhao J., Bailis W., Cao G., Kroehling L., Chen Y., Wang G., Broughton J.P., Chen Y.G., Kluger Y., Simon M.D., Chang H.Y., Yin Z. and Flavell R.A. (2017). m(6)A mRNA methylation controls T cell homeostasis by targeting the IL-7/STAT5/SOCS pathways. *Nature* 548(7667): 338-342.
- Li L., Zang L., Zhang F., Chen J., Shen H., Shu L., Liang F., Feng C., Chen D., Tao H., Xu T., Li Z., Kang Y., Wu H., Tang L., Zhang P., Jin P., Shu Q. and Li X. (2017). Fat mass and obesity-associated (FTO) protein regulates adult neurogenesis. *Human molecular genetics* 26(13): 2398-2411.
- Li M., Zhao X., Wang W., Shi H., Pan Q., Lu Z., Perez S.P., Suganthan R., He C., Bjørås M. and Klungland A. (2018). Ythdf2-mediated m(6)A mRNA clearance modulates neural development in mice. *Genome Biol* 19(1): 69.
- Li X., Ma S. and Yi C. (2016). Pseudouridine: the fifth RNA nucleotide with renewed interests. *Current Opinion in Chemical Biology* 33: 108-116.
- Li X., Xiong X., Wang K., Wang L., Shu X., Ma S. and Yi C. (2016). Transcriptome-wide mapping reveals reversible and dynamic N(1)-methyladenosine methylome. *Nature chemical biology* 12(5): 311-316.
- Li X., Xiong X., Zhang M., Wang K., Chen Y., Zhou J., Mao Y., Lv J., Yi D., Chen X.W., Wang C., Qian S.B. and Yi C. (2017). Base-Resolution Mapping Reveals Distinct m(1)A Methylome in Nuclear- and Mitochondrial-Encoded Transcripts. *Mol Cell* 68(5): 993-1005 e1009.
- Li X., Yang L. and Chen L.-L. (2018). The Biogenesis, Functions, and Challenges of Circular RNAs. *Molecular Cell* 71(3): 428-442.
- Li X., Zhu P., Ma S., Song J., Bai J., Sun F. and Yi C. (2015). Chemical pulldown reveals dynamic pseudouridylation of the mammalian transcriptome. *Nature Chemical Biology* 11: 592.
- Li Y., Song M.-G. and Kiledjian M. (2008). Transcript-specific decapping and regulated stability by the human Dcp2 decapping protein. *Molecular and cellular biology* 28(3): 939-948.
- Li Y., Wang X., Li C., Hu S., Yu J. and Song S. (2014). Transcriptome-wide N6-methyladenosine profiling of rice callus and leaf reveals the presence of tissue-specific competitors involved in selective mRNA modification. *RNA biology* 11(9): 1180-1188.
- Liao S., Sun H. and Xu C. (2018). YTH Domain: A Family of N(6)-methyladenosine (m(6)A) Readers. *Genomics, proteomics & bioinformatics* 16(2): 99-107.
- Lichinchi G., Gao S., Saletore Y., Gonzalez G.M., Bansal V., Wang Y., Mason C.E. and Rana T.M. (2016). Dynamics of the human and viral m(6)A RNA methylomes during HIV-1 infection of T cells. *Nat Microbiol* 1: 16011-16011.
- Lichinchi G., Zhao B.S., Wu Y., Lu Z., Qin Y., He C. and Rana T.M. (2016). Dynamics of Human and Viral RNA Methylation during Zika Virus Infection. *Cell Host Microbe* 20(5): 666-673.
- Licht K., Kapoor U., Mayrhofer E. and Jantsch M.F. (2016). Adenosine to Inosine editing frequency controlled by splicing efficiency. *Nucleic acids research* 44(13): 6398-6408.
- Liddicoat B.J., Piskol R., Chalk A.M., Ramaswami G., Higuchi M., Hartner J.C., Li J.B., Seeburg P.H. and Walkley C.R. (2015). RNA editing by ADAR1 prevents MDA5 sensing of endogenous dsRNA as nonself. *Science (New York, N.Y.)* 349(6252): 1115-1120.
- Lim J., Ha M., Chang H., Kwon S.C., Simanshu D.K., Patel D.J. and Kim V.N. (2014). Uridylation by TUT4 and TUT7 marks mRNA for degradation. *Cell* 159(6): 1365-1376.
- Lim L.P. and Burge C.B. (2001). A computational analysis of sequence features involved in recognition of short introns. *Proceedings of the National Academy of Sciences* 98(20): 11193-11198.
- Lin S., Choe J., Du P., Triboulet R. and Gregory R.I. (2016). The m(6)A Methyltransferase METTL3 Promotes Translation in Human Cancer Cells. *Mol Cell* 62(3): 335-345.
- Lin Z., Hsu P.J., Xing X., Fang J., Lu Z., Zou Q., Zhang K.-J., Zhang X., Zhou Y., Zhang T., Zhang Y., Song W., Jia G., Yang X., He C. and Tong M.-H. (2017). Mettl3-/Mettl14-mediated mRNA N(6)-methyladenosine modulates murine spermatogenesis. *Cell research* 27(10): 1216-1230.
- Linder B., Grozhik A.V., Olarerin-George A.O., Meydan C., Mason C.E. and Jaffrey S.R. (2015). Single-nucleotide-resolution mapping of m6A and m6Am throughout the transcriptome. *Nature methods* 12(8): 767-772.
- Linder B. and Jaffrey S.R. (2019). Discovering and Mapping the Modified Nucleotides That Comprise the Epitranscriptome of mRNA. *Cold Spring Harbor Perspectives in Biology* 11(6).
- Liscovitch-Brauer N., Alon S., Porath H.T., Elstein B., Unger R., Ziv T., Admon A., Levanon E.Y., Rosenthal J.J.C. and Eisenberg E. (2017). Trade-off between Transcriptome Plasticity and Genome Evolution in Cephalopods. *Cell* 169(2): 191-202.e111.
- Littlefield J.W. and Dunn D.B. (1958). The occurrence and distribution of thymine and three methylated-adenine bases in ribonucleic acids from several sources. *Biochemical Journal* 70(4): 642-651.
- Littleton J.T., Bellen H.J. and Perin M.S. (1993). Expression of synaptotagmin in *Drosophila* reveals transport and localization of synaptic vesicles to the synapse. *Development* 118(4): 1077-1088.
- Liu B., Merriman D.K., Choi S.H., Schumacher M.A., Plangger R., Kreutz C., Horner S.M., Meyer K.D. and Al-Hashimi H.M. (2018). A potentially abundant junctional RNA motif stabilized by m(6)A and Mg(2+). *Nature Communications* 9: 2761.
- Liu F., Clark W., Luo G., Wang X., Fu Y., Wei J., Wang X., Hao Z., Dai Q., Zheng G., Ma H., Han D., Evans M., Klungland A., Pan T. and He C. (2016). ALKBH1-Mediated tRNA Demethylation Regulates Translation. *Cell* 167(3): 816-828.e816.
- Liu H., Begik O., Lucas M.C., Ramirez J.M., Mason C.E., Wiener D., Schwartz S., Mattick J.S., Smith M.A. and Novoa E.M. (2019). Accurate detection of m(6)A RNA modifications in native RNA sequences. *Nature communications* 10(1): 4079-4079.
- Liu J., Li K., Cai J., Zhang M., Zhang X., Xiong X., Meng H., Xu X., Huang Z., Peng J., Fan J. and Yi C. (2020). Landscape and Regulation of m(6)A and m(6)Am Methylome across Human and Mouse Tissues. *Mol Cell* 77(2): 426-440.e426.
- Liu J., Zhu Y., Luo G.-Z., Wang X., Yue Y., Wang X., Zong X., Chen K., Yin H., Fu Y., Han D., Wang Y., Chen D. and He C. (2016). Abundant DNA 6mA methylation during early embryogenesis of zebrafish and pig. *Nature Communications* 7(1): 13052.
- Liu J.Z., Yue Y.N., Han D.L., Wang X., Fu Y., Zhang L., Jia G.F., Yu M., Lu Z.K., Deng X., Dai Q., Chen W.Z. and He C. (2014). A METTL3-

- METTL14 complex mediates mammalian nuclear RNA N6-adenosine methylation. *Nature Chemical Biology* 10(2): 93-95.
- Liu N., Dai Q., Zheng G., He C., Parisien M. and Pan T. (2015). N6-methyladenosine-dependent RNA structural switches regulate RNA-protein interactions. *Nature* 518: 560.
- Liu N., Parisien M., Dai Q., Zheng G., He C. and Pan T. (2013). Probing N6-methyladenosine RNA modification status at single nucleotide resolution in mRNA and long noncoding RNA. *RNA (New York, N.Y.)* 19(12): 1848-1856.
- Liu N., Zhou K.I., Parisien M., Dai Q., Diatchenko L. and Pan T. (2017). N6-methyladenosine alters RNA structure to regulate binding of a low-complexity protein. *Nucleic Acids Research* 45(10): 6051-6063.
- Liu X.-M., Zhou J., Mao Y., Ji Q. and Qian S.-B. (2019). Programmable RNA N 6-methyladenosine editing by CRISPR-Cas9 conjugates. *Nature chemical biology* 15(9): 865-871.
- Liu X., Lai W., Li Y., Chen S., Liu B., Zhang N., Mo J., Lyu C., Zheng J., Du Y.-R., Jiang G., Xu G.-L. and Wang H. (2020). N6-methyladenine is incorporated into mammalian genome by DNA polymerase. *Cell Research*.
- Liu Y.-Q., Bai G., Zhang H., Su D., Tao D.-C., Yang Y., Ma Y.-X. and Zhang S.-Z. (2010). Human RING finger protein ZNF645 is a novel testis-specific E3 ubiquitin ligase. *Asian J Androl* 12(5): 658-666.
- Liu Z.-X., Li L.-M., Sun H.-L. and Liu S.-M. (2018). Link Between m6A Modification and Cancers. *Frontiers in Bioengineering and Biotechnology* 6(89).
- Livneh I., Moshitch-Moshkovitz S., Amariglio N., Rechavi G. and Dominissini D. (2020). The m(6)A epitranscriptome: transcriptome plasticity in brain development and function. *Nat Rev Neurosci* 21(1): 36-51.
- Lobel J.H. and Gross J.D. (2020). Pat1 increases the range of decay factors and RNA bound by the Lsm1-7 complex. *bioRxiv: 2020.2004.2007.029900*.
- Loos R.J.F. and Yeo G.S.H. (2014). The bigger picture of FTO: the first GWAS-identified obesity gene. *Nature reviews. Endocrinology* 10(1): 51-61.
- Louloupi A., Ntini E., Conrad T. and Ørom U.A.V. (2018). Transient N6-Methyladenosine Transcriptome Sequencing Reveals a Regulatory Role of m6A in Splicing Efficiency. *Cell Reports* 23(12): 3429-3437.
- Luo G.-Z., MacQueen A., Zheng G., Duan H., Dore L.C., Lu Z., Liu J., Chen K., Jia G., Bergelson J. and He C. (2014). Unique features of the m6A methylome in Arabidopsis thaliana. *Nature Communications* 5(1): 5630.
- Luo S. and Tong L. (2014). Molecular basis for the recognition of methylated adenines in RNA by the eukaryotic YTH domain. *Proceedings of the National Academy of Sciences of the United States of America* 111(38): 13834-13839.
- Luo W., Guo F., McMahon A., Couvartier S., Jin H., Diaz M., Fieldsend A., Weerapana E. and Rosbash M. (2018). NonA and CPX Link the Circadian Clockwork to Locomotor Activity in Drosophila. *Neuron* 99(4): 768-780.e763.
- Luo Y., Na Z. and Slavoff S.A. (2018). P-Bodies: Composition, Properties, and Functions. *Biochemistry* 57(17): 2424-2431.
- Lupas A., Van Dyke M. and Stock J. (1991). Predicting coiled coils from protein sequences. *Science* 252(5009): 1162-1164.
- Ma C., Chang M., Lv H., Zhang Z.-W., Zhang W., He X., Wu G., Zhao S., Zhang Y., Wang D., Teng X., Liu C., Li Q., Klungland A., Niu Y., Song S. and Tong W.-M. (2018). RNA m(6)A methylation participates in regulation of postnatal development of the mouse cerebellum. *Genome biology* 19(1): 68-68.
- Ma H., Wang X., Cai J., Dai Q., Natchiar S.K., Lv R., Chen K., Lu Z., Chen H., Shi Y.G., Lan F., Fan J., Klaholz B.P., Pan T., Shi Y. and He C. (2019). N6-Methyladenosine methyltransferase ZCCHC4 mediates ribosomal RNA methylation. *Nature Chemical Biology* 15(1): 88-94.
- Ma X., Renda M.J., Wang L., Cheng E.C., Niu C., Morris S.W., Chi A.S. and Krause D.S. (2007). Rbm15 modulates Notch-induced transcriptional activation and affects myeloid differentiation. *Molecular and cellular biology* 27(8): 3056-3064.
- Malbec L., Zhang T., Chen Y.-S., Zhang Y., Sun B.-F., Shi B.-Y., Zhao Y.-L., Yang Y. and Yang Y.-G. (2019). Dynamic methylome of internal mRNA N7-methylguanosine and its regulatory role in translation. *Cell Research* 29(11): 927-941.
- Marengere L.E.M. and Pawson T. (1994). Structure and function of SH2 domains. *Journal of Cell Science* 1994(Supplement 18): 97-104.
- Martinez F.J., Pratt G.A., Van Nostrand E.L., Batra R., Huelga S.C., Kapeli K., Freese P., Chun S.J., Ling K., Gelboin-Burkhardt C., Fijany L., Wang H.C., Nussbacher J.K., Broski S.M., Kim H.J., Lardelli R., Sundararaman B., Donohue J.P., Javaherian A., Lykke-Andersen J., Finkbeiner S., Bennett C.F., Ares M., Jr., Burge C.B., Taylor J.P., Rigo F. and Yeo G.W. (2016). Protein-RNA Networks Regulated by Normal and ALS-Associated Mutant HNRNPA2B1 in the Nervous System. *Neuron* 92(4): 780-795.
- Martinez J. and Tuschl T. (2004). RISC is a 5' phosphomonoester-producing RNA endonuclease. *Genes & Development* 18(9): 975-980.
- Marygold S.J., Attrill H. and Lasko P. (2017). The translation factors of *Drosophila melanogaster*. *Fly (Austin)* 11(1): 65-74.
- Masamha C.P., Xia Z., Yang J., Albrecht T.R., Li M., Shyu A.-B., Li W. and Wagner E.J. (2014). CFIm25 links alternative polyadenylation to glioblastoma tumour suppression. *Nature* 510(7505): 412-416.
- Matera A.G. and Wang Z. (2014). A day in the life of the spliceosome. *Nature Reviews Molecular Cell Biology* 15: 108.
- Mauer J., Luo X., Blanjoie A., Jiao X., Grozhik A.V., Patil D.P., Linder B., Pickering B.F., Vasseur J.J., Chen Q., Gross S.S., Elemento O., Debart F., Kiledjian M. and Jaffrey S.R. (2017). Reversible methylation of m(6)Am in the 5' cap controls mRNA stability. *Nature* 541(7637): 371-375.
- Mauer J., Sindelar M., Despic V., Guez T., Hawley B.R., Vasseur J.-J., Rentmeister A., Gross S.S., Pellizzoni L., Debart F., Goodarzi H. and Jaffrey S.R. (2019). FTO controls reversible m6Am RNA methylation during snRNA biogenesis. *Nature Chemical Biology* 15(4): 340-347.
- Meissner A., Mikkelsen T.S., Gu H., Wernig M., Hanna J., Sivachenko A., Zhang X., Bernstein B.E., Nusbaum C., Jaffe D.B., Gnirke A., Jaenisch R. and Lander E.S. (2008). Genome-scale DNA methylation maps of pluripotent and differentiated cells. *Nature* 454: 766.
- Mendel M., Chen K.-M., Homolka D., Gos P., Pandey R.R., McCarthy A.A. and Pillai R.S. (2018). Methylation of Structured RNA by the m⁶A Writer METTL16 Is Essential for Mouse Embryonic Development. *Molecular Cell* 71(6): 986-1000.e1011.
- Meng T.-G., Lu X., Guo L., Hou G.-M., Ma X.-S., Li Q.-N., Huang L., Fan L.-H., Zhao Z.-H., Ou X.-H., OuYang Y.-C., Schatten H., Li L., Wang Z.-B. and Sun Q.-Y. (2019). Mettl14 is required for mouse postimplantation development by facilitating epiblast maturation. *The FASEB Journal* 33(1): 1179-1187.
- Menon K.P., Carrillo R.A. and Zinn K. (2013). Development and plasticity of the *Drosophila* larval neuromuscular junction. *Wiley Interdiscip Rev Dev Biol* 2(5): 647-670.
- Merkin J., Russell C., Chen P. and Burge C.B. (2012). Evolutionary dynamics of gene and isoform regulation in Mammalian tissues. *Science (New York, N.Y.)* 338(6114): 1593-1599.
- Merkurjev D., Hong W.T., Iida K., Oomoto I., Goldie B.J., Yamaguti H., Ohara T., Kawaguchi S.Y., Hirano T., Martin K.C., Pellegrini M. and Wang D.O. (2018). Synaptic N(6)-methyladenosine (m(6)A) epitranscriptome reveals functional partitioning of localized transcripts. *Nat Neurosci* 21(7): 1004-1014.
- Messerschmidt D.M., Knowles B.B. and Solter D. (2014). DNA methylation dynamics during epigenetic reprogramming in the germline and preimplantation embryos. *Genes & Development* 28(8): 812-828.
- Metzger E., Wang S., Urban S., Willmann D., Schmidt A., Offermann A., Allen A., Sum M., Obier N., Cottard F., Ulferts S., Preca B.-T., Hermann B., Maurer J., Greschik H., Hornung V., Einsle O., Perner S., Imhof A., Jung M. and Schüle R. (2019). KMT9 monomethylates histone H4 lysine 12 and controls proliferation of prostate cancer cells. *Nature Structural & Molecular Biology* 26(5): 361-371.
- Metzger M.B., Hristova V.A. and Weissman A.M. (2012). HECT and RING finger families of E3 ubiquitin ligases at a glance. *Journal of Cell Science* 125(3): 531-537.
- Meyer K.D. (2019). DART-seq: an antibody-free method for global m6A detection. *Nature Methods* 16(12): 1275-1280.
- Meyer K.D. (2019). m(6)A-mediated translation regulation. *Biochim Biophys Acta Gene Regul Mech* 1862(3): 301-309.

- Meyer K.D., Patil D.P., Zhou J., Zinoviev A., Skabkin M.A., Elemento O., Pestova T.V., Qian S.B. and Jaffrey S.R. (2015). 5' UTR m(6)A Promotes Cap-Independent Translation. *Cell* 163(4): 999-1010.
- Meyer K.D., Saletore Y., Zumbo P., Elemento O., Mason C.E. and Jaffrey S.R. (2012). Comprehensive Analysis of mRNA Methylation Reveals Enrichment in 3' UTRs and near Stop Codons. *Cell* 149(7): 1635-1646.
- Micura R., Pils W., Höbartner C., Grubmayr K., Ebert M.-O. and Jaun B. (2001). Methylation of the nucleobases in RNA oligonucleotides mediates duplex-hairpin conversion. *Nucleic Acids Research* 29(19): 3997-4005.
- Miller M.A. and Olivas W.M. (2011). Roles of Puf proteins in mRNA degradation and translation. *Wiley Interdisciplinary Reviews: RNA* 2(4): 471-492.
- Milyaev N., Osumi-Sutherland D., Reeve S., Burton N., Baldock R.A. and Armstrong J.D. (2011). The Virtual Fly Brain browser and query interface. *Bioinformatics* 28(3): 411-415.
- Mira-Bontenbal H. and Gribnau J. (2016). New Xist-Interacting Proteins in X-Chromosome Inactivation. *Current Biology* 26(8): R338-R342.
- Mishina Y. and He C. (2006). Oxidative dealkylation DNA repair mediated by the mononuclear non-heme iron AlkB proteins. *J Inorg Biochem* 100(4): 670-678.
- Mitchell A.L., Attwood T.K., Babbitt P.C., Blum M., Bork P., Bridge A., Brown S.D., Chang H.-Y., El-Gebali S., Fraser M.I., Gough J., Haft D.R., Huang H., Letunic I., Lopez R., Luciani A., Madeira F., Marchler-Bauer A., Mi H., Natale D.A., Necci M., Nuka G., Orengo C., Pandurangan A.P., Paysan-Lafosse T., Pesce S., Potter S.C., Qureshi M.A., Rawlings N.D., Redaschi N., Richardson L.J., Rivoire C., Salazar G.A., Sangrador-Vegas A., Sigrist C.J.A., Sillitoe I., Sutton G.G., Thanki N., Thomas P.D., Tosatto S.C.E., Yong S.-Y. and Finn R.D. (2019). InterPro in 2019: improving coverage, classification and access to protein sequence annotations. *Nucleic acids research* 47(D1): D351-D360.
- Modic M., Ule J. and Sibley C.R. (2013). CLIPing the brain: studies of protein-RNA interactions important for neurodegenerative disorders. *Molecular and cellular neurosciences* 56: 429-435.
- Mohapatra S.S., Fioravanti A. and Biondi E.G. (2014). DNA methylation in *Caulobacter* and other Alphaproteobacteria during cell cycle progression. *Trends in Microbiology* 22(9): 528-535.
- Moindrot B., Cerase A., Coker H., Masui O., Grijzenhout A., Pintacuda G., Schermelleh L., Nesterova Tatyana B. and Brockdorff N. (2015). A Pooled shRNA Screen Identifies Rbm15, Spen, and Wtap as Factors Required for Xist RNA-Mediated Silencing. *Cell Reports* 12(4): 562-572.
- Molinie B., Wang J., Lim K.S., Hillebrand R., Lu Z.-X., Van Wittenberghe N., Howard B.D., Daneshvar K., Mullen A.C., Dedon P., Xing Y. and Giallourakis C.C. (2016). m(6)A-LAIC-seq reveals the census and complexity of the m(6)A epitranscriptome. *Nature methods* 13(8): 692-698.
- Mondo S.J., Dannebaum R.O., Kuo R.C., Louie K.B., Bewick A.J., LaButti K., Haridas S., Kuo A., Salamov A., Ahrendt S.R., Lau R., Bowen B.P., Lipzen A., Sullivan W., Andreopoulos B.B., Clum A., Lindquist E., Daum C., Northen T.R., Kunde-Ramamoorthy G., Schmitz R.J., Gryganskyi A., Culley D., Magnuson J., James T.Y., O'Malley M.A., Stajich J.E., Spatafora J.W., Visel A. and Grigoriev I.V. (2017). Widespread adenine N6-methylation of active genes in fungi. *Nature Genetics* 49: 964.
- Moschall R., Gaik M. and Medenbach J. (2017). Promiscuity in post-transcriptional control of gene expression: *Drosophila* sex-lethal and its regulatory partnerships. *FEBS Letters* 591(11): 1471-1488.
- Motorin Y. (2015). RNA Modification. *eLS*.
- Motorin Y. and Helm M. (2010). tRNA Stabilization by Modified Nucleotides. *Biochemistry* 49(24): 4934-4944.
- Motorin Y. and Helm M. (2011). RNA nucleotide methylation. *Wiley Interdisciplinary Reviews: RNA* 2(5): 611-631.
- Motorin Y. and Helm M. (2019). Methods for RNA Modification Mapping Using Deep Sequencing: Established and New Emerging Technologies. *Genes* 10(1): 35.
- Mugridge J.S., Collier J. and Gross J.D. (2018). Structural and molecular mechanisms for the control of eukaryotic 5'-3' mRNA decay. *Nature Structural & Molecular Biology* 25(12): 1077-1085.
- Mukherjee M., Chow S.Y., Yusoff P., Seetharaman J., Ng C., Sinniah S., Koh X.W., Asgar N.F.M., Li D., Yim D., Jackson R.A., Yew J., Qian J., Iyu A., Lim Y.P., Zhou X., Sze S.K., Guy G.R. and Sivaraman J. (2012). Structure of a novel phosphotyrosine-binding domain in Hakai that targets E-cadherin. *The EMBO Journal* 31(5): 1308-1319.
- Müller-McNicol M., Botti V., de Jesus Domingues A.M., Brandl H., Schwich O.D., Steiner M.C., Curk T., Poser I., Zarnack K. and Neugebauer K.M. (2016). SR proteins are NXF1 adaptors that link alternative RNA processing to mRNA export. *Genes & development* 30(5): 553-566.
- Murthy K.G., Park P. and Manley J.L. (1991). A nuclear micrococcal-sensitive, ATP-dependent exoribonuclease degrades uncapped but not capped RNA substrates. *Nucleic acids research* 19(10): 2685-2692.
- Musheev M.U., Baumgärtner A., Krebs L. and Niehrs C. (2020). The origin of genomic N(6)-methyl-deoxyadenosine in mammalian cells. *Nature chemical biology* 16(6): 630-634.
- Nachtergaele S. and He C. (2018). Chemical Modifications in the Life of an mRNA Transcript. *Annu Rev Genet* 52: 349-372.
- Naftelberg S., Schor I.E., Ast G. and Kornblihtt A.R. (2015). Regulation of Alternative Splicing Through Coupling with Transcription and Chromatin Structure. *Annual Review of Biochemistry* 84(1): 165-198.
- Nagengast A.A., Stitzinger S.M., Tseng C.-H., Mount S.M. and Salz H.K. (2003). Sex-lethal splicing autoregulation in vivo: interactions between SEX-LETHAL, the U1 snRNP and U2AF underlie male exon skipping. *Development* 130(3): 463-471.
- Narayan P. and Rottman F. (1988). An in vitro system for accurate methylation of internal adenosine residues in messenger RNA. *Science* 242(4882): 1159-1162.
- Natchiar S.K., Myasnikov A.G., Kratzat H., Hazemann I. and Klaholz B.P. (2017). Visualization of chemical modifications in the human 80S ribosome structure. *Nature* 551: 472.
- Nayler O., Hartmann A.M. and Stamm S. (2000). The ER repeat protein YT521-B localizes to a novel subnuclear compartment. *The Journal of cell biology* 150(5): 949-962.
- Nayler O., Strätling W., Bourquin J.P., Staglar I., Lindemann L., Jasper H., Hartmann A.M., Fackelmayer F.O., Ullrich A. and Stamm S. (1998). SAF-B protein couples transcription and pre-mRNA splicing to SAR/MAR elements. *Nucleic acids research* 26(15): 3542-3549.
- Niessen M., Schneiter R. and Nothiger R. (2001). Molecular identification of virilizer, a gene required for the expression of the sex-determining gene Sex-lethal in *Drosophila melanogaster*. *Genetics* 157(2): 679-688.
- Nikalayevich E. and Ohkura H. (2015). The NuRD nucleosome remodelling complex and NHK-1 kinase are required for chromosome condensation in oocytes. *Journal of cell science* 128(3): 566-575.
- Nishikura K. (2015). A-to-I editing of coding and non-coding RNAs by ADARs. *Nature Reviews Molecular Cell Biology* 17: 83.
- Niu C., Zhang J., Breslin P., Onciu M., Ma Z. and Morris S.W. (2009). c-Myc is a target of RNA-binding motif protein 15 in the regulation of adult hematopoietic stem cell and megakaryocyte development. *Blood* 114(10): 2087-2096.
- Niu Y., Wan A., Lin Z., Lu X. and Wan G. (2018). N (6)-Methyladenosine modification: a novel pharmacological target for anti-cancer drug development. *Acta pharmaceutica Sinica*. B 8(6): 833-843.
- Nojima T., Gomes T., Grosso Ana Rita F., Kimura H., Dye Michael J., Dhir S., Carmo-Fonseca M. and Proudfoot Nicholas J. (2015). Mammalian NET-Seq Reveals Genome-wide Nascent Transcription Coupled to RNA Processing. *Cell* 161(3): 526-540.
- Nojima T., Rebelo K., Gomes T., Grosso A.R., Proudfoot N.J. and Carmo-Fonseca M. (2018). RNA Polymerase II Phosphorylated on CTD Serine 5 Interacts with the Spliceosome during Co-transcriptional Splicing. *Molecular Cell* 72(2): 369-379.e364.
- O'Brown Z.K. and Greer E.L. (2016). N6-Methyladenine: A Conserved and Dynamic DNA Mark. *Advances in experimental medicine and biology* 945: 213-246.
- O'Farrell H.C., Scarsdale J.N. and Rife J.P. (2004). Crystal structure of KsgA, a universally conserved rRNA adenine dimethyltransferase in *Escherichia coli*. *J Mol Biol* 339(2): 337-353.

- O'Grady P.M. and DeSalle R. (2018). Phylogeny of the Genus *Drosophila*. *Genetics* 209(1): 1-25.
- Oesterreich F.C., Herzl L., Straube K., Hujer K., Howard J. and Neugebauer K.M. (2016). Splicing of Nascent RNA Coincides with Intron Exit from RNA Polymerase II. *Cell* 165(2): 372-381.
- Oh J.-M., Di C., Venters C.C., Guo J., Arai C., So B.R., Pinto A.M., Zhang Z., Wan L., Younis I. and Dreyfuss G. (2017). U1 snRNP telescripting regulates a size-function-stratified human genome. *Nature structural & molecular biology* 24(11): 993-999.
- Okano M., Bell D.W., Haber D.A. and Li E. (1999). DNA Methyltransferases Dnmt3a and Dnmt3b Are Essential for De Novo Methylation and Mammalian Development. *Cell* 99(3): 247-257.
- Ong C., Yung L.-Y., Cai Y., Bay B.-H. and Baeg G. (2014). *Drosophila melanogaster* as a model organism to study nanotoxicity. *Nanotoxicology* 9: 1-8.
- Ortega A., Niksic M., Bachi A., Wilm M., Sanchez L., Hastie N. and Valcarcel J. (2003). Biochemical function of female-lethal (2)D/Wilms' tumor suppressor-1-associated proteins in alternative pre-mRNA splicing. *J Biol Chem* 278(5): 3040-3047.
- Ovcharenko A. and Rentmeister A. (2018). Emerging approaches for detection of methylation sites in RNA. *Open biology* 8(9): 180121.
- Pabis M., Neufeld N., Steiner M.C., Bojic T., Shav-Tal Y. and Neugebauer K.M. (2013). The nuclear cap-binding complex interacts with the U4/U6-U5 tri-snRNP and promotes spliceosome assembly in mammalian cells. *RNA (New York, N.Y.)* 19(8): 1054-1063.
- Palladino M.J., Keegan L.P., O'Connell M.A. and Reenan R.A. (2000). A-to-I Pre-mRNA Editing in *Drosophila* Is Primarily Involved in Adult Nervous System Function and Integrity. *Cell* 102(4): 437-449.
- Pan Q., Shai O., Lee L.J., Frey B.J. and Blencowe B.J. (2008). Deep surveying of alternative splicing complexity in the human transcriptome by high-throughput sequencing. *Nature Genetics* 40: 1413.
- Pan T. (2018). Modifications and functional genomics of human transfer RNA. *Cell Research* 28(4): 395-404.
- Park J.W., Parisky K., Celotto A.M., Reenan R.A. and Graveley B.R. (2004). Identification of alternative splicing regulators by RNA interference in *Drosophila*. *Proceedings of the National Academy of Sciences of the United States of America* 101(45): 15974-15979.
- Parker K.A. and Steitz J.A. (1989). Determination of RNA-protein and RNA-ribonucleoprotein interactions by nuclease probing. *Methods in enzymology*, Academic Press. 180: 454-468.
- Parker M.T., Knop K., Sherwood A.V., Schurch N.J., Mackinnon K., Gould P.D., Hall A.J.W., Barton G.J. and Simpson G.G. (2020). Nanopore direct RNA sequencing maps the complexity of *Arabidopsis* mRNA processing and m6A modification. *eLife* 9: e49658.
- Parker R. and Song H. (2004). The enzymes and control of eukaryotic mRNA turnover. *Nature Structural and Molecular Biology* 11: 121.
- Patil D.P., Chen C.-K., Pickering B.F., Chow A., Jackson C., Guttman M. and Jaffrey S.R. (2016). m(6)A RNA methylation promotes XIST-mediated transcriptional repression. *Nature* 537(7620): 369-373.
- Patil D.P., Pickering B.F. and Jaffrey S.R. (2017). Reading m6A in the Transcriptome: m6A-Binding Proteins. *Trends in Cell Biology* 28(2): 113-127.
- Penalva L.O., Ruiz M.F., Ortega A., Granadino B., Vicente L., Segarra C., Valcarcel J. and Sanchez L. (2000). The *Drosophila* fl(2)d gene, required for female-specific splicing of Sxl and tra pre-mRNAs, encodes a novel nuclear protein with a HQ-rich domain. *Genetics* 155(1): 129-139.
- Penalva L.O. and Sánchez L. (2003). RNA binding protein sex-lethal (Sxl) and control of *Drosophila* sex determination and dosage compensation. *Microbiol. Mol. Biol. Rev.* 67(3): 343-359.
- Pendleton K.E., Chen B., Liu K., Hunter O.V., Xie Y., Tu B.P. and Conrad N.K. (2017). The U6 snRNA m6A Methyltransferase METTL16 Regulates SAM Synthetase Intron Retention. *Cell* 169(5): 824-835.e814.
- Penn J.K.M., Graham P., Deshpande G., Calhoun G., Chaouki A.S., Salz H.K. and Schedl P. (2008). Functioning of the *Drosophila* Wilms'-tumor-1-associated protein homolog, Fl(2)d, in Sex-lethal-dependent alternative splicing. *Genetics* 178(2): 737-748.
- Penzo M., Guerrieri A.N., Zacchini F., Treré D. and Montanaro L. (2017). RNA Pseudouridylation in Physiology and Medicine: For Better and for Worse. *Genes* 8(11): 301.
- Perry R.P. and Kelley D.E. (1974). Existence of methylated messenger RNA in mouse L cells. *Cell* 1(1): 37-42.
- Perry R.P., Kelley D.E., Friderici K. and Rottman F. (1975). The methylated constituents of L cell messenger RNA: evidence for an unusual cluster at the 5' terminus. *Cell* 4(4): 387-394.
- Piccolo L.L., Corona D. and Onorati M.C. (2014). Emerging roles for hnRNPs in post-transcriptional regulation: what can we learn from flies? *Chromosoma* 123(6): 515-527.
- Piekna-Przybylska D., Decatur W.A. and Fournier M.J. (2008). The 3D rRNA modification maps database: with interactive tools for ribosome analysis. *Nucleic Acids Res Database* (Database issue): D178-183.
- Pinello N., Sun S. and Wong J.J.-L. (2018). Aberrant expression of enzymes regulating m(6)A mRNA methylation: implication in cancer. *Cancer biology & medicine* 15(4): 323-334.
- Ping X.L., Sun B.F., Wang L., Xiao W., Yang X., Wang W.J., Adhikari S., Shi Y., Lv Y., Chen Y.S., Zhao X., Li A., Yang Y., Dahal U., Lou X.M., Liu X., Huang J., Yuan W.P., Zhu X.F., Cheng T., Zhao Y.L., Wang X.Q., Danielsen J.M.R., Liu F. and Yang Y.G. (2014). Mammalian WTAP is a regulatory subunit of the RNA N6-methyladenosine methyltransferase. *Cell Research* 24(2): 177-189.
- Pitman J.L., Tsai C.-C., Edeen P.T., Finley K.D., Evans R.M. and McKeown M. (2002). DSF nuclear receptor acts as a repressor in culture and in vivo. *Developmental biology* 245(2): 315-328.
- Poock B., Triphan T., Neuser K. and Strauss R. (2008). Locomotor control by the central complex in *Drosophila*-An analysis of the tay bridge mutant. *Developmental neurobiology* 68(8): 1046-1058.
- Polevoda B., Span L. and Sherman F. (2006). The Yeast Translation Release Factors Mrf1p and Sup45p (eRF1) Are Methylated, Respectively, by the Methyltransferases Mtq1p and Mtq2p. *Journal of Biological Chemistry* 281(5): 2562-2571.
- Pontier D., Picart C., El Baidouri M., Roudier F., Xu T., Lahmy S., Llauro C., Azevedo J., Laudí M., Attina A., Hirtz C., Carpentier M.-C., Shen L. and Lagrange T. (2019). The m⁶A pathway protects the transcriptome integrity by restricting RNA chimera formation in plants. *Life Science Alliance* 2(3): e201900393.
- Porath H.T., Carmi S. and Levanon E.Y. (2014). A genome-wide map of hyper-edited RNA reveals numerous new sites. *Nature Communications* 5: 4726.
- Poritsanos N.J., Lew P.S., Fischer J., Mobbs C.V., Nagy J.I., Wong D., Rütger U. and Mizuno T.M. (2011). Impaired hypothalamic Fto expression in response to fasting and glucose in obese mice. *Nutrition & diabetes* 1(10): e19.
- Potapov V., Fu X., Dai N., Corrêa I.R., Jr., Tanner N.A. and Ong J.L. (2018). Base modifications affecting RNA polymerase and reverse transcriptase fidelity. *Nucleic Acids Res* 46(11): 5753-5763.
- Pradhan S.J., Nesler K.R., Rosen S.F., Kato Y., Nakamura A., Ramaswami M. and Barbee S.A. (2012). The conserved P body component HPat/Pat1 negatively regulates synaptic terminal growth at the larval *Drosophila* neuromuscular junction. *Journal of cell science* 125(Pt 24): 6105-6116.
- Pratanwanich P.N., Yao F., Chen Y., Koh C.W.Q., Hendra C., Poon P., Goh Y.T., Yap P.M.L., Yuan C.J., Chng W.J., Ng S., Thiery A., Goh W.S.S. and Göke J. (2020). Detection of differential RNA modifications from direct RNA sequencing of human cell lines. *bioRxiv*: 2020.2006.2018.160010.
- Presente A., Andres A. and Nye J.S. (2001). Requirement of Notch in adulthood for neurological function and longevity. *Neuroreport* 12(15): 3321-3325.
- Prokop A. and Technau G.M. (1994). Normal Function of the mushroom body defect Gene of *Drosophila* Is Required for the Regulation of the Number and Proliferation of Neuroblasts. *Developmental Biology* 161(2): 321-337.
- Proudfoot N.J. (2016). Transcriptional termination in mammals: Stopping the RNA polymerase II juggernaut. *Science (New York, N.Y.)* 352(6291): aad9926-aad9926.
- Qu Z. and Adelson D.L. (2012). Evolutionary conservation and functional roles of ncRNA. *Frontiers in genetics* 3: 205-205.

- Radlinska M., Bujnicki J.M. and Piekawicz A. (1999). Structural characterization of two tandemly arranged DNA methyltransferase genes from *Neisseria gonorrhoeae* MS11: N4-cytosine specific M.NgoMXV and nonfunctional 5-cytosine-type M.NgoMorf2P. *Proteins: Structure, Function, and Bioinformatics* 37(4): 717-728.
- Rafalska I., Zhang Z., Benderska N., Wolff H., Hartmann A.M., Brack-Werner R. and Stamm S. (2004). The intranuclear localization and function of YT521-B is regulated by tyrosine phosphorylation. *Human Molecular Genetics* 13(15): 1535-1549.
- Raffel G.D., Chu G.C., Jesneck J.L., Cullen D.E., Bronson R.T., Bernard O.A. and Gilliland D.G. (2009). Ott1 (Rbm15) is essential for placental vascular branching morphogenesis and embryonic development of the heart and spleen. *Molecular and cellular biology* 29(2): 333-341.
- Raffel G.D., Mercher T., Shigematsu H., Williams I.R., Cullen D.E., Akashi K., Bernard O.A. and Gilliland D.G. (2007). Ott1(Rbm15) has pleiotropic roles in hematopoietic development. *Proc Natl Acad Sci U S A* 104(14): 6001-6006.
- Ragab A., Thompson E.C. and Travers A.A. (2006). High mobility group proteins HMGD and HMGZ interact genetically with the Brahma chromatin remodeling complex in *Drosophila*. *Genetics* 172(2): 1069-1078.
- Raina M. and Ibba M. (2014). tRNAs as regulators of biological processes. *Frontiers in genetics* 5: 171-171.
- Ramaswami G. and Li J.B. (2016). Identification of human RNA editing sites: A historical perspective. *Methods (San Diego, Calif.)* 107: 42-47.
- Rana A.P. and Tuck M.T. (1990). Analysis and in vitro localization of internal methylated adenine residues in dihydrofolate reductase mRNA. *Nucleic Acids Research* 18(16): 4803-4808.
- Rauch S., He C. and Dickinson B.C. (2018). Targeted m6A reader proteins to study epitranscriptomic regulation of single RNAs. *Journal of the American Chemical Society* 140(38): 11974-11981.
- Rauch S., He E., Srien C., Zhou H., Zhang Z. and Dickinson B.C. (2019). Programmable RNA-Guided RNA Effector Proteins Built from Human Parts. *Cell* 178(1): 122-134.e112.
- Reed R. (1989). The organization of 3' splice-site sequences in mammalian introns. *Genes & Development* 3(12b): 2113-2123.
- Reim I., Mattow J. and Saumweber H. (1999). The RRM Protein NonA from *Drosophila* Forms a Complex with the RRM Proteins Hrb87F and S5 and the Zn Finger Protein PEP on hnRNA. *Experimental Cell Research* 253(2): 573-586.
- Reuter J.S. and Mathews D.H. (2010). RNAstructure: software for RNA secondary structure prediction and analysis. *BMC Bioinformatics* 11(1): 129.
- Rintala-Dempsey A.C. and Kothe U. (2017). Eukaryotic stand-alone pseudouridine synthases - RNA modifying enzymes and emerging regulators of gene expression? *RNA biology* 14(9): 1185-1196.
- Roost C., Lynch S.R., Batista P.J., Qu K., Chang H.Y. and Kool E.T. (2015). Structure and thermodynamics of N6-methyladenosine in RNA: a spring-loaded base modification. *Journal of the American Chemical Society* 137(5): 2107-2115.
- Rot G., Wang Z., Huppertz I., Modic M., Lenče T., Hallegger M., Haberman N., Curk T., von Mering C. and Ule J. (2017). High-Resolution RNA Maps Suggest Common Principles of Splicing and Polyadenylation Regulation by TDP-43. *Cell Reports* 19(5): 1056-1067.
- Rottman F.M., Bokar J.A., Narayan P., Shambaugh M.E. and Ludwiczak R. (1994). N6-Adenosine methylation in mRNA: Substrate specificity and enzyme complexity. *Biochimie* 76(12): 1109-1114.
- Roundtree I.A., Evans M.E., Pan T. and He C. (2017). Dynamic RNA Modifications in Gene Expression Regulation. *Cell* 169(7): 1187-1200.
- Roundtree I.A., Luo G.-Z., Zhang Z., Wang X., Zhou T., Cui Y., Sha J., Huang X., Guerrero L., Xie P., He E., Shen B. and He C. (2017). YTHDC1 mediates nuclear export of N6-methyladenosine methylated mRNAs. *eLife* 6: e31311.
- Roy B. and Jacobson A. (2013). The intimate relationships of mRNA decay and translation. *Trends in genetics* : TIG 29(12): 691-699.
- Ruppert M., Franz M., Saratsis A., Velo Escarcena L., Hendrich O., Gooi L.M., Schwenkert I., Klebes A. and Scholz H. (2017). Hangover Links Nuclear RNA Signaling to cAMP Regulation via the Phosphodiesterase 4d Ortholog *dunce*. *Cell Reports* 18(2): 533-544.
- Ruszkowska A., Ruszkowski M., Dauter Z. and Brown J.A. (2018). Structural insights into the RNA methyltransferase domain of METTL16. *Scientific Reports* 8: 5311.
- Růžička K., Mi Z., Ana C., Zsuzsanna B., Muhammad K., Mária S., Dominique E., Sedeer E.S., Hongying L., Silin Z., Geert D.J., P. M.N., Jan H., Ykä H. and G. F.R. (2017). Identification of factors required for m6A mRNA methylation in Arabidopsis reveals a role for the conserved E3 ubiquitin ligase HAKAI. *New Phytologist* 215(1): 157-172.
- Safra M., Nir R., Farouq D., Vainberg Slutskin I. and Schwartz S. (2017a). TRUB1 is the predominant pseudouridine synthase acting on mammalian mRNA via a predictable and conserved code. *Genome Research* 27(3): 393-406.
- Safra M., Sas-Chen A., Nir R., Winkler R., Nachshon A., Bar-Yaacov D., Erlacher M., Rossmanith W., Stern-Ginossar N. and Schwartz S. (2017b). The m1A landscape on cytosolic and mitochondrial mRNA at single-base resolution. *Nature* 551: 251.
- Saito K., Sakaguchi Y., Suzuki T., Suzuki T., Siomi H. and Siomi M.C. (2007). Pimet, the *Drosophila* homolog of HEN1, mediates 2'-O-methylation of Piwi-interacting RNAs at their 3' ends. *Genes & development* 21(13): 1603-1608.
- Saletore Y., Meyer K., Korlach J., Vilfan I.D., Jaffrey S. and Mason C.E. (2012). The birth of the Epitranscriptome: deciphering the function of RNA modifications. *Genome biology* 13(10): 175-175.
- Salz H.K. (1992). The genetic analysis of *snf*: a *Drosophila* sex determination gene required for activation of *Sex-lethal* in both the germline and the soma. *Genetics* 130(3): 547-554.
- Salz H.K. (2011). Sex determination in insects: a binary decision based on alternative splicing. *Current opinion in genetics & development* 21(4): 395-400.
- Sanchez-Pulido L. and Andrade-Navarro M.A. (2007). The FTO (fat mass and obesity associated) gene codes for a novel member of the non-heme dioxygenase superfamily. *BMC Biochem* 8: 23-23.
- Sapiro A.L., Freund E.C., Restrepo L., Qiao H.-H., Bhat A., Li Q., Ni J.-Q., Mosca T.J. and Li J.B. (2020). Zinc Finger RNA-Binding Protein Zn72D Regulates ADAR-Mediated RNA Editing in Neurons. *Cell Reports* 31(7): 107654.
- Sas-Chen A., Thomas J.M., Matzov D., Taoka M., Nance K.D., Nir R., Bryson K.M., Shachar R., Liman G.L.S., Burkhart B.W., Gamage S.T., Nobe Y., Briney C.A., Levy M.J., Fuchs R.T., Robb G.B., Hartmann J., Sharma S., Lin Q., Florens L., Washburn M.P., Isobe T., Santangelo T.J., Shalev-Benami M., Meier J.L. and Schwartz S. (2020). Dynamic RNA acetylation revealed by quantitative cross-evolutionary mapping. *Nature*.
- Sashital D.G., Venditti V., Angers C.G., Cornilescu G. and Butcher S.E. (2007). Structure and thermodynamics of a conserved U2 snRNA domain from yeast and human. *RNA (New York, N.Y.)* 13(3): 328-338.
- Schapira A.H. and Jenner P. (2011). Etiology and pathogenesis of Parkinson's disease. *Movement Disorders* 26(6): 1049-1055.
- Schlackow M., Nojima T., Gomes T., Dhir A., Carmo-Fonseca M. and Proudfoot N.J. (2017). Distinctive Patterns of Transcription and RNA Processing for Human lincRNAs. *Molecular Cell* 65(1): 25-38.
- Schmidt W., Arnold H.H. and Kersten H. (1975). Biosynthetic pathway of ribothymidine in *B. subtilis* and *M. lysodeikticus* involving different coenzymes for transfer RNA and ribosomal RNA. *Nucleic Acids Res* 2(7): 1043-1051.
- Schoenberg D.R. and Maquat L.E. (2012). Regulation of cytoplasmic mRNA decay. *Nature Reviews Genetics* 13: 246.
- Scholler E., Weichmann F., Treiber T., Ringle S., Treiber N., Flatley A., Feederle R., Bruckmann A. and Meister G. (2018). Interactions, localization, and phosphorylation of the m(6)A generating METTL3-METTL14-WTAP complex. *RNA* 24(4): 499-512.
- Schossere M., Minois N., Angerer T.B., Amring M., Dellago H., Harreither E., Calle-Perez A., Pircher A., Gerstl M.P., Pfeifenberger S., Brandl C., Sonntagbauer M., Kriegner A., Linder A., Weinhäusel A., Mohr T., Steiger M., Mattanovich D., Rinnerthaler M., Karl T., Sharma S., Entian K.-D., Kos M., Breitenbach M., Wilson I.B.H., Polacek N., Grillari-Voglauer R., Breitenbach-Koller L. and Grillari J. (2015). Methylation of ribosomal RNA by NSUN5 is a conserved mechanism

- modulating organismal lifespan. *Nature communications* 6: 6158-6158.
- Schultz C., Hilfiker A. and Nothiger R. (1998). virilizer regulates Sex-lethal in the germline of *Drosophila melanogaster*. *Development* 125(8): 1501-1507.
- Schunter S., Villa R., Flynn V., Heidelberger J.B., Classen A.-K., Beli P. and Becker P.B. (2017). Ubiquitylation of the acetyltransferase MOF in *Drosophila melanogaster*. *PLOS ONE* 12(5): e0177408.
- Schwartz S., Agarwala S.D., Mumbach M.R., Jovanovic M., Mertins P., Shishkin A., Tabach Y., Mikkelsen T.S., Satija R., Ruvkun G., Carr S.A., Lander E.S., Fink G.R. and Regev A. (2013). High-resolution mapping reveals a conserved, widespread, dynamic meiotically regulated mRNA methylation program. *Cell* 155(6): 1409-1421.
- Schwartz S., Bernstein D.A., Mumbach M.R., Jovanovic M., Herbst R.H., León-Ricardo B.X., Engreitz J.M., Guttman M., Satija R., Lander E.S., Fink G. and Regev A. (2014a). Transcriptome-wide mapping reveals widespread dynamic-regulated pseudouridylation of ncRNA and mRNA. *Cell* 159(1): 148-162.
- Schwartz S., Mumbach M.R., Jovanovic M., Wang T., Maciag K., Bushkin G.G., Mertins P., Ter-Ovanesyan D., Habib N., Cacchiarelli D., Sanjana N.E., Freinkman E., Pacold M.E., Satija R., Mikkelsen T.S., Hacohen N., Zhang F., Carr S.A., Lander E.S. and Regev A. (2014b). Perturbation of m6A writers reveals two distinct classes of mRNA methylation at internal and 5' sites. *Cell Rep* 8(1): 284-296.
- Schwenkert I., Eltrop R., Funk N., Steinert J.R., Schuster C.M. and Scholz H. (2008). The hangover gene negatively regulates bouton addition at the *Drosophila* neuromuscular junction. *Mechanisms of Development* 125(8): 700-711.
- Scutenaire J., Deragon J.-M., Jean V., Benhamed M., Raynaud C., Favory J.-J., Merret R. and Bousquet-Antonelli C. (2018). The YTH Domain Protein ECT2 is an m6A Reader Required for Normal Trichome Branching in *Arabidopsis*. *The Plant Cell*.
- Segura-Aguilar J. and Paris I. (2014). Mechanisms of dopamine oxidation and parkinson's disease. *Handbook of Neurotoxicity*. New York, NY, Springer: 865-883.
- Sekelsky J. (2017). DNA Repair in *Drosophila*: Mutagens, Models, and Missing Genes. *Genetics* 205(2): 471-490.
- Sendinc E., Valle-Garcia D., Dhall A., Chen H., Henriques T., Navarrete-Perea J., Sheng W., Gygi S.P., Adelman K. and Shi Y. (2019). PCIF1 Catalyzes m6Am mRNA Methylation to Regulate Gene Expression. *Mol Cell* 75(3): 620-630.e629.
- Seong K.-H., Ogashiwa T., Matsuo T., Fuyama Y. and Aigaki T. (2001). Application of the gene search system to screen for longevity genes in *Drosophila*. *Biogerontology* 2(3): 209-217.
- Sergiev P.V., Serebryakova M.V., Bogdanov A.A. and Dontsova O.A. (2008). The ybiN gene of *Escherichia coli* encodes adenine-N6 methyltransferase specific for modification of A1618 of 23 S ribosomal RNA, a methylated residue located close to the ribosomal exit tunnel. *J Mol Biol* 375(1): 291-300.
- Seugnet L., Galvin J.E., Suzuki Y., Gottschalk L. and Shaw P.J. (2009). Persistent short-term memory defects following sleep deprivation in a *Drosophila* model of Parkinson disease. *Sleep* 32(8): 984-992.
- Shah J.C. and Clancy M.J. (1992). IME4, a gene that mediates MAT and nutritional control of meiosis in *Saccharomyces cerevisiae*. *Molecular and cellular biology* 12(3): 1078-1086.
- Sharma S., Langhendries J.-L., Watzinger P., Kötter P., Entian K.-D. and Lafontaine D.L.J. (2015). Yeast Kre33 and human NAT10 are conserved 18S rRNA cytosine acetyltransferases that modify tRNAs assisted by the adaptor Tan1/THUMP1. *Nucleic acids research* 43(4): 2242-2258.
- Shatkin A.J. (1974). Animal RNA viruses: genome structure and function. *Annu Rev Biochem* 43(0): 643-665.
- Shen L., Liang Z., Gu X., Chen Y., Teo Zhi Wei N., Hou X., Cai Weiling M., Dedon Peter C., Liu L. and Yu H. (2016). N6-Methyladenosine RNA Modification Regulates Shoot Stem Cell Fate in *Arabidopsis*. *Developmental Cell* 38(2): 186-200.
- Sheth U. and Parker R. (2003). Decapping and decay of messenger RNA occur in cytoplasmic processing bodies. *Science (New York, N.Y.)* 300(5620): 805-808.
- Shi H., Wang X., Lu Z., Zhao B.S., Ma H., Hsu P.J., Liu C. and He C. (2017). YTHDF3 facilitates translation and decay of N6-methyladenosine-modified RNA. *Cell Research* 27: 315.
- Shi H., Wei J. and He C. (2019). Where, when, and how: context-dependent functions of RNA methylation writers, readers, and erasers. *Molecular cell* 74(4): 640-650.
- Shi H., Zhang X., Weng Y.-L., Lu Z., Liu Y., Lu Z., Li J., Hao P., Zhang Y., Zhang F., Wu Y., Delgado J.Y., Su Y., Patel M.J., Cao X., Shen B., Huang X., Ming G.-I., Zhuang X., Song H., He C. and Zhou T. (2018). m6A facilitates hippocampus-dependent learning and memory through YTHDF1. *Nature*.
- Shi W.-Y. and Skeath J.B. (2004). The *Drosophila* RCC1 homolog, Bjl, regulates nucleocytoplasmic transport and neural differentiation during *Drosophila* development. *Developmental Biology* 270(1): 106-121.
- Shima H., Matsumoto M., Ishigami Y., Ebina M., Muto A., Sato Y., Kumagai S., Ochiai K., Suzuki T. and Igarashi K. (2017). S-Adenosylmethionine Synthesis Is Regulated by Selective N(6)-Adenosine Methylation and mRNA Degradation Involving METTL16 and YTHDC1. *Cell Rep* 21(12): 3354-3363.
- Shu X., Cao J., Cheng M., Xiang S., Gao M., Li T., Ying X., Wang F., Yue Y., Lu Z., Dai Q., Cui X., Ma L., Wang Y., He C., Feng X. and Liu J. (2020). A metabolic labeling method detects m6A transcriptome-wide at single base resolution. *Nature Chemical Biology*.
- Shukla S. and Oberdoerffer S. (2012). Co-transcriptional regulation of alternative pre-mRNA splicing. *Biochimica et biophysica acta* 1819(7): 673-683.
- Sibley C.R., Emmett W., Blazquez L., Faro A., Haberman N., Briese M., Trabzuni D., Ryten M., Weale M.E., Hardy J., Modic M., Curk T., Wilson S.W., Plagnol V. and Ule J. (2015). Recursive splicing in long vertebrate genes. *Nature* 521: 371.
- Sigrist C.J.A., de Castro E., Cerutti L., Cucho B.A., Hulo N., Bridge A., Bougueleret L. and Xenarios I. (2013). New and continuing developments at PROSITE. *Nucleic acids research* 41(Database issue): D344-D347.
- Silva S.M.d. (2017). Characterization of mammalian RNA Exonuclease 5/NEF-sp as a testis-specific 3' → 5' exonuclease.
- Singh A.K. and Lakhota S.C. (2015). Dynamics of hnRNPs and omega speckles in normal and heat shocked live cell nuclei of *Drosophila melanogaster*. *Chromosoma* 124(3): 367-383.
- Sinsimer K.S., Jain R.A., Chatterjee S. and Gavis E.R. (2011). A late phase of germ plasm accumulation during *Drosophila* oogenesis requires lost and rumpelstiltskin. *Development* 138(16): 3431-3440.
- Siomi M.C., Zhang Y., Siomi H. and Dreyfuss G. (1996). Specific sequences in the fragile X syndrome protein FMR1 and the FXR proteins mediate their binding to 60S ribosomal subunits and the interactions among them. *Molecular and Cellular Biology* 16(7): 3825-3832.
- Sledz P. and Jinek M. (2016). Structural insights into the molecular mechanism of the m(6)A writer complex. *eLife* 5.
- Slobodin B., Bahat A., Sehrawat U., Becker-Herman S., Zuckerman B., Weiss A.N., Han R., Elkon R., Agami R., Ulitsky I., Shachar I. and Dikstein R. (2020). Transcription Dynamics Regulate Poly(A) Tails and Expression of the RNA Degradation Machinery to Balance mRNA Levels. *Mol Cell* 78(3): 434-444.e435.
- Slobodin B., Han R., Calderone V., Vrieland J.A.F.O., Loayza-Puch F., Elkon R. and Agami R. (2017). Transcription Impacts the Efficiency of mRNA Translation via Co-transcriptional N6-adenosine Methylation. *Cell* 169(2): 326-337.e312.
- Small T.W., Bolender Z., Bueno C., O'Neil C., Nong Z., Rushlow W., Rajakumar N., Kandel C., Strong J., Madrenas J. and Pickering J.G. (2006). Wilms' tumor 1-associating protein regulates the proliferation of vascular smooth muscle cells. *Circulation research* 99(12): 1338-1346.
- Small T.W. and Pickering J.G. (2009). Nuclear degradation of Wilms tumor 1-associating protein and survivin splice variant switching underlie IGF-1-mediated survival. *J Biol Chem* 284(37): 24684-24695.
- Smemo S., Tena J.J., Kim K.-H., Gamazon E.R., Sakabe N.J., Gómez-Marín C., Aneas I., Credidio F.L., Sobreira D.R., Wasserman N.F., Lee J.H., Puvion-Vandier V., Tam D., Shen M., Son J.E., Vakili N.A., Sung H.-K.,

- Naranjo S., Acemel R.D., Manzanares M., Nagy A., Cox N.J., Hui C.-C., Gomez-Skarmeta J.L. and Nóbrega M.A. (2014). Obesity-associated variants within FTO form long-range functional connections with IRX3. *Nature* 507(7492): 371-375.
- Smeyne M. and Smeyne R.J. (2013). Glutathione metabolism and Parkinson's disease. *Free Radical Biology and Medicine* 62: 13-25.
- Solberg A., Robertson A.B., Aronsen J.M., Rognum Ø., Sjaastad I., Wisløff U. and Klungland A. (2013). Deletion of mouse Alkbh7 leads to obesity. *Journal of Molecular Cell Biology* 5(3): 194-203.
- Soldano A., Worpenberg L., Paolantoni C., Longhi S., Mulorz M.M., Lence T., Wessels H.-H., Aiello G., Notarangelo M., Sutandy F.R., Scheibe M., Edupuganti R.R., Busch A., Mockel M.M., Vermeulen M., Butter F., König J., Ohler U., Dieterich C., Quattrone A. and Roignant J.-Y. (2020). The m6A reader Ythdf restricts axonal growth in *Drosophila* through target selection modulation of the Fragile X mental retardation protein. *bioRxiv*: 2020.2003.2004.976886.
- Solomon O., Oren S., Safran M., Deshet-Unger N., Akiva P., Jacob-Hirsch J., Cesarkas K., Kabesa R., Amariglio N., Unger R., Rechavi G. and Eyal E. (2013). Global regulation of alternative splicing by adenosine deaminase acting on RNA (ADAR). *RNA* 19(5): 591-604.
- Sommer S., Lavi U. and Darnell J.E. (1978). The absolute frequency of labeled N-6-methyladenosine in HeLa cell messenger RNA decreases with label time. *Journal of Molecular Biology* 124(3): 487-499.
- Song J. and Yi C. (2019). Reading Chemical Modifications in the Transcriptome. *Journal of Molecular Biology*.
- Song M.-G. and Kiledjian M. (2007). 3' Terminal oligo U-tract-mediated stimulation of decapping. *RNA* 13(12): 2356-2365.
- Songe-Møller L., van den Born E., Leihne V., Vågbø C.B., Kristoffersen T., Krokan H.E., Kirpekar F., Falnes P.Ø. and Klungland A. (2010). Mammalian ALKBH8 possesses tRNA methyltransferase activity required for the biogenesis of multiple wobble uridine modifications implicated in translational decoding. *Molecular and cellular biology* 30(7): 1814-1827.
- Spenkuch F., Motorin Y. and Helm M. (2015). Pseudouridine: still mysterious, but never a fake (uridine)! *RNA biology* 11(12): 1540-1554.
- Spitale R.C., Flynn R.A., Zhang Q.C., Crisalli P., Lee B., Jung J.-W., Kuchelmeister H.Y., Batista P.J., Torre E.A., Kool E.T. and Chang H.Y. (2015). Structural imprints in vivo decode RNA regulatory mechanisms. *Nature* 519(7544): 486-490.
- Sproat B.S., Lamond A.I., Beijer B., Neuner P. and Ryder U. (1989). Highly efficient chemical synthesis of 2'-O-methyloligoribonucleotides and tetrabiotinylated derivatives; novel probes that are resistant to degradation by RNA or DNA specific nucleases. *Nucleic acids research* 17(9): 3373-3386.
- Spychala A. and Rüter U. (2019). FTO affects hippocampal function by regulation of BDNF processing. *PLoS one* 14(2): e0211937-e0211937.
- Squires J.E., Patel H.R., Nusch M., Sibbritt T., Humphreys D.T., Parker B.J., Suter C.M. and Preiss T. (2012). Widespread occurrence of 5-methylcytosine in human coding and non-coding RNA. *Nucleic acids research* 40(11): 5023-5033.
- Standart N. and Weil D. (2018). P-Bodies: Cytosolic Droplets for Coordinated mRNA Storage. *Trends in Genetics* 34(8): 612-626.
- Stoilov P., Rafalska I. and Stamm S. (2002). YTH: a new domain in nuclear proteins. *Trends Biochem Sci* 27(10): 495-497.
- Stoltzfus C.M. and Dane R.W. (1982). Accumulation of spliced avian retrovirus mRNA is inhibited in S-adenosylmethionine-depleted chicken embryo fibroblasts. *Journal of virology* 42(3): 918-931.
- Strauss R. (2002). The central complex and the genetic dissection of locomotor behaviour. *Current Opinion in Neurobiology* 12(6): 633-638.
- Strauss R., Hanesch U., Kinkelin M., Wolf R. and Heisenberg M. (1992). No-bridge of *Drosophila melanogaster*: portrait of a structural brain mutant of the central complex. *J Neurogenet* 8(3): 125-155.
- Strauss R. and Pichler J. (1998). Persistence of orientation toward a temporarily invisible landmark in *Drosophila melanogaster*. *Journal of Comparative Physiology A* 182(4): 411-423.
- Strick T.R., Croquette V. and Bensimon D. (2000). Single-molecule analysis of DNA uncoiling by a type II topoisomerase. *Nature* 404(6780): 901-904.
- Su C.-H., D.D. and Tarn W.-Y. (2018). Alternative Splicing in Neurogenesis and Brain Development. *Frontiers in molecular biosciences* 5: 12-12.
- Su Z., Han L. and Zhao Z. (2011). Conservation and divergence of DNA methylation in eukaryotes: new insights from single base-resolution DNA methylomes. *Epigenetics* 6(2): 134-140.
- Suissa Y., Ordan E., Deshpande G. and Gerlitz O. (2011). Males and females: Creating differences while maintaining the similarities. *Fly (Austin)* 5(1): 25-28.
- Sun H., Zhang M., Li K., Bai D. and Yi C. (2019). Cap-specific, terminal N(6)-methylation by a mammalian m(6)Am methyltransferase. *Cell research* 29(1): 80-82.
- Sutandy F.X., Hildebrandt A. and König J. (2016). Profiling the Binding Sites of RNA-Binding Proteins with Nucleotide Resolution Using iCLIP. *Methods in molecular biology (Clifton, N.J.)* 1358: 175-195.
- Sutcliffe B., Forero M.G., Zhu B., Robinson I.M. and Hidalgo A. (2013). Neuron-type specific functions of DNT1, DNT2 and Spz at the *Drosophila* neuromuscular junction. *PLoS one* 8(10): e75902-e75902.
- Swenson J.M., Colmenares S.U., Strom A.R., Costes S.V. and Karpen G.H. (2016). The composition and organization of *Drosophila* heterochromatin are heterogeneous and dynamic. *eLife* 5: e16096.
- T Surosky R. and Esposito R. (1992). Early meiotic transcripts are highly unstable in *Saccharomyces cerevisiae*.
- Takeichi M. (1995). Morphogenetic roles of classic cadherins. *Current Opinion in Cell Biology* 7(5): 619-627.
- Tanabe A., Tanikawa K., Tsunetomi M., Takai K., Ikeda H., Konno J., Torigoe T., Maeda H., Kutomi G., Okita K., Mori M. and Sahara H. (2016). RNA helicase YTHDC2 promotes cancer metastasis via the enhancement of the efficiency by which HIF-1 α mRNA is translated. *Cancer Letters* 376(1): 34-42.
- Tanaka T. and Weisblum B. (1975). Systematic difference in the methylation of ribosomal ribonucleic acid from gram-positive and gram-negative bacteria. *J Bacteriol* 123(2): 771-774.
- Tang C., Klukovich R., Peng H., Wang Z., Yu T., Zhang Y., Zheng H., Klungland A. and Yan W. (2018). ALKBH5-dependent m6A demethylation controls splicing and stability of long 3'-UTR mRNAs in male germ cells. *Proceedings of the National Academy of Sciences of the United States of America* 115(2): E325-E333.
- Tennessen J.M. and Thummel C.S. (2011). Coordinating growth and maturation - insights from *Drosophila*. *Current biology : CB* 21(18): R750-R757.
- Tessarz P., Santos-Rosa H., Robson S.C., Sylvesters K.B., Nelson C.J., Nielsen M.L. and Kouzarides T. (2014). Glutamine methylation in histone H2A is an RNA-polymerase-I-dedicated modification. *Nature* 505(7484): 564-568.
- Theler D., Dominguez C., Blatter M., Boudet J. and Allain F.H. (2014). Solution structure of the YTH domain in complex with N6-methyladenosine RNA: a reader of methylated RNA. *Nucleic Acids Res* 42(22): 13911-13919.
- Thul P.J., Åkesson L., Wiking M., Mahdessian D., Geladaki A., Ait Blal H., Alm T., Asplund A., Björk L., Breckels L.M., Bäckström A., Danielsson F., Fagerberg L., Fall J., Gatto L., Gnann C., Hober S., Hjelmare M., Johansson F., Lee S., Lindskog C., Mulder J., Mulvey C.M., Nilsson P., Oksvold P., Rockberg J., Schütten R., Schwenk J.M., Sivertsson Å., Sjöstedt E., Skogs M., Stadler C., Sullivan D.P., Tegel H., Winsnes C., Zhang C., Zwahlen M., Mardinoglu A., Pontén F., von Feilitzen K., Lilley K.S., Uhlén M. and Lundberg E. (2017). A subcellular map of the human proteome. *Science* 356(6340): eaal3321.
- Timinkas A., Butkus V. and Janulaitis A. (1995). Sequence motifs characteristic for DNA [cytosine-N4] and DNA [adenine-N6] methyltransferases. Classification of all DNA methyltransferases. *Gene* 157(1): 3-11.
- Tissot M. and Stocker R.F. (2000). Metamorphosis in *Drosophila* and other insects: the fate of neurons throughout the stages. *Progress in Neurobiology* 62(1): 89-111.
- Toba G., Ohsako T., Miyata N., Ohtsuka T., Seong K.-H. and Aigaki T. (1999). The gene search system: a method for efficient detection and rapid molecular identification of genes in *Drosophila melanogaster*. *Genetics* 151(2): 725-737.
- Toczydłowska-Socha D., Zielinska M.M., Kurkowska M., Astha, Almeida C.F., Stefaniak F., Purta E. and Bujnicki J.M. (2018). Human RNA cap1 methyltransferase CMTr1 cooperates with RNA helicase DHX15 to

- modify RNAs with highly structured 5' termini. Philosophical transactions of the Royal Society of London. Series B, Biological sciences 373(1762): 20180161.
- Todd A.G., Lin H., Ebert A.D., Liu Y. and Androphy E.J. (2013). COPI transport complexes bind to specific RNAs in neuronal cells. *Human molecular genetics* 22(4): 729-736.
- Tollervey D., Lehtonen H., Jansen R., Kern H. and Hurt E.C. (1993). Temperature-sensitive mutations demonstrate roles for yeast fibrillarlin in pre-rRNA processing, pre-rRNA methylation, and ribosome assembly. *Cell* 72(3): 443-457.
- Truman J.W. (1990). Metamorphosis of the central nervous system of *Drosophila*. *Journal of Neurobiology* 21(7): 1072-1084.
- Tsujikawa K., Koike K., Kitae K., Shinkawa A., Arima H., Suzuki T., Tsuchiya M., Makino Y., Furukawa T., Konishi N. and Yamamoto H. (2007). Expression and sub-cellular localization of human ABH family molecules. *J Cell Mol Med* 11(5): 1105-1116.
- Tuck M.T. (1992). Partial purification of a 6-methyladenine mRNA methyltransferase which modifies internal adenine residues. *Biochemical Journal* 288(Pt 1): 233-240.
- Turner-Evans D.B. and Jayaraman V. (2016). The insect central complex. *Curr Biol* 26(11): R453-457.
- Tyanova S., Temu T., Sinitcyn P., Carlson A., Hein M.Y., Geiger T., Mann M. and Cox J. (2016). The Perseus computational platform for comprehensive analysis of (prote)omics data. *Nature Methods* 13(9): 731-740.
- Ueda Y., Ooshio I., Fusamae Y., Kitae K., Kawaguchi M., Jingushi K., Hase H., Harada K., Hirata K. and Tsujikawa K. (2017). AlkB homolog 3-mediated tRNA demethylation promotes protein synthesis in cancer cells. *Scientific reports* 7: 42271-42271.
- Ule J. and Darnell R.B. (2006). RNA binding proteins and the regulation of neuronal synaptic plasticity. *Current Opinion in Neurobiology* 16(1): 102-110.
- Urbonavicius J., Skouloubris S., Myllykallio H. and Grosjean H. (2005). Identification of a novel gene encoding a flavin-dependent tRNA:m5U methyltransferase in bacteria--evolutionary implications. *Nucleic acids research* 33(13): 3955-3964.
- Valcárcel J., Singh R., Zamore P.D. and Green M.R. (1993). The protein Sex-lethal antagonizes the splicing factor U2AF to regulate alternative splicing of transformer pre-mRNA. *Nature* 362(6416): 171-175.
- van der Feltz C. and Hoskins A.A. (2019). Structural and functional modularity of the U2 snRNP in pre-mRNA splicing. *Critical Reviews in Biochemistry and Molecular Biology* 54(5): 443-465.
- van Tran N., Ernst F.G.M., Hawley B.R., Zorbas C., Ulryck N., Hackert P., Bohnsack K.E., Bohnsack M.T., Jaffrey S.R., Graille M. and Lafontaine D.L.J. (2019). The human 18S rRNA m6A methyltransferase METTL5 is stabilized by TRMT112. *Nucleic Acids Research* 47(15): 7719-7733.
- Vazquez-Pianzola P. and Suter B. (2012). Conservation of the RNA Transport Machineries and Their Coupling to Translation Control across Eukaryotes. *Comp Funct Genomics* 2012: 287852.
- Vázquez M., Moore L. and Kennison J.A. (1999). The trithorax group gene *osa* encodes an ARID-domain protein that genetically interacts with the brahma chromatin-remodeling factor to regulate transcription. *Development* 126(4): 733-742.
- Venables J.P., Tazi J. and Juge F. (2012). Regulated functional alternative splicing in *Drosophila*. *Nucleic acids research* 40(1): 1-10.
- Venters C.C., Oh J.-M., Di C., So B.R. and Dreyfuss G. (2019). U1 snRNP Telescripting: Suppression of Premature Transcription Termination in Introns as a New Layer of Gene Regulation. *Cold Spring Harbor Perspectives in Biology* 11(2).
- Vespa L., Vachon G., Berger F., Perazza D., Faure J.D. and Herzog M. (2004). The immunophilin-interacting protein AtFIP37 from *Arabidopsis* is essential for plant development and is involved in trichome endoreduplication. *Plant physiology* 134(4): 1283-1292.
- Vuong C.K., Black D.L. and Zheng S. (2016). The neurogenetics of alternative splicing. *Nature reviews. Neuroscience* 17(5): 265-281.
- Walters B.J., Mercaldo V., Gillon C.J., Yip M., Neve R.L., Boyce F.M., Frankland P.W. and Josselyn S.A. (2017). The Role of The RNA Demethylase FTO (Fat Mass and Obesity-Associated) and mRNA Methylation in Hippocampal Memory Formation. *Neuropsychopharmacology : official publication of the American College of Neuropsychopharmacology* 42(7): 1502-1510.
- Wan C., Borgeson B., Phanse S., Tu F., Drew K., Clark G., Xiong X., Kagan O., Kwan J., Bezginov A., Chessman K., Pal S., Cromar G., Papoulas O., Ni Z., Boutz D.R., Stoilova S., Havugimana P.C., Guo X., Mally R.H., Sarov M., Greenblatt J., Babu M., Derry W.B., Tillier E.R., Wallingford J.B., Parkinson J., Marcotte E.M. and Emili A. (2015). Panorama of ancient metazoan macromolecular complexes. *Nature* 525(7569): 339-344.
- Wang C.-X., Cui G.-S., Liu X., Xu K., Wang M., Zhang X.-X., Jiang L.-Y., Li A., Yang Y., Lai W.-Y., Sun B.-F., Jiang G.-B., Wang H.-L., Tong W.-M., Li W., Wang X.-J., Yang Y.-G. and Zhou Q. (2018). METTL3-mediated m6A modification is required for cerebellar development. *PLoS biology* 16(6): e2004880-e2004880.
- Wang C., Zhu Y., Bao H., Jiang Y., Xu C., Wu J. and Shi Y. (2016). A novel RNA-binding mode of the YTH domain reveals the mechanism for recognition of determinant of selective removal by Mmi1. *Nucleic Acids Research* 44(2): 969-982.
- Wang E.T., Sandberg R., Luo S., Khrebtkova I., Zhang L., Mayr C., Kingsmore S.F., Schroth G.P. and Burge C.B. (2008). Alternative isoform regulation in human tissue transcriptomes. *Nature* 456: 470.
- Wang F., Minakhina S., Tran H., Changela N., Kramer J. and Steward R. (2018). Tet protein function during *Drosophila* development. *PLOS ONE* 13(1): e0190367.
- Wang G., He Q., Feng C., Liu Y., Deng Z., Qi X., Wu W., Mei P. and Chen Z. (2014). The atomic resolution structure of human AlkB homolog 7 (ALKBH7), a key protein for programmed necrosis and fat metabolism. *The Journal of biological chemistry* 289(40): 27924-27936.
- Wang P., Duxtader K.A. and Nam Y. (2016). Structural Basis for Cooperative Function of Mettl3 and Mettl14 Methyltransferases. *Molecular cell* 63(2): 306-317.
- Wang X., Feng J., Xue Y., Guan Z., Zhang D., Liu Z., Gong Z., Wang Q., Huang J., Tang C., Zou T. and Yin P. (2016). Structural basis of N(6)-adenosine methylation by the METTL3-METTL14 complex. *Nature* 534(7608): 575-578.
- Wang X., Lu Z., Gomez A., Hon G.C., Yue Y., Han D., Fu Y., Parisien M., Dai Q., Jia G., Ren B., Pan T. and He C. (2013). N6-methyladenosine-dependent regulation of messenger RNA stability. *Nature* 505: 117.
- Wang X., Lu Z., Gomez A., Hon G.C., Yue Y., Han D., Fu Y., Parisien M., Dai Q., Jia G., Ren B., Pan T. and He C. (2014). N6-methyladenosine-dependent regulation of messenger RNA stability. *Nature* 505(7481): 117-120.
- Wang X., Zhao Boxuan S., Roundtree Ian A., Lu Z., Han D., Ma H., Weng X., Chen K., Shi H. and He C. (2015). N6-methyladenosine Modulates Messenger RNA Translation Efficiency. *Cell* 161(6): 1388-1399.
- Wang Y., Li Y., Toth J.I., Petroski M.D., Zhang Z. and Zhao J.C. (2014). N6-methyladenosine modification destabilizes developmental regulators in embryonic stem cells. *Nature cell biology* 16(2): 191-198.
- Wang Y., Li Y., Yue M., Wang J., Kumar S., Wechsler-Reya R.J., Zhang Z., Ogawa Y., Kellis M., Duester G. and Zhao J.C. (2018). N(6)-methyladenosine RNA modification regulates embryonic neural stem cell self-renewal through histone modifications. *Nat Neurosci* 21(2): 195-206.
- Wang Y., Xiao Y., Dong S., Yu Q. and Jia G. (2020). Antibody-free enzyme-assisted chemical approach for detection of N(6)-methyladenosine. *Nature chemical biology*.
- Wang Z., Kayikci M., Briese M., Zarnack K., Luscombe N.M., Rot G., Zupan B., Curk T. and Ule J. (2010). iCLIP predicts the dual splicing effects of TIA-RNA interactions. *Plos Biol* 8(10): e1000530.
- Wang Z., Tang K., Zhang D., Wan Y., Wen Y., Lu Q. and Wang L. (2017). High-throughput m6A-seq reveals RNA m6A methylation patterns in the chloroplast and mitochondria transcriptomes of *Arabidopsis thaliana*. *PLoS one* 12(11): e0185612-e0185612.
- Warda A.S., Kretschmer J., Hackert P., Lenz C., Urlaub H., Höbartner C., Sloan Katherine E. and Bohnsack Markus T. (2017). Human METTL16 is a N6-methyladenosine (m6A) methyltransferase that targets pre-mRNAs and various non-coding RNAs. *EMBO reports* 18(11): 2004-2014.

- Waterhouse A.M., Procter J.B., Martin D.M.A., Clamp M. and Barton G.J. (2009). Jalview Version 2—a multiple sequence alignment editor and analysis workbench. *Bioinformatics* 25(9): 1189-1191.
- Webster M.W., Chen Y.-H., Stowell J.A.W., Alhusaini N., Sweet T., Graveley B.R., Collier J. and Passmore L.A. (2018). mRNA Deadenylation Is Coupled to Translation Rates by the Differential Activities of Ccr4-Not Nucleases. *Molecular cell* 70(6): 1089-1100.e1088.
- Wei C.-M., Gershowitz A. and Moss B. (1975). Methylated nucleotides block 5' terminus of HeLa cell messenger RNA. *Cell* 4(4): 379-386.
- Wei C.M., Gershowitz A. and Moss B. (1976). 5'-Terminal and internal methylated nucleotide sequences in HeLa cell mRNA. *Biochemistry* 15(2): 397-401.
- Wei C.M. and Moss B. (1974). Methylation of newly synthesized viral messenger RNA by an enzyme in vaccinia virus. *Proc Natl Acad Sci U S A* 71(8): 3014-3018.
- Wei C.M. and Moss B. (1975). Methylated nucleotides block 5'-terminus of vaccinia virus messenger RNA. *Proceedings of the National Academy of Sciences of the United States of America* 72(1): 318-322.
- Wei H.-H., Fan X.-J., Hu Y., Tian X.-X., Guo M., Fang Z.-Y., Wu P., Gao S.-X., Peng C., Yang Y. and Wang Z. (2020). A systematic survey of PRMT interactomes reveals key roles of arginine methylation in the global control of RNA splicing and translation. *bioRxiv*: 746529.
- Wei J. and He C. (2019). Site-specific m⁶A editing. *Nature chemical biology* 15(9): 848-849.
- Wei J., Liu F., Lu Z., Fei Q., Ai Y., He P.C., Shi H., Cui X., Su R., Klungland A., Jia G., Chen J. and He C. (2018). Differential m⁶A, m⁶Am, and m¹A Demethylation Mediated by FTO in the Cell Nucleus and Cytoplasm. *Molecular Cell* 71(6): 973-985.e975.
- Wei L.-H., Song P., Wang Y., Lu Z., Tang Q., Yu Q., Xiao Y., Zhang X., Duan H.-C. and Jia G. (2018). The m⁶A Reader ECT2 Controls Trichome Morphology by Affecting mRNA Stability in Arabidopsis. *The Plant Cell*.
- Weintraub H., Palter K. and Van Lente F. (1975). Histones H2a, H2b, H3, and H4 form a tetrameric complex in solutions of high salt. *Cell* 6(1): 85-110.
- Wen J., Lv R., Ma H., Shen H., He C., Wang J., Jiao F., Liu H., Yang P., Tan L., Lan F., Shi Y.G., He C., Shi Y. and Diao J. (2018). Zc3h13 Regulates Nuclear RNA m⁶A Methylation and Mouse Embryonic Stem Cell Self-Renewal. *Molecular Cell* 69(6): 1028-1038.e1026.
- Weng Y.L., Wang X., An R., Cassin J., Vissers C., Liu Y., Liu Y., Xu T., Wang X., Wong S.Z.H., Joseph J., Dore L.C., Dong Q., Zheng W., Jin P., Wu H., Shen B., Zhuang X., He C., Liu K., Song H. and Ming G.L. (2018). Epi-transcriptomic m⁶A Regulation of Axon Regeneration in the Adult Mammalian Nervous System. *Neuron* 97(2): 313-325 e316.
- Whitworth A.J., Theodore D.A., Greene J.C., Beneš H., Wes P.D. and Pallanck L.J. (2005). Increased glutathione S-transferase activity rescues dopaminergic neuron loss in a Drosophila model of Parkinson's disease. *Proceedings of the National Academy of Sciences* 102(22): 8024-8029.
- Widagdo J., Zhao Q.Y., Kempen M.J., Tan M.C., Ratnu V.S., Wei W., Leighton L., Spadaro P.A., Edson J., Anggono V. and Bredy T.W. (2016). Experience-Dependent Accumulation of N⁶-Methyladenosine in the Prefrontal Cortex Is Associated with Memory Processes in Mice. *The Journal of neuroscience : the official journal of the Society for Neuroscience* 36(25): 6771-6777.
- Wojtas M.N., Pandey R.R., Mendel M., Homolka D., Sachidanandam R. and Pillai R.S. (2017). Regulation of m⁶A Transcripts by the 3'→5' RNA Helicase YTHDC2 Is Essential for a Successful Meiotic Program in the Mammalian Germline. *Mol Cell* 68(2): 374-387 e312.
- Worpenberg L., Jakobi T., Dieterich C. and Roignant J.-Y. (2019). Identification of Methylated Transcripts Using the TRIBE Approach. *Epi-transcriptomics: Methods and Protocols*. N. Wajapeyee et al. New York, NY, Springer New York: 89-106.
- Wright A. and Vissel B. (2012). The essential role of AMPA receptor GluR2 subunit RNA editing in the normal and diseased brain. *Front Mol Neurosci* 5: 34-34.
- Wu H. and Zhang Y. (2014). Reversing DNA methylation: mechanisms, genomics, and biological functions. *Cell* 156(1-2): 45-68.
- Wu T.P., Wang T., Seetin M.G., Lai Y., Zhu S., Lin K., Liu Y., Byrum S.D., Mackintosh S.G., Zhong M., Tackett A., Wang G., Hon L.S., Fang G., Swenberg J.A. and Xiao A.Z. (2016). DNA methylation on N⁶-adenine in mammalian embryonic stem cells. *Nature* 532: 329.
- Wu Y., Zhang J., Peng B., Tian D., Zhang D., Li Y., Feng X., Liu J., Li J., Zhang T., Liu X., Lu J., Chen B. and Wang S. (2019). Generating viable mice with heritable embryonically lethal mutations using the CRISPR-Cas9 system in two-cell embryos. *Nature communications* 10(1): 2883-2883.
- Xia H., Zhong C., Wu X., Chen J., Tao B., Xia X., Shi M., Zhu Z., Trudeau V.L. and Hu W. (2018). Methyl3 Mutation Disrupts Gamete Maturation and Reduces Fertility in Zebrafish. *Genetics* 208(2): 729-743.
- Xiang J.-F., Yang Q., Liu C.-X., Wu M., Chen L.-L. and Yang L. (2018). N⁶-Methyladenosines Modulate A-to-I RNA Editing. *Molecular Cell* 69(1): 126-135.e126.
- Xiang Y., Laurent B., Hsu C.-H., Nachtergaele S., Lu Z., Sheng W., Xu C., Chen H., Ouyang J., Wang S., Ling D., Hsu P.-H., Zou L., Jambhekar A., He C. and Shi Y. (2017). RNA m⁶A methylation regulates the ultraviolet-induced DNA damage response. *Nature* 543(7646): 573-576.
- Xiao C.-L., Zhu S., He M., Chen D., Zhang Q., Chen Y., Yu G., Liu J., Xie S.-Q., Luo F., Liang Z., Wang D.-P., Bo X.-C., Gu X.-F., Wang K. and Yan G.-R. (2018). N⁶-Methyladenine DNA Modification in the Human Genome. *Molecular Cell* 71(2): 306-318.e307.
- Xiao N., Laha S., Das S.P., Morlock K., Jesneck J.L. and Raffel G.D. (2015). Ott1 (Rbm15) regulates thrombopoietin response in hematopoietic stem cells through alternative splicing of c-Mpl. *Blood* 125(6): 941-948.
- Xiao W., Adhikari S., Dahal U., Chen Y.S., Hao Y.J., Sun B.F., Sun H.Y., Li A., Ping X.L., Lai W.Y., Wang X., Ma H.L., Huang C.M., Yang Y., Huang N., Jiang G.B., Wang H.L., Zhou Q., Wang X.J., Zhao Y.L. and Yang Y.G. (2016). Nuclear m⁶A Reader YTHDC1 Regulates mRNA Splicing. *Mol Cell* 61(4): 507-519.
- Xie Q., Wu T.P., Gimple R.C., Li Z., Prager B.C., Wu Q., Yu Y., Wang P., Wang Y., Gorkin D.U., Zhang C., Dowiak A.V., Lin K., Zeng C., Sui Y., Kim L.J.Y., Miller T.E., Jiang L., Lee C.H., Huang Z., Fang X., Zhai K., Mack S.C., Sander M., Bao S., Kerstetter-Fogle A.E., Sloan A.E., Xiao A.Z. and Rich J.N. (2018). N⁶-methyladenine DNA Modification in Glioblastoma. *Cell* 175(5): 1228-1243.e1220.
- Xu C., Liu K., Ahmed H., Loppnau P., Schapira M. and Min J. (2015). Structural Basis for the Discriminative Recognition of N⁶-Methyladenosine RNA by the Human YT521-B Homology Domain Family of Proteins. *J Biol Chem* 290(41): 24902-24913.
- Xu C., Wang X., Liu K., Roundtree I.A., Tempel W., Li Y., Lu Z., He C. and Min J. (2014). Structural basis for selective binding of m⁶A RNA by the YTHDC1 YTH domain. *Nature Chemical Biology* 10: 927.
- Xu K., Yang Y., Feng G.-H., Sun B.-F., Chen J.-Q., Li Y.-F., Chen Y.-S., Zhang X.-X., Wang C.-X., Jiang L.-Y., Liu C., Zhang Z.-Y., Wang X.-J., Zhou Q., Yang Y.-G. and Li W. (2017). Methyl3-mediated m⁶A regulates spermatogonial differentiation and meiosis initiation. *Cell Research* 27: 1100.
- Xu L., Liu X., Sheng N., Oo K.S., Liang J., Chionh Y.H., Xu J., Ye F., Gao Y.-G., Dedon P.C. and Fu X.-Y. (2017). Three distinct 3-methylcytidine (m³C) methyltransferases modify tRNA and mRNA in mice and humans. *The Journal of biological chemistry* 292(35): 14695-14703.
- Yan D. and Perrimon N. (2015). spenito is required for sex determination in Drosophila melanogaster. *Proceedings of the National Academy of Sciences of the United States of America* 112(37): 11606-11611.
- Yang J.-Y., Zong C.S., Xia W., Wei Y., Ali-Seyed M., Li Z., Broglio K., Berry D.A. and Hung M.-C. (2006). MDM3 promotes cell motility and invasiveness by regulating E-cadherin degradation. *Molecular and cellular biology* 26(19): 7269-7282.
- Yang X., Yang Y., Sun B.-F., Chen Y.-S., Xu J.-W., Lai W.-Y., Li A., Wang X., Bhattarai D.P., Xiao W., Sun H.-Y., Zhu Q., Ma H.-L., Adhikari S., Sun M., Hao Y.-J., Zhang B., Huang C.-M., Huang N., Jiang G.-B., Zhao Y.-L., Wang H.-L., Sun Y.-P. and Yang Y.-G. (2017). 5-methylcytosine promotes mRNA export - NSUN2 as the methyltransferase and ALYREF as an m⁵C reader. *Cell research* 27(5): 606-625.
- Yang Y., Hsu P.J., Chen Y.-S. and Yang Y.-G. (2018). Dynamic transcriptomic m⁶A decoration: writers, erasers, readers and functions in RNA metabolism. *Cell Research* 28(6): 616-624.

- Yazdani U., Huang Z. and Terman J.R. (2008). The glucose transporter (GLUT4) enhancer factor is required for normal wing positioning in *Drosophila*. *Genetics* 178(2): 919-929.
- Ye F., Chen E.R. and Nilsen T.W. (2017). Kaposi's Sarcoma-Associated Herpesvirus Utilizes and Manipulates RNA N(6)-Adenosine Methylation To Promote Lytic Replication. *Journal of virology* 91(16): e00466-00417.
- Yee B., Pratt G., Graveley B., Van Nostrand E. and Yeo G. (2018). RBP-Maps enables robust generation of splicing regulatory maps. *RNA*.
- Yi H., Park J., Ha M., Lim J., Chang H. and Kim V.N. (2018). PABP Cooperates with the CCR4-NOT Complex to Promote mRNA Deadenylation and Block Precocious Decay. *Molecular Cell* 70(6): 1081-1088.e1085.
- Yoon K.J., Ringeling F.R., Vissers C., Jacob F., Pokrass M., Jimenez-Cyrus D., Su Y.J., Kim N.S., Zhu Y.H., Zheng L.L., Kim S., Wang X.Y., Dore L.C., Jin P., Regot S., Zhuang X.X., Canzar S., He C., Ming G.L. and Song H.J. (2017). Temporal Control of Mammalian Cortical Neurogenesis by m(6)A Methylation. *Cell* 171(4): 877-+.
- Yu B., Yang Z., Li J., Minakhina S., Yang M., Padgett R.W., Steward R. and Chen X. (2005). Methylation as a Crucial Step in Plant microRNA Biogenesis. *Science* 307(5711): 932-935.
- Yu C.-T. and Allen F.W. (1959). Studies of an isomer of uridine isolated from ribonucleic acids. *Biochimica et Biophysica Acta* 32: 393-406.
- Yu G., Wang L.G. and He Q.Y. (2015). ChIPseeker: an R/Bioconductor package for ChIP peak annotation, comparison and visualization. *Bioinformatics* 31(14): 2382-2383.
- Yu J., Chen M., Huang H., Zhu J., Song H., Zhu J., Park J. and Ji S.J. (2018). Dynamic m6A modification regulates local translation of mRNA in axons. *Nucleic Acids Res* 46(3): 1412-1423.
- Yuan B.-F. (2017). Liquid Chromatography-Mass Spectrometry for Analysis of RNA Adenosine Methylation. *RNA Methylation: Methods and Protocols*. A. Lusser. New York, NY, Springer New York: 33-42.
- Yue Y., Liu J., Cui X., Cao J., Luo G., Zhang Z., Cheng T., Gao M., Shu X., Ma H., Wang F., Wang X., Shen B., Wang Y., Feng X., He C. and Liu J. (2018). VIRMA mediates preferential m(6)A mRNA methylation in 3'UTR and near stop codon and associates with alternative polyadenylation. *Cell discovery* 4: 10-10.
- Zabzhinsky D., Slobodin B., Rapaport D. and Gerst J.E. (2016). An Essential Role for COPI in mRNA Localization to Mitochondria and Mitochondrial Function. *Cell reports* 15(3): 540-549.
- Zaccara S. and Jaffrey S.R. (2020). A Unified Model for the Function of YTHDF Proteins in Regulating m(6)A-Modified mRNA. *Cell*.
- Zearfoss N.R., Deveau L.M., Clingman C.C., Schmidt E., Johnson E.S., Massi F. and Ryder S.P. (2014). A conserved three-nucleotide core motif defines Musashi RNA binding specificity. *The Journal of biological chemistry* 289(51): 35530-35541.
- Zemach A., McDaniel I.E., Silva P. and Zilberman D. (2010). Genome-Wide Evolutionary Analysis of Eukaryotic DNA Methylation. *Science* 328(5980): 916-919.
- Zentner G.E. and Henikoff S. (2013). Regulation of nucleosome dynamics by histone modifications. *Nature Structural & Molecular Biology* 20: 259.
- Zhai B., Villén J., Beausoleil S.A., Mintseris J. and Gygi S.P. (2008). Phosphoproteome analysis of *Drosophila melanogaster* embryos. *Journal of proteome research* 7(4): 1675-1682.
- Zhang C., Chen Y., Sun B., Wang L., Yang Y., Ma D., Lv J., Heng J., Ding Y., Xue Y., Lu X., Xiao W., Yang Y.G. and Liu F. (2017). m(6)A modulates haematopoietic stem and progenitor cell specification. *Nature* 549(7671): 273-276.
- Zhang C. and Jia G. (2018). Reversible RNA Modification N1-methyladenosine (m1A) in mRNA and tRNA. *Genomics, Proteomics & Bioinformatics* 16(3): 155-161.
- Zhang C., Samanta D., Lu H., Bullen J.W., Zhang H., Chen I., He X. and Semenza G.L. (2016). Hypoxia induces the breast cancer stem cell phenotype by HIF-dependent and ALKBH5-mediated m⁶A-demethylation of NANOG mRNA. *Proceedings of the National Academy of Sciences of the United States of America* 113(14): E2047-E2056.
- Zhang F., Kang Y., Wang M., Li Y., Xu T., Yang W., Song H., Wu H., Shu Q. and Jin P. (2018). Fragile X mental retardation protein modulates the stability of its m6A-marked messenger RNA targets. *Human molecular genetics* 27(22): 3936-3950.
- Zhang F., Zhang Y.-C., Liao J.-Y., Yu Y., Zhou Y.-F., Feng Y.-Z., Yang Y.-W., Lei M.-Q., Bai M. and Wu H. (2019). The subunit of RNA N6-methyladenosine methyltransferase OsFIP regulates early degeneration of microspores in rice. *PLoS genetics* 15(5): e1008120.
- Zhang G., Huang H., Liu D., Cheng Y., Liu X., Zhang W., Yin R., Zhang D., Zhang P., Liu J., Li C., Liu B., Luo Y., Zhu Y., Zhang N., He S., He C., Wang H. and Chen D. (2015). N6-Methyladenine DNA Modification in *Drosophila*. *Cell* 161(4): 893-906.
- Zhang L., Tran N.T., Su H., Wang R., Lu Y., Tang H., Aoyagi S., Guo A., Khodadadi-Jamayran A., Zhou D., Qian K., Hricik T., Côté J., Han X., Zhou W., Laha S., Abdel-Wahab O., Levine R.L., Raffel G., Liu Y., Chen D., Li H., Townes T., Wang H., Deng H., Zheng Y.G., Leslie C., Luo M. and Zhao X. (2015). Cross-talk between PRMT1-mediated methylation and ubiquitylation on RBM15 controls RNA splicing. *eLife* 4.
- Zhang L.S., Liu C., Ma H., Dai Q., Sun H.L., Luo G., Zhang Z., Zhang L., Hu L., Dong X. and He C. (2019). Transcriptome-wide Mapping of Internal N(7)-Methylguanosine Methylome in Mammalian mRNA. *Mol Cell* 74(6): 1304-1316.e1308.
- Zhang S., Zhao B.S., Zhou A., Lin K., Zheng S., Lu Z., Chen Y., Sulman E.P., Xie K., Böglér O., Majumder S., He C. and Huang S. (2017). m(6)A Demethylase ALKBH5 Maintains Tumorigenicity of Glioblastoma Stem-like Cells by Sustaining FOXM1 Expression and Cell Proliferation Program. *Cancer cell* 31(4): 591-606.e596.
- Zhang Y., Liu T., Meyer C.A., Eeckhoutte J., Johnson D.S., Bernstein B.E., Nussbaum C., Myers R.M., Brown M., Li W. and Liu X.S. (2008). Model-based analysis of ChIP-Seq (MACS). *Genome Biol* 9(9): R137.
- Zhang Y., Sun L., Gao X., Guo A., Diao Y. and Zhao Y. (2019). RNF43 ubiquitinates and degrades phosphorylated E-cadherin by c-Src to facilitate epithelial-mesenchymal transition in lung adenocarcinoma. *BMC cancer* 19(1): 670.
- Zhang Y., Wang X., Zhang X., Wang J., Ma Y., Zhang L. and Cao X. (2019). RNA-binding protein YTHDF3 suppresses interferon-dependent antiviral responses by promoting FOXO3 translation. *Proceedings of the National Academy of Sciences* 116(3): 976-981.
- Zhang Z., Wang M., Xie D., Huang Z., Zhang L., Yang Y., Ma D., Li W., Zhou Q., Yang Y.-G. and Wang X.-J. (2018). METTL3-mediated N6-methyladenosine mRNA modification enhances long-term memory consolidation. *Cell Research*.
- Zhao B.S., Roundtree I.A. and He C. (2017a). Post-transcriptional gene regulation by mRNA modifications. *Nature reviews. Molecular cell biology* 18(1): 31-42.
- Zhao B.S., Wang X., Beadell A.V., Lu Z., Shi H., Kuuspalu A., Ho R.K. and He C. (2017b). m(6)A-dependent maternal mRNA clearance facilitates zebrafish maternal-to-zygotic transition. *Nature* 542(7642): 475-478.
- Zhao X., Yang Y., Sun B.-F., Shi Y., Yang X., Xiao W., Hao Y.-J., Ping X.-L., Chen Y.-S., Wang W.-J., Jin K.-X., Wang X., Huang C.-M., Fu Y., Ge X.-M., Song S.-H., Jeong H.S., Yanagisawa H., Niu Y., Jia G.-F., Wu W., Tong W.-M., Okamoto A., He C., Rendtlew Danielsen J.M., Wang X.-J. and Yang Y.-G. (2014). FTO-dependent demethylation of N6-methyladenosine regulates mRNA splicing and is required for adipogenesis. *Cell research* 24(12): 1403-1419.
- Zheng G., Dahl J.A., Niu Y., Fedorcsak P., Huang C.-M., Li C.J., Vågbo C.B., Shi Y., Wang W.-L., Song S.-H., Lu Z., Bosmans R.P.G., Dai Q., Hao Y.-J., Yang X., Zhao W.-M., Tong W.-M., Wang X.-J., Bogdan F., Furu K., Fu Y., Jia G., Zhao X., Liu J., Krokan H.E., Klungland A., Yang Y.-G. and He C. (2013). ALKBH5 is a mammalian RNA demethylase that impacts RNA metabolism and mouse fertility. *Molecular cell* 49(1): 18-29.
- Zhong S., Li H., Bodi Z., Button J., Vespa L., Herzog M. and Fray R.G. (2008). MTA is an Arabidopsis messenger RNA adenosine methylase and interacts with a homolog of a sex-specific splicing factor. *The Plant cell* 20(5): 1278-1288.
- Zhou C., Molinie B., Daneshvar K., Pondick J.V., Wang J., Van Wittenbergh N.O., Xing Y., Giallourakis C.C. and Mullen A.C. (2017). Genome-wide maps of m6A circRNAs identify widespread and cell-type-specific methylation patterns that are distinct from mRNAs. *Cell reports* 20(9): 2262-2276.

- Zhou J., Wan J., Shu X.E., Mao Y., Liu X.-M., Yuan X., Zhang X., Hess M.E., Brüning J.C. and Qian S.-B. (2018). N6-methyladenosine guides mRNA alternative translation during integrated stress response. *Molecular cell* 69(4): 636-647. e637.
- Zhou K.I., Shi H., Lyu R., Wylder A.C., Matuszek Z., Pan J.N., He C., Parisien M. and Pan T. (2019). Regulation of Co-transcriptional Pre-mRNA Splicing by m6A through the Low-Complexity Protein hnRNPG. *Molecular Cell*.
- Zhou Z., Licklider L.J., Gygi S.P. and Reed R. (2002). Comprehensive proteomic analysis of the human spliceosome. *Nature* 419: 182.
- Zhu T., Roundtree I.A., Wang P., Wang X., Wang L., Sun C., Tian Y., Li J., He C. and Xu Y. (2014). Crystal structure of the YTH domain of YTHDF2 reveals mechanism for recognition of N6-methyladenosine. *Cell Research* 24(12): 1493-1496.
- Zhuang M., Li X., Zhu J., Zhang J., Niu F., Liang F., Chen M., Li D., Han P. and Ji S.-J. (2019). The m6A reader YTHDF1 regulates axon guidance through translational control of Robo3.1 expression. *Nucleic Acids Research*.
- Zou S., Toh J.D.W., Wong K.H.Q., Gao Y.-G., Hong W. and Woon E.C.Y. (2016). N(6)-Methyladenosine: a conformational marker that regulates the substrate specificity of human demethylases FTO and ALKBH5. *Scientific reports* 6: 25677-25677.
- Žylicz J.J., Bousard A., Žumer K., Dossin F., Mohammad E., da Rocha S.T., Schwalb B., Syx L., Dingli F., Loew D., Cramer P. and Heard E. (2019). The Implication of Early Chromatin Changes in X Chromosome Inactivation. *Cell* 176(1): 182-197.e123.
- Zylka M.J., Simon J.M. and Philpot B.D. (2015). Gene length matters in neurons. *Neuron* 86(2): 353-355.

Appendix 1 - Research article

Lence T, Akhtar J, Bayer M, Schmid K, Spindler L, Ho CH, Kreim N, Andrade-Navarro MA, Poeck B, Helm M, Roignant JY (2016). m⁶A modulates neuronal functions and sex determination in *Drosophila*. *Nature*, Dec 8;540(7632):242-247. doi: 10.1038/nature2056.

m⁶A modulates neuronal functions and sex determination in *Drosophila*

Tina Lence 1, Junaid Akhtar 1, Marc Bayer 1, Katharina Schmid 2, Laura Spindler 3, Cheuk Hei Ho 4, Nastasja Kreim 1, Miguel A. Andrade-Navarro 1,5, Burkhard Poeck 3, Mark Helm 2 & Jean-Yves Roignant 1

1 - Institute of Molecular Biology (IMB), 55128 Mainz, Germany.

2 - Institute of Pharmacy and Biochemistry, Johannes Gutenberg University of Mainz, 55128 Mainz, Germany.

3 - Institute of Zoology III (Neurobiology), Johannes Gutenberg University of Mainz, 55128 Mainz, Germany.

4 - Kimmel Center for Biology and Medicine of the Skirball Institute, NYU School of Medicine, Department of Cell Biology, 540 First Avenue, New York, New York 10016, USA.

5 - Faculty of Biology, Johannes Gutenberg University of Mainz, 55128 Mainz, Germany.

Published: Nature, Vol 540, 8 December 2016, doi:10.1038/nature20568

N⁶-methyladenosine RNA (m⁶A) is a prevalent messenger RNA modification in vertebrates. Although its functions in the regulation of post-transcriptional gene expression are beginning to be unveiled, the precise roles of m⁶A during development of complex organisms remain unclear. Here we carry out a comprehensive molecular and physiological characterization of the individual components of the methyltransferase complex, as well as of the YTH domain-containing nuclear reader protein in *Drosophila melanogaster*. We identify the member of the split ends protein family, Spenito, as a novel bona fide subunit of the methyltransferase complex. We further demonstrate important roles of this complex in neuronal functions and sex determination, and implicate the nuclear YT521-B protein as a main m⁶A effector in these processes. Altogether, our work substantially extends our knowledge of m⁶A biology, demonstrating the crucial functions of this modification in fundamental processes within the context of the whole animal.

RNA modifications represent a critical layer of epigenetic regulation of gene expression¹. m⁶A is among the most abundant modifications in the mammalian system^{2,3}. m⁶A distribution has been determined in several organisms and cell types, including human, mouse, rice and yeast^{4–7}. The modification is found in a subset of the RRACH consensus sites (R, purine; H, non-guanine base) and is enriched around stop codons, in the 3'-untranslated regions (3'UTRs) and within long internal exons. m⁶A was shown to control several post-transcriptional processes, including pre-mRNA splicing, mRNA decay and translation^{4,5,8–16}, which are mediated in part via conserved members of the YTH protein family^{4,17}. The methyltransferase complex catalysing m⁶A formation in mammals consists of methyltransferase-like 3 (METTL3), methyltransferase-like 14 (METTL14) and a stabilizing factor called Wilms' tumour 1-associated protein (WTAP)^{9,11,18,19}. In mammals, m⁶A can be reverted into adenosine via two identified demethylases: fat mass and obesity associated factor (FTO)^{20–22} and AlkB homologue 5 (ALKBH5)²³.

Several studies have uncovered crucial roles for METTL3 during development and cell differentiation. Knockout of *Mettl3* in murine naive embryonic stem cells blocks differentiation^{24,25}, while its deletion in mice causes early embryonic lethality. Similarly, in *Drosophila*, loss of the *METTL3* orthologue *Ime4* is reported to be semi-lethal during development, with adult escapers having reduced fertility owing to impaired Notch signalling²⁶. Depletion of the *METTL3* orthologue *MTA* in *Arabidopsis thaliana* also affects embryonic development^{27,28}, while in yeast *ime4* has an essential role during meiosis^{29–31}. All of these observations indicate the importance of m⁶A in the gonads and during early embryogenesis. Recent crystal structure studies investigated the molecular activities of the two predicted catalytic proteins^{32,33}; however, their respective roles *in vivo* remain unclear. Here we characterize members of the methyltransferase complex in *Drosophila* and identify the split ends (SPEN) family protein, Spenito (Nito), as a novel bona fide subunit. Expression of complex components is substantially enriched in the nervous system, and flies with mutations in *Ime4* and *Mettl14* suffer from impaired neuronal functions. Methyltransferase complex components also

influence the female-specific splicing of *Sex-lethal* (*Sxl*), revealing a role in fine-tuning sex determination and dosage compensation. Notably, knockout of the nuclear m⁶A reader YT521-B resembles the loss of the catalytic subunits, implicating this protein as a main effector of m⁶A *in vivo*.

m⁶A is enriched in the nervous system

To investigate potential functions of m⁶A in *Drosophila*, we monitored its levels on mRNA samples isolated at different developmental stages of wild-type flies using mass spectrometry (Fig. 1a and Extended Data Fig. 1a, b). We find that m⁶A is remarkably enriched in early embryo-genesis but drops dramatically 2 h after fertilization and remains low throughout the rest of embryogenesis and early larval stages. During the third larval instar, m⁶A rises again to reach a peak at pupal phases. While the overall level of m⁶A decreases in adults, it remains substantially elevated in heads and ovaries. A phylogenetic analysis of the *Drosophila* METTL3 orthologue *Ime4* (Extended Data Fig. 1c) identifies two closely related factors, CG7818 and CG14906. Depletion of *Ime4* and CG7818 in embryonic-derived Schneider (S2R+) cells decreases m⁶A levels by about 70%, whereas depletion of CG14906 had no effect (Fig. 1b and Extended Data Fig. 1d). These results indicate that *Ime4* and CG7818 are required to promote m⁶A activity in *Drosophila*. Because of its sequence and functional conservation with human METTL14, CG7818 was renamed dMettl14. Fl(2)d and Virilizer (*Vir*) are the *Drosophila* homologues of WTAP and KIAA1429, respectively, which are integral components of the complex in mammals⁶. Both transcripts follow the same developmental distribution as other methyltransferase complex components and their depletion also affects m⁶A levels (Fig. 1a, b and Extended Data Fig. 1d–f). *Ime4* and Fl(2)d co-immunoprecipitate with dMettl14 in an RNA-independent manner (Fig. 1c). Likewise, *Vir*, Fl(2)d and *Ime4* are found in the same complex (Extended Data Fig. 1g). Notably, Fl(2)d depletion reduces the interaction between *Ime4* and dMettl14 (Extended Data Fig. 1h), confirming its proposed role as a stabilizing factor. All components localize in the nucleus and are ubiquitously expressed in early embryonic stages (data not shown) but show substantial enrichment in the neuroectoderm at later stages (Fig. 1d, e). Altogether, our results demonstrate the

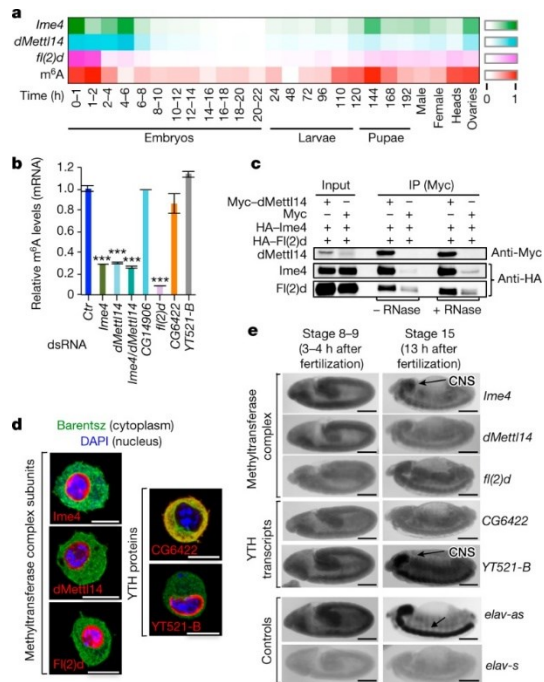


Figure 1 | *Drosophila* m6A methyltransferase complex is enriched in the nervous system.

a, Heatmap shows relative mRNA expression of methyltransferase complex subunits and m6A levels during development. **b**, m6A liquid chromatography tandem-mass spectrometry (LC-MS/MS) quantification in different knockdown conditions. *Ctrl*, control. Bar chart represents the mean \pm standard deviation (s.d.) of three technical measurements from three biological replicates. $***P < 0.0001$ (one-way analysis of variance (ANOVA), Tukey's post-hoc analysis). **c**, Lysates from S2R+ cells expressing indicated proteins were immunoprecipitated using Myc beads. HA, haemagglutinin. **d**, Immunostaining of indicated proteins in S2R+ cells. DAPI, 4',6-diamidino-2-phenylindole. Scale bars, 10 μ m. **e**, *In situ* RNA hybridization. *elav-positive* (*elav-as*) and -negative (*elav-s*) controls are shown. CNS, central nervous system. Scale bars, 100 μ m.

existence of a conserved functional methyltransferase complex in *Drosophila* and reveal its particular abundance in the nervous system.

YT521-B mediates m6A-dependent splicing

To obtain insight into the transcriptome-wide m6A distribution in S2R+ cells, we performed methylated RNA immunoprecipitation followed by sequencing (MeRIP-seq) (Extended Data Fig. 2a, b). In total, 1,120 peaks representing transcripts of 812 genes were identified (Supplementary Table 1). The consensus sequence RRACH is present in most m6A peaks ($n = 1,027$, 92% of all peaks) (Fig. 2a). Additional sequences are also enriched, suggesting their potential involvement in providing specificity to the methyltransferase complex (Extended Data Fig. 2c). As shown in other species, enrichment near start and stop codons was observed (Fig. 2b, c). We next performed transcriptome analyses in S2R+ cells lacking m6A components (Extended Data Fig. 3a–c). Knockdown of *Fl(2)d* leads to strong changes in gene expression ($n = 2,129$ differentially expressed genes; adjusted P value < 0.05 ; Fig. 2d, e and Supplementary Table 2), while knockdowns of *Ime4* and *dMett14* have milder effects. Gene ontology analyses revealed that genes involved in diverse metabolic processes, anion transport and cell adhesion are significantly overrepresented (Extended Data Fig. 4). Despite the fact that S2R+ cells are of non-neuronal origin, the affected genes are also enriched for neuronal functions, including roles in axon

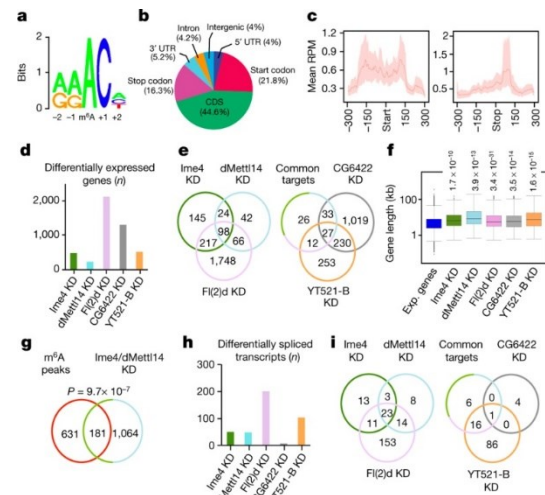


Figure 2 | m6A controls alternative splicing via YT521-B.

a, Sequence logo of deduced consensus motif for most m6A peaks centred on the modified adenosine. **b**, Pie chart of m6A peak distribution in distinct transcript segments. Start codon (± 300 bp window around start), CDS (coding sequence (CDS) excluding 300 bp after start and 300 bp before stop), stop codon (± 300 bp window around stop). **c**, Normalized m6A read counts in a ± 300 bp window around start (left) and stop codons (right) for all transcripts detected. RPM, reads per million. **d**, Number of differentially expressed genes upon knockdown (KD) of indicated proteins. **e**, Venn diagrams representing common targets between methyltransferase complex components and YTH proteins. **f**, Boxplots of gene length for all expressed (Exp.) genes (average coverage >1 read per kilobase per million mapped reads (RPKM) in control conditions) and differentially expressed genes in each knockdown. Distributions were compared to all expressed genes using the Wilcoxon rank sum test. Expressed genes were downsampled to the same number of genes as in the given knockdown. **g**, Venn diagram showing the overlap of differentially regulated and/or spliced genes in *Ime4/dMett14* double knockdown with genes containing m6A peaks. **h**, Number of differentially spliced genes upon knockdown of methyltransferase components and YTH proteins. **i**, Venn diagrams showing number of common targets between methyltransferase complex components and YTH proteins.

guidance and synapse activity. Consistent with the larger average size of neuronal genes³⁴, affected genes are significantly larger than the non-affected ones (Fig. 2f). We next compared the genes affected upon *Ime4/dMett14* double knockdown with the m6A profile. Overall, about 15% of the affected genes contain at least one m6A peak (Fig. 2g). We find a slight but significant positive influence of m6A on mRNA levels (P value = 9.9×10^{-4}) (Extended Data Fig. 3d) and this effect seems independent of the location of the m6A peak along the transcript (Extended Data Fig. 3e). Several splicing changes upon knockdown of individual complex components were also observed (Fig. 2h, i). *fl(2)d* itself is among the affected transcripts in any of the knockdowns tested (Extended Data Fig. 5). Generally, each knockdown results in alternative 5' splice site usage and intron retention (Extended Data Fig. 3f), which was also observed in human cells⁴. YTH proteins are critical readers of m6A in mammals. While vertebrates contain five proteins of this family, only two members exist in flies, CG6422 and YT521-B (Extended Data Fig. 6a). We find that CG6422 is localized in the cytoplasm and strongly enriched during the first 2 h after fertilization but then declines and remains at low levels during development and adulthood. By contrast, YT521-B is strictly nuclear and shows strong enrichment in the embryonic nervous system and adult brains (Fig. 1d, e and Extended Data Fig. 6b). Using dot-blot assays and pull-down experiments we confirmed that YT521-B binds m6A in *Drosophila* (Extended Data Fig. 6c, d). RNAsequencing (RNA-seq) experiments show that depletion of CG6422 only marginally affects splicing (Fig. 2h) while YT521-B knockdown significantly impairs this process (103

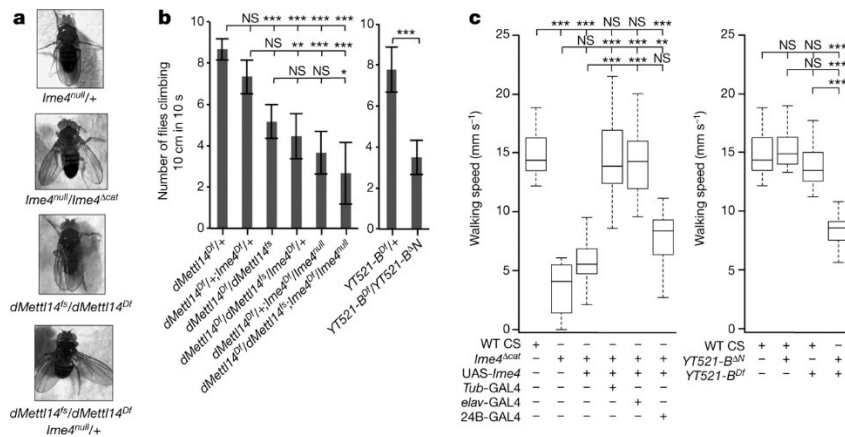


Figure 3 | YT521-B and the methyltransferase complex control fly behaviour.

a, Adult flies of indicated genotypes. **b**, Bars represent the mean \pm s.d. of female flies ($n = 10$ per condition) that climb over 10 cm in 10 s (six independent measurements). $*P < 0.01$; $**P < 0.001$; $***P < 0.0001$; NS, not significant (one-way ANOVA, Tukey's post-hoc analysis). Student's t -test was used for YT521-B analysis. **c**, Walking speed of indicated females ($n = 15$ per condition) measured in Buridan's paradigm. Kruskal–Wallis analysis with Bonferroni correction (*Ime4*) and one-way ANOVA, Bonferroni post-hoc analysis (YT521-B) were used. Boxes signify 25%/75% quartiles, thick lines indicate medians, and whiskers show maximum interquartile range $\times 1.5$. $*P < 0.0$, $**P < 0.01$, $***P < 0.001$; NS, not significant; WT-CS, wild-type *Canton-S* flies.

differentially regulated splicing events; adjusted P value < 0.1). The overlap of mis-spliced events between YT521-B knockdown and knockdown of methyltransferase complex subunits is about 70% (Fig. 2i), revealing that YT521-B might be the main mediator of m6A function in pre-mRNA splicing.

m6A components modulate fly behaviour

To investigate potential roles of m6A during *Drosophila* development, we generated *Ime4*- and *dMettl14*-knockout flies (Extended Data Fig. 7a, b, d). Two deletions in *Ime4* were created, removing the entire coding sequence (*Ime4*^{null}) or only the C-terminal part containing the catalytic domain (*Ime4*^{Δcat}). We find that flies homozygous for either mutant allele as well as transheterozygous flies survive until adulthood. We did not observe encapsulation defects in ovaries as previously shown using different alleles²⁶ (Extended Data Fig. 8a). However, the mutant flies have a reduced lifespan and exhibit multiple behavioural defects: flight and locomotion are severely affected and they spend more time grooming (Fig. 3b, c and Extended Data Fig. 8b). They also display a mild held-out wing appearance resulting from failure to fold their wings together over the dorsal surface of the thorax and abdomen (Fig. 3a). *dMettl14* mutant flies have normal wings but their locomotion is also deficient (Fig. 3a, b). To test whether *Ime4* and *dMettl14* can compensate for each other *in vivo*, we generated double-mutant animals. Removing one copy of *Ime4* in the *dMettl14* mutant background mimics the held-out wing phenotype observed upon loss of *Ime4* (Fig. 3a). Double-homozygous mutants give similar phenotypes as the *Ime4* single knockout, albeit with increased severity (Fig. 3b). Altogether, these phenotypic analyses strongly suggest that *Ime4* and *dMettl14* control similar physiological processes *in vivo*, indicating that they probably regulate common targets. Furthermore, the function of *Ime4* appears to be slightly predominant over *dMettl14* and most activities require its catalytic domain. To quantify the locomotion phenotype better, the so-called Buridan's paradigm^{35,36} was applied. We find that the activity and walking speed of *Ime4* mutant flies is reduced by twofold compared with control flies (Fig. 3c and Extended Data Fig. 8c). In addition, orientation defects were observed. All phenotypes were rescued by ubiquitous (*Tub-GAL4*) and neuronal (*elav-GAL4*), but not mesodermal (*24B10-GAL4*) expression of

Ime4 complementary DNA (Fig. 3c and Extended Data Fig. 8c). These findings demonstrate that m6A controls *Drosophila* behaviour by specifically influencing neuronal functions. To investigate potential neurological defects underlying the behavioural phenotype, we examined the neuromuscular junction (NMJ) of *Ime4*-mutant larvae. Notably, NMJ synapses grow exuberantly in the *Ime4* mutant, displaying a 1.5-fold increase in the number of boutons and a 1.3-fold increase of active zones per bouton (Extended Data Fig. 7e), indicating that *Ime4* may regulate locomotion via control of synaptic growth at the NMJ. To identify target genes involved in locomotion, adult heads of 1–2-day-old female flies were dissected and subjected to RNA-seq. In total, 1,681 genes display significant changes in expression and splicing upon *Ime4* loss of function (adjusted P value < 0.05). Notably, many of the affected genes control fly locomotion ($n = 193$; Supplementary Table 6). We next compared the list of affected genes with our MeRIP data from S2R+ cells and identified a dozen locomotion-related genes as potential direct targets of m6A (Supplementary Table 7). Hence, it is likely that more than a single gene accounts for the locomotion phenotype observed in the absence of a functional methyltransferase complex.

m6A components modulate splicing of *Sxl* transcripts

Among the top hits showing changes in alternative splicing upon *Ime4* knockout was *Sxl*, encoding a master regulator of sex determination and dosage compensation³⁷ (Fig. 4a). *Sxl* is expressed in both females and males, but the transcript in males contains an additional internal exon introducing a premature stop codon. To confirm the role of *Ime4* and potentially *dMettl14* in *Sxl* splicing, we analysed RNA extracts from the heads of both sexes by polymerase chain reaction with reverse transcription (RT-PCR). While splicing is unaffected in males, mutant females of both genotypes show inclusion of the male-specific exon and decrease of the female-specific isoform (Fig. 4b, c). We found that this decrease is less pronounced when analysing isoform levels from whole flies, possibly reflecting the specific enrichment of m6A in the brain (Extended Data Fig. 9a). Consistent with our findings, splicing of two *Sxl* target transcripts, *transformer* (*tra*) and *msl-2*, is also altered (Extended Data Fig. 9b, c). These results indicate that the methyltransferase complex facilitates splicing of *Sxl* pre-mRNA, suggesting a role in sex determination and dosage

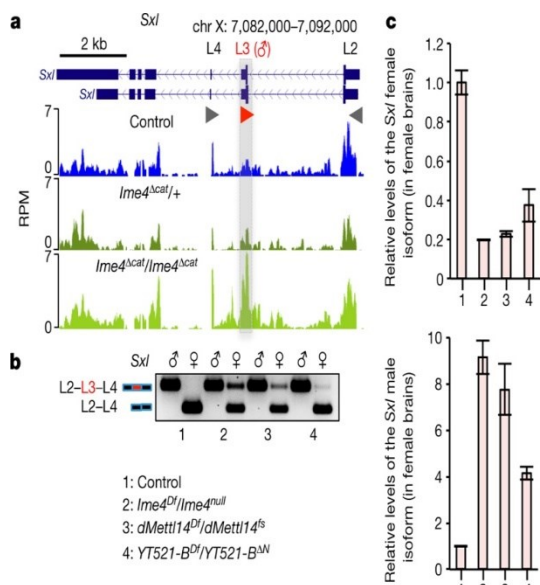


Figure 4 | YT521-B and the methyltransferase complex regulate *Sxl* splicing.

a, RNA-seq data from control *w¹¹¹⁸*, heterozygous and homozygous *Ime4* heads. Arrowheads display the primers used for quantification in **b** and **c**. chr, chromosome; L2, late exon 2; L3, late exon 3; L4, late exon 4. **b**, Spliced isoforms for *Sxl* were monitored by semi-quantitative RT-PCR using RNA extracts from male and female heads. The genotypes used are indicated below. **c**, RT-qPCR quantification of the *Sxl* female and male isoforms from RNA extracts of female heads using primers L2 and L4 (top), as well as L2 and L3 (bottom). Error bars show mean \pm s.d. of three technical replicates from three biological experiments.

compensation. To validate this hypothesis, we tested whether *Ime4* genetically interacts with *Sxl*. Transheterozygous *Ime4* females were crossed with males carrying a deficiency in the *Sxl* locus and the survival rate of the progeny was quantified for both sexes. Females lacking one wildtype copy of both *Ime4* and *Sxl* had severely reduced survival, while males were unaffected (Extended Data Fig. 9d). This effect probably arises from impairment of the dosage compensation pathway. Thus, these findings indicate that *Ime4* interacts with *Sxl* to control female survival.

Loss of *YT521-B* resembles m6A phenotypes

Given that *YT521-B* specifically recognizes m6A and influences most m6A-dependent splicing events in S2R⁺ cells, we investigated whether its deletion *in vivo* mimics the knockout of members of the methyltransferase complex. A deletion in the *YT521-B* locus that disrupts expression of both *YT521-B* isoforms was generated (Extended Data Fig. 7c). Similar to *Ime4* and *dMettl14* mutants, *YT521-B* mutant flies survive until adulthood but exhibit flight defects and poor locomotion (Fig. 3b, c and Extended Data Fig. 6e). Comparison of the transcriptome of *Ime4*-knockout with *YT521-B*-knockout female flies identified 397 splicing events regulated by *Ime4* and, among those, 243 (61% of *Ime4*-affected events) are also regulated by *YT521-B* (Extended Data Fig. 9e, f), indicating a similar overlap as from S2R⁺ cells. While alternative 5' splice site usage is not specifically enriched *in vivo*, intron retention is still overrepresented (Extended Data Fig. 9g). Notably, loss of *YT521-B* also leads to the male-specific splicing of *Sxl*, *tra* and *msl-2* and to the decrease of the female-specific *Sxl* isoform in females (Fig. 4b, c and Extended Data Fig. 9b, c). Collectively, these experiments strongly suggest that the m6A methyltransferase complex regulates adult locomotion and sex determination primarily via *YT521-B* binding to m6A.

Nito is a novel component of the m6A complex

To investigate the mechanisms of *YT521-B*-mediated splicing control, we searched for specific interacting partners using stable isotope labelling with amino acids in cell culture (SILAC)-based quantitative proteomics upon immunoprecipitation of a Myc-tagged *YT521-B* protein from S2R⁺ cells. We identified 73 factors that show more than twofold enrichment in the *YT521-B*-Myc sample (Extended Data Fig. 10a and Supplementary Table 8). Almost half ($n = 30$) are predicted mRNA-binding proteins. To investigate whether some of these mRNA-binding proteins regulate m6A-dependent splicing, we depleted them in S2R⁺ cells and assessed the effects on *fl(2)d* splicing. Notably, three proteins, *Hrb27C*, *Qkr58E-1* and *Nito*, were found to similarly control *fl(2)d* splicing (Extended Data Fig. 10b). Expanding this analysis to six additional m6A-regulated splicing events reveals that *Hrb27C* and *Qkr58E-1* regulate only a subset, while loss of *Nito* consistently leads to similar splicing defects as observed upon depletion of *YT521-B* and members of the methyltransferase complex (Fig. 5a and Extended Data Fig. 10c–f). To get further insights into the interplay between *YT521-B* and the three mRNA-binding proteins, we performed co-immunoprecipitation experiments. While *Qkr58E-1* interacts with *YT521-B* in an RNA-independent fashion, interactions with *Hrb27C* and *Nito* could not be reproduced (Extended Data Fig. 10g, h and data not shown). However, we found that *Nito* interacts with both *Fl(2)d* and *Ime4* independently of the presence of RNA (Fig. 5b). These findings indicate that *Nito* might be a component of the methyltransferase complex. Accordingly, *nito* mRNA expression correlates with m6A levels during development (Extended Data Fig. 10i) and *Nito* knockdown leads to a severe m6A decrease (Fig. 5c). This decrease is not an indirect consequence of reduced levels of methyltransferase complex components upon *Nito* knockdown (Extended Data Fig. 10j). Finally, *YT521-B* binding to mRNA depends on the presence of *Nito* (Fig. 5d). Collectively, these results demonstrate that *Nito* is a bona fide member of the m6A methyltransferase complex.

Discussion

Components of the methyltransferase complex were shown to be essential during early development of various organisms. In contrast to these studies, our analysis argues against a vital role for *Ime4* in *Drosophila* as both our deletion alleles give rise to homozygous adults without prominent lethality during development. This cannot be explained by compensation via *dMettl14*, as its knockout produces similar effects as the *Ime4* knockout. Furthermore, depleting both genes only slightly intensifies the locomotion phenotype without affecting fly survival, supporting the idea that *Ime4* and *dMettl14* act together to regulate the same target genes. Accordingly, loss of either component *in vivo* dramatically affects stability of the other (Extended Data Fig. 1i). Loss of function of either of the methyltransferases produces severe behavioural defects. All of them can be rescued by specific expression of *Ime4* cDNA in the nervous system of *Ime4* mutants, indicating neuronal functions. This is consistent with the substantial enrichment of m6A and its writer proteins in the embryonic neuroectoderm, as well as with the affected genes upon depletion in S2R⁺ cells. Our analyses further reveal notable changes in the architecture of NMJs, potentially explaining the locomotion phenotype. In the mouse, m6A is enriched in the adult brain⁵, whereas in zebrafish, *METTLL3* and *WTAP* show high expression in the

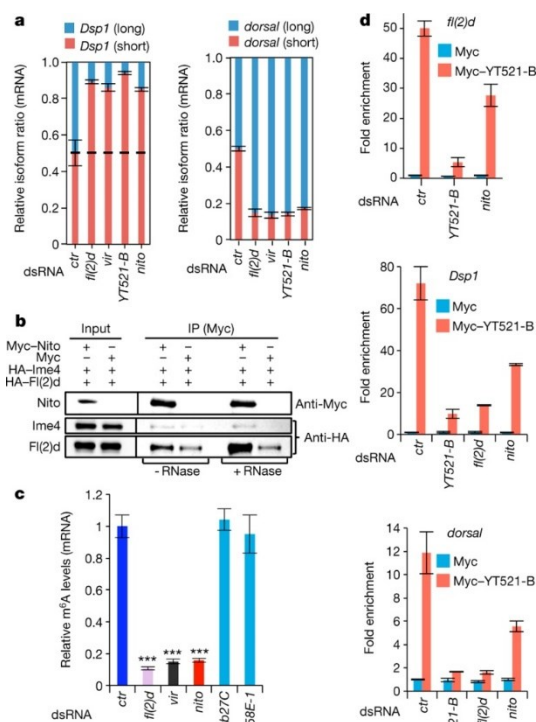


Figure 5 | Nito is a novel member of the methyltransferase complex. **a**, RT-qPCR quantification of splicing isoforms of *Dsp1* and *dorsal* transcripts upon knockdown of indicated proteins. Bars charts show mean \pm s.d. of three technical replicates from two biological experiments. *ctr.*, control. **b**, Lysates from S2R+ cells expressing the indicated proteins were immunoprecipitated (IP) using Myc beads. **c**, LC-MS/MS quantification of m6A levels in mRNA depleted for the indicated proteins. Bar chart represents the mean \pm s.d. of three technical measurements from two biological replicates. *** $P < 0.0001$ (one-way ANOVA, Tukey's post-hoc analysis). **d**, RT-qPCR quantification of fold enrichment over input of m6A-regulated transcripts in RNA immunoprecipitation with Myc-YT521-B, after depletion of indicated proteins. Error bars represent the mean \pm s.d. of three technical measurements from two biological replicates.

brain region of the developing embryo 19. Furthermore, a crucial role for the mouse m6A demethylase FTO in the regulation of the dopaminergic pathway was clearly demonstrated 22. Thus, together with previous studies, our work reveals that m6A RNA methylation is a conserved mechanism of neuronal mRNA regulation contributing to brain function. We find that *Ime4* and *dMettl14* also control the splicing of the *Sxl* transcript, encoding for the master regulator of sex determination in *Drosophila*. This is in agreement with the previously demonstrated roles of *Fl(2)d* and *Vir* in this process 38,39. However, in contrast to these mutants, mutants for *Ime4*, *dMettl14* and *YT521-B* are mostly viable, ruling out an essential role in sex determination and dosage compensation. Only when one copy of *Sxl* is removed, *Ime4* mutant females start to die. Notably, m6A effect on *Sxl* appears more important in the brain compared to the rest of the organism, possibly allowing fly survival in the absence of this modification. Our targeted screen identifies Nito as a bona fide methyltransferase complex subunit. The vertebrate homologue of Nito, RBM15, was recently shown to affect *XIST* gene silencing via recruitment of the methyltransferase complex to *XIST* RNA, indicating that its role in m6A function and dosage compensation is conserved 40. In summary, this study provides a comprehensive *in vivo* characterization of m6A biogenesis and function in *Drosophila*, demonstrating the crucial importance of the methyltransferase complex in controlling neuronal functions and fine-tuning sex determination via its nuclear reader YT521-B.

Received 24 March; accepted 21 October 2016.
Published online 30 November 2016.

Acknowledgements We would like to thank the Bloomington *Drosophila* Stock Center for fly reagents; the *Drosophila* Genomics Resource Center at Indiana University for plasmids; The Developmental Studies Hybridoma Bank and the Lehmann laboratory for antibodies; M. Soller for sharing unpublished data; members of the J.-Y.R. laboratory for helpful discussion; A. Dold and V. Morin for experimental help; the IMB Genomics; the IMB Genomics, Proteomics and Bioinformatics Core facilities for support; and Bioinformatics Core facilities for support; and R. Ketting, N. Soshnikova, R. Strauss, J. Treisman and K. Zarnack for critical reading of the manuscript. Research in the laboratory of J.-Y.R. is supported by the Marie Curie CIG 334288 and the Deutsche Forschungsgemeinschaft (DFG) SPP1935 grant RO 4681/4-1. L.S. is funded by the Rhineland-Palatinate program Gene RED. The project was also supported by a DFG grant (HE 3397/13-1, SPP1784) to M.H.

Author Contributions T.L. and J.-Y.R. conceived the idea. T.L. designed and performed the experiments. J.A. performed the YT521-B RNA immunoprecipitation experiment and M.B. generated the *YT521-B* allele. K.S. and M.H. performed the LC-MS/MS quantification of m6A levels. L.S. and B.P. carried out the Buridan analysis. C.H.H. performed NMJ staining and analysis. M.A.A.-N. performed the phylogenetic analysis. N.K. performed the computational analysis. T.L. and J.-Y.R. wrote the manuscript with input from all authors.

Author Information Reprints and permissions information is available at www.nature.com/reprints. The authors declare no competing financial interests. Readers are welcome to comment on the online version of the paper. Correspondence and requests for materials should be addressed to J.-Y.R. (j.roignant@imb-mainz.de).

METHODS

Drosophila stocks and genetics. *Drosophila melanogaster w1118*, *Canton-S* and *Oregon-R* were used as wild-type controls. Other fly stocks used were *tub-GAL4*, *elavC155-GAL4*, *how24B-GAL4*, *Df(3R)Exel6197*, *Df(2L)BSC200/Cyo*, *Df(3L)Exel6094* (Bloomington *Drosophila* Stock Center). *UAS-Ime4-HA/Cyo* flies were generated by injection of UAS *Ime4-HA* vector at Bestgene. Mutant alleles for *Ime4*, *dMettl14*, *fl(2)d* and *YT521-B* were generated using the CRISPR-Cas9 system following the previously described procedure 41. Two independent guide RNAs (gRNAs) per gene were designed using the gRNA design tool: <http://www.crisprflydesign.org/> (Supplementary Table 9). Oligonucleotides were annealed and cloned into pBfV-U6.2 vector (National Institute of Genetics, Japan). Vectors were injected into embryos of *y2 cho2 v1*; *attP40(U6.2-w-ex3-2)* flies. Positive recombinant males were further crossed with *y2 cho2 v1*; *attP40(nos-Cas9)/Cyo* females. Males carrying *nos-Cas9* and U6-gRNA transgenes were screened for the expected deletion and further crossed with the balancer strain *AptXa/CyoGFP-TM6c*. *Ime4Δcat* allele was obtained using gRNA sequences (GGACTCTTCCGCGCTACAG and GGCTCACACGGACGAATCTC). A deletion of 569 bp (607–1,175 bp in the genome region chr3R:24032157..24034257, genome assembly BDGP release 6) was produced. *Ime4null* allele was obtained using gRNA sequences (GGCCCTTTTAACGTCTTGA and GGCTCACACGGACGAATCTC) and produced a deletion of 1,291 bp (1,876–3,166 bp in the genome region chr3R:24030157..24034257). *dMettl14fs* allele was obtained using gRNA sequences (GGTCCCTCAGGAAGGTCG and GGACCAACATTAACAAGCC) and produced a 2-nucleotide frame shift at position 227 of the coding sequence, leading to a premature stop codon at amino acid position 89. *YT521-BΔN* allele was obtained using gRNA sequences (GGCATTAATTGTGTGGACAC and GGCTGTGTCGATCCTCGGTATC) and produced a deletion of 602 bp (133–734 bp in the genome region chr3L:3370451..3374170 (reverse complemented)).

Phylogenetic analysis. The phylogenetic trees were constructed with ClustalX42 from multiple sequence alignments generated with MUSCLE43 of the *Drosophila* sequences with homologues from representative species. **Cell line.** *Drosophila* S2R+ are embryonic-derived cells obtained from *Drosophila* Genomics Resource Center (DGRC; FlyBase accession FBtc0000150). The presence of Mycoplasma contamination was not tested.

Cloning. The plasmids used for immunohistochemistry and co-immunoprecipitation assays in *Drosophila* S2R+ cells were constructed by cloning the corresponding cDNA in the pPAC vector44 with N-terminal Myc tag and the Gateway-based vectors with N-terminal Flag-Myc tag (pPFMW) as well as C-terminal HA tag (pPWH) (obtained from *Drosophila* Genomics Resource Center at Indiana University).

Climbing test. Two-to-three-day-old flies were gender-separated and placed into measuring cylinders to assess their locomotion using the climbing assay reported previously45. Flies were tapped to the bottom and the number of flies that climb over the 10 cm threshold in 10 s interval were counted. Ten female f/flies were used per experiment and six independent measurements were performed.

Staging. Staging experiment was performed using *Drosophila melanogaster w1118* flies that were kept in a small fly cage at 25 °C. Flies laid embryos on big apple juice plates that were exchanged every 2 h. Before each start of collection, 1 h pre-laid embryos were discarded to remove all retained eggs and embryos from the collection. All the resultant plates with embryos of 1 h or 2 h lay were further incubated at 25 °C between 0 h and 20 h, with 2 h increments, to get all embryonic stages. For the collection of larval stages, L1 larvae (~30 larvae/stage) were transferred onto a new apple juice plate and were further incubated at 25 °C till they reached a defined age (24 to 110 h, 2 h intervals). Similarly, pupal stages were obtained by the transfer of L3 larvae (~30/stage) in a fresh vial, that were kept at 25 °C and left to develop into defined stage between 144 and 192 h in 2 h increments. One-to-three-day-old adults were collected and gender separated. Heads and ovaries from 50 females were also collected. A total of three independent samples were collected for each *Drosophila* stage as well as for heads and ovaries. Samples from the staging experiment were used for RNA extraction to analyse m6A abundance in mRNA and expression levels of different transcripts during *Drosophila* development.

RNA isolation and measurement of RNA levels. Total RNA from S2R+ cells was isolated using Trizol reagent (Invitrogen) and DNA was removed with DNase-I treatment (NEB). mRNA was purified with Oligotex mRNA Kit (Qiagen) or by using two rounds of purification with Dynabeads Oligo (dT)25 (Invitrogen). cDNA for RT-qPCR was prepared using M-MLV Reverse Transcriptase (Promega) and transcript levels were quantified using Power SYBR Green PCR Master Mix (Invitrogen) and the oligonucleotides indicated in Supplementary Table 9. For RNA isolation from fly heads, 20 female flies were collected in 1.5 ml Eppendorf tubes and flash frozen in liquid nitrogen. Heads were first removed from the body by spinning the flies on vortex and then collected via the 0.63 mm sieve at 4 °C. Fly heads were homogenized using a pestle and total RNA was isolated with Trizol reagent. DNA was removed by DNase-I treatment and RNA was further purified using RNeasy Kit (Qiagen). RNA from adult flies and dissected ovaries was prepared as described earlier by skipping the head separation step.

RT-PCR. Two-to-three-day-old flies were collected and their RNA isolated as described earlier. Following cDNA synthesis PCR was performed using the oligonucleotides described in Supplementary Table 9 to analyse *Sxl*, *tra* and *msl-2* splicing.

RNA in situ hybridization. For *in situ* hybridization *Drosophila melanogaster w1118* flies were kept at 25 °C in conical flasks with apple juice agar plates and embryos were collected every 24 h. Embryos were transferred in a sieve and dechorionated for 2 min in 50% sodium hypochloride. After 5 min wash in water, embryos were permeabilized with PBST (0.1% Tween X-100 in PBS) for 5 min. Embryos were transferred in 1:1 mixture of heptane (Sigma) and 8% formaldehyde (Sigma) and fixed for 20 min with constant shaking at room temperature. After fixation the lower organic phase was removed and 1 volume of MeOH was added to the aqueous phase containing fixed embryos. Following 5 min of extensive shaking all liquid was removed and embryos were washed 3 times with 100% MeOH. At this point embryos were stored at -20 °C or used for further analysis. For *in situ* hybridization MeOH was gradually

replaced with PBST with 10 min washes and with three final washes in PBST. Embryos were further washed for 10 min at room temperature with 50% HB4 solution (50% formamide, 5 × SSC, 50 μg/ml heparin, 0.1% Tween, 5 mg/ml torula yeast extract) diluted in PBST. Blocking was performed with HB4 solution, first for 1 h at room temperature and next for 1 h at 65 °C. *In situ* probes were prepared with DIG RNA labelling Kit (Roche) following the manufacturer's protocol. Two microlitres of the probe were diluted in 200 μl of HB4 solution, heated up to 65 °C to denature the RNA secondary structure and added to blocked embryos for further overnight incubation at 65 °C. The next day, embryos were washed 2 times for 30 min at 65 °C with formamide solution (50% formamide, 1 × SSC in PBST) and further 3 times for 20 min at room temperature with PBST. Embryos were then incubated with anti-DIG primary antibody (Roche) diluted in PBST (1:2,000) for 2 h at room temperature and later washed 5 times for 30 min with PBST. In order to develop the staining, embryos were rinsed with AP buffer (100 mM Tris pH 9.5, 50 mM MgCl₂, 100 mM NaCl, 0.1% Tween) and incubated with NBT/BCIP solution in AP buffer (1:100 dilution) until the intense staining was observed. Reaction was stopped with several 15 min PBST washes. Prior to mounting, embryos were incubated in 20% glycerol and later visualized on Leica M205-FA stereomicroscope.

YT521-B RNA immunoprecipitation. S2R+ cells were depleted for the indicated proteins with two treatments of double-stranded RNA (dsRNA). Four days after treatment Myc-tagged YT521-B was transfected along with the control Myc construct. Seventy-two hours after transfection, cells were fixed with 1% formaldehyde at room temperature for 10 min and harvested as described previously46. Extracted nuclei were subjected to 13 cycles of sonication on a bioruptor (Diagnode), with 30 s “ON”/“OFF” at high settings. Nuclear extracts were incubated overnight with 4 μg of anti-Myc 9E10 antibody (Enzo Life Sciences). Immunoprecipitation was performed as described previously 46 except that samples were DNase-treated (NEB) instead of RNase-treated and subjected to proteinase K treatment for reversal of crosslinks, 1 h at 65 °C. RNase inhibitors (Murine RNase Inhibitor, NEB) were used in all steps of the protocol at a concentration of 40 U/ml.

Generation of antibodies. Antibodies against Ime4 and dMettl14 were generated at Eurogentec. For anti-Ime4 sera guinea pig was immunized with a 14 amino acid-long peptide (163–177 amino acids (AA)); for anti-dMettl14 sera rabbit was immunized with a 14 amino acid-long peptide (240–254 AA). Both serums were affinity-purified using peptide antigens crosslinked to sepharose columns.

Immunostaining. For ovary immunostaining, ovaries from 3–5-day-old females were dissected in ice-cold PBS and fixed in 5% formaldehyde for 20 min at room temperature. After a 10 min wash in PBT1% (1% Triton X-100 in PBS), ovaries were further incubated in PBT1% for 1 h at room temperature. Ovaries were then blocked with PBTB (0.2% Triton, 1% BSA in PBS) for 1 h at room temperature and later incubated with the primary antibodies in PBTB overnight at 4 °C: rabbit anti-Vasa, 1:250 (gift from Lehmann laboratory), mouse anti-ORB 1:30 (#6H4 DSHB). The following day, ovaries were washed 2 times for 30 min in PBTB and blocked with PBTB containing 5% donkey serum (Abcam) for 1 h at room temperature. Secondary antibody was added later in PBTB with donkey serum and ovaries were incubated for 2 h at room temperature. Five washing steps of 30 min were performed with 0.2% Triton in PBT and ovaries were mounted onto slides in Vectashield (Vector Labs). For NMJ staining, third instar larvae were dissected in calcium free HL-3 saline and fixed in 4% paraformaldehyde in PBT (PBS + 0.05% Triton X-100). Larvae were then washed briefly in 0.05% PBT for 30 min and incubated overnight at 4 °C with the following primary antibodies: rabbit anti-synaptotagmin, 1:2,000 (ref. 47); mouse anti-DLG, 1:100 (#4F3, DSHB); TRITC-conjugated anti-HRP, 1:200 (Jackson ImmunoResearch). Secondary antibodies conjugated to Alexa-488 (goat anti-rabbit, Jackson ImmunoResearch) and Alexa-647 (goat anti-mouse, Jackson ImmunoResearch) were used at a concentration of 1:200 and incubated at room temperature for 2 h. Larvae were finally mounted in Vectashield. For staining of *Drosophila* S2R+ cells, cells were transferred to the poly-lysine pre-treated 8-well chambers (Ibidi) at the density of 2 × 10⁵ cells/well. After 30 min, cells were washed with 1 × DPBS (Gibco), fixed with 4%

formaldehyde for 10 min and permeabilized with PBST (0.2% Triton X-100 in PBS) for 15 min. Cells were incubated with mouse anti-Myc (1:2000; #9E10, Enzo) in PBST supplemented with 10% of donkey serum at 4 °C, overnight. Cells were washed 3 × for 15 min in PBST and then incubated with secondary antibody and 1 × DAPI solution in PBST supplemented with 10% of donkey serum for 2 h at 4 °C. After three 15 min washes in PBST, cells were imaged with Leica SP5 confocal microscope using ×63 oil immersion objective.

NMJ analysis. Images from muscles 6–7 (segment A3) were acquired with a Leica Confocal Microscope SP5. Serial optical sections at 512 × 512 or 1,024 × 1,024 pixels were obtained at 0.38 μm with the ×63 objective. Different genotypes were processed simultaneously and imaged using identical confocal acquisition parameters for comparison. Bouton number was quantified in larval abdominal segment A3, muscles 6 and 7, of wandering third instar larvae. ImageJ software (version 1.49) was used to measure the area of the synaptotagmin-positive area.

Cell culture, RNA interference and transfection. *Drosophila* S2R+ cells were grown in Schneider's medium (Gibco) supplemented with 10% FBS (Sigma) and 1% penicillin-streptomycin (Sigma). For RNA interference (RNAi) experiments, PCR templates for the dsRNA were prepared using T7 megascript Kit (NEB). dsRNA against bacterial β-galactosidase gene (*lacZ*) was used as a control for all RNA interference (RNAi) experiments. S2R+ cells were seeded at the density of 106 cells/ml in serum-free medium and 7.5 μg of dsRNA was added to 106 cells. After 6 h of cell starvation, serum supplemented medium was added to the cells. dsRNA treatment was repeated after 48 and 96 h and cells were collected 24 h after the last treatment. Effectene (Qiagen) was used to transfect vector constructs in all overexpression experiments following the manufacturer's protocol.

Co-immunoprecipitation assay and western blot analysis. For the co-immunoprecipitation assay, different combinations of vectors with indicated tags were co-transfected in S2R+ cells seeded in a 10 cm cell culture dish as described earlier. Forty-eight hours after transfection cells were collected, washed with DPBS and pelleted by 10 min centrifugation at 400g. The cell pellet was lysed in 1 ml of lysis buffer (50 mM Tris-HCl, pH 7.4, 150 mM NaCl, 0.05% NP-40) supplemented with protease inhibitors (1 μg/ml leupeptin, 1 μg/ml pepstatin, 1 μg/ml aprotinin and 1 mM PMSF) and rotated head-over-tail for 30 min at 4 °C. Nuclei were collected by 10 min centrifugation at 1,000g at 4 °C re-suspended in 300 μl of lysis buffer and sonicated with 5 cycles of 30 s ON, 30 s OFF low power setting. Cytoplasmic and nuclear fractions were joined and centrifuged at 18,000g for 10 min at 4 °C to remove the remaining cell debris. Protein concentrations were determined using Bradford reagent (BioRad). For immunoprecipitation, 2 mg of proteins were incubated with 7 μl of anti-Myc antibody coupled to magnetic beads (Cell Signaling) in lysis buffer and rotated head-over-tail overnight at 4 °C. The beads were washed 3 times for 15 min with lysis buffer and immunoprecipitated proteins were eluted by incubation in 1 × NuPAGE LDS buffer (ThermoFischer) at 70 °C for 10 min. Eluted immunoprecipitated proteins were removed from the beads and DTT was added to 10% final volume. Immunoprecipitated proteins and input samples were analysed by western blot after incubation at 70 °C for additional 10 min. For western blot analysis, proteins were separated on 7% SDS-PAGE gel and transferred on Nitrocellulose membrane (BioRad). After blocking with 5% milk in PBST (0.05% Tween in PBS) for 1 h at room temperature, the membrane was incubated with primary antibody in blocking solution overnight at 4 °C. Primary antibodies used were: mouse anti-Myc 1:2,000 (#9E10, Enzo); mouse anti-HA 1:1,000 (#16B12, COVANCE); mouse anti-Tubulin 1:2,000 (#903401, Biolegend); guinea pig anti-Ime4 1:500 and rabbit anti-dMett14 1:250. The membrane was washed 3 times in PBST for 15 min and incubated 1 h at room temperature with secondary antibody in blocking solution. Protein bands were detected using SuperSignal West Pico Chemiluminescent Substrate (Thermo Scientific).

In vitro pull-down assay. S2R+ cells were transfected with either Myc-YT521-B of Myc-GFP constructs. Forty-eight hours after transfection cells were collected, washed with PBS and pelleted by centrifugation at 400g for 10 min. The cell pellet was lysed and

processed in 1 ml of pull-down lysis buffer (10 mM Tris-HCl, pH 7.4, 150 mM NaCl, 2 mM EDTA, 0.5% Triton-X100, 0.5 mM DTT). For individual pull-down, 1.5 mg of protein were incubated with either 3 μg of biotinylated RNA probe of *bPRL* containing m6A or not, or without probe, as a control in 0.5 ml of pull-down buffer supplemented with protease inhibitor mix and 10 U of Murine RNase Inhibitor (NEB) and incubated for 2 h at 4 °C. Five microliters of Streptavidin beads (M-280, Invitrogen) were added and pull-down samples were incubated for an additional 1 h at 4 °C. After 3 washes of 15 min with pulldown buffer, beads were re-suspended in 400 μl of pull-down buffer. One-hundred microlitres was used for RNA isolation and dot blot analysis of recovered RNA probes with anti Strep-HRP. The remaining 300 μl of the beads was collected on the magnetic rack and immunoprecipitated proteins were eluted by incubation in 1 × SDS buffer (ThermoFischer) at 95 °C for 10 min. Immunoprecipitated proteins as well as input samples were analysed by western blot.

Dot blot assays. Serial dilutions of biotinylated RNA probe of *bPRL* containing m6A or A were spotted and crosslinked on nitrocellulose membrane (Biorad) with ultraviolet 245 light (3 × 150 mJ/cm²). RNA loading was validated with methylene blue staining. Membranes were blocked with 5% milk in PBST for 1 h at room temperature and washed in PBST before incubation with the proteins of interest. S2R+ cells were transfected with either Myc-YT521-B or Myc-GFP constructs. Forty-eight hours after transfection cells were collected, washed with PBS and pelleted by centrifugation at 400g for 10 min. The cell pellet was lysed in 1 ml of lysis buffer (10 mM Tris-HCl, pH 7.4, 150 mM NaCl, 0.5% NP-40). Three milligrams of the protein lysate were mixed with 2% BSA in lysis buffer and incubated with the membrane overnight at 4 °C. For control dot-blot rabbit anti-m6A antibody (Synaptic Systems) was used. The next day membranes were washed 3 times in lysis buffer. Membranes with bound proteins were further crosslinked with ultraviolet 245 light (3 × 150 mJ/cm²) and analysed using anti-Myc antibody.

SILAC experiment and LC-MS/MS analysis. For SILAC experiments, S2R+ cells were grown in Schneider medium (Dundee Cell) supplemented with either heavy (Arg8, Lys8) or light amino acids (Arg0, Lys0) (Sigma). For the forward experiment, Myc-YT521-B was transfected in heavy-labelled cells and Myc-alone in light-labelled cells. The reverse experiment was performed vice versa. The co-immunoprecipitation experiment was done as described earlier. Before elution, beads of the heavy and light lysates were combined in 1:1 ratio and eluted with 1 × NuPAGE LDS buffer that was subject to MS analysis as described previously 48. Raw files were processed with MaxQuant (version 1.5.2.8) and searched against the Uniprot database of annotated *Drosophila* proteins (*Drosophila melanogaster*: 41,850 entries, downloaded 8 January 2015).

LC-MS/MS analysis of m6A levels. mRNA samples from S2R+ cells depleted for the indicated proteins or from *Drosophila* staging experiments were prepared following the aforementioned procedure. Three-hundred nanograms of purified mRNA was further digested using 0.3 U Nuclease P1 from *Penicillium citrinum* (Sigma-Aldrich, Steinheim, Germany) and 0.1 U Snake venom phosphodiesterase from *Crotalus adamanteus* (Worthington, Lakewood, USA). RNA and enzymes were incubated in 25 mM ammonium acetate, pH 5, supplemented with 20 μM zinc chloride for 2 h at 37 °C. Remaining phosphates were removed by 1 U FastAP (Thermo Scientific, St Leon-Roth, Germany) in a 1 h incubation at 37 °C in the manufacturer supplied buffer. The resulting nucleoside mix was then spiked with 13C stable isotope labelled nucleoside mix from *Escherichia coli* RNA as an internal standard (SIL-IS) to a final concentration of 6 ng/μl for the sample RNA and 10 ng/μl for the SIL-IS. For analysis, 10 μl of the before mentioned mixture were injected into the LC-MS/MS machine. Generation of technical triplicates was obligatory. All mRNA samples were analysed in biological triplicates, except for the *ctr*, *nito*, *vir*, *hrb27C* and *qkr58E-1* knockdown samples, which were measured as biological duplicates. LC separation was performed on an Agilent 1200 series instrument, using 5 mM ammonium acetate buffer as solvent A and acetonitrile as buffer B. Each run started with 100% buffer A, which was decreased to 92% within 10 min. Solvent A was further reduced to 60% within another 10 min. Until minute 23 of the run, solvent A

was increased to 100% again and kept at 100% for 7 min to re-equilibrate the column (Synergi Fusion, 4 μ M particle size, 80 Å pore size, 250 \times 2.0 mm, Phenomenex, Aschaffenburg, Germany). The ultraviolet signal at 254 nm was recorded via a DAD detector to monitor the main nucleosides. MS/MS was then conducted on the coupled Agilent 6460 Triple Quadrupole (QQQ) mass spectrometer equipped with an Agilent JetStream ESI source which was set to the following parameters: gas temperature, 350 °C; gas flow, 8 l/min; nebulizer pressure, 50 psi; sheath gas temperature, 350 °C; sheath gas flow, 12 l/min; and capillary voltage, 3,000 V. To analyse the mass transitions of the unlabelled m⁶A and all 13C m⁶A simultaneously, we used the dynamic multiple reaction monitoring mode. Mass transitions, retention times and QQQ parameters are listed in Supplementary Table 10. The quantification was conducted as described previously⁴⁹. Briefly, the amount of adenosine was evaluated by the external linear calibration of the area under the curve (AUC) of the ultraviolet signal. The amount of modification was calculated by linear calibration of the SIL-IS in relation to m⁶A nucleoside. The R² of both calibrations was at least 0.998 (see Extended Data Fig. 1a, b). Knowing both amounts, the percentage of m⁶A/A could be determined.

MeRIP. MeRIP was performed using the previously described protocol⁵⁰ with the following modifications. Eight micrograms of purified mRNA from *Drosophila* S2R+ cells was incubated with 5 μ g of anti-m⁶A antibody (Synaptic Systems) in MeRIP buffer (150 mM NaCl, 10 mM Tris-HCl pH 7.4, 0.1% NP-40) supplemented with 5 U/ml of Murine RNase inhibitor (NEB) for 2 h at 4 °C. In control MeRIP experiment, no antibody was used in the reaction mixture. Five microlitres of A+G magnetic beads were added to all MeRIP samples for 1 h at 4 °C. On bead digestion with RNase T1 (Thermo Fisher) at final concentration 0.1 U/ml was performed for 15 min at room temperature. Beads with captured RNA fragments were then immediately washed 3 times with 500 μ l of ice-cold MeRIP buffer and further eluted with 100 μ l of elution buffer (0.02 M DTT, 150 mM NaCl, 50 mM Tris-HCl pH 7.4, 1 mM EDTA, 0.1% SDS, 5 U/ml Proteinase K) at 42 °C for 5 min. Elution step was repeated 4 times and 500 μ l of acidic phenol/chloroform pH 4.5 (Ambion) was added to 400 μ l of the combined eluate per sample to extract captured RNA fragments. Samples were mixed and transferred to Phase Lock Gel Heavy tubes (SPrime) and centrifuged for 5 min at 12,000g. Aqueous phase was precipitated overnight, –80 °C. On the following day, samples were centrifuged, washed twice with 80% EtOH and re-suspended in 10 μ l of RNase-free H₂O (Ambion). Recovered RNA was analysed on RNA Pico Chip (Agilent) and concentrations were determined with RNA HS Qubit reagents. Since no RNA was recovered in the MeRIP control samples, libraries were prepared with 30 ng of duplicate MeRIPs and duplicate input mRNA samples. MeRIP-qPCR was performed on the fraction of eluted immunoprecipitated RNA and an equal amount of input mRNA. cDNA for RT-qPCR was prepared using M-MLV Reverse Transcriptase (Promega) and transcript levels were quantified using Power SYBR Green PCR Master Mix (Invitrogen) using oligonucleotides indicated in Supplementary Table 9.

Lifespan assay. For lifespan assay, 2–3-day-old flies were gender-separated and kept at 25 °C in flasks with apple juice medium (<20 flies/tube). Number of flies tested: females (37, *Ime4Acat/Ime4Acat*; 57, *Tubulin-GAL4/UAS-Ime4*); males (33, *Ime4Acat/Ime4Acat*; 41, *Tubulin-GAL4/UAS-Ime4*). To monitor their survival rate over time, flies were counted and transferred into a new tube every 2 days.

Buridan paradigm. Behavioural tests were performed on 2–5-day-old females with *Canton-S* as wild-type control. Wings were cut under cold anaesthesia to one-third of their length on the evening before the experiment. Walking and orientation behaviour was analysed using Buridan's paradigm as described³⁶. Dark vertical stripes of 12° horizontal viewing angle were shown on opposite sides of an 85-mm diameter platform surrounded by water. The following parameters were extracted by a video-tracking system (5 Hz sampling rate): total fraction of time spent walking (activity), mean walking speed taken from all transitions of a fly between the visual objects, and number of transitions between the two stripes. The visual orientation capacity (mean angular deviation) of the flies was assessed by comparing all 0.2-s path increments per fly (4,500 values in 15 min) to the respective direct path towards the angular-wise closer of the two dark stripes. All statistical groups were tested

for normal distribution with the Shapiro–Wilk test. Multiple comparisons were performed using the Kruskal–Wallis ANOVA or oneway ANOVA with a post-hoc Bonferroni correction. $n = 15$ for all genotypes. The sample size was chosen based on a previous study⁵¹ and its power was validated with result analysis. Blinding was applied during the experiment.

RNA-seq. For samples from S2R+ cells and for full fly RNA samples, Illumina TruSeq Sequencing Kit (Illumina) was used. For *Drosophila* head samples, NEBNext Ultra Directional RNA Kit (NEB) was used. Libraries were prepared following the manufacturer's protocol and sequenced on Illumina HiSeq 2500. The read-length was 71 bp paired end. For MeRIP, NEBNext Ultra Directional Kit was used omitting the RNA fragmentation step for recovered MeRIP samples and following the manufacturer's protocol for input samples. Libraries were sequenced on an Illumina MiSeq as 68 bp single read in one pool on two flow cells.

Computational analysis. The RNA-seq data was mapped against the *Drosophila* genome assembly BDGP6 (Ensembl release 79) using STAR52 (version 2.4.0). After mapping, the bam files were filtered for secondary alignments using samtools (version 1.2). Reads on genes were counted using htseq-count (version 0.6.1p1). After read counting, differential expression analysis was done between conditions using DESeq2 (version 1.6.3) and filtered for a false discovery rate (FDR) < 5%. Differential splicing analysis was performed using rMATS (3.0.9) and filtered for FDR < 10%. The data from fly heads were treated as above but cleaned for mitochondrial and rRNA reads after mapping before further processing. The sample *Ime4hom_3* was excluded as an outlier from differential expression analysis. The MeRIP-seq data were processed following the same protocol as the RNA samples for mapping and filtering of the mapped reads. After mapping, peaks were called using MACS (version 1.4.1)⁵³. The genome size used for the MACS was adjusted to reflect the mappable transcriptome size based on Ensembl-annotated genes (Ensembl release 79). After peak calling, peaks were split into subpeaks using PeakSplitter (version 1.0, <http://www.ebi.ac.uk/research/bertone/software>). Consensus peaks were obtained by intersecting subpeaks of both replicates (using BEDTools, version 2.25.0). For each consensus peak, the coverage was calculated as counts per million (CPM) for each of the samples and averaged for input and MeRIP samples. Fold changes for MeRIP over input were calculated based on these. Peaks were filtered for a minimal fold change of 1.3 and a minimal coverage of 3 CPM in at least one of the samples. Peaks were annotated using the ChIPseeker and the GenomicFeatures package (based on R/Bioconductor) 54.

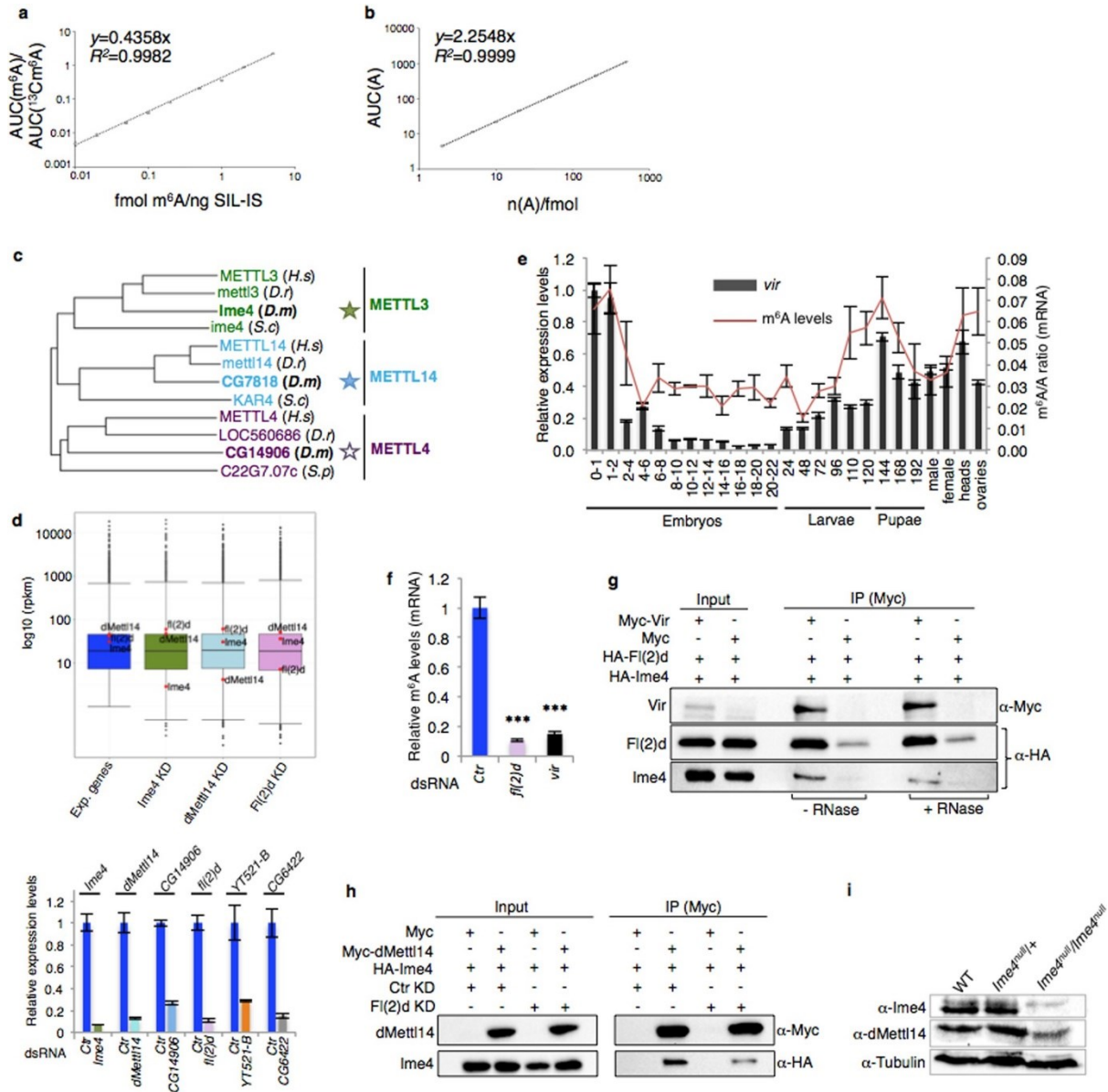
Statistics. In the Buridan paradigm, normality was tested for every dataset; different tests were used depending on the outcome. For not normally distributed data, Kruskal–Wallis test and Wilcoxon test were used. For normally distributed data, Bartlett test was applied to check for homogeneity of variances. ANOVA and *t*-test were used. Bonferroni corrections were applied. For climbing assays, normality was tested for every dataset. Homogeneity of variances were analysed with Levene's test. One-way ANOVA test with Tukey's post-hoc test was performed for multiple comparisons and Student's *t*-test when two data sets were compared. For m⁶A level measurement, normality was tested for every dataset. Homogeneity of variances were analysed with Levene's test. One-way ANOVA test with Tukey's post-hoc test was performed for multiple comparisons.

Randomization. Randomization was used for selection of female flies of chosen genotype for climbing tests, Buridan paradigm and RNA sequencing experiments. Randomized complete block design was applied to ensure the equal number of flies per test group. Complete randomization was applied for selection of larvae or flies of the chosen genotype for lifespan assay and NMJ staining experiment.

Data availability statement. The data that support the findings of this study have been deposited in the NCBI Gene Expression Omnibus (GEO) under accession number GSE79297. All other relevant data are available from the corresponding author.

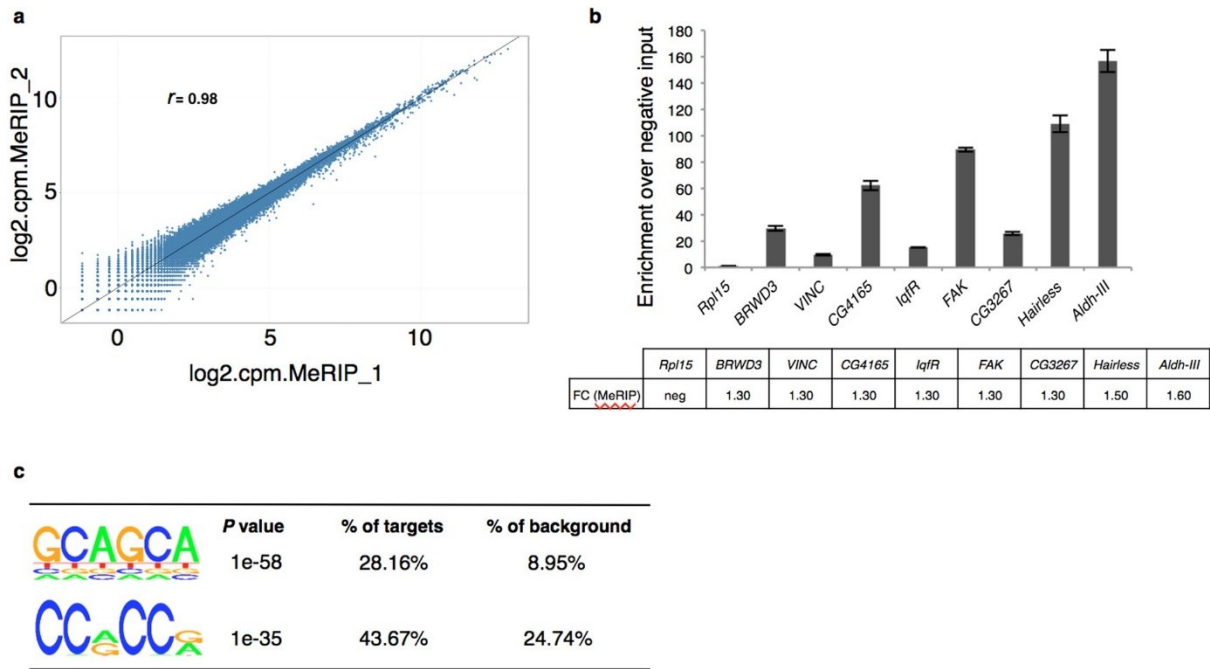
1. Motorin, Y. & Helm, M. RNA nucleotide methylation. *Wiley Interdiscip. Rev. RNA* 2, 611–631 (2011).
2. Fu, Y., Dominissini, D., Rechavi, G. & He, C. Gene expression regulation mediated through reversible m⁶A RNA methylation. *Nature Rev. Genet.* 15, 293–306 (2014).

3. Meyer, K. D. & Jaffrey, S. R. The dynamic epitranscriptome: N⁶-methyladenosine and gene expression control. *Nature Rev. Mol. Cell Biol.* **15**, 313–326 (2014).
4. Dominissini, D. *et al.* Topology of the human and mouse m⁶A RNA methylomes revealed by m⁶A-seq. *Nature* **485**, 201–206 (2012).
5. Meyer, K. D. *et al.* Comprehensive analysis of mRNA methylation reveals enrichment in 3' UTRs and near stop codons. *Cell* **149**, 1635–1646 (2012).
6. Schwartz, S. *et al.* High-resolution mapping reveals a conserved, widespread, dynamic mRNA methylation program in yeast meiosis. *Cell* **155**, 1409–1421 (2013).
7. Li, Y. *et al.* Transcriptome-wide N⁶-methyladenosine profiling of rice callus and leaf reveals the presence of tissue-specific competitors involved in selective mRNA modification. *RNA Biol.* **11**, 1180–1188 (2014).
8. Lin, S. & Gregory, R. I. Methyltransferases modulate RNA stability in embryonic stem cells. *Nature Cell Biol.* **16**, 129–131 (2014).
9. Schwartz, S. *et al.* Perturbation of m⁶A writers reveals two distinct classes of mRNA methylation at internal and 5' sites. *Cell Reports* **8**, 284–296 (2014).
10. Wang, X. *et al.* N⁶-methyladenosine-dependent regulation of messenger RNA stability. *Nature* **505**, 117–120 (2014).
11. Wang, Y. *et al.* N⁶-methyladenosine modification destabilizes developmental regulators in embryonic stem cells. *Nature Cell Biol.* **16**, 191–198 (2014).
12. Alarcón, C. R. *et al.* HNRNPA2B1 is a mediator of m⁶A-dependent nuclear RNA processing events. *Cell* **162**, 1299–1308 (2015).
13. Liu, N. *et al.* N⁶-methyladenosine-dependent RNA structural switches regulate RNA–protein interactions. *Nature* **518**, 560–564 (2015).
14. Meyer, K. D. *et al.* 5' UTR m⁶A promotes Cap-independent translation. *Cell* **163**, 999–1010 (2015).
15. Wang, X. *et al.* N⁶-methyladenosine modulates messenger RNA translation efficiency. *Cell* **161**, 1388–1399 (2015).
16. Zhou, J. *et al.* Dynamic m⁶A mRNA methylation directs translational control of heat shock response. *Nature* **526**, 591–594 (2015).
17. Wang, X. & He, C. Reading RNA methylation codes through methyl-specific binding proteins. *RNA Biol.* **11**, 669–672 (2014).
18. Liu, J. *et al.* A METTL3–METTL14 complex mediates mammalian nuclear RNA N⁶-adenosine methylation. *Nature Chem. Biol.* **10**, 93–95 (2014).
19. Ping, X. L. *et al.* Mammalian WTAP is a regulatory subunit of the RNA N⁶-methyladenosine methyltransferase. *Cell Res.* **24**, 177–189 (2014).
20. Jia, G. *et al.* N⁶-methyladenosine in nuclear RNA is a major substrate of the obesity-associated FTO. *Nature Chem. Biol.* **7**, 885–887 (2011).
21. Fu, Y. *et al.* FTO-mediated formation of N⁶-hydroxymethyladenosine and N⁶-formyladenosine in mammalian RNA. *Nature Commun.* **4**, 1798 (2013).
22. Hess, M. E. *et al.* The fat mass and obesity associated gene (*Fto*) regulates activity of the dopaminergic midbrain circuitry. *Nature Neurosci.* **16**, 1042–1048 (2013).
23. Zheng, G. *et al.* ALKBH5 is a mammalian RNA demethylase that impacts RNA metabolism and mouse fertility. *Mol. Cell* **49**, 18–29 (2013).
24. Batista, P. J. *et al.* m⁶A RNA modification controls cell fate transition in mammalian embryonic stem cells. *Cell Stem Cell* **15**, 707–719 (2014).
25. Geula, S. *et al.* m⁶A mRNA methylation facilitates resolution of naïve pluripotency toward differentiation. *Science* **347**, 1002–1006 (2015).
26. Hongay, C. F. & Orr-Weaver, T. L. *Drosophila* Inducer of Meiosis 4 (*IME4*) is required for Notch signaling during oogenesis. *Proc. Natl Acad. Sci. USA* **108**, 14855–14860 (2011).
27. Zhong, S. *et al.* MTA is an *Arabidopsis* messenger RNA adenosine methylase and interacts with a homolog of a sex-specific splicing factor. *Plant Cell* **20**, 1278–1288 (2008).
28. Bodi, Z. *et al.* Adenosine methylation in *Arabidopsis* mRNA is associated with the 3' end and reduced levels cause developmental defects. *Front. Plant Sci.* **3**, 48 (2012).
29. Shah, J. C. & Clancy, M. J. *IME4*, a gene that mediates MAT and nutritional control of meiosis in *Saccharomyces cerevisiae*. *Mol. Cell Biol.* **12**, 1078–1086 (1992).
30. Clancy, M. J., Shambaugh, M. E., Timpte, C. S. & Bokar, J. A. Induction of sporulation in *Saccharomyces cerevisiae* leads to the formation of N⁶-methyladenosine in mRNA: a potential mechanism for the activity of the *IME4* gene. *Nucleic Acids Res.* **30**, 4509–4518 (2002).
31. Agarwala, S. D., Blitzblau, H. G., Hochwagen, A. & Fink, G. R. RNA methylation by the MIS complex regulates a cell fate decision in yeast. *PLoS Genet.* **8**, e1002732 (2012).
32. Wang, P., Doxtader, K. A. & Nam, Y. Structural basis for cooperative function of Mettl3 and Mettl14 methyltransferases. *Mol. Cell* **63**, 306–317 (2016).
33. Wang, X. *et al.* Structural basis of N⁶-adenosine methylation by the METTL3–METTL14 complex. *Nature* **534**, 575–578 (2016).
34. Gabel, H. W. *et al.* Disruption of DNA-methylation-dependent long gene repression in Rett syndrome. *Nature* **522**, 89–93 (2015).
35. Götz, K. G. Visual guidance in *Drosophila*. *Basic Life Sci.* **16**, 391–407 (1980).
36. Strauss, R., Hanesch, U., Kinkelin, M., Wolf, R. & Heisenberg, M. No-bridge of *Drosophila melanogaster*: portrait of a structural brain mutant of the central complex. *J. Neurogenet.* **8**, 125–155 (1992).
37. Clough, E. & Oliver, B. Genomics of sex determination in *Drosophila*. *Brief. Funct. Genomics* **11**, 387–394 (2012).
38. Granadino, B., Campuzano, S. & Sánchez, L. The *Drosophila melanogaster* *fl(2)d* gene is needed for the female-specific splicing of Sex-lethal RNA. *EMBO J.* **9**, 2597–2602 (1990).
39. Hilfiker, A., Amrein, H., Dübendorfer, A., Schneiter, R. & Nöthiger, R. The gene *virilizer* is required for female-specific splicing controlled by *Sxl*, the master gene for sexual development in *Drosophila*. *Development* **121**, 4017–4026 (1995).
40. Patil, D. P. *et al.* m⁶A RNA methylation promotes XIST-mediated transcriptional repression. *Nature* **537**, 369–373 (2016).
41. Kondo, S. & Ueda, R. Highly improved gene targeting by germline-specific Cas9 expression in *Drosophila*. *Genetics* **195**, 715–721 (2013).
42. Larkin, M. A. *et al.* Clustal W and Clustal X version 2.0. *Bioinformatics* **23**, 2947–2948 (2007).
43. Edgar, R. C. MUSCLE: multiple sequence alignment with high accuracy and high throughput. *Nucleic Acids Res.* **32**, 1792–1797 (2004).
44. Astigarraga, S., Hofmeyer, K., Farajian, R. & Treisman, J. E. Three *Drosophila* liprins interact to control synapse formation. *J. Neurosci.* **30**, 15358–15368 (2010).
45. Bahadorani, S. & Hilliker, A. J. Cocoa confers life span extension in *Drosophila melanogaster*. *Nutr. Res.* **28**, 377–382 (2008).
46. Oktaba, K. *et al.* Dynamic regulation by polycomb group protein complexes controls pattern formation and the cell cycle in *Drosophila*. *Dev. Cell* **15**, 877–889 (2008).
47. Littleton, J. T., Bellen, H. J. & Perin, M. S. Expression of synaptotagmin in *Drosophila* reveals transport and localization of synaptic vesicles to the synapse. *Development* **118**, 1077–1088 (1993).
48. Bluhm, A., Casas-Vila, N., Scheibe, M. & Butter, F. Reader interactome of epigenetic histone marks in birds. *Proteomics* **16**, 427–436 (2016).
49. Kellner, S. *et al.* Absolute and relative quantification of RNA modifications via biosynthetic isotopomers. *Nucleic Acids Res.* **42**, e142 (2014).
50. Deng, X. *et al.* Widespread occurrence of N⁶-methyladenosine in bacterial mRNA. *Nucleic Acids Res.* **43**, 6557–6567 (2015).
51. Poeck, B., Triphan, T., Neuser, K. & Strauss, R. Locomotor control by the central ccomplex in *Drosophila*—An analysis of the *tay bridge* mutant. *Dev. Neurobiol.* **68**, 1046–1058 (2008). 10.1002/dneu.20643
52. Dobin, A. *et al.* STAR: ultrafast universal RNA-seq aligner. *Bioinformatics* **29**, 15–21 (2013).
53. Zhang, Y. *et al.* Model-based analysis of ChIP-Seq (MACS). *Genome Biol.* **9**, R137 (2008).
54. Yu, G., Wang, L. G. & He, Q. Y. ChIPseeker: an R/Bioconductor package for ChIP peak annotation, comparison and visualization. *Bioinformatics* **31**, 2382–2383 (2015).



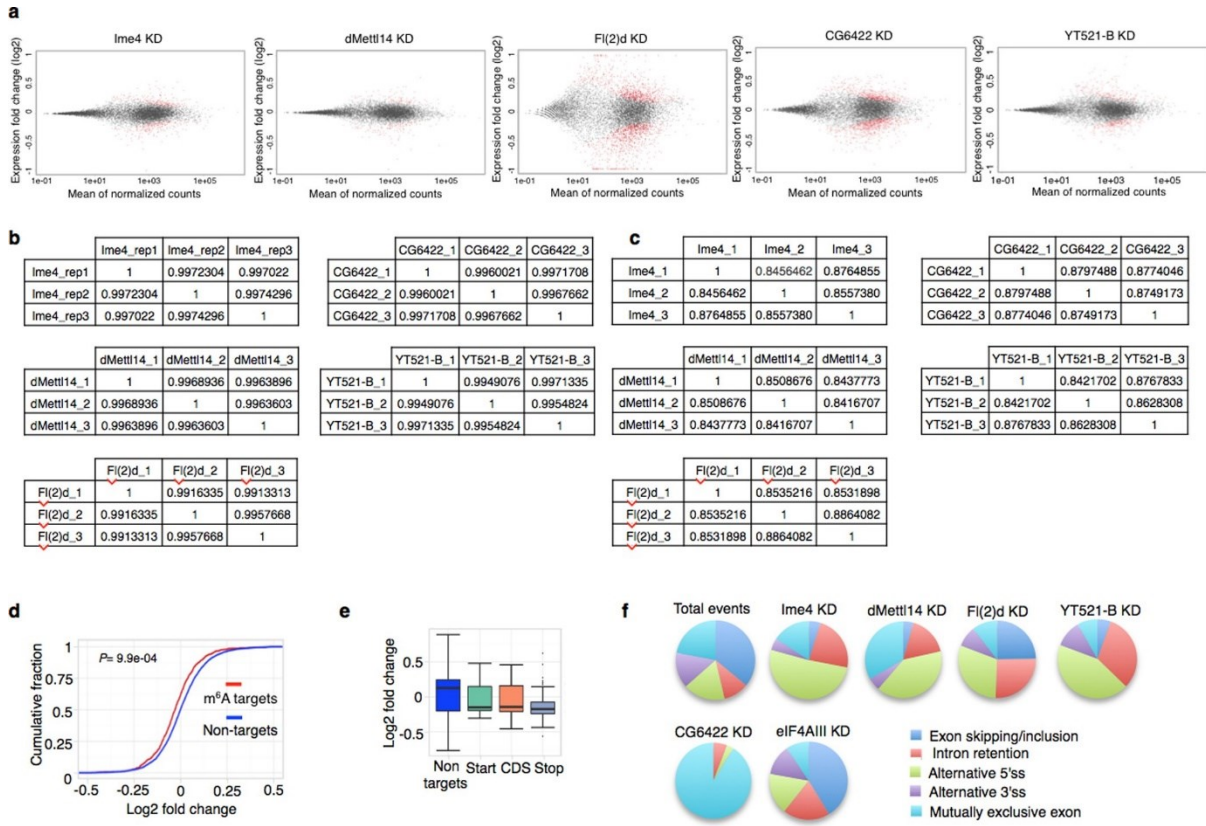
Extended Data Figure 1 | Characterization of the *Drosophila* m⁶A methyltransferase complex.

a, Calibration curve for m⁶A nucleoside versus stable isotope labelled internal standard from digested *Escherichia coli* RNA. Areas under the curve (AUCs) are taken from MS/MS chromatograms. Amounts of 1–500 fmol m⁶A were evaluated. **b**, Calibration curve for external calibration of adenosine (A) nucleoside from 2–500 pmol. AUCs are extracted from chromatograms generated by ultraviolet detection. **c**, Phylogenetic analysis of METTL3 homologues. Each *Drosophila* (*D.m*) sequence clusters with the corresponding human (*H.s*), *Danio rerio* (*D.r*) and fungal orthologue. Fungi probably lost ancestral versions of individual methyltransferases with these families, with *Schizosaccharomyces pombe* (*S.p*) keeping only one orthologue (METTL4) and *Saccharomyces cerevisiae* (*S.c*) keeping the two other (METTL3 and METTL14). METTL3, METTL14 and METTL4 orthologues are indicated in green, blue and purple, respectively. See Methods for details about the tree construction. **d**, Box plots of average expression (rpkm) for all genes expressed by at least 1 rpkm in different conditions. Red dots indicate the position of m⁶A components in comparison to other expressed genes. Bottom, relative expression of target genes upon different knockdowns (KDs). The mean \pm s.d. of three technical measurements from three biological replicates is shown. **e**, Relative *vir* mRNA expression and levels of m⁶A in mRNA during *Drosophila* development. Number of hours post-fertilization for different embryo, larval and pupal stages is indicated on the x axis. *vir* expression correlates with m⁶A levels. The mean \pm s.d. of three technical measurements from three biological replicates is shown. **f**, LC-MS/MS quantification of m⁶A levels in either control samples or in mRNA extracts depleted for the indicated proteins. *Vir* depletion affects m⁶A levels to the same extent as FI(2)d knockdown. The mean \pm s.d. of three technical measurements from three biological replicates is shown for *fl(2)d* and mean \pm s.d. of three technical measurements from two biological replicates for *vir*. **g**, Co-immunoprecipitation of Myc–Vir with HA–Ime4 and HA–FI(2)d. Extracts from S2R+ cells expressing HA-tagged proteins either with Myc alone or with Myc–Vir were immunoprecipitated using Myc-specific beads. Expression of indicated proteins was monitored by western blot analysis using anti-Myc and anti-HA antibodies. RNaseT1 treatment before immunoprecipitation is indicated at the bottom. **h**, Co-immunoprecipitation studies were carried out with lysates prepared from S2R+ cells co-expressing Myc–dMettl14 and HA–Ime4 upon control (Ctr) or FI(2)d knockdown. For control experiments, S2R+ cells were transfected with Myc alone and HA–Ime4. Lysates were immunoprecipitated using anti-Myc antibody and then detected with anti-Myc and anti-HA antibodies. Knockdown of FI(2)d weakens the interaction between Ime4 and dMettl14. **i**, Western blots showing Ime4 and dMettl14 protein expression levels in extracts from indicated genotypes. Tubulin is used as a loading control.



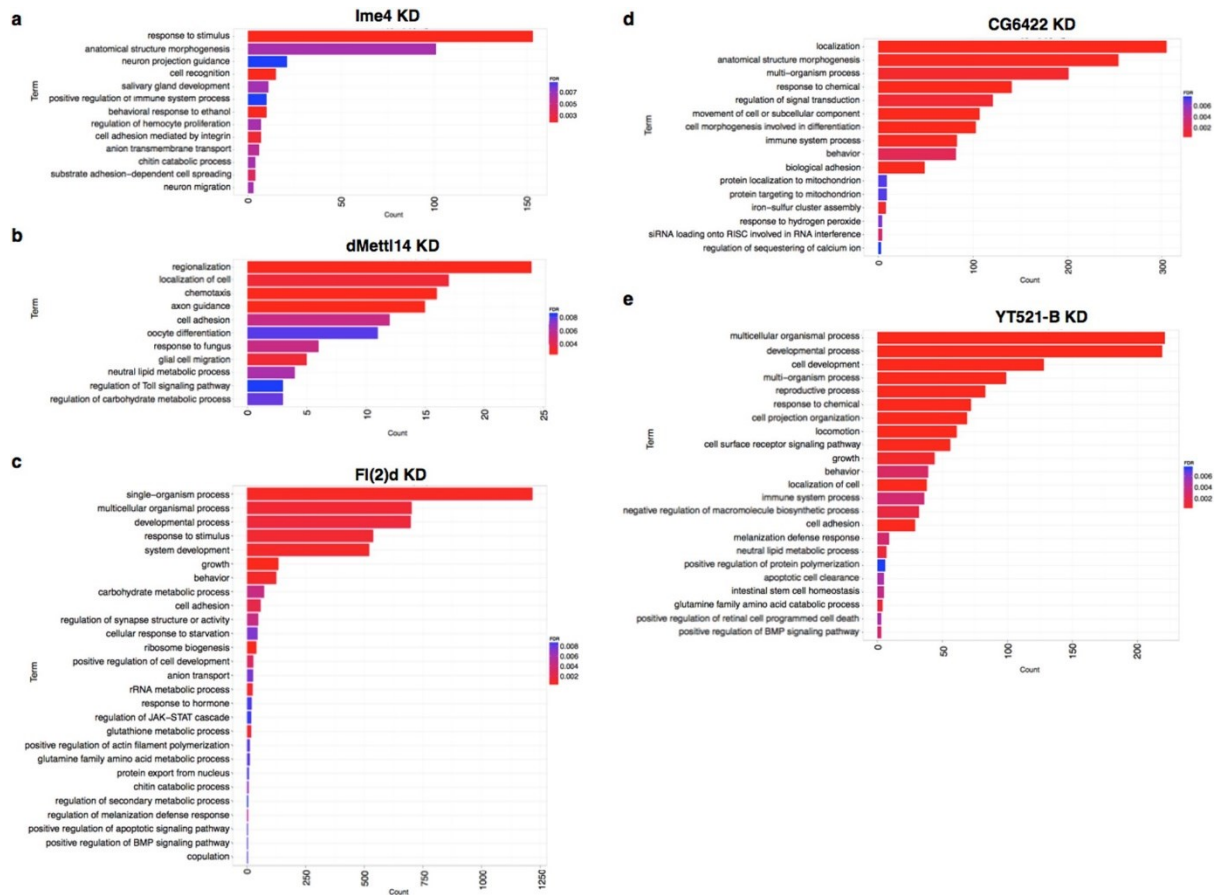
Extended Data Figure 2 | m⁶A quantification, MeRIP-seq validation and sequence features of m⁶A sites in *Drosophila* mRNA.

a, Scatter plot of counts per million (CPM) values for intersected MeRIP peaks. The peaks have at least a support of 3 CPM in one of the replicates. **b**, qPCR validation of MeRIP peaks. Enrichment is calculated over a negative region in the *Rpl15* transcript. The mean \pm s.d. of three technical measurements from two replicates is shown. **c**, Sequence motifs enriched in a fraction of m⁶A peaks, analysis performed by Homer.



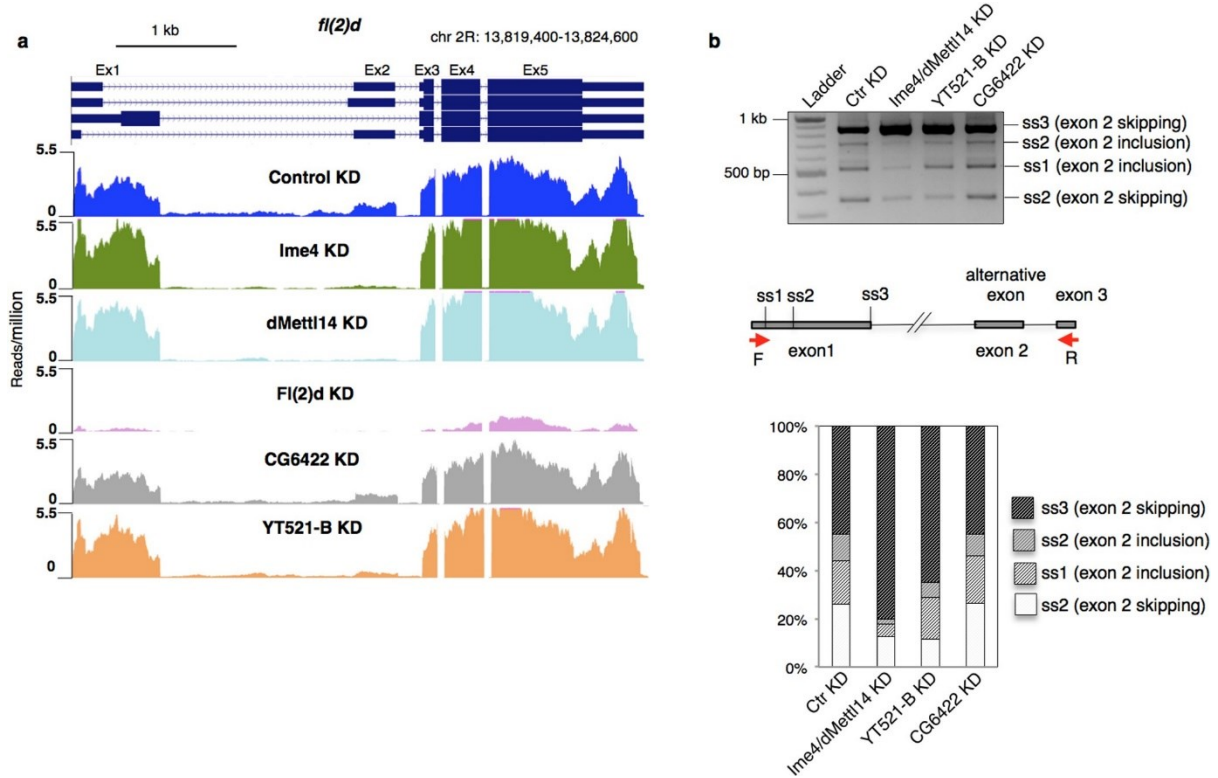
Extended Data Figure 3 | Significant fold changes and correspondence between biological replicates of RNA-seq data.

a, Average versus mean– difference plots (MA-plots) show the moderated estimation of fold change and dispersion for RNA-seq data in the different knockdown conditions (adjusted P value < 0.05). The significant values are highlighted in red. **b**, Spearman sample-to-sample correlation based on gene expression profiles. **c**, Spearman sample-to-sample correlation based on splicing levels. **d**, Empirical cumulative distribution function (ECDF) plot of fold changes (\log_2) upon lme4/dMettl14 double knockdown over control separated between m⁶A targets and non-targets. Values are shown between -0.5 and 0.5 . The distributions were compared using Wilcoxon rank sum test (P value = 9.9×10^{-4}). **e**, Fold change upon lme4/dMettl14 double knockdown versus control separated into genes without m⁶A peaks (non-targets) or containing m⁶A peaks within the CDS (CDS) or within a 300-bp window around the start or stop codon. Only genes considered for differential expression testing according to DESeq2 default filters are shown. **f**, Representation of differentially spliced events in the different knockdowns. Selection of 5' alternative splice sites and increase in intron retention are the two most enriched classes. Classification of splicing changes upon knockdown of the unrelated EJC component eIF4AIII is shown for comparison.



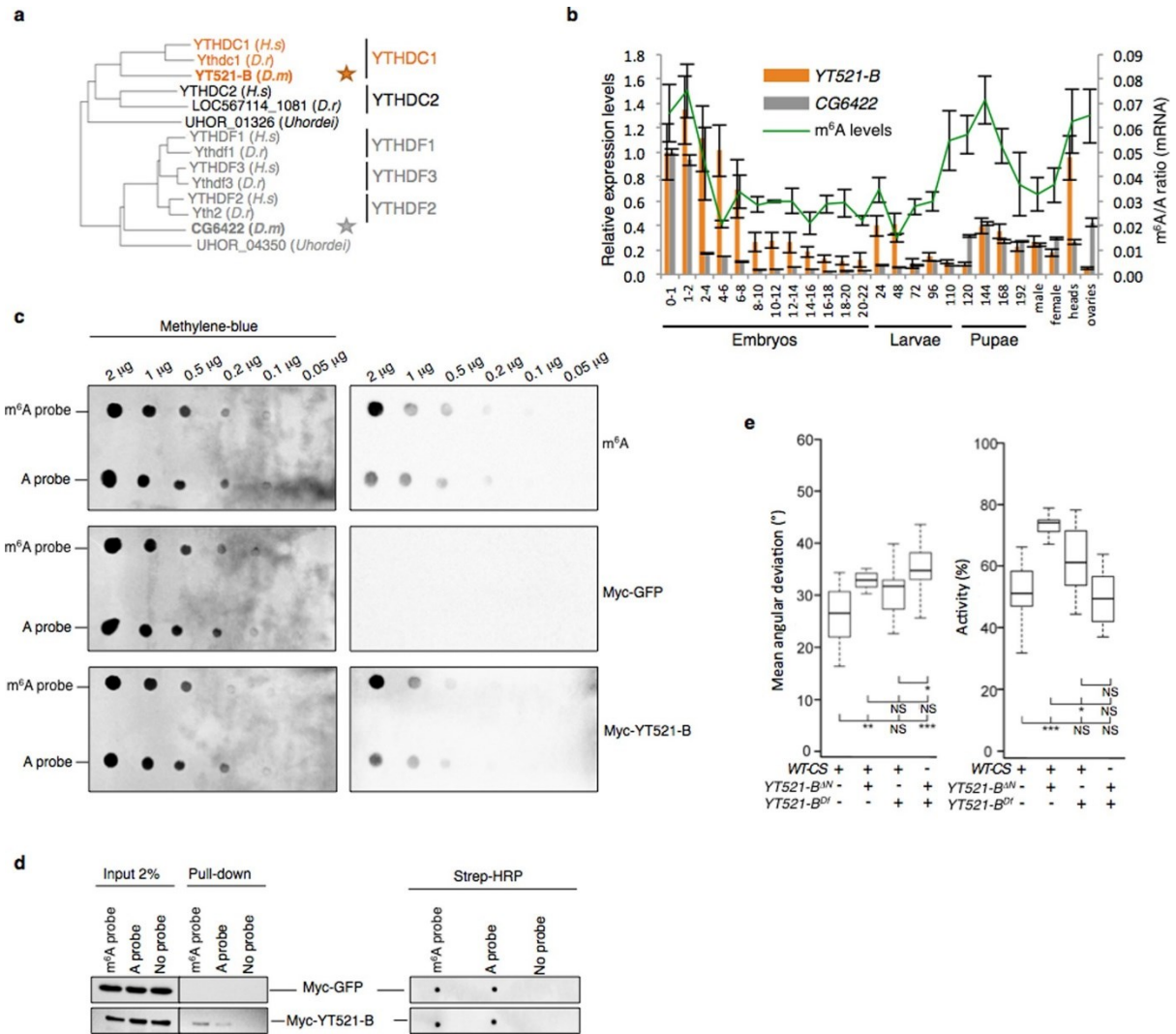
Extended Data Figure 4 | Gene ontology term enrichment analysis.

a–e. Significant GO terms (adjusted P value < 0.05) of differentially expressed genes in Ime4 knockdown (**a**), dMettl14 knockdown (**b**), Fl(2)d knockdown (**c**), CG6422 knockdown (**d**) and YT521-B knockdown (**e**) cells versus control S2R+ cells. Analysis was performed using the Bioconductor package of GOSTats.



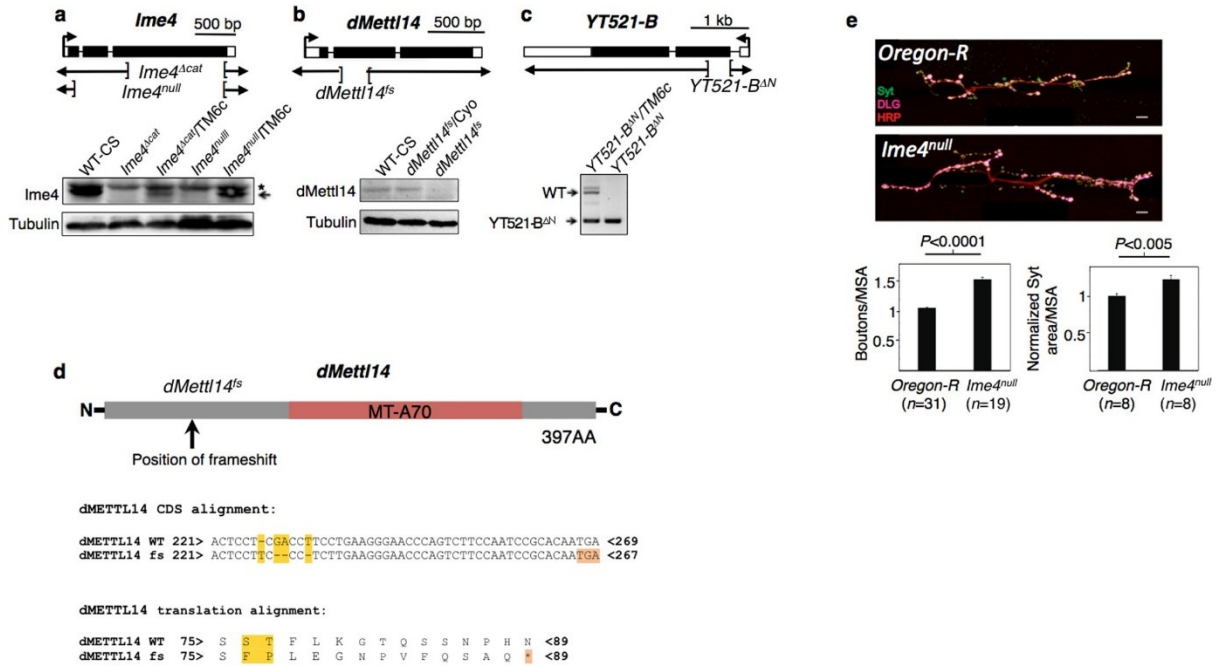
Extended Data Figure 5 | m6A nuclear components control *fl(2)d* splicing.

a, UCSC Genome Browser screenshots of *fl(2)d* showing normalized RNA-seq data from control and indicated knockdown samples in S2R⁺ cells. The gene architecture of *fl(2)d* is shown at the top, with thin blue boxes representing the 5' and 3' UTRs, thick blue boxes representing the CDS, and thin lines representing introns. Exon numbers are indicated at the top. Signals are displayed as RPM. **b**, Usage of different 5' splice sites in exon 1 of *fl(2)d* transcript and skipping of exon 2 upon different knockdowns. Analysis by semi-quantitative RT-PCR using primers in exon 1 and 3 (red arrows in the scheme). Quantification is indicated underneath the gel. ss1, splice site 1; ss2, splice site 2; ss3, splice site 3.



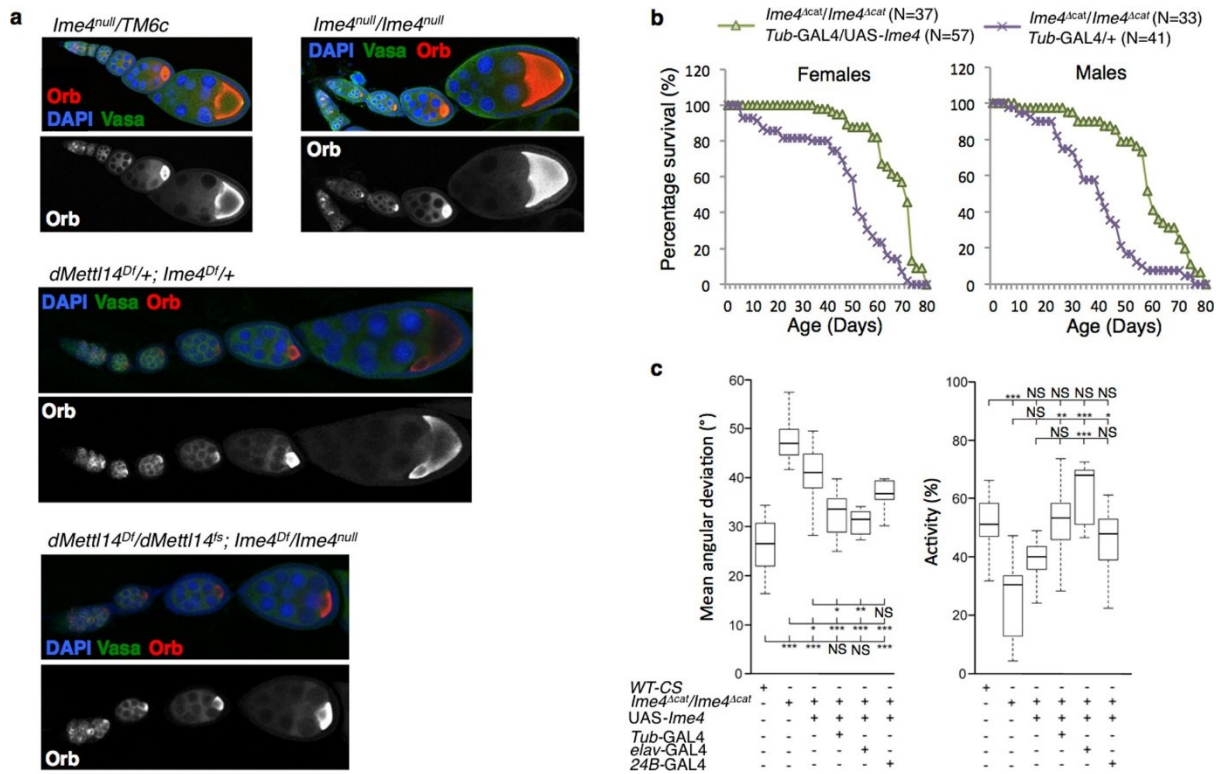
Extended Data Figure 6 | Characterization of *Drosophila* YTH components.

a, Phylogenetic analysis. Sequences from *Ustilago hordei* (a basidiomycota fungi) were used, in the absence of appropriate sequences from *S. cerevisiae*, and worked as outliers for each cluster to show the separation between the two major groups. **b**, Relative expression of *YT521-B* and *CG6422* transcripts and levels of m⁶A in mRNA during *Drosophila* development. Number of hours post-fertilization for different embryo, larval and pupal stages is indicated on the x axis. The mean \pm s.d. of three technical measurements from three biological replicates is shown. **c**, Dot-blot assay using biotinylated probe from *prolactin* transcripts with or without m⁶A RNA modification. Protein extracts from S2R⁺ cells transfected with either Myc-GFP or Myc-YT521-B were analysed for binding specificity to the crosslinked probes. Left, methylene-blue staining of crosslinked probes. Right, immunostaining using anti-Myc or anti-m⁶A antibody. YT521-B protein shows the same enrichment to the methylated probe as anti-m⁶A antibody. **d**, Pull-down using biotinylated m⁶A probe from *prolactin* transcripts and protein extracts from S2R⁺ cells transfected with either Myc-GFP or Myc-YT521-B. The same probe lacking the methylation was used as a negative control. Left, western blot using anti-Myc antibody. Right, dot blot using anti-Strep-HRP antibody. The binding of Myc-YT521-B is increased with the methylated probe. Three independent experiments show similar results. **e**, Walking behaviour in Buridan's paradigm in heterozygous and transheterozygous *YT521-B* mutants. Left, median angular displacements from the direct approach to one of the stripes. Right, median fraction of time spent walking during a 15 min test period (Kruskal-Wallis analysis of variance with a Bonferroni correction). Fifteen female flies per genotype were used in both assays. NS, not significant; **P* < 0.05; ***P* < 0.01; ****P* < 0.001.



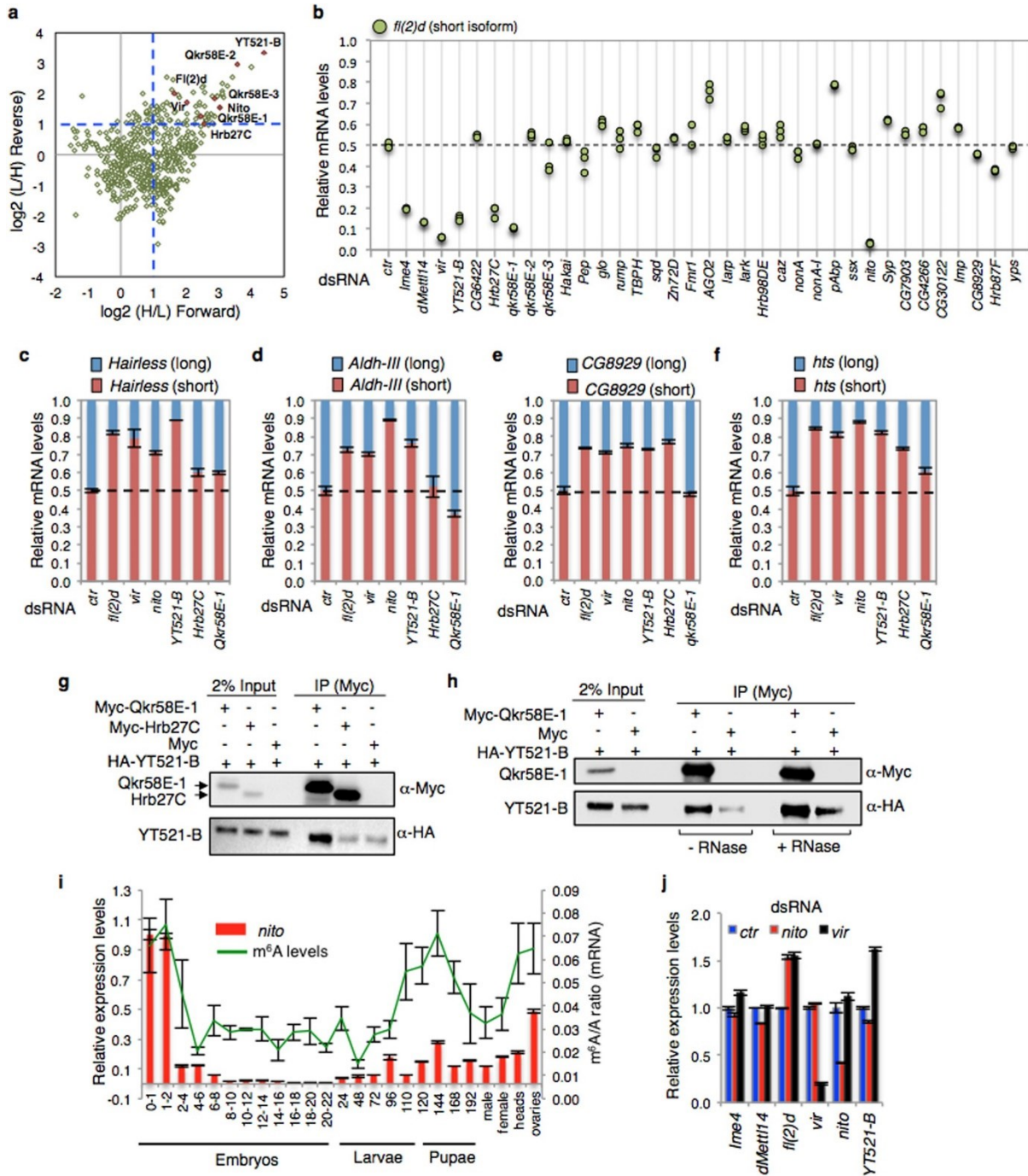
Extended Data Figure 7 | Genetic characterization of *Ime4*, *dMettl14* and *YT521-B*.

a–c, Top, *Ime4* (**a**), *dMettl14* (**b**) and *YT521-B* (**c**) loci with indicated deletions. Bottom, loss of function for *Ime4* and *dMettl14* were monitored by western blot using respective endogenous antibodies, while anti-Tubulin antibody was used as a loading control. To analyse *YT521-B* deletion, PCR using genomic DNA from heterozygous or homozygous *YT521-B^{ΔN}* mutant flies was loaded on agarose gel. **d**, Scheme of the *dMettl14* protein showing the conserved MT-A70 domain. The frameshift position caused by the guide RNA-induced deletions and the molecular nature of the allele are indicated below. **e**, Representative confocal images of muscle-6/7 NMJ synapses of abdominal hemisegment A2 for the indicated genotypes labelled with anti-DLG (magenta), anti-Synaptotagmin (green) and HRP (red) to reveal the synaptic vesicles and the neuronal membrane. Bottom, quantification of normalized bouton number (total number of boutons/muscle surface area ($\mu\text{m}^2 \times 1,000$)) and normalized Synaptotagmin area (total Synaptotagmin-positive area (μm^2)/muscle surface area ($\mu\text{m}^2 \times 1,000$)) of NMJ 6/7 in A3 of the indicated genotypes. Error bars show mean \pm s.e.m. *P* values were determined with a Student's *t*-test. The number of boutons and of active zones per boutons are increased upon *Ime4* knockout. MSA, muscle surface area.



Extended Data Figure 8 | *Ime4* mutant flies have reduced locomotion and shortened lifespan but apparent normal ovarian development.

a, Ovarian immunostaining of indicated genotypes. DAPI (blue) stains nucleus, Vasa protein (Vasa) (green) shows the germ cells and Orb protein (Orb) (red) the oocyte. Only one oocyte per egg chamber is seen in control and mutant ovaries, arguing against encapsulation defects. **b**, Survival curves of adult *Drosophila*. The lifespan of *Ime4^{scat}* mutant flies (purple) and *Ime4^{scat}* mutant flies expressing *Ime4* cDNA ubiquitously (*Tub-GAL4*) in neurons (*elav-GAL4*) or in muscles (*24B-GAL4*). Left, median angular displacements from the direct approach to one of the stripes. Right, median fraction of time spent walking during a 15 min test period. Fifteen female flies per genotype. NS, not significant; * $P < 0.05$, ** $P < 0.01$, *** $P < 0.001$ (Kruskal–Wallis analysis of variance with a Bonferroni correction).



Extended Data Figure 10 | RNA interference screen identifies Nito as a new member of the methyltransferase complex.

a, SILAC-coupled mass spectrometry analysis using YT521-B-Myc as a bait. Scatterplot of normalized forward versus inverted reverse experiments plotted on a log₂ scale. The threshold was set to a twofold enrichment (blue dashed line). Proteins in the top right quadrant are enriched in both duplicates. **b**, mRNA quantification of *fl(2)d* isoforms after knockdown of potential YT521-B-interacting proteins. Three proteins, Hrb27C, Qkr58E-1 and Nito, in addition to m6A components, control *fl(2)d* splicing in the same direction. Data points of three technical replicates are shown. **c-f**, mRNA quantification of m6A-regulated transcripts including *Hairless* (**a**), *Aldh-III* (**b**), *CG8929* (**c**), *his* (**d**) upon knockdown of indicated components. Nito controls m6A splicing events. The quantification of three technical replicates from two biological experiments is shown as mean \pm s.d. **g**, Co-immunoprecipitation studies were carried out with lysates prepared from S2R⁺ cells co-expressing Myc-Qkr58E-1, Myc-Hrb27C and HA-YT521-B. For control, S2R⁺ cells were transfected with Myc alone and HA-YT521-B. Myc-containing proteins were immunoprecipitated using a Myc antibody and then immunoblotted with anti-Myc and anti-HA antibodies. **h**, Co-immunoprecipitation of Myc-Qkr58E-1 with HA-YT521-B with or without RNaseT1. Extracts from S2R⁺ cells expressing HA-YT521-B either with Myc control or with Myc-Qkr58E-1 were immunoprecipitated using Myc-specific beads. Expression of indicated proteins was monitored by immunoblotting using anti-Myc and anti-HA antibodies. **i**, Relative *nito* mRNA expression and levels of m⁶A in mRNA during *Drosophila* development. Number of hours post-fertilization for different embryo, larval and pupal stages is indicated on the x axis. *nito* expression correlates with m⁶A levels. The mean \pm s.d. of three technical measurements from three biological replicates are shown. **j**, Relative expression of indicated transcripts upon control, Nito and Vir knockdown. Vir and Nito knockdowns do not reduce expression of other components of the methyltransferase complex. The mean \pm s.d. of three technical measurements from two biological replicates is shown.

Appendix 2 - Research article

Knuckles P*, **Lence T***, Haussmann IU, Jacob D, Kreim N, Carl SH, Masiello I, Hares T, Villaseñor R, Hess D, Andrade-Navarro MA, Biggiogera M, Helm M, Soller M, Bühler M# and Roignant J-Y# (2018). Zc3h13/Flacc is required for adenosine methylation by bridging the mRNA binding factor Rbm15/Spenito to the m⁶A machinery component Wtap/Fl(2)d. *Genes Dev*, Mar 1;32(5-6):415-429. doi: 10.1101/gad.309146.117.

* - indicates equal contribution

- indicates joint correspondence

Creative Commons License:

This article, published in Genes & Development, is available under a Creative Commons License (Attribution 4.0 International), as described at: creativecommons.org/licenses/by-nc/4.0/.

Zc3h13/Flacc is required for adenosine methylation by bridging the mRNA-binding factor Rbm15/Spenito to the m⁶A machinery component Wtap/Fl(2)d

Philip Knuckles,^{1,2,12} Tina Lence,^{3,12} Irmgard U. Haussmann,^{4,5} Dominik Jacob,⁶ Nastasja Kreim,⁷ Sarah H. Carl,^{1,8} Irene Masiello,^{3,9} Tina Hares,³ Rodrigo Villaseñor,^{1,2,11} Daniel Hess,¹ Miguel A. Andrade-Navarro,^{3,10} Marco Biggiogera,⁹ Mark Helm,⁶ Matthias Soller,⁴ Marc Bühler,^{1,2} and Jean-Yves Roignant³

¹Friedrich Miescher Institute for Biomedical Research, 4058 Basel, Switzerland; ²University of Basel, Basel 4002, Switzerland; ³Institute of Molecular Biology, 55128 Mainz, Germany; ⁴School of Life Science, Faculty of Health and Life Sciences, Coventry University, Coventry CV1 5FB, United Kingdom; ⁵School of Biosciences, College of Life and Environmental Sciences, University of Birmingham, Edgbaston, Birmingham B15 2TT, United Kingdom; ⁶Institute of Pharmacy and Biochemistry, Johannes Gutenberg University of Mainz, 55128 Mainz, Germany; ⁷Bioinformatics Core Facility, Institute of Molecular Biology, 55128 Mainz, Germany; ⁸Swiss Institute of Bioinformatics, Basel 4058, Switzerland; ⁹Laboratory of Cell Biology and Neurobiology, Department of Animal Biology, University of Pavia, Pavia 27100, Italy; ¹⁰Faculty of Biology, Johannes Gutenberg University of Mainz, 55128 Mainz, Germany

N⁶-methyladenosine (m⁶A) is the most abundant mRNA modification in eukaryotes, playing crucial roles in multiple biological processes. m⁶A is catalyzed by the activity of methyltransferase-like 3 (Mettl3), which depends on additional proteins whose precise functions remain poorly understood. Here we identified Zc3h13 (zinc finger CCCH domain-containing protein 13)/Flacc [Fl(2)d-associated complex component] as a novel interactor of m⁶A methyltransferase complex components in *Drosophila* and mice. Like other components of this complex, Flacc controls m⁶A levels and is involved in sex determination in *Drosophila*. We demonstrate that Flacc promotes m⁶A deposition by bridging Fl(2)d to the mRNA-binding factor Nito. Altogether, our work advances the molecular understanding of conservation and regulation of the m⁶A machinery.

[**Keywords:** Zc3h13; Flacc; m⁶A; methyltransferase complex; RNA modifications; sex determination]

Supplemental material is available for this article.

Received October 31, 2017; revised version accepted February 12, 2018.

In the past years, N⁶-methyladenosine (m⁶A) RNA has emerged as an abundant and dynamically regulated modification throughout the transcriptome (Dominissini et al. 2012; Meyer et al. 2012). m⁶A affects almost every stage of mRNA metabolism, and its absence is associated with various defects in meiosis, embryonic stem cell (ESC) differentiation, DNA repair, circadian rhythm, neurogenesis, dosage compensation, and sex determination (for a recent review, see Roignant and Soller 2017; Zhang et al. 2017). Alteration of m⁶A levels also promotes glioblastoma progression and is linked to poor prognosis in myeloid leukemia (Barbieri et al. 2017; Cui et al. 2017; Jaffrey and Kharas 2017; Kwok et al. 2017; Li et al. 2017; Vu et al. 2017; Weng et al. 2018).

Formation of m⁶A is catalyzed by the activity of methyltransferase-like 3 (METTL3; also called MT-A70) (Bokar et al. 1997), which physically interacts with METTL14 (Liu et al. 2014; Ping et al. 2014; Schwartz et al. 2014; Wang et al. 2014), Wilms tumor 1-associated protein (WTAP) (Zhong et al. 2008; Agarwala et al. 2012), Vir-like m⁶A methyltransferase-associated (KIAA1429/VIRMA) (Schwartz et al. 2014), and RNA-binding motif 15 (RBM15) and its paralog, RBM15B (Patil et al. 2016). *Drosophila* has corresponding homologs Mettl3, Mettl14, Fl(2)d, Virilizer (Vir), and Spenito (Nito) (Lence et al. 2017). Recent crystal structural studies investigated the molecular activities of the two predicted methyltransferases METTL3 and METTL14 (Sledz and Jinek 2016; Wang et al. 2016a,b). Only METTL3 was shown to contain the catalytic activity and form a stable heterodimer with METTL14, which was required to enhance METTL3

¹¹Present address: Department of Molecular Mechanisms of Disease, University of Zurich, 8057 Zürich, Switzerland.

¹²These authors contributed equally to this work.

Corresponding authors: jroignant@imb-mainz.de, marc.buehler@fmi.ch
Article published online ahead of print. Article and publication date are online at <http://www.genesdev.org/cgi/doi/10.1101/gad.309146.117>. Freely available online through the *Genes & Development* Open Access option.

© 2018 Knuckles et al. This article, published in *Genes & Development*, is available under a Creative Commons License (Attribution 4.0 International), as described at <http://creativecommons.org/licenses/by/4.0/>.

Knuckles et al.

enzymatic activity by binding substrate RNA and positioning the methyl group for transfer to adenosine. In addition, WTAP [Fl(2)d] ensures the stability and localization of the heterodimer to nuclear speckles (Ping et al. 2014; Lence et al. 2016). VIRMA (Vir) is essential for m⁶A deposition, but its molecular function is currently unknown. Last, RBM15 and RBM15B (Nito) have been suggested to recruit the methyltransferase complex to its target transcripts via direct binding to U-rich sequences on mRNA. In humans, this function is important to control m⁶A promoted X-chromosome inactivation via *XIST*-mediated transcriptional repression (Patil et al. 2016). In *Drosophila*, Nito promotes m⁶A function in the sex determination and dosage compensation pathways (Lence et al. 2016).

To date, it is unknown how Nito in *Drosophila* interacts with other members of the methyltransferase writer complex to ensure their recruitment to mRNA targets. Although, in human cells, RBM15/15B were reported to interact with METTL3 in a WTAP-dependent manner (Patil et al. 2016), it is unclear whether this interaction is conserved in other organisms. In order to address these questions, we performed interactome analyses from *Mus musculus* and *Drosophila melanogaster* cell extracts using Rbm15 and Nito as bait, respectively. We identified mouse zinc finger CCCH domain-containing protein 13 (Zc3h13) and its fly homolog, CG7358, which we named Fl(2)d-associated complex component (Flacc), as novel interactors of the m⁶A writer machinery. A lack of these proteins dramatically reduces m⁶A levels in both organisms. Consistent with the role of m⁶A in sex determination in *Drosophila*, Flacc depletion results in aberrant splicing of *Sex lethal* (*Sxl*) and leads to transformations of female into male-like structures. Moreover, we demonstrate that Flacc interacts with Nito and Fl(2)d and serves as an adaptor between these two proteins, thereby stabilizing the complex and promoting m⁶A deposition on mRNA.

Results

Zc3h13 interacts with the m⁶A machinery

In our recent work, we identified Nito as a novel interactor of the m⁶A methyltransferase complex (Lence et al. 2016). Because the role of the mouse Nito homolog protein Rbm15 appears to be evolutionarily conserved in regard to m⁶A deposition (Patil et al. 2016), we sought to identify interaction partners to obtain further insights into Rbm15's function. To this end, we tagged endogenous Rbm15 with the Flag-Avi tag using CRISPR-Cas9 genome editing in mouse ESCs (mESCs) that express the bacterial *BirA* ligase (Supplemental Fig. S1A, B; Flehr and Buhler 2015). Subsequently, we performed tandem affinity purification (TAP) coupled to liquid chromatography and mass spectrometry (TAP-LC-MS). We found that Rbm15 copurifies with Wtap, Virma, and Hakai (Fig. 1A) under stringent conditions (350 mM NaCl), demonstrating that these proteins stably interact with each other. Hakai was found recently to interact with other

subunits of the m⁶A methyltransferase complex in plants (Ruzicka et al. 2017). Interestingly, we also observed Zc3h13 among the top hits. Although it was reported to interact with WTAP in human cells, it has not been linked previously to adenosine methylation (Horiuchi et al. 2013; Wan et al. 2015).

Previous work suggested that the interaction of the heterodimer Mettl3/14 with Wtap, Virma, and Rbm15 is important to guide the methylation complex to its targets and correctly methylate mRNA (Ping et al. 2014; Schwartz et al. 2014; Patil et al. 2016). To test whether the Zc3h13-containing protein complex described above interacts with Mettl3/14 in mice, we also endogenously tagged Mettl3 with the Flag-Avi tag in mESCs (Supplemental Fig. S1A, B) and performed TAP-LC-MS. Consistent with previous reports, we found that Mettl3 copurifies with Mettl14, Wtap, Virma, Rbm15, and Hakai (Fig. 1B; Supplemental Fig. S2A). Importantly, we also recovered peptides from Zc3h13 (Fig. 1B; Supplemental Fig. S2A). Whereas these interactions resisted 350 mM NaCl, only the Mettl3/Mettl14 interaction remained at 500 mM NaCl (Fig. 1B). These results indicate the existence of two stable protein complexes (Mettl3/Mettl14 and Rbm15/Zc3h13/Wtap/Virma/Hakai), which we refer to as the m⁶A-METTL complex (MAC) and the m⁶A-METTL-associated complex (MACOM), respectively.

To gain further insight into the relative amounts of MAC to MACOM, we performed intensity-based absolute quantification (iBAQ) analysis on TAP-LC-MS data from endogenously tagged Mettl3. We observed comparable stoichiometry between the bait (Mettl3) and Mettl14. In contrast, Wtap and other MACOM components were <1% abundant compared with Mettl3 and Mettl14 (Supplemental Fig. S2B), an observation that we interpret as a sign of a weak and/or short-lived interaction. Alternatively, the abundance of MAC bound to MACOM could be very scarce relative to the level of each independent complex. Regardless of the precise mechanism, because components of both complexes are required to install m⁶A, we propose that MAC and MACOM interact with each other in order to deposit the methylation.

The Drosophila Zc3h13 homolog *Flacc* interacts with components of the m⁶A methyltransferase complex

To address whether Nito interacts with the same set of proteins that we identified in mice, we took an approach very similar to that described above using extracts from *Drosophila* S2R⁺ cells. We used stable isotope labeling of amino acids in cell culture (SILAC)-based quantitative proteomics. A Myc-tagged version of Nito was used to perform coimmunoprecipitation experiments from S2R⁺ cells. In total, we identified 40 factors that showed >1.5-fold enrichment in the Nito-Myc precipitate in comparison with control cells transfected with Myc alone (Fig. 1C; Supplemental Table 1). In agreement with mouse Rbm15 proteomic analysis, the homolog of Wtap in *Drosophila* Fl(2)d, was among the top candidates. We also found the previously reported m⁶A writers Vir and Hakai (refer to Fig. 1F for *M. musculus* and *D. melanogaster*

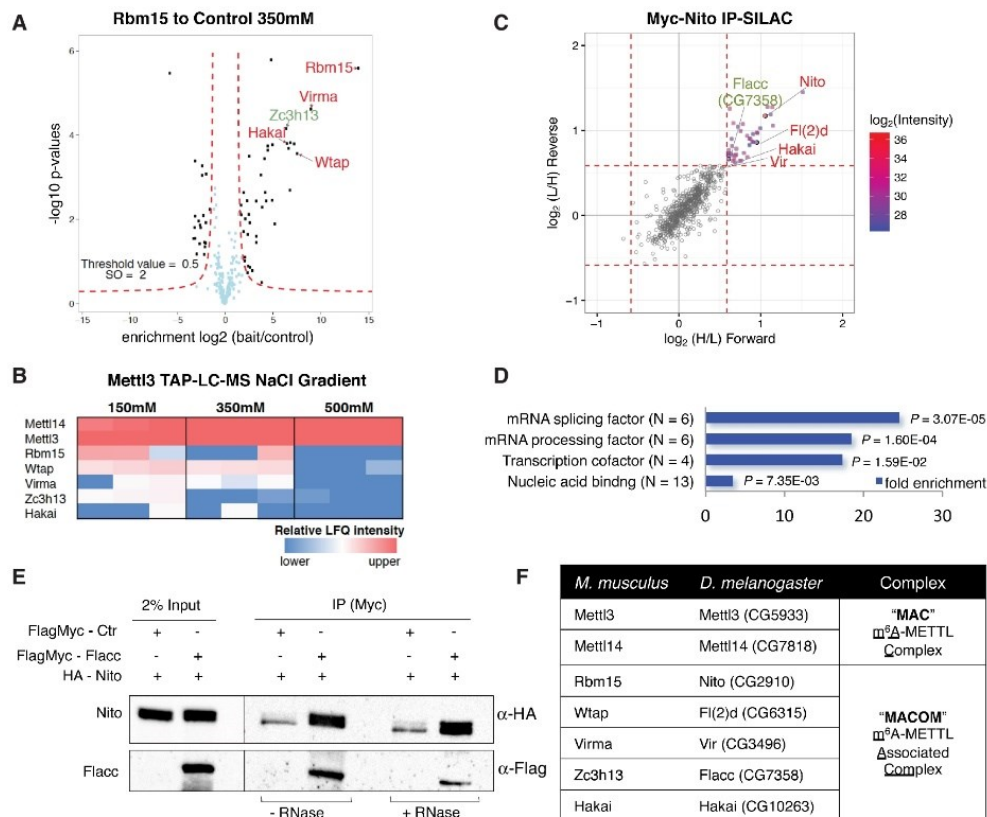
Zc3h13/Flacc is required for m⁶A biogenesis

Figure 1. Zc3h13/Flacc interacts with the m⁶A machinery. (A) TAP-LC-MS/MS of endogenously Flag-Avi-tagged Rbm15 mESCs. Parental cells were used as background control, and proteins were purified in the presence of 350 mM NaCl. Highlighted in the volcano plot are enriched proteins previously identified as Mettl3 interactors (red) as well as Zc3h13 (green). (B) Heat map comparing relative label-free quantification (LFQ) intensities of selected Mettl3-bound proteins across increasing NaCl concentrations. Statistical analysis was done with Perseus (see the Materials and Methods for details). MS raw data were deposited in ProteomeXchange. (C,D) Stable isotope labeling of amino acids in cell culture (SILAC) coupled to MS analysis using Nito-Myc as bait. Scatter plot of normalized forward versus inverted reverse experiments plotted on a log₂ scale. The threshold was set to a 1.5-fold enrichment (red dashed line). Proteins in the *top right* quadrant of C are enriched in both replicates. Gene ontology (GO) term analysis (Tyanova et al. 2016) for enriched proteins is shown in D. (E) Coimmunoprecipitation experiments were carried out with lysates prepared from S2R⁺ cells transfected with FlagMyc-Flacc and HA-Nito. In control lanes, S2R⁺ cells were transfected with FlagMyc alone and an identical HA-containing protein. Extracts were immunoprecipitated with Myc antibody and immunoblotted using Flag and HA antibodies. Two percent of input was loaded. The same experiment was repeated in the presence of RNaseT1. Nito and Flacc interact with each other in an RNA-independent manner. (F) Table representing orthologous proteins of the m⁶A-METTL complex (MAC) and the m⁶A-METTL-associated complex (MACOM) in mice and flies.

nomenclature of m⁶A factors). We observed an overall enrichment for mRNA-binding proteins (Fig. 1D) and, importantly, Flacc, which is the closest homolog of Zc3h13. To confirm the interaction of this protein with Nito, we generated tagged proteins and performed coimmunoprecipitation assays. These experiments confirmed that Flacc interacts with Nito and that this occurs in an RNA-independent manner (Fig. 1E). To verify that Flacc interacts with other components of the m⁶A methyltransferase complex, we immunoprecipitated Flacc-Myc and tested for the presence of Vir and Fl(2)d. As shown in Supplemental Figure S3, A and B, Flacc interacts with both proteins independently of RNA, indicating that it might

be a novel regulator of the m⁶A pathway. In contrast to mouse Zc3h13 (see below), however, Flacc does not contain a zinc finger motif (Supplemental Fig. S4).

Zc3h13/Flacc regulates the m⁶A pathway

To test whether Zc3h13 is necessary for adenosine methylation in mice, we measured global m⁶A levels by LC-MS/MS in Zc3h13 knockout mESCs (Supplemental Fig. S1C). We found an 80% reduction of m⁶A, similar to isogenic Mettl3 knockout mESCs (Fig. 2A). Consistent with a global reduction in m⁶A levels, Zc3h13 knockout cells

Knuckles et al.

displayed a drastic change in morphology, reminiscent of *Mettl3* knockout, with loss of dome-shaped colony formation and an overall increase in cell size (data not shown). In addition, we performed m⁶A RNA immunoprecipitation coupled to deep sequencing (m⁶A-RIP-seq) on oligo-dT-selected mRNA from wild-type, *Mettl3* knockout, and *Zc3h13* knockout mESCs. As observed with *Mettl3* knockout cells, ablation of *Zc3h13* resulted in a drastic reduction of m⁶A enrichment, particularly at the 3' end of target mRNAs (Fig. 2B,C). Hence, we conclude that *Zc3h13* is essential for m⁶A installation in mESCs. To investigate evolutionary conservation of this activity in *Drosophila*, we quantified m⁶A levels using LC-MS/MS analysis upon Flacc depletion in *Drosophila* S2R⁺ cells. Similar to the reduction observed upon knockdown of other m⁶A components, depletion of Flacc also resulted in strongly reduced m⁶A levels (Fig. 2D; Supplemental Fig. S5A). This was not due to

an indirect effect on expression of other components of the methyltransferase complex (Supplemental Fig. S5B–D). In agreement with decreased m⁶A levels, we found that binding of the reader protein Ythdc1 to its target transcripts was reduced in the absence of Flacc (Fig. 2E; Supplemental Fig. S3C,D). Together, these results demonstrate that *Zc3h13* and its *Drosophila* ortholog, Flacc, are novel and essential components of the m⁶A pathways in mice and flies.

Flacc is required for pre-mRNA splicing

To further corroborate Flacc as a bona fide m⁶A writer, we tested whether it was required to control m⁶A splicing-related events. As reported previously, splicing of several transcripts, including *AldhIII*, *Dsp1*, and *Hairless*, is dependent on the m⁶A pathway (Lence et al. 2016).

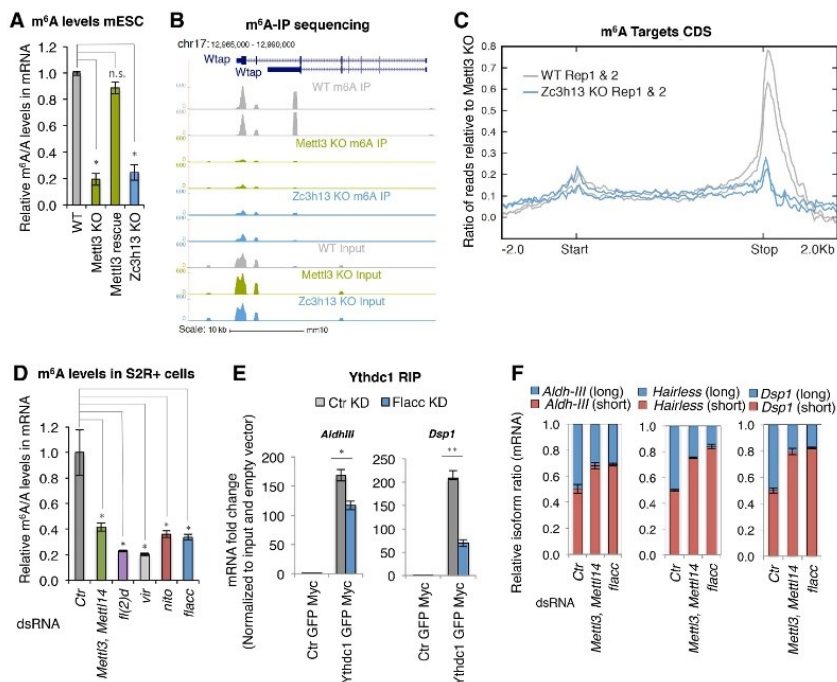


Figure 2. Flacc/Zc3h13 regulates the m⁶A pathway. [A] LC-MS/MS quantification of m⁶A levels in mRNA extracts from wild-type mESCs, *Mettl3* knockout and *Mettl3* knockout plasmid rescue, and *Zc3h13* knockout cells. The mean of two biological replicates and three independent measurements is shown. Errors bars indicate standard deviation (SD). (*) $P < 0.01$; (n.s.) not significant, Student's *t*-test. [B] University of California at Santa Cruz genome browser shots of m⁶A immunoprecipitation profiles of RNA isolated from *Mettl3* knockout, *Zc3h13* knockout, and wild-type cells and input samples for each genetic background at the *Wtap*-encoding locus. Scale is mapped reads in 100-base-pair (bp) bins normalized to mean library size. [C] Metaplot depicting reads from m⁶A immunoprecipitations at target genes (defined as genes overlapping or within 500 bp of MACS-identified peaks of m⁶A immunoprecipitation/input in wild-type cells) aligned to the coding sequence ("start" and "stop" refer to translation start and stop, respectively). [D] LC-MS/MS quantification of m⁶A levels in either control samples or mRNA extracts depleted for the indicated proteins in S2R⁺ cells. The bar chart shows the mean of three biological replicates and three independent measurements. Errors bars indicate SD. (*) $P < 0.01$, Student's *t*-test. Knockdown of the indicated proteins significantly reduces m⁶A levels. [E] Fold enrichment of m⁶A-regulated transcripts (*Aldh-III* and *Dsp1*) over input in Myc-Ythdc1 RIP after control or Flacc depletion. The bar chart shows the mean of three biological replicates. Errors bars indicate SD. (*) $P < 0.01$; (**) $P < 0.001$, Student's *t*-test. Loss of Flacc affects Ythdc1 binding. [F] Relative isoform quantification of m⁶A-regulated genes (*Aldh-III*, *Hairless*, and *Dsp1*) upon depletion of the indicated components. Flacc is required for m⁶A-dependent splicing events.

Remarkably, depletion of Flacc affected all of those transcripts (Fig. 2F; Supplemental Fig. S5E). We next expanded this analysis to a transcriptome-wide level, which revealed that depletion of Flacc in S2R⁺ cells leads to changes in gene expression and splicing that substantially overlap with changes observed upon knockdown of other m⁶A writers (Fig. 3A; Supplemental Fig. S6A; Supplemental Tables 3–8). In particular, the Flacc-depleted transcriptome clusters very closely with Fl(2)d- and Vir-depleted transcriptomes (Fig. 3B). Notably, Nito depletion induced greater changes and poorly clustered with the others, suggesting that Nito might be pleiotropic. Regardless of Nito's potential role in other pathways, common misregulated genes among components of the MACOM are larger than the average gene size (Fig. 3C) and are significantly methylated (61.5%; $P = 6.94 \times 10^{-31}$) (Fig. 3D). Importantly, differentially expressed genes generally change in the

same direction upon the different knockdowns, confirming that MACOM components belong to the same complex and share similar functions (Fig. 3E). We noticed that common up-regulated genes tend to be larger ($P = 2.9 \times 10^{-40}$) and more methylated compared with down-regulated ones (78.2% [$P = 6.12 \times 10^{-31}$] vs. 44.5% [$P = 0.086$]) (Fig. 3C,D). Up-regulated genes were enriched for processes involved in embryonic development as well as epithelial cell differentiation and migration (Fig. 3F). Thus, it is possible that down-regulated genes, which are mostly enriched for metabolic processes, are affected indirectly (Fig. 3F).

We next performed similar analysis with respect to splicing changes. We found that knockdown of each of the known m⁶A writer components, including Flacc, resulted in an increase of both alternative 5' splice site usage and intron retention (Supplemental Fig. S6A,B). Moreover,

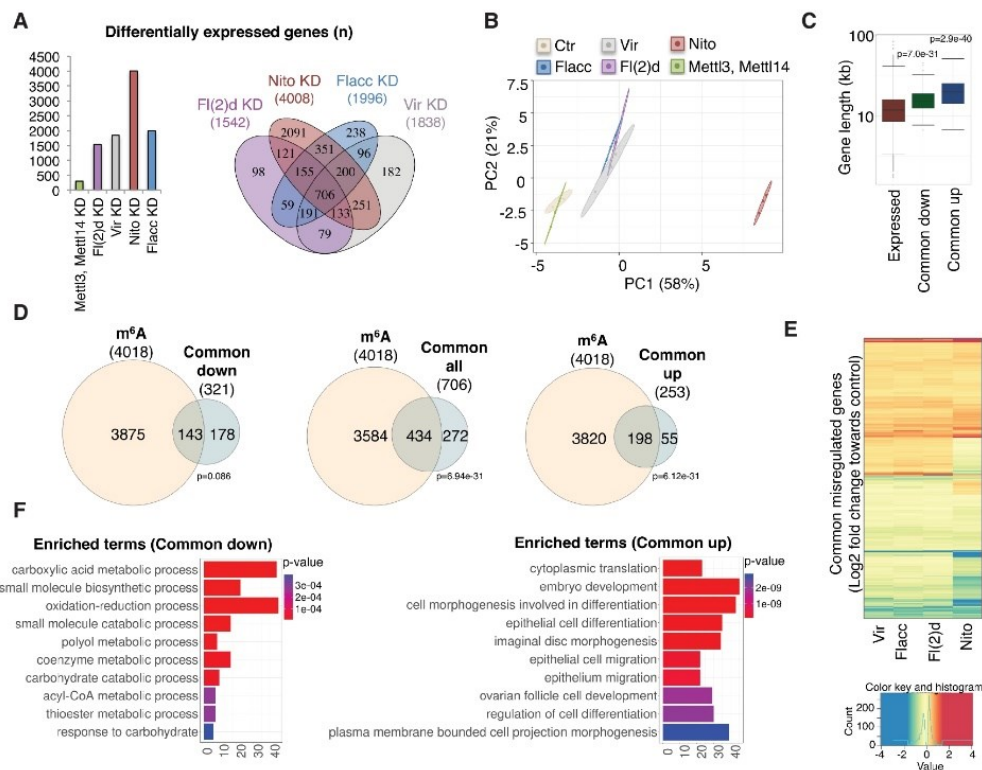


Figure 3. Flacc regulates common transcripts with other components of the m⁶A complex. (A) Number of differentially expressed genes (5% false discovery rate [FDR]) upon knockdown of the indicated proteins (left) and common differentially expressed targets regulated by components of MACOM (right). (B) Scatter plot of the first two principal components of a principal component analysis (PCA) of the 500 most variable genes in all conditions. The biological replicates are indicated in the same color, with elliptical areas representing the SD of the two depicted components. (C) Gene length distribution for genes tested in the differential expression analysis and the differential expressed genes up-regulated or down-regulated in all conditions. The distributions were tested for difference using the Kolmogorov-Smirnov test. (D) Overlap between common up, down, or all differentially expressed genes and genes annotated to have m⁶A-modified transcripts (according to methylation individual nucleotide resolution cross-linking immunoprecipitation data from Kan et al. 2017). The significance of the overlap was tested using a hypergeometric test. (E) Fold change (\log_2) expression of commonly misregulated genes. The heat map is clustered according to rows and columns. The color gradient was adjusted to display the 1% lowest/highest values within the most extreme color (lowest values as the darkest blue and highest values as the darkest red). (F) The GO term analysis of common up-regulated and down-regulated genes performed using the package ClusterProfiler. The top 10 GO terms are displayed.

Knuckles et al.

most common misspliced transcripts upon knockdown of MACOM components are methylated (82.2%; $P = 1.3 \times 10^{-8}$), show similar splicing defects, and are enriched for neuronal processes, which is consistent with our previous findings (Supplemental Fig. S6C–E; Lence et al. 2016). Of note, knockdown of *Mettl3/Mettl14* generally produces less effect compared with knockdown of MACOM components. This may be explained by residual m⁶A activity upon knockdown of the methyltransferases. Alternatively, MACOM components may have additional functions beyond m⁶A activity (see also the Discussion).

Flacc subcellular localization and expression through development

To further investigate the role of Flacc in *Drosophila*, we examined its subcellular localization as well as its developmental expression profile. We observed that Flacc is strictly localized in the nucleus in S2R⁺ cells (Supplemental Fig. S7A) and that its transcript is broadly expressed during embryogenesis but shows enrichment in the neuroectoderm (Supplemental Fig. S7B). Overall, *flacc* mRNA follows the same distribution as transcripts of other subunits of the methyltransferase complex (Lence et al. 2016) and as m⁶A levels in mRNA. An exception is the stage of maternal-to-zygotic transition (2 h after fertilization), where a boost of *flacc* expression is observed while m⁶A is rapidly decreasing (Supplemental Fig. S7C), suggesting that Flacc might have an additional function in early embryogenesis.

Flacc is required for sex determination and dosage compensation via Sxl alternative splicing

Components of the m⁶A machinery were shown previously to affect sex determination and dosage compensation in *Drosophila* via the control of *Sxl* alternative splicing (Hausmann et al. 2016; Lence et al. 2016; Kan et al. 2017). To address whether Flacc bears similar functions, we depleted its products by expressing corresponding dsRNA in both the legs and genital discs using the *dome*-GAL4 driver. Strikingly, these females displayed clear transformations into male structures, as shown previously for Nito (Fig. 4A; Yan and Perrimon 2015). This is illustrated by the appearance of sex combs in the forelegs of females that were depleted for Flacc. The phenotype was observed in ~20% of females examined (Fig. 4B). Using a dsRNA that targets a distinct region of *flacc* (GD35212), the penetrance was even increased to all female escapers (Fig. 4B; Supplemental Fig. S7D). Furthermore, typical female external structures, such as vaginal bristles, were absent on the same individuals (Fig. 4A). Altogether, these data indicate that Flacc plays a major role in the control of sex determination in flies.

To address how Flacc affects sex determination, we tested whether alternative splicing of *Sxl*, the master regulator of sex determination and dosage compensation, was affected. RNA extracts from fly heads depleted by RNAi for Fl(2)d, Nito, or Flacc were subjected to reverse transcription followed by PCR using primers spanning the

common exons 2 and 4. While the male-specific exon 3 is absent in control female heads, it was clearly included upon the loss of components of the m⁶A machinery, including Flacc (Fig. 4C). This experiment indicates that Flacc regulates sex determination and dosage compensation via *Sxl* alternative splicing, as shown previously for other m⁶A writers.

To confirm the effect of Flacc on sex determination via *Sxl* alternative splicing observed when using RNAi, we analyzed a lethal *flacc* mutant allele harboring a stop codon at amino acid 730 (Fig. 4D). Reducing one copy of m⁶A components [*Mettl3*, *Mettl14*, *fl(2)d*, *vir*, *nito*, or *Ythdc1*] in a sensitized background (heterozygous for *Sxl* and *daughterless*) significantly alters female viability (Fig. 4E). We showed previously for the *Mettl3* allele that this is due to activation of dosage compensation in females (Hausmann et al. 2016). Consistent with its role in N⁶-adenosine methylation, we found that removing one copy of the *flacc* allele results in female lethality (Fig. 4E). Likewise, the female-lethal single amino acid substitution allele *vir2F* interferes with *Sxl* recruitment, resulting in impaired *Sxl* autoregulation and inclusion of the male-specific exon (Hilfiker et al. 1995). We observed that female lethality of these alleles was rescued by *flacc* and *nito* double heterozygosity, further confirming the involvement of Flacc in *Sxl* alternative splicing (Fig. 4F).

Zc3h13/Flacc stabilizes Wtap/Fl(2)d–Rbm15/Nito interaction

To obtain insights into the molecular function of Flacc, we investigated interactions between m⁶A writers in the absence of Flacc. We found previously that knockdown of Fl(2)d diminishes the interaction between *Mettl3* and *Mettl14* (Lence et al. 2016). Interestingly, we found that this interaction is not affected upon Flacc knockdown (Supplemental Fig. S8A,B). However, we observed that depleting Flacc almost completely abolished the association between Nito and Fl(2)d (Fig. 5A), whereas interactions between Vir and different isoforms of Fl(2)d as well as Vir and Nito were not affected (Supplemental Fig. S8C–F). Interactions between Nito and *Mettl3/Mettl14* were also not compromised upon depletion of Flacc (Supplemental Fig. S8G,H). This indicates that Flacc stabilizes the complex and might serve as an adapter that connects the RNA-binding protein Nito to Fl(2)d. If this prediction was true, depletion of Flacc should prevent binding of Fl(2)d, but not Nito, to its mRNA targets. To test this hypothesis, we performed RNA immunoprecipitation (RIP) experiments to monitor the binding of these components to well-characterized m⁶A targets in the presence or absence of Flacc. As shown in Figure 5B, binding of Fl(2)d to *AldhIII*, *Hairless*, and *Dsp1* mRNA was strongly decreased upon Flacc knockdown, whereas Nito binding was only slightly affected. Thus, we conclude that Flacc serves as an adapter between Fl(2)d and the mRNA-recruiting factor RBM15/Nito.

To test functional conservation of Flacc, we cloned a human isoform of ZC3H13 and probed for the interaction between Nito and Fl(2)d upon depletion of endogenous

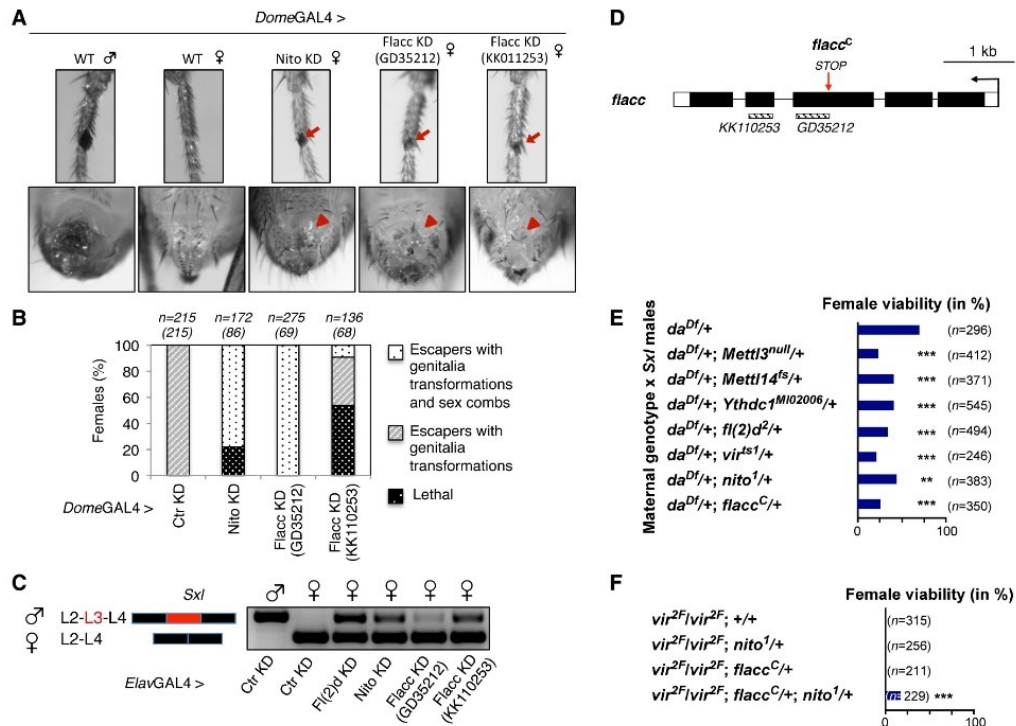
Zc3h13/Flacc is required for m⁶A biogenesis

Figure 4. Flacc is required for sex determination via control of *Sxl* alternative splicing. (A,B) *dome*-GAL4-driven expression of shRNA or dsRNA in genital discs and first pair of leg discs against Nito or Flacc, respectively. (Top) Forelegs of a wild-type male fly and female flies depleted for Nito or Flacc show the appearance of male-specific sex comb bristles (red arrow). (Bottom) Depletion of Nito or Flacc results in transformations of female genitalia and loss of vaginal bristles (red arrowhead). (B) Quantification of female survival and transformations in escapers upon depletion of Nito or Flacc using the *dome*-GAL4 driver. (n) The number of analyzed flies with the expected number of escapers in brackets. Depletion of Nito and Flacc results in a high level of transformation in female genitalia and the appearance of male-specific sex combs on forelegs. (C) Semiquantitative RT-PCR analysis of *Sxl* isoforms in male and female heads from flies depleted for Fl(2)d, Nito, or Flacc, respectively, using the *Elav*-GAL4 driver. Inclusion of male-specific exon L3 is observed in flies lacking m⁶A components. (D) The *flacc* locus (*flacc^C*) with a premature stop codon at amino acid Leu730. Sites of dsRNA fly lines KK110253 and GD35212 are shown below gene loci. (E) Viability of female flies from a cross of the indicated genotypes mated with *Sxl*^{7B/C} males. The loss of one copy of *flacc* significantly reduces female survival in a genetic background where one copy of *Sxl* and *da* are absent. The same compromised survival is observed for other m⁶A components [*Mettl3*, *Mettl14*, *Ythdc1*, *fl(2)d*, *vir*, and *nito*]. Viability was calculated from the numbers of females compared with males, and statistical significance was determined by a χ^2 test (Graphpad Prism). (F) The viability of female flies with homozygous *vir2F* mutation can be rescued by the loss of a single copy of *flacc* and *nito*. Viability was calculated from the numbers of homozygous *vir2F* females compared with heterozygous balancer-carrying siblings, and statistical significance was determined by a χ^2 test (Graphpad Prism).

Flacc protein in *Drosophila* S2R⁺ cells. Remarkably, expression of ZC3H13 was sufficient to re-establish the interaction between Nito and Fl(2)d (Fig. 5C,D; Supplemental Fig. S8I–K) even though the two orthologs bear low sequence similarity at the amino acid level (21% identity). These results hint at a conserved role of this newly characterized protein in stabilizing interactions within the MACOM. To address this more directly, we generated *Zc3h13* knockout mESCs that express Flag-Avi-tagged Rbm15 and performed TAP-LC-MS/MS experiments. Starting with both whole-cell extracts and nuclear fractions, Rbm15 interaction with Wtap was markedly reduced (Fig. 6A,B; Supplemental Fig. S9A,B), which is consistent with observations in the fly knockdown experiments [Nito and Fl(2)d, respectively]. Furthermore, the

reduced interaction was not attributable to a global decrease of Wtap or other components of MACOM (Supplemental Fig. S9C). As an alternative approach to test MACOM integrity, we used a protein fragment complementation assay (Dixon et al. 2016), generating fusion constructs of Rbm15 and Wtap to NanoBiT subunits. The optimal combination of fusions reconstituted the luciferase signal when transfected into wild-type cells (Wtap N-terminally tagged with the small nanoluciferase subunit and Rbm15 C-terminally tagged with the large nanoluciferase subunit) (Fig. 6C; Supplemental Fig. S9D–F). The relative luciferase signal intensity was strikingly reduced when fusion constructs were transfected in *Zc3h13* knockout but not in *Mettl3* knockout, discarding a secondary effect of global m⁶A loss (Fig. 6C). Taken

Knuckles et al.

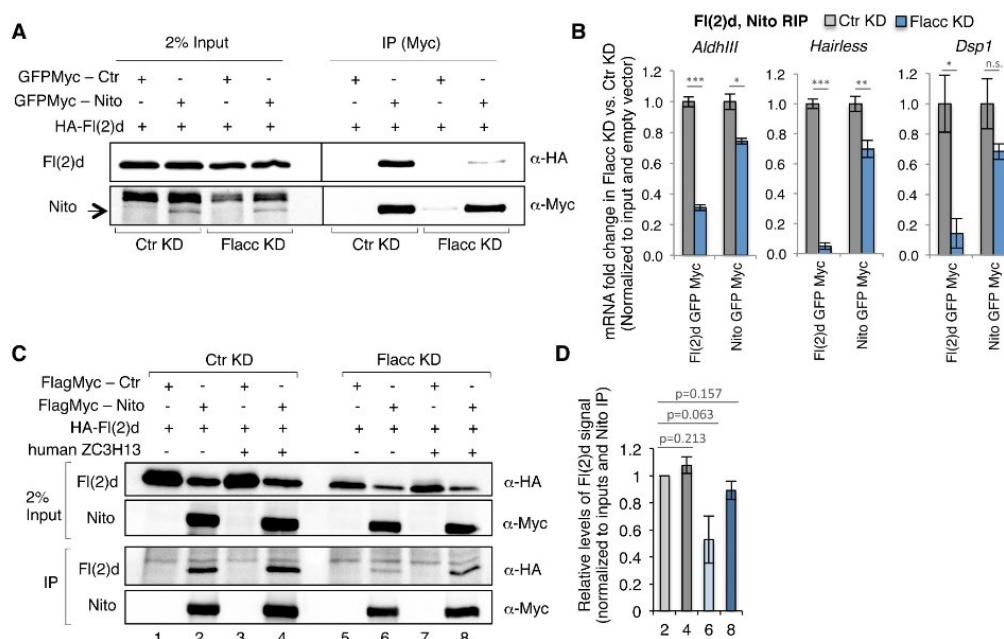


Figure 5. Flacc bridges the methyltransferase complex to mRNA targets via binding to Nito. (A) Coimmunoprecipitation experiments were carried out with lysates prepared from S2R⁺ cells transfected with GFPMyC-Nito and Fl(2)d-HA. In control lanes, S2R⁺ cells were transfected with Myc alone and an identical HA-containing protein. Extracts were immunoprecipitated with Myc antibody and immunoblotted using Myc and HA antibodies. Two percent of input was loaded. The same experiment was repeated in Flacc knockdown conditions. Interaction between Nito and Fl(2)d is strongly reduced upon depletion of Flacc. (B) Fold enrichment of m⁶A-regulated transcripts (*Aldh1l1*, *Hairless*, and *Dsp1*) over input in Myc-Fl(2)d and Myc-Nito RIP upon depletion of Flacc or in control conditions. The bar chart shows the mean of three biological replicates. Errors bars indicate SD. (*) $P < 0.01$; (**) $P < 0.001$; (***) $P < 0.0001$; (n.s.) not significant, Student's *t*-test. Loss of Flacc strongly affects Fl(2)d binding and, to a milder extent, binding of Nito to m⁶A-regulated transcripts. (C, D) Coimmunoprecipitation experiments were carried out with lysates prepared from S2R⁺ cells transfected with either FlagMyC-Nito or Fl(2)d-HA. In control lanes, S2R⁺ cells were transfected with FlagMyC alone and an identical HA-containing protein. Extracts were immunoprecipitated with Flag antibody and immunoblotted using Myc and HA antibodies. Two percent of input was loaded. The same experiment was performed upon depletion of Flacc. Human ZC3H13 was transfected in an identical set of experiments. The interaction between Nito and Fl(2)d is strongly reduced upon loss of Flacc (lane 6) but can be rescued upon expression of human ZC3H13 protein (lane 8). Quantification of two replicates is shown in D.

together, these findings suggest that Zc3h13 acts as an adapter that connects the RNA-binding protein Rbm15 to Wtap also in mammals.

Discussion

Our study identified a novel interactor of the m⁶A methyltransferase complex, which is conserved in *Drosophila* and mice. Its function in the m⁶A pathway is essential in both species, as its absence results in dramatic reduction of m⁶A levels. The facts that the human homolog was found recently in interactome studies with WTAP (Horiuchi et al. 2013; Wan et al. 2015) and that it can rescue the interaction between Fl(2)d and Nito in *Drosophila* suggest that it has a similar role in human cells. Despite this functional conservation, the protein sequence identity among different homologs is rather weak (Supplemental Fig. S4). Mouse Zc3h13 contains several additional domains as compared with Flacc. In partic-

ular, it differs by the presence of a zinc finger domain, which is present in a common ancestor but was lost in dipterian (Supplemental Fig. S4). Other species such as *Ciona intestinalis* also lack the zinc finger motif. In addition, the zinc finger motif can be found in two variants across evolution: one short and one long. As zinc finger motifs are commonly involved in nucleic acid binding or protein-protein interactions, it will be interesting to address the functional importance of this domain when present in the protein. Of note, Zc3h13 appears completely absent in nematodes, as is also the case for Mett13 (Dezi et al. 2016), possibly indicating that these two proteins have co-evolved for the regulation of adenosine methylation.

Our work strongly supports the existence of at least two distinct stable complexes that interact weakly to regulate m⁶A biogenesis. This result is consistent with earlier studies by Rottman and colleagues (Bokar et al. 1997), who isolated two protein components using an in vitro methylation assay and HeLa cell nuclear extracts, which are readily dissociable under nondenaturing conditions.

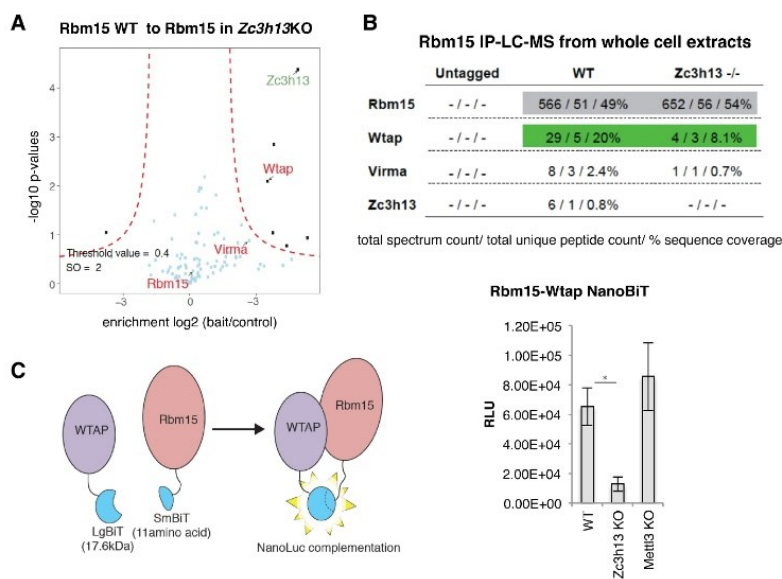
Zc3h13/Flacc is required for m⁶A biogenesis

Figure 6. Zc3h13 stabilizes the interaction between RBM15 and WTAP. (A,B) Comparison of TAP-LC-MS/MS of endogenously Flag-Avi-tagged Rbm15 mESCs in either a wild-type or a *Zc3h13* knockout background. Rbm15 and associated proteins were purified in the presence of 350 mM NaCl. (A) Volcano plot showing enriched proteins in wild-type cells (right) versus *Zc3h13* knockout cells (left). (B) Table of spectral counts, unique peptides, and percentage coverage of TAP-LC-MS/MS data in A. (C) Split luciferase NanoBiT assay examining the interaction of mouse Rbm15 and Wtap. (Left) Scheme representing luciferase reconstitution upon transfection of large (LgBiT) and small (SmBiT) NanoLuc subunit fusions and the interaction of Rbm15 and WTAP. (Right) Comparison of Rbm15–Wtap NanoBiT NanoLuc signal in wild-type and *Zc3h13* and *Mettl3* knockout cells. The mean of three independent experiments, three transfections each, is shown. Errors bars indicate SD. (*) $P = 0.026$, calculated using two-tailed Student's *t*-test.

Gel filtration and gradient glycerol sedimentation estimated molecular weights of 200 and 875 kDa (Bokar et al. 1997). While biochemical characterization will be required to address the exact identity of the different complex components, recent biochemical analysis suggests that the 200-kDa complex consists of Mettl3 and Mettl14 (Liu et al. 2014). Although the exact composition of the larger complex is currently unknown, we postulate that it is probably MACOM, consisting of Wtap, Virma, Hakai, Rbm15, and Zc3h13. The calculated total molecular weight of these proteins (600 kDa) is lower than that of the large complex (875 kDa), which suggests the presence of other factors or the inclusion of some subunits in multiple copies. For instance, recombinant WTAP can form aggregates, suggesting the possibility of higher complex organization (Liu et al. 2014). Finally, the existence of two complexes is also supported by our genetic analyses, which show that the knockout of *Mettl3* and *Mettl14* results in viable animals, while loss of function of *fl(2)d*, *vir*, *nito*, and *flacc* is lethal during development. This indicates that the MACOM acts beyond m⁶A methylation via Mettl3 (Fig. 7).

The physiological role of ZC3H13 in human cells has been poorly investigated. Recent reports suggest that mutant ZC3H13 facilitates glioblastoma progression and schizophrenia (Oldmeadow et al. 2014; Chow et al. 2017). It is possible that these diseases originate from misregulation of the m⁶A pathway upon ZC3H13 alteration. For instance, the association of m⁶A with cancer progression, in particular with glioblastoma and acute myeloid leukemia, has been demonstrated recently (Barbieri et al. 2017; Cui et al. 2017; Jaffrey and Kharas 2017; Kwok et al. 2017; Li et al. 2017; Vu et al. 2017; Zhang et al. 2017; Weng et al. 2018). Likewise, m⁶A plays an important role in cortical neurogenesis in the human fore-

brain (Yoon et al. 2017), a region of the brain that has been associated previously with schizophrenia (Heimer 2000). Hence, future studies should determine whether the role of ZC3H13 in these diseases is connected to its m⁶A-dependent function.

Materials and methods

mESC culture and genome editing

mESCs (129xC57Bl/6 genetic background; kindly provided by D. Schübeler of the Friedrich Miescher Institute for Biomedical Research) were cultured on gelatin-coated dishes in mES medium (DMEM; Gibco, 21969-035) supplemented with 15% FBS (Gibco), 1× nonessential amino acids (Gibco), 1 mM sodium pyruvate (Gibco), 2 mM L-glutamine (Gibco), 0.1 mM 2-mercaptoethanol (Sigma), 50 mg/mL penicillin, 80 mg/mL streptomycin, MycoZap prophylactic, and LIF conditioned medium at 37°C in 5% CO₂. Cultured cells were routinely tested for mycoplasma contamination using the VenorGeM mycoplasma detection kit according to manufacturer's recommendation (Sigma). For endogenous gene tagging using SpCas9-2A-mCherry (Knuckles et al. 2017), Rosa26: BirA-V5-expressing cells (RosaB) were transfected with 2 µg of SpCas9-sgRNA-2A-mCherry and 500 ng of ssODN as a donor when integration was desired. Small guide RNA constructs were generated as described in Knuckles et al. (2017). The ssODNs were synthesized as Ultramers by Integrated DNA Technologies, and their sequences are listed in Supplemental Table 2. All transfections were carried out using Lipofectamine 3000 reagent (Invitrogen). Twenty-four hours after transfection, mCherry-positive edited cells were sorted on a BD FACSAria III cell sorter (Becton Dickinson). mESCs were then sparsely seeded for clonal expansion, and then clones were individually picked, split, and screened by PCR for the desired mutation or integration. For tagging of Mettl3 and Rbm15, clones were subsequently screened by Western blotting using anti Flag (Sigma) or HRP-coupled streptavidin to confirm expression of endogenously tagged

Knuckles et al.

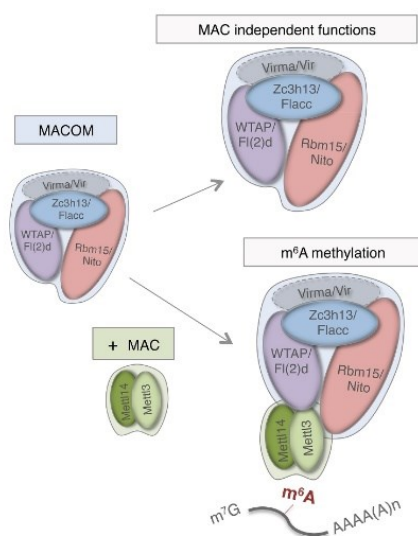


Figure 7. Schematic representation of the role of the MACOM and the MAC. The MACOM can regulate gene expression in two ways: either on its own (MAC-independent functions) or by interacting with MAC components (m^6A methylation). Flacc (Zc3h13) is a novel component of the MACOM that stabilizes the interaction between Fl(2)d and Nito (Wtap and Rbm15) proteins, thereby ensuring deposition of m^6A to targeted transcripts.

proteins. For Zc3h13 knockout lines, two independent single guide RNA (sgRNA) constructs were transfected to target sequences flanking exons 9–10, leading to a frameshift mutation and nonfunctional truncated protein. Deletion was confirmed via Western blotting using an anti-Zc3h13 antibody (Abcam, ab70802). Sequences of small guide RNAs are described in Supplemental Table 2.

Drosophila stocks and genetics

D. melanogaster w^{1118} was used as the wild-type control. Other fly stocks used were Fl(2)d shRNA [HMC03833; Bloomington *Drosophila* Stock Center [BDSC], 55674], Nito shRNA [HMS00166; obtained from *Drosophila* RNAi Screening Center [DRSC] [Harvard]], and Flacc dsRNA [GD35212 and KK110253; obtained from Vienna *Drosophila* Resource Center [VDRC]]. For genetic interaction studies, we used *Mett13^{met1}* [Haussmann et al. 2016], *Mett14^{fs}* [Lence et al. 2016], *Ythdc1^{M102006}* [Bloomington], *fl(2)d²* [Bloomington], *vir^{ts1}* [kind gift from Jamilla Horabin], *nito¹* [Yan and Perrimon 2015], and *flacc* mutant allele *CG7358^C* [Bloomington]. To remove *daughterless*, *Df(2L)BSC209* [Bloomington] was used. Driver lines used in this study were *dome-GAL4* [kind gift from Erika Bach, New York University Langone Medical Center] and *elav-GAL4* [Bloomington]. For the analysis of male-to-female transformations, flies of selected genotypes were chosen randomly.

Drosophila cell line

Drosophila S2R⁺ cells were embryonic-derived cells obtained from the *Drosophila* Genomics Resource Center [DGRC; at Indiana University; FlyBase accession FBtc0000150]. Mycoplasma

contamination was not present (verified by analyzing the RNA sequencing [RNA-seq] data from the cell line).

Cloning

The plasmids used for immunohistochemistry and coimmunoprecipitation assays in *Drosophila* S2R⁺ cells were constructed by cloning the corresponding cDNA in the pPAC vector [Lence et al. 2016] with an N-terminal Myc tag and the Gateway-based vectors with an N-terminal Flag-Myc tag (pPFMW) as well as a C-terminal HA tag (pPWH) [obtained from the DGRC at Indiana University].

TAP and MS

One confluent 15-cm dish of mESCs per sample was resuspended in 1 mL of ice-cold TAP lysis buffer (150–500 mM NaCl [depending on the experiment], 20 mM Tris-HCl at pH 7.5, 0.5% NP-40, 1 mM EDTA, 10% glycerol, 1 mM DTT supplemented with protease inhibitor cocktail [Roche]) after 0.25% trypsin/EDTA dissociation and PBS wash. Samples were shaken at 1000 rpm for 30 min at 4°C. Lysate was cleared by centrifugation at maximum speed at 4°C on a tabletop centrifuge. The protein concentration of each sample was determined using Bradford assay (Bio-Rad dye). Equal amounts of lysate (5 mg) from the control sample (parental untagged cells) and the bait protein sample (gene-tagged cells) were normalized by adding an appropriate amount of cold TAP lysis buffer to each sample to adjust the final sample concentration to ~5 mg/mL. Equilibrated Flag M2 Dynabeads (10 μ L of packed bead slurry per 5 mg of protein per sample; Sigma) previously washed twice with 1 mL of cold TAP lysis buffer were added to 5 mg/mL lysate. Tubes containing beads and lysates were incubated overnight at 4°C with end-over-end rotation.

The next day, Dynabeads were washed four times with TAP buffer for 10 min followed by three 15-min elutions of bound proteins with 3xFlag peptide (final concentration of 0.3 mg/mL in TAP buffer; Sigma). Next, elutions were pooled and added to the TAP-washed streptavidin Dynabeads (Thermo Fisher) and incubated overnight at 4°C with rotation. The next day, streptavidin Dynabeads were washed four times with TAP buffer for 10 min followed by a wash with TAP buffer without NP-40. The enriched proteins were digested directly on the Dynabeads with 0.1 mg/mL trypsin in digestion buffer (50 mM Tris at pH 8.0, 1 mM CaCl₂, 1 mM TCEP).

The generated peptides were acidified with TFA to a final concentration of 0.8% and analyzed by capillary LC-MS/MS with an EASY-nLC 1000 using the two-column setup [Thermo Scientific]. The peptides were loaded with 0.1% formic acid and 2% acetonitrile in H₂O onto a peptide trap [Acclaim PepMap 100, 75 μ m \times 2 cm, C18, 3 μ m, 100 Å] at a constant pressure of 800 bars. Peptides were separated at a flow rate of 150 nL/min with a linear gradient of 2%–6% buffer B (0.1% formic acid in acetonitrile) in buffer A (0.1% formic acid) for 3 min followed by a linear increase from 6% to 22% in 40 min, 22% to 28% in 9 min, 28% to 36% in 8 min, and 36% to 80% in 1 min, and the column was finally washed for 14 min at 80% B on a 50- μ m \times 15-cm ES801 C18, 2- μ m, 100 Å column [Thermo Scientific] mounted on a DPV ion source [New Objective] connected to an Orbitrap Fusion mass spectrometer [Thermo Scientific]. The data were acquired using 120,000 resolution for the peptide measurements in the Orbitrap and a top T (3-sec) method with HCD fragmentation for each precursor and fragment measurement in the ion trap according to the recommendations of the manufacturer [Thermo Scientific].

Zc3h13/Flacc is required for m⁶A biogenesis

Protein identification and relative quantification of the proteins were done with MaxQuant version 1.5.3.8 using Andromeda as the search engine (Cox et al. 2011) and label-free quantification (LFQ) (Cox et al. 2014) as described in Hubner et al. (2010). The mouse subset of UniProt version 2015_01 combined with the contaminant database from MaxQuant was searched, and the protein and peptide false discovery rates (FDRs) were set to 0.01. All MaxQuant parameters are in the uploaded parameter file mqpar.xml.

Statistical analysis was done in Perseus (version 1.5.2.6) (Cox et al. 2011, 2014; Tyanova et al. 2016). Results were filtered to remove reverse hits, contaminants, and peptides found in only one sample. Missing values were imputed, and potential interactors were determined using *t*-test and visualized by a volcano plot. Significance lines corresponding to a given FDR were determined by a permutation-based method (Tusher et al. 2001). Threshold values (FDR) were selected between 0.005 and 0.05 and SO (curve bend) between 0.2 and 2 and are shown in the corresponding figures. Results were exported from Perseus and visualized using statistical computing language R.

All MS raw data were deposited in ProteomeXchange (data set PXD008111).

iBAQ analysis

iBAQ was performed as described in Schwanhauser et al. (2011) to evaluate protein abundances in the MAC and the MACOM in *Mettl3* TAP-LC-MS experiments.

m⁶A-RIP

Total RNA from mESCs was isolated using Absolutely RNA Microprep kit (Stratagene) followed by mRNA selection using double Oligo d(T)23 (New England Biolabs) purification. Five micrograms of mRNA was incubated with 4 μ g of anti-m⁶A antibody (polyclonal rabbit, Synaptic Systems, catalog no. 202 003) in m⁶A immunoprecipitation buffer (150 mM NaCl, 10 mM Tris-HCl at pH 7.4, 0.1% NP-40) supplemented with 5 U/mL murine RNase inhibitor (New England Biolabs) for 2 h at 4°C. Ten microliters of protein G magnetic beads (Invitrogen) was added to all m⁶A immunoprecipitation samples for 2 h at 4°C. On-bead digestion with RNase T1 (Thermo Fisher) at a final concentration 0.1 U/mL was performed for 15 min at room temperature. Beads with captured RNA fragments were then immediately washed twice with 500 μ L of ice-cold m⁶A immunoprecipitation buffer and twice with room temperature m⁶A immunoprecipitation buffer and further eluted with 100 μ L of elution buffer (20 mM DTT, 150 mM NaCl, 50 mM Tris-HCl at pH 7.4, 1 mM EDTA, 0.1% SDS, 5 U/mL proteinase K) for 5 min at 42°C. The elution step was repeated four times, and 600 μ L of acidic phenol/chloroform (pH 4.5) (Ambion) was added to 400 μ L of the combined eluate per sample in order to extract captured RNA fragments. Samples were mixed and transferred to Phase Lock Gel Heavy tubes (5Prime) and centrifuged at 12,000g for 5 min. Aqueous phase was precipitated overnight at -80°C. On the following day, samples were centrifuged, washed twice with 80% EtOH, and resuspended in 15 μ L of RNase-free H₂O (Ambion). Recovered RNA was analyzed on RNA Pico Chip (Agilent), and concentrations were determined with RNA HS Qubit reagents. Since no RNA was recovered in the m⁶A immunoprecipitation no-antibody control samples, libraries were prepared with 30 ng of two independent m⁶A immunoprecipitations performed on RNA from wild-type and *Mettl3* and *Zc3h13* knockout cells. For every condition, input material (200 ng of mRNA) was also sequenced. Both m⁶A immunoprecipitations

and inputs were sequenced using the NEBNext RNA directional library preparation kit.

m⁶A RIP sequencing analysis

MACS2 was used to call peaks of m⁶A enrichment for wild-type immunoprecipitation versus input samples using the default parameters. Peaks were assigned to overlapping gene bodies within 500 base pairs (bp). The intersection of the resulting gene lists (3285 genes) was taken as the set of m⁶A target genes.

BigWig files for each sample were created using the qExportWig function from the QuasR package in R (Cox et al. 2011). Read counts were binned in 50-bp windows, and counts for each sample were scaled to the mean aligned library size of all samples. The deepTools suite was used for metagene analysis (Ramirez et al. 2016). The bigwigCompare function was used to calculate the log₂ ratio between each wild-type or *Zc3h13* knockout sample and the *Mettl3* knockout samples. m⁶A target CDS regions were scaled to 5 kb, and m⁶A enrichment versus *Mettl3* knockout was calculated in 50-bp bins across scaled target regions as well as 2 kb upstream and downstream using the computeMatrix command.

NanoBiT protein complementation assay

Fusion constructs of mouse Rbm15 and Wtap to NanoBiT subunits were generated as follows: Full-length Rbm15- and Wtap-coding sequences were amplified with the oligonucleotides indicated in Supplemental Table 2 from poly-A-selected mRNA using NEBNext High-Fidelity 2X PCR master mix (New England Biolabs). Overhangs with homology to destination vectors (pBiT1.1-C, pBiT2.1-C, pBiT1.1-N, and pBiTN.1-C; Promega) were included in oligonucleotide sequences. Gel-purified PCR products were cloned into EcoRI sites using NEBuilder HiFi DNA assembly kit (New England Biolabs) following the manufacturer's recommendations. The optimal combinations of N-terminal- or C-terminal-tagged fusions to small or large subunits were determined through transfection of 20,000 wild-type mESCs per well with Lipofectamine 3000 reagent (Invitrogen) seeded in 96-well tissue culture plates (Corning, catalog no. 3917). Measurements were performed using the Nano-Glo live-cell assay system (Promega) and measured in a microplate luminometer (Berthold, LB960). The Rbm15/Wtap fusion combination yielding the highest luciferase activity was then transfected into distinct mESC genetic backgrounds, and the expression level of the fusion construct was quantified via RT-qPCR using oligonucleotides described in Supplemental Table 2.

Drosophila staging

The staging experiment was performed as described previously (Lence et al. 2016) using *D. melanogaster* w¹¹¹⁸ flies. A total of three independent samples was collected for each *Drosophila* stage as well as for heads and ovaries. Samples from the staging experiment were used for RNA extraction to analyze m⁶A abundance in mRNA and expression levels of different transcripts during *Drosophila* development.

RNA isolation and mRNA purification

Total RNA from S2R⁺ cells was isolated using Trizol reagent (Invitrogen), and DNA was removed with DNase I treatment (New England Biolabs). Fly heads from 3- to 5-d-old flies were separated and homogenized in Trizol prior to RNA isolation. mRNA

Knuckles et al.

was isolated by two rounds of purification with Dynabeads Oligo d(T)25 (New England Biolabs).

RT-PCR

cDNA was prepared using M-MLV reverse transcriptase (Promega). Transcript levels were quantified using Power SYBR Green PCR master mix (Invitrogen) and the oligonucleotides indicated in Supplemental Table 2. RT-PCR was performed using the oligonucleotides described in Supplemental Table 2 to analyze *Sxl* splicing.

RNA in situ hybridization

In situ hybridization was performed as described previously (Lence et al. 2016). In situ probes were prepared with DIG RNA-labeling kit (Roche) following the manufacturer's protocol. Oligos used for the probes are listed in Supplemental Table 2.

RIP

S2R⁺ cells were transfected with Myc-tagged constructs using Effectene reagent. Seventy-two hours after transfection, cells were washed with ice-cold PBS and collected by centrifugation at 1000g for 5 min. The cell pellet was lysed in 1 mL of lysis buffer (50 mM Tris-HCl at pH 7.4, 150 mM NaCl, 0.05% NP-40) supplemented with protease inhibitors, rotated head over tail for 30 min at 4°C, and centrifuged at 18,000g for 10 min at 4°C to remove the remaining cell debris. Protein concentrations were determined using Bradford reagent (Bio-Rad). For RIP, 2 mg of protein was incubated with 2 µg of anti-Myc antibody coupled to protein G magnetic beads (Invitrogen) in lysis buffer and rotated head over tail for 4 h at 4°C. The beads were washed three times with lysis buffer for 5 min. One-fourth of the immunoprecipitated protein-RNA complexes were eluted by incubation in 1× NuPAGE LDS buffer (Thermo Fisher) for 10 min at 70°C for protein analysis. RNA from the remaining protein-RNA complexes was further isolated using Trizol reagent. qPCR was performed with the oligos listed in Supplemental Table 2.

Immunostaining

For staining of *Drosophila* S2R⁺ cells, cells were transferred to the polylysine-pretreated eight-well chambers (Ibidi) at a density of 2×10^5 cells per well. After 30 min, cells were washed with 1× DPBS (Gibco), fixed with 4% formaldehyde for 10 min, and permeabilized with PBST (0.2% Triton X-100 in PBS) for 15 min. Cells were incubated with mouse anti-Myc (1:2000; Enzo, 9E10) in PBST supplemented with 10% donkey serum overnight at 4°C. Cells were washed three times for 15 min in PBST and then incubated with secondary antibody and 1× DAPI solution in PBST supplemented with 10% donkey serum for 2 h at 4°C. After three 15-min washes in PBST, cells were imaged with a Leica SP5 confocal microscope using a 63× oil immersion objective.

Western blotting

Proteins were extracted for 30 min on ice, the lysates were centrifuged at 16,000g for 5 min at 4°C, and protein concentration in the supernatant was determined using the Bio-Rad protein assay. Protein samples were separated on NuPAGE-Novex Bis-Tris 4%–12% gradient gels (Invitrogen) in MOPS buffer for 40 min at 200 V. Semidry transfer to nitrocellulose membrane (Whatman) was performed for 40 min at 15 V. Membranes were blocked for 30 min in 2% nonfat dry milk and TBS–0.05% Tween 20

(TBST) and incubated with primary antibodies overnight at 4°C (Mettl3 [Protein Tech, 15073], Rbm15 [Abcam, ab70549], Zc3h13 [Abcam, ab70802], Hakai [Aviva Systems Biology, Cbl11 ARP39622], Wtap [Protein Tech, 60188], and Tubulin [Abcam, clone YL1/2]). Signal was detected with corresponding HRP-conjugated secondary antibodies and Immobilon Western Chemiluminescent HRP substrate (Millipore).

Cell culture, RNAi, and transfection

Drosophila S2R⁺ cells were grown in Schneider's medium (Gibco) supplemented with 10% FBS (Sigma) and 1% penicillin-streptomycin (Sigma). For RNAi experiments, PCR templates were prepared using the oligonucleotides indicated in Supplemental Table 2. dsRNA were prepared using T7 megascript kit (New England Biolabs). dsRNA against the bacterial β-galactosidase gene (*lacZ*) was used as a control for all RNAi experiments. S2R⁺ cells were seeded at a density of 10⁶ cells per milliliter in serum-free medium, and 7.5 µg of dsRNA was added to 10⁶ cells. After 6 h of cell starvation, serum-supplemented medium was added to the cells. dsRNA treatment was repeated after 48 and 96 h, and cells were collected 24 h after the last treatment. Effectene (Qiagen) was used to transfect vector constructs in all overexpression experiments following the manufacturer's protocol.

Coimmunoprecipitation assay and Western blot analysis

For the coimmunoprecipitation assay, different combinations of vectors with the indicated tags were cotransfected in S2R⁺ cells. Forty-eight hours after transfection, cells were collected, washed with DPBS, and pelleted by centrifugation at 400g for 10 min. The cell pellet was lysed in 1 mL of lysis buffer (50 mM Tris-HCl at pH 7.4, 150 mM NaCl, 0.05% NP-40) supplemented with protease inhibitors and rotated head over tail for 30 min at 4°C. Nuclei were collected by centrifugation at 1000g for 10 min at 4°C, resuspended in 300 µL of lysis buffer, and sonicated with five cycles of 30 sec on and 30 sec off at the low power setting. Cytoplasmic and nuclear fractions were joined and centrifuged at 18,000g for 10 min at 4°C to remove the remaining cell debris. Protein concentrations were determined using Bradford reagent (Bio-Rad). For immunoprecipitation, 2 mg of proteins was incubated with 2 µg of anti-Myc antibody coupled to protein G magnetic beads (Invitrogen) in lysis buffer and rotated head over tail overnight at 4°C. The beads were washed three times for 15 min with lysis buffer, and immunoprecipitated proteins were eluted by incubation in 1× NuPAGE LDS buffer (Thermo Fisher) for 10 min at 70°C. Eluted immunoprecipitated proteins were removed from the beads, and DTT was added to 10% final volume. Immunoprecipitated proteins and input samples were analyzed by Western blot after incubation for an additional 10 min at 70°C.

For Western blot analysis, proteins were separated on a 7% SDS-PAGE gel and transferred to a nitrocellulose membrane (Bio-Rad). After blocking with 5% milk in 0.05% Tween in PBS for 1 h at room temperature, the membrane was incubated with primary antibody in blocking solution overnight at 4°C. Primary antibodies used were mouse anti-Flag (1:2000; Sigma, M2-F1804), mouse anti-Myc (1:2000; Enzo, 9E10), mouse anti-HA (1:1000; Covance, 16B12), mouse anti-Tubulin (1:2000; Biolegend, 903401), mouse anti-Fl(2)d (1:500; Developmental Studies Hybridoma Bank, 9G2), and rabbit anti-Mettl14 and guinea pig anti-Mettl3 (1:500) (Lence et al. 2016). The membrane was washed three times in PBST for 15 min and incubated for 1 h at room temperature with secondary antibody in blocking solution. Protein bands were detected using SuperSignal West Pico chemiluminescent substrate (Thermo Scientific).

Zc3h13/Flacc is required for m⁶A biogenesis*SILAC experiment and LC-MS/MS analysis*

For SILAC experiments, S2R⁺ cells were grown in Schneider medium (Dundee Cell) supplemented with either heavy (Arg8 and Lys8) (Cambridge Isotope Laboratories) or light (Arg0 and Lys0) (Sigma) amino acids. For the forward experiment, Myc-Nito was transfected in heavy-labeled cells, and Myc alone was transfected in light-labeled cells. The reverse experiment was performed vice versa. The coimmunoprecipitation experiment was done as described earlier. Before elution, beads of the heavy and light lysates were combined in a 1:1 ratio and eluted with 1× NuPAGE LDS buffer that was subjected to MS analysis as described previously (Bluhm et al. 2016). Raw files were processed with MaxQuant (version 1.5.2.8) and searched against the UniProt database of annotated *Drosophila* proteins (*D. melanogaster*: 41,850 entries, downloaded January 8, 2015).

LC-MS/MS analysis of m⁶A levels

Three-hundred nanograms of purified mRNA was digested using 0.3 U of nuclease P1 from *Penicillium citrinum* (Sigma-Aldrich) and 0.1 U of snake venom phosphodiesterase from *Crotalus adamanteus* (Worthington). RNA and enzymes were incubated in 5 mM ammonium acetate (pH 5.3) for 2 h at 37°C. The remaining phosphates were removed by 1 U of FastAP (Thermo Scientific) in a 1-h incubation at 37°C in 10 mM ammonium acetate (pH 8). The resulting nucleoside mix was then spiked with ¹³C stable isotope-labeled nucleoside mix from *Escherichia coli* RNA as an internal standard (SIL-IS) to a final concentration of 6 ng/μL for the sample RNA and 2 ng/μL for the SIL-IS. For analysis, 10 μL of the previously mentioned mixture was injected into the LC-MS/MS machine. Generation of technical triplicates was obligatory. Mouse mRNA samples were analyzed in biological duplicates, and fly samples were analyzed in triplicates. LC separation was performed on an Agilent 1200 series instrument using 5 mM ammonium acetate buffer as solvent A and acetonitrile as buffer B. Each run started with 100% buffer A, which was decreased to 92% within 10 min. Solvent A was further reduced to 60% within another 10 min. Until minute 23 of the run, solvent A was increased to 100% again and kept at 100% for 7 min to re-equilibrate the column (Synergi Fusion; 4 μm particle size, 80 Å pore size, 250 × 2.0 mm; Phenomenex). The ultraviolet signal at 254 nm was recorded via a DAD detector to monitor the main nucleosides.

MS/MS was then conducted on the coupled Agilent 6460 triple-quadrupole (QQQ) mass spectrometer equipped with an Agilent JetStream ESI source that was set to the following parameters: gas temperature, 350°C; gas flow, 8 L/min; nebulizer pressure, 50 psi; sheath gas temperature, 350°C; sheath gas flow, 12 L/min; and capillary voltage, 3000 V. To analyze the mass transitions of the unlabeled m⁶A and all ¹³C m⁶A simultaneously, we used the dynamic multiple reaction monitoring mode. The quantification was conducted as described previously (Kellner et al. 2014).

RNA-seq and computational analysis

Illumina TruSeq sequencing kit (Illumina) was used for RNA-seq and computational analysis. The RNA libraries were sequenced on a NextSeq500 with a read length of 85 bp. The data were mapped against Ensembl release 90 of *D. melanogaster* using STAR (version 2.5.1b). Counts per gene were derived using featureCounts (version 1.5.1). Differential expression analysis was performed using DESeq2 (version 1.16.1) and filtered for an FDR <5%. Differential splicing analysis was performed using rMATS (version 3.2.5) and filtered for an FDR <10%. Sequencing depth-normalized coverage tracks were generated using Bedtools (ver-

sion 2.25.0), Samtools (version 1.3.1), and Kentutils (version 302). The heat map of the fold change (log₂) of commonly misregulated genes was clustered according to rows and columns. The color gradient was adjusted to display the 1% lowest/highest values within the most extreme color (lowest values as the darkest blue and highest values as the darkest red). Splice events for different knockdown conditions are represented by pie charts. “Control” depicts the detected splice events, on average, in all of the comparisons of control versus knockdown. The pie charts for the individual knockdowns depict the amount of significantly different splicing events with a FDR value <10%. The gene ontology (GO) term analysis was performed using the package ClusterProfiler. The GO terms were semantic similarity-reduced using the “simplify” function of the package. The genes tested in all of the conditions were used as a background gene set. Default parameters were used for the analysis. We defined the set of genes that was analyzed for differential expression (in any condition) and whose transcripts contained m⁶A (according to Kan et al. 2017). The significance of the overlap of these genes with the genes commonly differentially regulated in the knockdowns (either commonly up-regulated, commonly down-regulated, or misregulated in all conditions) or commonly misspliced in all conditions was tested using a hypergeometric test.

Phylogenetic analysis

The phylogenetic tree was constructed with ClustalX from multiple sequence alignments generated with MUSCLE of the *Drosophila* sequence with orthologs from human and other representative species.

Statistics

For m⁶A level measurements, data sets were compared using two-tailed Student's *t*-test for unequal variances. Normality was verified, and homogeneity of variances was analyzed with Levene's test. RIP-qPCR, ZC3H13 rescue quantification, split luciferase NanoBiT assay, and in vivo Flacc knockdown validation data sets were compared using two-tailed Student's *t*-test for equal variances. Statistical significance of fly viability was determined by a χ^2 test (GraphPad Prism). Statistical tests used for RNA-seq and m⁶A-RIP data analysis, TAP-MS analysis, iBAQ analysis, and SILAC experiments are described in detail in the relevant sections of the Materials and Methods.

Data availability

The data that support the findings of this study have been deposited in the NCBI Gene Expression Omnibus (GEO) under accession number GSE106614. All other relevant data are available from the corresponding author.

Acknowledgments

We thank the Bloomington *Drosophila* Stock Center and the Vienna *Drosophila* Resource Center for fly reagents, the *Drosophila* Genomics Resource Center at Indiana University for plasmids, members of the Bühler and Roignant laboratories for helpful discussion, Vytautas Iesmantavicius from the Protein Analysis Facility at Friedrich Miescher Institute for help with MS data analysis, and the Genomics and Bioinformatics Institute of Molecular Biology (IMB) Core Facilities for great support. Support by the IMB Proteomics Core Facility is gratefully acknowledged (the instrument is funded by Deutsche Forschungsgemeinschaft

Knuckles et al.

INST 247/766-1 FUGG). In particular, we thank Anja Freiwald from the IMB Proteomics Core Facility for sample preparation, and Dr. Mario Dejung from the Proteomics Core Facility for data processing and generating the scatter plot. Research in the laboratory of J.-Y.R. is supported by the Deutsche Forschungsgemeinschaft (DFG) RO 4681/5-1 and the Epitrans COST action (CA16120). Work performed in M. Bühler's laboratory was supported by the Novartis Research Foundation and the Swiss Science Foundation National Centre of Competence in Research RNA and Disease (grant no. 141735). Work performed in M.S.'s laboratory was supported by the Biotechnology and Biological Sciences Research Council. The project was also supported by the DFG SPP1784 grant to M.H.

Author contributions: P.K., T.L., M. Bühler, and J.-Y.R. conceived the study. P.K., T.L., I.U.H., D.J., I.M., T.H., R.V., D.H., M. Biggiogera, M.H., M.S., M. Bühler, and J.-Y.R. performed the methodology. N.K. performed the computational analysis of the RNA-seq data. S.H.C. performed the computational analysis of the methylated RIP sequencing data. M.A.A.-N. performed the phylogenetic analysis. P.K. and T.L. wrote the draft of the manuscript. All authors reviewed and edited the manuscript. M. Bühler, and J.-Y.R. supervised the study.

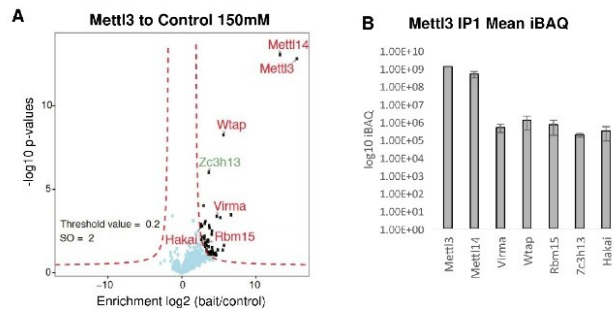
References

- Agarwala SD, Blitzblau HG, Hochwagen A, Fink GR. 2012. RNA methylation by the MIS complex regulates a cell fate decision in yeast. *PLoS Genet* **8**: e1002732.
- Barbieri I, Tzelepis K, Pandolfini L, Shi J, Millan-Zambrano G, Robson SC, Aspris D, Migliori V, Bannister AJ, Han N, et al. 2017. Promoter-bound METTL3 maintains myeloid leukaemia by m(6)A-dependent translation control. *Nature* **552**: 126–131.
- Bluhm A, Casas-Vila N, Scheibe M, Butter F. 2016. Reader interactome of epigenetic histone marks in birds. *Proteomics* **16**: 427–436.
- Bokar JA, Shambaugh ME, Polayes D, Matera AG, Rottman FM. 1997. Purification and cDNA cloning of the AdoMet-binding subunit of the human mRNA (N6-adenosine)-methyltransferase. *RNA* **3**: 1233–1247.
- Chow RD, Guzman CD, Wang G, Schmidt F, Youngblood MW, Ye L, Errami Y, Dong MB, Martinez MA, Zhang S, et al. 2017. AAV-mediated direct in vivo CRISPR screen identifies functional suppressors in glioblastoma. *Nat Neurosci* **20**: 1329–1341.
- Cox J, Neuhauser N, Michalski A, Scheltema RA, Olsen JV, Mann M. 2011. Andromeda: a peptide search engine integrated into the MaxQuant environment. *J Proteome Res* **10**: 1794–1805.
- Cox J, Hein MY, Luber CA, Paron I, Nagaraj N, Mann M. 2014. Accurate proteome-wide label-free quantification by delayed normalization and maximal peptide ratio extraction, termed MaxLFQ. *Mol Cell Proteomics* **13**: 2513–2526.
- Cui Q, Shi H, Ye P, Li L, Qu Q, Sun G, Sun G, Lu Z, Huang Y, Yang CG, et al. 2017. m⁶A RNA methylation regulates the self-renewal and tumorigenesis of glioblastoma stem cells. *Cell Rep* **18**: 2622–2634.
- Dezi V, Ivanov C, Haussmann IU, Soller M. 2016. Nucleotide modifications in messenger RNA and their role in development and disease. *Biochem Soc Trans* **44**: 1385–1393.
- Dixon AS, Schwinn MK, Hall MP, Zimmerman K, Otto P, Lubben TH, Butler BL, Binkowski BF, Machleidt T, Kirkland TA, et al. 2016. NanoLuc complementation reporter optimized for accurate measurement of protein interactions in cells. *ACS Chem Biol* **11**: 400–408.
- Dominissini D, Moshitch-Moshkovitz S, Schwartz S, Salmon-Divon M, Ungar L, Osenberg S, Cesarkas K, Jacob-Hirsch J, Amariglio N, Kupiec M, et al. 2012. Topology of the human and mouse m⁶A RNA methylomes revealed by m⁶A-seq. *Nature* **485**: 201–206.
- Flemr M, Buhler M. 2015. Single-step generation of conditional knockout mouse embryonic stem cells. *Cell Rep* **12**: 709–716.
- Haussmann IU, Bodi Z, Sanchez-Moran E, Mongan NP, Archer N, Fray RG, Soller M. 2016. m⁶A potentiates Sxl alternative pre-mRNA splicing for robust *Drosophila* sex determination. *Nature* **540**: 301–304.
- Heimer L. 2000. Basal forebrain in the context of schizophrenia. *Brain Res Brain Res Rev* **31**: 205–235.
- Hilfiker A, Amrein H, Dubendorfer A, Schneiter R, Nothiger R. 1995. The gene *virilizer* is required for female-specific splicing controlled by Sxl, the master gene for sexual development in *Drosophila*. *Development* **121**: 4017–4026.
- Horiuchi K, Kawamura T, Iwanari H, Ohashi R, Naito M, Kodama T, Hamakubo T. 2013. Identification of Wilms' tumor 1-associated protein complex and its role in alternative splicing and the cell cycle. *J Biol Chem* **288**: 33292–33302.
- Hubner NC, Bird AW, Cox J, Spletstoeser B, Bandilla P, Poser I, Hyman A, Mann M. 2010. Quantitative proteomics combined with BAC TransgeneOmics reveals in vivo protein interactions. *J Cell Biol* **189**: 739–754.
- Jaffrey SR, Kharas MG. 2017. Emerging links between m⁶A and misregulated mRNA methylation in cancer. *Genome Med* **9**: 2.
- Kan L, Grozhik AV, Vedanayagam J, Patil DP, Pang N, Lim KS, Huang YC, Joseph B, Lin CJ, Despici V, et al. 2017. The m⁶A pathway facilitates sex determination in *Drosophila*. *Nat Commun* **8**: 15737.
- Kellner S, Ochel A, Thuring K, Spenkuch F, Neumann J, Sharma S, Entian KD, Schneider D, Helm M. 2014. Absolute and relative quantification of RNA modifications via biosynthetic isotopomers. *Nucleic Acids Res* **42**: e142.
- Knuckles P, Carl SH, Musheev M, Niehrs C, Wenger A, Buhler M. 2017. RNA fate determination through cotranscriptional adenosine methylation and microprocessor binding. *Nat Struct Mol Biol* **24**: 561–569.
- Kwok CT, Marshall AD, Rasko JE, Wong JJ. 2017. Genetic alterations of m⁶A regulators predict poorer survival in acute myeloid leukemia. *J Hematol Oncol* **10**: 39.
- Lence T, Akhtar J, Bayer M, Schmid K, Spindler L, Ho CH, Kreim N, Andrade-Navarro MA, Poeck B, Helm M, et al. 2016. m⁶A modulates neuronal functions and sex determination in *Drosophila*. *Nature* **540**: 242–247.
- Lence T, Soller M, Roignant JY. 2017. A fly view on the roles and mechanisms of the m⁶A mRNA modification and its players. *RNA Biol* **14**: 1232–1240.
- Li Z, Weng H, Su R, Weng X, Zuo Z, Li C, Huang H, Nachtergaele S, Dong L, Hu C, et al. 2017. FTO plays an oncogenic role in acute myeloid leukemia as a N⁶-methyladenosine RNA demethylase. *Cancer Cell* **31**: 127–141.
- Liu J, Yue Y, Han D, Wang X, Fu Y, Zhang L, Jia G, Yu M, Lu Z, Deng X, et al. 2014. A METTL3–METTL14 complex mediates mammalian nuclear RNA N6-adenosine methylation. *Nat Chem Biol* **10**: 93–95.
- Meyer KD, Saletore Y, Zumbo P, Elemento O, Mason CE, Jaffrey SR. 2012. Comprehensive analysis of mRNA methylation reveals enrichment in 3' UTRs and near stop codons. *Cell* **149**: 1635–1646.
- Oldmeadow C, Mossman D, Evans TJ, Holliday EG, Tooney PA, Cairns MJ, Wu J, Carr V, Attia JR, Scott RJ. 2014. Combined analysis of exon splicing and genome wide polymorphism data predict schizophrenia risk loci. *J Psychiatr Res* **52**: 44–49.

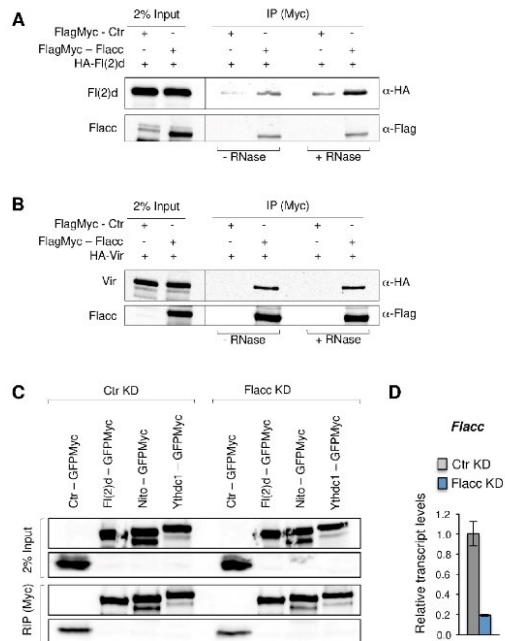
Zc3h13/Flacc is required for m⁶A biogenesis

- Patil DP, Chen CK, Pickering BF, Chow A, Jackson C, Guttman M, Jaffrey SR. 2016. m⁶A RNA methylation promotes XIST-mediated transcriptional repression. *Nature* **537**: 369–373.
- Ping XL, Sun BF, Wang L, Xiao W, Yang X, Wang WJ, Adhikari S, Shi Y, Lv Y, Chen YS, et al. 2014. Mammalian WTAP is a regulatory subunit of the RNA N⁶-methyladenosine methyltransferase. *Cell Res* **24**: 177–189.
- Ramirez F, Ryan DP, Gruning B, Bhardwaj V, Kilpert F, Richter AS, Heyne S, Dundar F, Manke T. 2016. deepTools2: a next generation web server for deep-sequencing data analysis. *Nucleic Acids Res* **44**: W160–W165.
- Roignant JY, Soller M. 2017. m⁶A in mRNA: an ancient mechanism for fine-tuning gene expression. *Trends Genet* **33**: 380–390.
- Ruzicka K, Zhang M, Campilho A, Bodi Z, Kashif M, Saleh M, Eeckhout D, El-Showk S, Li H, Zhong S, et al. 2017. Identification of factors required for m⁶A mRNA methylation in *Arabidopsis* reveals a role for the conserved E3 ubiquitin ligase HAKAI. *New Phytol* **215**: 157–172.
- Schwanhauser B, Busse D, Li N, Dittmar G, Schuchhardt J, Wolf J, Chen W, Selbach M. 2011. Global quantification of mammalian gene expression control. *Nature* **473**: 337–342.
- Schwartz S, Mumbach MR, Jovanovic M, Wang T, Maciag K, Bushkin GG, Mertins P, Ter-Ovanesyan D, Habib N, Cacchiarelli D, et al. 2014. Perturbation of m⁶A writers reveals two distinct classes of mRNA methylation at internal and 5' sites. *Cell Rep* **8**: 284–296.
- Sledz P, Jinek M. 2016. Structural insights into the molecular mechanism of the m⁶A writer complex. *eLife* **5**: e18434.
- Tusher VG, Tibshirani R, Chu G. 2001. Significance analysis of microarrays applied to the ionizing radiation response. *Proc Natl Acad Sci* **98**: 5116–5121.
- Tyanova S, Temu T, Sinitcyn P, Carlson A, Hein MY, Geiger T, Mann M, Cox J. 2016. The Perseus computational platform for comprehensive analysis of (prote)omics data. *Nat Methods* **13**: 731–740.
- Vu LP, Pickering BF, Cheng Y, Zaccara S, Nguyen D, Minuesa G, Chou T, Chow A, Saletore Y, MacKay M, et al. 2017. The N⁶-methyladenosine (m⁶A)-forming enzyme METTL3 controls myeloid differentiation of normal hematopoietic and leukemia cells. *Nat Med* **23**: 1369–1376.
- Wan C, Borgeson B, Phanse S, Tu F, Drew K, Clark G, Xiong X, Kagan O, Kwan J, Bezginov A, et al. 2015. Panorama of ancient metazoan macromolecular complexes. *Nature* **525**: 339–344.
- Wang Y, Li Y, Toth JJ, Petroski MD, Zhang Z, Zhao JC. 2014. N⁶-methyladenosine modification destabilizes developmental regulators in embryonic stem cells. *Nat Cell Biol* **16**: 191–198.
- Wang P, Doxtader KA, Nam Y. 2016a. Structural basis for cooperative function of Mettl3 and Mettl14 methyltransferases. *Mol Cell* **63**: 306–317.
- Wang X, Feng J, Xue Y, Guan Z, Zhang D, Liu Z, Gong Z, Wang Q, Huang J, Tang C, et al. 2016b. Structural basis of N⁶-adenosine methylation by the METTL3–METTL14 complex. *Nature* **534**: 575–578.
- Weng H, Huang H, Wu H, Qin X, Zhao BS, Dong L, Shi H, Skibbe J, Shen C, Hu C, et al. 2018. METTL14 inhibits hematopoietic stem/progenitor differentiation and promotes leukemogenesis via mRNA m(6)A modification. *Cell Stem Cell* **22**: 191–205 e199.
- Yan D, Perrimon N. 2015. spenito is required for sex determination in *Drosophila melanogaster*. *Proc Natl Acad Sci* **112**: 11606–11611.
- Yoon KJ, Ringeling FR, Vissers C, Jacob F, Pokrass M, Jimenez-Cyrus D, Su Y, Kim NS, Zhu Y, Zheng L, et al. 2017. Temporal control of mammalian cortical neurogenesis by m⁶A methylation. *Cell* **171**: 877–889.e17.
- Zhang S, Zhao BS, Zhou A, Lin K, Zheng S, Lu Z, Chen Y, Sulman EP, Xie K, Bogler O, et al. 2017. m⁶A demethylase ALKBH5 maintains tumorigenicity of glioblastoma stem-like cells by sustaining FOXM1 expression and cell proliferation program. *Cancer Cell* **31**: 591–606.e6.
- Zhong S, Li H, Bodi Z, Button J, Vespa L, Herzog M, Fray RG. 2008. MTA is an *Arabidopsis* messenger RNA adenosine methylase and interacts with a homolog of a sex-specific splicing factor. *Plant Cell* **20**: 1278–1288.

Knuckles_Lence309146_FigS2

**Supplemental Figure 2. Flacc/Zc3h13 regulates the m⁶A pathway, supporting data I**

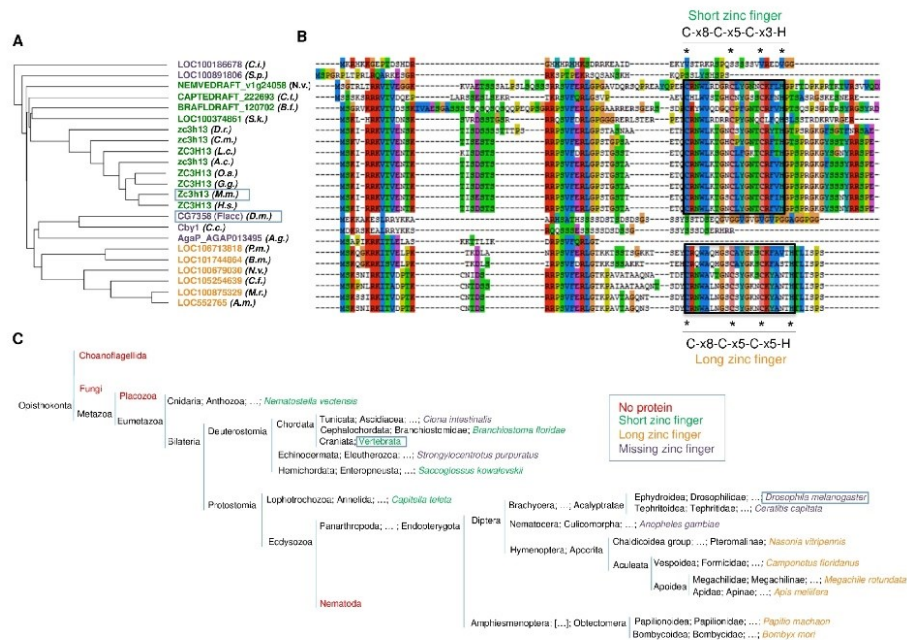
(A) TAP-LC-MS/MS of endogenously FLAG-Avi tagged Mettl3 mESC's compared to Parental untagged in presence of 150mM NaCl. Highlighted are enriched proteins (red) including novel protein Zc3h13 (green). (B) iBAQ values for selected proteins for (A).



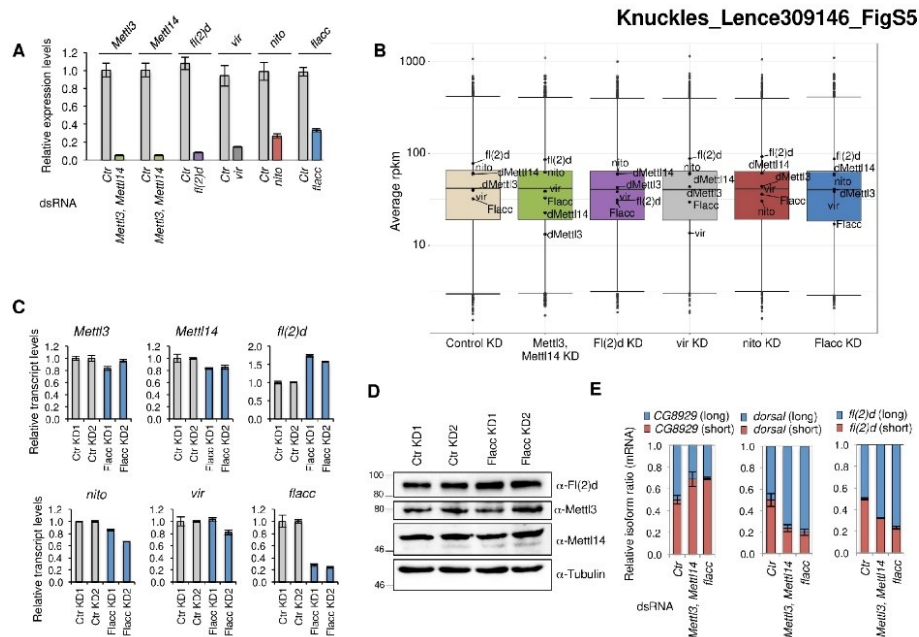
Supplemental Figure 3. Flacc/Zc3h13 regulates the m⁶A pathway, supporting data II

(A and B) Co-immunoprecipitation experiments were carried out with lysates prepared from S2R+ cells, transfected with FlagMyc-Flacc and HA-Fl(2)d (A) or HA-Vir (B). In control lanes, S2R+ cells were transfected with FlagMyc alone and identical HA-containing protein. Extracts were immunoprecipitated with Myc antibody and immunoblotted using Flag and HA antibodies. 2% of input was loaded. The same experiment was repeated in the presence of RNaseT1. Fl(2)d and Vir interact with Flacc in an RNA independent manner. (C and D) Western blot validation of RNA immunoprecipitation experiments, which were carried out with lysates prepared from S2R+ cells, transfected with GFPMyc-tagged control, Fl(2)d, Nito and Ythdc1 constructs. Extracts were immunoprecipitated with Myc antibody and immunoblotted using Myc antibody. 2% of input was loaded. The same experiment was performed upon Flacc depletion. Relative expression of *flacc* levels is shown in (D).

Knuckles_Lence309146_FigS4

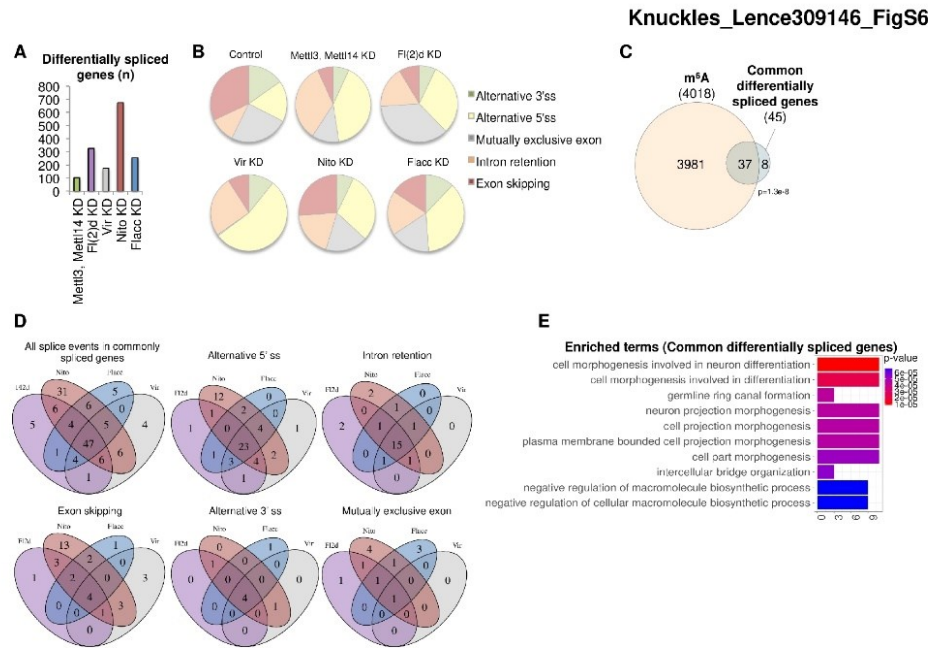
**Supplemental Figure 4. Phylogenetic characterization of ZC3H13 proteins.**

(A) Phylogenetic tree of the full sequence alignment of orthologs of ZC3H13 in 23 species. The labels indicate the gene names (from the NCBI's Entrez database) and the abbreviated species name. (B) N-terminal part of the multiple sequence alignment used to construct the phylogenetic tree, including the zinc-finger (boxes). (C) Tree of the 23 species included in the phylogenetic analyses. Coloring indicates whether the indicated taxa or species contain a ZC3H13 ortholog, and whether the ortholog has the zinc finger or not. The names of 15 species are displayed. The vertebrates included, whose names were not displayed, were: *Danio rerio*, *Callorhinchus milii*, *Latimeria chalumnae*, *Anolis carolinensis*, *Ornithorhynchus anatinus*, *Gallus gallus*, *Mus musculus* and *Homo sapiens*. See methods for details.



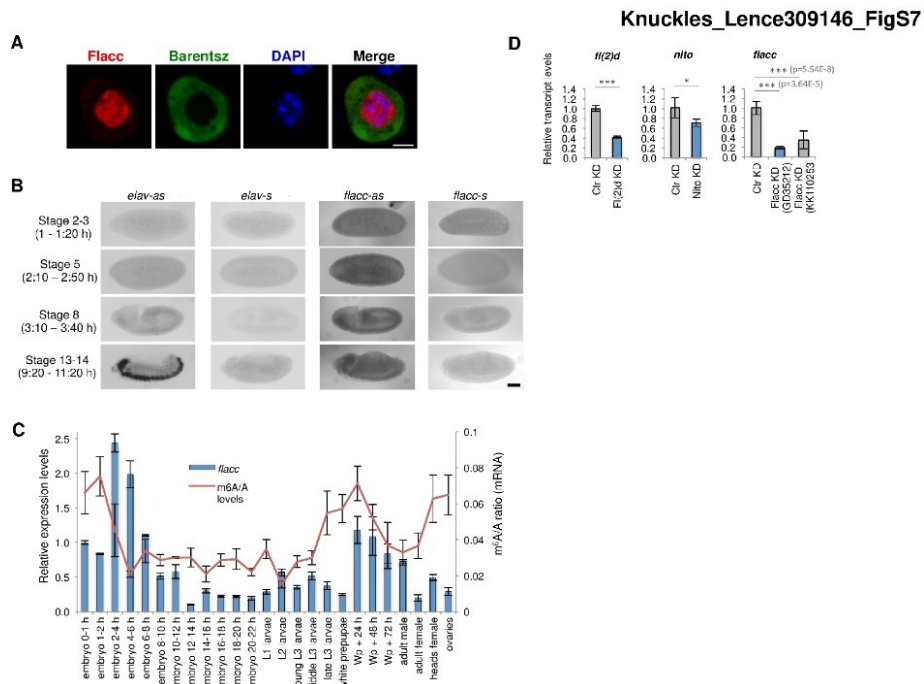
Supplemental Figure 5. Flacc regulates common transcripts with other components of the m⁶A complex, supporting data I

(A) Relative expression of indicated transcripts upon control (LacZ), Mett13, Mett14, Vir, Nito and Flacc KD. The mean standard deviation of three technical measurements from three biological replicates is shown. (B) Boxplots of average expression (rpkm) within replicates for all genes expressed by at least 1 rpkm in the different conditions. The black dots indicate the expression of m⁶A components in comparison to other expressed genes. (C) Relative expression of indicated transcripts upon control (LacZ) and Flacc KD. (D) WB for Mett13, Mett14 and Fl(2)d in control (LacZ) and Flacc KD. (E) (A) Relative isoform quantification of m⁶A-regulated genes (*CG8929*, *dorsal*, *fl(2)d*) upon depletion of indicated components. Flacc is required for m⁶A-dependent splicing events.

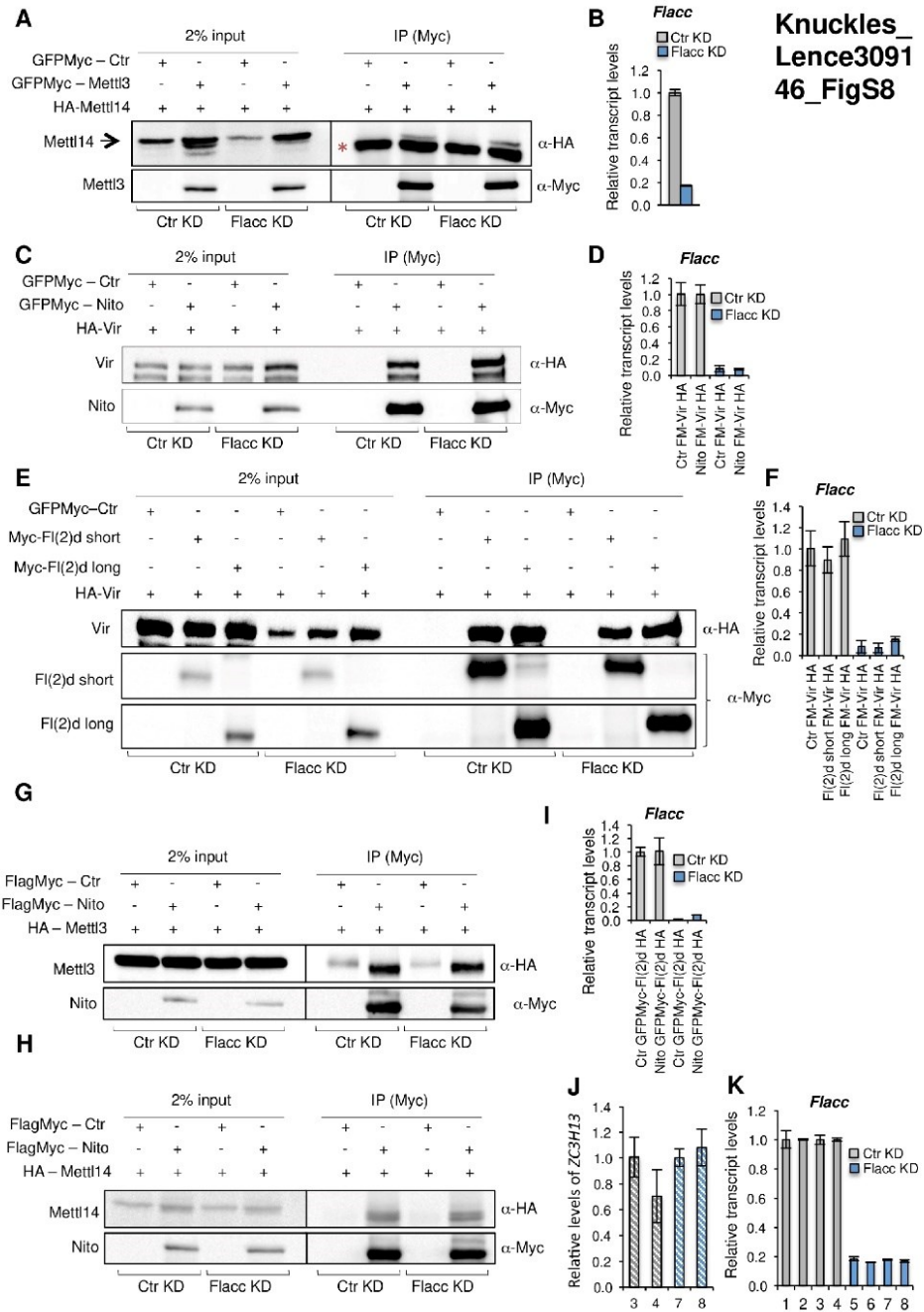


Supplemental Figure 6. Flacc regulates common transcripts with other components of the m⁶A complex, supporting data II

(A) Number of differentially spliced genes upon KD of indicated proteins. (B) Distribution of splicing events in the different KD conditions. The pie chart for “Control” depicts the detected splice events on average in all the comparisons “control vs. KD”. The pie charts for the individual KD depict the amount of significantly different splicing events with a FDR value below 10%. Intron retention and alternative 5' splice site usage are over-represented upon KD of m⁶A components. (C) Overlap between common differentially spliced genes and m⁶A-containing genes (miCLIP data from (Kan et al. 2017)). The significance of the overlap was tested using a hypergeometric test. Most commonly differentially spliced genes are methylated. (D) Venn diagrams of common differentially spliced events regulated by components of MACOM complex (E) The GO term analysis of common differentially spliced genes, performed using the package ClusterProfiler. Top 10 GO-terms are displayed.



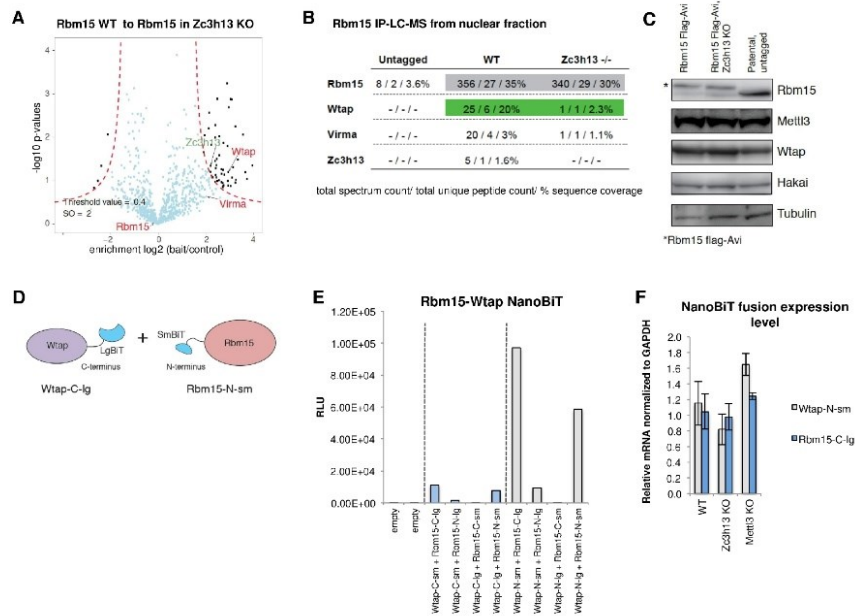
Supplemental Figure 7. Flacc sub-cellular localization and expression through development
(A) Immunostaining of Myc-tagged Flacc protein in S2R+ cells. GFP-tagged Barentsz was used as a cytoplasmic marker. Scale bar, 5 μm . **(B)** *in situ* RNA hybridization of *flacc* (*flacc-as*), *flacc* control (*flacc-s*), *elav* positive control (*elav-as*) and *elav* negative control (*elav-s*) are shown. Scale bars, 100 μm . **(C)** Relative *flacc* mRNA expression and levels of m⁶A in mRNA during *Drosophila* development. Number of hours post-fertilization for different embryo, larval and pupal stages is indicated below. The mean with standard deviation of three technical measurements from three biological replicates is shown. **(D)** Relative expression of indicated transcripts in fly heads upon control, Fl(2)d, Nito or Flacc KD. The mean of three technical measurements from two biological replicates is shown. Errors bars indicate standard deviation (s.d.). *, P<0.01; ***, P<0.0001 (Student's t-test).



Supplemental Figure 8. Flacc depletion does not interfere with interactions between two methyltransferases or between Vir and Fl(2)d.

(A-F) Co-immunoprecipitation experiments were carried out with lysates prepared from S2R+ cells, transfected with either GFPMyC-Mettl3 and Mettl14-HA (A), or Myc-Nito and Vir-HA (C), or Myc-Fl(2)d short isoform, Myc-Fl(2)d long isoform and Vir-HA (E). In control lanes, S2R+ cells were transfected with GFPMyC alone and identical HA-containing proteins. Extracts were immunoprecipitated with Myc antibody and immunoblotted using Myc and HA antibodies. 2% of input was loaded. The same experiments were performed upon depletion of Flacc. Interactions between Mettl3 and Mettl14, and Fl(2)d and Vir do not depend on the presence of Flacc (A, C and E). Relative expression of *flacc* levels is shown in (B, D and F). Star indicates IgG band in figure (A). (G and H) Co-immunoprecipitation experiments were carried out with lysates prepared from S2R+ cells, transfected with either FlagMyC-Nito and Mettl3-HA (A), or FlagMyC-Nito and Mettl14-HA (C). In control lanes, S2R+ cells were transfected with GFPMyC alone and identical HA-containing proteins. Extracts were immunoprecipitated with Myc antibody and immunoblotted using Myc and HA antibodies. 2% of input was loaded. The same experiments were performed upon depletion of Flacc. Interactions between Nito and Mettl3/Mettl14 are not affected by depletion of Flacc. (I) Related to Figure 5A. Relative levels of *flacc* in indicated samples. The mean with standard deviation of three technical measurements is shown. (J and K) Related to Figure 5C. Relative levels of human ZC3H13 transfected in indicated samples (J) and Relative levels of *flacc* in indicated samples (K). The mean with standard deviation of three technical measurements from two biological replicates is shown.

Knuckles_Lence309146_FigS9

**Supplemental Figure 9. Zc3h13 stabilizes the interaction between Rbm15 and Wtap.**

(A and B) Comparison of TAP-LC-MS/MS of endogenously FLAG-Avi tagged Rbm15 mESC's in either a WT or *Zc3h13* KO background. Rbm15 and associated proteins were purified from nuclear fractions of lysates. (A) Volcano plot showing enriched proteins in WT cells (right) vs *Zc3h13* KO cells. (B) Table of spectral counts, unique peptides and % coverage of TAP-LC-MS/MS data in (A). (C) Western blot analysis comparing parental untagged, FLAG-Avi tagged Rbm15 and FLAG-Avi tagged Rbm15 *Zc3h13* KO mESCs levels of Rbm15, Mettl3, Wtap and Hakai, Tubulin was used as loading control). * Denotes shift in Rbm15 due to FLAG-Avi tag. (D) Split luciferase NanoBiT assay examining mouse Rbm15 and Wtap. Scheme depicting example fusion constructs generated to determine optimal configuration of fusion proteins. e.g. Wtap-C-Ig is C-terminally tagged Wtap fused to the large subunit of NanoLuc. (E) Luciferase assays comparing all possible LgBit and SmBit NanoLuc subunit fusions to Rbm15 and Wtap to determine which combination provides the strongest signal. (F) RT-qPCR measurements of Wtap-N-sm and Rbm15-C-Ig fusion constructs in WT, *Zc3h13* KO and *Mettl3* KO backgrounds.

Kan L, Grozhik AV, Vedanayagam J, Patil DP, Pang N, Lim KS, Huang YC, Joseph B, Lin CJ, Despic V et al. 2017. The m(6)A pathway facilitates sex determination in *Drosophila*. *Nature communications* **8**: 15737.



Zc3h13/Flacc is required for adenosine methylation by bridging the mRNA-binding factor Rbm15/Spenito to the m⁶A machinery component Wtap/FI(2)d

Philip Knuckles, Tina Lence, Irmgard U. Haussmann, et al.

Genes Dev. 2018, **32**: originally published online March 13, 2018
Access the most recent version at doi:[10.1101/gad.309146.117](https://doi.org/10.1101/gad.309146.117)

Supplemental Material	http://genesdev.cshlp.org/content/suppl/2018/03/13/gad.309146.117.DC1
References	This article cites 48 articles, 9 of which can be accessed free at: http://genesdev.cshlp.org/content/32/5-6/415.full.html#ref-list-1
Creative Commons License	This article, published in <i>Genes & Development</i> , is available under a Creative Commons License (Attribution 4.0 International), as described at http://creativecommons.org/licenses/by/4.0/ .
Email Alerting Service	Receive free email alerts when new articles cite this article - sign up in the box at the top right corner of the article or click here .

A promotional banner for EXIQON and QIAGEN. The left side features a blue background with a grid of dots and the text 'Boost NGS microRNA profiling. Read about 3 methods tested'. The right side shows the EXIQON logo with the tagline 'Now a QIAGEN company' and the QIAGEN logo.

Acknowledgements



Thank you all!

Hvala vsem!

Ko hodiš, pojdi zmeraj do konca.

*Spomladi do rožne cvetice,
poleti do zrele pšenice,
jeseni do polne police,
pozimi do snežne kraljice,
v knjigi do zadnje vrstice,
v življenju do prave resnice,
v sebi do rdečice
čez eno in drugo lice.*

*A če ne prideš ne prvič, ne drugič
do krova in pravega kova,
poskusi vnovič in zopet in znova.*

(Tone Pavček, Popotnik)

When you walk, follow your way to the end.

*In spring, to the rose in flower,
in summer to the ripened wheat,
in autumn, to the well-stocked shelf,
in winter, to the snow-white queen,
in a book, to the last line recorded,
in life, to the very truth,
and in yourself – to a colour shed
over your cheeks blushing red.*

*If you've failed the first time, the second time, then,
in attaining sorts and summits you pursue,
try again, once more, and anew.*

(Tone Pavček, The Wayfarer)
